Mathematical Problems in Engineering

Coordinated Control and Estimation of Multiagent Systems with Engineering Applications

Guest Editors: Housheng Su, Michael Z. Q. Chen, Qing Hui, Wei Zhang, and Fanglai Zhu

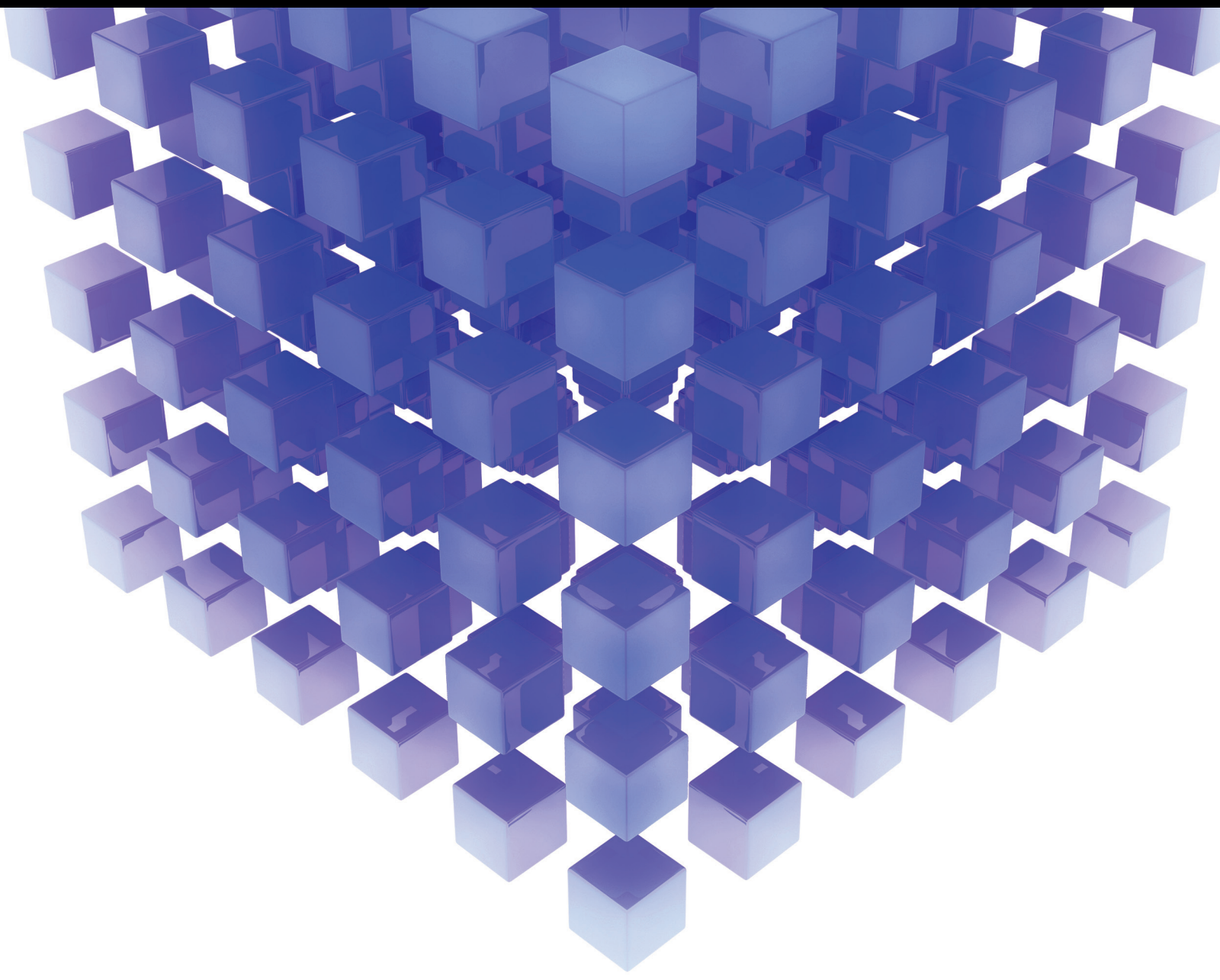

Coordinated Control and Estimation of Multiagent Systems with Engineering Applications

Mathematical Problems in Engineering

Coordinated Control and Estimation of Multiagent Systems with Engineering Applications

Guest Editors: Housheng Su, Michael Z. Q. Chen, Qing Hui, Wei Zhang, and Fanglai Zhu

Editorial Board

Contents

Hindawi Publishing Corporation
Mathematical Problems in Engineering
Volume 2015, Article ID 105827, 2 pages
http://dx.doi.org/10.1155/2015/105827

Editorial

Coordinated Control and Estimation of Multiagent Systems with Engineering Applications

Housheng Su,[1] Michael Z. Q. Chen,[2] Qing Hui,[3] Wei Zhang,[4] and Fanglai Zhu[5]

[1]*School of Automation, Huazhong University of Science and Technology, Wuhan 430074, China*
[2]*Department of Mechanical Engineering, The University of Hong Kong, Pokfulam Road, Hong Kong*
[3]*Department of Mechanical Engineering, Texas Tech University, Lubbock, TX, USA*
[4]*Laboratory of Intelligent Control and Robotics, Shanghai University of Engineering Science, Shanghai 201620, China*
[5]*College of Electronics and Information Engineering, Tongji University, Shanghai 200092, China*

Correspondence should be addressed to Housheng Su; houshengsu@qq.com

Received 14 December 2014; Accepted 14 December 2014

Recently, coordinated control and estimation problems have attracted a great deal of attention in different fields especially in biology, physics, computer science, and control engineering. Coordinated control and estimation problems have prominent characteristics of distributed control, local interaction, and self-organization. Research on multiagent coordinated control and estimation problems not only helps better understand the mechanisms of natural collective phenomena but also benefits the applications of cyberphysical systems.

This special issue focuses on theoretical and technological achievements in cooperative multiagent Systems. It contains twenty-six papers, the contents of which are summarized below.

(1) *Coordinated Control of Multiagent Systems and Synchronization of Complex Networks*. D. Yang and X. Liu "Distributed Robust Attitude Tracking of Multiple Spacecraft with Disturbances and Unmodelled Dynamics" investigated the distributed robust attitude tracking problem of multiple spacecraft subject to disturbances and unmodelled dynamics using the relative attitudes and relative angular velocities of neighbors. L. Ma et al. "Distributed Multiagent Control Approach for Multitarget Tracking" presented a novel control approach in distributed manner for multitarget tracking by providing a suboptimal multiagent control solution by maximizing the local Rényi divergence. F. Jiang et al. "Extremum Seeking Based Fault-Tolerant Cooperative Control for Multiagent Systems" proposed a novel fault tolerant cooperative control strategy for multiagent systems, and a real-time adaptive extremum seeking algorithm is utilized for adaptive approximation of fault parameter.

H. Zhou et al. "Flocking Control of Multiple Mobile Agents with the Rules of Avoiding Collision" investigated the flocking and the coordinative control problems of multiple mobile agents with the rules of avoiding collision. L. Wang et al. "Adaptive Synchronization via State Predictor on General Complex Dynamic Networks" discussed the adaptive synchronization of general complex dynamic networks via state predictor based on the fixed topology for nonlinear dynamical systems. W. Hu et al. "Impulsive Containment Control in Nonlinear Multiagent systems with Time-Delay" studied the containment control problems of nonlinear multiagent systems with time-delay via impulsive algorithms under both fixed and switching topologies. J. Ma et al. "Distributed Event-Triggered Control of Multiagent Systems with Time-Varying Topology" investigated the consensus of first-order discrete-time multiagent systems with time-varying interaction topology. C. Xu et al. "Pinning-Like Adaptive Consensus for Networked Mobile Agents with Heterogeneous Nonlinear Dynamics" studied the adaptive consensus for networked mobile agents with heterogeneous nonlinear dynamics. B. Liu et al. "Consensus of the Multiagent System with a Dynamic Leader Based on Directed Topology Using Laplace Transform" investigated the consensus of the multiagent system with directed topology and a dynamic leader. B. Liu et al. "Consensus of Multiagent Systems with Directed Topology and Communication Time Delay Bases on the

Laplace Transform" investigated the consensus problem of multiagent systems with directed topologies by proposing a new method, the Laplace transform, to study the consensus of multiagent systems. Y.-J. Sun et al. "Consensus Analysis for a Class of Heterogeneous Multiagent Systems with Time Delay Based on Frequency Domain Method" investigated the consensus problem of heterogeneous multiagent systems composed of first-order and second-order agent based on frequency domain method. The sufficient consensus conditions were obtained. M. Yu et al. "Average Consensus in Multiagent Systems with the Problem of Packet Losses When Using the Second-Order Neighbors' Information" investigated the average consensus of multiagent systems with the problem of packet losses when both the first-order and the second-order neighbors' information are used.

(2) *Distributed Estimation and Control for Mobile Sensor Networks*. Y. Bo et al. "Improved Different Dimensional Sensors Combined Space Registration Algorithm" studied a method based on the state value and space deviation of federated filtering of unscented Kalman filter and standard Kalman filter, which conduces to real time registering of system deviation of radar and IF sensors. B. Yan et al. "Robust Fault Detection for a Class of Uncertain Nonlinear Systems Based on MultiObjective Optimization" presented a robust fault detection scheme for a class of nonlinear systems with uncertainty. The proposed approach utilizes robust control theory and parameter optimization algorithm to design the gain matrix of fault tracking approximator (FTA) for fault detection. The design of the gain matrix of FTA takes into account the robustness of residual signals to system uncertainty and sensitivity of residual signals to system faults simultaneously, which leads to a multiobjective optimization problem. Then, the detectability of system faults is analyzed by investigating the threshold of residual signals. W. Liu et al. "Energy-Efficient Node Scheduling Method for Cooperative Target Tracking in Wireless Sensor Networks" proposed an energy-efficient node scheduling method is proposed to minimize energy consumption while ensuring the tracking accuracy. The proposed scheduling method can keep the tracking accuracy while minimizing energy consumption and the NP-complete nature is avoided. B. Yan et al. "Distributed Fault Detection for a Class of Nonlinear Stochastic Systems" presented a novel distributed fault detection strategy for a class of nonlinear stochastic systems, in which a nonlinear fault detection filter was constructed to provide estimation of unmeasurable system states and residual signals using outputs of the consensus filter.

(3) *Applications of Coordinated Control of Complex Networked Systems*. L. Qin et al. "Distributed Multiagent for NAO Robot Joint Position Control Based on Echo State Network" studied the joints position control of NAO robot. X. Dongdong et al. "The Study on Detection Method of Water Vapor on Boundary Layer Based on Multiagent System" proposed a method of detecting water vapor on boundary layer based on multiagent system. G. Chen et al. "A Core Model for Parts Suppliers Selecting Method in Manufacturing Supply Chain" proposed a core model for parts suppliers selecting method in manufacturing supply chain. H. Zhang et al. "Data Fusion Based Thermal Sensors for Mass Flow Measurement in Pneumatic Conveying" investigated the mass flow measurement of the gas-solid two-phase flow in pneumatic conveyor and proposed a new data fusion method based on the thermal sensors. D. Wang and S. Wu "Design of the Congestion Control for TCP/AQM Network with Time-Delay" designed congestion controller for TCP/AQM (transmission control protocol/Active queue management) networks using model following control, the equilibrium of a class of TCP/AQM network with time-delay was investigated, and the effect of communication time-delay on the stability was addressed. C. Zhang et al. "Hybrid Structure Based Tracking and Consensus for Multiple Motors" investigated a hybrid structure based synchronous control strategy for multimotor system of shaftless-driven printing press. S. Deng et al. "Solving the Fuzzy Bilevel Linear Programming with Multiple Followers through Structured Element Method" showed that the fuzzy bilevel linear programming with multiple followers (MFFBLP) model optimal solution was equivalent to the optimal solution of the bilevel linear programming with multiple followers by using fuzzy structured element theory. W. Zeng et al. "Risk-Sensitive Multiagent Decision-Theoretic Planning Based on MDP and One-Switch Utility Functions" studied multiagent decision-theoretic planning under Markov decision processes (MDPs) framework with considering the change of agent's risk attitude as his wealth level varies. C. Xie and J. Ren "A Dynamical Reliability Prediction Algorithm for Composite Service" proposed a new reliability predicting algorithm for composite services. Comparing with the traditional reliability model, the new dynamic reliability approach is more flexible, which does not recompute reliability for all composite units and only computes the reliability of the effected composite units. D. Sun and X. Kou "Punishment Effect of Prisoner Dilemma Game Based on a New Evolution Strategy Rule" discussed the effect of the punishment in the Prisoner's Dilemma Game and proposed a new evolution strategy rule which can reflect the external factor for both players in the evolution game.

Note that the selected topics and papers are not a comprehensive representation of the area covered by the special issue. Note, however, that the published papers in this special issue do provide some recent advances in the field of multiagent systems, which could benefit the current research in some way.

Acknowledgments

We would like to thank all the authors for their contributions and acknowledge all the reviewers for their time and effort in assessing the manuscripts.

Housheng Su
Michael Z. Q. Chen
Qing Hui
Wei Zhang
Fanglai Zhu

Hindawi Publishing Corporation
Mathematical Problems in Engineering
Volume 2015, Article ID 903682, 10 pages
http://dx.doi.org/10.1155/2015/903682

Research Article

Distributed Multiagent Control Approach for Multitarget Tracking

Liang Ma, Kai Xue, and Ping Wang

College of Mechanical and Electrical Engineering, Harbin Engineering University, Harbin, Heilongjiang 150001, China

Correspondence should be addressed to Liang Ma; mllx01161110@hotmail.com

Received 24 July 2014; Accepted 19 September 2014

Academic Editor: Housheng Su

In multiagent systems, tracking multiple targets is challenging for two reasons: firstly, it is nontrivial to dynamically deploy networked agents of different types for utility optimization; secondly, information fusion for multitarget tracking is difficult in the presence of uncertainties, such as data association, noise, and clutter. In this paper, we present a novel control approach in distributed manner for multitarget tracking. The control problem is modelled as a partially observed Markov decision process, which is a NP-hard combinatorial optimization problem, by seeking all possible combinations of control commands. To solve this problem efficiently, we assume that the measurement of each agent is independent of other agents' behavior and provide a suboptimal multiagent control solution by maximizing the local Rényi divergence. In addition, we also provide the SMC implementation of the sequential multi-Bernoulli filter so that each agent can utilize the measurements from neighbouring agents to perform information fusion for accurate multitarget tracking. Numerical studies validate the effectiveness and efficiency of our multiagent control approach for multitarget tracking.

1. Introduction

Advances in microelectromechanical systems have significantly boosted the development of multiagent systems in the past two decades. Low-cost agents, for example, robots, unmanned vehicles, or autonomous platforms, with high mobility, various sensing types, and powerful communication ability, are capable of different tasks in complex environment, for example, environmental monitoring, target localization and tracking, and event recognition [1, 2]. Multiagent coordinated control, as the fundamental problems in multiagent system, has received increasing research interest for utility optimization recently [3–5]. An area that benefits greatly from multiagent system is target tracking [6]. However, very little progress has been made in this direction since it is an extremely challenging problem in two aspects: multiagent control and information fusion for multitarget tracking.

The multiagent control problem in essence is a decision making issue which is to fulfill a given task in an optimal/suboptimal way. In this paper, we study the multiagent control problem particularly for multitarget tracking including accurate estimation of both target number and the location of each target. In the literature, researchers and practitioners have done extensive work on the agent control problem. Olfati-Saber et al. [6] established a consensus based Kalman filter for distributed single target tracking. In [7], multiagent control is performed by path following of a virtual leader. Olfati-Saber [8] provided flocking algorithms in both theory and applications to handle large number of agents. Unfortunately, none of them fit for the multitarget tracking issue well.

Recently, random finite set (RFS) based Bayesian framework has opened doors for multisensor multiobject system and provides elegant mathematical tools to address multitarget tracking problem in multiagent systems [9]. The probability hypothesis density (PHD) [10], cardinalized PHD (CPHD) [11], and multi-Bernoulli filter [12] have been developed as approximations under different posterior assumptions. Gaussian mixture and particle implementation of these filters have been shown to be effective in different tracking applications [13–17]. Using tools from FISST, agent control can pose as a partially observed Markov decision process (POMDP) [18], which has been shown to be effective in a single agent case in recent works [19, 20].

In this paper, we will further extend the work in [19, 20] to a more general problem: multiagent control for multitarget tracking, which is far more difficult than the single agent control case. We first model the multiagent coordinated control problem as a 1-step look-ahead POMDP since the multiple-step look-ahead is computationally intractable and show it is a NP combinatorial optimization problem when seeking all possible combinations of admissible control commands. Hence, we propose a suboptimal solution under the assumption that the measurements of each agent are independent of other agents' behavior. The multiagent coordinated control is decoupled into distributed control of each agent by maximizing the local Rényi divergence between prior and posterior multitarget probability density. Besides, we present the sequential Monte Carlo (SMC) implementation of the sequential multi-Bernoulli filter for each agent to utilize measurements from neighbouring agents. Numerical simulations demonstrate the effectiveness and efficiency of our approach.

The remainder of this paper is organized as follows. Section 2 presents some preliminary knowledge of RFS based Bayesian framework to lay a foundation for the rest of this paper. In Section 3, we illustrate the distributed agent control approach and present its implementation in detail. Section 4 provides the information fusion scheme for multitarget tracking for each agent to utilize measurements from other agents. Section 5 provides numerical results that verify the proposed agent control and multitarget tracking approach.

2. Preliminary Knowledge of RFS Based Bayesian Framework

This section provides the basic concepts and notations of RFS based Bayesian framework. Section 2.1 gives a general description of RFS and how to model multitarget by multi-Bernoulli RFS. Then, the RFS based Bayesian filtering is provided thereafter in Section 2.2.

2.1. Multi-Bernoulli RFS. A random finite set (RFS) is a random variable that takes values as unordered finite sets. The randomness of an RFS refers to two aspects: the set cardinality (number of elements of the set) is random; each element in the set is also a random variable. The probabilistic description of RFS has been studied regarding various types of probability distributions such as multi-Bernoulli (or Bernoulli) RFS, IID (short for independent identically distributed) cluster RFS, and Poisson RFS [21]. Here, we introduce the multi-Bernoulli RFS for multitarget state modelling, which offers a better alternative than the Poisson RFS and IID cluster RFS in applications with highly nonlinear model and/or nonhomogeneous sensor type [12].

Assume the dimension of target state is n; then, the target state space is denoted by $\mathcal{X} \subseteq \mathbb{R}^n$. A multi-Bernoulli RFS X on $\mathcal{X}$ is a union of a fixed number of independent Bernoulli RFSs $X^{(j)}$ with existence probability $r^{(j)} \in (0,1)$ and probability density $p^{(j)}$ (defined on $\mathcal{X}$), $j = 1, \ldots, M$; that is, $X = \cup_{j=1}^{M} \{X^{(j)}\}$.

Use a Bernoulli set for modelling a single target; then, the multitarget state can be modeled as multi-Bernoulli RFS Ξ with probability density given in [12] as follows:

$$f\left(\{\mathbf{x}_1, \ldots, \mathbf{x}_n\}\right) = f(\emptyset) \cdot \sum_{(r^{(j)}, p^{(j)}) \in \Xi} \left(\prod_{i=1}^{n} \frac{r^{(j)} p^{(j)}(\mathbf{x}_i)}{1 - r^{(j)}} \right), \quad (1)$$

where $r^{(j)}$ and $p^{(j)}$, respectively, represent the existence probability and distribution of the jth target and $f(\emptyset) = \prod_{j=1}^{M}(1 - r^{(j)})$. It is clear that the multitarget density can be completely specified by multi-Bernoulli parameter set $\{(r^{(j)}, p^{(j)})\}_{j=1}^{M}$. Hence, let us denote the multitarget density at time k by $\pi_k = \{(r_k^{(j)}, p_k^{(j)})\}_{j=1}^{M_k}$ for short in the following content.

2.2. Multisource Multiobject Bayesian Framework. Stochastic filtering in Bayesian framework has developed in decades [22]. Under the assumption of linear model and Gaussian distribution, Kalman filter is derived [23] and has been widely used for tracking since then. To extend the standard Bayesian framework to a multisource multitarget version, we need the help of RFS modelling. Let X_k and Z_k denote the state set and observation set, respectively, as follows:

$$\begin{aligned} X_k &= \left\{\mathbf{x}_{k,1}, \ldots, \mathbf{x}_{k,N_k}\right\}, \\ Z_k &= \left\{Z_k^1, \ldots, Z_k^W\right\}, \end{aligned} \quad (2)$$

where W is the total number of agents (we treat each agent as a single sensor) and $Z_k^i = \{\mathbf{z}_k^i, \ldots, \mathbf{z}_{k,M_{k,i}}^i\}$ for $i = 1, \ldots, W$. N_k is the time-varying cardinality of targets, while $M_{k,i}$ is the cardinality of the measurement set generated by agent i.

Using the RFS representation, the movement of multiobject can be described using two parts: an RFS for survival targets from previous time step S_k and an RFS for spontaneous birth targets at current time Γ_k. Thus, at time k, we have the predicted RFS $X_k = S_k \cup \Gamma_k$. The RFS for measurements Z_k^i of agent i can be represented as a union of two parts: target-generated measurements Θ_k^i and clutter K_k^i; thus, $Z_k^i = \Theta_k^i \cup K_k^i$.

Given the specific type of RFS, the Bayesian framework for optimal estimation via RFS which is the same form as the classical Bayesian filtering is given as follows:

$$\begin{aligned} &f_{k|k-1}\left(X \mid Z_{1:k-1}\right) \\ &\quad = \int f_{k|k-1}\left(X \mid X'\right) f_{k-1}\left(X' \mid Z_{1:k-1}\right) \delta X', \\ &f_k\left(X \mid Z_{1:k}\right) = \frac{f_k\left(Z_k \mid X\right) f_{k|k-1}\left(X \mid Z_{1:k-1}\right)}{\int f_k\left(Z_k \mid X\right) f_{k|k-1}\left(X \mid Z_{1:k-1}\right) \delta X}, \end{aligned} \quad (3)$$

which represent the prediction and update process of Bayesian recursion via set integrals, respectively. Under different assumptions of the RFS type, the PHD, CPHD, and multi-Bernoulli filter have been derived from (3) by finite set statistics [9]. Notice that the integrals in (3) are FISST set integrals (see [9–11] for details).

3. POMDP Based Distributed Multiagent Control Approach

In this section, we first illustrate multiagent control in the framework of a POMDP in Section 3.1. Section 3.2 provides maximizing expected Rényi divergence between prior and posterior multitarget density as the objective function for the control scheme. By assuming the measurement of each agent is independent of other agents' behavior, we propose a distributed agent control approach by maximizing the local Rényi divergence in Section 3.3.

3.1. POMDP Based Multiagent Control. We begin with the notations of using a POMDP as the solution for multiagent control. At time k, denote the control command of agent i by $\mathbf{u}_k^i \in \mathbf{U}_k^i$, where $\mathbf{U}_k^i$ is the set of all admissible control commands for agent i. Let $\mathcal{U}_k \in \mathbb{U}_k$ denote the multiagent control command, and $\mathbb{U}_k$ is the set of all possible control command combinations. Then, $\mathcal{U}_k = \{\mathbf{u}_k^1, \ldots, \mathbf{u}_k^i, \ldots, \mathbf{u}_k^W\}$ for $i = 1, \ldots, W$ and W is the total number of agents.

Define $\mathcal{D}(\mathcal{V}, f, Z)$ as the objective function dependent on multiagent control command $\mathcal{V}$, multitarget density f, and the associated measurement set Z when control command $\mathcal{V}$ was applied. The aim of multiagent control is to find the optimal multiagent control command $\mathcal{U}_k$ by maximizing/minimizing the statistical expectation of predefined objective function $\mathcal{D}(\mathcal{V}, f, Z)$ as

$$\begin{aligned}\mathcal{U}_k = \arg \max_{\mathcal{V} \in \mathbb{U}_k} (\min) \mathbf{E} \\ \times \left[\mathcal{D}\left(\mathcal{V}, f_{k-1}\left(X_{k-1} \mid Z_{0:k-1}, \mathcal{U}_{0:k-1}\right), Z_k\left(\mathcal{V}\right)\right)\right],\end{aligned} \tag{4}$$

where $f_{k-1}(X_{k-1} \mid Z_{0:k-1}, \mathcal{U}_{0:k-1})$ represents the multitarget posterior density after applying a sequence of multiagent control commands $\mathcal{U}_0, \ldots, \mathcal{U}_{k-1}$. Remark that the general formulation of POMDP is a p-step future decision process of which the computational cost would grow exponentially with the number of future steps. In this paper, we only consider a one-step future decision described by (4) as an approximation.

3.2. Global Objective Function. As shown in (4), the objective function plays a crucial role in POMDP based multiagent control problem. Information theoretic method is a typical objective function for sensor management. Here, we propose maximizing the information gain of multitarget prior and posterior density as the objective function for tracking. The Rényi divergence, also known as alpha divergence, measures the information gain between any two probability densities. The objective function for multitarget tracking is given as follows:

$$\begin{aligned}\mathcal{R}\left(\mathcal{U}_k\right) = \frac{1}{\alpha - 1} \\ \times \log\left(\left(\int \left[g_{k+1}\left(Z_{k+1} \mid X_{k+1}, \mathcal{U}_k\right)\right]^{\alpha}\right.\right. \\ \left.\left. \times f_{k+1|k}\left(X_{k+1} \mid Z_{1:k}\right) \delta X_{k+1}\right) \\ \times \left(\left[p\left(Z_{k+1} \mid Z_{1:k}, \mathcal{U}_k\right)\right]^{\alpha}\right)^{-1}\right),\end{aligned} \tag{5}$$

where $p(Z_{k+1} \mid Z_{1:k}, \mathcal{U}_k) = \int g_{k+1}(Z_{k+1} \mid X_{k+1}, \mathcal{U}_k) f_{k+1|k}(X_{k+1} \mid Z_{1:k}) \delta X$ and α is a parameter that determines how much we emphasize the tails of two densities in the metric. Notice that the Rényi divergence becomes the Kullback-Leibler discrimination and Hellinger affinity, respectively, when $\alpha \to 1$ and $\alpha = 0.5$ [24].

To compute the expectation of (5), we introduce the SMC implementation of the objective function. At time k, assume that the multitarget predicted density $f_{k+1|k}(X_k \mid Z_{1:k})$ is given in SMC form; that is, $f_{k+1|k}(X_k \mid Z_{1:k}) = \sum_{j=1}^{S} \omega^j \cdot \delta_{X_{k+1}^j}(X)$, where each multitarget particle $X_{k+1}^j = \{\mathbf{x}_{k+1,1}^j, \ldots, \mathbf{x}_{k+1,n_k^j}^j\}$, $n_{k+1}^j = |X_{k+1}^j|$ is the number of targets, $\mathbf{x}_{k+1,i}^j$ for $i = 1, \ldots, n_{k+1}^j$ represent target position in the state space, and ω^j is the weight associated to particle X_{k+1}^j. Notice that X_{k+1}^j is a particle sampled from a RFS, which accounts for the randomness of both the cardinality and target positions of particle X_{k+1}^j. Given the Bayesian prediction and update equations (3), we obtain

$$\begin{aligned}&\mathbf{E}\left[\mathcal{R}\left(\mathcal{U}_k, Z_{k+1}\right)\right] \\ &= \frac{1}{(\alpha - 1)} \log \frac{\sum_{j=1}^{S} \omega^j \left[g_{k+1}\left(Z_{k+1} \mid X_{k+1}^j, \mathcal{U}_k\right)\right]^{\alpha}}{\left[\sum_{j=1}^{S} \omega^j g_{k+1}\left(Z_{k+1} \mid X_{k+1}^j, \mathcal{U}_k\right)\right]^{\alpha}},\end{aligned} \tag{6}$$

where the multisensor multitarget likelihood function dependent on multiagent control $g_{k+1}(Z_{k+1} \mid X_{k+1}^j, \mathcal{U}_k)$ is given by

$$g_{k+1}\left(Z_{k+1} \mid X_{k+1}^j, \mathcal{U}_k\right) = \prod_{i=1}^{W} g_{k+1}^i\left(Z_{k+1}^i \mid X_{k+1}^j, \mathcal{U}_k\right) \tag{7}$$

and the single-sensor multitarget likelihood function dependent on multiagent control $g_{k+1}^i(Z_{k+1}^i \mid X_{k+1}^j, \mathcal{U}_k)$ is given in [9] as follows:

$$\begin{aligned}&g_{k+1}^i\left(Z_{k+1}^i \mid X_{k+1}^j, \mathcal{U}_k\right) \\ &= f_c\left(Z_{k+1}^i\right)\left(1 - p_D^i\right)^{n_{k+1}^j} \\ &\times \sum_{\theta} \prod_{l:\theta(l)>0} \frac{p_D^i g_{k+1}^i\left(\mathbf{z}_{\theta(l)}^i \mid \mathbf{x}_{k+1,l}^j, \mathcal{U}_k\right)}{\left(1 - p_D^i\right) \lambda c\left(\mathbf{z}_{\theta(l)}^i\right)},\end{aligned} \tag{8}$$

where $g_{k+1}^i(\mathbf{z}_{\theta(l)}^i \mid \mathbf{x}_{k+1,l}^j, \mathcal{U}_k)$ is the standard single-sensor single-target likelihood function described by the measurement model of agent i; $f_c(Z_{k+1}^i)$ is the probability density of clutter RFS and $f_c(Z_{k+1}^i) = e^{-\lambda} \prod_{\mathbf{z}^i \in Z_{k+1}^i} \lambda c(\mathbf{z}^i)$ for Poisson RFS; λ is the clutter rate, while $c(\cdot)$ is the probability distribution of clutter; $l : \theta(l) > 0$ represents all possible associations

between the particle set X_{k+1}^j and the measurement set Z_{k+1}^i; that is, $\theta : \{1, \ldots, n_{k+1}^j\} \rightarrow \{0, 1, \ldots, M_{k,i}\}$. Notice that (6) is a multisensor multitarget case, whereas the derivation is similar to the single sensor case in [19]. Thus, we directly omit the tedious proof here.

3.3. Distributed Agent Control. Even though multiagent control can be described as a POMDP given by (4) and (5), it is still intractable to achieve the global optimum of defined objective function for two reasons: firstly, searching all admissible control command combinations is a NP-hard combinatorial optimization problem [25]; secondly, global optimization requires the existence of a centralized fusion center that receives information from all agents, which is unrealistic for most large-scale multiagent systems. Hence, we propose a distributed sensor control method that compromises the local optimum of the global objective function, which is computationally tractable and convenient to implement.

Instead of computing the global information gain, we consider finding the optimal command for each individual agent. Similar to (5), the Rényi divergence for the ith agent is given by

$$\begin{aligned}&\mathbf{E}\left[\mathscr{R}^i\left(\mathbf{u}_k^i, Z_{k+1}\right)\right]\\&\quad= \frac{1}{(\alpha-1)}\log\frac{\sum_{j=1}^S \omega^j\left[g_{k+1}\left(Z_{k+1}\mid X_{k+1}^j, \mathbf{u}_k^i\right)\right]^\alpha}{\left[\sum_{j=1}^S \omega^j g_{k+1}\left(Z_{k+1}\mid X_{k+1}^j, \mathbf{u}_k^i\right)\right]^\alpha}.\end{aligned} \tag{9}$$

Assume that measurement set generated by one agent is independent of other agents' behaviour; then, the multisensor multitarget likelihood function $g_{k+1}(Z_{k+1} \mid X_{k+1}^j, \mathbf{u}_k^i)$ in (9) can be written as follows:

$$\begin{aligned}&g_{k+1}\left(Z_{k+1}\mid X_{k+1}^j, \mathbf{u}_k^i\right)\\&\quad= \prod_{l=1}^W g_{k+1}^l\left(Z_{k+1}^l\mid X_{k+1}^j, \mathbf{u}_k^i\right)\\&\quad= g_{k+1}^i\left(Z_{k+1}^i\mid X_{k+1}^j, \mathbf{u}_k^i\right)\prod_{l=1, l\neq i}^W g_{k+1}^l\left(Z_{k+1}^l\mid X_{k+1}^j\right),\end{aligned} \tag{10}$$

where $g_{k+1}^l(Z_{k+1}^l \mid X_{k+1}^j, \mathbf{u}_k^i) = g_{k+1}^l(Z_{k+1}^l \mid X_{k+1}^j)$ for $l \neq i$. The future measurement Z_{k+1} is generated assuming no clutter and unity detection rate as illustrated in [20]. For agent i, Z_{k+1}^i is predicted based on the multitarget state and possible control command $\mathbf{u}_k^i$, while Z_{k+1}^l for $l \neq i$ is predicted based on the multitarget state and current location of agent l. Therefore, we can find the optimal control command for each individual agent and then combine them together to form the total control command set, which is given as follows:

$$\mathbf{u}_k^i = \arg\max_{\mathbf{u}\in\mathbf{V}_k} \mathbf{E}\left[\mathscr{R}^i\left(\mathbf{u}, Z_{k+1}\right)\right], \tag{11}$$

$$\mathscr{U}_k = \bigcup_{i=1}^W \left\{\mathbf{u}_k^i\right\}. \tag{12}$$

Remark 1. Equation (9) is exactly a particular case of (6) by assuming all agents except agent i stay still at current time. The proposed distributed control approach is a suboptimal solution of (6) by seeking its local optimum, and the local optimum means that $\mathbf{u}_k^i$ is optimal given all other agents keep still.

When computing the optimal command of agent i, the distributed agent control given by (11) approximates the likelihood function $g_{k+1}^l(Z_{k+1}^l \mid X_{k+1}^j)$ via using current locations of agent l for $l \neq i$. Hence, we refer to (9) as the "local Rényi divergence" in this paper.

The proposed distributed control approach can significantly reduce the computational cost to perform real-time agent control. For illustration, assume that all agents have the same number of possible control command denoted by m; the computation complexity of our control approach is $\mathcal{O}(W \cdot m)$ which is much smaller than $\mathcal{O}(m^W)$ by searching all control combinations, especially in large-scale multiagent system.

Generally speaking, each agent can only communicate with its neighbouring W_k' agents and obtain their current locations $\mathbf{s}_k^l$ as well as their measurement model $g^l(\mathbf{z} \mid \mathbf{x})$ for $l = 1, \ldots, W_k'$. Here, we assume that the information received by each agent is accurate without any input saturation. For a more challenging case that there is input saturation described in [26, 27], the topic is beyond the scope of this paper. The neighbouring relationship may change over time due to the relative movement of agents. Algorithm 1 provides the SMC implementation of proposed distributed control for each agent by maximizing the local Rényi divergence.

4. Multisensor Fusion for Multi-Target Tracking

As mentioned before, the multi-Bernoulli filter outweighs the PHD/CPHD filter in the SMC implementation for nonlinear problem since the state extraction in multi-Bernoulli filter is not dependent upon the heuristics in clustering but is dependent only on the Bernoulli parameters. Hence, the multi-Bernoulli filter has been used extensively in computer vision [16, 17], robot SLAM [28], and sensor network [29]. Besides, the state-of-the-art development of the multi-Bernoulli filter offers the power to directly produce tracks of individual targets, which is known as the labelled multi-Bernoulli filter in the community [30].

In this section, we first briefly review the cardinality-balanced multi-Bernoulli filter given in [12] in Section 4.1. Then, Section 4.2 provides the sequential update scheme for information fusion of multiple sensors.

4.1. Cardinality-Balanced Multi-Bernoulli Filter

Prediction. At time k, if the posterior multitarget density is multi-Bernoulli given by $\pi_k = \{(r_k^{(j)}, p_k^{(j)})\}_{j=1}^{M_k}$ and the density of new births is also multi-Bernoulli $\pi_{\Gamma,k+1} = \{(r_{\Gamma,k+1}^{(j)}, p_{\Gamma,k+1}^{(j)})\}_{j=1}^{M_{\Gamma,k+1}}$, then the predicted density is given by

$$\pi_{k+1|k} = \left\{\left(r_{k+1|k}^{(j)}, p_{k+1|k}^{(j)}\right)\right\}_{j=1}^{M_k} \cup \left\{\left(r_{\Gamma,k+1}^{(j)}, p_{\Gamma,k+1}^{(j)}\right)\right\}_{j=1}^{M_{\Gamma,k+1}}, \tag{13}$$

Input: predicted multi-target density $\pi_{k+1|k}$, neighbouring agents $\mathbf{s}_k^l$ and $g^l(\mathbf{z} \mid \mathbf{x})$ for $l = 1, \ldots, W_k'$
(1) Sampling the multi-object state space $\{X_{k+1|k}^j\}_{j=1}^S \sim \pi_{k+1|k}$;
(2) Compute predicted estimation: target number $\widehat{n}_{k+1|k}$ and state $\widehat{X}_{k+1|k} = \cup_{j=1}^{\widehat{n}_{k+1|k}} \{\mathbf{x}_{k+1|k}^j\}$;
(3) **for** $l = 1, \ldots, W_k'$ **do**
(4) Predict Z_{k+1}^l based on $\widehat{X}_{k+1|k}$ and $g^l(\mathbf{z} \mid \mathbf{x})$;
(5) Compute single-sensor multi-target likelihood given by (8) to obtain $\{g(Z_{k+1}^l \mid X_{k+1|k}^j)\}_{j=1}^S$;
(6) **end for**
(7) **for** each $\mathbf{u}_k^i \in \mathbf{U}_k^i$ **do**
(8) Predict Z_{k+1}^i based on $\mathbf{u}_k^i$ and $g^i(\mathbf{z} \mid \mathbf{x})$;
(9) Compute single-sensor multi-target likelihood given by (8) to obtain $\{g(Z_{k+1}^i \mid X_{k+1|k}^j, \mathbf{u}_k^i)\}_{j=1}^S$;
(10) Compute multi-sensor multi-target likelihood given by (10) to obtain $\{g(Z_{k+1} \mid X_{k+1|k}^j, \mathbf{u}_k^i)\}_{j=1}^S$;
(11) Compute the value $\rho(\mathbf{u}_k^i) = \mathbf{E}[\mathscr{R}^i]$ given by (9);
(12) **end for**
Output: $\widehat{\mathbf{u}}_k^i = \arg\max \rho(\mathbf{u}_k^i)$

Algorithm 1: Control law of agent i.

where for survival targets

$$r_{k+1|k}^{(j)} = r_k^{(j)} \cdot \left\langle p_k^{(j)}, p_{S,k} \right\rangle,$$
$$p_{k+1|k}^{(j)}(\mathbf{x}) = \frac{\left\langle f_{k+1|k}(x \mid \cdot), p_k^{(j)} p_{S,k} \right\rangle}{\left\langle p_k^{(j)}, p_{S,k} \right\rangle}. \tag{14}$$

And, for new born targets, $r_{\Gamma,k+1}^{(j)}, p_{\Gamma,k+1}^{(j)}(\mathbf{x})$ are prior existence probability and distribution of birth model.

Update. At time $k+1$, if the predicted multitarget density is multi-Bernoulli $\pi_{k+1|k} = \{(r_{k+1|k}^{(j)}, p_{k+1|k}^{(j)})\}_{j=1}^{M_{k+1|k}}$, the output of corrector is composed of legacy tracks and measurement-updated tracks as

$$\pi_{k+1} = \left\{\left(r_{L,k+1}^{(j)}, p_{L,k+1}^{(j)}\right)\right\}_{j=1}^{M_{k+1|k}} \cup \left\{\left(r_{U,k+1}(\mathbf{z}), p_{U,k+1}(\cdot \mid \mathbf{z})\right)\right\}_{\mathbf{z} \in Z_k}, \tag{15}$$

where

$$r_{L,k+1}^{(j)} = r_{k+1|k}^{(j)} \frac{1 - \left\langle p_{k+1|k}^{(j)}, p_{D,k+1} \right\rangle}{1 - r_{k+1|k}^{(j)} \left\langle p_{k+1|k}^{(j)}, p_{D,k+1} \right\rangle},$$
$$p_{L,k+1}^{(j)}(\mathbf{x}) = p_{k+1|k}^{(j)}(\mathbf{x}) \frac{1 - p_{D,k+1}(\mathbf{x})}{1 - \left\langle p_{k+1|k}^{(j)}, p_{D,k+1} \right\rangle},$$
$$r_{U,k+1}(\mathbf{z}) = \left(\sum_{j=1}^{M_{k+1|k}} \frac{r_{k+1|k}^{(j)} \left(1 - r_{k+1|k}^{(j)}\right) \left\langle p_{k+1|k}^{(j)}, \psi_{k+1,\mathbf{z}} \right\rangle}{\left(1 - r_{k+1|k}^{(j)} \left\langle p_{k+1|k}^{(j)}, p_{D,k+1} \right\rangle\right)^2} \right) \times \left(\kappa_{k+1}(\mathbf{z}) + \sum_{j=1}^{M_{k+1|k}} \frac{r_{k+1|k}^{(j)} \left\langle p_{k+1|k}^{(j)}, \psi_{k+1,\mathbf{z}} \right\rangle}{1 - r_{k+1|k}^{(j)} \left\langle p_{k+1|k}^{(j)}, p_{D,k+1} \right\rangle} \right)^{-1},$$
$$p_{U,k+1}(\mathbf{z}) = \frac{\sum_{j=1}^{M_{k+1|k}} \left(r_{k+1|k}^{(j)} / \left(1 - r_{k+1|k}^{(j)}\right)\right) p_{k+1|k}^{(j)}(\mathbf{x}) \psi_{k+1,\mathbf{z}}(\mathbf{x})}{\sum_{j=1}^{M_{k+1|k}} \left(r_{k+1|k}^{(j)} / \left(1 - r_{k+1|k}^{(j)}\right)\right) \left\langle p_{k+1|k}^{(j)}, \psi_{k+1,\mathbf{z}} \right\rangle},$$
$$\psi_{k+1,\mathbf{z}}(\mathbf{x}) = g_{k+1}(\mathbf{z} \mid \mathbf{x}) p_{D,k+1}(\mathbf{x}); \tag{16}$$

p_S and p_D are probability of survival and detection. The inner product $\langle \cdot, \cdot \rangle$ is defined between two real valued functions β and γ by $\langle \beta, \gamma \rangle = \int \beta(x)\gamma(x)dx$. Note that, without loss of generality, we refer to the cardinality-balanced multi-Bernoulli filter as "multi-Bernoulli" filter for simplicity in this paper.

4.2. Sequential Multisensor Multi-Bernoulli Filter. In multisensor multitarget tracking scenario, there is no unified multisensor fusion method which is tractable and computationally acceptable. Sequential update has been widely used and verified to be a good approximation for information fusion of multiple sensors. Here, multitarget tracking in multiagent network is implemented via multi-Bernoulli filter with sequential update scheme based on the SMC implementation.

Suppose that, at time k, the posterior multitarget density is given as $\{r_k^{(j)}, p_k^{(j)}\}_{j=1}^{M_k}$, and the distribution of each target is given by a set of weighted particles $p_k^{(j)}(\mathbf{x}) = \sum_{i=1}^{L_k^{(j)}} \omega_{i,k}^{(j)} \cdot \delta_{\mathbf{x}_{i,k}^{(j)}}(\mathbf{x})$. Then, we give the SMC implementation of sequential multisensor multi-Bernoulli filter in Algorithm 2. We refer the readers to Section 4.1 of [12] for detailed equations.

The superscript $^{(j),l}$ in Algorithm 2 represents the predicted jth Bernoulli set updated with the lth sensor. To avoid the infinite growth of multi-Bernoulli set number, those with existence probability less than a predefined threshold (e.g., 0.001) are removed. Meanwhile, the particle number is limited between $L_{\min}$ and $L_{\max}$, in case that sampling is not enough or resampling reallocates too many particles. The number of particles for each Bernoulli set is proportional to each target existence $r_k^{(j)}$ during the resampling step. With

Prediction:

Input: $\pi_k = \{r_k^{(j)}, p_k^{(j)}\}_{j=1}^{M_k}$

(1) **for** Survival targets: $j = 1, \ldots, M_k$ **do**

(2) for $i = 1, \ldots, L_k^{(j)}$, sample $x_{S,i,k+1|k}^{(j)}$, compute weight $\omega_{S,i,k+1|k}^{(j)}$ and normalization $\widetilde{\omega}_{S,i,k+1|k}^{(j)}$

(3) compute $r_{S,k+1|k}^{(j)}$, $p_{S,k+1|k}^{(j)}(\mathbf{x})$

(4) **end for**

(5) **for** newborn targets: $j = 1, \ldots, M_{\Gamma,k+1}$ **do**

(6) for $i = 1, \ldots, L_{\Gamma,k}^{(j)}$, sample $x_{\Gamma,i,k+1}^{(j)}$, compute weight $\omega_{\Gamma,i,k+1}^{(j)}$ and normalization $\widetilde{\omega}_{\Gamma,i,k+1}^{(j)}$

(7) compute $r_{\Gamma,k+1}^{(j)}$, $p_{\Gamma,k+1}^{(j)}(\mathbf{x})$

(8) **end for**

Output: $\pi_{k+1|k} = \{(r_{k+1|k}^{(j)}, p_{k+1|k}^{(j)})\}_{j=1}^{M_k} \cup \{(r_{\Gamma,k+1}^{(j)}, p_{\Gamma,k+1}^{(j)})\}_{j=1}^{M_{\Gamma,k+1}}$

Update:

Input: $\pi_{k+1|k} = \{r_{k+1|k}^{(j)}, p_{k+1|k}^{(j)}\}_{j=1}^{M_{k+1|k}}$; neighbouring agents $\mathbf{s}_k^l$, $g^l(\mathbf{z} \mid \mathbf{x})$ and Z_{k+1}^l for $l = 1, \ldots, W_k'$

(1) **for** $l = 1, \ldots, W_k'$ **do**

(2) **for** Legacy targets: $j = 1, \ldots, M_{k+1|k}$ **do**

(3) compute $\omega_{L,i,k+1}^{(j),l}$ and normalization $\widetilde{\omega}_{L,i,k+1}^{(j),l}$, compute pseudo-likelihood $\varrho_{L,k+1}^{(j),l}$

(4) compute $r_{L,k+1}^{(j),l}$, $p_{L,k+1}^{(j),l}(\mathbf{x})$

(5) **end for**

(6) **for** $\mathbf{z} \in Z_{k+1}^l$ **do**

(7) **for** Measurement-updated targets: $j = 1, \ldots, M_{k+1|k}$ **do**

(8) compute $\omega_{U,i,k+1}^{(j),l}(\mathbf{z})$ and normalization $\widetilde{\omega}_{U,i,k+1}^{(j),l}(\mathbf{z})$, compute pseudo-likelihood $\varrho_{U,k+1}^{(j),l}(\mathbf{z})$

(9) compute $r_{U,k+1}^{(j),l}(\mathbf{z})$, $p_{U,k+1}^{(j),l}(\mathbf{x}; \mathbf{z})$

(10) **end for**

(11) **end for**

(12) $\pi_{k+1|k} = \{(r_{L,k+1}^{(j),l}, p_{L,k+1}^{(j),l})\}_{j=1}^{M_{k+1|k}} \cup \{(r_{U,k+1}^{l}(\mathbf{z}), p_{U,k+1}^{l}(\cdot \mid \mathbf{z}))\}_{\mathbf{z} \in Z_{k+1}^l}$

(13) **end for**

Output: $\pi_{k+1} = \{(r_{L,k+1}^{(j),W_k'}, p_{L,k+1}^{(j),W_k'})\}_{j=1}^{M_{k+1|k}} \cup \{(r_{U,k+1}^{W_k'}(\mathbf{z}), p_{U,k+1}^{W_k'}(\cdot \mid \mathbf{z}))\}_{\mathbf{z} \in Z_{k+1}^{W_k'}}$

Algorithm 2: SMC sequential multisensor multi-Bernoulli filter.

a given existence threshold 0.75, those sets with $r_k^{(j)}$ over 0.75 are true tracks, while the others are not. Notice that the multi-Bernoulli filter we adopt here cannot produce tracks directly, and it can be replaced by the labelled multi-Bernoulli filter to produce individual tracks at the cost of some extra computation.

5. Simulation

In order to demonstrate the performance of proposed multi-agent control approach for multitarget tracking, we present numerical results for a planar multitarget tracking scenario in multiagent system where three controllable moving observers, two equipped with range-only sensors and one with a bearing-only sensor, are placed in a specified surveillance area of size $[0, 1000\,\mathrm{m}] \times [0, 1000\,\mathrm{m}]$ to estimate the number of targets as well as their positions. Each agent shares its current locations, sensor type, and observations with the other agents. It is intuitive that the initial positions of agents have an impact on the agent control and target tracking procedure. However, we are not going to involve the network topology issue in this paper since our approach is supposed to act independently from the network topology which is different from the method described in [31, 32].

There are unknown and time-varying numbers of targets observed in clutter for each agent. Assume that targets move according to the nearly constant velocity model given by

$$\mathbf{x}_k = F\mathbf{x}_{k-1} + G\mathbf{w}_{v,k}, \tag{17}$$

where $\mathbf{x}_k = [p_{x,k}, v_{x,k}, p_{y,k}, v_{y,k}]^T$; $\mathbf{p}_k = [p_{x,k}, p_{y,k}]^T$ are planar position and $\mathbf{v}_k = [v_{x,k}, v_{y,k}]^T$ are planar velocity, respectively, along x-coordinate, y-coordinate. $F = I_2 \otimes \left[\begin{smallmatrix} 1 & T \\ 0 & 1 \end{smallmatrix}\right]$; $G = I_2 \otimes \left[\begin{smallmatrix} T^2/2 \\ T \end{smallmatrix}\right]$. I_2 is 2×2 identity matrix and $\otimes$ denotes Kronecker product. T is the sampling period, and $\mathbf{w}_{v,k} \sim \mathcal{N}(\mathbf{0}, Q_k)$ is a 2×1 IID Gaussian noise. Assume process noise is time-invariant and identical for both $v_{x,k}$ and $v_{y,k}$; then, $Q = \sigma_v^2 I_2$, where σ_v is the standard deviation.

Measurement of sensor l originated from target with state $\mathbf{x}_k$ is noisy vector of range or bearing measurement, and the measurement model for range-only sensor is given by

$$\mathbf{z}_{r,k}^l = \left\| \mathbf{p}_k - \mathbf{s}_l \right\| + w_r^l \tag{18}$$

and, for bearing-only sensor,

$$\mathbf{z}_{\phi,k}^l = \arctan \frac{y_l - p_{y,k}}{x_l - p_{x,k}} + w_\phi^l, \tag{19}$$

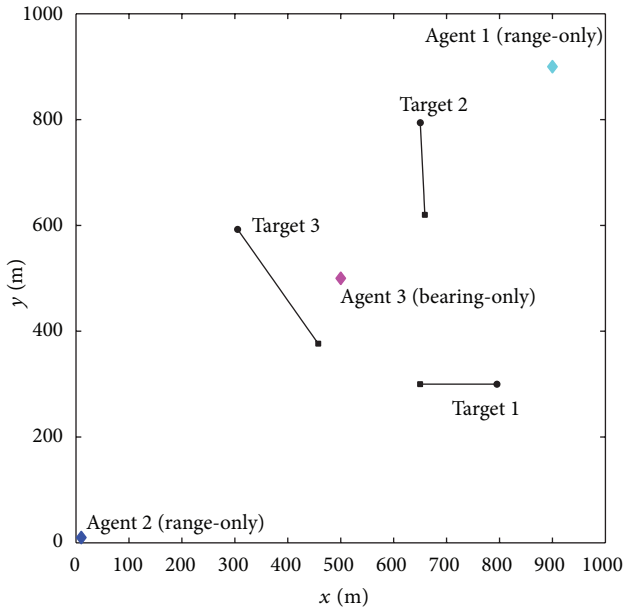

FIGURE 1: Target tracks. Start/stop positions for each track are shown with •/■. Colored ♦ are initial locations of agents.

where $\mathbf{s}_k^l = [x_k^l, y_k^l]$ is the location of agent l and $\|\mathbf{p}_k - \mathbf{s}_k^l\| = \sqrt{(x_k^l - p_{x,k})^2 + (y_k^l - p_{y,k})^2}$ is the Euclidean distance between sensor l and the target. w_r^l is zero mean Gaussian noise $\mathcal{N}(\cdot; 0, (\sigma_r^l)^2)$ and w_ϕ^l is also zero mean Gaussian noise $\mathcal{N}(\cdot; 0, (\sigma_\phi^l)^2)$. The standard derivations of w_r^l and w_ϕ^l are, respectively, given by σ_r^l and σ_ϕ^l as follows:

$$\begin{aligned} \sigma_{r,k}^l &= \sigma_0 + \beta_r \|\mathbf{p}_k - \mathbf{s}_l\|^2 \\ \sigma_{\phi,k}^l &= \sigma_1 + \beta_\phi \|\mathbf{p}_k - \mathbf{s}_l\|, \end{aligned} \tag{20}$$

with $\sigma_0 = 1\,\text{m}$, $\beta_r = 5 \times 10^{-5}\,\text{m}^{-1}$, $\sigma_1 = \pi/180\,\text{rad}$, and $\beta_\phi = 10^{-5}\,\text{rad} \cdot \text{m}^{-1}$.

Targets can appear or disappear in the scene at any time, and survival probability $p_S = 0.95$ for each existing target. New born targets appear spontaneously according to $\gamma_k = 0.2\mathcal{N}(\cdot; \bar{\mathbf{x}}, Q)$. Three targets are presented as illustrated in Figure 1, where $\bar{\mathbf{x}}_1 = [800\,\text{m};\ -5\,\text{m/s};\ 300\,\text{m};\ 0\,\text{m/s}]^T$, $\bar{\mathbf{x}}_2 = [650\,\text{m};\ 0.5\,\text{m/s};\ 800\,\text{m};\ -6\,\text{m/s}]^T$, and $\bar{\mathbf{x}}_3 = [300\,\text{m};\ 5\,\text{m/s};\ 600\,\text{m};\ -8\,\text{m/s}]^T$, respectively, for each target, and $Q = \text{diag}([50\,\text{m}, 2\,\text{m/s}, 50\,\text{m}, 2\,\text{m/s}]^2)$ are identical for all three targets.

The probability of detection for both range-only sensor and bearing-only sensor is modelled by

$$p_D(\mathbf{x}_k) = \begin{cases} 0.99 & \|\mathbf{p}_k - \mathbf{s}_l\| \le R_0 \\ \max\{0, 0.99 - c\|\mathbf{p}_k - \mathbf{s}_l\|\} & \|\mathbf{p}_k - \mathbf{s}_l\| \ge R_0, \end{cases} \tag{21}$$

with $R_0 = 320\,\text{m}$ and $c = 0.002\,\text{m}^{-1}$. The clutter rate of each sensor $\lambda_c = 5$ per scan. The standard derivation of process noise $\sigma_v = 1\,\text{m/s}$ for both $v_{x,k}$ and $v_{y,k}$. Given the current agent location $\mathbf{s}_k^l$, the set of admissible control commands for each agent is computed as $\mathbf{U}_k^l = \{[x_k^l + i\Delta_R \cos(j\Delta_\phi), y_k^l + i\Delta_R \cos(j\Delta_\phi)]\}_{i=0,\ldots,N_\phi}^{j=0,\ldots,N_R}$, where $\Delta_\phi = 2\pi/N_\phi$ and $\Delta_R = 30\,\text{m}$ are for angular and radial step size. $N_R = 2$ and $N_\phi = 8$ here.

The initial locations of agents are shown in Figure 1, and each agent runs for 30 scans with sampling period $T = 1\,\text{s}$. Birth intensity for the multi-Bernoulli filter is approximated using adaptive target birth intensity sampling technique described in [33]. $L_{\min} = 300$ and $L_{\max} = 500$ are the minimum and maximum particle numbers of each Bernoulli set for track maintenance.

Since each agent shares its location and observation with other two agents, agents have pretty much the same performance in this scene. Hence, we take agent 3 (bearing-only) as an example to illustrate the tracking procedure. Figure 2 presents three key frames of one trial run of the proposed control and tracking approach. It is clear that, with the movement of agents, scattered particles converge to the ground truth locations of targets. This is because each agent is moving forward to a more informative direction so that "ghost" particles that are not generated by actual targets can be quickly eliminated by the multisensor fusion scheme. As a result, the estimation of target positions is getting more accurate over time. Besides, it can be seen from Figure 2(c) that the trajectories of agents are different for their distinctive initial locations and sensor types.

Due to stochastic nature of our control and tracking approach, we adopt 1000 Monte Carlo runs to evaluate their performance. The optimal subpattern assignment (OSPA) metric composed of location error and cardinality error is used for tracking performance evaluation [34]. Figure 3 shows the OSPA distance of our approach, ($c = 100\,\text{m}$, $p = 1$) from 1000 Monte Carlo runs, from which we can see that the OSPA distance converges with the movement of agents over time. The location error is reduced gradually since each agent is obtaining more informative measurements to lower the covariance of position estimation, while the estimation of target number quickly converges to a relatively low value. The average computation time for a single run is only approximately 0.82 s (algorithm is implemented in MATLAB 2012a on a PC with 8 GB RAM and Intel Core i7-4770k CPU). Several runs have been recorded in videos attached as Supplementary Material (available online at http://dx.doi.org/10.1155/2015/903682) for demonstration.

6. Conclusion

In this paper, we propose a novel distributed multiagent control approach by maximizing the local Rényi divergence. The SMC implementation of the sequential multi-Bernoulli filter is provided for each agent to utilize the information from neighbouring agents. Simulation results demonstrate that

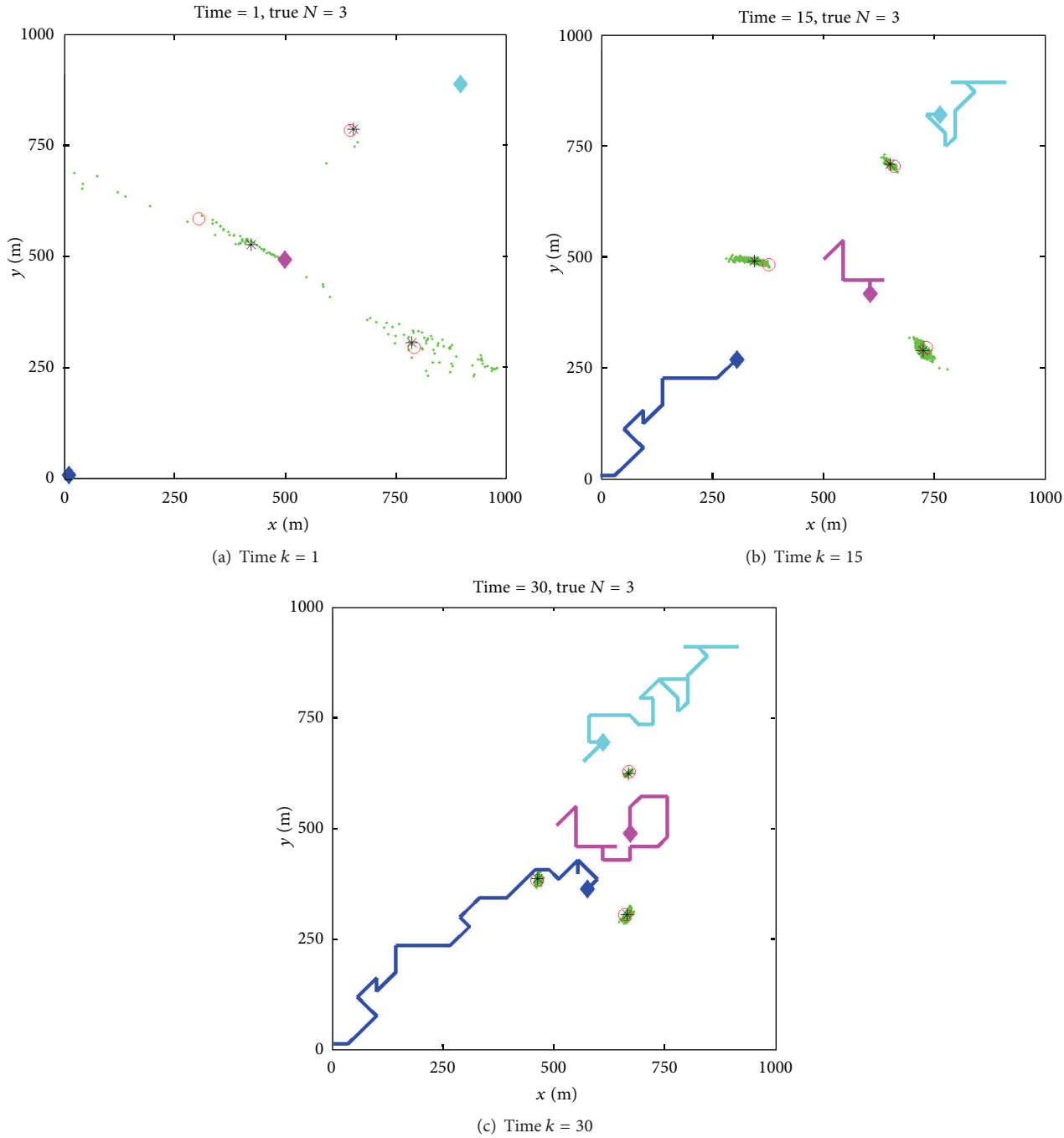

(a) Time $k = 1$

(b) Time $k = 15$

(c) Time $k = 30$

FIGURE 2: One trial result. Green dots are for particles. Colored ♦ are current locations of agents. Red ◦ are ground truth of target stop positions, while black ∗ are for target estimation.

the proposed approach is capable of distributed multitarget tracking via effective sensor control.

Our future work is to use convex relaxation method for seeking global optimal solution for multiagent control and compare with the approach proposed in this paper. We also need to consider more challenging measurement model, such as time-difference-of-arrival measurement or Doppler measurement, which depends on the behavior of multiple agents.

Conflict of Interests

The authors declare that there is no conflict of interests regarding the publication of this paper.

Acknowledgments

Liang Ma got financial support from the Program of China Scholarships Council (no. 201206680025). This work is

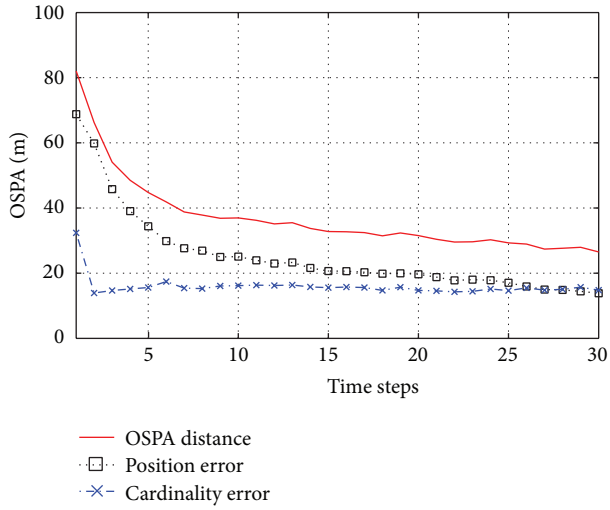

Figure 3: OSPA distance.

sponsored by the Fundamental Research Funds for the Central Universities (HEUCF130703).

References

[1] J. Ferber, *Multi-Agent Systems: An Introduction to Distributed Artificial Intelligence*, Addison-Wesley, Reading, Mass, USA, 1999.

[2] J. Yick, B. Mukherjee, and D. Ghosal, "Wireless sensor network survey," *Computer Networks*, vol. 52, no. 12, pp. 2292–2330, 2008.

[3] M. Ji and M. Egerstedt, "Distributed coordination control of multiagent systems while preserving connectedness," *IEEE Transactions on Robotics*, vol. 23, no. 4, pp. 693–703, 2007.

[4] H. Su, X. Wang, and Z. Lin, "Flocking of multi-agents with a virtual leader," *IEEE Transactions on Automatic Control*, vol. 54, no. 2, pp. 293–307, 2009.

[5] X. Wang and H. Su, "Pinning control of complex networked systems: a decade after and beyond," *Annual Reviews in Control*, vol. 38, no. 1, pp. 103–111, 2014.

[6] R. Olfati-Saber, J. A. Fax, and R. M. Murray, "Consensus and cooperation in networked multi-agent systems," *Proceedings of the IEEE*, vol. 95, no. 1, pp. 215–233, 2007.

[7] M. B. Egerstedt and X. Hu, *Formation Constrained Multi-Agent Control*, 2001.

[8] R. Olfati-Saber, "Flocking for multi-agent dynamic systems: algorithms and theory," *IEEE Transactions on Automatic Control*, vol. 51, no. 3, pp. 401–420, 2006.

[9] R. P. Mahler, *Statistical Multisource-Multitarget Information Fusion*, Artech House, Boston, Mass, USA, 2007.

[10] R. P. S. Mahler, "Multitarget bayes filtering via first-order multitarget moments," *IEEE Transactions on Aerospace and Electronic Systems*, vol. 39, no. 4, pp. 1152–1178, 2003.

[11] R. Mahler, "PHD filters of higher order in target number," *IEEE Transactions on Aerospace and Electronic Systems*, vol. 43, no. 4, pp. 1523–1543, 2007.

[12] B.-T. Vo, B.-N. Vo, and A. Cantoni, "The cardinality balanced multi-target multi-Bernoulli filter and its implementations," *IEEE Transactions on Signal Processing*, vol. 57, no. 2, pp. 409–423, 2009.

[13] E. Maggio, E. Piccardo, C. Regazzoni, and A. Cavallaro, "Particle PHD filtering for multi-target visual tracking," in *Proceedings of the IEEE International Conference on Acoustics, Speech and Signal Processing (ICASSP '07)*, pp. I1101–I1104, April 2007.

[14] B.-N. Vo, B.-T. Vo, N.-T. Pham, and D. Suter, "Joint detection and estimation of multiple objects from image observations," *IEEE Transactions on Signal Processing*, vol. 58, no. 10, pp. 5129–5141, 2010.

[15] V. C. Ravindra, L. Svensson, L. Hammarstrand, and M. Morelande, "A cardinality preserving multitarget multi-Bernoulli RFS tracker," in *Proceedings of the 15th International Conference on Information Fusion (FUSION '12)*, pp. 832–839, September 2012.

[16] R. Hoseinnezhad, B.-N. Vo, B.-T. Vo, and D. Suter, "Visual tracking of numerous targets via multi-Bernoulli filtering of image data," *Pattern Recognition*, vol. 45, no. 10, pp. 3625–3635, 2012.

[17] R. Hoseinnezhad, B.-N. Vo, and B.-T. Vo, "Visual tracking in background subtracted image sequences via multi-Bernoulli filtering," *IEEE Transactions on Signal Processing*, vol. 61, no. 2, pp. 392–397, 2013.

[18] R. P. Mahler, "Global posterior densities for sensor management," in *Acquisition, Tracking, and Pointing XII*, vol. 3365 of *Proceedings of SPIE*, pp. 252–263, 1998.

[19] B. Ristic and B.-N. Vo, "Sensor control for multi-object state-space estimation using random finite sets," *Automatica*, vol. 46, no. 11, pp. 1812–1818, 2010.

[20] H. G. Hoang and B. T. Vo, "Sensor management for multi-target tracking via multi-Bernoulli filtering," *Automatica*, vol. 50, no. 4, pp. 1135–1142, 2014.

[21] B. Ristic, B.-T. Vo, B.-N. Vo, and A. Farina, "A tutorial on Bernoulli filters: theory, implementation and applications," *IEEE Transactions on Signal Processing*, vol. 61, no. 13, pp. 3406–3430, 2013.

[22] A. H. Jazwinski, *Stochastic Processes and Filtering Theory*, Courier Dover, 2007.

[23] R. E. Kalman, "A new approach to linear filtering and prediction problems," *Journal of Fluids Engineering*, vol. 82, no. 1, pp. 35–45, 1960.

[24] A. O. Hero III, C. M. Kreucher, and D. Blatt, *Information Theoretic Approaches to Sensor Management*, Springer, 2008.

[25] C. Boutilier, "Planning, learning and coordination in multiagent decision processes," in *Proceedings of the 6th Conference on Theoretical Aspects of Rationality and Knowledge (TARK '96)*, pp. 195–210, Morgan Kaufmann, 1996.

[26] H. Su, M. Z. Chen, J. Lam, and Z. Lin, "Semi-global leader-following consensus of linear multi-agent systems with input saturation via low gain feedback," *IEEE Transactions on Circuits and Systems I: Regular Papers*, vol. 60, no. 7, pp. 1881–1889, 2013.

[27] H. Su, M. Z. Q. Chen, X. Wang, and J. Lam, "Semiglobal observer-based leader-following consensus with input saturation," *IEEE Transactions on Industrial Electronics*, vol. 61, no. 6, pp. 2842–2850, 2014.

[28] J. Mullane, B.-N. Vo, M. Adams, and B.-T. Vo, "Random finite sets for robot mapping and slam," *Springer Tracts in Advanced Robotics*, vol. 72, 2011.

[29] A. K. Gostar, R. Hoseinnezhad, and A. Bab-Hadiashar, "Robust multi-bernoulli sensor selection for multi-target tracking in sensor networks," *IEEE Signal Processing Letters*, vol. 20, no. 12, pp. 1167–1170, 2013.

[30] S. Reuter, B.-T. Vo, B.-N. Vo, and K. Dietmayer, "The labeled multi-Bernoulli filter," *IEEE Transactions on Signal Processing*, vol. 62, no. 12, pp. 3246–3260, 2014.

[31] H. Su, X. Wang, and G. Chen, "Rendezvous of multiple mobile agents with preserved network connectivity," *Systems & Control Letters*, vol. 59, no. 5, pp. 313–322, 2010.

[32] H. Su, G. Chen, X. Wang, and Z. Lin, "Adaptive second-order consensus of networked mobile agents with nonlinear dynamics," *Automatica*, vol. 47, no. 2, pp. 368–375, 2011.

[33] B. Ristic, D. Clark, B.-N. Vo, and B.-T. Vo, "Adaptive target birth intensity for PHD and CPHD filters," *IEEE Transactions on Aerospace and Electronic Systems*, vol. 48, no. 2, pp. 1656–1668, 2012.

[34] D. Schuhmacher, B.-T. Vo, and B.-N. Vo, "A consistent metric for performance evaluation of multi-object filters," *IEEE Transactions on Signal Processing*, vol. 56, no. 8, part 1, pp. 3447–3457, 2008.

Hindawi Publishing Corporation
Mathematical Problems in Engineering
Volume 2015, Article ID 529538, 9 pages
http://dx.doi.org/10.1155/2015/529538

Research Article

Flocking Control of Multiple Mobile Agents with the Rules of Avoiding Collision

Hongtao Zhou, Wenfeng Zhou, and Wei Zeng

School of Automation, Huazhong University of Science and Technology, Wuhan 430074, China

Correspondence should be addressed to Wenfeng Zhou; 963474063@qq.com

Received 10 July 2014; Accepted 1 September 2014

Academic Editor: Wei Zhang

This paper investigates the flocking and the coordinative control problems of multiple mobile agents with the rules of avoiding collision. We propose a set of control laws using hysteresis in adding new links and applying new potential function to guarantee that the fragmentation of the network can be avoided, under which all agents approach a common velocity vector, and asymptotically converge to a fixed value of interagent distances and collisions between agents can be avoided throughout the motion. Furthermore, we extend the flocking algorithm to solve the flocking situation of the group with a virtual leader agent. The laws can make all agents asymptotically approach the virtual leader and collisions can be avoided between agents in the motion evolution. Finally, some numerical simulations are showed to illustrate the theoretical results.

1. Introduction

In recent years, the problem of coordinated motion of multiple mobile agents, especially the flocking control [1–3], has attracted a lot of attention among researchers. Researchers structure a distributed model that simulates these behaviors such as flocks, herds, and schools [3–21]. The wide attention and research on this issue get a good application in biology, social behavior, statistical physics, control engineering, and other fields [2–11]. Most previous works of flocking algorithm are based on the assumption that the network topologies are always connected [12, 13]. However, in fact, it is difficult to ensure that network maintains connection at all times even if the initial network is connected [14]. Therefore, there is great realistic significance to find out an algorithm that ensures that the connectivity requirement of the network is always satisfied. Fortunately, a connectivity preserving flocking algorithm for network topologies with distributed control was studied in [14–17]. Under the condition that the initial network is connected, the author applies appropriate weight for network edge to make the network maintain connection. In [2, 16], in order to maintain network connectivity, the method of measuring the local network was applied. In [17], using the potential function method was considered. However, these methods were designed for single-integrator dynamics. In [13], the author first proposed a distributed connected algorithm for the second-order network system. With the algorithm, collisions between agents can be avoided in the motion evolution.

In this work, we consider how to maintain network connectivity by constructing artificial potential function and investigating the flocking algorithm with avoiding collision rules. This algorithm is using hysteresis in adding new links [14] and applying new potential function method to maintain network connectivity. The major difference from the algorithm which was considered in [13, 15] is that we choose the new potential function. Furthermore, the situation of multiagent systems with a virtual leader is further investigated. We conclude that, in the case that the initial network is connected, the laws can make all agents approach a common velocity vector and asymptotically converge to a fixed value of interagent distances and collisions between agents can be avoided throughout the motion.

The rest of this paper is organized as follows. We define the multiagent flocking problem in Section 2, and some background on Graphs, Laplacian, and Reynolds model is presented in this section. In Section 3 we propose a new flocking algorithm and its results analyses are presented.

Then, some numerical simulation examples are presented in Section 4. Finally, some conclusions are made in Section 5.

2. Problem Formulation

2.1. Background. In order to improve the understanding of the flocking control problem and facilitate the narrative for the next part, some basic knowledge including the undirected graph $G(t)$, Laplacian matrix, and Reynolds model is introduced as follows.

2.1.1. Algebraic Graph Theory. Assume that each agent has the same sensing radius r, for given constants $\varepsilon \in (0, r]$ and $\varepsilon_0 \in (0, r)$, satisfying $\varepsilon_0 \leq \varepsilon$. Consider the agent i as a node and use undirected edge link node i and other nodes which can be sensing. Thus, the graph consisting of a set of nodes $V = \{1, \ldots, N\}$ and a time-varying set of edges $E(t) = \{(i, j) \in V \times V : i \sim j\}$ can be expressed as an undirected graph $G(t)$ at time t, and the detailed meaning is as follows [15, 22]:

(i) the initial edges are satisfied with $E(0) = \{(i, j) \mid \|s_i(0) - s_j(0)\| < r, i, j \in V\}$;

(ii) if the inequality $r \leq \|s_i(0) - s_j(0)\|$ is reasonable, we have $(i, j) \notin E(t)$;

(iii) if $r - \varepsilon > \|s_i(0) - s_j(0)\|$ and $(i, j) \notin E(t^-)$, a new edge is generated between agent i and agent j.

Here, $s_i(t)$ denotes the position vector of agent i and $\| \bullet \|$ expresses the Euclidean norm. The description of whether there exist edges between agent i and agent j at time t can use a symmetric indicator function $\sigma(i, j) \in \{0, 1\}$, and we can describe it as follows:

$$\sigma(i, j)[t] = k, \quad k = 0, 1. \tag{1}$$

Here, if $((\sigma(i, j)[t^-] = 0) \cap (r - \varepsilon \leq \|s_i(t) - s_j(t)\| < r)) \cup (\|s_i(t) - s_j(t)\| \geq r)$, means that there is no edge between agent i and agent j at time t, then $k = 0$. If $((\sigma(i, j)[t^-] = 0) \cap (r - \varepsilon \leq \|s_i(t) - s_j(t)\| < r)) \cup (\|s_i(t) - s_j(t)\| < r - \varepsilon)$, scilicet that exist edge between agent i and agent j at time t, then $k = 1$.

The above imply that a new edge will be added when the distance between the two agents is less than induction radius r.

2.1.2. Laplacian. Define the Laplacian of agent i as $L = D - A$, where A is the adjacency matrix of graph $G(t)$ such that [13]

$$A = \left[a_{ij}\right] \in R^{n \times n}, \quad a_{ij} = \begin{cases} 1, & \text{if } (u, v) \in G(E) \\ 0, & \text{otherwise,} \end{cases} \tag{2}$$

where $D = \text{diag}\{d_i, i \in V\}$, $d_i = \sum_{j \in N_i} a_{ij}$, $i = l, 2, \ldots, N$, is the sum of ith row element of matrix A. Obviously, the sum is zero of all row elements for Laplacian. Furthermore, Laplacian is a positive semidefinite matrix that satisfies the following sum-of-squares property [14]:

$$Z^T L Z = \frac{1}{2} \sum_{(i,j) \in \varepsilon} a_{ij} \left(z_j - z_i\right)^2, \quad z \in R^n. \tag{3}$$

For a given undirected graph $G(t)$, the Laplace matrix is symmetrical, and the nonnegative adjacency matrix A satisfies $A^T = A$.

2.1.3. Reynolds Model. In 1986, Reynolds introduced three heuristic rules that led to creating the first computer animation of flocking [3]. Then, researchers used the name Reynolds model that describes the rules. The flocking algorithm that will be proposed is based on these rules. Here, we list three flocking rules of Reynolds [4].

(i) Flock centering: attempt to stay close to nearby agents.

(ii) Velocity matching: attempt to match velocity with nearby agents.

(iii) Collision avoidance: avoid collisions with nearby agents.

2.2. Problem Description. In our background, the Reynolds model was proposed based on the position and velocity of agents; consider a group of mobile agents moving in a n-dimensional Euclidean space. Let $\dot{s}_i \in R^n$ and $v_i \in R^n$ denote the position vector and velocity vector of agent i, $i = 1, 2, \ldots, N$, respectively. The motion equations of each agent are described by the following double integrator:

$$\begin{aligned} \dot{s}_i &= v_i, \\ \dot{v}_i &= u_i, \end{aligned} \tag{4}$$

where $u_i \in R^n$ denotes the energy control input of agent i, $i = 1, 2, \ldots, N$. The value of the position vector and the velocity vector of each agent is stored in the form of matrix; define

$$s = \begin{bmatrix} s_1 \\ s_2 \\ \vdots \\ s_N \end{bmatrix}, \qquad v = \begin{bmatrix} v_1 \\ v_2 \\ \vdots \\ v_N \end{bmatrix}. \tag{5}$$

Then, the problems of flocking control can consider how to design the control input u_i value, which can make all agent motion satisfy the three rules of Reynolds.

The control purpose of this work is to make all agents approach a uniform velocity and asymptotically converge to a fixed value of interagent distances, and collisions can be avoided among agents in the motion evolution. Namely, for all $i, j \in V$, we require $v_i(t) - v_j(t) \to 0$ and $s_i(t) - s_j(t) \to k_{ij}$, and here $k_{ij} \in R^n$ is offset constants. In general, we want the final desired formation that satisfies equation $s_1(t) = s_2(t) = s_3(t) = \cdots = s_n(t)$. In order to achieve this goal, the control input u_i is designed as follows:

$$u_i = f_i + h_i. \tag{6}$$

And consider the situation of the group with a virtual leader agent; the control input u_i in this case can be described as follows:

$$u_i = f_i + h_i + \gamma_i \tag{7}$$

where $f_i \in R^n$ is the gradient-base term and its action is enforced on each agent that asymptotically converges to the fixed value of interagent distances, ensures the network connectivity, and avoids collision between agents. The middle item of (7) $h_i \in R^n$ acts as a damping force, which makes every agent attempt to consistent velocity with nearby agent. And $\gamma_i \in R^n$ is the navigational feedback term, which enforces that all agents are aware of the virtual leader.

3. Flocking Algorithms

3.1. Without a Virtual Leader. We have assumed that multiple mobile agents are moving in n-dimensional Euclidean space; consider the fact that the agent can only sense other agents in its epsilon neighborhood because of the limited awareness of each agent. So we define $N_i(t) = \{j \mid \sigma(i,j)[t] = 1,\ j \neq i,\ j = 1, \ldots N\}$ stand for the epsilon neighborhood of agent i at time t. The control input (6) for agent i is governed by

$$u_i = \sum_{j \in N_i} \omega_{ij} v_j - \sum_{j \in N_i} \left(\nabla_{s_i} \psi \left(\left\| s_{ij} \right\| \right) + \omega_{ij} v_i \right), \tag{8}$$

where $s_{ij} = (s_i - s_j)$ and weight number $w_{ij} = w_{ji} > 0$. The $\psi(\|s_{ij}\|)$ where in (8) is nonnegative artificial potential function, which independent variables is the distance $\|s_{ij}\|$ between agent i and agent j; here $\|s_{ij}\| \in [0, r]$. It has the following properties:

(i) the potential function $\psi(\|s_{ij}\|)$ achieves its unique minimum value when $\|s_{ij}\|$ reaches a desired distance;

(ii) if $\|s_{ij}\| \to 0$ and $\|s_{ij}\| \to r$, the potential function $\psi(\|s_{ij}\|) \to \infty$.

We can know that no distance between agents will tend to 0 or r at all times, which implies that any two agents can attract each other and collisions can be avoided by constructing $\psi(\|s_{ij}\|)$. One example to meet the above features of artificial potential function is as follows:

$$\psi \left(\left\| s_{ij} \right\| \right) = \begin{cases} \dfrac{1}{\left\| s_{ij} \right\|} + \dfrac{1}{r - \left\| s_{ij} \right\|}, & \left\| s_{ij} \right\| \in (0, r) \\ +\infty, & \left\| s_{ij} \right\| = r \text{ or } \left\| s_{ij} \right\| = 0. \end{cases} \tag{9}$$

For the physical properties of the dynamic agent, we define the total energy of agent system as follows:

$$Q = -\frac{1}{2} \sum_{i=1}^{N} \sum_{j \in N_i} \psi \left(\left\| s_{ij} \right\| \right) + v_i^T v_i. \tag{10}$$

It shows that Q is the sum of the total potential energy and the total relative kinetic energy among agents. Define the initial energy $Q_0 = Q(s(0), v(0))$; it is easy to see that Q is a positive semidefinite function.

For the convenience of description, denote the velocity and position of the center of mass (COM) of all agents as follows [22]:

$$\overline{v} = \frac{\sum_{i=1}^{N} v_i}{N}, \qquad \overline{s} = \frac{\sum_{i=1}^{N} s_i}{N}. \tag{11}$$

Considering a group of N agents with dynamic motion (4) steered by protocol (8) in combination with the artificial potential function which we have put forward, the following conclusion can be got based on the above description.

Theorem 1. *Assume that the initial energy $Q_0 = Q(s(0), v(0))$ and the initial network $G(0)$ are finite and connected, respectively. Then, one has the main result: (i) for all $t \geq 0$, the $G(t)$ will maintain connection; (ii) the velocity $\overline{v}$ of the COM remains the same for all $t \geq 0$; (iii) all agents approach a uniform velocity $\overline{v}$ and asymptotically converge to the fixed value of interagent distances; (iv) collisions among agents can be avoided.*

Proof. Part one of Theorem 1 is proved first. We can speculate that the topology of $G(t)$ is fixed at the time period $[t_{k-1}, t_k)$ under the assumption that $G(t)$ switches at time t_k ($k = 1, 2, \ldots, N$). In view of initial energy Q_0 is finite, and we obtain the time derivative of energy equation $Q(t)$ in $[t_0, t_1)$ as follows:

$$\begin{aligned} \dot{Q}(t) &= \frac{1}{2} \sum_{i=1}^{N} \sum_{j \in N_i} \dot{\psi} \left(\left\| s_{ij} \right\| \right) + \sum_{i=1}^{N} v_i^T \dot{v}_i \\ &= \sum_{i=1}^{N} v_i^T \left(\sum_{j \in N_i} \nabla_{s_i} \psi \left(\left\| s_{ij} \right\| \right) - \sum_{j \in N_i} \nabla_{s_i} \psi \left(\left\| s_{ij} \right\| \right) \right. \\ &\qquad \left. - \sum_{j \in N_i} \omega_{ij} \left(v_i - v_j \right) \right) \\ &= \sum_{i=1}^{N} v_i^T \sum_{j \in N_i} \omega_{ij} \left(v_j - v_i \right) \\ &= -v^T \left[L(t) \otimes I_n \right] v. \end{aligned} \tag{12}$$

One has $\dot{Q}(t) \leq 0$ in the time $[t_0, t_1)$ because of the fact that $L(t)$ is positive semidefinite [14], and it means that the following inequality is established at the time period

$$Q_{\max} \geq Q_0 \geq Q(t). \tag{13}$$

According to the definition of the artificial potential function, it is easy to know $\psi(r) > Q_{\max} \geq Q_0$. Therefore, all existing edge-distances will not tend to r in $[t_0, t_1)$ from the definition of artificial potential function, which implies that fragmentation of existing edges will be avoided at time t_1. Hence, the edge number of the interaction network must be increased. The potential energy, which comes from the new edges, is a limited value because of the effect of hysteresis.

Using a similar analysis method, we can obtain the time derivative of $Q(t)$, and the following equation exists in time period $[t_{k-1}, t_k)$:

$$\dot{Q}(t) = -v^T \left[L(t) \otimes I_n \right] v \leq 0. \tag{14}$$

Based on this fact, the inequation is reasonable in $[t_{k-1}, t_k)$ $(k = 1, 2, \ldots, N)$ as follows:

$$Q_{\max} > Q_{(t_{k-1})} \geq Q(t). \tag{15}$$

It is obvious that all existing edge-distances will not tend to r in $[t_{k-1}, t_k)$, which implies that fragmentation of existing edges will be avoided at time t_k. Therefore, $Q_{\max} \geq Q(t_k)$.

According to the above analysis, we know that $G(0)$ is connected and no edge in $E(0)$ will be fragmented, and it proves that $G(t)$ maintains connection for all $t \geq 0$.

In what follows, we will give the proof procedure of parts (ii) and (iii).

Let us consider that there are n_k edges being added to the dynamic network at t_k; it is easy to know that

$$0 < n_k \leq \left(\frac{N(N-1)}{2} - (N-1) \right) \triangleq M. \tag{16}$$

From (9) and (15), we have

$$Q(t_k) \leq Q_0 + (n_1 + n_2 + n_3 + \cdots + n_k)\, \psi(\|r - \varepsilon\|). \tag{17}$$

Combined with (16), clearly, $Q_{\max} \geq Q(t)$ for all time $t \geq 0$. Hence, we can define the positive invariant set Ω that goes with above analysis. Consider the following:

$$\Omega = \left\{ \hat{s} \in D_g, v \in R^{Nn} \mid Q(\hat{s}, v) \leq Q_{\max} \right\}. \tag{18}$$

Here, $D_g = \{\hat{s} \in R^{N^2 n} \mid \|s_{ij}\| \in [0, r), \forall (i,j) \in E(t)\}$, $\hat{s} = [s_{11}^T, \ldots, s_{1N}^T, \ldots, s_{N1}^T, \ldots, s_{NN}^T]$, and $v = [v_1^T, v_2^T, \ldots, v_N^T]^T$.

The inequality $\|s_{ij}\| \leq (N-1)r$ is reasonable for all agents i and j under the fact that $G(t)$ always maintains connection. From $Q(t) \leq Q_{\max}$, we have $v_i^T v_i \leq 2Q_{\max}$ or $\|v_i\| \leq \sqrt{2Q_{\max}}$, and it means that the positive invariant set Ω is compact. Note that network $G(t)$ is a fixed topology; combining with LaSalle's invariance principle [23], we know that the value of each solution lies in set Ω that tends to the range of the invariant set

$$S = \left\{ \hat{s} \in D_g, v \in R^{Nn} \mid \dot{Q} = 0 \right\}. \tag{19}$$

From (14), we can get

$$\dot{Q}(t) = -v^T [L(t) \otimes I_n] v = \frac{1}{2} \sum_{(i,j) \in E} w_{ij} \left\| v_j - v_i \right\|^2. \tag{20}$$

It is easy to see that $\dot{Q} = 0$ if and only if $v_1 = v_2 = \cdots = v_N$, which shows that all agents approach a uniform velocity $\overline{v}$.

For given conditions $w_{ij} = w_{ji}$ and $\psi(\|s_{ij}\|) = \psi(\|s_{ji}\|)$ and the control input (8), we have

$$\begin{aligned} \dot{\overline{u}} = \dot{\overline{v}} &= \frac{\sum_{i=1}^N u_i}{N} \\ &= -\frac{1}{N} \sum_{i=1}^N \left(\sum_{j \in N_i(t)} \nabla_{s_i} \psi\left(\left\| s_{ij} \right\| \right) \right. \\ &\qquad \left. + \sum_{j \in N_i(t)} w_{ij} \left(v_i - v_j \right) \right) = 0. \end{aligned} \tag{21}$$

This formula implies that part (ii) of Theorem 1 is established.

From the control input (8), we have

$$\begin{aligned} u_i = \dot{v}_i &= -\sum_{j \in N_i(t)} \nabla_{s_i} \psi\left(\left\| s_{ij} \right\| \right) \\ &= -\sum_{j \in N_i(t)} \frac{\partial \psi\left(\left\| s_{ij} \right\| \right)}{\partial \left\| s_{ij} \right\|} \cdot \frac{1}{\left\| s_{ij} \right\|} \left(s_i - s_j \right), \quad i = 1, \ldots, N. \end{aligned} \tag{22}$$

In a stable state, clearly $v_1 = v_2 = \cdots = v_N = \overline{v}$, which implies that $\dot{v}_i = \dot{\overline{v}} = 0$ for all $i \in V$. We can rewrite (22) in a matrix form such that

$$-\left[\widehat{L(t)} \otimes I_n \right] s = 0. \tag{23}$$

Here $s = [s_1^T, s_2^T, \ldots, s_N^T]$, the element of matrix $\widehat{L(t)} = [\widehat{l_{ij}}]$ is $\widehat{l_{ij}} = (\partial \psi(\|s_{ij}\|)/\partial \|s_{ij}\|) \cdot (1/\|s_{ij}\|)$, and $\widehat{l_{ii}} = -\sum_{j=1, j \neq N}^N ((\partial \psi(\|s_{ij}\|)/\partial \|s_{ij}\|) \cdot (1/\|s_{ij}\|))$. For a given initial network and combining the definition of Laplacian matrix $\widehat{L(t)} \otimes I_n$, one has $s_1 = s_2 = \cdots = s_N$, and it means that part (iii) is reasonable.

At the end of Section 3, we prove part (iv). According to the set $\Omega = \{\hat{s} \in D_g, v \in R^{Nn} \mid Q(\hat{s}, v) \leq Q_{\max}\}$, it is easy to know that $Q \leq Q_{\max}$ for all $t \geq 0$. Hence, we can deduce that $\lim_{\|s_{ij}\| \to 0} \psi(\|s_{ij}\|) = \infty$ combines with the definition of artificial potential function. Thus, collisions between any two agents can be avoided. □

3.2. With a Virtual Leader. The situation of multiagent systems (4) with a virtual leader is considered in this subsection. The control input is governed by

$$u_i = -\sum_{j \in N_i} \nabla_{s_i} \psi\left(\left\| s_{ij} \right\| \right) - \sum_{j \in N_i} \omega_{ij} \left(v_i - v_j \right) - c_1 \left(v_i - v_\gamma \right), \tag{24}$$

where v_γ denotes the velocity of the virtual leader agent and it is a constant vector. If $c_1 = 1$, it means that agent i has the information of the virtual leader, and otherwise $c_1 = 0$. The last item in the equation has the same role of the γ_i in (7).

We define the total energy of agent system as follows:

$$U = \frac{1}{2} \left(\sum_{i=1}^N \sum_{j \in N_i(t)} \psi\left(\left\| s_{ij} \right\| \right) + \sum_{i=1}^N \left(v_i - v_\gamma \right)^T \left(v_i - v_\gamma \right) \right). \tag{25}$$

It shows that U is the sum of the total interrelated kinetic energy and the total potential energy between the virtual leader and the agents of dynamic network, and it satisfies the feature of positive semidefinite function. In this work, we will choose the artificial potential function $\psi(\|s_{ij}\|)$ which satisfies the property defined in Section 2.

Similar to the analysis of flocking behavior without the virtual leader, considering a group of N agents with dynamic motion (4) steered by protocol (24) in combination with the artificial potential function which we have put forward, we can get the following conclusion.

Theorem 2. *Assume that the initial energy $Q_0 = Q(s(0), v(0))$ and the initial network $G(0)$ are finite and connected, respectively. Then, the following hold: (i) the $G(t)$ will maintain connection for all $t \geq 0$; (ii) all agents approach a uniform velocity v_γ and asymptotically converge to the fixed value of interagent distances; (iii) collisions can be avoided between any agents; (iv) the velocity of the COM will exponentially converge to the desired velocity v_γ, and the group keeps on moving with the velocity v_γ all the following time.*

Proof. Part one of Theorem 2 is proved first.

Assume that $s_i = s_i - v_\gamma t$ represents the position difference and $\tilde{v}_i = v_i - v_\gamma$ represents the velocity difference between agent i of the network and virtual leader. The kinetic equation of agent i is given by

$$\begin{aligned} \dot{\tilde{s}}_i &= \tilde{v}_i \\ \dot{\tilde{v}}_i &= u_i, \quad i = 1, \ldots, N. \end{aligned} \tag{26}$$

According to the definition of $\psi(\|s_{ij}\|)$, we have $\psi(\|s_{ij}\|) = \psi(\|\tilde{s}_{ij}\|)$; therefore, the control input (24) can be rewritten as follows:

$$u_i = -\sum_{j \in N_i} \nabla_{\tilde{s}_i} \psi \left\|\tilde{s}_{ij}\right\| - \sum_{j \in N_i} \omega_{ij} \left(\tilde{v}_i - \tilde{v}_j\right) - c_1 \tilde{v}_i. \tag{27}$$

The energy equation (25) can be rewritten as follows:

$$U = \frac{1}{2} \sum_{i=1}^{N} \left(\sum_{j \in N_i} \psi \left(\left\|s_{ij}\right\| \right) \right) + \tilde{v}_i^T \tilde{v}_i. \tag{28}$$

Referencing the proof of part (i) of Theorem 1, we obtain the time derivative of energy equation $U(t)$ at the time $[t_{k-1}, t_k)$:

$$\begin{aligned} \dot{U}(t) &= \frac{1}{2} \sum_{i=1}^{N} \sum_{j \in N_i} \dot{\psi} \left(\left\|s_{ij}\right\| \right) + \sum_{i=1}^{N} \tilde{v}_i^T \dot{\tilde{v}}_i \\ &= -\tilde{v}^T \left[\left(L(t) + c_1 I_N \right) \otimes I_n \right] \tilde{v} \leq 0. \end{aligned} \tag{29}$$

It is clear that $U(t) \leq 0$, which implied that the following inequality is existing in $[t_{k-1}, t_k)$, $(k = 1, 2, \ldots, N)$. Consider the following:

$$U(t) \leq U_{(t_{k-1})} < U_{\max}. \tag{30}$$

Hence, all existing edge-distances will not tend to radius r in $[t_{k-1}, t_k)$, $(k = 1, 2, \ldots, N)$, which implies that fragmentation of existing edges will be avoided at time t_1; thus $U(t_k) \leq U_{\max}$. We further understand that $G(0)$ is connected and no edge in $E(0)$ will be fragmentated, and it ensures that $G(t)$ maintains connection for all $t \geq 0$.

Then, we give the proof procedure of part (ii). We can get that the positive invariant set is

$$\Omega = \left\{ \hat{s} \in D_g, v \in R^{Nn} \mid U(\hat{s}, v) \leq U_{\max} \right\}, \tag{31}$$

where $D_g = \{\hat{s} \in R^{N^2 n} \mid \|s_{ij}\| \in [0, r), \forall (i, j) \in E(t)\}$, $\hat{\tilde{s}} = [\tilde{s}_{11}^T \tilde{s}_{11}^T, \ldots, \tilde{s}_{1N}^T, \ldots, \tilde{s}_{N1}^T, \ldots, \tilde{s}_{NN}^T]$, $U_{\max} \triangleq U_0 + (1/2N^2 - 3/2N + 1)\psi(\|r - \varepsilon\|)$, and $\tilde{v} = [\tilde{v}_1^T, \tilde{v}_2^T, \ldots, \tilde{v}_N^T]^T$.

The following equation is given combined with LaSalle's invariance principle [23]:

$$\begin{aligned} \dot{U}(t) &= -\tilde{v}^T \left[L(t) + c_1 I_N \otimes I_n \right] \tilde{v} \\ &= -\tilde{v}^T \left[L(t) \otimes I_n \right] \tilde{v} - c_1 \tilde{v}^T \tilde{v} = 0. \end{aligned} \tag{32}$$

Hence $\tilde{v}_1 = \tilde{v}_2 = \cdots = \tilde{v}_N = 0$, and it means that $v_1 = v_2 = \cdots = v_N = v_\gamma$, which implies that all agents approach a uniform velocity v_γ.

We now prove part (iii) of Theorem 2. According to the set $\Omega = \{\hat{s} \in D_g, v \in R^{Nn} \mid U(\hat{s}, v) \leq U_{\max}\}$, it is easy to know that $U \leq U_{\max}$ for all $t \geq 0$. However, we can deduce $\lim_{\|s_{ij}\| \to 0} \psi(\|s_{ij}\|) = \infty$ from the definition of artificial potential function. Thus collisions will be avoided among agents.

At the end of this section, we will prove part (iv). We can get the following equation from the control protocol (24):

$$\begin{aligned} \dot{\overline{v}} &= \frac{\sum_{i=1}^{N} u_i}{N} \\ &= -\frac{1}{N} \sum_{i=1}^{N} \sum_{j \in N_i} \nabla_{s_i} \psi \left(\left\|s_{ij}\right\| + \sum_{j \in N_i} \omega_{ij} \left(v_i - v_j\right) \right. \\ &\qquad \left. + c_1 \left(v_i - v_\gamma\right) \right) \\ &= -c_1 \overline{v} + c_1 v_\gamma. \end{aligned} \tag{33}$$

□

We can get the solution of the equation

$$\overline{v} = v_\gamma + \left(\overline{v}(0) - v_\gamma \right) e^{-c_1 t}, \tag{34}$$

which implies that the initial velocity of the COM will exponentially converge to the desired velocity v_γ.

4. Numerical Simulation

In this section, several numerical examples of the proposed control laws are presented to illustrate the rationality of the theoretical analysis.

4.1. Flocking without a Virtual Leader. The simulation is performed with 10 agents moving in a two-dimensional Euclidean space under the control protocol (8). All initial positions are chosen randomly from the plane $[0, 8] \times [0, 8]$, and initial velocities of the 10 agents are set with arbitrary directions and magnitudes within the plane $[0, 4] \times [0, 4]$. The potential function which is selected for the control protocol (8) with the sensing radius $r = 4$ and the switching

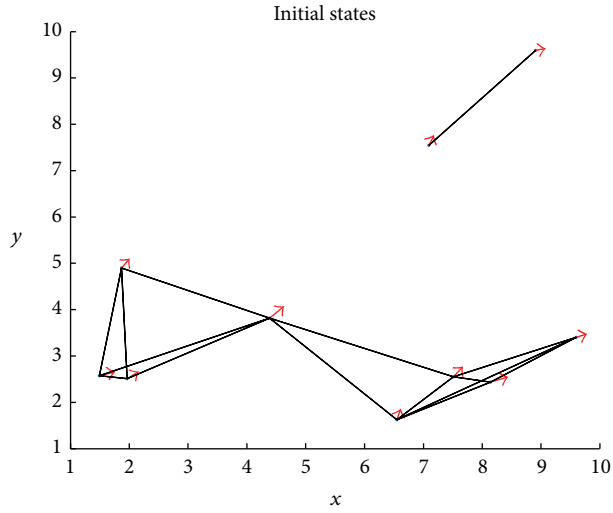

Figure 1: Initial states.

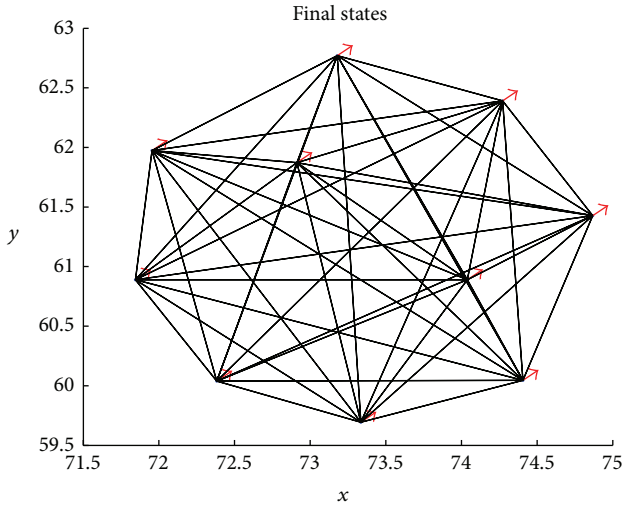

Figure 2: Final states.

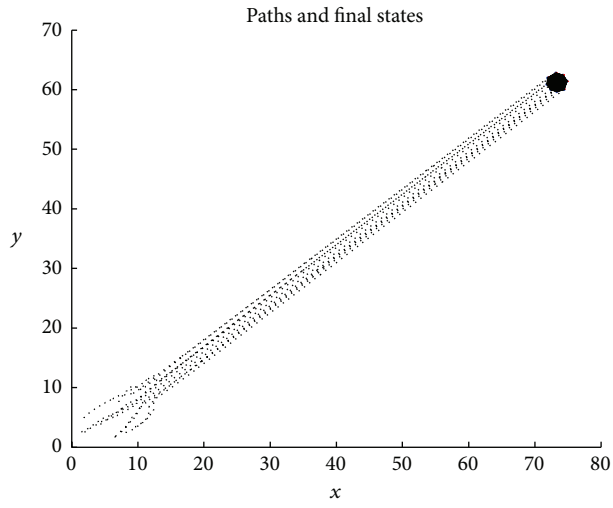

Figure 3: Paths and final states.

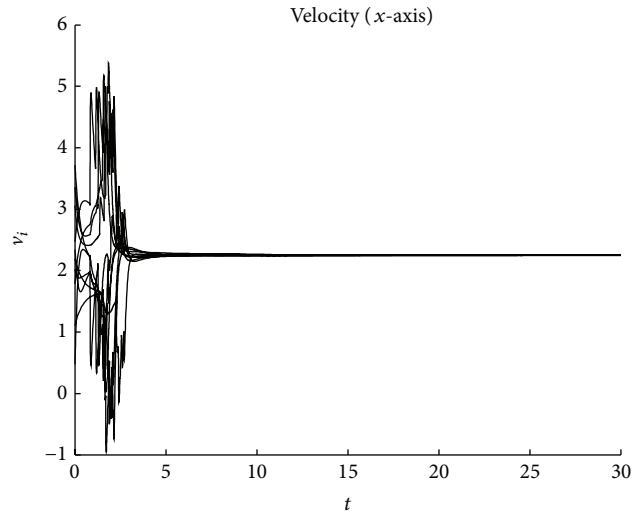

Figure 4: Velocity convergence without virtual leader (x-axis).

threshold dictating is $\varepsilon = 0.1$, the difference between r and ε is the threshold of add edges. The simulation results are shown as follows in the figures. The initial states of each agent are shown in Figure 1; the black lines represent existing neighboring relations between agent i and agent j at time t, and the blue point and the solid lines with arrows represent the multiagent and the direction of velocity, respectively. Figure 2 shows the final states of the 10 agents with the control protocol (8), which showed that all agents eventually move in the same direction. The paths and final states of the agents' motion that evolve according to the control protocol (8) are captured in Figure 3, where the dotted line represents the path of each agent. Figures 4 and 5 describe the convergence process of the agents velocity over the x-axis and the y-axis. It is clearly known that all agents approach a uniform velocity $\bar{v}$. The convergence process of position over the x-axis and the y-axis is demonstrated in Figures 6 and 7. We can know clearly that all agents asymptotically converge to the stabilization of interagent distances.

4.2. Flocking with a Virtual Leader. This simulation is performed with a virtual leader and 10 agents moving in a two-dimensional Euclidean space under the control protocol (24). The choice of initial positions and initial velocities of the 10 agents is the same with the simulation of the flocking without a virtual leader. The initial position and velocity of the virtual leader are chosen randomly. Here we set $s_\gamma = [10, 10]^T$ and $v_\gamma = [3, 3]^T$, respectively. The radius for interagent sensing and communication is $r = 4$ and we will perform the simulation with $\varepsilon = 0.1$. The initial states of each agent are shown in Figure 8; the pink hexagons represent the virtual leader and its velocity vector is described as the solid lines with arrows. Figure 9 shows the final states of the 10 agents with the control protocol (24), which showed that all agents eventually move in the same direction of the virtual leader. The paths and final states of the agents' motion that evolve according to the control protocol (24) are captured in Figure 10.

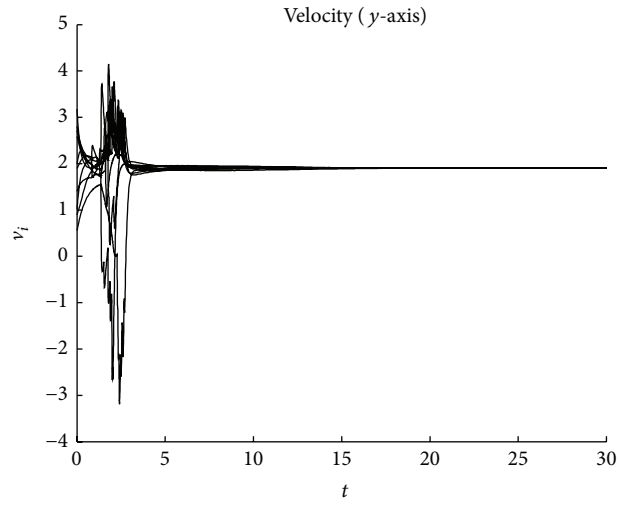

Figure 5: Velocity convergence without virtual leader (y-axis).

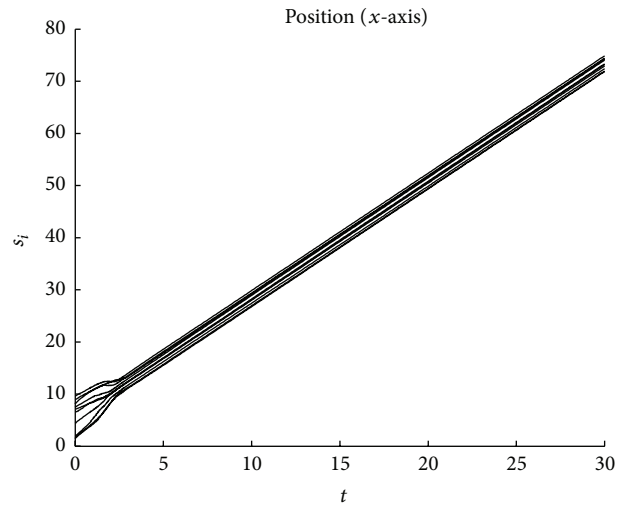

Figure 6: The process of position convergence for $\varepsilon = 0.1$ (x-axis).

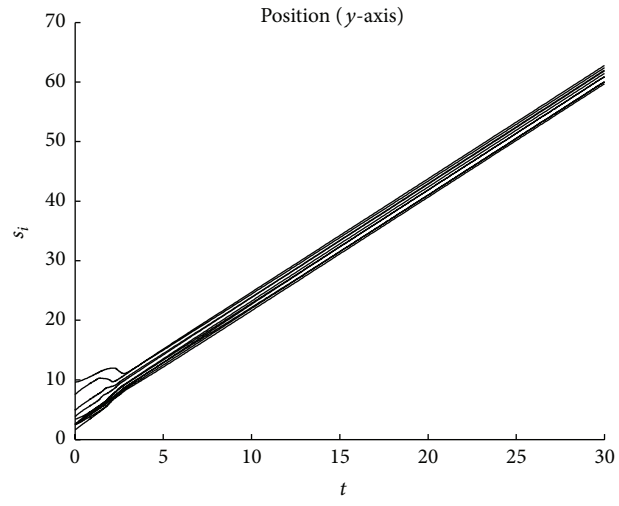

Figure 7: The process of position convergence for $\varepsilon = 0.1$ (y-axis).

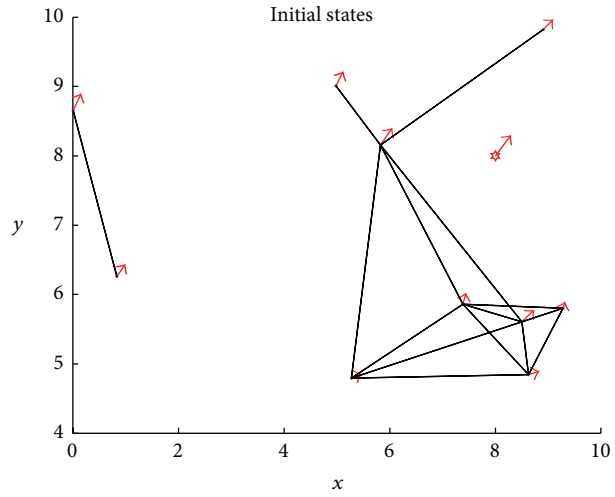

Figure 8: Initial states with a virtual leader.

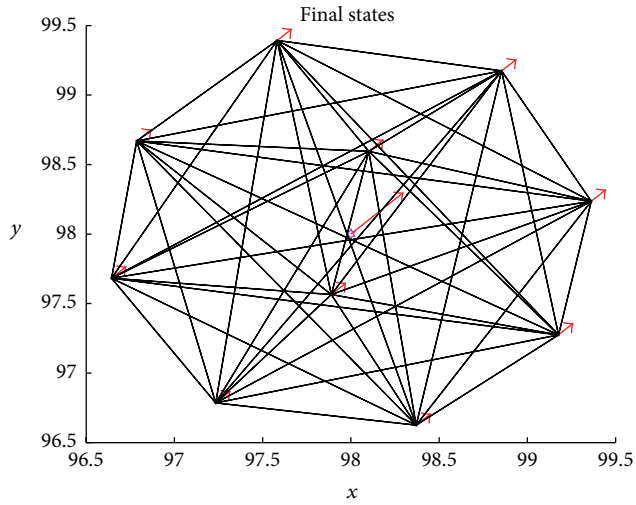

Figure 9: Final states with a virtual leader.

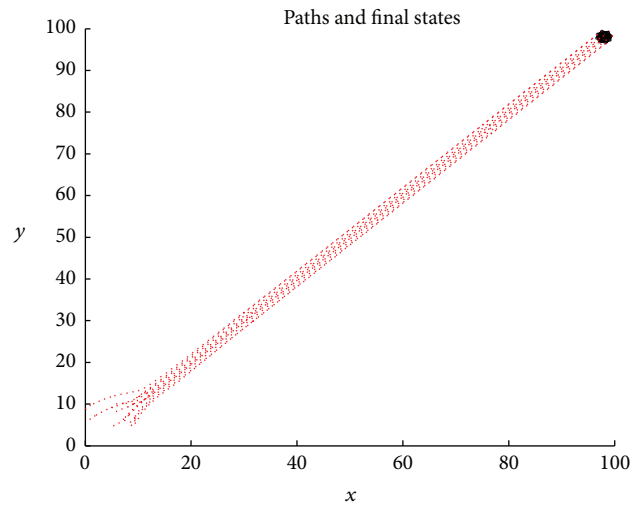

Figure 10: Paths and final states.

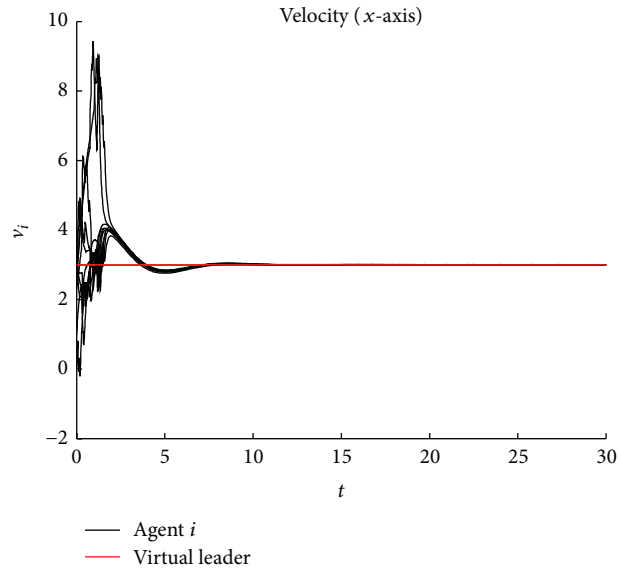

Figure 11: Velocity convergence with a virtual leader (x-axis).

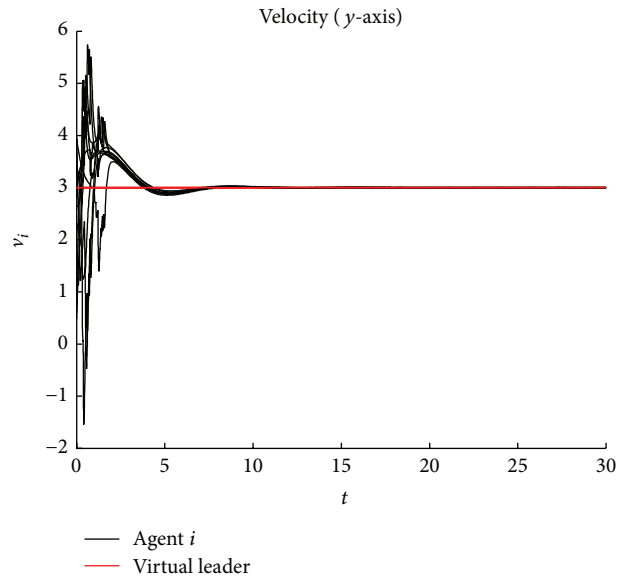

Figure 12: Velocity convergence with a virtual leader (y-axis).

Figures 11 and 12 describe the convergence process of the agents velocity over the x-axis and the y-axis, where the dotted line represents the path of the ten agents and the red solid line represents the virtual leader, which makes it clearly known that all agents approach the velocity v_γ of virtual leader and the group with the virtual leader keeps on moving at this velocity v_γ all the time. The convergence process of position over the x-axis and the y-axis is demonstrated in Figures 13 and 14. These figures are in close agreement with our theoretical predictions in Theorem 2.

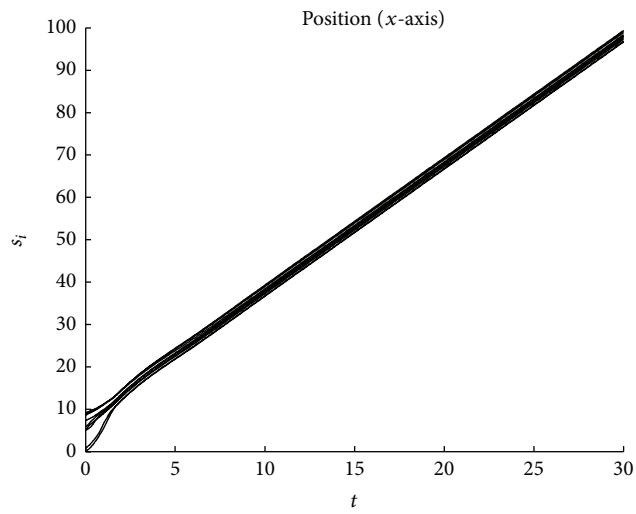

Figure 13: The process of position convergence (x-axis).

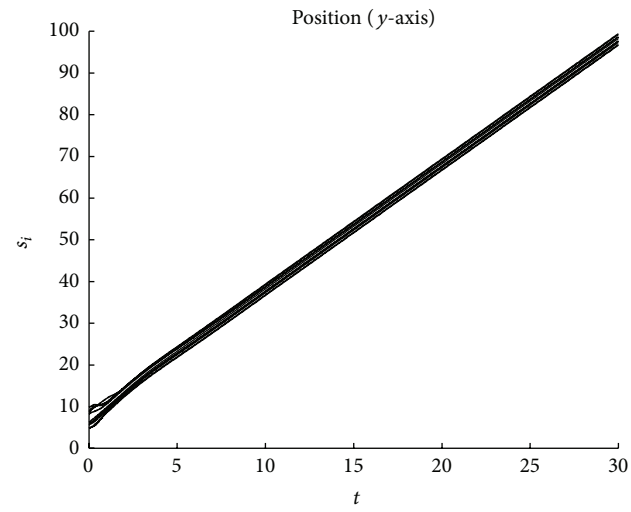

Figure 14: The process of position convergence (y-axis).

5. Conclusion

In this paper, we have investigated the flocking and the coordinative control problems of mobile autonomous agents with preserved network connectivity and proposed the flocking algorithm with avoiding collision rules. This algorithm has proposed using hysteresis in adding new links and applying new potential function method to ensure that the network always stays connected and collisions between agents can be avoided. The extended application of the flocking algorithm with a virtual leader has been investigated. The simulation has proved that the laws can make all agents approach a common velocity vector and asymptotically converge to the fixed value of interagent distances and collisions between any agents can be avoided throughout the motion. The laws also satisfy the situation that there exists a virtual leader in the group of all agents, and it is proved that the value of desired velocity of the group is the same as that of the virtual leader. Future work

will pay attention to the situation of how to make the network topology be connected as the initial network is not satisfied.

Conflict of Interests

The authors declare that there is no conflict of interests regarding the publication of this paper.

Acknowledgment

This work was supported in part by the National Natural Science Foundation of China, Grant no. 61473129.

References

[1] E. Shaw, "Fish in school," *Natural History*, vol. 84, no. 8, pp. 40–45, 1975.

[2] D. P. Spanos and R. M. Murray, "Robust connectivity of networked vehicles," in *Proceedings of the 43rd IEEE Conference on Decision and Control (CDC '04)*, vol. 3, pp. 2893–2898, December 2004.

[3] C. W. Reynolds, "Flocks, herds, and schools: a distributed behavioral model," *Computer Graphics*, vol. 21, no. 4, pp. 25–34, 1987.

[4] R. Olfati-Saber, "Flocking for multi-agent dynamic systems: algorithms and theory," *IEEE Transactions on Automatic Control*, vol. 51, no. 3, pp. 401–420, 2006.

[5] H.-S. Su and W. Zhang, "Second-order consensus of multiple agents with coupling delay," *Communications in Theoretical Physics*, vol. 51, no. 1, pp. 101–109, 2009.

[6] H. Su, G. Chen, X. Wang, and Z. Lin, "Adaptive second-order consensus of networked mobile agents with nonlinear dynamics," *Automatica*, vol. 47, no. 2, pp. 368–375, 2011.

[7] L. Cheng, Z.-G. Hou, M. Tan, Y. Lin, and W. Zhang, "Neural-network-based adaptive leader-following control for multiagent systems with uncertainties," *IEEE Transactions on Neural Networks*, vol. 21, no. 8, pp. 1351–1358, 2010.

[8] K. Sakurama and K. Nakano, "Path tracking control of lagrange systems with obstacle avoidance," *International Journal of Control, Automation and Systems*, vol. 10, no. 1, pp. 50–60, 2012.

[9] H. Su, N. Zhang, M. Z. Chen, H. Wang, and X. Wang, "Adaptive flocking with a virtual leader of multiple agents governed by locally Lipschitz nonlinearity," *Nonlinear Analysis. Real World Applications. An International Multidisciplinary Journal*, vol. 14, no. 1, pp. 798–806, 2013.

[10] W. Ren, "On consensus algorithms for double-integrator dynamics," *IEEE Transactions on Automatic Control*, vol. 53, no. 6, pp. 1503–1509, 2008.

[11] A. Zalesky, A. Fornito, and E. Bullmore, "On the use of correlation as a measure of network connectivity," *NeuroImage*, vol. 60, no. 4, pp. 2096–2106, 2012.

[12] Y. Cao and W. Ren, "Distributed coordinated tracking with reduced interaction via a variable structure approach," *IEEE Transactions on Automatic Control*, vol. 57, no. 1, pp. 33–48, 2012.

[13] M. M. Zavlanos, A. Jadbabaie, and G. J. Pappas, "Flocking while preserving network connectivity," in *Proceedings of the 46th IEEE Conference on Decision and Control*, pp. 2919–2924, December 2007.

[14] H. Su, X. Wang, and G. Chen, "Rendezvous of multiple mobile agents with preserved network connectivity," *Systems and Control Letters*, vol. 59, no. 5, pp. 313–322, 2010.

[15] M. Ji and M. Egerstedt, "Distributed coordination control of multiagent systems while preserving connectedness," *IEEE Transactions on Robotics*, vol. 23, no. 4, pp. 693–703, 2007.

[16] M. Wang, H. Su, M. Zhao, M. Z. Q. Chen, and H. Wang, "Flocking of multiple autonomous agents with preserved network connectivity and heterogeneous nonlinear dynamics," *Neurocomputing*, vol. 115, pp. 169–177, 2013.

[17] M. C. de Gennaro and A. Jadbabaie, "Decentralized control of connectivity for multi-agent systems," in *Proceedings of the 45th IEEE Conference on Decision and Control (CDC '06)*, vol. 45, pp. 3628–3633, December 2006.

[18] A. Jadbabaie, J. Lin, and A. S. Morse, "Coordination of groups of mobile autonomous agents using nearest neighbor rules," *IEEE Transactions on Automatic Control*, vol. 48, no. 6, pp. 988–1001, 2003.

[19] R. Olfati-Saber and R. M. Murray, "Consensus problems in networks of agents with switching topology and time-delays," *IEEE Transactions on Automatic Control*, vol. 49, no. 9, pp. 1520–1533, 2004.

[20] H. Su, X. Wang, and Z. Lin, "Flocking of multi-agents with a virtual leader," *IEEE Transactions on Automatic Control*, vol. 54, no. 2, pp. 293–307, 2009.

[21] H. Su, M. Z. Chen, J. Lam, and Z. Lin, "Semi-global leader-following consensus of linear multi-agent systems with input saturation via low gain feedback," *IEEE Transactions on Circuits and Systems. I. Regular Papers*, vol. 60, no. 7, pp. 1881–1889, 2013.

[22] L. Wang, H. Shi, and T. Chu, "Flocking control of groups of mobile autonomous agents via local feedback," in *Proceedings of the IEEE International Symposium on Intelligent Control*, pp. 441–446, June 2005.

[23] H. K. Khalil, *Nonlinear Systems*, Prentice Hall, Upper Saddle River, NJ, USA, 3rd edition, 2002.

Hindawi Publishing Corporation
Mathematical Problems in Engineering
Volume 2015, Article ID 945493, 7 pages
http://dx.doi.org/10.1155/2015/945493

Research Article

Distributed Multiagent for NAO Robot Joint Position Control Based on Echo State Network

Ling Qin[1,2] and Bo Lei[3]

[1]*School of Automation, Huazhong University of Technology and Science, Wuhan 430074, China*
[2]*Hubei Key Laboratory of Advanced Technology for Automotive Components, Wuhan University of Technology, Wuhan 430070, China*
[3]*School of Mechanical and Electronic Information, University of Geosciences, Wuhan 430074, China*

Correspondence should be addressed to Ling Qin; qinling@whut.edu.cn

Received 25 July 2014; Accepted 29 October 2014

Academic Editor: Wei Zhang

Based on echo state networks, the joints position control of NAO robot is studied in this paper. The process to control the robot position can be divided into two phases. The senor parameters are released during the first phase. Depending on the dynamic coupling effect between the angle acceleration of passive joint and the torque of active joint, passive joint can be controlled indirectly to the desired position along the desired trajectory. The ESN control rules during the first phase are described and ESN controller is designed to control the motion of passive joint. The brake is locked during the second phase; then active joint is controlled to the desired position. The experimental control system based on PMAC controller is designed and developed. Finally, the joint position control of the NAO robot is achieved successfully by experiments. Echo state networks utilized incremental updates driven by new sensor readings and massive short memory with history inputs; thus varying communication rates can help imitate human upper limb motion based on wearable sensors to obtain human joint angles.

1. Introduction

Humanoid robot is very common in our daily life. It can communicate with humans, respond to the surrounding environment, and complete kinds of work instead of humans. In addition, it plays an important role in exploring human interaction and cognitive processes. In robotics technology, there is much space for improvement, because it is hard to keep balance and stability of the robot at any moment, especially during movement. Path planning is one of difficult and hot spots in biped robot research. The researchers also devoted themselves to studying it.

Park and Rhee [1] observed that the zero moment point (ZMP) forward constantly on human movement; on this basis, according to the hip position and the free leg configuration, they implemented a fuzzy-logic to generate the ZMP trajectory. But the scheme was just simulated on a 7-degree-of-freedom biped robot. Lee et al. [2] simplified the dominant dynamics into a simply linear inverted pendulum model (LIPM). Under the designed conditions, the choice of ZMP function was determined with five parameters, and then the walking pattern was formed; finally the goal to perform complex tasks was achieved. In order to reduce several difficulties brought about by the uncertainty world model and unknown environment, García et al. [3] presented an estimator that depends on sensor fusion strategy; it was able to filter out low frequency and high frequency.

Based on the NAO robot platform, Gouaillier et al. [4] proposed a new walking method. They added trapezoid function to joint trajectory calculation, compensated joints that are not up to the specified location, and introduced trunk error feedback to form the close-loop achieved NAO robot dynamic humanoid walk. Strom et al. [5] proposed an omnidirectional walk for NAO based on ZMP and preview controller. They firstly confirmed the following parameters: leg trajectories in initial frame, foot frame, and center of mass (CoM) frame, and then, combining with a series of steps, specified CoM trajectory. Next they adopted preview control for walking, which suits fast-moving environment. Besides, Kulk and Welsh [6] achieved move smoothly by setting the NAO robot motor in a low stiffness.

With the upgrading of the study level, researchers are constantly expanding their research directions. To imitate human movement seems to become a new content.

As early as in 1999, Dasgupta and Nakamura [7] had already begun to study driving robot by human motion data. They attached markers at the limbs and joints of human, using the VICOT-370 system from Oxford metrics to obtain the human motion data. In 2003, a system that imitates human dance motions [8] was raised. According to motion features which can be obtained from analyzing limbs motion track, then calculated joint angle sequence of the robot. At the same time, based on ZMP, it moved the waist trajectory for keeping the balance and stability of the robot. Suleiman et al. [9] also focused their energies on studying imitation of human captured motions. They used a virtual actor to provide the joint value as motions, took the physical limitations of the humanoid robot as an optimization problem, and finally based on an optimization framework to realize the upper body imitate motion of humanoid.

Infrared camera has been used to obtain the location of human [10] successfully. Firstly it used the motion information in the virtual human model and calculated the gait information with the aid of related professional software and then derived the NAO robot. Ude et al. [11] suggested transforming human motion information obtained from an optical tracking device into a high-dimensional trajectory for the humanoid robot; then b-spline wavelet analysis is used to remove noise. But the method based on static motion capture device is difficult to realize when used in the real-time control in a lab environment. The most direct way to get the joint information is to adopt ewearable sensor devices [12]. ENC-03J sensor is produced by Japan Murata, which is composed of a gyroscope and an accelerometer. Gyroscope and accelerometer signals are amplified and filtered before output to remove electrical noise.

In this paper, our main contribution is to realize the humanoid robot to imitate human upper limb motion in real-time based on ESN (Figure 3). We tie the wearable sensors to the upper limb to get motion information. And then with the help of specialized software platform, such as Choregraphe developed by Aldebaran-Robotics Company and Visual Studio, the corresponding data is relayed to the humanoid robot. Ultimately we complete the real-time trajectory imitation of the humanoid robot.

2. Method

This section provides the basic concepts and notations of joint motion of NAO robot based echo state network. Section 2.1 gives a general description of NAO robot and how to control the robot by traditional ways. Then, the basic architecture of echo state network is introduced in the paper in Section 2.2. Finally, the joint motion control based echo state network is provided thereafter in Section 2.3.

2.1. NAO Robot. NAO robot is more popular humanoid robot nowadays. It stands 57 cm high and weighs 4.5 kg and has 25 degrees of freedom. NAO was developed by Aldebaran-Robotics Company with the latest technology and a variety of sensors, so it can ensure the fluency of motion. The more important feature of NAO is the embedded software. With the software, NAO can do voice synthesis, acoustic positioning, detect the visual image and shape with color, and detect obstacles based on dual-channel ultrasonic system. Human body can be simplified as a model that can be described as in Figure 1, which contains 12 main body joints.

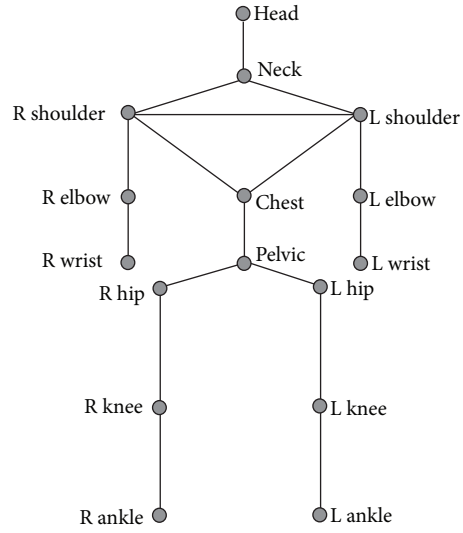

Figure 1: Human bones simplified model.

The purpose of this paper is to drive the robot arm joint, mapped to the human body, corresponding to the upper arm joint of the human body. So we tied the MTi sensors on human upper limb to obtain joints movement data. And we make sure the joint of human and NAO robot is the same.

As for the wearable sensors, we adopt the Xsens sensors-MTi. It is a miniature gyroscope enhanced heading measurement system that integrates MEMS inertial measurement sensors. The internal low-power signal processor provides three-dimensional orientations of no drift and corrected 3D acceleration, 3D angular velocity, and 3D magnetic field data. Now it is broadly used in robot fields.

MTi's coordinate system is shown in Figure 2 and aligns with the MTi sensor equipment enclosure. When starting collecting data, the initial position of the MTi sensor is marked as the coordinate direction of the current experiment. We can use the MTi sensor directly with its function of RS232, which can meet the real-time requirements of our experiment. Then we can obtain the data from the serial port with the MTi binary communication protocol using flow (free-running) operation or polling (request) mode. The initialization of the MTi sensor devices is done on the computer programming. It is quite easy to achieve with the Xsens code examples. The MTi sensors have a variety of output modes; researchers can choose the mode according to their needs. In this paper, we choose the Euler Angle output mode. The output format is roll, pitch, and yaw; all data elements are four-byte floating point.

Because human is more flexible, the activity scope is relatively larger than robot; when the human body joint

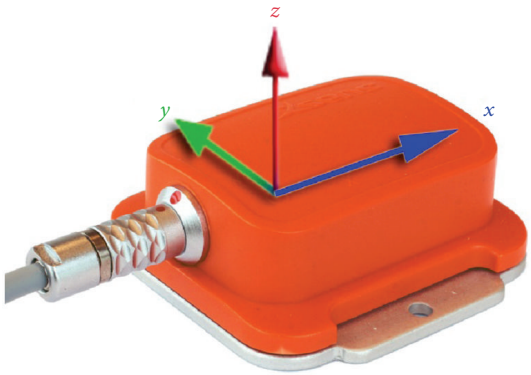

Figure 2: MTi with sensor-fixed coordinate system overlaid (S).

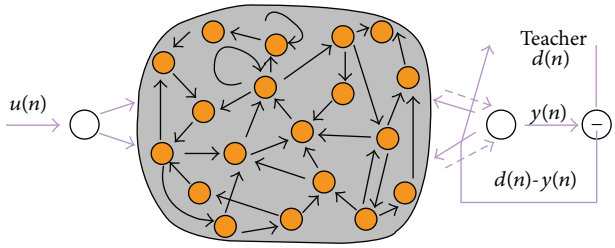

Figure 3: Basic ESN architecture.

movement value exceeds the limit value of the NAO robot, the NAO robot will take the angle value as the maximum. In order to achieve data-driven robot, the joint data obtained by the MTi sensors is assigned to a target angle, with the NAO robot's angle function method; the target angle values will be sent to the NAO robot. We can complete the programming of the NAO robot motion control based on VS platform and implement this program under the chorographer. Then call the program with port and IP address by the DOS command.

The dynamic equation of NAT robot is given as

$$m(\theta)\ddot{\theta} + F\left(\theta, \dot{\theta}\right)\dot{\theta} + f\left(\dot{\theta}\right) = \tau, \tag{1}$$

where m is the mass and inertia matrix, F is the stiffness matrix, f is the damping matrix, and τ is the NAO robot joint matrix. And the dynamic equation is described as matrix as

$$\begin{pmatrix} m_{11} & m_{12} \\ m_{21} & m_{22} \end{pmatrix} \begin{pmatrix} \ddot{\theta}_1 \\ \ddot{\theta}_2 \end{pmatrix} + \begin{pmatrix} F_1 \\ F_2 \end{pmatrix} \begin{pmatrix} \dot{\theta}_1 \\ \dot{\theta}_2 \end{pmatrix} + \begin{pmatrix} f_1 \\ f_2 \end{pmatrix} = \begin{pmatrix} \tau_1 \\ 0 \end{pmatrix}. \tag{2}$$

2.2. Brief Formal Description on ESN. More formally, an ESN consisted of K input units, N internal units, and L output units. Then, activation of input, internal, and output units at time step t is $u(t) = \{u_1(t), \ldots, u_k(t)\}$, $x(t) = \{x_1(t), \ldots, x_N(t)\}$, and $y(t) = \{y_1(t), \ldots, y_L(t)\}$, respectively. Connection weights between units are kept in four connection matrices. There are $K \times N$ weights in the input weight matrix $W^{\text{in}} = (w_{ij}^{\text{in}})$, $N \times N$ weights in the internal weight matrix $W = (w_{ij}^{\text{in}})$, $L \times (K + N + L)$ weights in the output weight matrix, and $L \times N$ weights in a matrix $W^{\text{back}} = (w_{ij}^{\text{back}})$ for connection projecting back from the output to internal units.

Table 1: Parameter settings for the reservoir of ESN.

Reservoir parameter	Values
State dimensionality	100
Sparseness	5%
Radius ρ	0.8
Input weight W^{in}	$[-0.2, 0.2]$, even distribution
Back weight W^{back}	$[-0.8, 0.8]$, even distribution

The activation of internal units was calculated as

$$x(t+1) = f\left(W^{\text{in}}u(t+1) + Wx(t) + W^{\text{back}}y(t)\right) \tag{3}$$

with $f = \{f_1, \ldots, f_N\}$ being the output functions of the internal units, a sigmoid function for the experiments in this paper. Similarly, the output was computed as

$$y(t+1) = f^{\text{out}}\left(W^{\text{out}}\left(u(t+1), x(t+1), y(t)\right)\right) \tag{4}$$

with $f^{\text{out}} = \{f^{\text{out}1}, \ldots, f^{\text{out}}{}_L\}$, the output functions of the output units and $\{u(t+1), x(t+1), y(t)\}$ the concatenation of input, internal, and previous output activation vector.

2.3. Motivation and Simulation on ESN. In order to get motion flatness and velocity continuity of NAO robot's joint, human body can be simplified as a model that contained 12 main body joints (Figure 3). And the inputs of ESN were the 12 main body joints, described as $u(t) = \{u_1(t), \ldots, u_{12}(t)\}$. The outputs of ESN were 3 main parameters, described as $y(t) = \{y_1(t), y_2(t), y_3(t)\}$.

First we created a random RNN with 800 neurons (called the "reservoir") and one output neuron. Importantly, the output neuron was equipped with random connections that project back into the reservoir. A 2500-step teacher sequence $d(1), \ldots, d(2500)$ was generated from the MGS equation and fed into the output neuron. This excited the internal neurons through the output feedback connections. After an initial transient, they started to exhibit systematic individual variations of the teacher sequence.

The fact that the internal neurons display systematic variants of the exciting external signal is constitutional for ESN: the internal neurons must work as "echo functions" for the driving signal. Not every randomly generated RNN has this property, but it can effectively be built into a reservoir. Figure 4 was the simulation for trace of NAO robot's legs. In the paper, the parameter settings for the robot's joint of NAO robot are shown in Table 1.

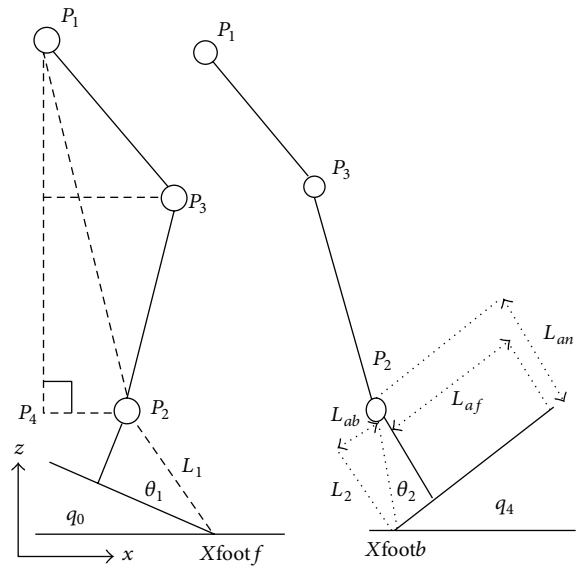

Figure 4: Trace of NAO's legs.

Figure 4 shows that the parameters of single joint are set. Taking the single joint of NAO robot as an example, the dynamic trace for passive joint is as shown in

$$\theta_2^d(t) = \begin{cases} \theta_2^0 & 0 \le t \le t_1 \\ \theta_2^0 + \left(\theta_2^{\text{end}} - \theta_2^0\right) \\ \quad \times \left[\dfrac{t - t_1}{t_2 - t_1} - \dfrac{1}{2\pi} \sin \dfrac{2\pi(t - t_1)}{t_2 - t_1}\right] & t_1 \le t \le t_2 \\ \theta_2^{\text{end}} & t_2 \le t \le t_3. \end{cases} \tag{5}$$

And for function (5), in this paper, the states for shift, velocity, and acceleration in the moving joint of NAO robot are set in

$$\begin{pmatrix} 2 & 1 & & & & & \\ \lambda_1 & 2 & \mu_1 & & & & \\ & \lambda_2 & 2 & \mu_2 & & & \\ & & \ddots & \ddots & \ddots & & \\ & & & \lambda_{n-1} & 2 & \mu_{n-1} & \\ & & & & 1 & 2 & \end{pmatrix} \begin{pmatrix} M_1 \\ M_2 \\ M_3 \\ \vdots \\ M_{n-1} \\ M_n \end{pmatrix}$$

$$= 6 \begin{pmatrix} \dfrac{f[x_1, x_2] - m_1}{h_1} \\ \dfrac{f[x_1, x_2, x_3]}{h_2} \\ \dfrac{f[x_2, x_3, x_4]}{h_3} \\ \vdots \\ \dfrac{f[x_{n-2}, x_{n-1}, x_n]}{h_{n-1}} \\ \dfrac{m_n - f[x_{n-1}, x_n]}{h_n} \end{pmatrix}. \tag{6}$$

3. Experiment

In this section, brief review the steps for collecting human pose data is given in Section 3.1. Then, Section 3.2 provides the sequential update scheme for the algorithm of multiple sensors.

3.1. Collecting Human Motion Data. Follow the steps below; our experiment of collecting human motion data goes on well.

(1) The initial position of the human body and NAO robot: to guarantee that the NAO robot can imitate human body movement accurately, we first make sure that the initial position of human body coordinates and the NAO should keep in the same position. This can be achieved through Choregraphe. In Choregraphe, processing the initialization instruction, the NAO robot will be at the zero position, as shown in Figure 5.

(2) Signal acquisition depended on MTi sensor: this paper puts forward a humanoid robot control system based on a wearable sensor. This system is not strictly limited by fixed motion analysis equipment. Wear the MTi sensor in the Shoulder joint, and as shown in Figure 6, just like the NAO robot. With the Visual Studio platform, we connect the computer and NAO robot. When ready, with the input validation rules, the MTi sensor begins to collect the shoulder joint data.

(3) Joint angle calculation and processing: the angle value of human shoulder joint obtained by the MTi sensor should be transformation and processing that will meet the NAO robot's requirements. On the right-handed Cartesian coordinate system, rotation about X, Y, and Z axis, respectively, called roll, pitch and yaw rotation. It is easy to express when the rotation is expressed as on a rotating shaft. Combined with the above formulas, it is easy to calculate the required angle value.

(4) Data driven NAO robot: with the existing NAO robot joint function, ready processed joint angle value is assigned to the NAO robot. This process needs using two software systems—Choregraphe and Visual Studio. The NAO robot can be connected by its IP address.

3.2. Algorithms. Inputs for ESN networks controller are joint sensors' information or datum of NAO robot. The difference of the different components of the range can reduce the studying accuracy and speed for networks. In order to improve better studying accuracy and speed for ESN, inputting datum for sensors must be normalized firstly with function (6) and then be linear transformation:

$$x_j' = \frac{\left(V_{\max} - x_j\right)}{\left(V_{\max} - V_{\min}\right)} \quad (j = 1, \ldots, 8). \tag{7}$$

In training, the inner neurons update as follow:

$$x(t+1) = f\left[W^{\text{in}} u(n+1) + Wx(n) + W^{\text{back}} d(n)\right], \tag{8}$$

where f is used as sigmoid function. When $t = 0$, the network begins to run and the state $x(0)$ is initialized randomly (here,

Input: $x(t+1) = f(W^{\text{in}}u(t+1) + Wx(t) + W^{\text{back}}y(t))$
(1) Initialize networks
(2) Linear transform inputs: $x'_j = (V_{\max} - x_j)/(V_{\max} - V_{\min})$
(2) Setting parameter for ESN: input weight W^{in}, back weight W^{back}, radius ρ
(3) Compute predicted estimation: sparseness
(4) Update: $x(t+1) = f(W^{\text{in}}u(t+1) + Wx(t) + W^{\text{back}}y(t))$
(5) Training
(6) **end for**
(7) **for** $n = 300, 301, \ldots, 2500$ **do**
(8) Getting Training MSE: $\text{MSE}_{\text{train}} = 1/1000 \sum_{n=300}^{2500} \{\tanh^{-1}[d(n)] - \tanh^{-1}[y(n)]\}^2$
(9) Getting Testing MSE: $\text{MSE}_{\text{test}} = 1/150 \sum_{n=1}^{150} \{\tanh^{-1}[d(n)] - \tanh^{-1}[y(n)]\}^2$
(10) **for** each n **do**
(11) **While** (MSE $\leqslant 0.8$) **then** to Step 7
(12) compute output value
(13) **end for**
Output: $y(t+1) = f^{\text{out}}(W^{\text{out}}(u(t+1), x(t+1), y(t)))$

Algorithm 1: Control law of joint motion.

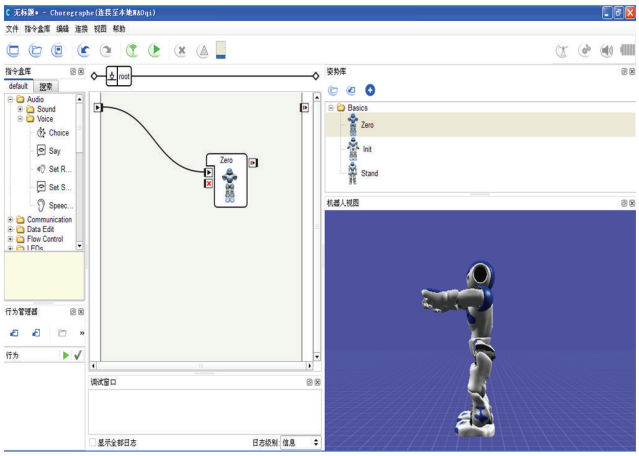

Figure 5: The zero position of the NAO robot.

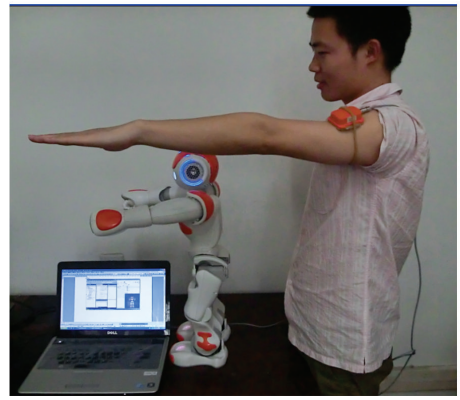

Figure 6: The initial position of human and NAO.

$x(0) = 0$), $d(n) = 0$. The training I/O date series is inputted in the network. Then DR is encouraged fully, which shows system dynamic characteristics (see Algorithm 1).

4. Analysis of Simulation

In order to demonstrate the performance of proposed multiagent control approach for joint motion of NAO robot, numerical results are presented in the paper for a planar multitarget tracking scenario in multiagent system where three controllable moving observers, two equipped with range-only sensors and one with a bearing-only sensor, are placed in a specified surveillance area to estimate the number of targets as well as their positions. Each joint shares its current locations, sensor type, and observations with the other agents. There are an unknown and time-varying number of targets observed in clutter for each agent.

A series of experiments are done to prove the reliability of this point proposed in this paper. The motion trace of NAO robot joint is shown in Figure 7. During the experiments, we constantly change the stop position of human right arm; the robot can imitate the human right arm movement accurately. Figure 8 shows that the passive robot's joints could be controlled more accurately along expecting trace with human pose data.

The simulation result is shown that the joint motion control based on ESN can get better motion flatness and velocity continuity.

5. Conclusions and Future Work

In this paper, we propose a novel joint motion control of NAO robot approach based on echo state network. Simulation results demonstrate that the proposed approach is capable of joint motion control via effective sensor control. Unfortunately, during the experiments, we cannot achieve the man-robot synchronization. There could be network reason for this. Or there may be a better way for data optimization. How to optimize the time question is the focus of our efforts in the future.

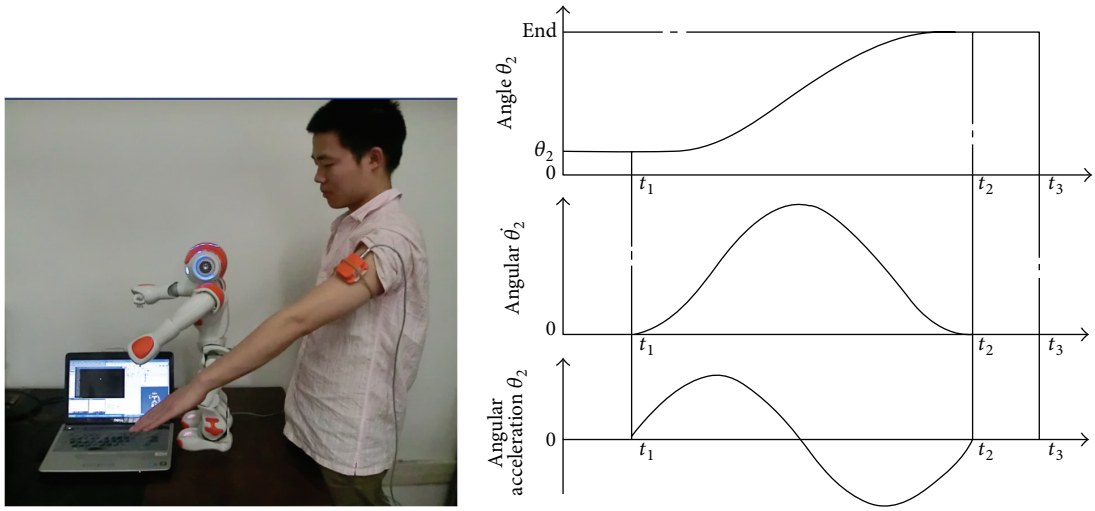

(a) (b)

Figure 7: (a) The results of the experiment. (b) The motion trace of NAO joint.

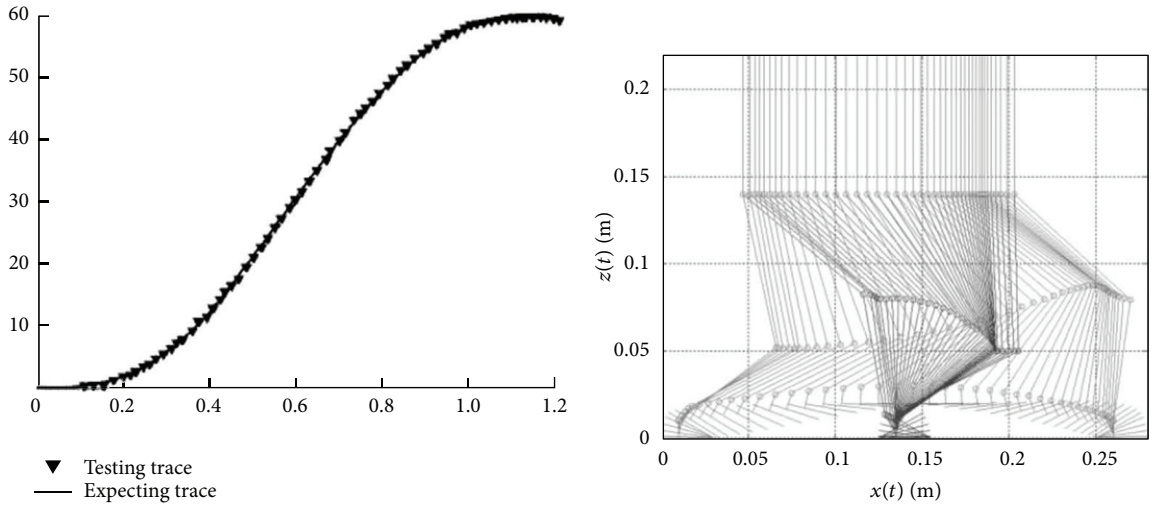

(a) (b)

Figure 8: (a) Joint motion trace of NAO robot. (b) Joint motion simulation of NAO robot.

Conflict of Interests

The authors declare that there is no conflict of interests regarding the publication of this paper.

References

[1] J. H. Park and Y. K. Rhee, "ZMP trajectory generation for reduced trunk motions of biped robots," in *Proceedings of the IEEE/RSJ International Conference on Intelligent Robots and Systems*, pp. 90–95, October 1998.

[2] B.-J. Lee, D. Stonier, Y.-D. Kim, J.-K. Yoo, and J.-H. Kim, "Modifiable walking pattern of a humanoid robot by using allowable ZMP variation," *IEEE Transactions on Robotics*, vol. 24, no. 4, pp. 917–925, 2008.

[3] J. G. García, A. Robertsson, J. G. Ortega, and R. Johansson, "Sensor fusion for compliant robot motion control," *IEEE Transactions on Robotics*, vol. 24, no. 2, pp. 430–441, 2008.

[4] D. Gouaillier, C. Collette, and C. Kilner, "Omni-directional closed-loop walk for NAO," in *Proceedings of the 10th IEEE-RAS International Conference on Humanoid Robots*, pp. 448–454, 2010.

[5] J. Strom, G. Slavov, and E. Chown, "Omnidirectional walking using ZMP and preview control for the NAO humanoid robot," in *RoboCup 2009: Robot Soccer World Cup XIII*, vol. 5949 of *Lecture Notes in Computer Science*, pp. 378–389, Springer, Berlin, Germany, 2010.

[6] J. Kulk and J. Welsh, "A low power walk for the NAO robot," in *Proceedings of the Australasian Conference on Robotics and Automation (ACRA '08)*, J. Kim and R. Mahony, Eds., December 2008.

[7] A. Dasgupta and Y. Nakamura, "Making feasible walking motion of humanoid robots from human motion capture data," in *Proceedings of the IEEE International Conference on Robotics and Automation (ICRA '99)*, pp. 1044–1049, May 1999.

[8] S. Nakaoka, A. Nakazawa, K. Yokoi, H. Hirukawa, and K. Ikeuchi, "Generating whole body motions for a biped humanoid robot from captured human dances," in *Proceedings of the IEEE International Conference on Robotics and Automation (ICRA '03)*, vol. 3, pp. 3905–3910, September 2003.

[9] W. Suleiman, E. Yoshida, F. Kanehiro, J.-P. Laumond, and A. Monin, "On human motion imitation by humanoid robot," in *Proceedings of the IEEE International Conference on Robotics and Automation (ICRA '08)*, pp. 2697–2704, Pasadena, Calif, USA, May 2008.

[10] P. L. Jean-Christophe, B. Olivier, and F. Jean-Guy, "From human motion captures to humanoid spatial coordination," *International Journal of Humanoid Robotics*, vol. 9, no. 3, Article ID 1250019, 2012.

[11] A. Ude, C. G. Atkeson, and M. Riley, "Programming full-body movements for humanoid robots by observation," *Robotics and Autonomous Systems*, vol. 47, no. 2-3, pp. 93–108, 2004.

[12] D. Roetenberg, H. Luinge, and P. Slycke, "Xsens MVN: full 6DOF human motion tracking using miniature inertial sensors," Tech. Rep., Sens Technologies, 2009.

Hindawi Publishing Corporation
Mathematical Problems in Engineering
Volume 2015, Article ID 941697, 7 pages
http://dx.doi.org/10.1155/2015/941697

Research Article

Distributed Robust Attitude Tracking of Multiple Spacecraft with Disturbances and Unmodelled Dynamics

Dapeng Yang and Xiangdong Liu

State Key Laboratory for Intelligent Control & Decision of Complex Systems, Beijing Institute of Technology, Beijing 100081, China

Correspondence should be addressed to Dapeng Yang; yangdp1988@163.com

Received 26 August 2014; Accepted 24 September 2014

Academic Editor: Housheng Su

This paper considers the distributed robust attitude tracking problem of multiple spacecraft subject to disturbances and unmodelled dynamics. We designed a distributed robust attitude controller for each spacecraft using the relative attitudes and relative angular velocities of neighbors to ensure that the attitude tracking errors between the leader and the followers converge to zero under the condition that the communication graph among the followers is undirected and connected and at least one follower has the access to the leader. The control algorithm achieves robust attitude tracking under the existence of the disturbances and unmodelled dynamics by selecting the control gains according to the given condition.

1. Introduction

In the recent ten years, many researchers of the control field began to study the coordinated control of multiagent systems because of its broad applications including formation, flocking, and cooperative control [1–4]. It is well-known that cooperative attitude control of multiple rigid bodies is an important research direction and has received much attention in the last decade. The existing literature of multiagent systems contains the work with integrator dynamics and general linear dynamics [1, 2, 4–6]. The topic of our paper, cooperative attitude tracking for multiple spacecraft, is more difficult. References [7–9] have considered the attitude control problem of single spacecraft or single rigid body by using some methods such as adaptive control and sliding mode control. For the attitude tracking problem of multiple rigid bodies or multiple spacecraft, distributed control strategies seem to be a proper method because there are some advantages such as less communication and decentralized computing [10].

Many researchers in the field of control engineering have considered the distributed attitude control problem of multiple rigid bodies. A leader-follower strategy for attitude coordination was studied in [11], while the cooperative attitude control problem was considered in [12]. The authors in [13] adopted the contraction analysis theory to guarantee the exponential convergence of attitude synchronization problem of multiple spacecraft. The communication topology in [13] is a bidirectional ring. Using quaternion to describe the spacecraft's attitude, [14] studied the distributed attitude synchronization problem. In contrast, the authors in [15] used modified Rodriguez parameters (MRPs) to represent the attitude of the spacecraft. Under the assumption that the communication topology is a directed spanning tree, [16] addressed the distributed attitude synchronization problem for multiple spacecraft with unknown inertia matrices. In a word, all the existing works above mainly considered the cases where the exact model knowledge of each spacecraft is known or the cases where the external disturbance does not exist. However, there might exist some disturbances and unmodelled dynamics in practical applications. References [17–19] considered the distributed coordinated control problem for multimanipulator systems or decentralized consensus problem for multiagent systems. The semiglobal leader-following consensus problem of linear multiagent systems with input saturation via low-gain feedback was investigated in [20, 21] based on state feedback and output feedback.

In this paper, we consider the distributed robust attitude tracking problem subject to disturbances and unmodelled dynamics for multiple spacecraft. In this paper, we adopt MRPs to describe the attitude for the spacecraft. We design

a robust controller for each spacecraft in a distributed manner using the relative attitudes and the angular velocities of neighbors. Under the assumption that the communication topology among the followers is undirected and at least one follower can get the information from the leader, the proposed controller could guarantee that the combined errors between the leader spacecraft and the follower spacecraft would converge to zero. Although [22, 23] dealt with the robust consensus tracking problem for multiagent system where the agent dynamics were restricted to being single or double integrators with disturbances and unmodelled dynamics. In contrast to [22, 23] which only considered the robust tracking problem with linear dynamics, this paper considers the attitude tracking problem of multiple spacecraft where the attitude dynamics of spacecraft are totally nonlinear. The proposed controller solves the robust attitude tracking problem in the presence of disturbances and unmodelled dynamics by selecting the control gains according to the given condition. Under the proposed control strategy, only a subgroup of the followers have the access to the leader; that is, the robust attitude tracking can be achieved using only the neighboring information.

The structure of this paper is arranged as follows. Some existing results and mathematical preliminaries are introduced in Section 2. Section 3 investigated the distributed robust attitude tracking controllers. Section 4 represents the simulation examples. The conclusion of this paper is Section 5.

2. Mathematical Preliminaries

2.1. Notation and Graph Theory. I_p means the identity matrix of dimension p. $\mathbf{R}^{n\times n}$ represent the set of $n \times n$ real matrices. Let T represent the transpose for real matrices. Let $A \otimes B$ be the Kronecker product of matrices A and B. Let $\|x\|$ be the 2-norm of a vector x. $\mathrm{diag}(A_1, \ldots, A_N)$ denotes a block-diagonal matrix with matrices A_i, on its diagonal, $i = 1, \ldots, N$. We say a vector $x \in \mathscr{L}_\infty$, when all the elements of x are bounded.

A directed graph $\mathscr{G}$ is a pair $(\mathscr{V}, \mathscr{E})$, where $\mathscr{V} = \{v_1, \ldots, v_N\}$ is a set of nodes and $\mathscr{E} \subseteq \mathscr{V} \times \mathscr{V}$ is a set of edges, in which an edge is represented by an ordered pair of distinct nodes. For an edge (v_i, v_j), we call node v_i the parent node, node v_j the child node, and v_i a neighbor of v_j. If $(i, j) \in \mathscr{E}$ means $(j, i) \in \mathscr{E}$, we say the graph is undirected. A path from node v_{i_1} to node v_{i_l} is a sequence of ordered edges of the form $(v_{i_k}, v_{i_{k+1}})$, $k = 1, \ldots, l-1$. The adjacency matrix $A = [a_{ij}] \in \mathbf{R}^{N\times N}$ associated with the directed graph $\mathscr{G}$ is defined by $a_{ii} = 0$, $a_{ij} = 1$ if $(v_j, v_i) \in \mathscr{E}$ and $a_{ij} = 0$ otherwise. The Laplacian matrix $L = [l_{ij}] \in \mathbf{R}^{N\times N}$ is defined as $l_{ii} = \sum_{j=0, j\neq i}^{N} a_{ij}$ and $l_{ij} = -a_{ij}$, $i \neq j$.

Lemma 1 (see [24]). *Zero is a simple eigenvalue of L and the associated eigenvector is $\mathbf{1}$ if and only if the undirected graph is connected, where $\mathbf{1} = [1, \ldots, 1]^T \in \mathbf{R}^N$ is a unitary column vector. All of the nonzero eigenvalues of L are real and positive for an undirected graph.*

2.2. Attitude Dynamics. In this paper, we consider the distributed robust attitude tracking problem for a group of $N + 1$ spacecrafts. We adopt MRPs to represent the attitude of a spacecraft with respect to the inertial frame. The MRP vector $\sigma_i \in \mathbf{R}^3$ is defined by $\sigma_i = \widehat{\mathbf{e}}_i \tan(\phi_i/4)$ for the ith spacecraft, where $\widehat{\mathbf{e}}_i$ is the Euler axis and ϕ_i is the Euler angle [25]. In our following discussion, it is assumed that the leader spacecraft is indexed by 0 and the follower spacecrafts are labeled by $1, \ldots, N$. For the ith follower spacecraft, the attitude dynamics is described by [26]

$$\begin{aligned} J_i\dot{\omega}_i &= -\omega_i^{\times} J_i\omega_i + u_i + f_i', \\ \dot{\sigma}_i &= G(\sigma_i)\,\omega_i, \quad i = 1, \ldots, N, \end{aligned} \tag{1}$$

where $J_i \in \mathbf{R}^{3\times 3}$ is the inertia matrix, $\omega_i \in \mathbf{R}^3$ denotes the attitude angular velocity with respect to the inertial frame in the body-fixed frame, $u_i \in \mathbf{R}^3$ is the control input, $\omega_i^{\times} \in \mathbf{R}^{3\times 3}$ is the skew-symmetric matrix such that $\omega_i^{\times} v = \omega_i \times v$ for any vector $v \in \mathbf{R}^3$, f_i' represents the disturbances and unmodelled dynamics, and

$$G(\sigma_i) = \frac{1}{2}\left(\frac{1 - \sigma_i^T\sigma_i}{2} I_3 + \sigma_i^{\times} + \sigma_i\sigma_i^T\right). \tag{2}$$

Rewrite the dynamics equation to get a simpler form as follows:

$$\begin{aligned} \dot{\omega}_i &= -J_i^{-1}\omega_i^{\times} J_i\omega_i + J_i^{-1}u_i + f_i, \\ \dot{\sigma}_i &= G_i\omega_i, \end{aligned} \tag{3}$$

where $f_i = J_i^{-1} f_i'$. Note that we define a new form $f_i(t)$ instead of $J_i^{-1} f_i'(t)$ to represent the disturbances and unmodelled dynamics, which does not affect the overall analysis in this paper. This modification is only for simplicity in the subsequent discussion. We assume that the leader is not a real spacecraft, but just a reference signal. So we do not consider the disturbances and unmodelled dynamics for the leader.

We assume that there is no access to any follower spacecraft from the leader. And the leader's information can only be obtained by a subset of the followers. We use an undirected graph to represent the communication topology of the N followers. The access of the followers to the leader is represented by a diagonal matrix $A_0 = \mathrm{diag}(a_{10}, \ldots, a_{N0}) \in \mathbf{R}^{N\times N}$. $a_{i0} = 1$, $i = 1, \ldots, N$, if the ith spacecraft has the access to the leader and $a_{i0} = 0$ otherwise. To facilitate the stability analysis of the closed-loop control system, we make the following assumptions on $f_i(t)$ and the communication graph among the $N + 1$ spacecraft. Our control objective is to drive the follower spacecraft's attitudes σ_i, $i = 1, \ldots, N$, to follow the leader spacecraft's attitude σ_0 in the presence of the disturbances and unmodelled dynamics existing in the follower spacecraft's attitude dynamics. It is reasonable that there exist external disturbances and parameter uncertainties in the attitude dynamics for the followers in some applications.

Assumption 2. The disturbances term $f_i(t)$ and the first-order and second-order time derivatives of $f_i(t)$ are bounded; that is, $f_i(t), \dot{f}_i(t), \ddot{f}_i(t) \in \mathscr{L}_\infty$, $i = 1, \ldots, N$.

Assumption 3. The graph $\mathcal{G}$ is connected and at least one follower has the access to the leader.

3. Main Results

This section considers the distributed robust attitude tracking problem for multiple spacecraft described by (3). The followers' attitudes are desired to follow the leader in the presence of the disturbances and unmodelled dynamics. Note that the attitude of the leader is a time-varying signal. The distributed attitude tracking problem is defined as follows.

Definition 4. The distributed robust attitude tracking problem is said to be solved, if the local control laws u_i, $i = 1, \ldots, N$, are designed for (3) in the presence of disturbances and unmodelled dynamics such that $\lim_{t\to\infty}\|\sigma_i - \sigma_0\| = 0$ and $\lim_{t\to\infty}\|\omega_i - \omega_0\| = 0$, $i = 1, \ldots, N$.

Using the local information available to the ith spacecraft, the angular velocity tracking error e_{ω_i}, the attitude tracking error e_{σ_i}, and the combined tracking error e_i for each follower spacecraft at each time are defined by

$$\begin{aligned} e_{\omega_i} &= \sum_{j=1}^{N} a_{ij}\left(\omega_i - \omega_j\right) + a_{i0}\left(\omega_i - \omega_0\right), \\ e_{\sigma_i} &= \sum_{j=1}^{N} a_{ij}\left(\sigma_i - \sigma_j\right) + a_{i0}\left(\sigma_i - \sigma_0\right), \\ e_i &= e_{\omega_i} + \alpha e_{\sigma_i}, \quad i, j = 1, \ldots, N, \end{aligned} \tag{4}$$

where a_{ij} is the (i, j)th element of the adjacency matrix and $\alpha \in \mathbf{R}$ is a positive constant.

A distributed robust attitude tracking controller is proposed for each follower as

$$\begin{aligned} u_i &= J_i\left(-\widehat{f}_i + \rho_i + a_{i0}\dot{\omega}_0 - k_c e_i - \alpha G_i \omega_i\right), \\ \dot{\widehat{f}}_i &= k_1 \dot{e}_i + k_2\,\mathrm{sgn}\left(e_i\right) + k_3 e_i, \quad i = 1, \ldots, N, \end{aligned} \tag{5}$$

using only the local information of neighboring spacecraft, where $\rho_i = J_i^{-1}\omega_i^{\times} J_i \omega_i$, k_c, k_1, k_2, and $k_3 \in \mathbf{R}$ are positive constant control gains to be determined and $\mathrm{sgn}(\cdot)$ is the sign function. Since the disturbances and unmodelled dynamics term f_i is unknown, we use its estimate $\widehat{f}_i$ to obtain the control law u_i. We can see that $\widehat{f}_i$ is calculated by the combined tracking error e_i for each spacecraft. To facilitate the further analysis, a group of concatenated vectors and diagonal matrices are defined as

$$\begin{aligned} \omega &= \left[\omega_1^T \ \cdots \ \omega_N^T\right]^T, \qquad \sigma = \left[\sigma_1^T \ \cdots \ \sigma_N^T\right]^T, \\ u &= \left[u_1^T \ \cdots \ u_N^T\right]^T, \qquad f = \left[f_1^T \ \cdots \ f_N^T\right]^T, \\ \widehat{f} &= \left[\widehat{f}_1^T \ \cdots \ \widehat{f}_N^T\right]^T, \qquad e_\omega = \left[e_{\omega_1}^T \ \cdots \ e_{\omega_N}^T\right]^T, \\ e_\sigma &= \left[e_{\sigma_1}^T \ \cdots \ e_{\sigma_N}^T\right]^T, \qquad e = \left[e_1^T \ \cdots \ e_N^T\right]^T, \\ \rho &= \left[\rho_1^T \ \cdots \ \rho_N^T\right]^T, \qquad G = \mathrm{diag}\left(G_1, \ldots, G_N\right), \\ J &= \mathrm{diag}\left(J_1, \ldots, J_N\right). \end{aligned} \tag{6}$$

Then, it can be derived that

$$\begin{aligned} e_\omega &= \left(M \otimes I_3\right)\omega - A_0 \otimes \omega_0, \\ e_\sigma &= \left(M \otimes I_3\right)\sigma - A_0 \otimes \sigma_0, \\ e &= e_\omega + \alpha e_\sigma \\ &= \left(M \otimes I_3\right)(\omega + \alpha\sigma) - A_0 \otimes \left(\omega_0 + \alpha\sigma_0\right), \end{aligned} \tag{7}$$

where $M \triangleq L + A_0$. The time derivative of the concatenated combined tracking error e is given by

$$\begin{aligned} \dot{e} &= \dot{e}_\omega + \alpha\dot{e}_\sigma \\ &= \left(M \otimes I_3\right)\left(-\rho + J^{-1}u + f + \alpha G\omega\right) \\ &\quad - A_0 \otimes \left(\dot{\omega}_0 + \alpha\dot{\sigma}_0\right) \\ &= \left(M \otimes I_3\right)\left(-\rho + J^{-1}J\left(-\widehat{f} + \rho + A_0 \otimes \dot{\omega}_0 \right.\right. \\ &\qquad \left.\left. - k_c e - \alpha G\omega\right) + f + \alpha G\omega\right) \\ &\quad - A_0 \otimes \left(\dot{\omega}_0 + \alpha\dot{\sigma}_0\right) \\ &= \left(M \otimes I_3\right)\left(f - \widehat{f} - k_c e + A_0 \otimes \dot{\omega}_0\right) \\ &\quad - A_0 \otimes \left(\dot{\omega}_0 + \alpha\dot{\sigma}_0\right). \end{aligned} \tag{8}$$

In addition, define a filtered tracking error $r(t) \in \mathbf{R}^{3\times N}$ by

$$k_c\left(M \otimes I_3\right)r = k_c\dot{e} + e, \tag{9}$$

deriving that $\dot{e} = (M \otimes I_3)r - (1/k_c)e$ and

$$\begin{aligned} r &= \left(M \otimes I_3\right)^{-1}\dot{e} + \frac{1}{k_c}\left(M \otimes I_3\right)^{-1}e \\ &= \int_0^t m\,d\tau - \widehat{f} - k_c e + \frac{1}{k_c}\left(M \otimes I_3\right)^{-1}e, \end{aligned} \tag{10}$$

where $\int_0^t m\,d\tau = f + A_0 \otimes \dot{\omega}_0 - (M \otimes I_3)^{-1}A_0 \otimes (\dot{\omega}_0 + \alpha\dot{\sigma}_0)$. Using $\dot{e} = (M \otimes I_3)r - (1/k_c)e$, the time derivative of r is given by

$$\begin{aligned} \dot{r} &= m - \dot{\widehat{f}} - k_c\dot{e} + \frac{1}{k_c}\left(M \otimes I_3\right)^{-1}\dot{e} \\ &= m - k_2\,\mathrm{sgn}\left(e\right) - k_3 e - k_1\left(M \otimes I_3\right)r + \frac{k_1}{k_c}e \\ &\quad - k_c\left(M \otimes I_3\right)r + e + \frac{1}{k_c}r - \frac{1}{k_c^2}\left(M \otimes I_3\right)^{-1}e. \end{aligned} \tag{11}$$

Remark 5. It can be concluded that the convergence of the filtered tracking error $r(t)$ guarantees the convergence of the concatenated combined tracking error $e(t)$, which can be proved using the Lyapunov-based analysis by selecting a Lyapunov function $V(e) = (1/2)e^T e$.

Lemma 6 (see [22]). *A function $s(t) \in \mathbf{R}$ defined as follows is positive semidefinite:*

$$s(t) = e(0)^T k_2 \operatorname{sgn}(e(0)) - e(0)^T m(0) - \int_0^t r^T (M \otimes I_3)(m - k_2 \operatorname{sgn}(e))\, d\tau, \tag{12}$$

if the control gains k_2 and k_c satisfy

$$k_2 > \|m(t)\| + k_c \|\dot{m}(t)\|. \tag{13}$$

Theorem 7. *Suppose that Assumptions 2 and 3 hold. The distributed robust attitude tracking problem of the spacecraft in* (3) *is solved by the distributed attitude tracking control law* (5) *if the control gains are selected such that*

$$k_2 > \|m(t)\| + k_c \|\dot{m}(t)\|, \quad k_3 = \frac{k_1}{k_c} + 1, \quad M \otimes I_3 - \frac{1}{k_c^2} I_{3\times N} > 0. \tag{14}$$

Proof. Note that $M = L + A_0$ and L is the Laplacian matrix associated with graph $\mathcal{G}$. Under the Assumption 2, M is positive definite [27]. Then, it can be seen that

$$\begin{aligned} e &= (M \otimes I_3)(\omega + \alpha\sigma) - A_0 \otimes (\omega_0 + \alpha\sigma_0) \\ &= (M \otimes I_3)(\omega + \alpha\sigma) - A_0 \otimes (\omega_0 + \alpha\sigma_0) \\ &\quad - L \otimes (\omega_0 + \alpha\sigma_0) \\ &= (M \otimes I_3)\left[(\omega + \alpha\sigma) - I_N \otimes (\omega_0 + \alpha\sigma_0)\right], \end{aligned} \tag{15}$$

where we have used the fact that $L \otimes (\omega_0 + \alpha\sigma_0) = (L \otimes I_3)(I_N \otimes (\omega_0 + \alpha\omega_0)) = 0$ because $\mathbf{1}$ is the eigenvector of the Laplacian matrix L associated with the simple eigenvalue 0 according to Lemma 1 and $I_N \otimes (\omega_0 + \alpha\omega_0) \in \operatorname{span}\{\mathbf{1}\}$. Then, it follows from (15) and the positive definiteness of the matrix M that $e = 0$ if and only if

$$\omega_0 + \alpha\sigma_0 = \cdots = \omega_N + \alpha\sigma_N, \tag{16}$$

which, as proved in [28], in turn implies that

$$\lim_{t\to\infty} \|\sigma_i - \sigma_0\| = 0, \quad \lim_{t\to\infty} \|\omega_i - \omega_0\| = 0, \quad i = 1, \ldots, N. \tag{17}$$

So, the distributed robust attitude tracking problem is solved if and only if $e(t) = 0$ as $t \to \infty$.

Choose the Lyapunov function candidate

$$V(t) = \frac{1}{2} e^T e + \frac{1}{2} r^T (M \otimes I_3) r + s, \tag{18}$$

where s is defined in (12). From Assumption 2, $f_i(t)$, $\dot{f}_i(t), \ddot{f}_i(t) \in L_\infty$, $i = 1, \ldots, N$, which implies that $\dot{F}$ and $\ddot{F}$ are both bounded. In view of the boundedness of the initial state of the leader spacecraft, we know that $\dot{\omega}_0(0), \ddot{\omega}_0(0), \dot{\sigma}_0(0), \ddot{\sigma}_0(0) \in L_\infty$. Based on the definition of $m(t)$ in (10), we can see that $\|m(t)\|$ and $\|\dot{m}(t)\|$ are both bounded. Then, it follows from Lemma 6, the positive definiteness of the matrix M, and the first condition in (14) that the Lyapunov function candidate $V(t)$ is positive definite. Then the time derivative of $V(t)$ along the trajectory of (10), (11), and (12) is given by

$$\begin{aligned} \dot{V}(t) &= e^T \dot{e} + r^T (M \otimes I_3)\dot{r} + \dot{s} \\ &= e^T \left((M \otimes I_3) r - \frac{1}{k_c} e\right) + r^T (M \otimes I_3) \\ &\quad \times \left(m - k_2 \operatorname{sgn}(e) - k_3 e - k_1 (M \otimes I_3) r + \frac{k_1}{k_c} e \right. \\ &\quad \left. - k_c (M \otimes I_3) r + e + \frac{1}{k_c} r - \frac{1}{k_c^2} (M \otimes I_3)^{-1} e\right) \\ &\quad - r^T (M \otimes I_3)(m - k_2 \operatorname{sgn}(e)). \end{aligned} \tag{19}$$

By using the second condition in (14), we can obtain that

$$\begin{aligned} \dot{V}(t) &= -\frac{1}{k_c} e^T e - k_1 r^T (M \otimes I_3)(M \otimes I_3) r \\ &\quad - k_c r^T (M \otimes I_3)\left((M \otimes I_3) - \frac{1}{k_c^2} I_{3\times N}\right) r \\ &\quad + r^T \left((M \otimes I_3) - \frac{1}{k_c^2} I_{3\times N}\right) e. \end{aligned} \tag{20}$$

Since

$$\begin{aligned} &r^T \left((M \otimes I_3) - \frac{1}{k_c^2} I_{3\times N}\right) e \\ &= -\frac{1}{2k_c}\left[e - k_c \left((M \otimes I_3) - \frac{1}{k_c^2} I_{3\times N}\right) r\right]^T \\ &\quad \times \left[e - k_c \left((M \otimes I_3) - \frac{1}{k_c^2} I_{3\times N}\right) r\right] \\ &\quad + \frac{1}{2k_c} k_c^2 r^T \left((M \otimes I_3) - \frac{1}{k_c^2} I_{3\times N}\right)^2 r + \frac{1}{2k_c} e^T e, \end{aligned} \tag{21}$$

it follows that

$$\begin{aligned} \dot{V}(t) &= -\frac{1}{k_c} e^T e - k_1 r^T (M \otimes I_3)(M \otimes I_3) r \\ &\quad - k_c r^T (M \otimes I_3)\left((M \otimes I_3) - \frac{1}{k_c^2} I_{3\times N}\right) r \end{aligned}$$

$$
\begin{aligned}
&- \frac{1}{2k_c}\left[e - k_c\left((M\otimes I_3) - \frac{1}{k_c^2}I_{3\times N}\right)r\right]^T \\
&\times \left[e - k_c\left((M\otimes I_3) - \frac{1}{k_c^2}I_{3\times N}\right)r\right] \\
&+ \frac{1}{2k_c}k_c^2 r^T\left((M\otimes I_3) - \frac{1}{k_c^2}I_{3\times N}\right)^2 r + \frac{1}{2k_c}e^T e \\
&= -\frac{1}{2k_c}e^T e - k_1 r^T (M\otimes I_3)(M\otimes I_3)r \\
&- \frac{1}{2k_c}\left[e - k_c\left((M\otimes I_3) - \frac{1}{k_c^2}I_{3\times N}\right)r\right]^T \\
&\times \left[e - k_c\left((M\otimes I_3) - \frac{1}{k_c^2}I_{3\times N}\right)r\right] \\
&- k_c r^T (M\otimes I_3)\left((M\otimes I_3) - \frac{1}{k_c^2}I_{3\times N}\right)r \\
&+ \frac{1}{2}k_c r^T\left((M\otimes I_3) - \frac{1}{k_c^2}I_{3\times N}\right)^2 r \\
&= -\frac{1}{2k_c}e^T e - k_1 r^T (M\otimes I_3)(M\otimes I_3)r \\
&- \frac{1}{2k_c}\left[e - k_c\left((M\otimes I_3) - \frac{1}{k_c^2}I_{3\times N}\right)r\right]^T \\
&\times \left[e - k_c\left((M\otimes I_3) - \frac{1}{k_c^2}I_{3\times N}\right)r\right] \\
&- k_c r^T\left[(M\otimes I_3)^2 - \frac{1}{k_c^2}(M\otimes I_3) - \frac{1}{2}(M\otimes I_3)^2\right. \\
&\qquad \left. - \frac{1}{2k_c^4}I_{3\times N} + \frac{1}{k_c^2}(M\otimes I_3)\right]r \\
&= -\frac{1}{2k_c}e^T e - k_1 r^T (M\otimes I_3)(M\otimes I_3)r \\
&- \frac{1}{2k_c}\left[e - k_c\left((M\otimes I_3) - \frac{1}{k_c^2}I_{3\times N}\right)r\right]^T \\
&\times \left[e - k_c\left((M\otimes I_3) - \frac{1}{k_c^2}I_{3\times N}\right)r\right] \\
&- \frac{1}{2}k_c r^T\left[(M\otimes I_3) + \frac{1}{k_c^2}I_{3\times N}\right] \\
&\times \left[(M\otimes I_3) - \frac{1}{k_c^2}I_{3\times N}\right]r,
\end{aligned}
\tag{22}
$$

where we have used the equation $M^T = M$ since the graph $\mathcal{G}$ is undirected.

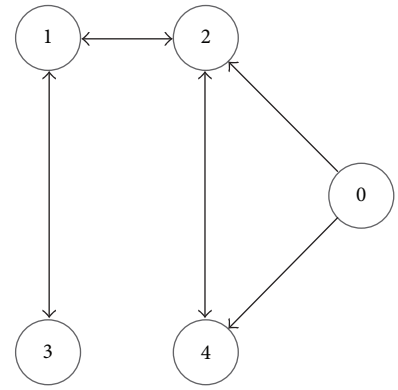

Figure 1: The communication topology of spacecraft.

In view of the third condition in (14), we obtain that $M\otimes I_3 - (1/k_c^2)I_{3\times N} > 0$. Then, if follows from (22) that $\dot{V}(t) \le 0$. Since $V(t) > 0$ and $\dot{V}(t) \le 0$, it is easy to see that $V(t) \le V(0) \in L_\infty$. From the definition of $V(t)$, we can see that $e(t), r(t) \in L_\infty$. Based on the boundedness of $f(t)$, $e(t)$, $\dot{\omega}_0(t)$, $\dot{\sigma}_0(t)$, (5), and (8), we can obtain $\widehat{f}(t), \dot{e}(t) \in L_\infty$. Then, it follows from (10) and the boundedness of $m(t)$, $\dot{\widehat{f}}(t)$, and $\dot{e}(t)$ that $\dot{r}(t) \in L_\infty$, which in turn guarantees that $\ddot{V}(t) = f(e, \dot{e}, r, \dot{r})$ is bounded. According to Barbalat's lemma [29], we get that $\dot{V}(t) \to 0$ as $t \to \infty$; that is, $\lim_{t\to\infty} e(t) = 0$, $i = 1, \ldots, N$. Thus, the distributed robust attitude tracking problem is solved. □

Remark 8. The cooperative attitude synchronization problem for multiple rigid bodies has been solved in [15, 30]. However, the authors in [15, 30] only considered the nominal model of the attitude dynamics, while in this paper the disturbances and unmodelled dynamics are contained during the analysis. This paper proposed a sufficient condition for achieving distributed robust attitude tracking between the following spacecraft and the leader, which is a more challenging task because of the disturbances and unmodelled dynamics.

Remark 9. Compared to [22, 31] where the robust consensus tracking problems were considered and the agent dynamics were restricted to being single or double integrator, this paper considers robust attitude tracking of multiple spacecraft where the attitude dynamics of spacecraft are nonlinear. Additionally, [32, 33] considered the rendezvous problem and the adaptive consensus problem for multiple mobile linear agents with preserved network connectivity, which is an interesting topic for the distributed cooperative control of multiple spacecraft. However, it is more challenging and cannot be obtained easily by extending the results in our paper. We will consider the network connectivity preserving case in our future research.

4. Simulation Examples

Consider a group of five spacecraft whose communication topology is given by Figure 1. The inertia matrices of the

Table 1: Spacecraft inertias.

Number	Parameters/(kg·m^2)
J_0	[1.1 0.35 0.45; 0.35 1.0 0.5; 0.45 0.5 1.3]
J_1	[1 0.1 0.1; 0.1 0.1 0.1; 0.1 0.1 0.9]
J_2	[1.5 0.2 0.3; 0.2 0.9 0.4; 0.3 0.4 2.0]
J_3	[0.8 0.1 0.2; 0.1 0.7 0.3; 0.2 0.3 1.1]
J_4	[1.2 0.3 0.7; 0.3 0.9 0.2; 0.7 0.2 1.4]

spacecraft are shown in Table 1. We choose the initial attitude $\sigma_i(0)$,$\omega_i(0)$, $i = 0, \ldots, 4$, randomly. In this section, we assume that the leader spacecraft's information can only be obtained by spacecrafts 1 and 2. We design the control input u_0 as

$$u_0 = J_0 \left[\rho_0 - k_0 \left(\omega_0 - \omega_0^d\right)\right], \tag{23}$$

where $\rho_0 = J_0^{-1}\omega_0^{\times} J_0\omega_0$ and $k_0 = \mathrm{diag}(1, 1, 1)$, to track a given angular velocity $\omega_0^d = [0.2\sin(0.3t); 0.1\sin(0.4t); 0.15\cos(0.5t)]$.

To verify the theoretical result of our paper, let the constants in Theorem 7 be $k_c = 10$, $k_1 = 0.1$, $k_2 = 0.003$, $k_3 = 1.01$, and $\alpha = 1$. The disturbances and unmodelled dynamics $f_i'(t)$, $i = 1, \ldots, 4$, for the follower spacecraft are given by

$$f_i'(t) = \begin{bmatrix} f_{i1}'(t) \\ f_{i2}'(t) \\ f_{i3}'(t) \end{bmatrix} = \begin{bmatrix} \left(0.03 - \dfrac{i}{100}\right)\sin(0.3t) \\ \left(0.04 - \dfrac{i}{100}\right)\cos(0.3t) \\ \left(0.03 - \dfrac{i}{100}\right)\sin\left(0.3t + \dfrac{\pi}{4}\right) \end{bmatrix}. \tag{24}$$

The attitudes and the attitude angular velocities of the five spacecrafts are shown in Figures 2 and 3, from which we can see that the distributed robust attitude tracking problem is solved provided that the disturbances and unmodelled dynamics exist in the attitude dynamics. The tracking errors e_i, $i = 1, \ldots, 4$, of the follower spacecraft are given in Figure 4, which clearly converge to zero as $t \to \infty$.

5. Conclusion

In this paper, we considered the distributed robust attitude tracking problem of multiple spacecraft with disturbances and unmodelled dynamics. We designed distributed robust controllers for multiple spacecraft based on the relative attitudes and relative attitude angular velocities of neighbors to track the leader's time-varying attitude in the presence of disturbances and unmodelled dynamics. The proposed control algorithm achieves robust attitude tracking for the case that the communication graph among follower spacecrafts is an undirected connected graph and at least one follower has the access to the leader by selecting the control

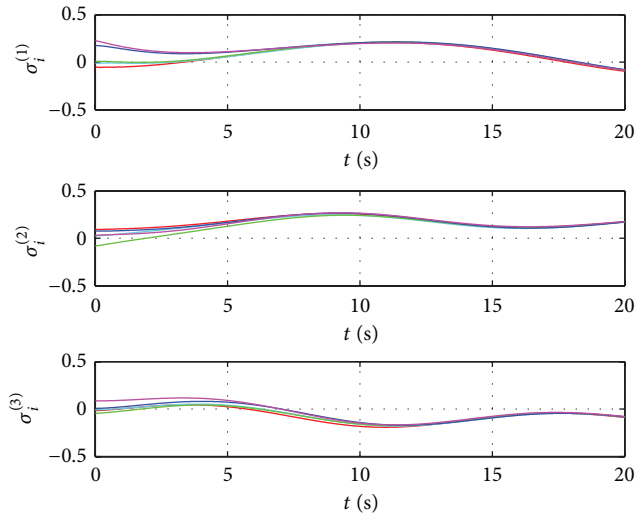

Figure 2: The attitudes under the robust controller (5).

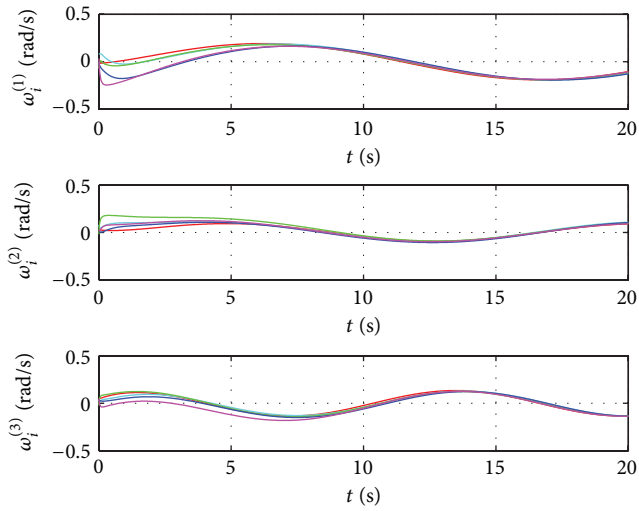

Figure 3: The angular velocities under the robust controller (5).

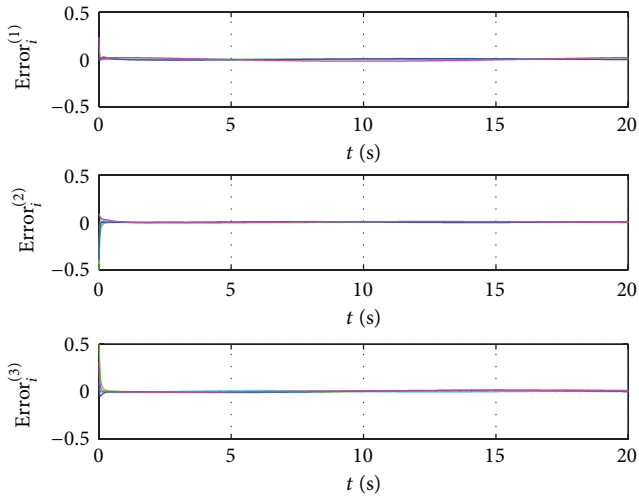

Figure 4: The tracking errors under the robust controller (5).

gains according to the given condition. The distributed robust attitude tracking of multiple spacecraft without velocity measurements and robust attitude tracking under directed communication topologies are interesting topics for future research.

Conflict of Interests

The authors declare that there is no conflict of interests regarding the publication of this paper.

References

[1] R. Olfati-Saber and R. M. Murray, "Consensus problems in networks of agents with switching topology and time-delays," *IEEE Transactions on Automatic Control*, vol. 49, no. 9, pp. 1520–1533, 2004.

[2] W. Ren and R. W. Beard, "Consensus seeking in multiagent systems under dynamically changing interaction topologies," *IEEE Transactions on Automatic Control*, vol. 50, no. 5, pp. 655–661, 2005.

[3] W. Ren, R. W. Beard, and E. M. Atkins, "Information consensus in multivehicle cooperative control," *IEEE Control Systems Magazine*, vol. 27, no. 2, pp. 71–82, 2007.

[4] Z. Li, Z. Duan, G. Chen, and L. Huang, "Consensus of multiagent systems and synchronization of complex networks: a unified viewpoint," *IEEE Transactions on Circuits and Systems I: Regular Papers*, vol. 57, no. 1, pp. 213–224, 2010.

[5] Y. Hong, G. Chen, and L. Bushnell, "Distributed observers design for leader-following control of multi-agent networks," *Automatica*, vol. 44, no. 3, pp. 846–850, 2008.

[6] Z. Li, Z. Duan, and G. Chen, "On H_∞ and H_2 performance regions of multi-agent systems," *Automatica*, vol. 47, no. 4, pp. 797–803, 2011.

[7] G. Q. Xing and S. A. Parvez, "Nonlinear attitude state tracking control for spacecraft," *Journal of Guidance, Control, and Dynamics*, vol. 24, no. 3, pp. 624–626, 2001.

[8] W. Luo, Y.-C. Chu, and K.-V. Ling, "Inverse optimal adaptive control for attitude tracking of spacecraft," *IEEE Transactions on Automatic Control*, vol. 50, no. 11, pp. 1639–1654, 2005.

[9] H. Wong, M. S. De Queiroz, and V. Kapila, "Adaptive tracking control using synthesized velocity from attitude measurements," *Automatica*, vol. 37, no. 6, pp. 947–953, 2001.

[10] W. Ren and R. Beard, *Distributed Consensus in Multi-Vehicle Cooperative Control: Theory and Applications*, Springer, 2008.

[11] P. K. C. Wang, F. Y. Hadaegh, and K. Lau, "Synchronized formation rotation and attitude control of multiple free-flying spacecraft," *Journal of Guidance, Control, and Dynamics*, vol. 22, no. 1, pp. 28–35, 1999.

[12] D. V. Dimarogonas, P. Tsiotras, and K. J. Kyriakopoulos, "Leader-follower cooperative attitude control of multiple rigid bodies," *Systems and Control Letters*, vol. 58, no. 6, pp. 429–435, 2009.

[13] S.-J. Chung, U. Ahsun, and J.-J. E. Slotine, "Application of synchronization to formation flying spacecraft: lagrangian approach," *Journal of Guidance, Control, and Dynamics*, vol. 32, no. 2, pp. 512–526, 2009.

[14] A. Abdessameud and A. Tayebi, "Attitude synchronization of a group of spacecraft without velocity measurements," *IEEE Transactions on Automatic Control*, vol. 54, no. 11, pp. 2642–2648, 2009.

[15] W. Ren, "Distributed cooperative attitude synchronization and tracking for multiple rigid bodies," *IEEE Transactions on Control Systems Technology*, vol. 18, no. 2, pp. 383–392, 2010.

[16] Z. Li and Z. Duan, "Distributed adaptive attitude synchronization of multiple spacecraft," *Science China Technological Sciences*, vol. 54, no. 8, pp. 1992–1998, 2011.

[17] Z. Hou, L. Cheng, M. Tan, and X. Wang, "Distributed adaptive coordinated control of multi-manipulator systems using neural networks," in *Robot Intelligence: An Advanced Knowledge Processing Approach*, pp. 49–69, Springer, London, UK, 2010.

[18] L. Cheng, Z.-G. Hou, M. Tan, Y. Lin, and W. Zhang, "Neural-network-based adaptive leader-following control for multiagent systems with uncertainties," *IEEE Transactions on Neural Networks*, vol. 21, no. 8, pp. 1351–1358, 2010.

[19] Z.-G. Hou, L. Cheng, and M. Tan, "Decentralized robust adaptive control for the multiagent system consensus problem using neural networks," *IEEE Transactions on Systems, Man, and Cybernetics Part B: Cybernetics*, vol. 39, no. 3, pp. 636–647, 2009.

[20] H. Su, M. Z. Q. Chen, J. Lam, and Z. Lin, "Semi-global leader-following consensus of linear multi-agent systems with input saturation via low gain feedback," *IEEE Transactions on Circuits and Systems I: Regular Papers*, vol. 60, no. 7, pp. 1881–1889, 2013.

[21] H. Su, M. Z. Q. Chen, X. Wang, and J. Lam, "Semiglobal observer-based leader-following consensus with input saturation," *IEEE Transactions on Industrial Electronics*, vol. 61, no. 6, pp. 2842–2850, 2014.

[22] G. Hu, "Robust consensus tracking for an integrator-type multi-agent system with disturbances and unmodelled dynamics," *International Journal of Control*, vol. 84, no. 1, pp. 1–8, 2011.

[23] G. Hu, "Robust consensus tracking of a class of second-order multi-agent dynamic systems," *Systems and Control Letters*, vol. 61, no. 1, pp. 134–142, 2012.

[24] R. Olfati-Saber, J. A. Fax, and R. M. Murray, "Consensus and cooperation in networked multi-agent systems," *Proceedings of the IEEE*, vol. 95, no. 1, pp. 215–233, 2007.

[25] M. D. Shuster, "Survey of attitude representations," *The Journal of the Astronautical Sciences*, vol. 41, no. 4, pp. 439–517, 1993.

[26] P. Tsiotras, "Further passivity results for the attitude control problem," *IEEE Transactions on Automatic Control*, vol. 43, no. 11, pp. 1597–1600, 1998.

[27] Y. Hong, J. Hu, and L. Gao, "Tracking control for multi-agent consensus with an active leader and variable topology," *Automatica*, vol. 42, no. 7, pp. 1177–1182, 2006.

[28] Z.-X. Li and B.-L. Wang, "Robust attitude tracking control of spacecraft in the presence of disturbances," *Journal of Guidance, Control, and Dynamics*, vol. 30, no. 4, pp. 1156–1159, 2007.

[29] J. Slotine and W. Li, *Applied Nonlinear Control*, Prentice Hall, 1991.

[30] Z. Meng, W. Ren, and Z. You, "Decentralized cooperative attitude tracking using modified Rodriguez parameters," in *Proceedings of the 48th IEEE Conference on Decision and Control held jointly with 28th Chinese Control Conference (CDC/CCC '09)*, pp. 853–858, December 2009.

[31] S. Khoo, L. Xie, and Z. Man, "Robust finite-time consensus tracking algorithm for multirobot systems," *IEEE/ASME Transactions on Mechatronics*, vol. 14, no. 2, pp. 219–228, 2009.

[32] H. Su, X. Wang, and G. Chen, "Rendezvous of multiple mobile agents with preserved network connectivity," *Systems & Control Letters*, vol. 59, no. 5, pp. 313–322, 2010.

[33] H. Su, G. Chen, X. Wang, and Z. Lin, "Adaptive second-order consensus of networked mobile agents with nonlinear dynamics," *Automatica*, vol. 47, no. 2, pp. 368–375, 2011.

Hindawi Publishing Corporation
Mathematical Problems in Engineering
Volume 2015, Article ID 530147, 11 pages
http://dx.doi.org/10.1155/2015/530147

Research Article

A Core Model for Parts Suppliers Selecting Method in Manufacturing Supply Chain

Guorong Chen,[1,2,3] Jiangyuan Zhao,[2] and Juli Deng[1]

[1]*School of Electronic and Information Engineering, Chongqing University of Science and Technology, Chongqing 401331, China*
[2]*CAIA, Dhurakij Pundit University, Bangkok 10210, Thailand*
[3]*Faculty of Engineering, University of Ottawa, Ottawa, ON, Canada K1N 6M9*

Correspondence should be addressed to Juli Deng; cwcgr@126.com

Received 3 June 2014; Revised 1 September 2014; Accepted 2 September 2014

Academic Editor: Housheng Su

Service-oriented manufacturing is the new development of manufacturing systems, and manufacturing supply chain service is also an important part of the service-oriented manufacturing systems; hence, the optimal selection of parts suppliers becomes one of key problems in the supply chain system. Complex network theories made a rapid progress in recent years, but the classical models such as BA model and WS model can not resolve the widespread problems of manufacturing supply chain, such as the repeated attachment of edge and fixed number of vertices, but edges increased with preferential connectivity, and flexible edges' probability. A core model is proposed to resolve the problem in the paper: it maps the parts supply relationship as a repeatable core; a vertex's probability distribution function integrating the edge's rate and vertex's degree is put forward; some simulations, such as the growth of core, the degree distribution characteristics, and the impacting of parameter, are carried out in our experiments, and the case study is set also. The paper proposed a novel model to analyze the manufacturing supply chain system from the insights of complex network.

1. Introduction

Manufacturing services spawned the manufacturing system's range, which needs the dominant firms collaborating with their parts suppliers beyond geographical boundaries, but how to select the most optimal parts suppliers in the supply chain becomes the new difficulty. In order to resolve the problem of optimal selecting part suppliers in manufacturing supply chain, many scholars devote their researches in the topics from those fields.

The first field is the cooperation models in the manufacturing supply chain. Holland proposed the mode of cooperation and collaboration of supply chain management [1]; Sarmah et al. went into the coordination models between the business entities to gain lower supply chain cost [2]. Kelle and Akbulut discussed the software tools of ERP in supply chain for information sharing, cooperation, and cost optimization [3]; Nagarajan and Sošić discussed the game-theoretic analysis method in cooperation supply chains [4]; Fiala discussed the information sharing between suppliers, manufacturers, distributors, retailers, and customers [5]; Savaskan et al. discussed the closed loop supply chain models with product remanufacturing [6]; Ma and Chen researched on the elements and characters in integrated logistics' supply chain [7]; Xu and Ma researched on the trust mechanism between enterprises in supply chain and suggested that the cultivation of mutual trust of enterprises is the core of supply chain management [8]; and Love et al. researched on the interorganizational relations in construction industry [9].

The second field is the dynamic analysis, evaluation methods, and the business forecasting in the supply chain. Liang et al. put forward nonlinear programming problems to solve the DEA (Data envelopment analysis) models for supply chain efficiency evaluation [10]; Leng and Zhu reviewed the side-payment contracts in two-person nonzero-sum supply chain games and discussed its application [11]; Zhu et al. researched on the confirmation of a measurement model for green supply chain management practices implementation

[12]; Cachon and Zipkin discussed the competitive and cooperative inventory policies in a two-stage supply chain [13]; Sarkis proposed a strategic decision framework for green supply chain management [14]; Huang et al. discussed an analysis of manufacturer-retailer supply chain coordination in cooperative advertising [15]; Ferguson discussed the "commitment time frame problem" between an end product manufacturer and a parts supplier [16]; Surana et al. researched the context of supply-chain networks [17]; Gupta and Maranas discussed the managing demand uncertainty method in supply chain planning and proposed a tool for evaluating and actively managing the exposure of enterprises assets (such as inventory levels and profit margins) to market uncertainties [18]; Kim et al. go through an empirical investigation in IT alignment between supply chain partners to enhance customer value creation [19]; and Connelly et al. discussed the perspectives of six prominent organizational theories, such as apply real options theory, internationalization theory, organizational economics, resource dependence theory, social network theory, and institutional theory, and how to effect the development of supply chain [20].

The third field is the complex network analysis approach and its applications. Stanley Milgram pointed out the famous theories of six degrees of separation; he observed that the distant of human in the world is about six degrees; Watts built a special website to check the theories [21]; and game of Kevin Bacon checked the theories as Bacon degree [22], and some scholars in Oakland University go through the theories as Erdos degree [23]; all of those experiments proved the theories are valid. Erdős and Rényi study the social network based on the perspective of graph theory for the first time in the world and published a famous paper on the evolution of random graphs [24]; Watts and Strogatz researched on the modeling of small-world networks, characteristics, and mechanism [25, 26]; Barabási and Albert studied some kinds of complex networks and put forward the statistical mechanism of small world networks, scale-free networks, complex networks, and evolutionary theory [27, 28]; Gregoriades A and Sutcliffe studied the reliability of complex systems based on load forecasting and planning methods [29]. Shi et al. studied the calculation model and vertex degree distribution of complex networks, such as clustering coefficient estimates [30, 31]; Wang research network synchronization and control technology [32]; Li and Chen studied the control principles and methods of complex networks [33]. Guoning and Zheren discussed the components product family relations, described the relationship between the network diagram of parts products using the weighted directed tree network method, calculated the statistical properties of the relationship between the network components, studied the revolution process of the parts products relationship network diagram, and proposed a prediction approach of the amount of parts [34]. The study is completely broken through the traditional way of manufacturing research information system and provides a guideline for our research.

From the reviews above, we can see that the complex network theory and its applications have made a rapid progress in recent years, and it can integrate the system engineering and topology and became a new approach to be used to analyze the part suppliers' optimal selecting problems of manufacturing supply chain.

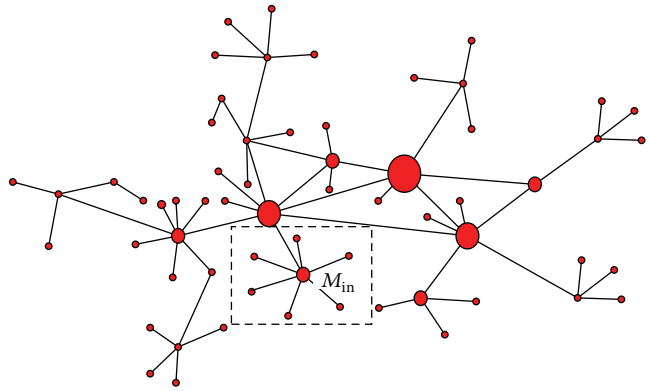

Figure 1: The supply relationship network.

But there have been rare reports of complex network theories applied in manufacturing supply chain. Based on the preliminary studies [35], this paper will focus on the part supplier's optimal selecting problems and presents a core model for the part suppliers optimal selecting problems in manufacturing supply chain. It will describe the application problem in Section 2; analyze the shortcomings of two classical complex network models named BA model and WS model in Section 3; put forward a core model, discuss the designs and description of the model, and present the probability formula of selecting part suppliers in detail in Section 4; and simulate the model and analyze the characteristics in Section 5.

2. The Problem Description

The supply relationship of parts in manufacturing system intertwined together and formed a complex relationship network. The dominant firm wants some parts for assembling its production. If there are many parts suppliers meeting the given quality and times requirements, the cost is the key factors to affect their decision that those parts suppliers should to be selected. Supposing the parts consisted of some parts, the parts are made up of subparts and so on; the supply relation forms a supply relationship network, so the manufacturing supply chain has the sketch as Figure 1.

It is not easy to resolve the suppliers selecting problem of the whole network. In the paper, we select one vertex that has many suppliers to analyze; other vertices' characteristics are easy to arrive using the same method.

3. The Relationship Model Researches and the New Characteristics of Manufacturing Supply Chain

Toward the manufacturing supply chain, the similar researches mainly were two famous models, WS model [25] and BA model [27].

3.1. The WS Model [25]. Watts and Strogatz reported the WS model firstly in their "Collective dynamics of 'small-world' networks" in 1998 (by Nature). Newman and Watts improved it as NW model in 1999 [36]. The WS model starts from a ring lattice with n vertices and k edges per vertex then rewire each edge at random with probability p. This model shows a graph between regularity ($p = 0$) and disorder ($p = 1$), for intermediate values of p, and the graph is a small-world network that is highly clustered like a regular graph, yet with small characteristic path length, like a random graph; it is shown in Figure 2. The characteristic can be used in large scale network, with some characteristic as that the number of vertices is fixed; number of edges is fixed, rewriting edges random.

3.2. The BA Model. The BA model is proposed by Barabási and Albert in their "Emergence of scaling in random networks" in 1999 (by Science) [27]. The BA model should meet two conditions: at first, the graph is opened and new vertices should continue to be added to the system; secondly, the attachment of the edges has the characteristic of preferential connectivity. So, the degree of vertices with rich-get-richer phenomenon can be detected easily in BA networks, and the growth process is shown as in Figure 3.

3.3. The Performances of Manufacturing Supply Chain Network. Now, let us trace the development of the manufacturing supply chain network from its origin. In Figure 1, at first, the vertex M_{in} is new one and has no parts supplier, which means the core diagram only has candidate vertices with degree 1; then, some parts need to be produced from the suppliers, which means some edges should be added in the network. Which are the next vertices to produce the parts? It may be decided by random at the first time, the following selections maybe select other vertices different from the first vertices; perhaps the new selection is more efficient than the first one. Then, a most efficiency route arrived; the follow-up selections will tend to the same route to produce the parts; the selection will strengthen the ability of the notes in the chains, the abilities improvement of the vertices will firm the tendency to form fixed manufacturing supply chains. From the description above, we can see that the manufacturing supply chain network has some characteristics different from the BA model and WS model (see Figures 2 and 3).

First, both models suppose that the edges attached any two vertices without any repetition, but, in the manufacturing supply chain system, the edges maybe reduplicate, and it usually is repeated many times with the development of the manufacturing supply chain.

Second, in WS model, the attachment probability of new edge is fixed and comes randomly; in BA model, the attachment probability of new edge is be added along with vertices and with preferential connectivity. But those cannot meet the real supply chain network's request, and the new edges add into the network with preferential connectivity but do not need to add new vertices, so the number of vertices is fixed but the edges will keep increasing with preferential connectivity.

Third, the WS model and the BA model suggested that the edges probability of attachment is constant, but, in supply chain network, because of the limitation of production ability and the distance between them, the probability usually changes periodically. So, it needs a new model to meet the needs of manufacturing supply chains.

4. The Core Model

4.1. The Core Model of Manufacturing Supply Chain. In order to resolve the problems mentioned in WS model and BA model, our model maps the supply relationship network from Figure 1 to the core diagram in Figure 4; in Figure 4(a), it constituted by some vertices and some edges that the core has one input vertex and has n selective supply vertices. The supply vertices may be defined as part suppliers; the edges may be defined as the costs between the input vertex/dominant firm M_{in} and the special supply vertex. In the selecting process, the director of edges directs the collected to the supply vertices. If it needs to decide the parts supplier of vertex M_k, the core iterated on the vertex M_k, as shown in Figure 4(b).

Now, towards Figure 4(a), if k_i is used to express the degrees set of vertex i, obviously, larger k_i means more experience to produce the candidate parts. The edge E_i is the supply relationships between the vertex E_i to the supply vertex M_i, and lower value of E_i shows that the transportation costs from vertex M_i to the supply vertex i are more cheap and means that vertex i tends to be selected as the candidate unit. The object of production scheduling is to optimize the manufacturing systems so as to produce the parts using the minimize costs in the given during time, and it may be described as the following formula:

$$O = \min\{O_1, O_2, O_3, \ldots, O_n\}, \quad (0 < i < n). \tag{1}$$

Therefore, O_i is the cost of vertex i.

4.2. The Vertex Probability Distribution in Manufacturing Supply Network. In order to describe the growing process of the manufacturing supply network, we supposed it satisfied the following 4 assumptions.

(1) The number of vertices in the network is fixed as N.

(2) It does not allow the edges' start and end to join the same vertices.

(3) The edges of network may grow freely only with preferential connectivity.

(4) The probability of changes meets a special function discussed next.

Supposing the core has m_0 edges initially, now m ($m < N$) new edges should be added into the core diagram every fixed time interval t. and the attachments should select the vertices with biggest probability. After time interval t, the edges in the network will be $m_0 + mt$ edges.

The first factor to be considered is the degree of vertex; it means the truth, cooperation times, or selection history.

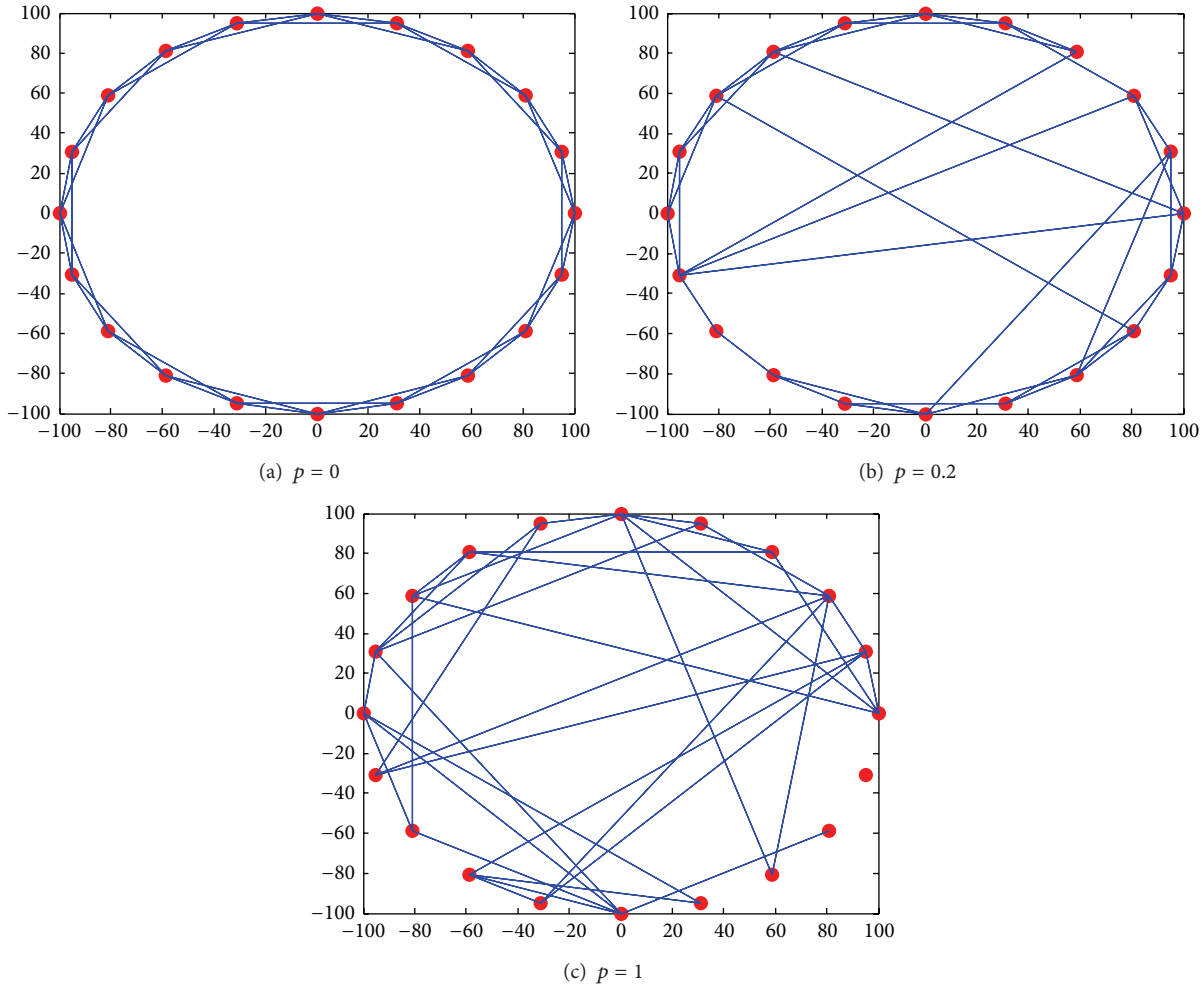

Figure 2: The WS model.

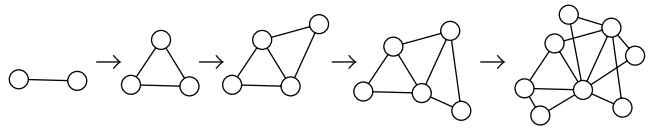

Figure 3: The growth of BA model.

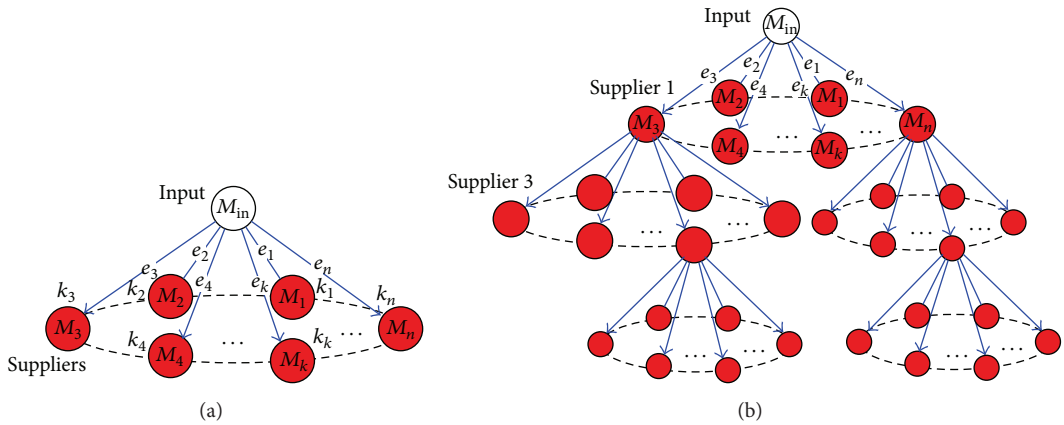

Figure 4: The core model.

Obviously, the selection process is a binomial distribution function, as in the following formula:

$$p\{X = t\} = k_i. \tag{2}$$

The normalized result is the following formula:

$$p_i = \frac{k_i}{\sum_{j=1}^{N} k_j}. \tag{3}$$

However, the degree can not involve all the factors. It is only an experiment index; a bigger degree means the supplier has more experiment of operation, or it has more relation resources or skills. The edges rate should to be taken into consideration, and it is a cost index; it is to be decided by such as transportation costs of the parts, ready resources, and other costs. So, the relationship between the vertices degree and the edges rates should be taken into consideration. The preresearch shows that it is a linear function if only it is taken into consideration one factor of the vertex degree or the edges rates individually. Toward the vertex, the vertex degree and the edges rates are a binomial distribution; the probability distribution meets the function as in formula

$$p\{X = i\} = k_i^{\tau} r_i^{1-\tau}, \quad (0 \le \tau \le 1). \tag{4}$$

The normalized results may be expressed as

$$p_i = \frac{k_i^{\tau} r_i^{1-\tau}}{\sum_{j=1}^{N} k_j^{\tau} r_j^{1-\tau}}, \quad (0 \le \tau \le 1), \tag{5}$$

where k_i is the degree of vertex i, it may be decided as the operation times, and it may be obtained by computing the indegree; hence, k_i may be computed as the following formula:

$$k_i = \sum_{j=1}^{t} k_{\text{in-}i}, \tag{6}$$

where r_i is the rate of the attachment, E_i means the costs attaching vertex i, and the affecting factor includes the diverting and other costs. Then, r_i is

$$r_i = \frac{1}{E_i}, \tag{7}$$

where τ is the adjustable parameter between k_i and r_i, and it make it easier to adjust the vertices' degree and the edge's rates.

Formula (5) gives us a quantitative method to compute the probability distribution of suppliers at a time point. Each supplier has different calculating result and the results will change along with time because k_i changes with the time.

If the time is unlimited, the parts supply chain plan tends to the most effective route, and other suppliers have no chances to obtain the orders. So, the operation cost is

$$C_{\min} = \sum_{j=1}^{N} C_{\text{Min-}i}, \quad (t\Gamma \le T). \tag{8}$$

Therefore, $C_{\text{Min-}i}$ is the minimizing vertex's cost of vertex i.

On the contrary, if the time is very urgent, the time should exceed the shortest time request so as to finish all the parts of the batch. Maybe, the cost is the largest one:

$$C_{\max} = \sum_{j=1}^{N} C_i, \quad \left(t\Gamma = \frac{T}{n}\right). \tag{9}$$

Therefore, $\sum_{j=1}^{N} C_i$ means all of the suppliers should work regardless of its inefficiency.

Usually, the optimal plan is between the two extreme cases, which means the operation tending to some effective suppliers and other suppliers may allocate fewer amounts of orders.

5. Simulation Study

Now, let us study the core model in simulation to check it. In our experience, the rate of edges (the reciprocal of transportation costs) came from random number between 0 and 1; each vertex has initial degree of 1.

5.1. The Growth Process of Core Model. The growth of core is studied first in our experiment, and the results are shown in Figures 5 and 6.

Where the adjustable parameter of degree and edge is $\tau = 0.1$, the rates of edge come from random number; the vertex's number is 20, and the number following the vertex name in Figure 5 is the vertex' degree.

From Figure 5, we can see that, with new edges added into the core model and the degree of core growing with the time, some vertices tend to grow, but other vertices' degree keeps constant. M6, M8, and M12 have the greatest degrees while degree = 1000, that means those suppliers may keep lowest costs, and they are the best selections. On the contrary, the degrees of M1, M2, M4, M5, M7, M9, and M20 are 1 or 2, which means those suppliers have seldom chances to cooperate with the center vertex M_{in}.

5.2. The Degree Distribution of the Core Model. The degree distribution of growing process is shown in Figure 6: it shows that the key suppliers have a small number, but those vertices supplied a large number of parts; on the contrary, a large number of other vertices only supplied few parts (Figures 6(a) and 6(b)). The number of suppliers and the numbers of vertices in a core show a power law, vertex with rich degree becomes richer (Figures 6(c) and 6(d)), and the reality is almost like it. If the supplier has no chance to attend the cooperation in the earlier time, it needs to have a much lower cost to attend the core later; the cooperation of core is decided by lower cost and more trust.

Figure 7 shows the cooperation tendency chart in the core: the suppliers in higher degree (Figure 7(a)) or hot color (Figure 7(b)) mean the supplier has closer cooperation relationship with the core center vertex.

Figure 5 shows the cooperation tendency chart in the core: the suppliers in higher degree (Figure 5(a)) or hot

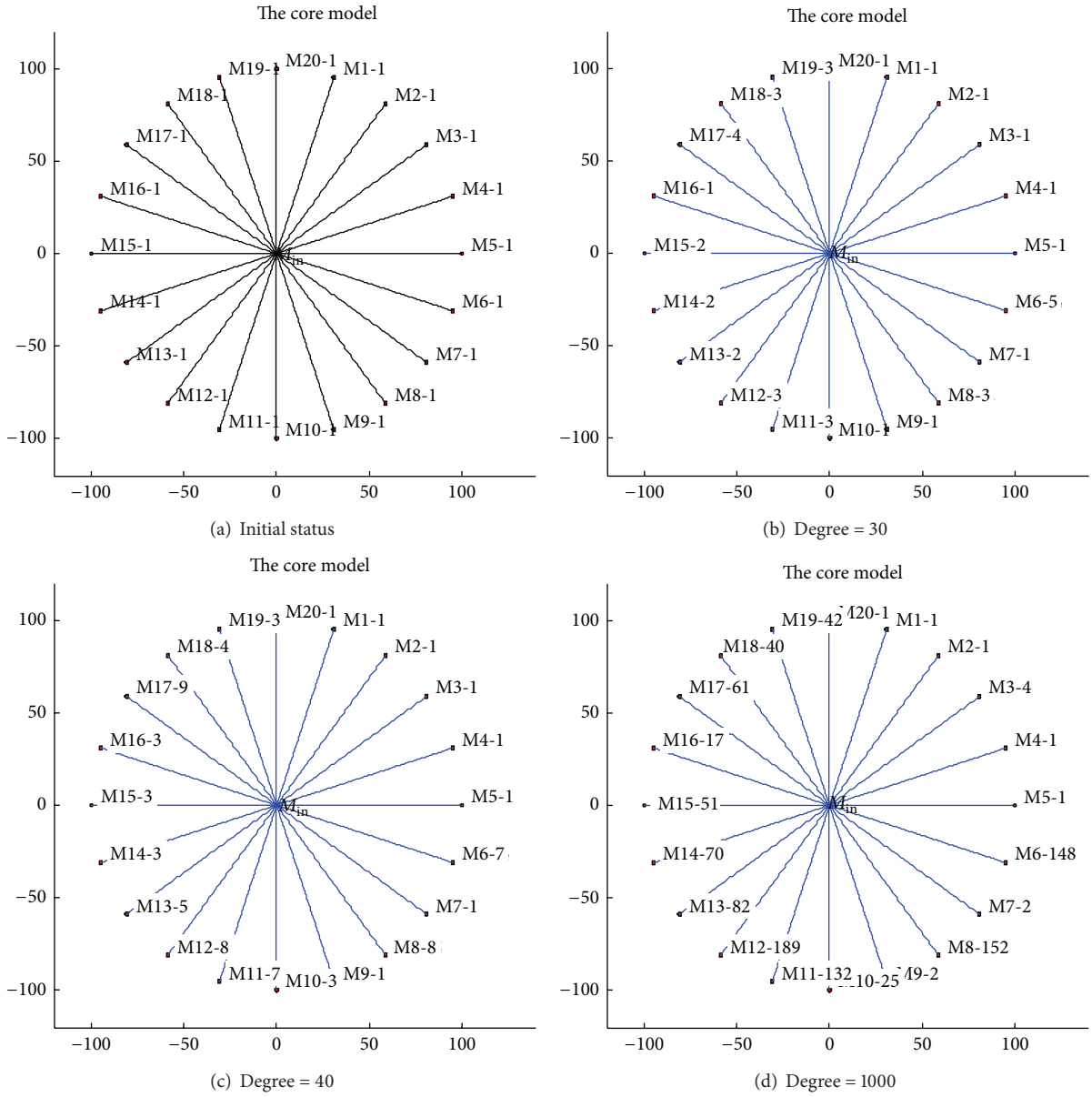

Figure 5: The growth of the core.

color (Figure 5(b)) mean the supplier has closer cooperation relationship with the core center vertex.

5.3. The Impact of Parameters

5.3.1. The Impact of Edge's Rate. Formula (5) shows that the edge's rate is one of the key factors for the core. The edge's rate comes from random number in our experiments above, and it affected the core chart which tends to smooth. What will happen if the edge's rate keeps constant? The experiment results show in Figure 8.

It shows that the degree distribution is a single peak function when the rates of edge are constant; it is obviously different from the rates of edge which are not constant. It may be explained from formula (5), while the rates of edge are constant means that the probability of vertex is only decided by the degree; once a vertex has a bigger degree than other vertices, the vertex's probability will be the biggest one in the core; other vertices have no chance to have the new edge.

5.3.2. The Impact of Adjustable Parameter. The adjustable parameter t adjusts the importance of vertex's rate and the degree; it can impact the selection of new edge's attachment. Figure 9 shows the action of adjustable parameter t from $t = 0$ to $t = 1$. While $t = 0$, the degree does not act on any action according to formula (5); the degree of the core is a random function, and the difference of vertex degree is wave in a narrow range (the wave motion is between 30 and 45 while $t = 0$, shown in Figure 9(a)); while $t = 1$, the edge's rate does not take action, and only one vertex degree keeps

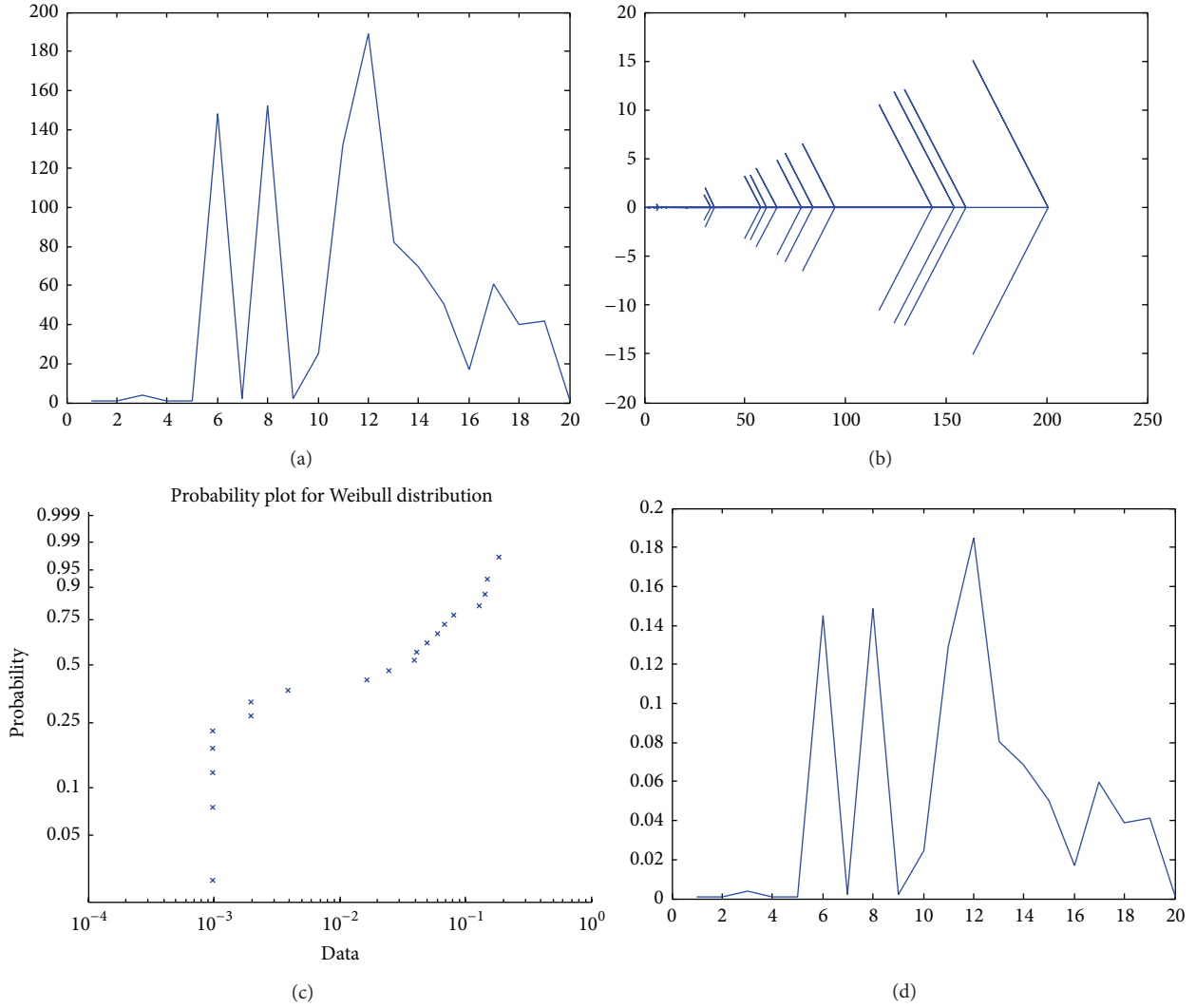

Figure 6: The degree distribution of the core while time = 1000.

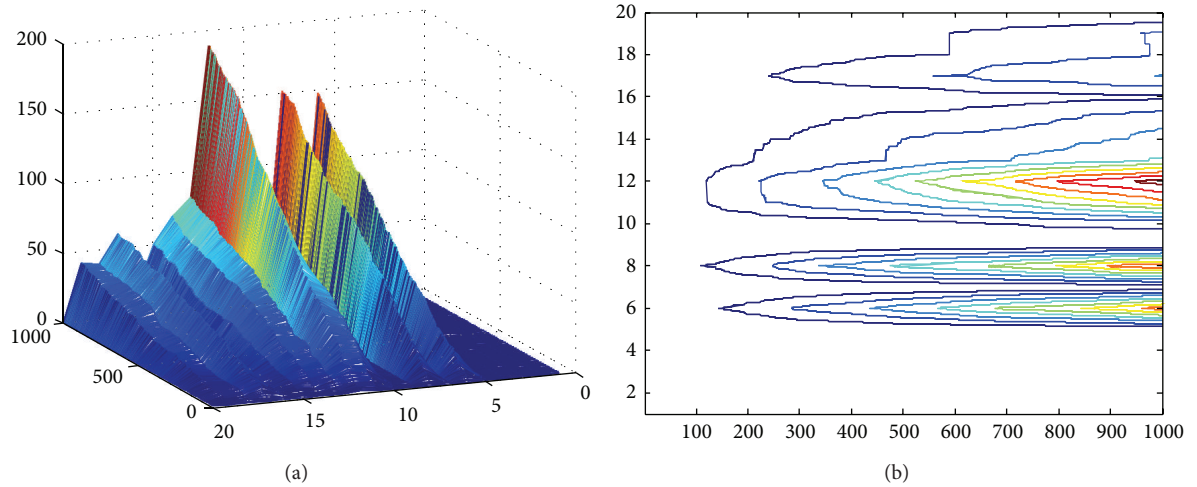

Figure 7: The cooperation relationship and tendency.

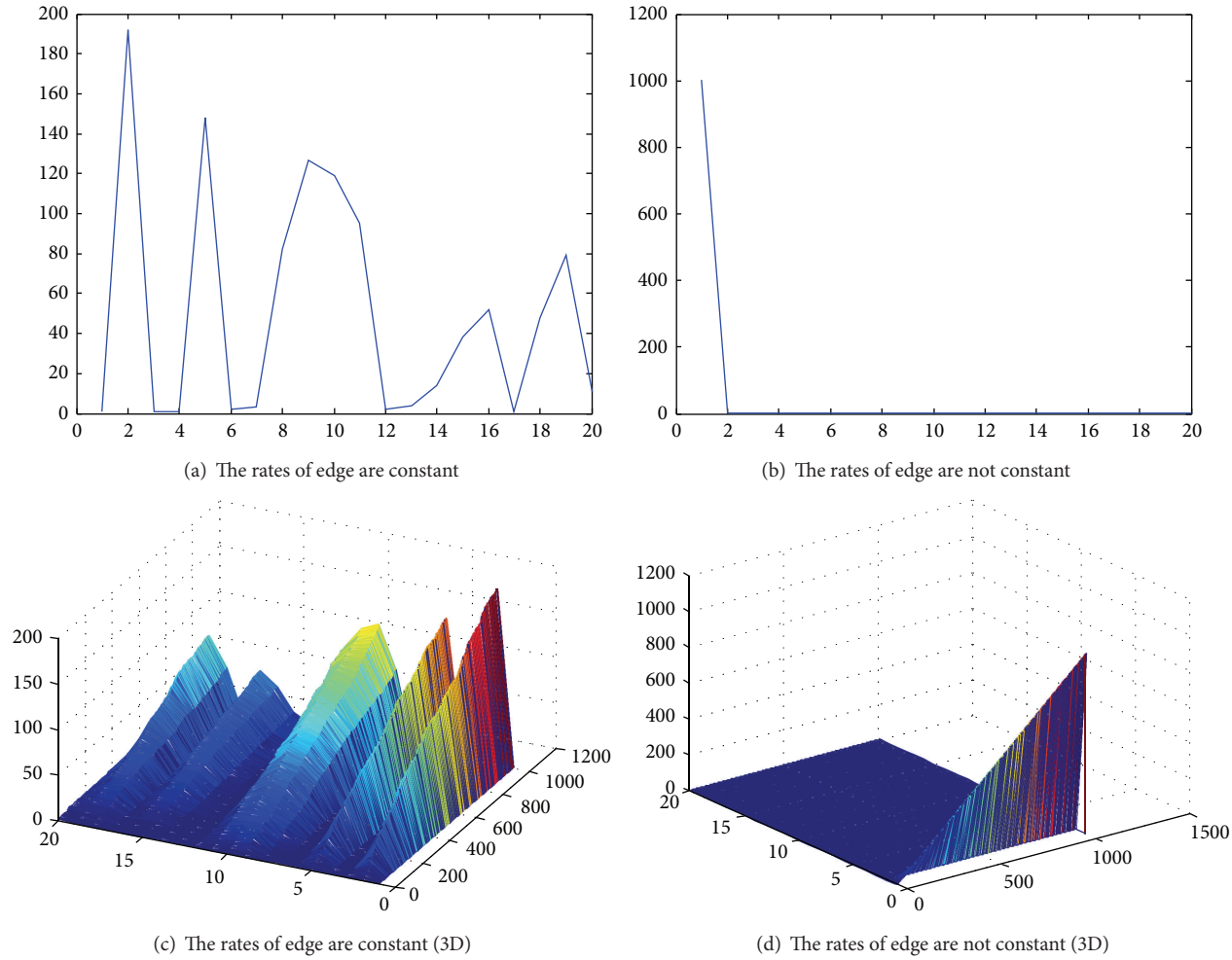

(a) The rates of edge are constant

(b) The rates of edge are not constant

(c) The rates of edge are constant (3D)

(d) The rates of edge are not constant (3D)

FIGURE 8: The impact of edge's rate.

increasing. With the value of t increasing, the wave motion of vertex's degree becomes more and more wider (the wave motion is amplified between 20 and 50 while $t = 0.01$, shown in Figure 9(b); between 1 and 200 while $t = 0.1$ in Figure 9(c); between 1 and 350 while $t = 0.2$ in Figure 9(d); between 1 and 1000 while $t \geqslant 0.5$ in Figures 9(e) and 9(f)). It also shows that degrees of vertex tend to difference, and the amount of suppliers attending to supply chain becomes more and more smaller; only one supplier supplies the parts while $t \geqslant 0.5$.

5.3.3. The Impact of Time/Experience. Figure 10 shows the growth process and tendency of the core with the time; the supply relationship is very chaotic at first, but it will tend to become different with the development of core; the supply relationship of the core tends to differentiation and stablility after a long time.

5.3.4. The Results of the Simulations. The simulations show that the supply chain is a power law network, and the selecting amount tends differently with the time. A little amount of vertices supply the most amount of parts; on the contrary, most of the vertices have little chances to attend the supply chain, and the supply relationship is the effect of Matthew; on the other hand, if a supplier improved their product and reduced the cost of parts, they have the chance to attend the supply chain network. So, the supply chain network is dynamic and clustered.

Formula (5) shows the directions of how to improve the chance of attending the supply chain: the first way is that the parts supplier keeps a closer relationship to the core firms in the network, which means that there is a larger k_i; another way is to keep a lower cost, which means that the supplier should reduce the cost of the parts, such as sale of lower parts price or producing the product locally (to reduce the transportation cost).

The simulations also show the difference between the model proposed in the paper and the traditional model: our model disclosed the running principle of the supply chain and gives the ways to how to improve the chance to obtain the orders, so it is a novel and practical method to analyze the supply chain.

6. Case Analyses

6.1. The IT Manufacturing Supply Chains Development at Chongqing China. The IT manufacturing industry of

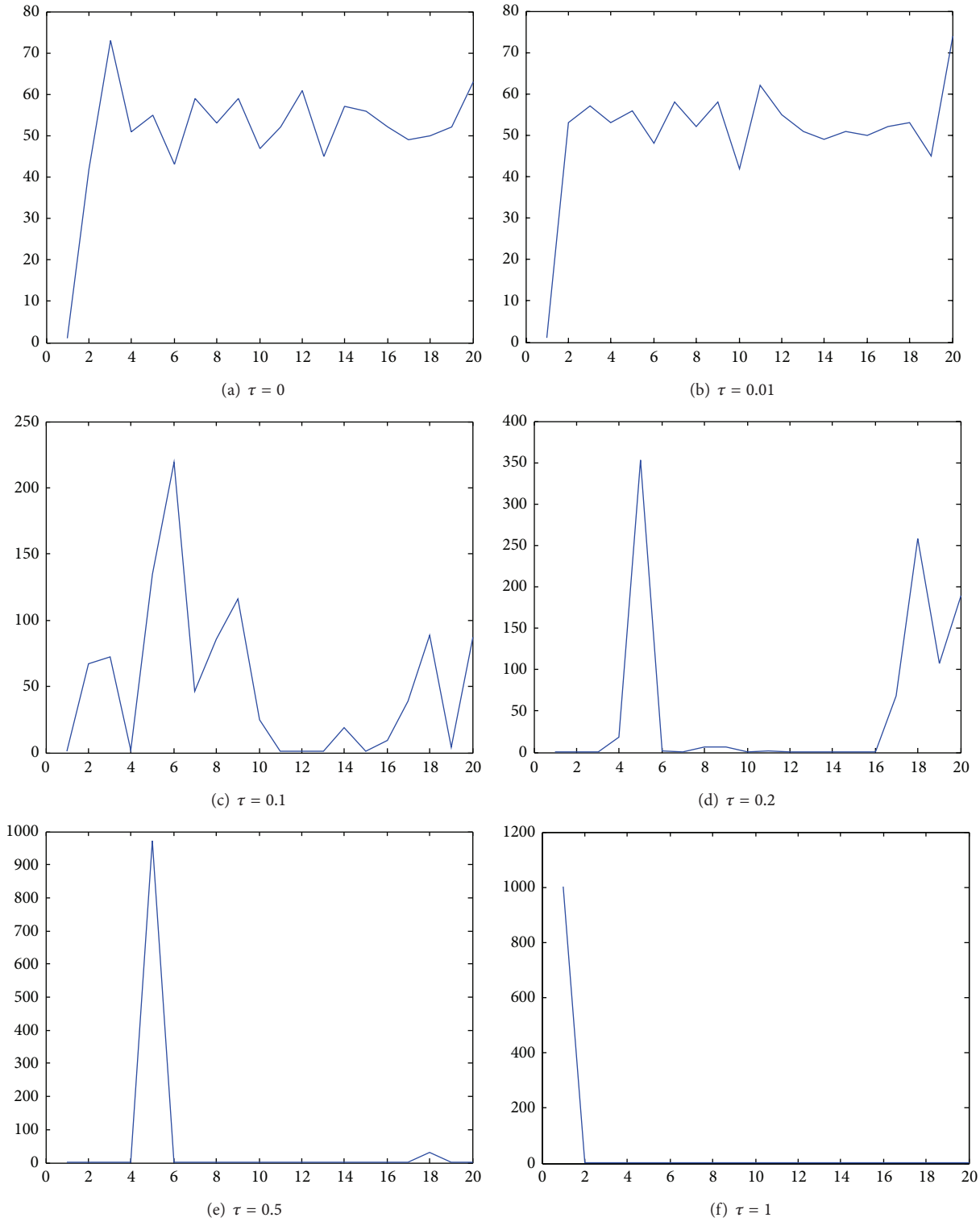

Figure 9: The impact of adjustable parameter.

Chongqing China was very weak at 2000, but it had a rapid expansion while Hewlett-Packard (Chongqing) Co., Ltd, and Acer (Chongqing) Co., Ltd, began to produce the notebook computer in recent years and the notebook computer accounts for one-fifth of global production [37, 38].

Why did it expand so quickly? It clustered 5 large computer enterprises, 6 large foundries, and 817 parts manufacturers in Xiyong Chongqing till February 11, 2014, and the industry gathering circle is about 1 hour drive. One very interesting phenomenon is that these companies are new plants

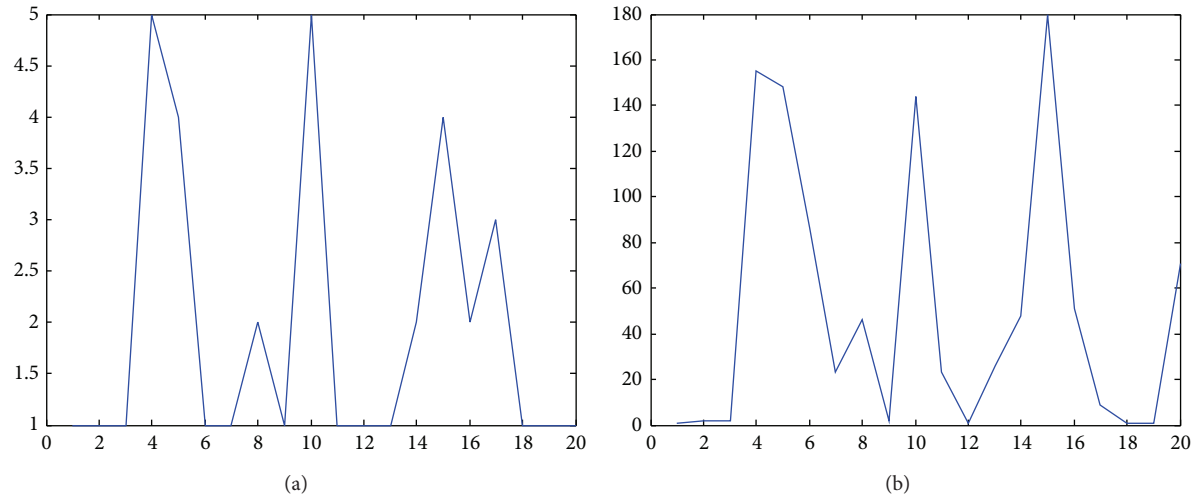

Figure 10: The growth process and tendency of the core.

following the large enterprises such as HP, Acer, and Cisco. The foundries and parts manufacturers built new production plant in Chongqing in order to decrease the transportation costs to the lowest level, so they have the lowest, calculated from formula (5); the lowest gained the biggest probability distribution, and they will obtain the greatest opportunities for cooperating with the large computer enterprises, and the industry aggregation phenomenon proved their action in practice.

6.2. Jiangmen Hi-Tech Development Zone. Jiangmen Hi-tech Development Zone began at 1992 [39]; it is one of the Hi-tech development zones of China. But the park was one of the worst Hi-tech development zones in China before 2010. It introduces itself as being able to serve for many industries, such as LED, advanced and other industries, but only a few enterprises grow up in the zone. Why is that? Because there almost are no large enterprises, and the products produced here need to be sold to the enterprises far away from there, which means the product costs have higher than other part suppliers; in other words, it has least probability distribution. In order to develop better, Jiangmen Hi-tech Development Zone replaned the industrial layout and direction and set up three professional parks, such as auto parts professional park; FAW Volkswagen and other auto manufacturers built their factories in the park; it speeded up all the auto parts development, so the professional park developed very fast in recent years; Jiangmen Hi-tech Development Zone is an important professional park in south China now.

7. Summary

Aiming at the three difficulties of classical complex network theories to resolve the optimal selection of parts suppliers, a core model is proposed in the paper after reviewing famous BA model and WS model; it maps the parts supply relationships of manufacturing supply chain as a repeatable core. A vertex's probability distribution formula is put forward; it mainly involves the edge's rate and vertex's degree. Some simulation studies, such as the growth of core, the degree distribution characteristics, and the impacting of parameter experiment, were carried out. At last, two cases were set out to prove the correctness in the paper. The core model can be used to resolve some difficulties—with repeating edge attachment, fixed vertices number but increasing edges with preferential connectivity, and flexible edges probability.

It did not consider the interactions of other cores and the consistency of costs in our experiments; the calculating results may be a little deviated, and we plan to resolve those problems in next steps.

Conflict of Interests

The authors declare that there is no conflict of interests regarding the publication of this paper.

Acknowledgments

This research is supported by the Natural Sciences Fund of China (Grant no. 51275547) and the Natural Science Fund Projects in Chongqing (Grant no. cstc2012gg-yyjs40019, CSTCjjA1481).

References

[1] C. P. Holland, "Cooperative supply chain management: the impact of interorganizational information systems," *The Journal of Strategic Information Systems*, vol. 4, no. 2, pp. 117–133, 1995.

[2] S. P. Sarmah, D. Acharya, and S. K. Goyal, "Buyer vendor coordination models in supply chain management," *European Journal of Operational Research*, vol. 175, no. 1, pp. 1–15, 2006.

[3] P. Kelle and A. Akbulut, "The role of ERP tools in supply chain information sharing, cooperation, and cost optimization," *International Journal of Production Economics*, vol. 93-94, pp. 41–52, 2005.

[4] M. Nagarajan and G. Sošić, "Game-theoretic analysis of cooperation among supply chain agents: review and extensions,"

European Journal of Operational Research, vol. 187, no. 3, pp. 719–745, 2008.

[5] P. Fiala, "Information sharing in supply chains," *Omega*, vol. 33, no. 5, pp. 419–423, 2005.

[6] R. C. Savaskan, S. Bhattacharya, and L. N. van Wassenhove, "Closed-loop supply chain models with product remanufacturing," *Management Science*, vol. 50, no. 2, pp. 239–252, 2004.

[7] S.-H. Ma and X.-Y. Chen, "The study for elements and characters of integrated logistics capability," *Chinese Journal of Management*, vol. 1, no. 1, pp. 107–111, 2004.

[8] S.-J. Xu and S.-H. Ma, "A study on trust crisis between inter-firm in supply chain in china," *Computer Integrated Manufacturing System*, vol. 8, no. 1, pp. 51–53, 2002.

[9] P. E. Love, Z. Irani, E. Cheng, and H. Li, "A model for supporting interorganizational relations in the supply chain," *Engineering Construction and Architectural Management*, vol. 9, no. 1, pp. 2–15, 2002.

[10] L. Liang, F. Yang, W. D. Cook, and J. Zhu, "DEA models for supply chain efficiency evaluation," *Annals of Operations Research*, vol. 145, pp. 35–49, 2006.

[11] M. Leng and A. Zhu, "Side-payment contracts in two-person nonzero-sum supply chain games: review, discussion and applications," *European Journal of Operational Research*, vol. 196, no. 2, pp. 600–618, 2009.

[12] Q. Zhu, J. Sarkis, and K.-H. Lai, "Confirmation of a measurement model for green supply chain management practices implementation," *International Journal of Production Economics*, vol. 111, no. 2, pp. 261–273, 2008.

[13] G. P. Cachon and P. H. Zipkin, "Competitive and cooperative inventory policies in a two-stage supply chain," *Management Science*, vol. 45, no. 7, pp. 936–953, 1999.

[14] J. Sarkis, "A strategic decision framework for green supply chain management," *Journal of Cleaner Production*, vol. 11, no. 4, pp. 397–409, 2003.

[15] Z. Huang, S. X. Li, and V. Mahajan, "An analysis of manufacturer-retailer supply chain coordination in cooperative advertising," *Decision Sciences*, vol. 33, no. 3, pp. 469–494, 2002.

[16] M. E. Ferguson, "When to commit in a serial supply chain with forecast updating," *Naval Research Logistics*, vol. 50, no. 8, pp. 917–936, 2003.

[17] A. Surana, S. Kumara, M. Greaves, and U. N. Raghavan, "Supply-chain networks: a complex adaptive systems perspective," *International Journal of Production Research*, vol. 43, no. 20, pp. 4235–4265, 2005.

[18] A. Gupta and C. D. Maranas, "Managing demand uncertainty in supply chain planning," *Computers and Chemical Engineering*, vol. 27, no. 8-9, pp. 1219–1227, 2003.

[19] D. Kim, S. T. Cavusgil, and E. Cavusgil, "Does IT alignment between supply chain partners enhance customer value creation? An empirical investigation," *Industrial Marketing Management*, vol. 42, no. 6, pp. 880–889, 2013.

[20] B. L. Connelly, D. J. Ketchen, and G. T. M. Hult, "Global supply chain management: toward a theoretically driven research agenda," *Global Strategy Journal*, vol. 3, no. 3, pp. 227–243, 2013.

[21] http://www.columbia.edu/cu/news/01/12/duncanWatts.html.

[22] http://www.cs.virginia.edu/oracle.

[23] http://www.oakland.edu/enp/erdpaths.

[24] P. Erdős and A. Rényi, "On the evolution of random graphs," *Magyar Tudományos Akadémia Matematikai Kutató Intézetének Közleményei*, vol. 5, pp. 17–61, 1960.

[25] D. J. Watts and S. H. Strogatz, "Collective dynamics of "small-world" networks," *Nature*, vol. 393, no. 6684, pp. 440–442, 1998.

[26] D. J. Watts, "The "new' science of networks," *Annual Review of Sociology*, vol. 30, pp. 243–270, 2004.

[27] A.-L. Barabási and R. Albert, "Emergence of scaling in random networks," *American Association for the Advancement of Science. Science*, vol. 286, no. 5439, pp. 509–512, 1999.

[28] R. Albert and A.-L. Barabási, "Statistical mechanics of complex networks," *Reviews of Modern Physics*, vol. 74, no. 1, pp. 47–97, 2002.

[29] A. Gregoriades and A. Sutcliffe, "Workload prediction for improved design and reliability of complex systems," *Reliability Engineering and System Safety*, vol. 93, no. 4, pp. 530–549, 2008.

[30] D. Shi, Q. Chen, and L. Liu, "Markov chain-based numerical method for degree distributions of growing networks," *Physical Review E*, vol. 71, no. 3, Article ID 036140, 9 pages, 2005.

[31] D. Shi, L. Liu, S. X. Zhu, and H. Zhou, "Degree distributions of evolving networks," *EPL (Europhysics Letters)*, vol. 76, no. 4, pp. 731–737, 2006.

[32] X. F. Wang, "Complex networks: topology, dynamics and synchronization," *International Journal of Bifurcation and Chaos*, vol. 12, no. 5, pp. 885–916, 2002.

[33] Z. Li and G. Chen, "Global synchronization and asymptotic stability of complex dynamical networks," *IEEE Transactions on Circuits and Systems II: Express Briefs*, vol. 53, no. 1, pp. 28–33, 2006.

[34] L. F. Y. Q. Q. Guoning and H. Zheren, "Universality analysis method of parts for product family based on complex network," *Chinese Journal of Mechanical Engineering*, vol. 11, article 014, 2005.

[35] C. Guorong, D. Juli, S. Jinliang, and Y. Ping, "Relationship network analysis of manufacturing system limited by business lines," *TELKOMNIKA Indonesian Journal of Electrical Engineering*, vol. 10, no. 6, pp. 1503–1509, 2012.

[36] M. E. J. Newman and D. J. Watts, "Renormalization group analysis of the small-world network model," *Physics Letters A*, vol. 263, no. 4–6, pp. 341–346, 1999.

[37] http://wjj.cq.gov.cn/cqgy/gygk/cqgyfzndbg/40451.htm.

[38] http://news.jrcq.cn/news/2014-02/11/1818.html.

[39] http://www.jip.gov.cn/default.html.

Hindawi Publishing Corporation
Mathematical Problems in Engineering
Volume 2015, Article ID 627479, 11 pages
http://dx.doi.org/10.1155/2015/627479

Research Article

Energy-Efficient Node Scheduling Method for Cooperative Target Tracking in Wireless Sensor Networks

Weirong Liu, Yun He, Xiaoyong Zhang, Fu Jiang, Kai Gao, and Jianming Xiao

School of Information Science and Engineering, Central South University, Changsha 410075, China

Correspondence should be addressed to Xiaoyong Zhang; zhangxy@csu.edu.cn

Received 25 July 2014; Revised 13 October 2014; Accepted 15 October 2014

Academic Editor: Wei Zhang

Using the sensor nodes to achieve target tracking is a challenging problem in resource-limited wireless sensor networks. The tracking nodes are usually required to consume much energy to improve the tracking performance. In this paper, an energy-efficient node scheduling method is proposed to minimize energy consumption while ensuring the tracking accuracy. Firstly, the Kalman-consensus filter is constructed to improve the tracking accuracy and predict the target position. Based on the predicted position, an adaptive node scheduling mechanism is utilized to adjust the sample interval and the number of active nodes dynamically. Rather than using traditional search algorithm, the scheduling problem is decomposed to decouple the sample interval and number of nodes. And the node index is mapped into real domain to get closed-form solution to decide the active nodes. Thus, the NP-complete nature is avoided in the proposed method. The proposed scheduling method can keep the tracking accuracy while minimizing energy consumption. Simulation results validate its effective performance for target tracking in wireless sensor networks.

1. Introduction

Wireless sensor network (WSN), which consists of tiny low-cost, energy-limited, and sensing range-limited nodes, has received extensive research in recent years. The nodes in WSN, equipped with one or more sensors, can sense, measure, and gather information from vicinal area. By utilizing the wireless RF module, these nodes can transmit the gathered information from local region to remote base station through node's multiple-hop relay. With the development of microelectronic technology, WSN has been deployed in various application scenarios to observe physical environmental change and detect events of interest [1].

In all kinds of practical scenarios, target tracking is one of the most important applications of WSN. Target tracking is a process of estimating or predicting the trajectories and velocities of some mobile targets by the sensor nodes in WSN collaboratively. The cooperation among sensor nodes could improve the accuracy of target's location or velocity. The targets of tracking can be any mobile objects, such as animals, humans, and vehicles [2].

With the development of WSN, numerous target tracking applications have emerged in many practical projects. For instance, PinPtr [3] is a counter-sniper system applied in military field to detect and locate enemy shooters. Underwater monitoring system in [4] developed a submarine platform to monitor coral reefs and fisheries. CenWits [5] is a search-and-rescue system utilizing static or mobile sensor nodes to locate stranded person in wreckage. ZebraNet system [6] consists of sensor nodes installed in animals to track and research the migration of wildlife populations. These projects have been used intensively in environmental detecting, industrial monitoring, disaster alerting, and healthcare [2].

Differing from the traditional target tracking, the target tracking using WSN brings up many challenges: keeping the tracking accuracy under the node's resources constraints. As most existing works have mentioned, the constraints of node resources, such as sensing range, communication bandwidth, and computation ability, are critical factors to keep accuracy and to save energy for target tracking in wireless sensor networks [7]. Recently, many researches have proposed algorithms to improve energy efficiency while keeping the target tracking accuracy.

Some researches focus on reducing the communication cost in target tracking. In [8], a heuristic algorithm to construct an efficient object tracking in wireless sensor networks

was developed, which formulates the minimizing communication cost as 0/1 integer programming problem, and a Lagrangian relaxation based heuristic algorithm was proposed to solve this optimization problem. In [9], a publish-and-subscribe method and drain-and-balance policy were described, respectively, to optimize the structure of network communication and reduce communication consumption. Reference [10] was considered to adjust physical topology of the sensor network, so the total communication cost was reduced. Although these works were devoted to reducing the energy consumption, they have limitation on network energy saving by just minimizing the communication cost, and they may also not be scalable enough.

Recently much attention has been focusing on sensor node scheduling to reduce energy for target tracking. The node scheduling can be classified into 2 categories: the random selection method and adaptive selection method. In random selection method, the sensing nodes are randomly selected according to a certain degree of probability; in adaptive selection method, the sensing nodes are selected according to the critical factors such as node type, detecting ability, and residual energy.

Random selection method has compared low scheduling cost and it is easy to deploy in real WSN. In [11], a probabilistic scheduling of the duty cycle of the sensors was provided in a sensor network deployed in an area of interest based on a Poisson distribution. Its tracking algorithm exploits signal from multiple sensor nodes in several modalities, relying on prior statistical information about target models. In [12], the authors describe the key ideas behind the CSP algorithms for distributed sensor networks and present how the CSP algorithms interface with the networking/routing algorithms. An entropy-based sensor selection heuristic algorithm for location-to-location was proposed in [13], which needs (1) a prior probability distribution of the target location and (2) the locations and the sensing models of a set of candidate sensors for selection. These works concentrated on improving the energy conservation by randomly selecting tasking sensors.

However, sensors' random sleep with a probability may not keep the target tracking accuracy because some sensors close to a target may be in sleep mode. Even in the target sensing region, there are not active nodes. But it is also sufficiently important to keep the performance of the target tracking. From this point of view, node selection along with the trajectory of moving target has aroused much interest. Some practical distributed sensor node selection algorithms have been proposed to improve energy efficiency with reliable tracking [14–18].

In [14], an energy-efficient selection of cooperative nodes was presented. According to the information utility and the remaining energy of sensor nodes, the authors in [10] constructed an objective function and proposed a dynamic node selection scheme based on genetic algorithms. Although the simulation results have shown its good effect, the node selection scheme based on genetic algorithms is difficult to apply in real applications and may not be suitable for the real-time requirement. The authors in [15] proposed an energy-efficient distributed adaptive multisensor scheduling for target tracking. The number of tasking sensors and the sampling time interval are taken into consideration. To select the tasking node, the leader needs to know its target detection probability which can be deduced from the target state equations. But this process may be somehow complex and requires implementing the Monte Carlo method. An adaptive sensor scheduling is formulated in [16], which contains two tracking modes: the fast tracking mode and the tracking maintenance mode. The energy conservation was achieved by adaptively adjusting the sampling time interval. But it is only applied to selected single tasking sensor at each sample interval. In [17, 18], the variable sampling interval was also adopted, but it cannot realize the joint optimization to energy.

Summarizing the above works, the main factors that influence position accuracy and energy efficiency of target tracking include the network communication topology, the sampling time interval, and the number of tasking sensors. The number of tasking sensors is directly related to the total energy consumption in tracking process. However, the current adaptive node selection method could not permit large candidate node set because of their high complexity.

Comprehending these factors, this paper aims to propose a novel node scheduling method with cooperative Kalman-consensus filter to reduce the energy consumption while keeping tracking accuracy. The Kalman-consensus filter is used to obtain the target state estimation and predict the next step position. The node selection problem is transformed into a convex optimization problem, which is decomposed, and a Lagrangian function is used to solve it.

The main contributions of this paper include (1) extending the classic Kalman filter to cooperative form, which can combine the local nodes' information to improve the tracking precision; (2) proposing a joint sample interval and node selection optimization scheme, which can realize the energy consumption minimum while keeping the tracking accuracy; (3) addressing the NP-hard joint optimization problem, adopting a map method to map the selecting factor to real domain; and utilizing gradient information to get the solution rapidly.

The rest of this paper is organized as follows. The problem formulation, dynamic model, and energy model are analyzed in Section 2. In Section 3, the novel node selection method is presented. Simulation results are proposed in Section 4. Finally, conclusion and future work are given in Section 5.

2. Problem Formulation

2.1. Target Model and Kalman-Consensus Filter (KCF). Considering that wireless sensor network is constructed by deploying n sensor nodes and a moving target, all cognitive sensors have the same sensing range and can jointly capture the target trajectory. The target model is taken as general linear model, like in [17]. A moving target with the system disturbance is described by the differential equation

$$x(k+1) = A(x(k))\, x(k) + B\omega(k), \tag{1}$$

where $x(k) = (q_x(k), p_x(k), q_y(k), p_y(k))^T$ denotes the state of the target at time k; $q = (q_x, q_y)^T$ and $p = (p_x, p_y)^T$ are

the coordinate and velocity of the target, respectively, in two-dimensional coordinate system; and $\omega(k)$ is the zero-mean Gaussian white noise with variance σ_0^2, which is the process noise.

The state matrix $A(x)$ is depicted as

$$A(x,\Delta t) = F(x)\otimes M_1(\Delta t) + \left(I_2 - F(x)\right)\otimes M_2,$$
$$M_1 = \begin{bmatrix} 1 & \varepsilon \\ 0 & 1 \end{bmatrix}, \qquad M_2 = \begin{bmatrix} 1 & \varepsilon \\ -\varepsilon c_1 & 1-\varepsilon c_2 \end{bmatrix}, \tag{2}$$
$$F(x) = \begin{bmatrix} \mu(x_1) & 0 \\ 0 & \mu(x_3) \end{bmatrix},$$

where ε is the step size and does not depend on the sampling time interval, which means that the target's motion is independent of the sensor's sampling frequency. $\mu(x)$ is defined by

$$\mu(x) = \frac{\rho(a+x) + \rho(a-x)}{2},$$
$$\rho(x) = \begin{cases} 1, & x \geq 0, \\ -1, & x < 0. \end{cases} \tag{3}$$

The matrix B is defined as

$$B = I_2 \otimes G, \quad G = \begin{bmatrix} \dfrac{\varepsilon^2\sigma_0}{2} \\ \varepsilon\sigma_0 \end{bmatrix}, \tag{4}$$

where $c_1, c_2 > 0$ are the parameters of a PD controller and "$\otimes$" denotes the Kronecker product of matrix.

The measurement model is given by

$$z_i(k) = Hx(k) + v_i(k), \tag{5}$$

where $x(k)$ is the state of the target, H is the observation model, and v_i is the measurement zero-mean Gaussian white noise of the sensor i with covariance R_i.

The Kalman-consensus filter (KCF) algorithm used in this paper is mainly referred to in [19] and operates as shown in Algorithm 1.

2.2. Sensor Detection Model. The binary detection model, described in most of the existing works [14, 20], assumes that if the target is within the sensing zone of a node, the detection of the target is successful. This is an ideal assumption to sensor's detection ability. Generally, there is always uncertainty when sensors perform the operation of detection. In this paper, the target probability detected by node s_i is

$$p(s_i) = \begin{cases} 0, & r_s + r_e \leq d(s_i, P), \\ e^{-\lambda\alpha^\beta}, & r_s - r_e \leq d(s_i, P) < r_s + r_e, \\ 1, & r_s - r_e \geq d(s_i, P), \end{cases} \tag{6}$$

where r_e ($r_e < r$) is the uncertainty measurement length of node s_i, $\alpha = d(s_i, P) - (r - r_e)$, and α and β are measurement parameters dependent on sensor type.

Based on this sensing model, for a target located in $P(x, y)$ detected by m sensors $s_1, s_2, \ldots, s_m$, the joint detection probability for these m tasking sensors is given by

$$P_d = 1 - \prod_{i=1}^{m} \left(1 - p(s_i)\right). \tag{7}$$

2.3. Tracking Error. According to [21], the estimated target state error covariance at k time step can be defined as

$$P(k \mid k) \equiv \left[\sigma_{ij}\right], \tag{8}$$

and the predicted target state error covariance can be calculated as

$$P(k \mid k) = \sum(\Delta t_k) = \begin{bmatrix} \sigma_{11} + 2\Delta t_k\sigma_{12} + \Delta t_k^2\sigma_{22} & \sigma_{13} + \Delta t_k(\sigma_{14} + \sigma_{23}) + \Delta t_k^2\sigma_{24} \\ \sigma_{13} + \Delta t_k(\sigma_{14} + \sigma_{23}) + \Delta t_k^2\sigma_{24} & \sigma_{33} + 2\Delta t_k\sigma_{34} + \Delta t_k^2\sigma_{44} \end{bmatrix}. \tag{9}$$

The predicted target state uncertainty is described as follows:

$$\begin{aligned} \phi(k+1 \mid k) &= \operatorname{trace}\left(\sum(\Delta t_k)\right) \\ &= (\sigma_{11} + \sigma_{33}) + (2\sigma_{12} + 2\sigma_{34})\Delta t_k \\ &\quad + (\sigma_{22} + \sigma_{44})\Delta t_k^2 + \frac{2}{3}q\Delta t_k^3. \end{aligned} \tag{10}$$

A threshold ϕ_0 is preset as the tracking accuracy. If the predicted target state uncertainty $\phi(k+1 \mid k)$ is less than ϕ_0, the tracking accuracy is supposed to be satisfied. Otherwise, it is deemed to be unsatisfied and needs to be improved.

2.4. Energy Model. At each tracking step, as the energy model in [22] shows, energy cost is mainly used in target detecting, data sending, data receiving, and data processing.

If the current tasking node i selects node j as the candidate sensor for the next tracking step, the energy cost by sending data from node i to node j is $E_t(i, j) = (e_t + e_d r_{ij}^\alpha) b_c$, where e_t and e_d are decided by the transmitter and r_{ij} is the distance between sensors i and j. α is known parameter that relies on channel characteristic, and b_c is the number of bits of the transmitted data.

The energy cost in receiving data by sensor node j is $E_r(j) = e_r b_c$, where e_r is decided by receiver installed in sensor node j. In a practical application, energy consumption mainly comes from communication between sensors. Hence,

Given the initial parameters $P_i = P_0, \overline{x}_i = x(0)$, for sensor node i at time step k

(1) Obtain measurement z_i with covariance R_i.

(2) Compute information vector and matrix of node i

$$u_i = H_i^T R_i^{-1} z_i$$
$$U_i = H_i^T R_i^{-1} H_i.$$

(3) Send message $m_i = (u_i, U_i, \overline{x}_i)$ to active neighbors.

(4) Receive messages from all active neighbors.

(5) Fuse information matrices and vectors

$$y_i = \sum_{j \in J_i} u_j, \qquad S_i = \sum_{j \in J_i} U_j.$$

(6) Compute the Kalman-consensus state estimation

$$M_i = (P_i^{-1} + S_i)^{-1},$$
$$\widehat{x}_i = \overline{x}_i + M_i(y_i - S_i \overline{x}_i) + \xi M_i \sum_{j \in N_i} (\overline{x}_j - \overline{x}_i),$$
$$\xi = 1/(\|M_i\| + 1)\ .$$

(7) Update the estimate state of the target

$$P_i \leftarrow A M_i A^T + BQB^T$$
$$\overline{x}_i \leftarrow A \widehat{x}_i$$

Algorithm 1: Kalman-consensus filter.

we treat the energy cost from sensing and processing as a union; that is, $E_s(j) = e_s b_s$. Let $E_i(k)$ be the remaining energy after $k-1$ time step that is also the available energy at k tracking step. Hence, the total energy cost for tasking sensor i is

$$E(j) = E_t(i, j) + E_r(j) + E_s(j) = e_0 + e_1 r_{ij}^{\alpha}, \tag{11}$$

where

$$e_0 = (e_t + e_r) b_c + e_s b_s,$$
$$e_1 = e_d b_c. \tag{12}$$

And the total energy consumed for a tracking step is given by

$$E_T = \sum_{i=1}^{N} \rho_i (e_0 + e_{hi}^{\alpha}), \tag{13}$$

where $\rho_i \in \{0, 1\}$ is the assignment index and it denotes by "1" being active to track target and by "0" sleeping to save energy. As the cluster header, the energy consumption for estimating state fusion and selecting the next tasking sensors as well as transmitting $\widehat{x}_t$ to receivers is

$$E(h) = \sum_{i \in G(k+1) - s_h} (e_t + e_d r_{hi}^{\alpha} + e_r) b_c, \tag{14}$$

where $G(k)$ represents the sensor cluster at k tracking step and s_k is the cluster header.

3. Adaptive Node Scheduling Method

3.1. Analysis of Target Tracking Process. Figure 1 shows a general target tracking scene in a wireless sensor network with uniform deployment sensor nodes. Sensor nodes will be active on demand following the target trajectory. To save energy, not all of the sensors in sensing zone are selected to detect the target. These selected sensors, at first, cooperate to generate an estimation of target position using Kalman-consensus filter algorithm. And then they send their estimation to cluster header for further fusion so that more accurate estimation of target position is achieved. The goal of the method is twofold: (i) generating the state estimation and predicting the position of dynamic target and (ii) selecting the tasking cluster and cluster header for the tracking step.

At the beginning of detecting, all sensors are in the sleep state initially, except for sensors that are on the borders of the sensor filed. The sensor nodes on borders that first found the target will broadcast the target information and start the tracking task. They will obtain the first measurement and calculate the target state estimation to select and activate the next tasking sensor nodes (including the cluster header) for the next sample interval. They will send their state prediction to the next tasking cluster.

At k tracking step, the selected sensor nodes in current active cluster perform the following sensing tasks:

(1) obtaining measurement $z(k)$ of target location with R;

(2) computing and updating the state estimation using Kalman-consensus filter;

(3) sending the updated state estimation $(P, \overline{x})$ to cluster header.

As for the cluster header, except for the above tasks, it needs to perform the following additional jobs:

(1) fusing the state estimation $(P, \overline{x})$ so that an accurate estimation of target position is achieved;

(2) calculating the sampling interval Δt for $k+1$ tracking step;

(3) selecting the tasking cluster for the step $k+1$;

(4) selecting a new cluster header for the new tasking cluster;

(5) transmitting the fused target estimation $\widehat{x}_t$ to the next tasking sensor nodes.

Once the sensor nodes in the tasking cluster at step k receive the estimation information from their cluster header to next cluster, they will turn into sleep mode at step $k+1$.

3.2. Adaptive Node Selection Combining with Kalman-Consensus Filter Algorithm (ANS-KCF). For the problem of node selection for distributed cooperative target tracking, the key issue is to form tasking sensor cluster dynamically, which directly related to energy consumption and tracking accuracy. The objective of proposed method is to minimize the energy cost of network under the condition of desired tracking error. In addition, the sampling time interval has a great influence on tracking accuracy and network energy cost. Actually, if the desired tracking performance is obtained, a bigger sampling time interval will be a better choice for energy saving.

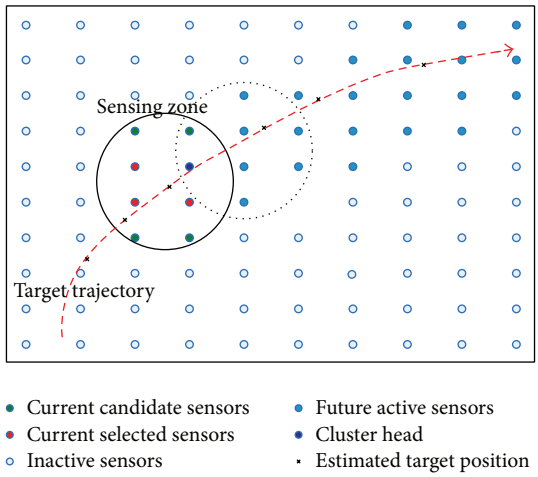

Figure 1: Target tracking scene in WSN.

The formation of next cluster candidate set includes two phases: the first phase is the target tracking, in which nodes that can detect the target are active; the second phase is the detection probability $p(s_i)$ calculating, which is calculated according to (6). Only these nodes whose detection probability is bigger than the threshold θ can be taken as the candidates. Hence, the set of candidate sensor nodes can be given by

$$V = \{s_i \mid p(s_i) > \varepsilon, \operatorname{dis}(s_i, \hat{x}_t) < r_s\}, \tag{15}$$

where $\hat{x}_t$ is the estimate position at k tracking step.

In order to better express the node selecting problem, the joint detection probability (7) to the following form is

$$P_d = 1 - \prod_{i=1}^{V} (1 - \rho_i p(s_i)). \tag{16}$$

Based on the sensor detection probability model and the energy model given previously, the node selection problem can be formulated as follows: at tracking step k, considering the target state estimation $\hat{x}_t$, its error covariance $P(k \mid k)$, and the sampling time interval Δt_k, the tasking sensors at tracking step $k+1$ are determined such that

$$\begin{aligned} &\min_{\rho_i, \Delta t_k} \quad J = \frac{1}{\Delta t_k} \sum_{i=1}^{|V|} \rho_i (e_0 + e_1 r_{hi}^{\alpha}) \\ &\text{subject to:} \ \phi(k+1 \mid k) \le \phi_0, \quad P_d \ge \theta_d, \end{aligned} \tag{17}$$

where θ_d is the preset joint detection threshold for multiple sensor nodes.

Because of the complexity in computing the detection probability P_d and the coupling effect of the sampling interval Δt_k and the selection of the tasking sensor nodes, a two-stage suboptimal algorithm is designed to approximate the original optimization problem (17).

As mentioned above, the fixed sampling time interval is not suitable for energy-efficient target tracking. We suppose that Δt_k is in the range $[T_{\min}, T_{\max}]$, where $T_{\min}$ is the given minimal sampling intervals and cannot be too small because it must be larger than the total duration span for tracking activities. A maximum sampling interval Δt_k is obtained to satisfy the given tracking accuracy specification ϕ_0. The corresponding suboptimization problem is

$$\begin{aligned} &\max \ (\Delta t_k) \\ &\text{s.t.} \quad \phi(k+1 \mid k) \le \phi_0. \end{aligned} \tag{18}$$

According to [15], the max Δt_k will be obtained at the constraint bound:

$$\phi(k+1 \mid k) = \phi_0. \tag{19}$$

By solving the following equation, we can get the suitable Δt_k^*. That is,

$$\begin{aligned} &\Delta t_k^* = \arg\max_{\Delta t_k} (\Delta t_k) \\ &\text{s.t.} \ \phi(k+1 \mid k) \le \phi_0. \end{aligned} \tag{20}$$

At the second stage, a number of sensors are selected based on the determined sampling interval Δt_k^* to form a temporary tasking cluster to achieve the target detection probability threshold. Therefore (17) can be rewritten as the decomposed problem; the second suboptimization problem can be expressed in the following mathematical form:

$$\begin{aligned} &\min_{\rho_i} \ J = \frac{1}{\Delta t_k^*} \sum_{i=1}^{V} \rho_i (e_0 + e_1 r_{hi}^{\alpha}) \\ &\text{s.t.} \quad P_d \ge \theta_d. \end{aligned} \tag{21}$$

Since $\partial J / \partial \rho_i > 0$ and $\partial P_d / \partial \rho_i > 0$, also $\partial^2 J / \partial \rho_i^2 = 0$ and $\partial^2 P_d / \partial \rho_i^2 = 0$. This can be solved systematically as a convex optimization problem [23] where index and constraints are convex with respect to ρ_i.

Then the resulting convex problem can be solved to find the minimum J and its corresponding parameters ρ_i for each node and for networks. We use the Lagrangian function as follows:

$$L(\rho_i, \lambda) = \sum_{i=1}^{V} \rho_i (e_0 + e_1 r_{hi}^{\alpha}) - \lambda (P_d - \theta_d), \tag{22}$$

where λ is the Lagrangian multiplier for the constraint in (21). Then the gradient for the Lagrangian function is

$$\frac{\partial L}{\partial \rho_i} = (e_0 + e_1 r_{hi}^{\alpha}) - \lambda p(s_i) \prod_{k!=i} (1 - \rho_k p(s_k)), \quad i \in V, \tag{23}$$

where V is the candidate sensor set described by (15). To select the suitable sensing nodes, there is no need to solve this equation, which is complex. The goal of proposed method is just to determine the priority of the candidate sensor nodes for target tracking. From the Karush-Kuhn-Tucker conditions and the gradient (23), we let

$$\frac{\partial L}{\partial \rho_j} = (e_0 + e_1 r_{hj}^{\alpha}) - \lambda p(s_j) \prod_{k!=j} (1 - \rho_k p(s_k)) = 0. \tag{24}$$

Then, for node i, the following can be obtained:

$$\frac{\left(e_0 + e_1 r_{hi}^{\alpha}\right)}{\prod_{k!=i,j}\left(1-\rho_k p\left(s_k\right)\right)} - \lambda p\left(s_i\right) = -\lambda p\left(s_i\right)\rho_j p\left(s_j\right). \quad (25)$$

And for node j, the following can be obtained:

$$\frac{\left(e_0 + e_1 r_{hj}^{\alpha}\right)}{\prod_{k!=i,j}\left(1-\rho_k p\left(s_k\right)\right)} - \lambda p\left(s_j\right) = -\lambda p\left(s_j\right)\rho_i p\left(s_i\right). \quad (26)$$

Therefore, the priority ratio (which is converse to the cost ratio) for node i and node j can be obtained as follows:

$$\begin{aligned}\frac{\rho_i}{\rho_j} &= \frac{\left(e_0 + e_1 r_{hj}^{\alpha}\right) - \lambda p\left(s_j\right)\prod_{k\neq i,j}\left(1-\rho_k p\left(s_k\right)\right)}{\left(e_0 + e_1 r_{hi}^{\alpha}\right) - \lambda p\left(s_i\right)\prod_{k\neq i,j}\left(1-\rho_k p\left(s_k\right)\right)} \\ &\triangleq \frac{\cos t\left(j\right)}{\cos t\left(i\right)}.\end{aligned} \quad (27)$$

From (27), the cost function can be defined as

$$\cos t\left(i\right) = \left(e_0 + e_1 r_{hi}^{\alpha}\right) - \lambda p\left(s_i\right)\prod_{k!=i,j}\left(1-\rho_k p\left(s_k\right)\right). \quad (28)$$

The cost function is the energy consumption under the target detection constraint if the nodes are selected.

The next stage is to determine the optimum λ and to select the sensor nodes for target tracking. The node with max remaining energy will be selected firstly and it can be taken as cluster header. Then, considering just two nodes (i.e., the other sensors are not selected yet), (26) can be simplified as

$$\cos t\left(i\right) = e_0 + e_1 r_{hi}^{\alpha} - \lambda p\left(s_i\right). \quad (29)$$

The optimal λ should be calculated and it may be a positive nonzero parameter or a zero parameter. Consider the complimentary slackness conditions:

$$\lambda\left(P_d - \theta_d\right) = 0 \longrightarrow \lambda = 0, \quad P_d > \theta_d, \quad (30a)$$

$$\lambda\left(P_d - \theta_d\right) = 0 \longrightarrow \lambda \neq 0, \quad P_d = \theta_d. \quad (30b)$$

If $\lambda = 0$ is the optimal solution, then, due to (30a), $P_d > \beta$ is satisfied. We also know that P_d is the increasing functions of ρ_j. Therefore, we can decrease ρ_j so that $P_d = \beta$ is satisfied. Under this reduction, we have smaller Pf and $e_0 + e_1 r_{hi}^{\alpha}$, which leads to a more desirable answer. In this way, λ is selected so that $P_d = \theta_d$ is satisfied. It is equal to (30b) condition. Thus, in this paper, the optimal λ is positive nonzero parameter and there is $P_d = \theta_d$.

In order to find the optimum λ we use an iterative bisection algorithm. We search through the algorithm to satisfy the optimal conditions stated before. At each iteration, cost functions $\cos t(*)$ for all sensors in (29) are calculated and sorted in ascending order. Then the sensors with the highest priority are selected until the global $P_d > \beta$ is satisfied. Then λ is updated according to the computed P_d and searching space is halved and the algorithm is repeated again.

This iterative algorithm ends when the accuracy of λ becomes smaller than ε. ε declares the resolution of the proposed algorithm. Noting that in each iteration, to obtain the optimal λ, if $P_d > \theta_d$, then λ is decreased and $P_d < \theta_d$; then λ is increased. It means that the proposed algorithm converges to the optimal λ which satisfied $P_d = \theta_d$.

Because the solving of optimum λ adopts bisection iteration, its order is $(\log_2(\lambda_{\max} - \lambda_{\min})/\varepsilon)$. For each iteration, the proposed algorithm has the linear complexity with the order of $O(N)$, since the cost functions for all sensors are computed. Thus, to solve the optimal nodes' schedule design, the complexity is $(N \cdot \log_2(\lambda_{\max} - \lambda_{\min})/\varepsilon)$. Then the optimal sample period is decided by iteration, which is a linear process with the order N_T. Because of the decoupling of node schedule and sample period in the proposed algorithm, the entire complexity of algorithm is $(N \cdot \log_2(\lambda_{\max} - \lambda_{\min})/\varepsilon + N_T)$. It must be mentioned that the cost of algorithm is mainly computing cost, whose energy consumption is minor compared to the energy consumption when the node participates in the target tracking.

In order to limit the search space of optimal λ, it is proper to find the $\lambda_{\max}$, which should guarantee the condition $0 < \lambda_{\text{optimal}} < \lambda_{\max}$; $\lambda_{\max}$ is obtained when priorities of selecting sensors are determined according to their $p(s_i)s$. We sort $p(s_i)s$ for all nodes; then the relation between cost functions of two nodes becomes

$$e_{\text{amp}} s_i^2 - \lambda_{\max} p\left(s_i\right) < e_{\text{amp}} s_{i-1}^2 - \lambda_{\max} p\left(s_{i-1}\right) \quad \forall i \in V. \quad (31)$$

Hence,

$$\lambda_{\max} > \frac{e_{\text{amp}}\left(s_i^2 - s_{i-1}^2\right)}{p\left(s_{i\max}\right) - p\left(s_{i-1\max}\right)} \quad \forall i \in V. \quad (32)$$

It means that $\lambda_{\max}$ should be selected according to (32) such that a suitable searching space is considered to find desirable answer.

Each node with the smaller cost function defined as (29) has the higher priority in target tracking. To determine the priority of tasking nodes, cost function in (29) is calculated for all of candidates in V and sorted in ascending order. Algorithm 2 is given to calculate the optimal λ and to select the tasking nodes from candidate sensor set.

4. Simulation Results

The intruder detection and tracking system in military is a representative application of target tracking. To avoid the sudden attack or surreptitious scout of enemy, the wireless sensor network is deployed in the buffer region between defensive line and the enemy. When the enemy combatants or vehicles enter the buffer region, the sensor network can detect these events and report the enemy position real time so that the troops can respond immediately.

To evaluate the performance of the proposed algorithm, the software MATLAB is used to simulate the intruder detection and tracking scene. The network scene is formed by sensing range-limited sensors and the monitoring area is 100 m × 100 m with coordinates from (−50, −50) to (50, 50), as shown in Figure 1. In the scene, a single moving target whose dynamics is given in (1) is tracked by 100 uniform distributed

$\lambda_{\min} = 0, \lambda_{\max} = 1, \mu$ is a small number
While (abs($\lambda_{\max} - \lambda_{\min}$) > μ)
  $\lambda = (\lambda_{\min} + \lambda_{\max})/2$
  Number of tasking node $n = 0, \Delta t_k = T_{\max}$
  Calculate $\cos t(i) = (e_0 + e_1 r_{hi}^{\alpha}) - \lambda p(s_i)$ for every node in V and sort it in ascending order
  While ($n <$ length(V))
    Compute P_d by using (16)
    If $P_d > \theta_d$, break
    Else $n = n + 1$,
    End;
    For $t = N_T$ to 1,
    Predict $\phi(k+1 \mid k)$ for sensor node s_n using Algorithm 1 with T_t
      If $\phi(k+1 \mid k) \le \phi_0$ and $T_t \le \Delta t_k$
        $\Delta t_k = T_t$, break
      End;
    End;
  End
  If $P_d > \theta_d$
    $\lambda_{\max} = \lambda$
  Else if $P_d < \theta_d$
    $\lambda_{\min} = \lambda$
  End
End

Algorithm 2: Adaptive node selection algorithm combining with Kalman-consensus filter (ANS-KCF).

sensor nodes. Each sensor node measures the position of the target in a 2D plane; that is,

$$H = \begin{bmatrix} 1 & 0 & 0 & 0 \\ 0 & 0 & 1 & 0 \end{bmatrix}. \tag{33}$$

It is assumed that all the sensors in the network have the same sensing parameters; that is, the sensing and communication range of each sensor are $r_s = 15$ and $r_c = 18$, respectively. The measurement and process noise statistics are $R_i = 9I_2$ and $Q = 25I_4$, respectively. The desired sensor detection threshold is assumed to be $\theta_d = 0.95$. The threshold of the tracking accuracy is also assumed to be $\phi_0 = 5$.

Firstly, the proposed method is tested and verified by comparing the estimated trajectory with real target trajectory. Figure 2 shows the estimated target trajectory of the proposed method. The target moves in sensing area for 40 s and forms a trajectory shown in Figure 2. It displays that the estimated trajectory is closely following the target trajectory. Furthermore, the tracking accuracy is shown in Figure 3. Obviously, the excellent tracking performance is obtained in simulation when using the proposed methods.

To display the performance more convincingly, the proposed tracking algorithm Kalman-consensus filter (KCF) is compared with EKF, and the accuracy of target tracking is evaluated using estimated trajectory and estimated error. Figures 4 and 6 list the estimated value of X coordinate and Y coordinate, respectively. And the corresponding estimated errors are shown in Figures 5 and 7, respectively.

From the deviation of estimated position and actual position described in Figures 4–7, both the proposed KCF and EKF can track target with small estimated error when target movement direction remains the same. But when the target

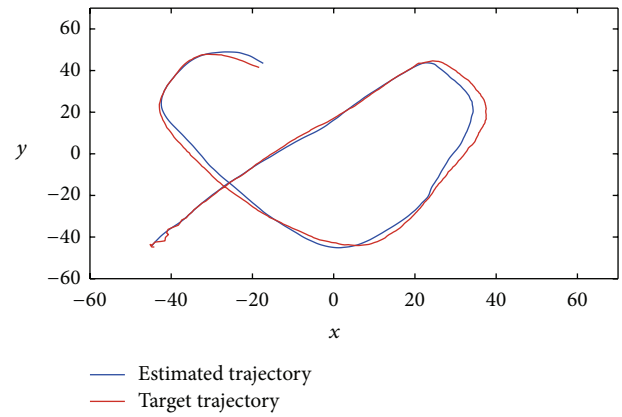

Figure 2: The comparison of estimated trajectory with the real target tracking trajectory.

direction changes, especially in the beginning of changes, the estimated trajectory with KCF is more close to the real target trajectory, and the estimated error is much smaller than EKF. Therefore, compared with the conventional EKF, the proposed scheme can achieve a better performance when the target changes directions dynamically, which is more practical in actual applications.

To implement the KCF, the local sensor nodes need to exchange their message packets, which include three parts: node information vector u_i, information matrix U_i, and the average target state value $\overline{x}_i$. For 2-dimensional target tracking, the exchanged data amount almost is less than 50 bytes. Every active node will broadcast the information. In target tracking process, the average number of the active nodes is

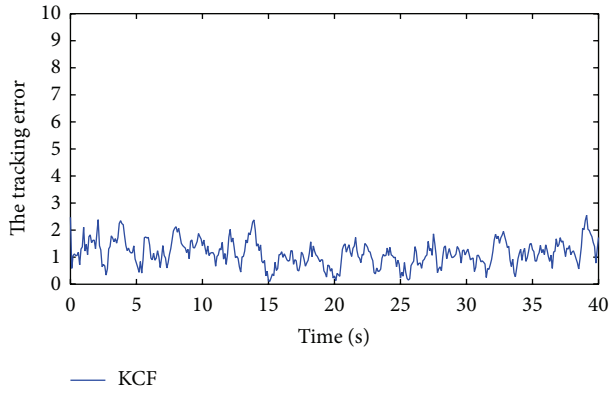

Figure 3: Tracking accuracy by using the proposed method.

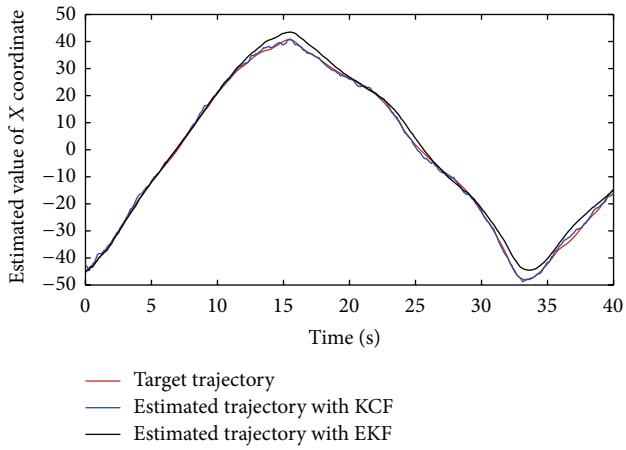

Figure 4: The comparison of the estimated value of X coordinate between KCF and EKF.

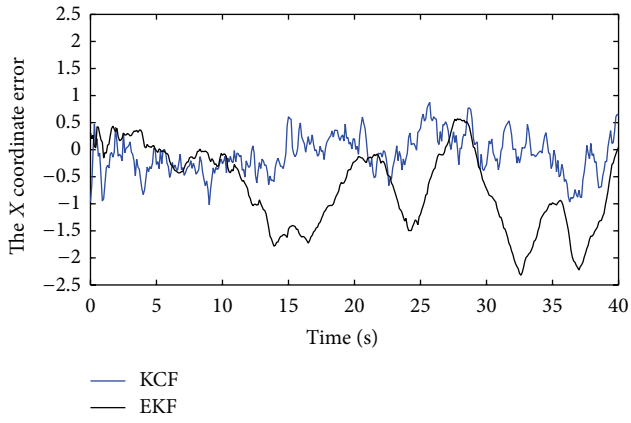

Figure 5: The comparison of the estimated error of X coordinate between KCF and EKF.

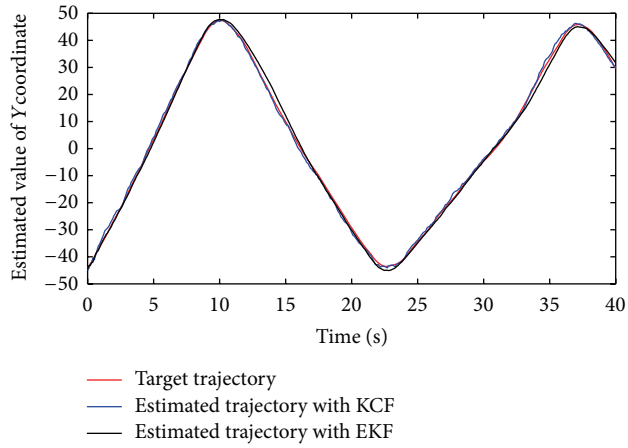

Figure 6: The comparison of the estimated value of Y coordinate between KCF and EKF.

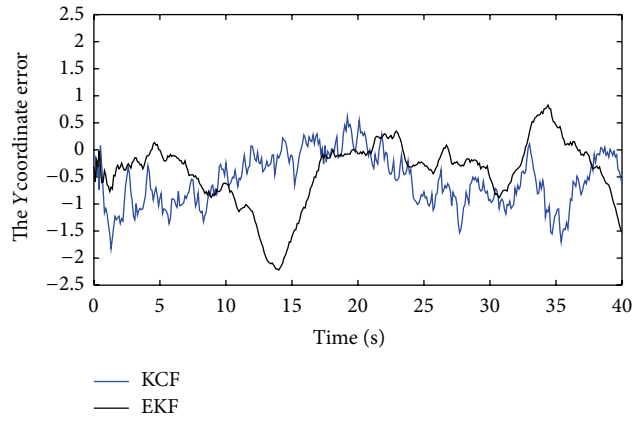

Figure 7: The comparison of the estimated error of Y coordinate between KCF and EKF.

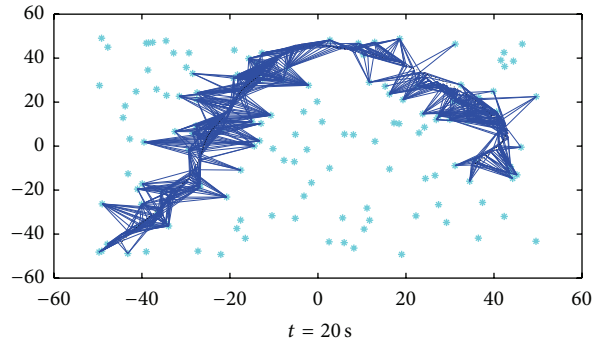

Figure 8: Target trajectory using random node selection with fixed number of sensor nodes for each sensing step.

limited to 10 due to the application of node selection. Thus the increased complexity is tolerable in practical tracking scene.

To improve the energy efficiency, the sensor node selection algorithm is introduced into target tracking. As described in the introduction, the node selection algorithm can be classified into two categories: random selection and adaptive selection. Figures 8 and 9 give the estimated target trajectories using random selection and adaptive selection, respectively. In these figures, the red dot denotes the estimated position and the blue line connects the sensor node to its estimation. From Figure 8, it is shown that the blue lines in Figure 8 are much denser than in Figure 9, which means

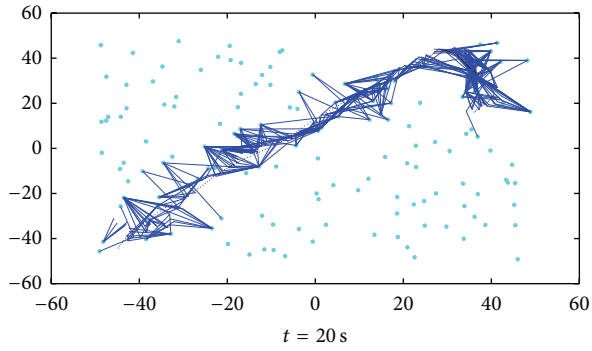

Figure 9: Target trajectory using the proposed adaptive node selection with various number of sensor nodes for each sensing step.

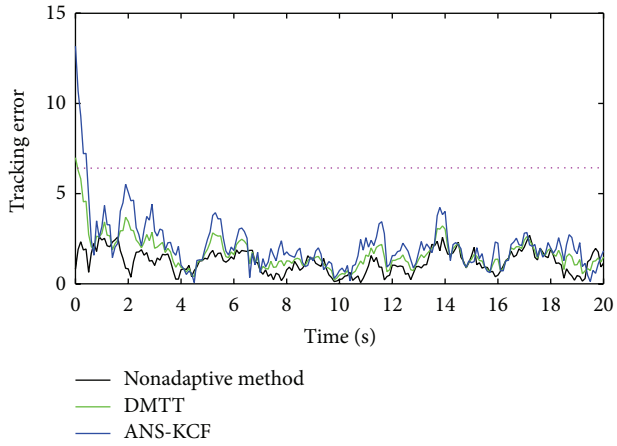

Figure 10: Tracking accuracy with nonadaptive, DMTT, and ANS-KCF methods.

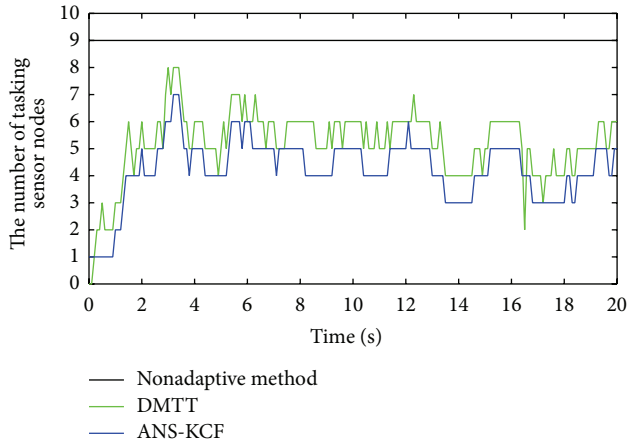

Figure 11: The number of tasking sensor nodes participating in the target tracking at different time for nonadaptive, DMTT, and ANS-KCF methods.

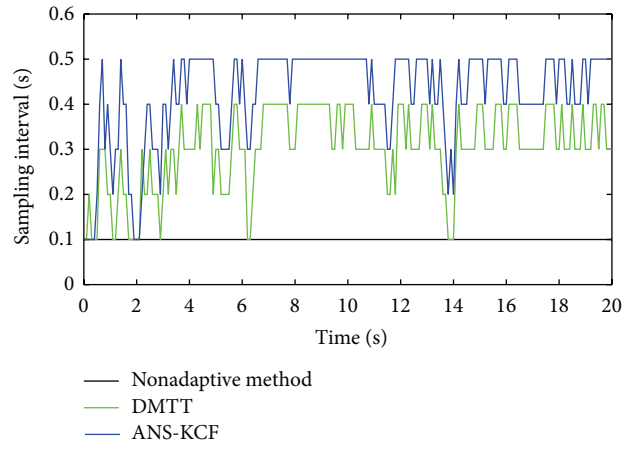

Figure 12: The sampling interval of tasking sensor nodes participating in the target tracking at different time for nonadaptive, DMTT, and ANS-KCF methods.

that the random selection algorithm uses more sensor nodes than the proposed adaptive node selection algorithm. But their tracking performance is similar. Thus some sensor nodes in random selection algorithm could not be necessary.

To represent this, Figure 10 displays the comparison of the tracking accuracy with nonadaptive and adaptive methods, DMTT algorithm, and the proposed ANS-KCF algorithm. As shown in Figure 10, nonadaptive algorithm indeed outperforms the nonadaptive methods in the tracking accuracy because the nonadaptive algorithm uses fixed sample frequency and has more sensor nodes that participate in target tracking. But the differences existing are minor. All the three methods can achieve the system requirement, but the proposed ANS-KCF algorithm can reduce the number of participating sensor nodes mostly, thus saving energy significantly.

Figures 11 and 12 show the number of tasking sensor nodes and the sampling interval of the three methods, respectively. For nonadaptive methods, the participating nodes' number and sampling interval are fixed. But for adaptive methods, in the beginning of tracking, just one sensor node found the target as shown in Figure 11. Thus just the smallest sampling interval was chosen to improve the tracking accuracy, as shown in Figure 12.

After that, the tracking accuracy is improved with the number of sensing nodes increasing. But the tracking process is tending towards stability with the tracking going on. Also from Figures 11 and 12, it is shown that the proposed algorithm ANS-KCF allows fewer nodes to participate in tracking and allows larger sample interval than DMTT, which illustrates that the proposed algorithm ANS-KCF has more energy consideration.

Finally the energy performance is evaluated. Figure 13 shows the energy consumption in target tracking using nonadaptive method with fixed number of active sensing nodes and uniform sampling interval, $\Delta t = 0.1$, and the target tracking using DMTT and the proposed algorithm ANS-KCF. The comparison results show that the energy consumption is smallest when the proposed algorithm ANS-KCF was adopted because it uses fewer nodes and larger sample interval to realize tracking.

Compared to nonadaptive algorithm, the proposed adaptive algorithm has node selection procedure, which will

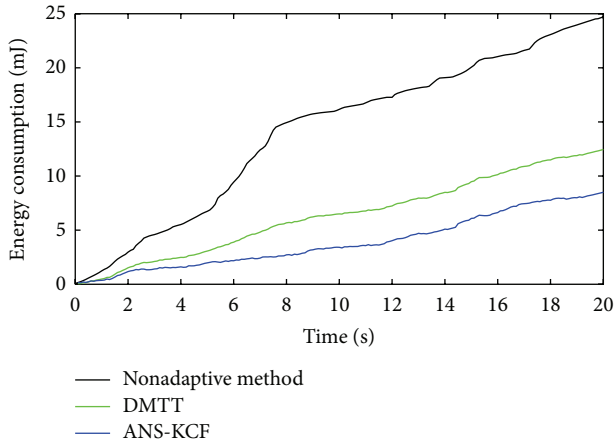

FIGURE 13: The comparison of the energy consumption for nonadaptive, DMTT, and ANS-KCF methods.

increase the implementation complexity. From the analysis of Section 3.2, the complexity of algorithm is $(N \cdot \log_2(\lambda_{\max} - \lambda_{\min})/\varepsilon + N_T)$, which mainly increases the computation consumption with polynomial order. Under the parameter setting of the simulation, the node selection can be implemented in real time. Compared to the saving energy, the computing consumption can be accepted.

5. Conclusion and Future Works

In this paper, we have proposed a novel adaptive node scheduling method for energy-efficient target tracking in wireless sensor networks. Firstly, the Kalman-consensus filter is improved to support the cooperative node tracking. Then the node scheduling problem with the energy and accuracy constraints is decomposed and analyzed by convex framework. The novelty of the proposed method lies in using index gradient rather than using brute research to decide the suitable sensor nodes. The method realizes the tradeoff between tracking accuracy and energy efficiency for resource-limited sensor networks. In our future work, we will focus on the scenario that the sensing range of a sensor will decay as energy consumption.

Conflict of Interests

The authors declare that there is no conflict of interests regarding the publication of this paper.

Acknowledgments

This work is partially supported by the National Natural Science Foundation of China (nos. 61003233, 61379111, and 61202342) and Specialized Research Fund for Doctoral Program of Higher Education (no. 20110162110042).

References

[1] J. Yick, B. Mukherjee, and D. Ghosal, "Wireless sensor network survey," *Computer Networks*, vol. 52, no. 12, pp. 2292–2330, 2008.

[2] P. Corke, T. Wark, R. Jurdak, W. Hu, P. Valencia, and D. Moore, "Environmental wireless sensor networks," *Proceedings of the IEEE*, vol. 98, no. 11, pp. 1903–1917, 2010.

[3] G. Simon, M. Maroti, A. Ledeczi et al., "Sensor network-based countersniper system," in *Proceedings of the 2nd International Conference on Embedded Networked Sensor Systems (SenSys '04)*, pp. 1–12, Baltimore, Md, USA, November 2004.

[4] I. Vasilescu, K. Kotay, D. Rus et al., "Data collection, storage, and retrieval with an underwater sensor network," in *Proceedings of the 3rd International Conference on Embedded Networked Sensor Systems*, pp. 154–165, ACM, 2005.

[5] J. H. Huang, S. Amjad, and S. Mishra, "Cenwits: a sensor-based loosely coupled search and rescue system using witnesses," in *Proceedings of the 3rd International Conference on Embedded Networked Sensor Systems*, pp. 180–191, ACM, 2005.

[6] P. Zhang, C. M. Sadler, S. A. Lyon, and M. Martonosi, "Hardware design experiences in ZebraNet," in *Proceedings of the 2nd International Conference on Embedded Networked Sensor Systems (SenSys '04)*, pp. 227–238, Baltimore, Md, USA, November 2004.

[7] O. Demigha, W.-K. Hidouci, and T. Ahmed, "On Energy efficiency in collaborative target tracking in wireless sensor network: a review," *IEEE Communications Surveys and Tutorials*, vol. 15, no. 3, pp. 1210–1222, 2013.

[8] K. J. Hintz, "A measure of the information gain attributable to cueing," *IEEE Transactions on Systems, Man and Cybernetics*, vol. 21, no. 2, pp. 434–442, 1991.

[9] F. Zhao, J. Shin, and J. Reich, "Information-driven dynamic sensor collaboration," *IEEE Signal Processing Magazine*, vol. 19, no. 2, pp. 61–72, 2002.

[10] J. Manyika and H. Durrant-Whyte, *Data Fusion and Sensor Management: A Decentralized Information-Theoretic Approach*, Prentice Hall PTR, Upper Saddle River, NJ, USA, 1995.

[11] R. R. Brooks, P. Ramanathan, and A. M. Sayeed, "Distributed target classification and tracking in sensor networks," *Proceedings of the IEEE*, vol. 91, no. 8, pp. 1163–1171, 2003.

[12] D. Li, K. D. Wong, Y. H. Hu, and A. M. Sayeed, "Detection, classification, and tracking of targets," *IEEE Signal Processing Magazine*, vol. 19, no. 2, pp. 17–29, 2002.

[13] H. Wang, G. Pottie, K. Yao, and D. Estrin, "Entropy-based sensor selection heuristic for target localization," in *Proceedings of the 3rd International Symposium on Information Processing in Sensor Networks (IPSN '04)*, pp. 36–45, ACM, April 2004.

[14] J. Chen, K. Cao, K. Li, and Y. Sun, "Distributed sensor activation algorithm for target tracking with binary sensor networks," *Cluster Computing*, vol. 14, no. 1, pp. 55–64, 2011.

[15] H. Rowaihy, S. Eswaran, M. Johnson et al., "A survey of sensor selection schemes in wireless sensor networks," in *Unattended Ground, Sea, and Air Sensor Technologies and Applications IX*, vol. 6562 of *Proceedings of SPIE*, Orlando, Fla, USA, April 2007.

[16] D. Guo and X. Wang, "Dynamic sensor collaboration via sequential Monte Carlo," *IEEE Journal on Selected Areas in Communications*, vol. 22, no. 6, pp. 1037–1047, 2004.

[17] R. Tharmarasa, T. Kirubarajan, and M. L. Hernandez, "Large-scale optimal sensor array management for multitarget tracking," *IEEE Transactions on Systems, Man and Cybernetics Part C: Applications and Reviews*, vol. 37, no. 5, pp. 803–814, 2007.

[18] Y. E. M. Hamouda and C. Phillips, "Adaptive sampling for energy-efficient collaborative multi-target tracking in wireless sensor networks," *IET Wireless Sensor Systems*, vol. 1, no. 1, pp. 15–25, 2011.

[19] R. Olfati-Saber, "Distributed Kalman filtering for sensor networks," in *Proceedings of the 46th IEEE Conference on Decision and Control*, pp. 5492–5498, 2007.

[20] N. Ahmed, S. S. Kanhere, and S. Jha, "Probabilistic coverage in wireless sensor networks," in *Proceedings of the IEEE 30th Anniversary Conference on Local Computer Networks*, vol. 8, p. 681, IEEE, 2005.

[21] W. Xiao, S. Zhang, J. Lin, and C. K. Tham, "Energy-efficient adaptive sensor scheduling for target tracking in wireless sensor networks," *Journal of Control Theory and Applications*, vol. 8, no. 1, pp. 86–92, 2010.

[22] M. Bhardwaj and A. P. Chandrakasan, "Bounding the lifetime of sensor networks via optimal role assignments," in *Proceedings of the IEEE information Conmmunication Conference (INFOCOM '02)*, pp. 1587–1596, New York, NY, USA, June 2002.

[23] T. Rappaport, *Wireless Communication: Principles and Practice*, Prentice Hall PTR, Upper Saddle River, NJ, USA, 2nd edition, 2001.

Hindawi Publishing Corporation
Mathematical Problems in Engineering
Volume 2015, Article ID 415734, 6 pages
http://dx.doi.org/10.1155/2015/415734

Research Article

Adaptive Synchronization via State Predictor on General Complex Dynamic Networks

Lijun Wang,[1] Pingnan Ruan,[1] Shuang Li,[2] and Xiao Han[2]

[1] *School of Economics and Management, Beijing University of Technology, Beijing 100022, China*
[2] *College of Science, North China University of Technology, Beijing 100144, China*

Correspondence should be addressed to Shuang Li; 374915249@qq.com

Received 25 June 2014; Accepted 14 August 2014

Academic Editor: Michael Chen

This paper considers the adaptive synchronization of general complex dynamic networks via state predictor based on the fixed topology for nonlinear dynamical systems. Using Lyapunov stability properties, it is proved that the complex dynamical networks with state predictor are asymptotically stable. Moreover, it is also shown that the rate of convergence of complex dynamical networks with state predictor is faster than the complex dynamical networks without state predictor.

1. Introduction

In recent years, the synchronization of complex dynamical networks has received more and more attention. The synchronous research can be applied in many fields, such as biology, smart city, computer, and the traffic [1–23].

It is well known that the complex network has a lot of nodes; however, in order to save an increasing number of energies, the pinning control is introduced to study the synchronization of complex dynamical networks. So far, the pinning control is a main tool by controlling a small number of nodes to steer the whole network. In [2], the pinning control of a continuous-time complex dynamical network with general coupling topologies was researched. The speed of synchronization is a significant issue, so, in [6], a state predictor was introduced. In [7], the adaptive synchronization of complex dynamical networks with state predictor was studied, therefore, this paper studies the problem using the pinning control.

This paper considers the adaptive synchronization of general complex dynamic networks via state predictor based on the fixed topology for nonlinear dynamical systems. With the limited information, state predictor can predict the future state of the nodes and its neighbors; therefore, general complex dynamic networks via state predictor can be faster to achieve synchronization.

This paper is organized as follows. Section 2 gives a model of the complex dynamical network. In addition, some preliminaries are introduced to prove the adaptive synchronization. Section 3 gives the main results and the theoretical analysis. The simulations of the theoretical results are given in Section 4. Finally, the conclusion is drawn in Section 5.

2. Preliminaries and Problem Statement

Consider a complex dynamical network described by

$$\begin{aligned}\dot{x}_i(t) = {} & f\left(x_i(t)\right) + \sum_{j=1}^{N} a_{ij}c_{ij}(t)\left[x_j(t) - x_i(t)\right] \\ & + \gamma \sum_{j\in\mathcal{N}_i} a_{ij}c_{ij}(t)\left(\dot{x}_i^p(t) - \dot{x}_j^p(t)\right) + u_i(t),\end{aligned} \tag{1}$$

where $x_i(t) = (x_{i1}(t), x_{i2}(t), \ldots, x_{in}(t))^T \in R^n$ $(i = 1, 2, \ldots, N)$ is the state vector of the ith node at time t, where t is the continuous time; $f_i : R^n \to R^n$ is a continuous function; N_i represents the neighbor node of i; a_{ij} typify the coupling weight between any two nodes, where $a_{ij} \geq 0$ and $a_{ii} = 0$; $c_{ij}(t)$ stands for the coupling strengths between node i and node j;

define the matrix of the weighted coupling configuration of the system as

$$U = \begin{bmatrix} a_{11}c_{11} & a_{12}c_{12} & \cdots & a_{1N}c_{1N} \\ a_{21}c_{21} & a_{22}c_{22} & \cdots & a_{2N}c_{2N} \\ \vdots & \vdots & \ddots & \vdots \\ a_{N1}c_{N1} & a_{N2}c_{N2} & \cdots & a_{NN}c_{NN} \end{bmatrix} \in R^{N\times N}, \quad (2)$$

with $a_{ii}c_{ii} = -\sum_{j=1, j\neq i}^{N} a_{ij}c_{ij}$.

Introduce the state predictor as

$$\dot{X}^p = -LX, \quad (3)$$

where $\dot{X}^p = (\dot{x}_1^p, \dot{x}_2^p, \ldots, \dot{x}_N^p)^T$, γ represents the impact factor of the state predictor.

Under the state predictor (3), network (1) can be written as

$$\begin{aligned} \dot{x}_i(t) = {} & f(x_i(t)) + \sum_{j=1}^{N} a_{ij}c_{ij}(t)\left[x_j(t) - x_i(t)\right] \\ & - \gamma\left[\sum_{j\in\mathcal{N}_i}\sum_{k\in\mathcal{N}_i} a_{ij}a_{ik}c_{ij}(t)c_{ik}(t)\left(x_i(t) - x_k(t)\right)\right. \\ & \left. - \sum_{j\in\mathcal{N}_i}\sum_{p\in\mathcal{N}_j} a_{ij}a_{jp}c_{ij}(t)c_{jp}(t)\left(x_j(t) - x_p(t)\right)\right] \\ & + u_i(t). \end{aligned} \quad (4)$$

The control input is designed as

$$u_i = -h_i c_i\left(x_i(t) - \overline{x}(t)\right), \quad (5)$$

where h_i is a binary number; if the ith agent is controlled, $h_i = 1$; otherwise $h_i = 0$. c_i is the feedback gain of position.

Definition 1. Network (4) is said to achieve synchronization if

$$\lim_{t\to\infty}\left\|x_i(t) - \overline{x}(t)\right\| = 0, \quad i = 1\cdots N, \quad (6)$$

where the homogeneous state satisfies

$$\dot{\overline{x}}(t) = f(\overline{x}(t), t) = 0. \quad (7)$$

The adaptive control at node i is designed as

$$\dot{c}_{ij}(t) = a_{ij}k_{ij}\left[x_i(t) - x_j(t)\right]^T P\left[x_i(t) - x_j(t)\right], \quad (8)$$

where $c_{ij}(0) \geq 0$.

In the following, some necessary assumptions and lemmas are stated.

Assumption 2 (see [10]). The continuous function $f_i : R^n \times [0, +\infty] \to R^n$ satisfies

$$\begin{aligned} & (x-y)^T P\left\{\left[f(x,t) - f(y,t)\right] - \Delta(x-y)\right\} \\ & \quad \leq -\omega(x-y)^T(x-y), \end{aligned} \quad (9)$$

for $\forall x, y \in R^n$. And

$$\begin{aligned} \Delta &= \operatorname{diag}\{\delta_1, \ldots, \delta_n\}, \\ P &= \operatorname{diag}\{p_1, \ldots, p_n\} \end{aligned} \quad (10)$$

are positive constant matrices, for the constant $\omega > 0$.

Lemma 3 (see [8]). *For any vectors $x, y \in R^n$ and positive-definite matrix $G \in R^{n\times n}$, the following matrix inequality holds:*

$$2x^T y \leq x^T G x + y^T G^{-1} y. \quad (11)$$

Lemma 4 (see [9]). *Suppose that a and b are vectors; then for any positive-definite matrix E, the following inequality holds:*

$$-2a^T b \leq \inf_{E>0}\left\{a^T E a + b^T E^{-1} b\right\}. \quad (12)$$

Lemma 5 (see [10]). *The following equation holds:*

$$\begin{aligned} & \sum_{i=1}^{N}(x_i - \overline{x})^T P \sum_{j=1, j\neq i}^{N} a_{ij}c_{ij}\left(x_i - x_j\right) \\ & \quad = \frac{1}{2}\sum_{i=1}^{N}\sum_{j=1, j\neq i}^{N} a_{ij}c_{ij}\left(x_i - x_j\right)^T P\left(x_i - x_j\right). \end{aligned} \quad (13)$$

Lemma 6 (see [18]). *For a connected graph which is undirected, the Laplace matrix is positive semidefinite matrix, and the minimum nonzero eigenvalue is the algebraic connectivity of L, as follows:*

$$\lambda_2(L) = \min_{x\neq 0, 1^T x = 0}\frac{x^T L x}{\|x\|^2}. \quad (14)$$

Lemma 7 (see [18]). *For a system which is similar to $\dot{x}_i = u_i$ $(i = 1, 2, \ldots, n)$, the evolution rate associated with the minimum nonzero eigenvalue λ_2. λ_2 describes the lower bound of convergence rate. Generally, the bigger the λ_2 is, the faster the system converges.*

3. Main Results

In the following, we will give the main result.

Theorem 8. *Consider network* (4) *with the state predictor* (3) *and N nodes steered by adaptive control* (8)*, under Assumption 2, and at least one node is selected to be controlled. Then, all nodes asymptotically synchronize with the given homogeneous stationary state:*

$$\lim_{t\to\infty}\left\|x_i(t) - \overline{x}(t)\right\| = 0. \quad (15)$$

Proof. Let $\widetilde{x}_i(t) \triangleq x_i(t) - \overline{x}(t)$. Construct the following Lyapunov function:

$$V(t) = V_1(t) + V_2(t), \quad (16)$$

where

$$V_1(t) = \frac{1}{2}\sum_{i=1}^{N} \widetilde{x}_i^T(t) P \widetilde{x}_i(t),$$
$$V_2(t) = \frac{1}{2}\sum_{i=1}^{N}\sum_{j\in\mathcal{N}_i} \frac{\left[c_{ij}(t) - m\right]^2}{2k_{ij}}. \tag{17}$$

Then

$$\begin{aligned}
\dot{V}_1(t) &= \sum_{i=1}^{N} \widetilde{x}_i^T P \Bigg[f(x_i(t)) + \sum_{j=1}^{N} a_{ij}c_{ij}(t)\left(x_j - x_i\right) \\
&\qquad + \gamma \sum_{j\in\mathcal{N}_i} a_{ij}c_{ij}(t)\left(\dot{x}_i^p(t) - \dot{x}_j^p(t)\right) \\
&\qquad + u_i(t) - f(\overline{x}(t)) \Bigg] \\
&= \sum_{i=1}^{N} \widetilde{x}_i^T P \Bigg[f(x_i(t)) + \sum_{j=1}^{N} a_{ij}c_{ij}(t)\left(x_j - x_i\right) \\
&\qquad - \gamma \Bigg[\sum_{j\in\mathcal{N}_i}\sum_{k\in\mathcal{N}_i} a_{ij}a_{ik}c_{ij}(t)c_{ik}(t)\left(x_i - x_k\right) \\
&\qquad\quad - \sum_{j\in\mathcal{N}_i}\sum_{p\in\mathcal{N}_j} a_{ij}a_{jp}c_{ij}(t)c_{jp}(t) \\
&\qquad\quad \times \left(x_j - x_p\right) \Bigg] \\
&\qquad - h_i c_i \widetilde{x}_i(t) - f(\overline{x}(t)) \Bigg] \\
&= \sum_{i=1}^{N} \widetilde{x}_i^T P \left[f(x_i(t)) - f(\overline{x}(t)) \right] \\
&\quad + \sum_{i=1}^{N} \widetilde{x}_i^T P \sum_{j=1}^{N} a_{ij}c_{ij}(t)\left(x_j - x_i\right) \\
&\quad - \sum_{i=1}^{N} \widetilde{x}_i^T P h_i c_i \widetilde{x}_i^T - \gamma \sum_{i=1}^{N} \widetilde{x}_i^T P \\
&\quad \times \sum_{j\in\mathcal{N}_i}\sum_{k\in\mathcal{N}_i} a_{ij}a_{ik}c_{ij}(t)c_{ik}(t)\left(\widetilde{x}_i - \widetilde{x}_k\right) \\
&\quad + \gamma \sum_{i=1}^{N} \widetilde{x}_i^T P \sum_{j\in\mathcal{N}_i}\sum_{p\in\mathcal{N}_j} a_{ij}a_{ip}c_{ij}(t)c_{ip}(t)\left(\widetilde{x}_j - \widetilde{x}_p\right) \\
&\le -\omega \sum_{i=1}^{N} \widetilde{x}_i^T \widetilde{x}_i + \sum_{i=1}^{N} \widetilde{x}_i^T P \Delta\widetilde{x}_i \\
&\quad + \sum_{i=1}^{N} \widetilde{x}_i^T P \sum_{j=1}^{N} a_{ij}c_{ij}(t)\left(x_j - x_i\right) \\
&\quad - \sum_{i=1}^{N} \widetilde{x}_i^T P h_i c_i \widetilde{x}_i^T - \gamma \sum_{i=1}^{N} \widetilde{x}_i^T P \\
&\quad \times \sum_{j\in\mathcal{N}_i}\sum_{k\in\mathcal{N}_i} a_{ij}a_{ik}c_{ij}(t)c_{ik}(t)\widetilde{x}_i \\
&\quad + \gamma \sum_{i=1}^{N} \widetilde{x}_i^T P \sum_{j\in\mathcal{N}_i}\sum_{k\in\mathcal{N}_i} a_{ij}a_{ik}c_{ij}(t)c_{ik}(t)\widetilde{x}_k \\
&\quad + \gamma \sum_{i=1}^{N} \widetilde{x}_i^T P \sum_{j\in\mathcal{N}_i}\sum_{p\in\mathcal{N}_j} a_{ij}a_{jp}c_{ij}(t)c_{jp}(t)\widetilde{x}_j \\
&\quad - \gamma \sum_{i=1}^{N} \widetilde{x}_i^T P \sum_{j\in\mathcal{N}_i}\sum_{p\in\mathcal{N}_j} a_{ij}a_{jp}c_{ij}(t)c_{jp}(t)\widetilde{x}_p \\
&\le -\omega \sum_{i=1}^{N} \widetilde{x}_i^T \widetilde{x}_i + \sum_{i=1}^{N} \widetilde{x}_i^T P \Delta\widetilde{x}_i \\
&\quad + \sum_{i=1}^{N} \widetilde{x}_i^T(t) P \sum_{j=1}^{N} a_{ij}c_{ij}(t)\left(x_j - x_i\right) \\
&\quad - \sum_{i=1}^{N} \widetilde{x}_i^T P h_i c_i \widetilde{x}_i - \gamma \sum_{i=1}^{N} \widetilde{x}_i^T P \\
&\quad \times \sum_{j\in\mathcal{N}_i}\sum_{k\in\mathcal{N}_i} a_{ij}a_{ik}c_{ij}(t)c_{ik}(t)\widetilde{x}_i \\
&\quad + \frac{1}{2}\gamma \sum_{i=1}^{N}\sum_{j\in\mathcal{N}_i}\sum_{k\in\mathcal{N}_i} \widetilde{x}_i^T P a_{ij}a_{ik}c_{ij}(t)c_{ik}(t)\widetilde{x}_i \\
&\quad + \frac{1}{2}\gamma \sum_{i=1}^{N}\sum_{j\in\mathcal{N}_i}\sum_{k\in\mathcal{N}_i} \widetilde{x}_k^T P a_{ij}a_{ik}c_{ij}(t)c_{ik}(t)\widetilde{x}_k \\
&\quad + \frac{1}{2}\gamma \sum_{i=1}^{N}\sum_{j\in\mathcal{N}_i}\sum_{p\in\mathcal{N}_j} \widetilde{x}_i^T P a_{ij}a_{jp}c_{ij}(t)c_{jp}(t)\widetilde{x}_i \\
&\quad + \frac{1}{2}\gamma \sum_{i=1}^{N}\sum_{j\in\mathcal{N}_i}\sum_{p\in\mathcal{N}_j} \widetilde{x}_j^T P a_{ij}a_{jp}c_{ij}(t)c_{jp}(t)\widetilde{x}_j \\
&\quad + \frac{1}{2}\gamma \sum_{i=1}^{N}\sum_{j\in\mathcal{N}_i}\sum_{p\in\mathcal{N}_j} \widetilde{x}_i^T P a_{ij}a_{jp}c_{ij}(t)c_{jp}(t)\widetilde{x}_i \\
&\quad + \frac{1}{2}\gamma \sum_{i=1}^{N}\sum_{j\in\mathcal{N}_i}\sum_{p\in\mathcal{N}_j} \widetilde{x}_p^T P a_{ij}a_{jp}c_{ij}(t)c_{jp}(t)\widetilde{x}_p \\
&= -\omega \sum_{i=1}^{N} \widetilde{x}_i^T \widetilde{x}_i + \sum_{i=1}^{N} \widetilde{x}_i^T P \Delta\widetilde{x}_i + \sum_{i=1}^{N} \widetilde{x}_i^T P
\end{aligned}$$

$$
\begin{aligned}
&\times \sum_{j=1}^{N} a_{ij}c_{ij}(t)\left(x_j - x_i\right) \\
&- \sum_{i=1}^{N} \widetilde{x}_i^T P h_i c_i \widetilde{x}_i - \frac{1}{2}\gamma \\
&\times \sum_{i=1}^{N} \sum_{j\in\mathcal{N}_i} \sum_{k\in\mathcal{N}_i} \widetilde{x}_i^T P a_{ij}a_{ik}c_{ij}(t)\, c_{ik}(t)\, \widetilde{x}_i \\
&+ \frac{1}{2}\gamma \sum_{i=1}^{N} \sum_{j\in\mathcal{N}_i} \sum_{k\in\mathcal{N}_i} \widetilde{x}_k^T P a_{ij}a_{ik}c_{ij}(t)\, c_{ik}(t)\, \widetilde{x}_k \\
&+ \gamma \sum_{i=1}^{N} \sum_{j\in\mathcal{N}_i} \sum_{p\in\mathcal{N}_j} \widetilde{x}_i^T P a_{ij}a_{jp}c_{ij}(t)\, c_{jp}(t)\, \widetilde{x}_i \\
&+ \frac{1}{2}\gamma \sum_{i=1}^{N} \sum_{j\in\mathcal{N}_i} \sum_{p\in\mathcal{N}_j} \widetilde{x}_j^T P a_{ij}a_{jp}c_{ij}(t)\, c_{jp}(t)\, \widetilde{x}_j \\
&+ \frac{1}{2}\gamma \sum_{i=1}^{N} \sum_{j\in\mathcal{N}_i} \sum_{p\in\mathcal{N}_j} \widetilde{x}_p^T P a_{ij}a_{jp}c_{ij}(t)\, c_{jp}(t)\, \widetilde{x}_p \\
&= -\omega \sum_{i=1}^{N} \widetilde{x}_i^T \widetilde{x}_i + \sum_{i=1}^{N} \widetilde{x}_i^T P \Delta \widetilde{x}_i \\
&+ \sum_{i=1}^{N} \widetilde{x}_i^T P \sum_{j=1}^{N} a_{ij}c_{ij}(t)\left(x_j - x_i\right) \\
&- \sum_{i=1}^{N} \widetilde{x}_i^T P h_i c_i \widetilde{x}_i + 2\gamma \sum_{i=1}^{N} \widetilde{x}_j^T P L_i^2 \widetilde{x}_j,
\end{aligned}
\tag{18}
$$

where $L_i = \sum_{j=1, j\neq i}^{N} a_{ij}c_{ij}(t)$, $i, j = 1, 2, \ldots, N$.

Consider the following:

$$
\begin{aligned}
&\dot{V}_2(t) \\
&= \frac{1}{2}\sum_{i=1}^{N} \sum_{j\in\mathcal{N}_i} \frac{\left(c_{ij} - m\right)\dot{c}_{ij}}{k_{ij}} \\
&= \frac{1}{2}\sum_{i=1}^{N} \sum_{j\in\mathcal{N}_i} \left(c_{ij} - m\right) a_{ij}\left[x_i - x_j\right]^T P \left[x_i - x_j\right] \\
&= \sum_{i=1}^{N} \widetilde{x}_i^T P \sum_{j\in\mathcal{N}_i} a_{ij}c_{ij}\left(x_i - x_j\right) \\
&\quad - m\sum_{i=1}^{N} \widetilde{x}_i^T P \sum_{j\in\mathcal{N}_i} a_{ij}\left(x_i - x_j\right).
\end{aligned}
$$

$$
\begin{aligned}
&\dot{V}_1(t) + \dot{V}_2(t) \\
&\leq -\omega \sum_{i=1}^{N} \widetilde{x}_i^T \widetilde{x}_i + \sum_{i=1}^{N} \widetilde{x}_i^T P \Delta \widetilde{x}_i - \sum_{i=1}^{N} \widetilde{x}_i^T P h_i c_i \widetilde{x}_i \\
&\quad + 2\gamma \sum_{i=1}^{N} \widetilde{x}_j^T P L_i^2 \widetilde{x}_j - m\sum_{i=1}^{N} \widetilde{x}_i^T P \sum_{j\in\mathcal{N}_i} a_{ij}\left(\widetilde{x}_i - \widetilde{x}_j\right) \\
&= \widetilde{x}^T \left[\left(I_N \otimes P\Delta + 2\gamma L^2 \otimes P\right)\right. \\
&\qquad \left. - \left(H \otimes P + mA \otimes P\right)\right] \widetilde{x} - \omega \sum_{i=1}^{N} \widetilde{x}_i^T x_i^T.
\end{aligned}
\tag{19}
$$

Since the positive constant m is sufficiently large, $\dot{V}(t) < 0$.

Therefore, $\lim_{t\to\infty} \|x_i(t) - \overline{x}(t)\| = 0$. □

Theorem 9. *Network* (4) *with the state predictor* (3) *is faster to achieve synchronization than the network without the state predictor.*

Proof. For the system with state predictor, the main difference is whether the system contains $\gamma \sum_{j\in\mathcal{N}_i} a_{ij}c_{ij}(t)(\dot{x}_i^p(t) - \dot{x}_j^p(t))$. We consider the minimum nonzero eigenvalue of state predictor. The Laplace matrix is positive semidefinite matrix, so there is a nonsingular matrix P that can make the Laplace matrix expressed as

$$
\gamma L^2 = P^{-1} \begin{bmatrix} \gamma\lambda_n^2 & & & \\ & \ddots & & \\ & & \gamma\lambda_2^2 & \\ & & & 0 \end{bmatrix} P, \quad 0 < \lambda_2 \leq \cdots \leq \lambda_n. \tag{20}
$$

Obviously, under the same conditions, a system with state predictor has greater minimum nonzero eigenvalue. According to Lemma 7, network (4) with the state predictor (3) is faster to achieve synchronization than the network without the state predictor. □

4. Simulations

In this section, a numerical simulation is given to illustrate the analytical results.

Consider a network with the undirected topology described as follows:

$$
A = \begin{bmatrix} 0 & 0.0964 & 0.0757 & 0.0570 \\ 0.0964 & 0 & 0.1199 & 0.1396 \\ 0.0757 & 0.1199 & 0 & 0.0581 \\ 0.0570 & 0.1396 & 0.0581 & 0 \end{bmatrix}, \tag{21}
$$

where each node is a Lorenz system:

$$
f(x(t)) = f\left(x^1, x^2, x^3\right) = \begin{cases} \dot{x}^1 = 10\left(x^2 - x^1\right) \\ \dot{x}^2 = 28x^1 - x^1x^3 - x^2 \\ \dot{x}^3 = x^1x^2 - \dfrac{8}{3}x^3. \end{cases} \tag{22}
$$

Figure 1 describes the error states on the x-axis, y-axis, and z-axis, respectively. From Figure 1, we can see that all nodes can synchronize with the synchronous state by degrees. In particular, under the same conditions, the network with a state predictor can be synchronized faster. It is shown in Figure 2.

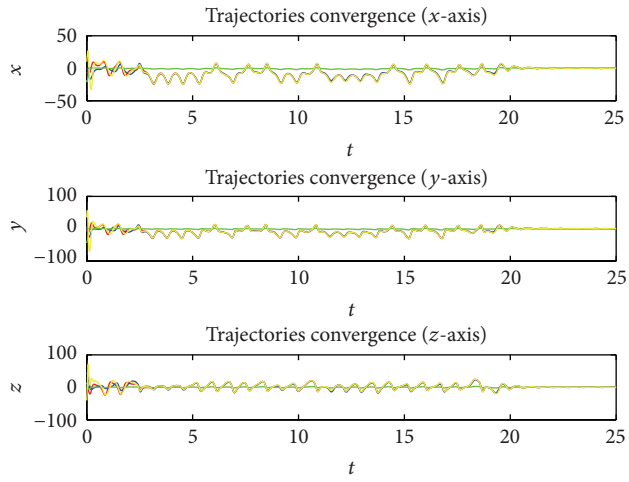

FIGURE 1: The dynamical network without a state predictor.

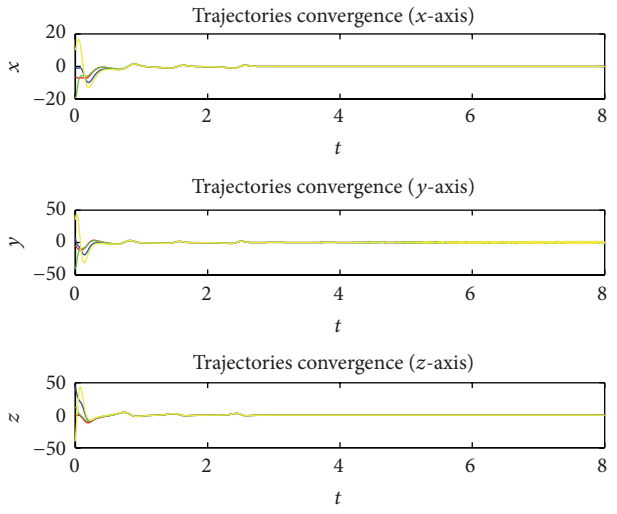

FIGURE 2: The dynamical network with a state predictor when $\gamma = 100$.

5. Conclusion

In this paper, we have investigated the state predictor problem for synchronization of complex dynamical networks in fixed topology. By introducing local adaptive strategies for the coupling strengths, we have proved that the complex dynamical networks are asymptotically stable. It is obvious that the rate of convergence of the network with a state predictor is faster than the network without a state predictor.

Conflict of Interests

The authors declare that there is no conflict of interests regarding the publication of this paper.

Acknowledgments

This work was supported in part by the National Natural Science Foundation of China under Grant no. 61304049, Technology Development Plan Project of Beijing Education Commission (no. KM201310009011).

References

[1] W. Yu, G. Chen, J. Lü, and J. Kurths, "Synchronization via pinning control on general complex networks," *SIAM Journal on Control and Optimization*, vol. 51, no. 2, pp. 1395–1416, 2013.

[2] L. Y. Xiang, Z. X. Liu, Z. Q. Chen, F. Chen, and Z. Z. Yuan, "Pinning control of complex dynamical networks with general topology," *Physica A: Statistical Mechanics and Its Applications*, vol. 379, no. 1, pp. 298–306, 2007.

[3] X. F. Wang and G. Chen, "Pinning control of scale-free dynamical networks," *Physica A*, vol. 310, no. 3-4, pp. 521–531, 2002.

[4] P. de Lellis, M. di Bernardo, and F. Garofalo, "Synchronization of complex networks through local adaptive coupling," *Chaos*, vol. 18, no. 3, Article ID 037110, 8 pages, 2008.

[5] H. Su, Z. Rong, M. Z. Q. Chen, X. Wang, G. Chen, and H. Wang, "Decentralized adaptive pinning control for cluster synchronization of complex dynamical net works," *IEEE Transactions on Systems, Man, and Cybernetics B: Cybernetics*, vol. 43, no. 1, pp. 394–399, 2013.

[6] Y. Xi, W. Huang, and X. Li, "Consensus of multi-agent system with state predictor," *Control and Decision*, vol. 25, no. 5, pp. 769–772, 2010.

[7] Y. Shi, B. Liu, and X. Han, "Adaptive synchronization of complex dynamical networks with state predictor," *Journal of Applied Mathematics*, vol. 2013, Article ID 394137, 8 pages, 2013.

[8] H. Su, X. Wang, and Z. Lin, "Flocking of multi-agents with a virtual leader," *IEEE Transactions on Automatic Control*, vol. 54, no. 2, pp. 293–307, 2009.

[9] H. Su, N. Zhang, M. Z. Q. Chen, and X. Wang, "Adaptive flocking with a virtual leader of multiple agents governed by locally Lipschitz nonlinearity," *Nonlinear Analysis: Real World Applications*, vol. 14, no. 1, pp. 798–806, 2013.

[10] H. Su, G. Chen, X. Wang, and Z. Lin, "Adaptive second-order consensus of networked mobile agents with nonlinear dynamics," *Automatica*, vol. 47, no. 2, pp. 368–375, 2011.

[11] B. Liu, W. Hu, J. Zhang, and H. Su, "Controllability of discrete-time multi-agent systems with multiple leaders on fixed networks," *Communications in Theoretical Physics*, vol. 58, no. 6, pp. 856–862, 2012.

[12] H. Su, M. Z. Q. Chen, J. Lam, and Z. Lin, "Semi-global leader-following consensus of linear multi-agent systems with input saturation via low gain feedback," *IEEE Transactions on Circuits and Systems. I. Regular Papers*, vol. 60, no. 7, pp. 1881–1889, 2013.

[13] B. Liu, X. Wang, and J. Zhang, "Adaptive pinning synchronization of the complex dynamical network," in *Proceedings of the International Conference on Automatic Control and Artificial Intelligence*, vol. 6, pp. 4173–4176, 2012.

[14] W. Yu, P. DeLellis, G. Chen, M. di Bernardo, and J. Kurths, "Distributed adaptive control of synchronization in complex networks," *IEEE Transactions on Automatic Control*, vol. 57, no. 8, pp. 2153–2158, 2012.

[15] W. Yu, G. Chen, and J. Lü, "On pinning synchronization of complex dynamical networks," *Automatica*, vol. 45, no. 2, pp. 429–435, 2009.

[16] Z. Hou, L. Cheng, and M. Tan, "Decentralized robust adaptive control for the multiagent system consensus problem using neural networks," *IEEE Transactions on Systems, Man, and Cybernetics B: Cybernetics*, vol. 39, no. 3, pp. 636–647, 2009.

[17] P. de Lellis, M. di Bernardo, and F. Garofalo, "Synchronization of complex networks through local adaptive coupling," *Chaos*, vol. 18, no. 3, Article ID 037110, 2008.

[18] Y. Xi, W. Huang, and X. Li, "Consensus of multi-agent system with state predictor," *Control and Decision*, vol. 25, no. 5, pp. 669–772, 2010.

[19] B. Tadić, S. Thurner, and G. J. Rodgers, "Traffic on complex networks: towards understanding global statistical properties from microscopic density fluctuations," *Physical Review E*, vol. 69, no. 3, Article ID 036102, 2004.

[20] G. Xi, W. Huang, and X. Li, "Consensus of multi-agent system with state predictor," *Control and Decision*, vol. 25, no. 5, pp. 669–772, 2010.

[21] L. Zhao, Y. Lai, K. Park, and N. Ye, "Onset of traffic congestion in complex networks," *Physical Review E—Statistical, Nonlinear, and Soft Matter Physics*, vol. 71, no. 2, Article ID 026125, 2005.

[22] Z. Gao, D. Kong, and C. Gao, "Modeling and control of complex dynamic systems: applied mathematical aspects," *Journal of Applied Mathematics*, vol. 2012, Article ID 869792, 5 pages, 2012.

[23] Z. Gao, D. Kong, C. Gao, and M. Chen, "Modeling and control of complex dynamic systems," *Journal of Applied Mathematics*, vol. 2013, Article ID 151372, 3 pages, 2013.

Hindawi Publishing Corporation
Mathematical Problems in Engineering
Volume 2015, Article ID 705725, 9 pages
http://dx.doi.org/10.1155/2015/705725

Research Article

Robust Fault Detection for a Class of Uncertain Nonlinear Systems Based on Multiobjective Optimization

Bingyong Yan, Huifeng Wang, and Huazhong Wang

Key Laboratory of Advanced Control and Optimization for Chemical Process of Ministry of Education, Department of Automation, East China University of Science and Technology, Shanghai 200237, China

Correspondence should be addressed to Huazhong Wang; hzwang@ecust.edu.cn

Received 30 August 2014; Accepted 12 October 2014

Academic Editor: Wei Zhang

A robust fault detection scheme for a class of nonlinear systems with uncertainty is proposed. The proposed approach utilizes robust control theory and parameter optimization algorithm to design the gain matrix of fault tracking approximator (FTA) for fault detection. The gain matrix of FTA is designed to minimize the effects of system uncertainty on residual signals while maximizing the effects of system faults on residual signals. The design of the gain matrix of FTA takes into account the robustness of residual signals to system uncertainty and sensitivity of residual signals to system faults simultaneously, which leads to a multiobjective optimization problem. Then, the detectability of system faults is rigorously analyzed by investigating the threshold of residual signals. Finally, simulation results are provided to show the validity and applicability of the proposed approach.

1. Introduction

In recent years, with the development of intelligent control technology and processing ability of microchips, modern dynamic systems are becoming more and more complex. Fault detection and identification (FDI) can be deployed for monitoring and reacting to the faults occurring in these modern dynamic systems, which has a broad range of applications including intelligent power grids, underwater robot, high voltage direct current transmission lines, and long transmission lines in pneumatic, chemical processes. Effective FDI schemes can ensure safety and reliability of complex dynamic systems. The most fundamental problem for FDI is to develop a fault diagnosis observer or fault diagnosis filter. Due to the development of various nonlinear or linear states observers, the model-based analytical redundancy approaches received more and more attention in the last two decades, including observer based method, parity space based method, eigenstructure assignment based method, and parameter identification based method and H_∞ filter based method [1–8].

Early fault diagnosis approaches often assumed the availability of an accurate dynamic system model. In practice, however, such an assumption can be invalid. The main reason is that unstructured modeling uncertainties are always unavoidable when modeling system mathematical structures. Therefore, there are a growing number of researchers focusing their interests on FDI for nonlinear systems with uncertainty. A novel integrated fault diagnosis and fault tolerant control algorithm for non-Gaussian singular time-delayed stochastic distribution control system was proposed based on iterative learning observer. The iterative learning observer was developed to obtain estimation of system faults. Recently in [9], the authors introduced a novel fault detection and diagnosis for nonlinear non-Gaussian dynamic processes using kernel dynamic independent component analysis method. Sensor fault diagnosis and identification in nonlinear plants were discussed in [10]. The faults under consideration in [10] were assumed to be abruptly occurring calibration errors. Thus, an adaptive particle filter was developed to diagnose sensor faults and compensate for their effects. Chen and Saif in [11] proposed an iterative learning observer (ILO) based fault diagnosis approach for fault detection, identification, and accommodation. The main characteristic of the ILO was that its states were updated or driven successively by the estimation errors of previous system outputs and control inputs. The observer gain matrix and adaptive adjusting rule of the fault estimator are investigated in detail.

In our previous work [12], a robust fault tracking approximator (RFTA) based fault detection and identification scheme for a class of nonlinear systems was developed and its stability properties were investigated as well. Due to the existence of unstructured modeling uncertainties, the convergence speed and fault tracking accuracy of the FTA will be influenced dramatically. The objective of this work is to extend the previous research results to a class of nonlinear systems with uncertainty and optimize the gain matrix of FTA. First of all, we decompose the fault diagnosis problem into a parameter optimization problem and a fault detection problem. The parameter optimization problem can be described as follows: by using robust control technology and parameter optimization algorithms, the gain matrix of FTA is designed to minimize the effects of system uncertainty on residual signals while maximizing the effects of system faults on residual signals. The design of the gain matrix of FTA takes into account the robustness to system uncertainty and sensitivity to system faults simultaneously, which leads to a multiobjective optimization problem. The fault detection problem can be described as follows: we detect the system faults according to the relationship between the calculated threshold and residual signals. The detectability of system faults is rigorously analyzed by investigating the threshold of residual signals. In the end, an illustrative example is proposed to demonstrate the validity and applicability of the proposed approach.

An outline of this paper is organized as follows. In Section 2, we define a class of uncertain nonlinear systems and present a multiobjective optimization problem. The design of gain matrix of FTA is investigated in Section 3. The calculation of threshold for fault detection is designed in Section 4. In Section 5, simulation results are reported illustrating the effectiveness of the proposed robust fault detection scheme. Some conclusion remarks are provided in Section 6.

2. Problem Formulation

Consider a class of uncertain nonlinear systems described by

$$\dot{x}(t) = Ax(t) + Bu(t) + g(x(t), t) + B_f f(t) + B_d d(t), \tag{1}$$

$$y(t) = Cx(t) + Du(t) + D_f f(t) + D_d d(t), \tag{2}$$

where $x(t) \in R^n$ is the system state vector, $u(t) \in R^p$ is the control input vector, $y(t) \in R^q$ is the measurement output vector, $d(t)$ is the system uncertainty that belongs to $L_2^m[0, +\infty]$, $f(t) \in R^m$ is the system fault to be detected, and $g(\cdot)$: is a known nonlinear function. A, B, B_f, B_d, C, D, D_f, and D_d are known parameter matrix with appropriate dimensions. We take the following assumptions.

Assumption 1. The observability matrix associated with the pair (A, C) is full rank.

Assumption 2. The function $d(t)$ in (1), representing the unstructured modeling uncertainty, is bounded by a known constant; that is, $\|d(t)\| \le L_w$.

Assumption 3. The nonlinear function $g(\cdot)$ satisfies Lipschitz condition; that is,

$$\|g(x(t), t) - g(y(t), t)\| \le \|\rho(x(t) - y(t))\| \quad \forall x(t), y(t) \in D, \tag{3}$$

where ρ is a known real constant. Throughout the paper, the notation $\|\cdot\|$ will be used to denote the Euclidean norm of a vector.

To detect a fault, the FTA is constructed as follows [12]:

$$\dot{\hat{x}}_k = A\hat{x}_k(t) + g(\hat{x}_k(t), t) + Bu_k(t) + B_f \hat{f}_k(t) + H(y(t) - \hat{y}(t)), \tag{4}$$

$$\hat{y}_k(t) = C\hat{x}_k(t) + Du_k(t), \tag{5}$$

$$e_k(t) = x_k(t) - \hat{x}_k(t), \tag{6}$$

$$r_k(t) = Ce_k(t), \tag{7}$$

$$\hat{f}_{k+1}(t) = \hat{f}_k(t) + \Gamma \dot{r}_k(t), \tag{8}$$

$$\|y_k(t) - \hat{y}_k(t)\|_\infty \le \gamma, \quad t \in [t_a, t_b], \tag{9}$$

where $\hat{x}_k(t) \in R^n$, $\hat{y}_k(t) \in R^q$ are estimated system state and output, respectively. k is the iteration index and γ is the given performance index. Γ is constant gain matrix, and its elements are within the scope $(0, 1)$. $\hat{f}_k(t)$ is virtual fault, which is an estimate of $f(t)$ and the value of $\hat{f}(t)$ is set to zero until a fault is detected. $e(t)$ denotes the system state estimation error. $e_k(t)$ denotes the estimation error of $e(t)$ after kth iterative operation. $r_k(t)$ denotes the estimation error of $r(t)$ after kth iterative operation. H is the gain matrix to be optimized. $r(t)$ is the so-called generated residual signal.

The basic idea behind the FTA is to adjust the virtual fault $\hat{f}_k(t)$ within a specified time horizon by using iterative learning algorithm such that the virtual fault can approximate the system fault $f(t)$ as closely as possible. Detailed description about the FTA can be found in [12].

From (4) we can clearly see that the value of gain matrix H will have a great influence on the convergence speed of FTA. As a result, the fault tracking accuracy will be influenced as well. In previous work [12], we have investigated the stability and fault tracking accuracy of the FTA on the assumption that the gain matrix is a prespecified value. However, the design of gain matrix H still remains unresolved. In this work, we will utilize multiobjective parameter optimization algorithm and robust control theory to optimize the gain matrix H.

3. Design of Gain Matrix

First, we convert the parameter optimization problem into a performance index optimization problem. Then, the design of gain matrix is given in terms of linear matrix inequality (LMI).

Define the state estimation error $e(t) = x(t) - \hat{x}(t)$, and then it follows from (1)–(7) that [13–17]

$$\begin{aligned}\dot{e}(t) &= (A - HC)e(t) + \left(B_f - HD_f\right)f(t) \\ &\quad + \left(B_d - HD_d\right)d(t) + g(x(t),t) - g(\hat{x}(t),t), \\ r(t) &= Ce(t) + D_f f(t) + D_d d(t),\end{aligned} \tag{10}$$

where gain matrix H is to be designed such that the system (10) is asymptotically stable. To optimize the gain matrix H, we propose the following performance index [18]:

$$J = \frac{\left\|T_{rd}\right\|_\infty}{\left\|T_{rf}\right\|_-}, \tag{11}$$

where T_{rd} denotes the transfer function from system uncertainty to residual signal and T_{rf} denotes the transfer function from system faults to residual signal. The objective of this parameter optimization problem is to maximize the effects of system faults on residual signals while minimizing the effects of system uncertainty on residual signals. Thus, it leads to the following optimization problem: finding a gain matrix H, such that the system (10) remains asymptotically stable, and the performance index $J = \|T_{rd}\|_\infty / \|T_{rf}\|_-$ is minimized.

Remark 4. The item $\|T_{rd}\|_\infty$ is used to measure the robustness of residual signals to system uncertainty, while the sensitivity of residual signals to system faults is measured by $\|T_{rf}\|_- = \inf_{f\in(0,\infty)} \underline{\sigma}[T_{rf}(jw)]$ and $\underline{\sigma}[T_{rf}(jw)]$ denotes the nonzero singular value of $T_{rf}(jw)$. The optimization problem described by (11) is actually a multiobjective optimization problem, and it can be formulated as follows: for a given constant $\gamma > 0$, $\beta > 0$, finding a gain matrix H, such that the system (10) remains asymptotically stable, and satisfying the following inequality [18]:

$$\|r(t)\|_\infty \le \gamma \|d(t)\|_\infty, \qquad \|r(t)\|_- > \beta \left\|f(t)\right\|_- \tag{12}$$

with (10); note that the dynamics of the residual signal depends not only on $f(t)$ and $d(t)$, but also on the nonlinear part: $g(x(t),t) - g(\hat{x}(t),t)$. So the traditional fault detection observer design methods cannot be used here. A novel method to design gain matrix H, meeting the performance index (12), is required. In this paper, we propose a method to resolve this problem in terms of LMIs.

Lemma 5 (see [18, 19]). *Let A and B be real matrices with appropriate dimensions. For any scalar $\varepsilon > 0$ and vectors $x, y \in R^n$, then*

$$2x^T ABy \le \varepsilon^{-1} x^T AA^T x + \varepsilon y^T B^T B y. \tag{13}$$

Theorem 6. *Given a constant $\gamma > 0$, in the condition of $f(t) = 0$, the system (10) is asymptotically stable and satisfies $\|r(t)\|_\infty \le \gamma \|d(t)\|_\infty$, if there exists a positive symmetrical matrix P, scalar $\varepsilon_1 > 0$, satisfying the following LMI:*

$$\begin{bmatrix} M_1 & M_3 & P \\ M_3^T & M_2 & 0 \\ P^T & 0 & -\varepsilon_1 I \end{bmatrix} < 0, \tag{14}$$

where

$$\begin{aligned} M_1 &= P(A - HC) + (A - HC)^T P + C^T C + \varepsilon_1 \rho^2 I, \\ M_2 &= D_d^T D_d - \gamma^2 I, \\ M_3 &= C^T D_d + P\left(B_d - HD_d\right). \end{aligned} \tag{15}$$

Proof. We choose a Lyapunov function of the form:

$$V(t) = e^T(t) Pe(t), \tag{16}$$

where P is a positive symmetrical matrix. In the fault-free case, when the system uncertainty $d(t) = 0$, we have

$$\begin{aligned} \dot{V}(t) &= e^T(t) P\dot{e}(t) + \dot{e}^T(t) Pe(t) \\ &= e^T(t) P\left[(A - HC)e(t) + g(x(t),t) - g(\hat{x}(t),t)\right] \\ &\quad + \left[(A - HC)e(t) + g(x(t),t) - g(\hat{x}(t),t)\right]^T Pe \\ &= e^T(t)\left[P(A - HC) + (A - HC)^T P\right]e(t) \\ &\quad + e^T(t) P\left[g(x(t),t) - g(\hat{x}(t),t)\right] \\ &\quad + \left[g(x(t),t) - g(\hat{x}(t),t)\right]^T eP. \end{aligned} \tag{17}$$

According to Lemma 5 and Assumption 3, we have

$$\begin{aligned} &2e^T(t) P\left[g(x(t),t) - g(\hat{x}(t),t)\right] \\ &\le \varepsilon_1^{-1} e^T(t) PP^T e(t) + \varepsilon_1 \left(g(x(t),t) - g(\hat{x}(t),t)\right)^T \\ &\quad \times \left(g(x(t),t) - g(\hat{x}(t),t)\right) \\ &\le \varepsilon_1^{-1} e^T(t) PP^T e(t) + \varepsilon_1 \rho^2 e^T(t) e(t). \end{aligned} \tag{18}$$

Thus:

$$\begin{aligned} \dot{V}(t) \le e^T(t)\Big[&P(A - HC) + (A - HC)^T P \\ &+ \varepsilon_1^{-1} PP^T + \varepsilon_1 \rho^2 I\Big] e(t). \end{aligned} \tag{19}$$

According to (14), we can obtain that $\dot{V}(t) \le 0$. So the system (10) is asymptotically stable in the condition of no fault.

When the system uncertainty $d(t) \ne 0$, define

$$H(e,d) = \dot{V}(t) + \|r(t)\|_\infty - \gamma^2 \|d(t)\|_\infty. \tag{20}$$

So we have

$$\begin{aligned} H(e,d) &= e^T(t) P\dot{e}(t) + \dot{e}^T(t) Pe(t) + e^T(t) C^T Ce(t) \\ &\quad + e^T(t) C^T D_d d(t) + d^T(t) D_d^T Ce(t) \\ &\quad + d^T(t) D_d^T D_d d(t) - \gamma^2 d^T(t) d(t) \\ &= e^T(t) P\left[(A - HC)e(t) + \left(B_d - HD_d\right)d(t)\right. \\ &\qquad \left. + g(x(t),t) - g(\hat{x}(t),t)\right] \\ &\quad + \left[(A - HC)e(t) + g(x(t),t) - g(\hat{x}(t),t)\right. \\ &\qquad \left. + \left(B_d - HD_d\right)d(t)\right]^T Pe(t) \end{aligned}$$

$$
\begin{aligned}
&+ e^T(t) C^T C e(t) + e^T(t) C^T D_d d(t) \\
&+ d^T(t) D_d^T C e(t) + d^T(t) D_d^T D_d d(t) \\
&- \gamma^2 d^T(t) d(t) \\
&\le e^T(t) \left[P(A - HC) + (A - HC)^T P + \varepsilon_1^{-1} P P^T \right. \\
&\qquad \left. + C^T C + \varepsilon_1 \rho^2 I \right] e(t) + e^T(t) \left[C^T D_d \right] d(t) \\
&+ d^T(t) \left[D_d^T C \right] e(t) + d^T(t) D_d^T D_d d(t) \\
&- \gamma^2 d^T(t) d(t) + e^T(t) \left[P(B_d - HD_d) \right] d(t) \\
&+ d^T(t) \left[(B_d - HD_d)^T P \right] e(t) \\
&= \begin{bmatrix} e(t) \\ d(t) \end{bmatrix}^T \begin{bmatrix} M_1 & M_3 \\ M_3^T & M_2 \end{bmatrix} \begin{bmatrix} e(t) \\ d(t) \end{bmatrix},
\end{aligned}
\tag{21}
$$

where

$$
\begin{aligned}
M_1 &= P(A - HC) + (A - HC)^T P + C^T C + \varepsilon_1^{-1} P P^T + \varepsilon_1 \rho^2 I, \\
M_2 &= D_d^T D_d - \gamma^2 I, \\
M_3 &= C^T D_d + P(B_d - HD_d).
\end{aligned}
\tag{22}
$$

According to (14) and Schur theory, we can obtain that

$$
H(e, d) = \dot{V}(t) + r^T(t) r(t) - \gamma^2 d^T(t) d(t) < 0. \tag{23}
$$

For any given time $t > 0$, integration of (23) from 0 to t yields

$$
\int_0^{+\infty} r^T(t) r(t) < \gamma^2 \int_0^{+\infty} d^T(t) d(t). \tag{24}
$$

Thus, the inequality $\|r(t)\|_\infty \le \gamma \|d(t)\|_\infty$ holds. This completes the proof. □

Theorem 7. *Given a constant $\beta > 0$, in the condition of $d(t) = 0$, the system (10) is asymptotically stable and satisfies $\|r(t)\|_- \ge \beta \|f(t)\|_-$, if there exists a positive symmetrical matrix Q, scalar $\eta_1 > 0$, satisfying the following LMI:*

$$
\begin{bmatrix} N_1 & N_3 & Q \\ N_3^T & N_2 & 0 \\ Q^T & 0 & -\eta_1 I \end{bmatrix} < 0, \tag{25}
$$

where

$$
\begin{aligned}
N_1 &= Q(A - HC) + (A - HC)^T Q - C^T C + \eta_1 \rho^2 I, \\
N_2 &= -D_f^T D_f + \beta^2 I, \\
N_3 &= -C^T D_f + Q\left(B_f - HD_f\right).
\end{aligned}
\tag{26}
$$

Proof. We choose a Lyapunov function of the form:

$$
V(t) = e^T(t) Q e(t), \tag{27}
$$

where Q is a positive symmetrical matrix. In the condition of $d(t) = 0$, when the system faults $f(t) = 0$, we have

$$
\begin{aligned}
\dot{V}(t) &= e^T(t) Q \dot{e}(t) + \dot{e}^T(t) Q e(t) \\
&= e^T(t) Q \left[(A - HC) e(t) + g(x(t), t) - g(\hat{x}(t), t) \right] \\
&\quad + \left[(A - HC) e(t) + g(x(t), t) - g(\hat{x}(t), t) \right]^T Q e \\
&= e^T(t) \left[Q(A - HC) + (A - HC)^T Q \right] e(t) \\
&\quad + e^T(t) Q \left[g(x(t), t) - g(\hat{x}(t), t) \right] \\
&\quad + \left[g(x(t), t) - g(\hat{x}(t), t) \right]^T e Q.
\end{aligned}
\tag{28}
$$

According to Lemma 5 and Assumption 3, we have

$$
\begin{aligned}
&2 e^T(t) Q \left[g(x(t), t) - g(\hat{x}(t), t) \right] \\
&\le \eta_1^{-1} e^T(t) Q Q^T e(t) + \eta_1 \left(g(x(t), t) - g(\hat{x}(t), t) \right)^T \\
&\quad \times \left(g(x(t), t) - g(\hat{x}(t), t) \right) \\
&\le \eta_1^{-1} e^T(t) Q Q^T e(t) + \eta_1 \rho^2 e^T(t) e(t).
\end{aligned}
\tag{29}
$$

Thus

$$
\begin{aligned}
\dot{V}(t) \le e^T(t) &\left[Q(A - HC) + (A - HC)^T Q \right. \\
&\left. + \eta_1^{-1} P P^T + \eta_1 \rho^2 I \right] e(t).
\end{aligned}
\tag{30}
$$

According to (25), we can obtain that $\dot{V}(t) \le 0$. So the system (10) is asymptotically stable in the condition of $f(t) = 0$.

When the system faults $f(t) \ne 0$, define

$$
H(e, f) = \dot{V}(t) + \beta^2 \|f(t)\|_\infty - \|r(t)\|_\infty. \tag{31}
$$

So we have

$$
\begin{aligned}
H(e, f) &= e^T(t) Q \dot{e}(t) + \dot{e}^T(t) Q e(t) - e^T(t) C^T C e(t) \\
&\quad - e^T(t) C^T D_f f(t) - f^T(t) D_f^T C e(t) \\
&\quad - f^T(t) D_f^T D_f f(t) + \beta^2 f^T(t) f(t) \\
&= e^T(t) Q \left[(A - HC) e(t) + \left(B_f - HD_f \right) f(t) \right. \\
&\qquad \left. + g(x(t), t) - g(\hat{x}(t), t) \right] \\
&\quad + \left[(A - HC) e(t) + g(x(t), t) - g(\hat{x}(t), t) \right. \\
&\qquad \left. + \left(B_f - HD_f \right) f(t) \right]^T Q e(t) - e^T(t) C^T C e(t) \\
&\quad - e^T(t) C^T D_f d(t) - f^T(t) D_f^T C e(t) \\
&\quad - f^T(t) D_f^T D_f f(t) + \beta^2 f^T(t) f(t) \\
&\le e^T(t) \left[Q(A - HC) + (A - HC)^T Q + \eta_1^{-1} Q Q^T \right. \\
&\qquad \left. - C^T C + \eta_1 \rho^2 I \right] e(t) - e^T(t) \left[C^T D_f \right] f(t)
\end{aligned}
$$

$$
\begin{aligned}
&- f^T(t)\left[D_f^T C\right] e(t) - f^T(t) D_f^T D_f f(t) \\
&+ \beta^2 f^T(t) f(t) - e^T(t)\left[Q\left(B_d - HD_d\right)\right] f(t) \\
&- f^T(t)\left[\left(B_f - HD_f\right)^T Q\right] e(t) \\
&= \begin{bmatrix} e(t) \\ f(t) \end{bmatrix}^T \begin{bmatrix} N_1 & N_3 \\ N_3^T & N_2 \end{bmatrix} \begin{bmatrix} e(t) \\ f(t) \end{bmatrix},
\end{aligned} \tag{32}
$$

where

$$
\begin{aligned}
N_1 &= Q(A - HC) + (A - HC)^T Q - C^T C \\
&\quad + \eta_1^{-1} Q Q^T + \eta_1 \rho^2 I, \\
N_2 &= -D_f^T D_f + \beta^2 I, \\
N_3 &= -C^T D_f + Q\left(B_f - HD_f\right).
\end{aligned} \tag{33}
$$

According to Schur theory, we can obtain that

$$
H(e, f) = \dot{V}(t) + \beta^2 f^T(t) f(t) - r^T(t) r(t) < 0. \tag{34}
$$

For any given time $t > 0$, integration of (34) from 0 to t yields

$$
\int_0^{+\infty} r^T(t) r(t) > \beta^2 \int_0^{+\infty} f^T(t) f(t). \tag{35}
$$

Thus, the inequality $\|r(t)\|_- > \beta \|f(t)\|_-$ holds. This completes the proof. □

Theorem 8. *Given constants $\gamma > 0$ and $\beta > 0$, the system (10) is asymptotically stable and satisfies $\|r(t)\|_\infty \le \gamma \|d(t)\|_\infty$ and $\|r(t)\|_- \ge \beta \|f(t)\|_-$, if there exist matrices P, Q, and H, scalar $\varepsilon_1 > 0$, $\eta_1 > 0$ satisfying matrix inequality:*

$$
\begin{bmatrix} M_1 & M_3 & P \\ M_3^T & M_2 & 0 \\ P^T & 0 & -\varepsilon_1 I \end{bmatrix} < 0, \qquad \begin{bmatrix} N_1 & N_3 & Q \\ N_3^T & N_2 & 0 \\ Q^T & 0 & -\eta_1 I \end{bmatrix} < 0, \tag{36}
$$

where

$$
\begin{aligned}
M_1 &= P(A - HC) + (A - HC)^T P + C^T C + \varepsilon_1 \rho^2 I, \\
M_2 &= D_d^T D_d - \gamma^2 I, \\
M_3 &= C^T D_d + P\left(B_d - HD_d\right), \\
N_1 &= Q(A - HC) + (A - HC)^T Q - C^T C + \eta_1 \rho^2 I, \\
N_2 &= -D_f^T D_f + \beta^2 I, \\
N_3 &= -C^T D_f + Q\left(B_f - HD_f\right).
\end{aligned} \tag{37}
$$

Proof. By combining Theorems 6 and 7, we have Theorem 8. This completes the proof. □

Remark 9. Theorem 6 considers the robustness of residual signals to system uncertainty, and Theorem 7 considers the sensitivity of residual signals to system faults. Theorem 8 investigates the optimization of gain matrix H by taking into account the robustness of residual signals to system uncertainty and sensitivity of residual signals to system faults simultaneously. If we iteratively use Theorem 8, we can get the optimized solution of the performance indices γ, β and gain matrix H by using LMI toolbox in MatLab.

4. Fault Detection Threshold

In the above sections, we have investigated the optimization of the value of gain matrix H in terms of LMIs. In this section, we will investigate the calculation of threshold for fault detection.

Theorem 10. *Suppose Assumptions 1–3 hold. Consider the dynamic system described by (1), (2) and the FTA described by (4)~(9); let the initial state and output of the FTA be $\hat{x}_k(0) = x(0)$, $\hat{y}_k(0) = y(0)$ $(k = 1, 2, \ldots)$, respectively. If the following inequality holds*

$$
\begin{aligned}
\left\|r_k(t)\right\| > L_w P \sup_{t,\tau\in[t_a,t_b]} &\left\|C\Phi(t,\tau)\left(B_d - HD_d\right)\right\| \\
&+ \left(\left(\sup_{t,\tau\in[t_a,t_b]} \left\|C\Phi(t,\tau)\right\| L_w P \right.\right. \\
&\qquad \left.\left. \times \sup_{t,\tau\in[t_a,t_b]} \left\|\Phi(t,\tau)\left(B_d - HD_d\right)\right\|\right) \right. \\
&\qquad \left. \times \left(\sup_{t,\tau\in[t_a,t_b]} \left\|\Phi(t,\tau)\right\|\right)^{-1}\right) \\
&\times \exp \rho \sup_{t,\tau\in[t_a,t_b]} \left\|\Phi(t,\tau)\right\| P
\end{aligned} \tag{38}
$$

then there is fault occurring in the system.

Proof. Without loss of generality, we assume $t \in [t_a, t_b]$ and $t_b - t_a = P$.

Subtracting (4) from system equation (1) and subtracting (5) from system equation (2) result in the estimation error dynamics:

$$
\begin{aligned}
\dot{e}(t) &= (A - HC) e(t) + \left(B_f - HD_f\right) f(t) \\
&\quad + \left(B_d - HD_d\right) d(t) + g(x(t), t) \\
&\quad - g(\hat{x}(t), t) - B_f \hat{f}(t), \\
r(t) &= Ce(t) + D_f f(t) + D_d d(t).
\end{aligned} \tag{39}
$$

In the condition of $\hat{f}(t) = 0$, we have

$$
\begin{aligned}
\dot{e}(t) &= (A - HC) e(t) + \left(B_f - HD_f\right) f(t) \\
&\quad + \left(B_d - HD_d\right) d(t) + g(x(t), t) - g(\hat{x}(t), t), \\
r(t) &= Ce(t) + D_f f(t) + D_d d(t).
\end{aligned} \tag{40}
$$

The solution of (40) is

$$e_k(t) = \Phi(t,t_a)\, e_k(t_a) + \int_{t_a}^{t} \Phi(t,\tau)\left[\left(B_f - HD_f\right) f(\tau) + g_k(x(\tau),\tau) - g_k(\hat{x}(\tau),\tau) + \left(B_d - HD_d\right) d(\tau)\right] d\tau, \tag{41}$$

$$r_k(t) = C\Phi(t,t_a)\, e_k(t_a) + \int_{t_a}^{t} C\Phi(t,\tau)\left[\left(B_f - HD_f\right) f(\tau) + g_k(x(\tau),\tau) - g_k(\hat{x}(\tau),\tau) + \left(B_d - HD_d\right) d(\tau)\right] d\tau, \tag{42}$$

where $\Phi(t) = L^{-1}[(sI - (A - HC))^{-1}]$; L^{-1} denotes inverse Laplacian transform.

Due to $\hat{x}_k(0) = x(0)$, $\hat{y}_k(0) = y(0)$ $(k = 1, 2, \ldots)$, we have

$$\hat{y}_{k+1}(t_a) = C\hat{x}_{k+1}(t_a) = C\hat{x}_k(t_a) = \hat{y}_k(t_a), \qquad r_k(t_a) = 0, \quad e_k(t_a) = 0. \tag{43}$$

Substituting (43) into (42) yields

$$r_k(t) = \int_{t_a}^{t} C\Phi(t,\tau)\left[\left(B_f - HD_f\right) f(\tau) + g_k(x(\tau),\tau) - g_k(\hat{x}(\tau),\tau) + \left(B_d - HD_d\right) d(\tau)\right] d\tau. \tag{44}$$

According to Assumptions 1–3, the time weighted norm of (44) is

$$\begin{aligned}\left\|r_k(t)\right\| &\le \int_{t_a}^{t} \left\|C\Phi(t,\tau)\left(B_f - HD_f\right) f(\tau)\right\| d\tau \\ &\quad + \int_{t_a}^{t} \left\|C\Phi(t,\tau)\left(g_k(x(\tau),\tau) - g_k(\hat{x}(\tau),\tau)\right)\right\| d\tau \\ &\quad + \int_{t_a}^{t} \left\|C\Phi(t,\tau)\left(B_d - HD_d\right)\right\| \left\|d(\tau)\right\| d\tau.\end{aligned} \tag{45}$$

In the condition of $f(t) = 0$, we have

$$\begin{aligned}\left\|r_k(t)\right\| &\le \int_{t_a}^{t} \left\|C\Phi(t,\tau)\left(g_k(x(\tau),\tau) - g_k(\hat{x}(\tau),\tau)\right)\right\| d\tau \\ &\quad + \int_{t_a}^{t} \left\|C\Phi(t,\tau)\left(B_d - HD_d\right)\right\| \left\|d(\tau)\right\| d\tau.\end{aligned} \tag{46}$$

According to (41), we have

$$\begin{aligned}\left\|e_k(t)\right\| &\le \int_{t_a}^{t} \rho \left\|\Phi(t,\tau)\right\| \left\|e_k(\tau)\right\| d\tau \\ &\quad + \int_{t_a}^{t} \left\|\Phi(t,\tau)\left(B_d - HD_d\right)\right\| \left\|d(\tau)\right\| d\tau \\ &\le \int_{t_a}^{t} \rho \left\|\Phi(t,\tau)\right\| \left\|e_k(\tau)\right\| d\tau \\ &\quad + L_w P \sup_{t,\tau\in[t_a,t_b]} \left\|\Phi(t,\tau)\left(B_d - HD_d\right)\right\|.\end{aligned} \tag{47}$$

Using Gronwall-Bellman inequality, (47) can be simplified as

$$\begin{aligned}\left\|e_k(t)\right\| &\le L_w P \sup_{t,\tau\in[t_a,t_b]} \left\|\Phi(t,\tau)\left(B_d - HD_d\right)\right\| \\ &\quad \times \exp\rho \sup_{t,\tau\in[t_a,t_b]} \left\|\Phi(t,\tau)\right\| (t - t_a),\end{aligned} \tag{48}$$

where exp denotes exponential function. Substituting (48) into (46) yields

$$\begin{aligned}\left\|r_k(t)\right\| &\le \int_{t_a}^{t} \left\|C\Phi(t,\tau)\left(g_k(x(\tau),\tau) - g_k(\hat{x}(\tau),\tau)\right)\right\| d\tau \\ &\quad + \int_{t_a}^{t} \left\|C\Phi(t,\tau)\left(B_d - HD_d\right)\right\| \left\|d(\tau)\right\| d\tau \\ &\le \int_{t_a}^{t} \rho \left\|C\Phi(t,\tau)\right\| \cdot \left\|e_k(t)\right\| d\tau \\ &\quad + \int_{t_a}^{t} \left\|C\Phi(t,\tau)\left(B_d - HD_d\right)\right\| \left\|d(\tau)\right\| d\tau \\ &\le L_w P \sup_{t,\tau\in[t_a,t_b]} \left\|C\Phi(t,\tau)\left(B_d - HD_d\right)\right\| \\ &\quad + \left(\left(\sup_{t,\tau\in[t_a,t_b]} \left\|C\Phi(t,\tau)\right\| L_w P \times \sup_{t,\tau\in[t_a,t_b]} \left\|\Phi(t,\tau)\left(B_d - HD_d\right)\right\|\right) \times \left(\sup_{t,\tau\in[t_a,t_b]} \left\|\Phi(t,\tau)\right\|\right)^{-1}\right) \\ &\quad \times \exp\rho \sup_{t,\tau\in[t_a,t_b]} \left\|\Phi(t,\tau)\right\| (t - t_a) \\ &\le L_w P \sup_{t,\tau\in[t_a,t_b]} \left\|C\Phi(t,\tau)\left(B_d - HD_d\right)\right\| \\ &\quad + \left(\left(\sup_{t,\tau\in[t_a,t_b]} \left\|C\Phi(t,\tau)\right\| L_w P \times \sup_{t,\tau\in[t_a,t_b]} \left\|\Phi(t,\tau)\left(B_d - HD_d\right)\right\|\right) \times \left(\sup_{t,\tau\in[t_a,t_b]} \left\|\Phi(t,\tau)\right\|\right)^{-1}\right) \\ &\quad \times \exp\rho \sup_{t,\tau\in[t_a,t_b]} \left\|\Phi(t,\tau)\right\| P.\end{aligned} \tag{49}$$

If faults occur in the system, then

$$\begin{aligned}\left\|r_k(t)\right\| > {} & L_w P \sup_{t,\tau\in[t_a,t_b]} \left\|C\Phi(t,\tau)\left(B_d - HD_d\right)\right\| \\ & + \left(\left(\sup_{t,\tau\in[t_a,t_b]} \left\|C\Phi(t,\tau)\right\| L_w P \right.\right. \\ & \qquad \left.\left. \times \sup_{t,\tau\in[t_a,t_b]} \left\|\Phi(t,\tau)\left(B_d - HD_d\right)\right\|\right) \\ & \qquad \times \left(\sup_{t,\tau\in[t_a,t_b]} \left\|\Phi(t,\tau)\right\|\right)^{-1}\right) \\ & \times \exp\rho \sup_{t,\tau\in[t_a,t_b]} \left\|\Phi(t,\tau)\right\| P.\end{aligned} \tag{50}$$

If the following inequality holds

$$\begin{aligned}\left\|r_k(t)\right\| \le {} & L_w P \sup_{t,\tau\in[t_a,t_b]} \left\|C\Phi(t,\tau)\left(B_d - HD_d\right)\right\| \\ & + \left(\left(\sup_{t,\tau\in[t_a,t_b]} \left\|C\Phi(t,\tau)\right\| L_w P \right.\right. \\ & \qquad \left.\left. \times \sup_{t,\tau\in[t_a,t_b]} \left\|\Phi(t,\tau)\left(B_d - HD_d\right)\right\|\right) \\ & \qquad \times \left(\sup_{t,\tau\in[t_a,t_b]} \left\|\Phi(t,\tau)\right\|\right)^{-1}\right) \\ & \times \exp\rho \sup_{t,\tau\in[t_a,t_b]} \left\|\Phi(t,\tau)\right\| P\end{aligned} \tag{51}$$

then there are no faults occurring in the system.

This completes the proof. □

In the presence of unstructured modeling uncertainty, we have to determine the upper bounds of the residual signals for fault detection, referred to as the threshold. Theorem 10 investigated the calculation of threshold for fault detection. Once the residual signals exceed the threshold, it indicates that system faults occur. If the residual signal is below the threshold, there is no fault occurring. Moreover, we can use the residual evaluation function $\|r(t)\|_2$ to detect system faults [20, 21].

5. Simulation Results

In this section, we use the proposed method to detect faults for a class of uncertain nonlinear systems. Let us consider the uncertain nonlinear system with parameters as follows:

$$\begin{aligned}\dot{x}(t) = {} & \begin{bmatrix}-0.38 & 0\\ 0 & -0.59\end{bmatrix} x(t) + \begin{bmatrix}1\\1\end{bmatrix} u \\ & + \begin{bmatrix}0.1\sin(t) & \\ & 0.1\sin(t)\end{bmatrix} x(t) \\ & + \begin{bmatrix}0.2\\0.2\end{bmatrix} d(t) + \begin{bmatrix}0.1\\0.1\end{bmatrix} f(t), \\ y(t) = {} & \begin{bmatrix}1 & 1\end{bmatrix} x(t) + 0.1 f(t) + 0.1 d(t).\end{aligned} \tag{52}$$

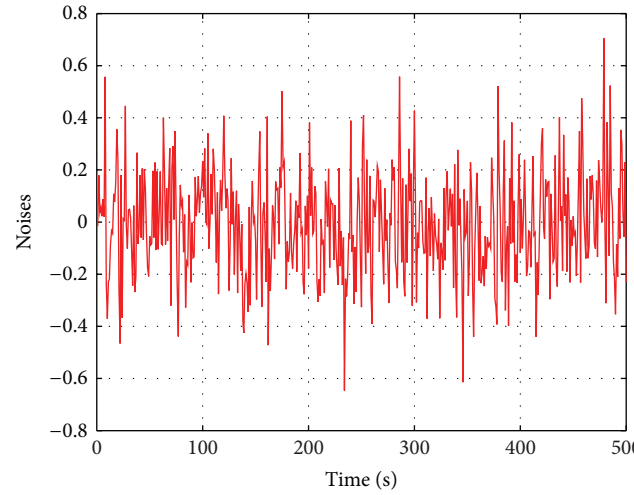

Figure 1: White noise signal.

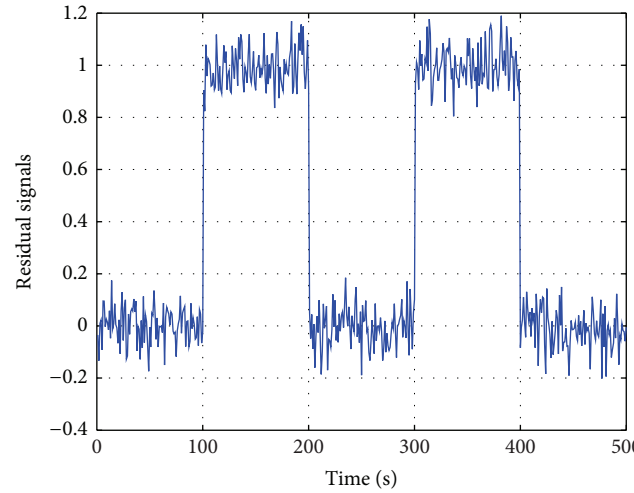

Figure 2: Generated residual signal.

Let $\gamma = 0.3$, let $\beta = 0.7$, and let $d(t)$ be white noise with energy 0.5. According to Theorem 8, the gain matrix of FTA can be determined: $H = [0.2071, 0.1832]^T$. According to Theorem 10, the threshold for fault detection is 0.426. The white noise signal, generated residual signal are shown in Figures 1 and 2, respectively.

From Figure 2, we can clearly see that the residual signal is below the threshold at time $t < 100$ s. Therefore, there is no fault occurring at time $t < 100$ s. At time $100\text{ s} < t < 200\text{ s}$, the residual signal exceeds the threshold; it indicates that system fault occurs. Next, we use residual evaluation function $\|r(t)\|_2$ to detect system faults. Figure 3 shows the evolution of residual evaluation function $\|r(t)\|_2$. From Figure 3 we can see that, at time $100\text{ s} < t < 200\text{ s}$, the residual evaluation function $\|r(t)\|_2$ jumps from 0.1 to 5.1; it indicates that system fault occurs. It can be seen from the simulation results that the proposed approach can improve not only the sensitivity of the FTA to system faults, but also the robustness of the FTA to systems uncertainty.

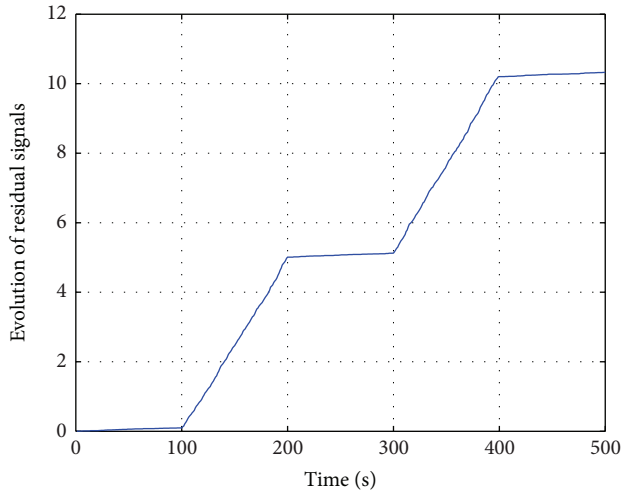

Figure 3: Evolution of residual evaluation function.

6. Conclusions

This paper has proposed a fault detection scheme for a class of uncertain nonlinear systems. The main contribution of this paper is to utilize robust control theory and multiobjective optimization algorithm to design the gain matrix of FTA. The gain matrix of FTA is designed to minimize the effects of system uncertainty on residual signals while maximizing the effects of system faults on residual signals. The calculation of the gain matrix is given in terms of LMIs formulations. The selection of threshold for fault detection is rigorously investigated as well. In the end, an illustrative example has demonstrated the validity and applicability of the proposed approach.

Conflict of Interests

The authors declare that there is no conflict of interests regarding the publication of this paper.

Acknowledgments

This work is supported by National Natural Science Foundation of China (nos. 51407078, 61201124) and Special Fund of East China University of Science and Technology for Basic Scientific Research (WJ1313004-1, WH1114027, H200-4-13192, and WH1414022).

References

[1] P. M. Frank, "Fault diagnosis in dynamic systems using analytical and knowledge-based redundancy—a survey and some new results," *Automatica*, vol. 26, no. 3, pp. 459–474, 1990.

[2] R. Isermann, "Process fault detection based on modeling and estimation methods: a survey," *Automatica*, vol. 20, no. 4, pp. 387–404, 1984.

[3] K. Zhang, B. Jiang, and V. Cocquempot, "Fast adaptive fault estimation and accommodation for nonlinear time-varying delay systems," *Asian Journal of Control*, vol. 11, no. 6, pp. 643–652, 2009.

[4] X. Zhang, T. Parisini, and M. M. Polycarpou, "Sensor bias fault isolation in a class of nonlinear systems," *IEEE Transactions on Automatic Control*, vol. 50, no. 3, pp. 370–376, 2005.

[5] A. T. Vemuri, "Sensor bias fault diagnosis in a class of nonlinear systems," *IEEE Transactions on Automatic Control*, vol. 46, no. 6, pp. 949–954, 2001.

[6] W. Zhang, X.-S. Cai, and Z.-Z. Han, "Robust stability criteria for systems with interval time-varying delay and nonlinear perturbations," *Journal of Computational and Applied Mathematics*, vol. 234, no. 1, pp. 174–180, 2010.

[7] L. Guo and H. Wang, "Fault detection and diagnosis for general stochastic systems using B-spline expansions and nonlinear filters," *IEEE Transactions on Circuits and Systems. I. Regular Papers*, vol. 52, no. 8, pp. 1644–1652, 2005.

[8] X. Zhang, M. M. Polycarpou, and T. Parisini, "Fault diagnosis of a class of nonlinear uncertain systems with Lipschitz nonlinearities using adaptive estimation," *Automatica*, vol. 46, no. 2, pp. 290–299, 2010.

[9] J. Fan and Y. Wang, "Fault detection and diagnosis of nonlinear non-Gaussian dynamic processes using kernel dynamic independent component analysis," *Information Sciences*, vol. 259, pp. 369–379, 2014.

[10] P. Tadić and Ž. Durović, "Particle filtering for sensor fault diagnosis and identification in nonlinear plants," *Journal of Process Control*, vol. 24, no. 4, pp. 401–409, 2014.

[11] W. Chen and M. Saif, "An iterative learning observer for fault detection and accommodation in nonlinear time-delay systems," *International Journal of Robust and Nonlinear Control*, vol. 16, no. 1, pp. 1–19, 2006.

[12] B. Yan, Z. Tian, and S. Shi, "A novel distributed approach to robust fault detection and identification," *International Journal of Electrical Power & Energy Systems*, vol. 30, no. 5, pp. 343–360, 2008.

[13] W. Zhang, H. Su, H. Wang, and Z. Han, "Full-order and reduced-order observers for one-sided Lipschitz nonlinear systems using Riccati equations," *Communications in Nonlinear Science and Numerical Simulation*, vol. 17, no. 12, pp. 4968–4977, 2012.

[14] W. Zhang, H.-S. Su, Y. Liang, and Z.-Z. Han, "Non-linear observer design for one-sided Lipschitz systems: an linear matrix inequality approach," *IET Control Theory and Applications*, vol. 6, no. 9, pp. 1297–1303, 2012.

[15] W. Zhang, H. Su, F. Zhu, and D. Yue, "A note on observers for discrete-time lipschitz nonlinear systems," *IEEE Transactions on Circuits and Systems II: Express Briefs*, vol. 59, no. 2, pp. 123–127, 2012.

[16] X. Zhang, M. M. Polycarpou, and T. Parisini, "A robust detection and isolation scheme for abrupt and incipient faults in nonlinear systems," *IEEE Transactions on Automatic Control*, vol. 47, no. 4, pp. 576–593, 2002.

[17] Y. Bingyong, T. Zuohua, and L. Dongmei, "Fault diagnosis for a class of nonlinear stochastic time-delay systems," *Control and Instruments in Chemical Industry*, vol. 34, no. 1, pp. 12–15, 2007.

[18] M. Zhong, S. X. Ding, J. Lam, and H. Wang, "An LMI approach to design robust fault detection filter for uncertain LTI systems," *Automatica*, vol. 39, no. 3, pp. 543–550, 2003.

[19] S. Xie, S. Tian, and Y. Fu, "A new algorithm of iterative learning control with forgetting factors," in *Proceedings of the 8th Control, Automation, Robotics and Vision Conference (ICARCV '04)*, vol. 1, pp. 625–630, 2004.

[20] H. Yang and M. Saif, "State observation, failure detection and isolation (FDI) in bilinear systems," *International Journal of Control*, vol. 67, no. 6, pp. 901–920, 1997.

[21] D. Yu and D. N. Shields, "A bilinear fault detection filter," *International Journal of Control*, vol. 68, no. 3, pp. 417–430, 1997.

Hindawi Publishing Corporation
Mathematical Problems in Engineering
Volume 2015, Article ID 783275, 8 pages
http://dx.doi.org/10.1155/2015/783275

Research Article

Extremum Seeking Based Fault-Tolerant Cooperative Control for Multiagent Systems

Fu Jiang, Xiaoyong Zhang, Wentao Yu, Heng Li, Jun Peng, and Yong He

School of Information Science and Engineering, Central South University, Changsha 410075, China

Correspondence should be addressed to Xiaoyong Zhang; zhangxy@csu.edu.cn

Received 18 July 2014; Revised 17 October 2014; Accepted 27 October 2014

Academic Editor: Fanglai Zhu

We propose a novel fault-tolerant cooperative control strategy for multiagent systems. A set of unknown input observers for each agent are constructed for fault detection. Then a real-time adaptive extremum seeking algorithm is utilized for adaptive approximation of fault parameter. We prove that the consensus can be still reached by regulating the interconnection weights and changing the connection topology of the fault agent. A numerical simulation example is given to illustrate the feasibility and effectiveness of the proposed method.

1. Introduction

Recent years have seen a growing interest in the cooperative control of multiagent systems [1, 2]. Cooperative multiagent system refers to the concept that multiple agents work together to complete a task or achieve a target state according to the cooperative control law [3]. With the rapid development of embedded systems, complex algorithms can be effectively implemented in multiagent systems.

In multiagent systems, a fault occurring in any agent may have an impact on other agents, which is different from the traditional faults occurring in isolated systems [4]. Moreover, when faults occur to agents, the topology of the multiagent system may change [5]. Therefore, fault detection should perform fast detecting to avoid affecting other agents, and fault-tolerant control should make the system has endurance to the failures while keeping the topology structure.

Fault detection of multiagent systems has to be completed before fault tolerance. In the last decade, scholars proposed different methods for fault detection, such as observer-based methods [6, 7], parity equation [8], and the identification-based method [9]. Shames et al. derived sufficient conditions for the existence of unknown input observers for second-order linear time invariant systems [6], which constituted the basis of the current study. Then, they extended these conditions to imprecise models [7]. For parity space method, residual errors are obtained by collecting system input and output. Chan et al. developed a parity space-based estimator, which is sensitive to specific faults [8]. The literature [9] overviewed the problem of identifying. The identification-based method means that residuals for output variables are generated with adaptive nonparametric or parametric models. However, all these methods need a great amount of computations and long computing time when the system has large numbers of agents, which are not acceptable for practice.

Once a faulty agent is detected, fault-tolerant control is taken for handling faults. In this paper, fault-tolerant control is divided into two steps, namely, fault parameter approximation and adjusting some interconnection weights. Adaptive fault parameter approximation is developed on the basis of parameter estimation. Generally, fault parameters are estimated using the nonlinear neural network [10, 11]. We transform the fault parameter approximation problem into the optimization problem by using extremum seeking. Compared with the classical neural network method, the advantages of the proposed approach are that the approximation is real-time and online without any offline training.

Moreover, the extremum seeking based parameter approximation is significantly simplified. The design process of extremum seeking does not call for the understanding of the input and output characteristics of the system [12, 13].

In step two, the faulty system is recovered by adjusting some weights of the cooperative protocol. There have been several studies in recovering faulty multiagent systems. Semsar-Kazerooni and Khorasani [14] and Azizi and Khorasani [15] used fault-tolerant control algorithms to recover an actuator fault detected by FDI. Furthermore, Azizi and Khorasani put forward a two-level architecture which contains partial recovery and cooperative recovery [15]. Yang et al. proposed a cooperative protocol to adjust fault parameters for a target aggregation problem of nonlinear multiagent systems [5]. However, in these studies, the cooperative fault-tolerant control was used to adjust interconnection weights without isolating out the faulty agent, which leads to a lot of calculation when faulty agent has a number of neighbors.

The rest of the paper is organized as follows. Section 2 provides some preliminary knowledge and formulates the problems. Section 3 focuses on fault detection. In Section 4, an adaptive fault parameter approximation algorithm using extremum seeking is proposed. In Section 5, the cooperative fault-tolerant control of multiagent systems is discussed. In Section 6, an example of a multiagent team is given to demonstrate the effectiveness of the proposed scheme. In Section 7, conclusion is drawn.

2. Preliminary Knowledge

Agents and their link topology are mapped based on the graph theory [16]. We consider a system constituted by n agents; $G(v, \varepsilon)$ is an undirected graph with vertex set v and edge set ε, where $i \in v$ represents agent i. The edge $(j, i) \in \varepsilon$ denotes a connection between agent j and agent i, and a_{ij} is the weight of the interconnection. The set $N_i = \{j \in v : \{i, j\} \in \varepsilon\}$ represents all the neighboring agents that are interconnected with i. Agent i is supposed to have a double-integrator dynamics:

$$\begin{aligned} \dot{p}_i(t) &= q_i(t), \\ \dot{q}_i(t) &= u_i(t), \end{aligned} \tag{1}$$

where $p_i(t) \in R$ and $q_i(t) \in R$ are the position and velocity of agent i and u_i is the controlled input based on the following formula:

$$\begin{aligned} u_i(t) = \sum_{j \in N_i} a_{ij} \left[\left(p_j(t) - p_i(t) \right) + \gamma \left(q_j(t) - q_i(t) \right) \right] \\ + \beta_i (t - T_i) f_i. \end{aligned} \tag{2}$$

Formula (2) achieves the position and velocity consensus. The term $\beta_i(t - T_i)$ characterizes the time jump function of an actuator fault, T_i denotes faulty time of agent i, *if* $t \geq T_i$, $\beta_i = 1$, *else* $\beta_i = 0$. The variable $f_i \in R$ is the fault parameter of agent i. The system dynamics in the presence of a fault are written as follows:

$$\begin{aligned} \dot{x}(t) &= Ax(t) + B_f f, \\ y(t) &= Cx(t), \end{aligned} \tag{3}$$

where $x = [p_1, p_2, \ldots, p_N, q_1, q_2, \ldots, q_N]^{\mathrm{T}}$, $f = [f_1, f_2, \ldots, f_N] \in R^n$, $A, C \in R^{2n \times 2n}$, $B_f \in R^{2n \times 2n}$, $x, y \in R^{2n}$, and $f \in R^{2n}$. We designed $C = I_{2n}$ (I_n means an identity matrix with the dimension $n \times n$) to observe all the states of the multiagent system. The following text gave some details of A for the velocity consensus and position consensus problems:

$$A = \begin{bmatrix} 0_n & I_n \\ -L & -B \end{bmatrix}, \quad \text{or} \quad A = \begin{bmatrix} 0_n & I_n \\ -L & -\gamma L \end{bmatrix}, \tag{4}$$

where $B = \mathrm{diag}(b, b, \ldots, b) \in R^{n \times n}$; L is the Laplacian matrix of the graph, where $l_{ij} = -a_{ij}$, *if* $(j, i) \in \varepsilon$, $i \neq j$ (otherwise, $l_{ij} = 0$), and $l_{ii} = -\sum_{i \neq j} l_{ij}$. By this definition, every row sum of the matrix L is zero, so the Laplacian matrix always has a zero eigenvalue, right eigenvector $v = (1, 1, \ldots, 1)^{\mathrm{T}}$, and $\mathrm{rank}(L) \leq n - 1$.

3. Fault Detection and Isolation

In this paper, a set of state observers are constructed for the second-order system using the unknown input observer (UIO) method. UIO refers to a robust fault diagnosis scheme for multiagent systems. Once an actuator failure is detected, residual errors are used to locate the faulty agent. In order to reduce the amount of calculation, only neighbors are observed for each agent. We rewrite (3) as

$$\begin{aligned} \dot{x}(t) &= Ax(t) + B_{f_{-i}} f_{-i}(t) + b_{f_i} \beta_i (t - T_i) f_i(t), \\ y(t) &= Cx(t), \end{aligned} \tag{5}$$

where $B_{f_{-i}}$ is B_f with the ith column deleted, b_{f_i} is the ith column of B_f, $f_{-i}(t)$ is f with the ith component deleted, and $f_i(t)$ is the ith component of f. Suppose graph $G(v, \varepsilon)$ is interconnected and the topology of the system is fixed.

A full-order observer for system (5) is described by

$$\begin{aligned} \dot{\chi}(t) &= F\chi(t) + TB_{f_{-i}} f_{-i}(t) + Ky(t), \\ \hat{x}(t) &= \chi(t) + Hy(t). \end{aligned} \tag{6}$$

Choosing the matrixes F, T, K, and H satisfies the following conditions:

$$\begin{aligned} F &= A - K_1 C - HCA, \qquad T = I - HC, \\ K &= K_1 + K_2, \qquad K_2 = FH, \qquad (HC - I) B_{f_{-i}} = 0. \end{aligned} \tag{7}$$

Then, there exists a UIO [7] for agent i as follows:

$$\begin{aligned} \dot{\chi}_i(t) &= F_i \chi_i(t) + T_i B_{f_{-i}} f_{-i}(t) + K_i y(t) \\ \hat{x}_i(t) &= \chi_i(t) + H_i y(t), \end{aligned} \tag{8}$$

where $\hat{x}_i(t) \in R^{2n}$ and $\chi_i(t) \in R^{2n}$ are the estimated state and the observer's state for agent i and F_i, T_i, K_i, and H_i are unknown matrices of appropriate dimension, which must be designed such that $\hat{x}_i$ will asymptotically converge to x. The unknown input observer is constructed to achieve the decoupling from $f_i(t)$, by designing matrixes F_i, T_i, K_i,

and H_i. Matrix F_i is a stability matrix; that is, it has all its eigenvalues in the left-hand side of the complex plane.

Thus, we can obtain the observer error and residual dynamics as

$$\begin{aligned} \dot{e}_i(t) &= F_i e_i(t) - T_i B_{f_{-i}} f_{-i}(t) \\ r_i(t) &= C e_i(t), \end{aligned} \tag{9}$$

where $e_i(t) = x(t) - \hat{x}_i(t)$ is the observer error and $r_i(t)$ is the corresponding residual, which is a fault indicator function that satisfies

$$\|r_i(t)\| = 0 \Longleftrightarrow \|f_{-i}(t)\| = 0. \tag{10}$$

The detection and isolation condition for fault $f_i(t)$ are given as follows:

$$\begin{aligned} \|r_i(t)\| &< \theta_{f_i}, \\ \|r_j(t)\| &\geq \theta_{f_j}, \end{aligned} \tag{11}$$

where θ_{f_i} and θ_{f_j} are isolation thresholds. If the above condition is satisfied, we can conclude that there is a fault affecting the system's ith component.

The proposed approach in this section is feasible if a single additive fault exists. In order to isolate multiple faults, one can repeat the abovementioned fault detection procedure for each of the potential fault combinations. We can derive similar observers for all faults and then adopt the detection and isolation condition to isolate each of them.

4. Extremum Seeking for Approximating Fault Parameters

4.1. Single Faulty Agent Case. The fault detection scheme makes use of observers called unknown input observer, as described in the previous section. Then residuals and their thresholds are designed to generate false alarms, which is used for fast network fault location. Under the assumption of only one faulty agent in the network (suppose the mth agent is faulty), the proposed extremum seeking framework is shown in Figure 1.

Theorem 1. *Let $J : R^n \to R$ be a sufficiently smooth objective function, and suppose the changing rate of fault parameter estimation $\hat{f}_m$ is much faster than the changing rate of fault parameter f_m:*

$$J\left(\hat{f}_m\right) = \left\| B_f^{-1}\left(\dot{\tilde{x}}(t) - A\tilde{x}(t)\right)\right\|^2, \tag{12}$$

where J has a global minimum ($\hat{f}_m^* = f_m$). Then with the fault parameter estimation scheme shown in Figure 1, $\hat{f}_m$ will converge to the extremum point $\hat{f}_m^*$.

Proof. Define the error between estimate state and real state by $\tilde{x}(t) = x(t) - \hat{x}(t)$:

$$\begin{aligned} \dot{\tilde{x}}(t) &= \dot{x}(t) - \dot{\hat{x}}(t) = A(x(t) - \hat{x}(t)) + B_f\left(f(t) - \hat{f}(t)\right) \\ &= A\tilde{x}(t) + B_f \tilde{f}(t). \end{aligned} \tag{13}$$

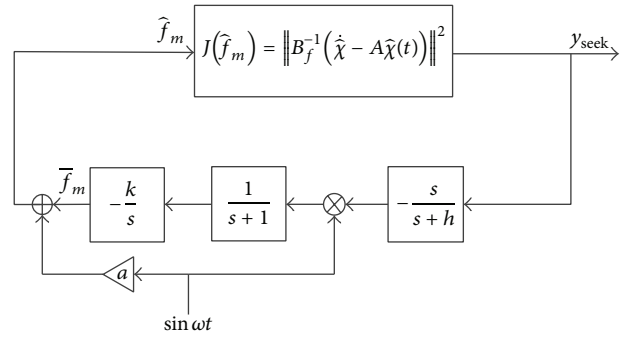

Figure 1: Structure of fault parameter estimation with extremum seeking.

Then we obtain

$$\begin{aligned} J\left(\hat{f}_m\right) &= \left\|B_f^{-1}\left(\dot{\tilde{x}}(t) - A\tilde{x}(t)\right)\right\|^2 = \left\|\tilde{f}(t)\right\|^2 \\ &= \left(\hat{f}_1 - f_1\right) + \cdots \left(\hat{f}_n - f_n\right) = \sum_{i=1}^{n}\left(\hat{f}_i - f_i\right)^2. \end{aligned} \tag{14}$$

From the definition above we have $J(f_m) = 0$, $J'' = 2$, and there is only one faulty agent in the network: $f_i = 0$ if $i \neq m$. Then formula (14) can be rewritten as

$$J\left(\hat{f}_m\right) = \sum_{i=1}^{n}\left(\hat{f}_i - f_i\right)^2 = J(f_m) + \frac{J''}{2}\left(\hat{f}_m - f_m\right)^2. \tag{15}$$

Denote the estimation error of $\hat{f}_m$ as $\tilde{f}_m = f_m - \overline{f}_m$, so we have

$$\tilde{f}_m = f_m - \hat{f}_m - a\sin(\omega t). \tag{16}$$

The dynamic model of the system can be summarized as follows:

$$\hat{f}_m = \overline{f}_m + a\sin(\omega t), \qquad \xi = [a\sin(\omega t)]\frac{s}{s+h} y_{\text{seek}}, \tag{17}$$

where $[a\sin(\omega t)]$ means the Laplace transforms of $a\sin(\omega t)$. Then we have

$$J\left(\hat{f}_m\right) = J(f_m) + \frac{J''}{2}\left(a\sin(\omega t) - \tilde{f}_m\right)^2. \tag{18}$$

Then we have

$$J\left(\hat{f}_m\right) = f_m + \frac{J''\tilde{f}_m^2}{2} - aJ''\tilde{f}_m\sin(\omega t) + \frac{a^2 J''\sin^2(\omega t)}{2}. \tag{19}$$

Then the signal which is processed with high-pass filter $s/(s+h)$ can be denoted as

$$\begin{aligned} &\frac{s}{s+h}\left[J\left(\hat{f}_m\right)\right] \\ &= \left[\frac{J''\tilde{f}_m^2}{2} - aJ''\tilde{f}_m\sin(\omega t) + \frac{a^2 J''\sin^2(\omega t)}{2}\right]. \end{aligned} \tag{20}$$

So we have

$$\xi = \frac{J''\widetilde{f}_m^2}{2}\sin(\omega t) - aJ''\widetilde{f}_m\sin^2(\omega t) + \frac{a^2J''\sin^3(\omega t)}{2},$$
$$\overline{f}_m = \left(-\frac{k}{s}\right)\frac{1}{s+1}\xi. \tag{21}$$

From $\widetilde{f}_m = f_m - \overline{f}_m$, we obtain

$$\dot{\widetilde{f}}_m = -\dot{\overline{f}}_m = -s\left(\left(-\frac{k}{s}\right)\frac{1}{s+1}\xi\right) = \frac{\beta}{s+1}\xi. \tag{22}$$

We arrive at

$$\begin{aligned}\dot{\widetilde{f}}_m &= \frac{k}{s+1}\left(\frac{J''\widetilde{f}_m^2}{2}\sin(\omega t) - aJ''\widetilde{f}_m \times\left(\frac{1-\cos(2\omega t)}{2}\sin^2(\omega t) + \frac{a^2J''\sin^3(\omega t)}{2}\right)\right)\\ &\approx -\frac{k}{2}aJ''\widetilde{f}_m = -ka\widetilde{f}_m.\end{aligned} \tag{23}$$

□

From formula (23), we find that the convergence rate is governed by the excitation signal gain a, integration time k, and the estimation error $\widetilde{f}_m$. However, to implement the algorithm, some suitable parameters have to be designed; for example, ω is designed large relative to k, a.

Remark 2. The principle of extremum seeking has been reported in the literature [12]. Since Wang and Krstic proved the stability of extremum seeking in 2000 [17], scholars have shown increasing interest in extremum seeking. In addition, $\sin\omega t$ (excitation signals) can be replaced by other excitation signals [13]. The assumption that the changing rate of $\widehat{f}_m$ is much faster than f_m can be fulfilled if the gain a and frequency ω of excitation signal are chosen large enough.

Remark 3. There are many other self-adapting algorithms to estimate fault parameters. However, comparing with extremum seeking, most of the algorithms are more difficult to design.

4.2. Multiple Faulty Agents Case. Theorem 1 gives the condition of parameter estimation when there is only a faulty agent in the network. When there are multiple faulty agents in the network, a multivariable extremum seeking parameter estimation scheme is proposed, which is concluded in Theorem 4.

Theorem 4. *Replace the excitation signals $a\sin\omega t$ and $\sin\omega t$ with excitation signals vector $S(t)$ and $M(t)$ in the structure of fault parameter estimation in Figure 1:*

$$\begin{aligned}S(t) &= \left[a_1\sin\omega_1 t\cdots a_n\sin\omega_n t\right]^T,\\ M(t) &= \left[\frac{2}{a_1}\sin(\omega_1 t)\cdots\frac{2}{a_n}\sin(\omega_n t)\right],\end{aligned} \tag{24}$$

where $\omega_i \neq \omega_j$ and $\omega_i + \omega_j \neq \omega_k$, J has a global minimum ($\widehat{f} = f$), and $\widehat{f}$ will converge to the extremum vector $\widehat{f}^*$.

Proof. From formula (14),

$$J(\widehat{f}_m) = \sum_{i=1}^{n}\left(\widehat{f}_i - f_i\right)^2. \tag{25}$$

The first derivative and second derivative of cost function are

$$\frac{\partial J}{\partial\widehat{f}_i} = 2\left(\widehat{f}_i - f_i\right), \qquad \frac{\partial^2 J}{\partial\widehat{f}_i^2} = 2, \qquad \frac{\partial^2 J}{\partial\widehat{f}_i\partial\widehat{f}_j} = 0. \tag{26}$$

The Hessian matrix is $H_e = \mathrm{diag}(2, 2, \ldots, 2)$, and formula (25) can be rewritten as

$$J(\widehat{f}) = J(f) + \frac{1}{2}\left(\widehat{f} - f\right)^{\mathrm{T}} H_e\left(\widehat{f} - f\right). \tag{27}$$

Denote the estimation error of $\widehat{f}$ as $\widetilde{f} = f - \overline{f}$, and we have

$$\begin{aligned}y_{\mathrm{seek}} &= \sum_{i=1}^{n}\left(\widetilde{f}_i - a_i\sin\omega_i t\right)^2\\ &= \sum_{i=1}^{n}\left(\widetilde{f}_i^2 - 2a_i\sin\omega_i t + a_i^2\sin^2\omega_i t\right)^2.\end{aligned} \tag{28}$$

Then we obtain

$$\begin{aligned}\xi &= M(t)\frac{s}{s+h}y_{\mathrm{seek}}\\ &= \left[\frac{2}{a_1}\sin(\omega_1 t)\,y_{\mathrm{seek}},\ldots,\frac{2}{a_n}\sin(\omega_n t)\,y_{\mathrm{seek}}\right],\\ \xi_i &= \frac{2}{a_i}\sin(\omega_i t)\,y_{\mathrm{seek}}\\ &= \frac{2}{a_i}\sin(\omega_i t)\sum_{i=1}^{n}\widetilde{f}_i^2 - 4\widetilde{f}_i\sin^2(\omega_i t) + 2a_i\sin^2(\omega_i t).\end{aligned} \tag{29}$$

We have

$$\begin{aligned}\overline{f}_i &= \frac{k}{s}\cdot\frac{1}{s+1}\xi_i\\ &= \frac{k}{s}\cdot\frac{1}{s+1}\times\left[\frac{2}{a_1}\sin(\omega_1 t)\sum_{i=1}^{n}\widetilde{f}_i^2 - 4\widetilde{f}_i\sin^2(\omega_i t) + 2a_i\sin^2(\omega_i t)\right]\\ &\approx -4\widetilde{f}_i\frac{k}{s},\end{aligned} \tag{30}$$

$$\dot{\widetilde{f}} = -4k\widetilde{f}_i. \tag{31}$$

□

From (31), we find that the convergence rate is governed by the integration time k and the estimation error $\widetilde{f}$.

5. Cooperative Weight Accommodation for Fault Tolerance

In this section, we primarily focus on the design of cooperative fault-tolerant control laws for multiagent systems. The system contains N agents with fixed connection topology. The connection matrix can be formulated as a Laplacian matrix, and the velocity of the ith agent is influenced by connection weight a_{ij}. When the unknown input observers detect a failure in the network, we can improve the influence of its nonfaulty neighbors on the faulty agent by adjusting the weight.

5.1. Single Faulty Agent Case. Weights a_{mj} and b_m are both positive constants. Based on (2), all agents asymptotically converge to the same velocity and reach the same position if there is no faulty agent. Agent m turns faulty at T_m and it was first isolated from the system. The new networked system without faulty agent can be written as a linear time invariant dynamical system as

$$\begin{aligned} \dot{x}_{-m} &= A_{-m}x, \\ y_{-m} &= C_{-m}x_{-m}, \end{aligned} \tag{32}$$

where $x_{-m} = [p_1, p_2, \ldots, p_{m-1}, p_{m+1}, \ldots, p_N, q_1, q_2, \ldots, q_{m-1}, q_{m+1}, \ldots, q_N]^{\mathrm{T}}$, $A_{-k}, C_{-k} \in R^{2(n-1)\times 2(n-1)}$, and $x, y \in R^{2(n-1)}$. All the eigenvalues of the matrix A_{-k} less than 0 guarantee the convergence to the target point. We defined the state of each agent as $x_i = [p_i, q_i]$, $x_t \in R^2$ as the target state. We defined $\widetilde{p}_i = p_i - p_0$, $\widetilde{q}_i = q_i - q_0$ and $\widetilde{x} = [\widetilde{p}_1, \widetilde{p}_2, \ldots, \widetilde{p}_{n-1}, \widetilde{q}_1, \widetilde{q}_2, \ldots, \widetilde{q}_{n-1}]$, and we have

$$\begin{aligned} \dot{\widetilde{p}}_i &= \dot{p}_i - \dot{p}_0 = q_i - q_0 = \widetilde{q}_i, \\ \dot{\widetilde{q}}_i &= \dot{q}_i - \dot{q}_0 = -b\widetilde{q}_0 + \sum_{j\in N_i} a_{ij}\left(\widetilde{p}_j - \widetilde{p}_i\right) - \sum_{j\in N_0} a_{0j}\widetilde{p}_j - f_0. \end{aligned} \tag{33}$$

The networked system without faulty agent can be written as a linear time invariant dynamical system:

$$\dot{\widetilde{x}} = A_1\widetilde{x} - A_2\widetilde{x} - f_e. \tag{34}$$

The following text gives some details of A_1 and A_2:

$$A_1 = \begin{bmatrix} 0 & I_{n-1} \\ -\widetilde{L} & -b \end{bmatrix}, \qquad A_2 = \begin{bmatrix} 0_{(n-1)(n-1)} \\ d \\ \vdots \\ d \end{bmatrix}, \tag{35}$$

where $d \in R^{n-1}$, $d = [d_1, d_2, \ldots, d_{n-1}]$, and $f_e = [0, 0, \ldots, 0, f_0, f_0, \ldots, f_0]^{\mathrm{T}}$.

Lemma 5. *The new system (34) achieves consensus asymptotically if and only if A_{-m} has exactly two zeros and all other eigenvalues have negative real parts, specifically,*

$$\begin{aligned} p_e(t) &= \frac{1}{n-1}\sum_{i=1}^{n-1} p_i(T_m) + \frac{1}{n-1}(t - T_m)\sum_{i=1}^{n-1} q_i(T_m), \\ q_{T_m} &= \frac{1}{n-1}\sum_{i=1}^{n-1} q_i(T_m). \end{aligned} \tag{36}$$

Theorem 6. *The faulty agent has an equilibrium state $\dot{q}_0 = 0$ when*

$$\sum_{j\in N_0} a_{0j}\overline{p}_j = -f_0, \tag{37}$$

where $a_{\min} \le a_{0j} \le a_{\max}$.

Proof. The new multiagent system is still able to converge to the target state $x_t = [p_t, q_t]$ after the faulty agent is isolated. For a faulty agent under u_i, the Lyapunov function is constructed as

$$V_0 = \frac{1}{2}\sum_{j=N_0} a_{0j}\left(p_e - \overline{p}_j - p_0\right)^2 + \frac{1}{2}q_0^2 \tag{38}$$

and the time derivative of V_0 is

$$\begin{aligned} \dot{V}_0 &= -\sum_{j\in N_0} a_{0j}\left(p_e - \overline{p}_j - p_0\right)q_0 \\ &\quad + q_0\left[-bq_0 + \sum_{j\in N_0} a_{0j}\left(p_j - p_0\right) + f_0\right] \\ &= \sum_{j\in N_0} a_{0j}\overline{p}_j q_0 - bq_0^2 + q_0 f_0. \end{aligned} \tag{39}$$

Then we have

$$\dot{V}_0 = \sum_{j\in N_0} a_{0j}\overline{p}_j q_0 - bq_0^2 + q_0 f_0 = -bq_0^2 \le 0. \tag{40}$$

□

5.2. Multiple Faulty Agent Case. As described above, all the faulty agents are isolated from the system. The faulty set is defined by $m = [m_1, m_2, \ldots, m_{nf}]$, where there are n_f faulty agents in the network. We defined $\widetilde{p}_{im_k} = p_i - p_{m_k}$, $\widetilde{q}_{im_k} = q_i - q_{m_k}$ and $\widetilde{x}_{mk} = [\widetilde{p}_{2mk}, \widetilde{p}_{2mk}, \ldots, \widetilde{p}_{(n-n_f)mk}, \widetilde{q}_{1mk}, \widetilde{q}_{2mk}, \ldots, \widetilde{q}_{(n-n_f)mk}]$. Then we have the following theorem.

Theorem 7. *For multiple faulty agents case, each faulty agent has an equilibrium state $\dot{q}_{mk} = 0$ when*

$$\sum_{j\in N_{mk}} a_{m_k j}\overline{p}_{jm_k} = -f_{mk}, \tag{41}$$

where $a_{\min} \le a_{mkj} \le a_{\max}$.

Proof. See Theorem 6. □

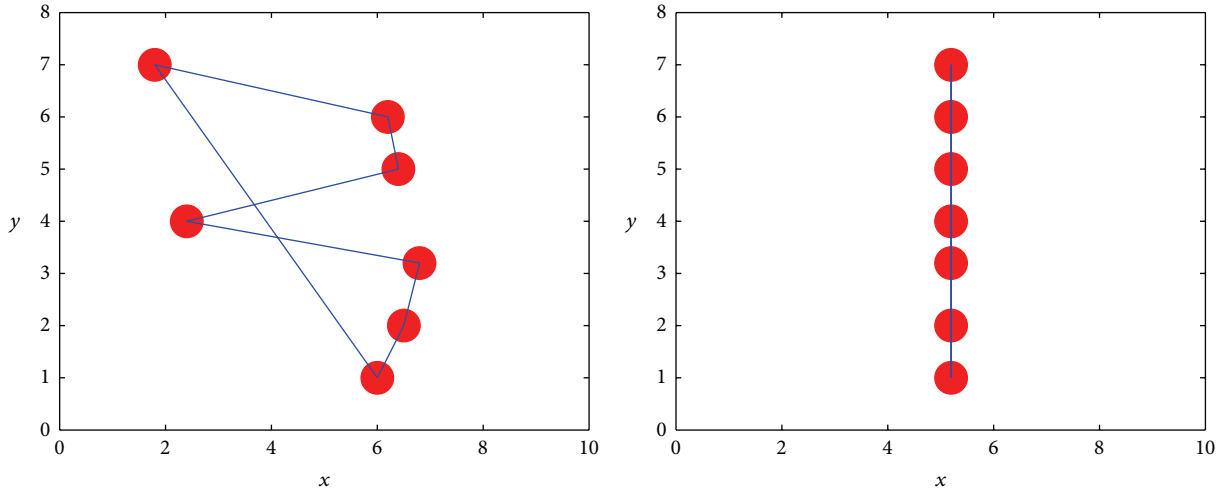

(a) Initial positions (b) Desired positions

Figure 2: Initial positions and desired positions of 7 agents.

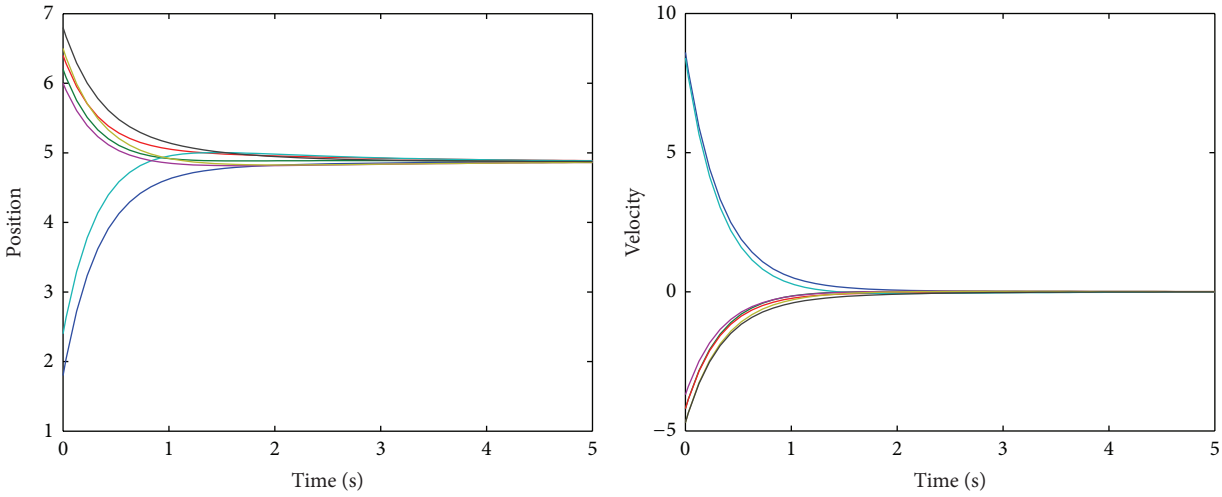

(a) Consensus of x-position without faulty agent (b) Consensus of velocity without faulty agent

Figure 3: The consensus process of seven agents.

6. Simulation

In this study, a cooperative multiagent team example is given to illustrate the feasibility and effectiveness of the proposed method. Seven agents communicate with each other to aggregate the consensus position. First, we build a set of unknown input observers for each agent. Then, we utilize extremum seeking to adaptively approximate the fault parameter. Finally, we use the fault tolerance method to recover the system.

As shown in Figure 2, seven agents will converge to the consensus state in x-label, where the position in y-label is fixed. The start position of the seven agents is $10 * \text{random}(1)$, where the start velocity is zero. The initialization parameters are $a_{ij} = 1$, $b = 1$, and $\gamma = 1$, so the second maximum eigenvalue of matrix A for the position consensus problem is $\text{Re}(\lambda) = -0.5$. At $T_2 = 16$ s, agent 2 gets faulty, and the faulty parameter is $f_2 = 2{,}5$. Figure 3 shows the x-position and velocity of seven agents, and all agents achieve target state consensus by cooperative control law. The final state of position is mean value of the initial positions, and the final state of velocity is zero for the initial velocity. When $t > T_2 = 16$ s, there was a deviation between real state and estimate state. In extremum seeking, we choose $\omega = 10$, $k = 0.001$, and $a = 0.1$. The seeking process is shown in Figure 4.

7. Conclusion

This paper proposes a new framework of fault detection and fault-tolerant control of multiagent systems. This paper mainly studies fault parameter approximation using extremum seeking and cooperative fault-tolerant control using

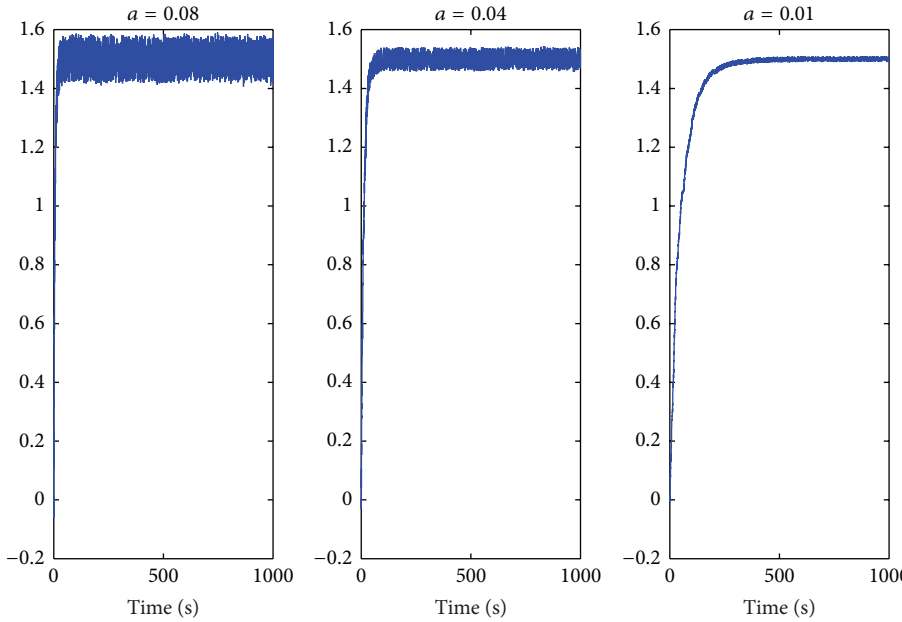

Figure 4: The search process of extremum seeking.

interconnection weights adjusting. Fault parameter approximation using extremum seeking simplifies the design process. Then, by adjusting some interconnection weights based on Lyapunov potential-energy function, we show that the target state is still reached.

Conflict of Interests

The authors declare that there is no conflict of interests regarding the publication of this paper.

Acknowledgments

The authors would like to acknowledge that this work was partially supported by the National Natural Science Foundation of China (Grant nos. 61202342, 61379111, 61402538 and 61403424) and Research Fund for the Doctoral Program of Higher Education of China (Grant nos. 20110162110042).

References

[1] R. Olfati-Saber, J. A. Fax, and R. M. Murray, "Consensus and cooperation in networked multi-agent systems," *Proceedings of the IEEE*, vol. 95, no. 1, pp. 215–233, 2007.

[2] W. Ren, R. W. Beard, and E. M. Atkins, "A survey of consensus problems in multi-agent coordination," in *Proceedings of the American Control Conference (ACC '05)*, Portland, Ore, USA, June 2005.

[3] P. R. Chandler, M. Pachter, and S. Rasmussen, "UAV cooperative control," in *Proceedings of the American Control Conference*, pp. 50–55, April 2001.

[4] P. Panagi and M. M. Polycarpou, "Distributed fault accommodation for a class of interconnected nonlinear systems with partial communication," *IEEE Transactions on Automatic Control*, vol. 56, no. 12, pp. 2962–2967, 2011.

[5] H. Yang, M. Staroswiecki, B. Jiang, and J. Liu, "Fault tolerant cooperative control for a class of nonlinear multi-agent systems," *Systems and Control Letters*, vol. 60, no. 4, pp. 271–277, 2011.

[6] I. Shames, A. M. Teixeira, H. Sandberg, and K. H. Johansson, "Distributed fault detection for interconnected second-order systems," *Automatica*, vol. 47, no. 12, pp. 2757–2764, 2011.

[7] I. Shames, A. M. H. Teixeira, H. Sandberg, and K. H. Johansson, "Distributed Fault Detection and Isolation with imprecise network models," in *Proceedings of the American Control Conference (ACC '12)*, pp. 5906–5911, June 2012.

[8] C. W. Chan, S. Hua, and Z. Hong-Yue, "Application of fully decoupled parity equation in fault detection and identification of DC motors," *IEEE Transactions on Industrial Electronics*, vol. 53, no. 4, pp. 1277–1284, 2006.

[9] S. Simani, C. Fantuzzi, and R. J. Patton, *Model-Based Fault Diagnosis in Dynamic Systems Using Identification Techniques*, Springer, London, UK, 2003.

[10] X. Zhang, M. M. Polycarpou, and T. Parisini, "Fault diagnosis of a class of nonlinear uncertain systems with Lipschitz nonlinearities using adaptive estimation," *Automatica*, vol. 46, no. 2, pp. 290–299, 2010.

[11] T. Jiang, K. Khorasani, and S. Tafazoli, "Parameter estimation-based fault detection, isolation and recovery for nonlinear satellite models," *IEEE Transactions on Control Systems Technology*, vol. 16, no. 4, pp. 799–808, 2008.

[12] Y. Tan, W. H. Moase, C. Manzie, D. Nešić, and I. M. Y. Mareels, "Extremum seeking from 1922 to 2010," in *Proceedings of the 29th Chinese Control Conference (CCC '10)*, pp. 14–26, Beijing, China, July 2010.

[13] Y. Tan, D. Nešić, and I. Mareels, "On the choice of dither in extremum seeking systems: a case study," *Automatica*, vol. 44, no. 5, pp. 1446–1450, 2008.

[14] E. Semsar-Kazerooni and K. Khorasani, "Team consensus for a network of unmanned vehicles in presence of actuator faults,"

IEEE Transactions on Control Systems Technology, vol. 18, no. 5, pp. 1155–1161, 2010.

[15] S. M. Azizi and K. Khorasani, "Cooperative fault accommodation in formation flying satellites," in *Proceedings of the 17th IEEE International Conference on Control Applications*, pp. 1127–1132, September 2008.

[16] R. Diestel, *Graph Theory*, vol. 173 of *Graduate Texts in Mathematics*, Springer.

[17] H.-H. Wang and M. Krstic, "Extremum seeking for limit cycle minimization," *IEEE Transactions on Automatic Control*, vol. 45, no. 12, pp. 2432–2437, 2000.

Hindawi Publishing Corporation
Mathematical Problems in Engineering
Volume 2015, Article ID 959570, 9 pages
http://dx.doi.org/10.1155/2015/959570

Research Article

Impulsive Containment Control in Nonlinear Multiagent Systems with Time-Delay

Wenshan Hu, Zhenhua Wang, Zhi-Wei Liu, and Hong Zhou

Department of Automation, Wuhan University, Wuhan 430072, China

Correspondence should be addressed to Zhi-Wei Liu; liuzw@whu.edu.cn

Received 12 June 2014; Accepted 8 August 2014

Academic Editor: Housheng Su

The containment control problems of nonlinear multiagent systems with time-delay via impulsive algorithms under both fixed and switching topologies are studied. By using the Lyapunov methods, several conditions are derived to achieve the containment control. It is shown that the states of the followers can converge into the convex hull spanned by the states of the leaders if every leader has directed paths to all the followers and the impulsive period is short enough. Finally, some simulations are conducted to verify the effectiveness of the proposed algorithms.

1. Introduction

Recently, the distribution cooperative control of the multiagent systems has attracted numerous researches due to the extensive applications in the scientific, engineering, biological aspects, and so forth [1–5]. The very essence of the distribution cooperative control lies in that none of the agents know the states of all the other agents exactly and every agent updates its own states based on the state information from its neighbors. Consensus problems, as a fundamental branch of cooperative control, have been investigated in many literatures with plenty of useful results obtained [6, 7]. In earlier times, the researches mainly focused on the consensus cases where there exists no more than one leader [8–11]. Zhu and Cheng in [8] considered the consensus of multiagent systems where there exists one leader. Su et al. in [9, 10] mainly investigated the leader-following consensus of linear multiagent systems with one leader and input saturation. Lu et al. [11] studied the finite-time distributed tracking control for multiagent systems with an active leader.

The investigations on consensus problems of multiple leaders [12–19], called containment control, are also significant because they are related with many practical applications, such as there are some agents equipped with the detective sensors, while the other less capable agents are driven into the convex hull spanning by the former agents such that all the agents can navigate their trip without any potential danger.

The proposed algorithms in [13, 14] are applied to multiagent systems with linear dynamics. These critical defects limit the validity of the proposed models because the nonlinear systems are ubiquitous in the real world [20–22]. In this paper, we deal with the containment control of the nonlinear multiagent systems. Compared with the continuous control algorithms [12–19], the impulsive algorithms have remarkable superiority as the impulsive controllers are usually simple and practical [23–26]. In many cases, to achieve the consensus, the continuous regulation and control are not necessary or impossible. Nevertheless, the impulsive algorithms just need to regulate and alter the states of the systems at the impulsive instants. Also, it can be easily seen that impulsive control is effective and efficient in the control of the multiagent systems to achieve consensus. In many real applications, due to the limited switching speed and the transmission of the signals, the next states of the dynamic systems may be concerned not only with the states at this time but also with states of the time before. It is practical and necessary to analyse the systems with time-delay. If the time-delay is not taken into consideration in the system models, inappropriate or even inaccurate results may be obtained. There are some works

[27, 28] that deal with the consensus or synchronization problem with time-delays.

Motivated by the aforementioned discussions, we investigate the achievement of the containment control for the nonlinear multiagent systems with time-delay under both fixed and switching topology in this paper. The proposed impulsive algorithm can achieve the containment control and some sufficient conditions are obtained, which show that, for specific dynamic systems, the containment control can be achieved if the control period of the impulsive algorithms and the feedback gain of the controller satisfy the given conditions. Finally, some numerical simulations are presented to verify the validity of the theoretical analysis.

The outline of this paper is organized as follows. In Section 2, we first give some preliminaries which are essential for the analyses of the multiagent systems. Then, the containment control of the nonlinear dynamic systems with internal time-delays under both fixed and switching topology via impulsive algorithms is considered. In Section 3, some simulations are presented to illustrate the theoretical results. Finally, some conclusions of this paper are drawn in Section 4.

The notions and symbols used in the paper are given as follows. $\mathbb{R}$ denotes the set of real numbers. Let I_N be the $N\times N$ identity matrix (or just I if no confusion), $\mathbf{1}_N = [1, 1, \ldots, 1]^T$. $\mathbf{0}_{N\times M}$ is the $N\times M$ matrix with all entries zero. $\|\cdot\|$ denotes the Euclidean norm. $\lambda_{\max}(A)$, $\lambda_{\min}(A)$ denote the maximum and minimum eigenvalue of the square matrix A, respectively.

2. Impulsive Containment Control for Nonlinear Systems with Internal Delay

First, we summarize some definitions and results from graph theory that will be used in the paper.

Let $\mathcal{G} = (\mathcal{V}, \mathcal{E}, \mathcal{A})$ be a weighted graph consisting of the set of nodes $\mathcal{V} = \{1, 2, \ldots, n\}$, the set of edges $\mathcal{E} \subset \mathcal{V} \times \mathcal{V}$, and a weighted adjacency matrix $\mathcal{A} = [a_{ij}]$, $i, j = 1, 2, \ldots, n$. If $(j, i) \in \mathcal{E}$, then $a_{ij} > 0$ and $a_{ji} > 0$; otherwise, $a_{ij} = a_{ji} = 0$ and the diagonal entries of $\mathcal{A}$ are zero; that is, $a_{ii} = 0$. A path from node i to node j is a sequence of edges $(i, p_1), (p_1, p_2), \ldots, (p_k, j)$, where $(i, p_1), (p_1, p_2), \ldots, (p_k, j) \in \mathcal{E}$. $\mathcal{N}_i$ denotes the set of the neighbors of node i, where $\mathcal{N}_i = \{j \in \mathcal{V} : (j, i) \in \mathcal{E}\}$. The Laplacian matrix of graph $\mathcal{G}$ is denoted by $L = [l_{ij}] \in \mathbb{R}^{n\times n}$, $l_{ii} = \sum_{j=1}^{n} a_{ij}$ and $l_{ij} = -a_{ij}$ for $i \neq j$.

2.1. Impulsive Containment Control for Nonlinear Dynamic Systems of Fixed Topology with Internal Delay. Consider a nonlinear dynamic multiagent system with $(M + N)$ agents. Assume that there are M leaders and N followers. An agent is a leader if the agent does not receive any information from others. Otherwise, it is a follower. The set of leaders is denoted by $\mathcal{M} = \{1, 2, \ldots, M\}$ and the set of followers is denoted by $\mathcal{N} = \{M+1, \ldots, M+N\}$. Let $\mathcal{V} = \mathcal{M} \cup \mathcal{N} = \{1, 2, \ldots, M+N\}$ be the set of all the agents. The communications among the $(M + N)$ agents are represented by a directed graph $\mathcal{G}$.

The dynamics of the nonlinear multiagent system with internal time-delay are given as follows:

$$\begin{aligned} \dot{x}_i(t) &= g\left(t, x_i(t), x_i(t-d)\right) + u_i(t), \quad i \in \mathcal{N}, \\ \dot{x}_i(t) &= g\left(t, x_i(t), x_i(t-d)\right), \quad i \in \mathcal{M}, \end{aligned} \tag{1}$$

where d is the internal delay and $x_i(t) \in \mathbb{R}^n$ and $u_i(t) \in \mathbb{R}^n$ are the state and control input of the ith agent, respectively. $g(\cdot, \cdot, \cdot) : \mathbb{R} \times \mathbb{R}^n \times \mathbb{R}^n \to \mathbb{R}^n$ is the nonlinear dynamic of the ith agent.

Assumption 1. The nonlinear function $g(t, x_i(t), x_i(t-d))$ in system (1) satisfies the convex Lipschitz condition. That is, there exist two positive numbers K and l, such that, for all $x_i, y_i, i = M+1, \ldots, M+N$,

$$\begin{aligned} &\left\| g\left(t, x_i, y_i\right) - \sum_{j=1}^{M} a_j g\left(t, x_j, y_j\right) \right\| \\ &\qquad \leqslant K \left\| x_i - \sum_{j=1}^{M} a_j x_j \right\| + l \left\| y_i - \sum_{j=1}^{M} a_j y_j \right\|, \end{aligned} \tag{2}$$

where $a_j \geqslant 0$, $j = 1, \ldots, M$ and $\sum_{j=1}^{M} a_j = 1$.

The initial states of the system (1) are

$$x_i(t) = o_i(t), \quad -d \leqslant t \leqslant 0, \ i \in \mathcal{V}, \tag{3}$$

where $o_i(t) \in C([-d, 0], \mathbb{R}^n)$ and $C([-d, 0], \mathbb{R}^n)$ is the n-dimensional vector space of continuous functions. In this paper, we consider the case of $n = 1$ and all the results will hold for $x_i(t), u_i(t) \in \mathbb{R}^n$ $(n > 1)$ by using the property of Kronecker product.

From the definitions of the leader and the follower, the Laplacian matrix of the graph $\mathcal{G}$ can be partitioned as

$$L = \begin{bmatrix} L_{11} & L_{12} \\ 0_{M\times N} & 0_{M\times M} \end{bmatrix}, \tag{4}$$

where L_{11} is a $N \times N$ matrix which denotes the communications among the followers. L_{12} is a $N \times M$ matrix which denotes the communications among the followers and leaders.

Assumption 2. In the graph $\mathcal{G}$, the communications among the followers are undirected and, for each follower, there exists at least one leader that has a directed path to that follower.

From the property of the Laplacian matrix, the following lemma can be obtained.

Lemma 3 (see [17]). *Let Assumption 1 hold. Then L_{11} is symmetric positive definite and all the entries of $-(L_{11}^{-1}L_{12})$ are nonnegative and $-(L_{11}^{-1}L_{12})\mathbf{1}_M = \mathbf{1}_N$.*

Definition 4 (see [29]). A subset C of $\mathbb{R}^N$ is said to be convex if $(1 - \lambda)x + \lambda y \in C$ whenever $x \in C$, $y \in C$, and $0 < \lambda < 1$.

The convex hull of a finite set of points $x_1, x_2, \ldots, x_q \in \mathbb{R}^N$ (q is a positive integer) is the minimal convex set containing all points in $\{x_1, x_2, \ldots, x_q\}$. We use $\mathrm{co}\{x_1, x_2, \ldots, x_q\}$ to denote it; that is,

$$\mathrm{co}\left\{x_1, x_2, \ldots, x_q\right\} = \left\{\sum_{j=1}^{q} a_j x_j \mid a_j \in \mathbb{R}, a_j \geqslant 0, \sum_{j=1}^{q} a_j = 1\right\}. \tag{5}$$

Definition 5. The containment control is achieved in system (1) if, for any initial conditions, $x_i(t) \in \mathrm{co}\{x_1(t), \ldots, x_M(t)\}$ as $t \to +\infty$, for all $i \in \mathcal{N}$. That is, each state of the followers will converge into the convex hull formed by the states of the leaders as $t \to +\infty$.

To achieve the containment control for the system (1), we propose the following impulsive algorithm:

$$u_i(t) = \sum_{k=1}^{\infty}\left[(-\alpha)\sum_{j=1}^{M+N} a_{ij}\left(x_i(t) - x_j(t)\right)\right]\delta\left(t - t_k\right), \quad i \in \mathcal{N}, \tag{6}$$

where $\alpha > 0$ is the feedback gain to be determined and $\mathcal{A} = [a_{ij}] \in \mathbb{R}^{n\times n}$ is the adjacency matrix associated with the graph $\mathcal{G}$. The impulsive instants are t_k, $k = 1, 2, \ldots$, $\lim_{k\to+\infty} t_k = +\infty$. That is, $t_1 < t_2 < \cdots < t_k < \cdots$ is the impulsive instant sequence, where $t_1 > t_0$; $t_0 = 0$ is the initial time. $\delta(\cdot)$ is the Dirac impulsive function.

Using the impulsive algorithm (6) in the system (1), we can obtain

$$\begin{aligned}
\dot{x}_i(t) &= g\left(t, x_i(t), x_i(t-d)\right), \quad t \neq t_k,\\
\Delta x_i\left(t_k\right) &= (-\alpha)\sum_{j=1}^{N+M} a_{ij}\left(x_i\left(t_k\right) - x_j\left(t_k\right)\right), \quad i \in \mathcal{N}\\
\dot{x}_i(t) &= g\left(t, x_i(t), x_i(t-d)\right), \quad t > 0,\ i \in \mathcal{M},
\end{aligned} \tag{7}$$

where $\Delta x_i(t_k) = x_i(t_k^+) - x_i(t_k)$ and $x_i(t_k^+) = \lim_{t\to t_k^+} x_i(t)$. Assume that $x_i(t)$ is left-hand continuous at $t = t_k$, $k = 1, 2, \ldots$; that is, $x_i(t_k^-) = x_i(t_k)$, where $x_i(t_k^-) = \lim_{t\to t_k^-} x_i(t)$, $i \in \mathcal{N}$. For simplification, we assume that $x_i(t)$, $i \in \mathcal{V}$, is continuous at the initial time $t_0 = 0$.

Assumption 6. The internal delay must be less than the impulsive period. That is, $0 \leqslant d \leqslant \tau_0$, where $t_{k+1} - t_k = \tau_0$, $k = 1, 2 \ldots$, is the impulsive period.

Let

$$\begin{aligned}
x_F(t) &= \left[x_{M+1}(t), \ldots, x_{M+N}(t)\right]^T,\\
x_L(t) &= \left[x_1(t), \ldots, x_M(t)\right]^T,\\
G_F(t) &= \left[g\left(t, x_{M+1}(t), x_{M+1}(t-d)\right), \ldots, g(t, x_{M+N}(t), x_{M+N}(t-d))\right]^T,\\
G_L(t) &= \left[g\left(t, x_1(t), x_1(t-d)\right), \ldots, g(t, x_M(t), x_M(t-d))\right]^T.
\end{aligned} \tag{8}$$

According to equality (4), the system (7) can be rewritten as

$$\begin{aligned}
\dot{x}_F(t) &= G_F(t), \quad t \neq t_k\\
\Delta x_F\left(t_k\right) &= -\alpha L_{11}\left[x_F\left(t_k\right) + L_{11}^{-1}L_{12}x_L\left(t_k\right)\right],\\
\dot{x}_L(t) &= G_L(t), \quad t > 0.
\end{aligned} \tag{9}$$

Let $\omega(t) = x_F(t) + (L_{11}^{-1}L_{12})x_L(t)$, $t \neq t_k$, and $\Delta\omega(t_k) = \Delta x_F(t_k) + (L_{11}^{-1}L_{12})\Delta x_L(t_k)$. Because $\Delta x_L(t_k) = 0$ and from equality (9), the following equations can be obtained:

$$\begin{aligned}
\dot{\omega}(t) &= G_F(t) + \left(L_{11}^{-1}L_{12}\right)G_L(t), \quad t \neq t_k,\\
\Delta\omega\left(t_k\right) &= -\alpha L_{11}\omega\left(t_k\right).
\end{aligned} \tag{10}$$

Remark 7. From Lemma 3, every entry in $-(L_{11}^{-1}L_{12})$ is nonnegative and $-(L_{11}^{-1}L_{12})\mathbf{1}_M = \mathbf{1}_N$. We can get that each entry of $(-L_{11}^{-1}L_{12})x_L(t)$ is the convex hull formed by the states of the leaders. So, the containment control is achieved if the system (10) is stable.

Theorem 8. *Suppose that Assumptions 1, 2, and 6 are satisfied. The system* (1) *using impulsive algorithm* (6) *achieves containment control, that is, $x_F(t) \to (-L_{11}^{-1}L_{12})x_L(t)$, as $t \to +\infty$, if the following conditions are satisfied:*

$$\frac{\lambda_{\max}(L_{11}) - \lambda_{\min}(L_{11})}{\lambda_{\max}(L_{11}) + \lambda_{\min}(L_{11})} \leqslant q < 1, \tag{11}$$

$$\frac{1-q}{\lambda_{\min}(L_{11})} \leqslant \alpha \leqslant \frac{1+q}{\lambda_{\max}(L_{11})}, \tag{12}$$

$$\tau_0 < \frac{-\ln(q)}{2(K+l)}, \tag{13}$$

where q is an auxiliary constant.

Proof. Construct a Lyapunov function $V(t) = \omega^T(t)\omega(t)$. Then $V(t)$ is piecewise continuous and positive definite. When $t \neq t_k$, we can get $\dot{V}(t) = 2\omega^T(t)\dot{\omega}(t)$. Let $\omega(t) = [\omega_1(t), \ldots, \omega_N(t)]^T$ and $\overline{\omega}(t) = [|\omega_1(t)|, \ldots, |\omega_N(t)|]^T$; then we can get $V(t) = \overline{\omega}^T(t)\overline{\omega}(t)$. From Assumption 1 and (10),

$$\dot{V}(t) \leqslant 2\overline{\omega}^T(t)\left(K\overline{\omega}(t) + l\overline{\omega}(t-d)\right) \tag{14}$$

can be obtained. That is,

$$\dot{V}(t) \leqslant 2K\overline{\omega}^T(t)\,\overline{\omega}(t) + 2l\overline{\omega}^T(t)\,\overline{\omega}(t-d). \tag{15}$$

It is obvious that

$$2\overline{\omega}^T(t)\,\overline{\omega}(t-d) \leqslant \overline{\omega}^T(t)\,\overline{\omega}(t) + \overline{\omega}^T(t-d)\,\overline{\omega}(t-d). \tag{16}$$

Combining inequalities (15) and (16) and the definition of $V(t)$, we can arrive at the following inequality:

$$\dot{V}(t) \leqslant (2K+l)\,V(t) + lV(t-d), \quad t \neq t_k. \tag{17}$$

From the definition of $V(t)$, we can obtain $V(t_k^+) = \omega^T(t_k^+)\omega(t_k^+)$. From system (10), it is easy to see that $\omega(t_k^+) = (I-\alpha L_{11})\omega(t_k)$. Thus,

$$\begin{aligned} V(t_k^+) &= \omega^T(t_k)\left(I-\alpha L_{11}\right)^T\left(I-\alpha L_{11}\right)\omega(t_k), \\ &\leqslant \lambda_{\max}^2\left(I-\alpha L_{11}\right)\omega^T(t_k)\,\omega(t_k). \end{aligned} \tag{18}$$

That is,

$$V(t_k^+) \leq \lambda_{\max}^2\left(I-\alpha L_{11}\right)V(t_k). \tag{19}$$

To prove that the Lyapunov function $V(t)$ is convergent, we construct an auxiliary variable ξ in the following form:

$$\begin{aligned} \dot{\xi}(t) &= (2K+l)\,\xi(t) + l\xi(t-d) + \mu, \quad t \neq t_k \\ \xi(t_k^+) &= \lambda_{\max}^2\left(I-\alpha L_{11}\right)\xi(t_k), \end{aligned} \tag{20}$$

where the initial states are $\xi(t) = \|o_\omega(t)\|^2$, $-d \leqslant t \leqslant 0$, and $\mu > 0$, where $o_\omega(t) = o_F(t) + (L_{11}^{-1}L_{12})o_L(t)$, $o_F(t) = [o_{M+1}(t), \ldots, o_{M+N}(t)]^T$, and $o_L(t) = [o_1(t), \ldots, o_M(t)]^T$.

Let

$$\begin{aligned} \dot{\eta}(t) &= (2K+l)\,\eta(t), \quad t \neq t_k, \\ \eta(t_k^+) &= \lambda_{\max}^2\left(I-\alpha L_{11}\right)\eta(t_k). \end{aligned} \tag{21}$$

From inequalities (17), (19), and (20), it is obvious that, for all $t > 0$, $0 \leqslant V(t) \leqslant \xi(t)$. And the solution of (20) satisfies the following integral equation:

$$\xi(t) = \phi(t,0)\,\xi(0) + \int_0^t \phi(t,s)\left[l\xi(s-d) + \mu\right]ds, \tag{22}$$

where $\phi(t,s)$, $(t,s \geqslant 0)$, is the state transition matrix of the system (21).

When $t_k < t < t_{k+1}$ and $t_{k-1} < s < t_k$, $k = 1, 2, \ldots$, we can arrive at

$$\phi(t,s) \leqslant e^{(2K+l)(t-s)}\lambda_{\max}^2\left(I-\alpha L_{11}\right). \tag{23}$$

From inequalities (11) and (12), we can obtain

$$\left|\lambda_{\max}\left(I-\alpha L_{11}\right)\right| \leqslant q < 1. \tag{24}$$

Let $a = -(2K+l) - \gamma/2$ and $2\ln(q)/\tau_0 = \gamma$. From condition (13), it is obvious that $\gamma < -4(K+l)$ and $a > 0$. Accordingly, inequality (23) can be rewritten:

$$\begin{aligned} \phi(t,s) &\leqslant e^{(-a-\gamma/2)(t-s)}\lambda_{\max}^2\left(I-\alpha L_{11}\right) \\ &< e^{-a(t-s)} \cdot e^{-(\gamma/2)\cdot 2\tau_0}\lambda_{\max}^2\left(I-\alpha L_{11}\right) \leqslant e^{-a(t-s)}. \end{aligned} \tag{25}$$

Thus, from equality (22), we can obtain

$$\xi(t) < e^{-at}\left\|o_\omega(t)\right\|^2_{\sup(-d\leqslant t\leqslant 0)} + \int_0^t e^{-a(t-s)}\left[l\xi(s-d) + \mu\right]ds \tag{26}$$

for $t \geqslant 0$.

Let $\varepsilon(\theta) = \theta - a + le^{\theta d}$. Then, $\varepsilon(\theta) = 0$ has a unique solution $\theta^* > 0$ because $\varepsilon(\theta)$ is a strictly monotonic function $\dot{\varepsilon}(\theta) = 1 + lde^{\theta d} > 0$ and $\varepsilon(0) = -a + l < 0$, $\varepsilon(+\infty) > 0$. According to $a - l > 0$ and $-\theta^* t > 0$ when $-d \leqslant t \leqslant 0$, we can get

$$\xi(t) < e^{-\theta^* t}\left\|o_\omega(t)\right\|^2_{\sup(-d\leqslant t\leqslant 0)} + \frac{\mu}{a-l}, \tag{27}$$

where $-d \leqslant t \leqslant 0$. And we can prove that inequality (27) is true for $t \geqslant 0$ in the following.

Suppose that inequality (27) is not held; there must exist a t_c such that

$$\xi(t_c) \geqslant e^{-\theta^* t_c}\left\|o_\omega(t)\right\|^2_{\sup(-d\leqslant t\leqslant 0)} + \frac{\mu}{a-l}, \tag{28}$$

$$\xi(t) < e^{-\theta^* t}\left\|o_\omega(t)\right\|^2_{\sup(-d\leqslant t\leqslant 0)} + \frac{\mu}{a-l}, \quad t < t_c. \tag{29}$$

However, from (26) and (29), we can obtain

$$\begin{aligned} \xi(t_c) &< e^{-at_c}\left(\left\|o_\omega(t)\right\|^2_{\sup(-d\leqslant t\leqslant 0)} + \frac{\mu}{a-l}\right) \\ &\quad + \int_0^{t_c} e^{-a(t_c-s)}\left[l\xi(s-d) + \mu\right]ds \\ &< e^{-at_c}\left(\left\|o_\omega(t)\right\|^2_{\sup(-d\leqslant t\leqslant 0)} + \frac{\mu}{a-l}\right) + e^{-at_c} \\ &\quad \times \int_0^{t_c} e^{as}\left[l\left(e^{-\theta^*(s-d)}\left\|o_\omega(t)\right\|^2_{\sup(-d\leqslant t\leqslant 0)} + \frac{\mu}{a-l}\right) + \mu\right]ds \\ &= e^{-at_c}\left[\left\|o_\omega(t)\right\|^2_{\sup(-d\leqslant t\leqslant 0)} + \frac{\mu}{a-l} + l\left\|o_\omega(t)\right\|^2_{\sup(-d\leqslant t\leqslant 0)}\right. \\ &\quad \times \int_0^{t_c} e^{as}\cdot e^{-\theta^*(s-d)}ds \\ &\quad \left. + \frac{l\mu}{a-l}\int_0^{t_c} e^{as}ds + \mu\int_0^{t_c} e^{as}ds\right]. \end{aligned} \tag{30}$$

Combine the fact that $le^{\theta^* d} = a - \theta^*$ and we can get

$$\xi(t_c) < e^{-\theta^* t_c}\left\|o_\omega(t)\right\|^2_{\sup(-d\leqslant t\leqslant 0)} + \frac{\mu}{a-l}, \tag{31}$$

which contradicts inequality (28). Thus, (27) can hold for $t > 0$.

As $\mu \to 0$, then

$$V(t) \leqslant \xi(t) < e^{-\theta^* t}\left\|o_\omega(t)\right\|^2_{\sup(-d\leqslant t\leqslant 0)}. \tag{32}$$

That is,

$$\|\omega(t)\| \leqslant \sup_{(-d\leqslant t\leqslant 0)} \left\|o_\omega(t)\right\| e^{-\theta^* t/2}. \tag{33}$$

This completes the proof. □

Remark 9. For the special case with only one leader, the final states of the followers will track the leader under the conditions in Theorem 8. That is, $x_i(t) \to x_l(t)$, as $t \to \infty$, where $i \in \mathcal{N}$ and $x_l(t)$ is the state of the leader.

2.2. Impulsive Containment Control for Nonlinear Dynamic Systems of Switching Topology with Internal Delay. In the following, we propose the impulsive algorithms to achieve the containment control for nonlinear systems with switching topologies.

Consider the nonlinear system (1) in the switching cases; the proposed impulsive algorithm is

$$u_i(t) = \sum_{k=1}^{\infty}\left[(-\beta)\sum_{j=1}^{M+N} a_{ij}(t)\left(x_i(t) - x_j(t)\right)\right]\delta(t-t_k), \quad i \in \mathcal{N}, \tag{34}$$

where $\beta > 0$ is the feedback gain.

Using the impulsive algorithm (34), the system (1) can be rewritten as

$$\begin{aligned} \dot{x}_i(t) &= g\left(t, x_i, x_i(t-d)\right), \quad t \neq t_k \\ \Delta x_i(t) &= (-\beta)\sum_{j=1}^{N+M} a_{ij}(t)\left(x_i(t) - x_j(t)\right), \\ & \qquad t = t_k,\ i \in \mathcal{N}, \quad k = 1, 2, \ldots \\ \dot{x}_i(t) &= g\left(t, x_i, x_i(t-d)\right), \quad t > 0,\ i \in \mathcal{M}, \end{aligned} \tag{35}$$

where $\Delta x_i(t_k) = x_i(t_k^+) - x_i(t_k)$ and assume that $x_i(t)$ is left-hand continuous at $t = t_k$, $k = 1, 2, \ldots$, $i \in \mathcal{N}$. Obviously, $x_i(t)$ is continuous when $t \in \mathcal{M}$. For simplicity, we assume that $x_i(t)$ is continuous at $t_0 = 0$, $i \in \mathcal{N}$.

Let

$$\begin{aligned} x_F(t) &= \left[x_{M+1}(t), \ldots, x_{M+N}(t)\right]^T, \\ x_L(t) &= \left[x_1(t), \ldots, x_M(t)\right]^T, \\ G_F(t) &= \left[g\left(t, x_{M+1}(t), x_{M+1}(t-d)\right), \ldots, \right. \\ &\qquad \left. g(t, x_{M+N}(t), x_{M+N}(t-d))\right]^T, \\ G_L(t) &= \left[g\left(t, x_{M+1}(t), x_{M+1}(t-d)\right), \ldots, \right. \\ &\qquad \left. g\left(t, x_{M+N}(t), x_{M+N}(t-d)\right)\right]^T, \\ \omega(t) &= x_F(t) + \left(L_{11}^{-1}(t) L_{12}(t)\right) x_L(t), \\ G_\omega(t) &= G_F(t) + \left(L_{11}^{-1}(t) L_{12}(t)\right) G_L(t). \end{aligned} \tag{36}$$

From (4) and (35), we can arrive at

$$\begin{aligned} \dot{\omega}(t) &= G_\omega(t), \quad t \in \left(t_{k-1}, t_k\right] \\ \Delta\omega(t) &= -\beta L_{11}(t)\,\omega(t), \quad t = t_k, \end{aligned} \tag{37}$$

where $k = 1, 2, \ldots$. The switching signal $\sigma : R^+ \mapsto \{1, 2, \ldots, m\}$, which is equivalent to $(t_{k-1}, t_k] \mapsto L_{11}(t) \in \{L_{11}^{(1)}, L_{11}^{(2)}, \ldots, L_{11}^{(m)}\}$, is a piecewise constant function. That is, the Lapacian matrix of the communication topologies is assumed to take from a set $\mathcal{L} = \{L^{(1)}, L^{(2)}, \ldots, L^{(m)}\}$ and the switching signal $\sigma : R^+ \mapsto \{1, 2, \ldots, m\}$ describes which communication topology is active in the time interval $(t_{k-1}, t_k]$. The communication topology is constant during $(t_{k-1}, t_k]$ and changes at t_k, $k = 1, 2, \ldots$. So, there exist m subsystems in the system (37); that is,

$$\begin{aligned} \dot{\omega}(t) &= G_\omega(t), \quad t \in \left(t_{k-1}, t_k\right], \\ \Delta\omega(t) &= -\beta L_{11}^{(i_k)}\omega(t), \quad t = t_k, \end{aligned} \tag{38}$$

where $i_k \in \{1, 2, \ldots, m\}$, $k = 1, 2, \ldots$.

To simplify the presentation, define the constant numbers γ that satisfy the following equality:

$$\gamma = \max_{1\leqslant i\leqslant m}\left\{\lambda_{\max}^2\left(I - \beta L_{11}^{(i)}\right)\right\}. \tag{39}$$

Theorem 10. *Suppose that Assumption 2 is satisfied in every subsystem of* (38) *and Assumptions 1 and 6 are held. The system* (1) *with switching topologies using impulsive algorithm* (34) *achieves the containment control if*

$$\max_{1\leqslant i\leqslant m}\left\{\lambda_{\max}^2\left(I - \beta L_{11}^{(i)}\right)\right\} < q^2. \tag{40}$$

That is,

$$\begin{aligned} &\frac{\max_{1\leqslant i\leqslant m}\left\{\lambda_{\max}\left(L_{11}^{(i)}\right)\right\} - \min_{1\leqslant i\leqslant m}\left\{\lambda_{\min}\left(L_{11}^{(i)}\right)\right\}}{\max_{1\leqslant i\leqslant m}\left\{\lambda_{\max}\left(L_{11}^{(i)}\right)\right\} + \min_{1\leqslant i\leqslant m}\left\{\lambda_{\min}\left(L_{11}^{(i)}\right)\right\}} \leqslant q < 1, \\ &\frac{1-q}{\min_{1\leqslant i\leqslant m}\left\{\lambda_{\min}\left(L_{11}^{(i)}\right)\right\}} \leqslant \beta \leqslant \frac{1+q}{\max_{1\leqslant i\leqslant m}\left\{\lambda_{\max}\left(L_{11}^{(i)}\right)\right\}}, \end{aligned} \tag{41}$$

$$\tau_0 < \frac{-\ln(q)}{2(K+l)}, \tag{42}$$

where q is an auxiliary constant.

Proof. Construct a Lyapunov function $V(t) = \omega^T(t)\omega(t)$; then $V(t)$ is piece continuous and positive definite. It is obvious that $V(t)$ is left-hand continuous at $t = t_k$, $k = 1, 2, \ldots$. Now consider the time interval $(t_{k-1}, t_k]$, $k = 1, 2, \ldots$. When $t \in (t_{k-1}, t_k]$, owing to Assumption 1, the differential of the $V(t)$ with regard to (38) is

$$\begin{aligned} \dot{V}(t) &= 2\omega^T(t)\,\dot{\omega}(t) = 2\overline{\omega}^T(t)\,\overline{G}_\omega(t) \\ &\leqslant 2\overline{\omega}^T(t)\left(K\overline{\omega}(t) + l\overline{\omega}(t-d)\right), \end{aligned} \tag{43}$$

where $\overline{G}_\omega(t) = [|\dot{\omega}_1(t)|, \ldots, |\dot{\omega}_N(t)|]^T$. It is obvious that

$$2\overline{\omega}^T(t)\,\overline{\omega}(t-d) \leqslant \overline{\omega}^T(t)\,\overline{\omega}(t) + \overline{\omega}^T(t-d)\,\overline{\omega}(t-d). \quad (44)$$

As a consequence, we obtain

$$\dot{V}(t) \leqslant (2K+l)V(t) + lV(t-d), \quad t \in (t_{k-1}, t_k]. \quad (45)$$

It follows from (38) that $\omega(t_k^+) = (I - \beta L_{11}^{(i_k)})\omega(t_k)$. Combine the definition of $V(t)$ and γ in equality (39); we can obtain

$$\begin{aligned} V(t_k^+) &= \omega^T(t_k^+)\left(I - \beta L_{11}^{(i_k)}\right)^2 \omega(t_k^+) \\ &\leqslant \lambda_{\max}^2\left(I - \beta L_{11}^{(i_k)}\right)\omega^T(t_k)\,\omega(t_k) \leqslant \gamma V(t_k), \end{aligned} \quad (46)$$

where $k = 1, 2, \ldots, i_k \in \{1, 2, \ldots, m\}$.

To prove the Lyapunov function $V(t)$ is convergent, we construct an auxiliary variable ξ in the following form:

$$\begin{aligned} \dot{\xi}(t) &= (2K+l)\xi(t) + l\xi(t-d) + \mu, \quad t \neq t_k, \\ \xi(t_k^+) &= \lambda_{\max}^2\left(I - \beta L_{11}^{(i_k)}\right)\xi(t_k), \end{aligned} \quad (47)$$

where the initial states of $\xi(t) = \|o_\omega(t)\|^2$, $-d \leqslant t \leqslant 0$, $\mu > 0$, $k = 1, 2, \ldots$, where $o_\omega(t) = o_F(t) + (L_{11}^{-1}(0)L_{12}(0))o_L(t)$, $o_F(t) = [o_{M+1}(t), \ldots, o_{M+N}(t)]^T$, $o_L(t) = [o_1(t), \ldots, o_M(t)]^T$.

Let

$$\begin{aligned} \dot{\eta}(t) &= (2K+l)\eta(t), \quad t \neq t_k \\ \eta(t_k^+) &= \lambda_{\max}^2\left(I - \beta L_{11}^{(i_k)}\right)\eta(t_k), \end{aligned} \quad (48)$$

where $k = 1, 2, \ldots$.

From (45), (46), and (47), it is obvious that, for all $t > 0$, $0 \leqslant V(t) \leqslant \xi(t)$. And the solution of (47) satisfies the following integral equation:

$$\xi(t) = \phi(t,0)\xi(0) + \int_0^t \phi(t,s)\left[l\xi(s-d) + \mu\right]ds, \quad (49)$$

where $\phi(t,s)$, $(t, s \geqslant 0)$, is the state transition matrix of the system (48).

When $t_k < t < t_{k+1}$ and $t_{k-1} < s < t_k$, we can arrive at

$$\phi(t,s) \leqslant e^{(2K+l)(t-s)}\lambda_{\max}^2\left(I - \beta L_{11}^{(i_k)}\right). \quad (50)$$

From inequalities (40) and (41), we can obtain

$$\left|\lambda_{\max}\left(I - \beta L_{11}^{(i_k)}\right)\right| \leqslant q < 1. \quad (51)$$

Let $a = -(2K + l) - \gamma/2$ and $2\ln(q)/\tau_0 = \gamma$. Then, from inequality (42), we can get $\gamma < -4(K + l)$ and $a > 0$. Accordingly, inequality (50) can be rewritten as follows:

$$\begin{aligned} \phi(t,s) &\leqslant e^{(-a-\gamma/2)(t-s)}\lambda_{\max}^2\left(I - \beta L_{11}^{(i_k)}\right) \\ &< e^{-a(t-s)} \cdot e^{-(\gamma/2)\cdot 2\tau_0}\lambda_{\max}^2\left(I - \beta L_{11}^{(i_k)}\right) = e^{-a(t-s)}. \end{aligned} \quad (52)$$

Thus, from (49), we can obtain

$$\xi(t) < e^{-at}\left\|o_\omega(t)\right\|^2_{\sup(-d\leqslant t\leqslant 0)} + \int_0^t e^{-a(t-s)}\left[l\xi(s-d) + \mu\right]ds. \quad (53)$$

Let $\varepsilon(\theta) = \theta - a + le^{\theta d}$. Then, $\varepsilon(\theta) = 0$ has a unique solution $\theta^* > 0$ because $\varepsilon(\theta)$ is a strictly monotonic function $\dot{\varepsilon}(\theta) = 1 + lde^{\theta d} > 0$ and $\varepsilon(0) = -a + l < 0$, $\varepsilon(+\infty) > 0$. It is obvious that the following inequality is satisfied:

$$\xi(t) < e^{-\theta^* t}\left\|o_\omega(t)\right\|^2_{\sup(-d\leqslant t\leqslant 0)} + \frac{\mu}{a-l}, \quad (54)$$

where $-d \leqslant t \leqslant 0$. Then we can prove that inequality

$$\xi(t) < e^{-\theta^* t}\left\|o_\omega(t)\right\|^2_{\sup(-d\leqslant t\leqslant 0)} + \frac{\mu}{a-l}, \quad t > 0, \quad (55)$$

is true in the following.

Suppose that inequality (55) is not held; there must be a t_c such that

$$\xi(t_c) \geqslant e^{-\theta^* t_c}\left\|o_\omega(t)\right\|^2_{\sup(-d\leqslant t\leqslant 0)} + \frac{\mu}{a-l}, \quad (56)$$

$$\xi(t_c) < e^{-\theta^* t}\left\|o_\omega(t)\right\|^2_{\sup(-d\leqslant t\leqslant 0)} + \frac{\mu}{a-l}, \quad t < t_c. \quad (57)$$

However, from (53) and (57), we can obtain

$$\xi(t_c) < e^{-\theta^* t_c}\left\|o_\omega(t)\right\|^2_{\sup(-d\leqslant t\leqslant 0)} + \frac{\mu}{a-l} \quad (58)$$

which contradict inequality (56). Thus, (55) can hold for $t > 0$.

As $\mu \to 0$,

$$V(t) \leqslant \xi(t) < e^{-\theta^* t}\left\|o_\omega(t)\right\|^2_{\sup(-d\leqslant t\leqslant 0)}. \quad (59)$$

That is,

$$\|\omega(t)\| \leqslant \left\|o_\omega(t)\right\|_{\sup(-d\leqslant t\leqslant 0)} e^{-\theta^* t/2}. \quad (60)$$

This completes the proof. □

Remark 11. For the special case with only one leader, the result obtained in Theorem 10 also holds. And the final states of the followers will track the leader's state.

Remark 12. The fixed communication topology in Section 2.1 can be viewed as a special case in the switching topology case. The achievement of the containment control in the fixed topology systems is the fundamental problem and it contributes to the proof procedure of the switching counterpart.

Remark 13. The design procedure of the impulsive controller in Theorem 8 is that first, according to the communication topology of the graph $\mathcal{G}$ and inequality (11), the region of q can be ascertained. Then, we choose an appropriate constant q. From conditions (12) and (13), we can derive the region of the feedback α and the impulsive period τ_0. Choosing the appropriate α and τ_0, the containment control can be achieved. The counterpart under switching topology in Theorem 10 is similar and we omit it.

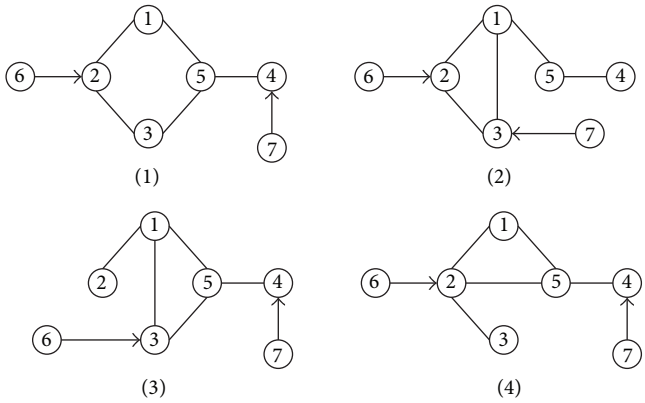

FIGURE 1: The interaction graphs.

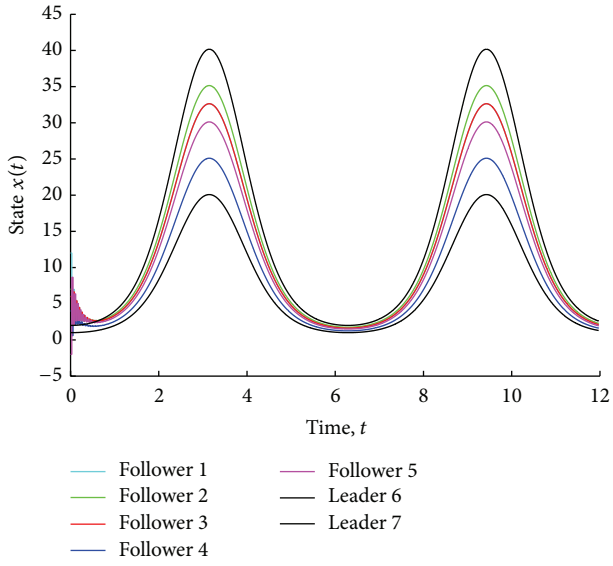

FIGURE 2: The states of the agents in system (1) with fixed topology using impulsive algorithm (6).

3. Simulations

In this section, we give some examples to verify the theoretical analysis. The communication graphs are shown in Figure 1. The agents labeled as 6 and 7 are the leaders and the agents labeled as 1, 2, 3, 4, and 5 are the followers.

Example 1. According to Figure 1, the communication graph (1) satisfies the Assumption 2. Consider that the system (1) with the nonlinear dynamic is $g(t, x_i(t), x_i(t-d)) = x_i(t)\sin(t) + 0.5x_i(t)\sin(t-d)$, $i \in \mathcal{V}$. Obviously, Assumption 1 is satisfied in the system and the corresponding parameters are $K = 1$ and $l = 0.5$, respectively. Using the proposed impulsive containment control algorithm (6), the simulation results are shown in Figure 2. From condition (11) in Theorem 8, the regions of q should be $0.8774 < q < 1$. In this case, we choose $q = 0.9$ and, according to conditions (12) and (13), it is obvious that the region of α and the impulsive period τ_0 are $0.3263 \leqslant \alpha \leqslant 0.4048$ and $\tau_0 < 0.0351$, respectively. We choose $\alpha = 0.38$ and $\tau_0 = 0.03$. Suppose the time-delay $d = 0.01$. Obviously, Assumption 6 is satisfied in the system (1). From Figure 2, it is obvious that the final states of the followers converge into the convex hull formed by the leaders.

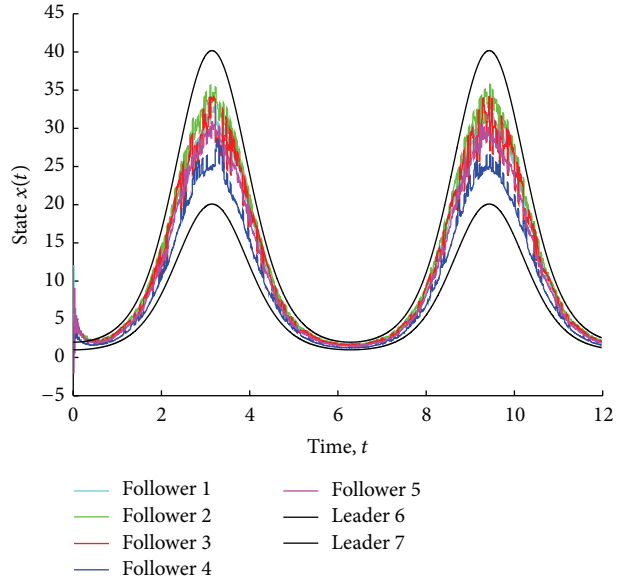

FIGURE 3: The states of the agents in system (1) with switching topologies using impulsive algorithm (34).

Example 2. The graphs of the communication topology are shown in Figure 1. Now consider the nonlinear system $g(t, x_i(t), x_i(t-d)) = x_i(t)\sin(t) + 0.5x_i(t)\sin(t-d)$, $i \in \mathcal{V}$, with switching topologies. It is clear that the four topologies in Figure 1 satisfy Assumption 2 and the dynamics of the system satisfy Assumption 1. In every time interval $(t_{k-1}, t_k]$, $k = 1, 2, \ldots$, the communication topology is chosen from Figure 1 randomly. Using the impulsive algorithm (34), the simulation result of the nonlinear system with switching topologies is shown in Figure 3. According to the conditions in Theorem 10, the region of q is $q > 0.9273$ and we choose $q = 0.93$. According to condition (41), the feedback gain β should choose from $0.3755 \leqslant \beta \leqslant 0.3907$ and we choose $\beta = 0.38$. From inequality (42), the impulsive period τ_0 should be less than 0.0242 and we choose $\tau_0 = 0.02$. And suppose that the time-delay $d = 0.01$, which satisfies Assumption 6. From Figure 3, we can get that the containment control is achieved and the follower's states converge into the convex hull spanned by the multiple leaders. The final states of the followers $x_F(t)$ converge to $(-L_{11}^{-1}(t)L_{12}(t))x_L(t)$ as $t \to +\infty$ and the states $(-L_{11}^{-1}(t)L_{12}(t))x_L(t)$ are time varying and nonsmooth.

4. Conclusions

This paper has considered the nonlinear multiagent systems with time-delay of multiple leaders. When the topologies in the nonlinear systems are fixed, an impulsive control

algorithm is proposed and some useful sufficient conditions to achieve containment control are obtained. Also, the nonlinear systems under switching topologies are considered. Using the proposed impulsive algorithms, the final states of all the followers will converge into the convex hull formed by the states of the leaders. Finally, some simulations are given to illustrate our theoretical analyses.

Conflict of Interests

The authors declare that there is no conflict of interests regarding the publication of this paper.

Acknowledgments

The work was supported partly by the National Natural Science Foundation of China under Grants 61374064, 61304152, and 61364017, the National Key Technology R&D Program of China 2013BAA01B01, and the China Postdoctoral Science Foundation funded Project 2012M511258 and 2013T60738.

References

[1] H. Su, X. Wang, and Z. Lin, "Flocking of multi-agents with a virtual leader," *IEEE Transactions on Automatic Control*, vol. 54, no. 2, pp. 293–307, 2009.

[2] H. Du and S. Li, "Attitude synchronization control for a group of flexible spacecraft," *Automatica*, vol. 50, no. 2, pp. 646–651, 2014.

[3] D. Yuan, D. W. Ho, and S. Xu, "Inexact dual averaging method for distributed multi-agent optimization," *Systems & Control Letters*, 2014.

[4] Z. Liu, Z. Guan, T. Li, X. Zhang, and J. Xiao, "Quantized consensus of multi-agent systems via broadcast gossip algorithms," *Asian Journal of Control*, vol. 14, no. 6, pp. 1634–1642, 2012.

[5] X. Lu, F. Austin, and S. Chen, "Formation control for second-order multi-agent systems with time-varying delays under directed topology," *Communications in Nonlinear Science and Numerical Simulation*, vol. 17, no. 3, pp. 1382–1391, 2012.

[6] R. Olfati-Saber and R. M. Murray, "Consensus problems in networks of agents with switching topology and time-delays," *IEEE Transactions on Automatic Control*, vol. 49, no. 9, pp. 1520–1533, 2004.

[7] W. Ren and R. W. Beard, "Consensus seeking in multiagent systems under dynamically changing interaction topologies," *IEEE Transactions on Automatic Control*, vol. 50, no. 5, pp. 655–661, 2005.

[8] W. Zhu and D. Cheng, "Leader-following consensus of second-order agents with multiple time-varying delays," *Automatica*, vol. 46, no. 12, pp. 1994–1999, 2010.

[9] H. Su, M. Z. Q. Chen, J. Lam, and Z. Lin, "Semi-global leader-following consensus of linear multi-agent systems with input saturation via low gain feedback," *IEEE Transactions on Circuits and Systems I: Regular Papers*, vol. 60, no. 7, pp. 1881–1889, 2013.

[10] H. Su, M. Chen, X. Wang, and J. Lam, "Semiglobal observer-based leader-following consensus with input saturation," *IEEE Transactions on Industrial Electronics*, vol. 61, pp. 2842–2850, 2014.

[11] X. Lu, R. Lu, S. Chen, and J. Lu, "Finite-time distributed tracking control for multi-agent systems with a virtual leader," *IEEE Transactions on Circuits and Systems I: Regular Papers*, vol. 60, no. 2, pp. 352–362, 2013.

[12] Y. Lou and Y. Hong, "Target containment control of multi-agent systems with random switching interconnection topologies," *Automatica*, vol. 48, no. 5, pp. 879–885, 2012.

[13] Z. Li, Z. Duan, W. Ren, and G. Feng, "Containment control of linear multi-agent systems with multiple leaders of bounded inputs using distributed continuous controllers," *International Journal of Robust and Nonlinear Control*, 2014.

[14] H. Liu, G. Xie, and L. Wang, "Containment of linear multi-agent systems under general interaction topologies," *Systems and Control Letters*, vol. 61, no. 4, pp. 528–534, 2012.

[15] J. Li, W. Ren, and S. Xu, "Distributed containment control with multiple dynamic leaders for double-integrator dynamics using only position measurements," *IEEE Transactions on Automatic Control*, vol. 57, no. 6, pp. 1553–1559, 2012.

[16] Z. Meng, W. Ren, and Z. You, "Distributed finite-time attitude containment control for multiple rigid bodies," *Automatica*, vol. 46, no. 12, pp. 2092–2099, 2010.

[17] H. Liu, G. Xie, and L. Wang, "Necessary and sufficient conditions for containment control of networked multi-agent systems," *Automatica*, vol. 48, no. 7, pp. 1415–1422, 2012.

[18] J. Mei, W. Ren, and G. Ma, "Distributed containment control for Lagrangian networks with parametric uncertainties under a directed graph," *Automatica*, vol. 48, no. 4, pp. 653–659, 2012.

[19] Y. Cao, W. Ren, and M. Egerstedt, "Distributed containment control with multiple stationary or dynamic leaders in fixed and switching directed networks," *Automatica*, vol. 48, no. 8, pp. 1586–1597, 2012.

[20] P. Wang and Y. Jia, "Distributed containment control of second-order multi-agent systems with inherent non-linear dynamics," *IET Control Theory & Applications*, vol. 8, no. 4, pp. 277–287, 2014.

[21] K. Liu, G. Xie, W. Ren, and L. Wang, "Consensus for multi-agent systems with inherent nonlinear dynamics under directed topologies," *Systems and Control Letters*, vol. 62, no. 2, pp. 152–162, 2013.

[22] W. Yu, G. Chen, and M. Cao, "Consensus in directed networks of agents with nonlinear dynamics," *IEEE Transactions on Automatic Control*, vol. 56, no. 6, pp. 1436–1441, 2011.

[23] Z. Liu, H. Zhou, Z. Guan, W. Hu, L. Ding, and W. Wang, "Distributed impulsive consensus of the multiagent system without velocity measurement," *Abstract and Applied Analysis*, vol. 2013, Article ID 825307, 8 pages, 2013.

[24] J. Lu, J. Kurths, J. Cao, N. Mahdavi, and C. Huang, "Synchronization control for nonlinear stochastic dynamical networks: pinning impulsive strategy," *IEEE Transactions on Neural Networks and Learning Systems*, vol. 23, no. 2, pp. 285–292, 2012.

[25] Z. Guan, D. J. Hill, and X. Shen, "On hybrid impulsive and switching systems and application to nonlinear control," *IEEE Transactions on Automatic Control*, vol. 50, no. 7, pp. 1058–1062, 2005.

[26] Z.-W. Liu, Z.-H. Guan, X. Shen, and G. Feng, "Consensus of multi-agent networks with aperiodic sampled communication via impulsive algorithms using position-only measurements," *Institute of Electrical and Electronics Engineers*, vol. 57, no. 10, pp. 2639–2643, 2012.

[27] Z.-H. Guan, Z.-W. Liu, G. Feng, and Y.-W. Wang, "Synchronization of complex dynamical networks with time-varying delays via impulsive distributed control," *IEEE Transactions on Circuits and Systems I: Regular Papers*, vol. 57, no. 8, pp. 2182–2195, 2010.

[28] G. Wen, Z. Duan, W. Yu, and G. Chen, "Consensus of second-order multi-agent systems with delayed nonlinear dynamics and intermittent communications," *International Journal of Control*, vol. 86, no. 2, pp. 322–331, 2013.

[29] R. T. Rockafellar, *Convex Analysis*, vol. 28 of *Princeton Mathematical Series*, Princeton University Press, Princeton, NJ, USA, 1997.

Hindawi Publishing Corporation
Mathematical Problems in Engineering
Volume 2015, Article ID 289825, 9 pages
http://dx.doi.org/10.1155/2015/289825

Research Article

Improved Different Dimensional Sensors Combined Space Registration Algorithm

Yuming Bo, Zhimin Chen, Mingfeng Yin, and Tianxiong Wang

School of Automation, Nanjing University of Science and Technology, Nanjing 210094, China

Correspondence should be addressed to Zhimin Chen; chenzhimin@188.com

Received 5 September 2014; Accepted 30 November 2014

Academic Editor: Michael Chen

To address the problem of deviation and registration of 3D radar and infrared sensor, this paper presents and improves a method based on the state value and space deviation of federated filtering of unscented Kalman filter and standard Kalman filter, which conduces to real time registering of system deviation of radar and IF sensors. In the method presented here, a covariance matching criteria-based approach was employed for judgment of filtering divergent trend, while self-adaptive attenuation factor was introduced for correction of the predicted error covariance so as to inhibit the divergent phenomenon. The experiment results indicated that the method presented here conduces to improvement of the precision and speed of space registration, showing practical value in deviation registration of 3D radars and infrared sensors.

1. Introduction

Heterogeneous multisensor system overcomes the defect of single sensor that can provide unilateral information of the tracking object image [1, 2]. However, employment of heterogeneous multisensor system in measurement requires calibration of the data information of such sensors. Due to the fact that the transferred data form, narration, and description of the environment by every sensor vary [2–4], if the space deviation undergoes information fusion directly without registration, then it may result in obvious tracking error or even the presence of multiple false points [5–8].

3D radar is able to provide the complete position information of the tracking objects. Nevertheless, since radar always radiates high-power magnetic wave into the air during working, it is apt to magnetic interference and attack by antiradiation missiles. Infrared sensors can be easily concealed and effective in resisting interference, yet unable to offer the distance data of the tracking object to the system [8]. Moreover, it can be easily influenced by climate due to over close distance. Deviation fusion mainly relies on two methods: least square method and exact maximum likelihood method [9]. Unfortunately, least square method overlooks the measurement noise of sensors and the impact of deviation relative to the common coordinate system of each sensor on information fusion. Exact maximum likelihood method though takes the measurement noise of sensors into consideration [10], yet fails to resolve the problem of error in coordinate conversion, which inevitably results in wrong data and inaccurate models [11]. Moreover, least square method and exact maximum likelihood method all require the sensors to be homogeneous sensors which are less capable in measurement of deviation registration among sensors at different dimensions.

To address the issues stated above, this paper employed an improved federated filter based on unscented and standard Kalman filters, the former wherein was used for accuracy estimation relying on its self-adaptive divergence-inhibition ability, the later wherein was used for deviation vector estimation depending on its high speed, thereby actualizing accurate registration of space deviation.

2. UKF (Unscented Kalman Filter)

Consider a discrete time nonlinear system as follows:

$$\begin{aligned} X(t_{k+1}) &= F(X(t_k)) + W(t_k), \\ Z(t_k) &= h(X(t_k)) + V(t_k), \end{aligned} \tag{1}$$

where in X_{k+1} is the state vector of the system, F is the state transition matrix, W_k is system process noise with $Q(t_k)$ as variance, and V_k is measurement noise with $R(t_k)$ as variance.

After state estimation of the above nonlinear system, the linear approximation in EKF (Extended Kalman Filter, EKF) algorithm was replaced by UT [12], and then the UKF [13] algorithm for nonlinear system state estimation was acquired [14]. Now simply after sigma point sampling of the system state vector, the process noise and measurement noise can be separated.

The detailed operation steps of UKF algorithm are given as follows.

Initializing:

$$\begin{aligned}\hat{x}(t_0) &= E[x(t_0)],\\ P(t_0) &= E\left[(x(t_0)-\hat{x}(t_0))(x(t_0)-\hat{x}(t_0))^T\right].\end{aligned} \tag{2}$$

Computing sigma point set:

$$\chi(t_k) = \left[\hat{x}(t_k) \quad \hat{x}(t_k) \pm ((L+\lambda)P(t_k))^{1/2}\right]. \tag{3}$$

Prediction updating:

$$\begin{aligned}\chi(t_{k+1} \mid t_k) &= F(\chi_k),\\ \hat{x}(t_{k+1} \mid t_k) &= \sum_{i=0}^{2n} W_i^m \chi_i(t_{k+1} \mid t_k),\\ P(t_{k+1} \mid t_k) &= \sum_{i=0}^{2L} W_i^c \left[\chi_i(t_{k+1} \mid t_k) - \hat{x}(t_{k+1} \mid t_k)\right]\\ &\quad \times \left[\chi_i(t_{k+1} \mid t_k) - \hat{x}(t_{k+1} \mid t_k)\right]^T + Q(t_{k+1}),\\ \hat{z}_i(t_{k+1} \mid t_k) &= h(\chi_i(t_{k+1} \mid t_k)),\\ \hat{z}(t_{k+1} \mid t_k) &= \sum_{i=0}^{2L} W_i^m \hat{z}_i(t_{k+1} \mid t_k).\end{aligned} \tag{4}$$

Measurement updating:

$$\begin{aligned}P_{zz}(t_{k+1}) &= \sum_{i=0}^{2L} W_i^c \left[\hat{z}_i(t_{k+1} \mid t_k) - \hat{z}^{(1)}(t_{k+1} \mid t_k)\right]\\ &\quad \times \left[\hat{z}_i(t_{k+1} \mid t_k) - \hat{z}(t_{k+1} \mid t_k)\right]^T + R(t_{k+1}),\\ P_{xz}(t_{k+1}) &= \sum_{i=0}^{2L} W_i^c \left[\chi_i(t_{k+1} \mid t_k) - \hat{x}(t_{k+1} \mid t_k)\right]\\ &\quad \times \left[\chi_i(t_{k+1} \mid t_k) - \hat{x}(t_{k+1} \mid t_k)\right]^T,\\ K(t_{k+1}) &= P_{xz}(t_{k+1})\left(P_{zz}(t_{k+1})\right)^{-1},\\ \hat{x}(t_{k+1}) &= \hat{x}(t_{k+1} \mid t_k) + K(t_{k+1}) \cdot \left[z(t_{k+1}) - \hat{z}(t_{k+1} \mid t_k)\right],\\ P(t_{k+1}) &= P(t_{k+1} \mid t_k) - K(t_{k+1})\left(P_{zz}(t_{k+1})^{-1}\right)\left(K(t_{k+1})\right)^T.\end{aligned} \tag{5}$$

3. Improved Unscented Kalman Filter

When UKF algorithm is applied to target tracking, the mathematical model of the studied object and the a priori knowledge of noise statistics should be known at first. If the filter was designed based on inaccurate mathematical model or noise statistics, then a larger state estimation error or even filter divergence can occur [15].

Divergence of UKF occurs frequently. A covariance registration criterion-based method was presented here for judgment of filter divergence trend:

$$\begin{aligned}&\left(z_k - h(\hat{x}_{k|k-1})\right)^T \left(z_k - h(\hat{x}_{k|k-1})\right)\\ &\quad \le S \operatorname{tr}\left[E\left(\left(z_k - h(\hat{x}_{k|k-1})\right)^T \left(z_k - h(\hat{x}_{k|k-1})\right)\right)\right],\end{aligned} \tag{6}$$

wherein S is the preset adjustability coefficients, $S \ge 1$; if the above equation is false, then adjust $P_{k|k-1}$ to be

$$\begin{aligned}P_{k|k-1} &= \lambda_k \sum_{0}^{2n} W_i \left[\chi_i(t_k \mid t_{k-1}) - \widehat{X}(t_k \mid t_{k-1})\right]\\ &\quad \times \left[\chi_i(t_k \mid t_{k-1}) - \widehat{X}(t_k \mid t_{k-1})\right] + Q_{k-1}.\end{aligned} \tag{7}$$

When the filtering diverges, attenuation factor calculation formula can be used to acquire self-adaptive weighting coefficient λ_k that can then be used for correction of $P_{k|k-1}$, accordingly increasing the use of the current observed quantity and inhibiting the filtering divergence. λ_k therein can be determined by the following equation:

$$\begin{aligned}\lambda_k &= \begin{cases}\lambda_0, & \lambda_0 \ge 1\\ 1, & \lambda < 1,\end{cases}\\ \lambda_0 &= \operatorname{tr}\left(C_{0,k} - R\right)^T\\ &\quad \times \left(\operatorname{tr}\left(\sum_{i=0}^{L} W_i \left[h(\chi_i(t_k \mid t_{k-1}) - \hat{z}_{k|k-1})\right]\right.\right.\\ &\quad \left.\left. \times \left[h(\chi_i(t_k \mid t_{k-1})) - \hat{z}_{k|k-1}\right]^T\right)\right)^{-1},\end{aligned} \tag{8}$$

$$C_{0,k} = \begin{cases}\left(z_k - h(\hat{x}_{k|k-1})\right)\left(z_k - h(\hat{x}_{k|k-1})\right)^T, & k = 1\\ \left(\rho C_{0,k} + \left(z_k - h(\hat{x}_{k|k-1})\right)\right.\\ \quad \times \left(z_k - h(\hat{x}_{k|k-1})\right)^T\big)\\ \quad \times (1+\rho)^{-1} & k > 1,\end{cases}$$

in which $0 < \rho < 1$ is the attenuation coefficient which can further enhance the rapid tracking ability of filter, normally the more it close to 1, the greater proportion of the information before moment k, and the influence of the current residual error vector can be highlighted better. This method shows good tracking ability of mutation state and keeps effective in tracking even though the filtering reaches a steady state.

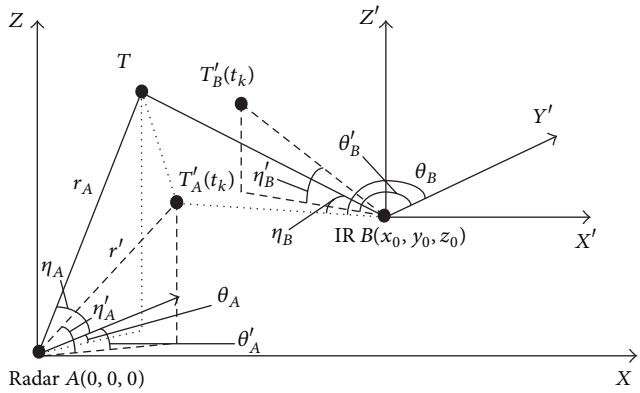

Figure 1: Improved heterogeneous sensor deviation registration model.

4. Establishment of Improved Heterogeneous Sensor Deviation Registration Model

3D radar and IR sensor B are tracking and detecting the same object T, the set relation of deviation registration is shown in Figure 1 It is assumed that radar A is located at the origin of the reference Cartesian coordinate system $(0, 0, 0)$, IR sensor B locating at (x_0, y_0, z_0) in the reference Cartesian coordinate system. Let Δt be the measurement time deviation, $(\Delta r_A, \Delta\theta_A, \Delta\eta_A)$ the system deviation of radar A (distance, azimuth angle, and pitch angle), and $(\Delta\theta_B, \Delta\eta_B)$ the system deviation (azimuth angle and pitch angle) of infrared B. Assuming the system deviation measurement random noises of 3D radar A and IR sensor B were $V_A = [v_{rA}, v_{\theta A}, v_{\eta A}]$ and $V_B = [v_{\theta B}, v_{\eta B}]$, respectively, wherein the subject means of V_A and V_B were 0, covariance was the Gaussian distribution of $R_A = \mathrm{diag}[\sigma^2_{rA}, \sigma^2_{\theta A}, \sigma^2_{\eta A}]$ and $R_B = \mathrm{diag}[\sigma^2_{\theta B}, \sigma^2_{\eta B}]$, in which σ^2_{rA} is the standard deviation of distance, $\sigma^2_{\theta A}$ is the standard deviation of radar azimuth angle, $\sigma^2_{\eta A}$ is the standard deviation of radar pitch angle, $\sigma^2_{\theta B}$ is the standard deviation of IR sensor azimuth angle, $\sigma^2_{\eta B}$ is the standard deviation of IR sensor pitch angle.

Supposing the true position coordinate of object T at t_k is $\{x(t_k), y(t_k), z(t_k)\}$, true polar coordinates of object relative to IR sensor B are $\{\theta_B(t_k), \eta_B(t_k)\}$ and measurement values of radar A and TR sensor B were $\{r'(t_k), \theta'_A(t_k), \eta'_A(t_k)\}$ and $\{\theta'_B(t_k), \eta'_B(t_k)\}$, respectively. The true polar coordinate value of object T relative to radar A is $\{r(t_k), \theta_A(t_k), \eta_A(t_k)\}$, and then (9) can be deduced:

$$\begin{aligned} r'_A(t_k) &= r_A(t_k) + \Delta r_A + v_{rA}, \\ \theta'_A(t_k) &= \theta_A(t_k) + \Delta\theta_A + v_{\theta A}, \\ \eta'_A(t_k) &= \eta_A(t_k) + \Delta\eta_A + v_{\eta A}, \\ \theta'_B(t_k) &= \theta_B(t_k) + \Delta\theta_B + v_{\theta B}, \\ \eta'_B(t_k) &= \eta_B(t_k) + \Delta\eta_B + v_{\eta B}. \end{aligned} \tag{9}$$

$$\begin{aligned} x'_A(t_k) &= r'_A(t_k)\sin\left(\theta'_A(t_k)\right)\cos\left(\eta'_A(t_k)\right) - \mu_1(t_k) \\ &= \left(r_A(t_k) + \Delta r_A\right)\sin\left(\theta_A(t_k) + \Delta\theta_A\right) \\ &\quad \cdot \cos\left(\eta_A(t_k) + \Delta\eta_A\right) - \mu_1(t_k), \\ y'_A(t_k) &= r'_A(t_k)\cos\left(\theta'_A(t_k)\right)\cos\left(\eta'_A(t_k)\right) - \mu_2(t_k) \\ &= \left(r_A(t_k) + \Delta r_A\right)\cos\left(\theta_A(t_k) + \Delta\theta_A\right) \\ &\quad \cdot \cos\left(\eta_A(t_k) + \Delta\eta_A\right) - \mu_2(t_k), \\ z'_A(t_k) &= r'_A(t_k)\sin\left(\theta'_A(t_k)\right) - \mu_1(t_k) \\ &= \left(r_A(t_k) + \Delta r_A\right)\sin\left(\theta_A(t_k) + \Delta\theta_A\right) - \mu_3(t_k). \end{aligned} \tag{11}$$

Convert (9) into the common reference coordinate system; then

Developing (11) using the transfer of axes polar coordinate-Cartesian coordinate and Taylor first approximation formula, (12) can be acquired as follows:

$$\begin{aligned} x'_A(t_k) &\approx x_A(t_k) + \frac{x_A(t_k)}{r_A(t_k)}\Delta r_A + y_A(t_k)\Delta\theta_A \\ &\quad - \frac{z_A(t_k)\cdot x_A(t_k)}{\sqrt{x^2_A(t_k) + y^2_A(t_k)}}\Delta\eta_A - \mu_1(t_k), \\ y'_A(t_k) &\approx y_A(t_k) + \frac{y_A(t_k)}{r_A(t_k)}\Delta r_A - x_A(t_k)\Delta\theta_A \\ &\quad - \frac{z_A(t_k)\cdot x_A(t_k)}{\sqrt{x^2_A(t_k) + y^2_A(t_k)}}\Delta\eta_A - \mu_2(t_k), \\ z'_A(t_k) &\approx z_A(t_k) + \frac{z_A(t_k)}{r_A(t_k)}\Delta r_A \\ &\quad + \sqrt{x^2_A(t_k) + y^2_A(t_k)}\Delta\eta - \mu_3(t_k), \end{aligned} \tag{12}$$

wherein $r_A(t_k) = \sqrt{x^2_A(t_k) + y^2_A(t_k) + z^2_A(t_k)}$.

For the same object, since the object positions in the common coordinate system are the same, thus the following equation is true:

$$\begin{aligned} x_A(t_k) &= r_A(t_k)\sin\left(\theta_A(t_k)\right)\cos\left(\eta_A(t_k)\right) \\ &= r_B(t_k)\sin\left(\theta_B(t_k)\right)\cos\left(\eta_B(t_k)\right) + x_0, \\ y_A(t_k) &= r_A(t_k)\cos\left(\theta_A(t_k)\right)\cos\left(\eta_A(t_k)\right) \\ &= r_B(t_k)\cos\left(\theta_B(t_k)\right)\cos\left(\eta_B(t_k)\right) + y_0, \\ z_A(t_k) &= r_A(t_k)\sin\left(\theta_A(t_k)\right) \\ &= r_B(t_k)\sin\left(\theta_B(t_k)\right) + z_0. \end{aligned} \tag{13}$$

Deducing from the equation above, we have

$$\theta_B(t_k) = \arctan\left(\frac{x_A(t_k) - x_0}{y_A(t_k) - y_0}\right),$$

$$\eta_B(t_k) = \arctan\left(\frac{z_A(t_k) - z_0}{\sqrt{[x_A(t_k) - x_0]^2 + [y_A(t_k) - y_0]}}\right). \tag{14}$$

Introducing the equation above into (10),

$$\theta'_B(t_k) = \arctan\left(\frac{x_A(t_k) - x_0}{y_A(t_k) - y_0}\right) + \Delta\theta_B + v_{\theta B},$$

$$\eta'_B(t_k) = \arctan\left(\frac{z_A(t_k) - z_0}{\sqrt{[x_A(t_k) - x_0]^2 + [y_A(t_k) - y_0]}}\right) + \Delta\eta_B + v_{\eta B}. \tag{15}$$

5. Heterogeneous Sensor Deviation Registration Steps

5.1. Vector Dimension Expansion. Different from the standard state filtering, since the algorithm given in this paper is the federated computation estimation of the object state and deviation registration, dimension expansion is performed here.

Firstly establishing dimension expansion vector $X(t_k) = [X^{(1)}(t_k)^T, X^{(2)}(t_k)^T]$, in which $X^{(1)}(t_k)$ is the state vector of the object, and $X^{(2)}(t_k) = [\Delta r_A \ \Delta\theta_A \ \Delta\eta_A \ \Delta\theta_B \ \Delta\eta_B]^T$ is the time and space deviation vector, then the system state equation in dimension expansion state is shown in

$$X(t_{k+1}) = \Phi X(t_k) + W(t_k), \tag{16}$$

wherein $\Phi = \left[\begin{smallmatrix} F & 0 \\ 0 & I \end{smallmatrix}\right]$, $W(t_k) = [\Gamma w(t_k) \ \ 0]$, and F and Γ are determined by the specific object motion model.

After dimension expansion, the system measurement vector is $Z(t_k) = [x'_A(t_k) \ \ y'_A(t_k) \ \ z'_A(t_k) \ \ \theta'_B(t_k) \ \ \eta'_B(t_k)]$, and the system measurement equation after dimension expansion is shown in

$$Z(t_k) = h(t_k) + V(t_k), \tag{17}$$

in which $h(t_k) = [h_1(t_k), h_2(t_k), h_3(t_k), h_4(t_k), h_5(t_k)]$. The specific forms can be referred to as (12) and (15). $V(t_k) = [0, 0, 0, v_{\theta B}, v_{\eta B}]^T$ is the measurement noise vector.

5.2. Computing Steps. The following equation can be deduced from (16):

$$X^{(2)}(t_{k+1}) = X^{(2)}(t_k). \tag{18}$$

From (18), registering deviation shows the features of fixed error and remains the same within a certain time.

Besides, from the measurement equations (17), (12), and (15), we can see that, relative to the object state vector $X^{(1)}(t_k)$, the measurement equation is nonlinear. But it is linear relative to space deviation vector $X^{(2)}(t_k)$. That is, measurement equation (17) can be developed into

$$Z(t_k) = H\left[X^{(1)}(t_k)\right] X^{(2)}(t_k) + V(t_k). \tag{19}$$

$H[X^{(1)}(t_k)]$ is the nonlinear function matrix of the state vector $X^{(1)}(t_k)$ of the object.

Therefore, giving a fixed dimension expansion state vector $X(t_k)$, the object state vector $X^{(1)}(t_k)$ can be estimated by improved UKF, and then KF can be used to estimate the space deviation vector $X^{(2)}(t_k)$. The specific steps are given as follows.

(1) Let the state vector mean be $\widehat{X}(t_k)$, and its corresponding covariance $P(t_k)$:

$$\widehat{X}(t_k) = \begin{bmatrix} \widehat{X}^{(1)}(t_k) \\ \widehat{X}^{(2)}(t_k) \end{bmatrix},$$

$$P(t_k) = \begin{bmatrix} P^{(1)}(t_k) & 0 \\ 0 & P^{(2)}(t_k) \end{bmatrix},$$

$$\widehat{X}(t_{k+1} \mid t_k) = \begin{bmatrix} \widehat{X}^{(1)}(t_{k+1} \mid t_k) \\ \widehat{X}^{(2)}(t_{k+1} \mid t_k) \end{bmatrix} = \begin{bmatrix} F\widehat{X}^{(1)}(t_k) \\ \widehat{X}^{(2)}(t_k) \end{bmatrix}, \tag{20}$$

$$P(t_{k+1} \mid t_k) = \begin{bmatrix} P^{(1)}(t_{k+1} \mid t_k) & 0 \\ 0 & P^{(2)}(t_{k+1} \mid t_k) \end{bmatrix} = \begin{bmatrix} FP^{(1)}(t_k)F^T + \Gamma Q_k \Gamma^T & 0 \\ 0 & P^{(2)}(t_k)F^T \end{bmatrix}.$$

(2) Sampling symmetric strategy can be used for computation of Sigma point $\chi_i(t_{k+1} \mid t_k)$ and the corresponding weight:

$$\chi_0(t_{k+1} \mid t_k) = \widehat{X}^{(1)}(t_{k+1} \mid t_k), \quad i = 0,$$

$$\chi_i(t_{k+1} \mid t_k) = \widehat{X}^{(1)}(t_{k+1} \mid t_k) + \left(\sqrt{(L_1 + \kappa)P^{(1)}(t_{k+1} \mid t_k)}\right)_i, \quad i = 1, \ldots, L_1,$$

$$\chi_{i+L_1}(t_{k+1} \mid t_k) = \widehat{X}^{(1)}(t_{k+1} \mid t_k) + \left(\sqrt{(L_1 + \kappa)P^{(1)}(t_{k+1} \mid t_k)}\right)_i, \quad i = 1, \ldots, L_1, \tag{21}$$

$$W_0 = \frac{\kappa}{L_1 + \kappa}, \quad i = 0,$$

$$W_i = \frac{1}{[2(L_1 + \kappa)]}, \quad i = 1, \ldots, L_1,$$

$$W_{i+L_1} = \frac{1}{[2(L_1 + \kappa)]}, \quad i = 1, \ldots, L_1,$$

wherein L_1 is the dimension of the object state vector $\widehat{X}^{(1)}(t_k)$, κ is the scale parameter, and $(\sqrt{(L_1+\kappa)P^{(1)}(t_{k+1} \mid t_k)})_i$ is the ith column of the matrix square root.

(3) Along the time update process, according to the state equation, the updated sigma point is

$$\chi_i(t_{k+1} \mid t_k) = F\chi_i(t_k), \quad i = 0, 1, \ldots, 2L_1. \tag{22}$$

(4) Compute the state variance prediction and covariance

$$\begin{aligned}
\widehat{X}^{(1)}(t_{k+1}t_k) &= \sum_{i=0}^{2L_1} W_i \chi_i(t_{k+1} \mid t_k), \\
P^{(1)}(t_{k+1} \mid t_k) &= \sum_{i=0}^{2L_1} W_i \left[\chi_i(t_{k+1} \mid t_k) - \widehat{X}^{(1)}(t_{k+1} \mid t_k)\right] \\
&\quad \times \left[\chi_i(t_{k+1} \mid t_k) - \widehat{X}^{(1)}(t_{k+1} \mid t_k)\right]^T + Q,
\end{aligned} \tag{23}$$

wherein Q is the covariance of process noise.

(5) If covariance is emanative, modify $P^{(1)}(t_{k+1} \mid t_k)$ according to (7), or otherwise take the next step.

The measurement prediction and covariance corresponding to sigma point are given as follows, respectively:

$$\widehat{Z}_i(t_{k+1} \mid t_k) = h\left(\chi_i(t_{k+1} \mid t_k)\right), \tag{24}$$

$$\begin{aligned}
\widehat{Z}^{(1)}(t_{k+1} \mid t_k) &= \sum_{i=0}^{2L_1} W_i \widehat{Z}_i(t_{k+1} \mid t_k), \\
P_{ZZ}^{(1)}(t_{k+1}) &= \sum_{i=0}^{2L_1} W_i \left[\widehat{Z}_i(t_{k+1} \mid t_k) - \widehat{Z}^{(1)}(t_{k+1} \mid t_k)\right] \\
&\quad \times \left[\widehat{Z}_i(t_{k+1} \mid t_k) - \widehat{Z}^{(1)}(t_{k+1} \mid t_k)\right]^T + R(t_{k+1}), \\
P_{XZ}^{(1)}(t_{k+1}) &= \sum_{i=0}^{2L_1} W_i \left[\chi_i(t_{k+1} \mid t_k) - \widehat{X}^{(1)}(t_{k+1} \mid t_k)\right] \\
&\quad \times \left[\chi_i(t_{k+1} \mid t_k) - \widehat{X}^{(1)}(t_{k+1} \mid t_k)\right]^T.
\end{aligned} \tag{25}$$

(6) Measurement updating is as follows:

$$\begin{aligned}
\widehat{X}^{(1)}(t_{k+1}) &= \widehat{X}^{(1)}(t_{k+1} \mid t_k) \\
&\quad + K^{(1)}(t_{k+1}) \cdot \left[Z(t_{k+1}) - \widehat{Z}^{(1)}(t_{k+1} \mid t_k)\right], \\
P^{(1)}(t_{k+1}) &= P^{(1)}(t_{k+1} \mid t_k) \\
&\quad - K^{(1)}(t_{k+1})\left(P_{ZZ}{}^{(1)}(t_{k+1})^{-1}\right)\left(K^{(1)}(t_{k+1})\right)^T, \\
K^{(1)}(t_{k+1}) &= P_{XZ}^{(1)}(t_{k+1})\left(P_{ZZ}^{(1)}(t_{k+1})\right)^{-1}.
\end{aligned} \tag{26}$$

Table 1: Comparison of simulation parameters by UNGM model.

	Algorithm	RMSE	Time (s)
$Q = 10$	UKF	3.1372	0.2890
	Improved UKF	2.2089	0.3156
$Q = 20$	UKF	5.2998	0.2874
	Improved UKF	2.7304	0.3237

(7) Then make use of Kalman filtering method to estimate space deviation vector. The specific steps are given as follows:

$$\begin{aligned}
K^{(2)}(t_{k+1}) &= P^{(2)}\left(\frac{t_{k+1}}{t_k}\right) H\left[\widehat{X}^{(1)}(t_{k+1})\right]^T \\
&\quad \cdot \left[H\left[\widehat{X}^{(1)}(t_{k+1})\right] P^{(2)}\left(\frac{t_{k+1}}{t_k}\right)\right. \\
&\quad \left. \cdot H\left[\widehat{X}^{(1)}(t_{k+1})\right]^T + R(t_{k+1})\right]^{-1}, \\
\widehat{X}^{(2)}(t_{k+1}) &= \widehat{X}^{(2)}\left(\frac{t_{k+1}}{t_k}\right) + K^{(2)}(t_{k+1}) \\
&\quad \cdot \left[z(t_{k+1}) - H\left[\widehat{X}^{(1)}(t_{k+1})\right] \widehat{X}^{(2)}\left(\frac{t_{k+1}}{t_k}\right)\right], \\
P^{(2)}(t_{k+1}) &= \left[I - K^{(2)}(t_{k+1}) H\left[\widehat{X}^{(1)}(t_{k+1})\right]\right] P^{(2)}(t_{k+1} \mid t_k).
\end{aligned} \tag{27}$$

6. Simulation Experiment

6.1. Univariate Nonstationary Growth Model. Choosing univariate nonstationary growth model [16], the process model and measurement model are given as follows:

$$\begin{aligned}
x(t) &= 0.5x(t-1) + \frac{25x(t-1)}{1 + [x(t-1)]^2} \\
&\quad + 8\cos[1.2(t-1)] + w(t), \\
z(t) &= \frac{x(t)^2}{20} + v(t).
\end{aligned} \tag{28}$$

$w(t)$ and $v(t)$ are zero-mean Gaussian noise. This system is highly nonlinear and the likelihood function presents bimodal [17, 18]. Using UKF and improved UKF to estimate the state, the formula of root-mean-square error is RMSE $= [(1/T)\sum_{t=1}^{T}(x_t - \overline{x}_t)^2]^{1/2}$. Giving the particle number $N = 100$, and process noise variance values $Q = 10$, $Q = 20$, and measurement noise variance $R = 1$, simulation is conducted. The results of a single simulation are shown in Figures 2–5. After 100 times of Monte Carlo simulation, the result is given in Table 1.

From the experimental result, it is apparent that giving different noise intensities, the errors of improved UKF algorithm are lower. In the above calculation, with respect to both precision and time, the improved UKF algorithm has the most desirable performance.

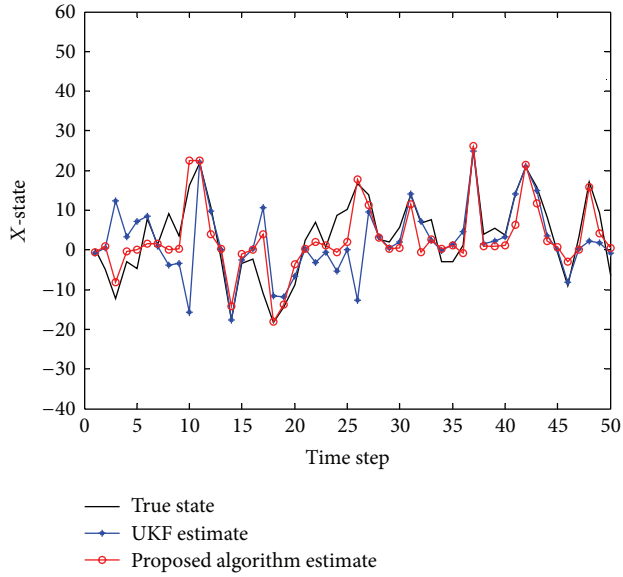

Figure 2: State estimation of different algorithm.

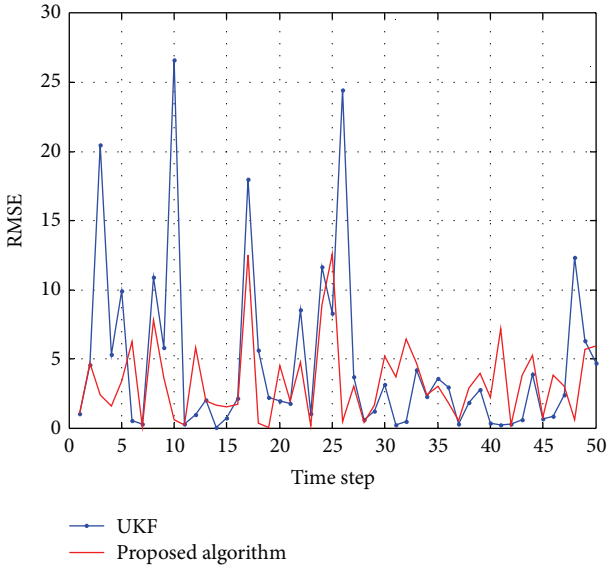

Figure 3: RMSE of different algorithm.

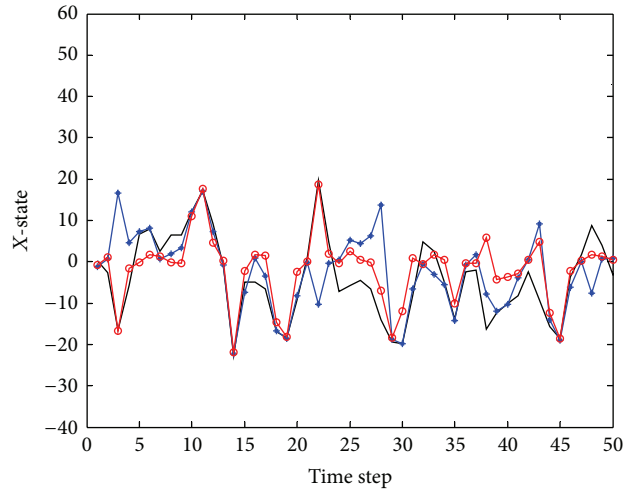

Figure 4: State estimation of different algorithm.

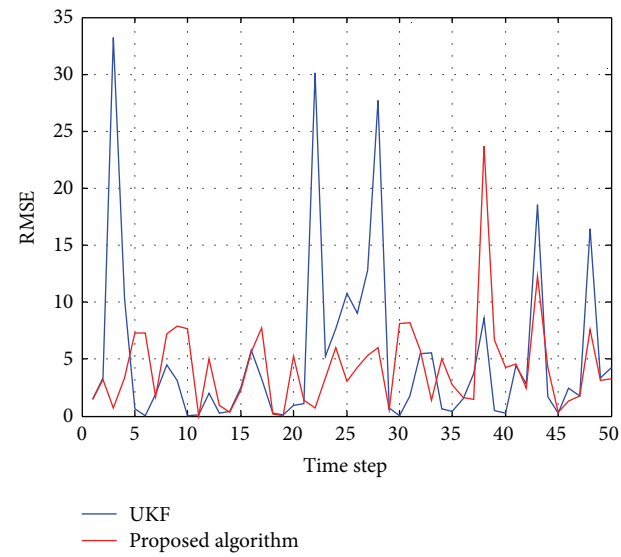

Figure 5: RMSE of different algorithm.

6.2. Deviation Registration Model. Assuming the tracked object is in uniform linear motion within 3D space, the initial position of the object was (20 km, 50 km, 0.5 km), speed (0.3 km/s, 0.3 km/s, 0 km/s), and process noise variance σ_v = 0.01 km. Also assuming radar A locating at the origin, and IF sensor B at position (5 km, 5 km, 0 km). Sampling cycle is T = 10 s and deviations of sensors are Δr_A = 1000 m, $\Delta\theta_A$ = 0.0175 rad, $\Delta\eta_A$ = 0.0175 rad, $\Delta\theta_B$ = 0.0175 rad, and $\Delta\eta_B$ = 0.0175 rad. Random noises of radar A and IF sensor B are R_A = diag[$(100\,\text{m})^2$, $(0.00087\,\text{rad})^2$, $(0.00087\,\text{rad})^2$] and R_B = diag[$(0.00087\,\text{rad})^2$, $(0.00087\,\text{rad})^2$], respectively.

In order to verify the effectiveness of the algorithm, UKF-based registration algorithm mentioned in literature [19] and the improved UKF and KF federated filtering-based registration algorithm presented here were employed, respectively, for carrying out 100 simulation experiments Monte Carlo, acquiring the following simulation results (Figures 6, 7, 8, 9 and 10).

The simulation results have indicated that the improved KF and KF federated filtering deviation registration method features better registering precision in distance deviation of radar, azimuth angle, and pitch angle deviations of both radar and IF than UKF-based deviation registering method. This is because the improved UKF presented here is making judgments of the filtering discrete trend based on measurement information and attenuation factor has been introduced to inhibit the discretion, which can not only guarantee

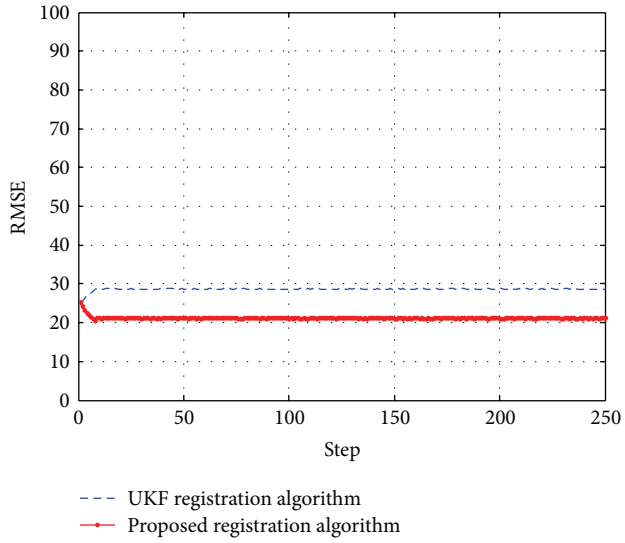

Figure 6: RMSE of the range bias estimation of radar.

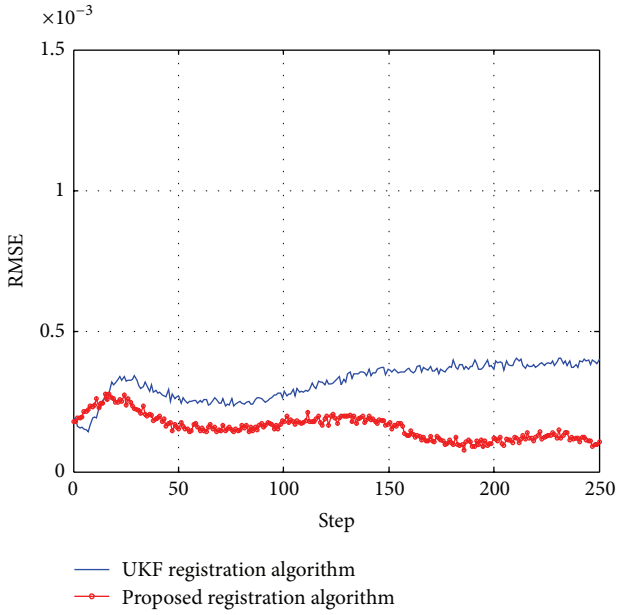

Figure 7: RMSE of the azimuth bias estimation of radar.

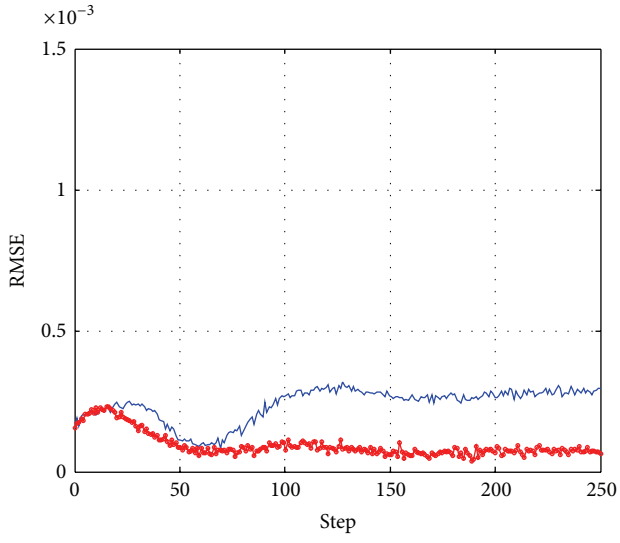

Figure 8: RMSE of the elevation bias estimation of radar.

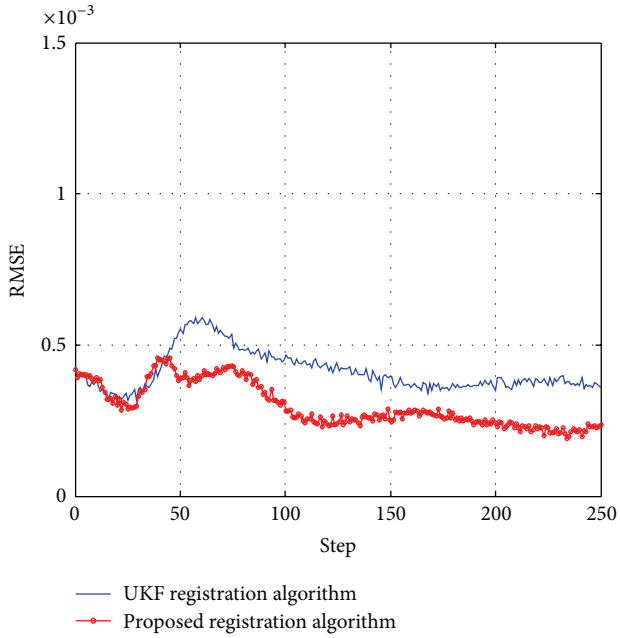

Figure 9: RMSE of the azimuth bias estimation of IR.

the positive semidefiniteness and positive definiteness of the noise variance matrix, but also effectively monitor the variance matrix. As a result the problem of instable filtering arising from inaccurate or unknown statistics of system noise can be effectively resolved, while the divergent speed and estimation precision can also be significantly enhanced. In addition, when the deviation vector is updated, KF can enable accurate computation of that since the deviation vector is linear. Therefore, the algorithm in this paper displays great advantages in registering precision.

In terms of real time, after repeated simulation experiment Monte Carlo and acquisition of the average value, average time consumption of UKF-based registering algorithm is 0.2836, whereas that of the method based on improved UKF and KF federated filtering is 0.2971. Apparently, compared with UKF-based deviation registering method, the computation complexity of federated filtering deviation registering method remains the same as UKF-based deviation registering method. This is because, in the improved UKF, in addition to real-time judgment of the filtering discrete trend, $P^{(1)}(t_{k+1} \mid t_k)$ also needs to be modified in a discrete situation. To analyze from a comprehensive perspective, the algorithm in this paper can well meet the requirement of high precise deviation registering. At the same time the real time can also be guaranteed.

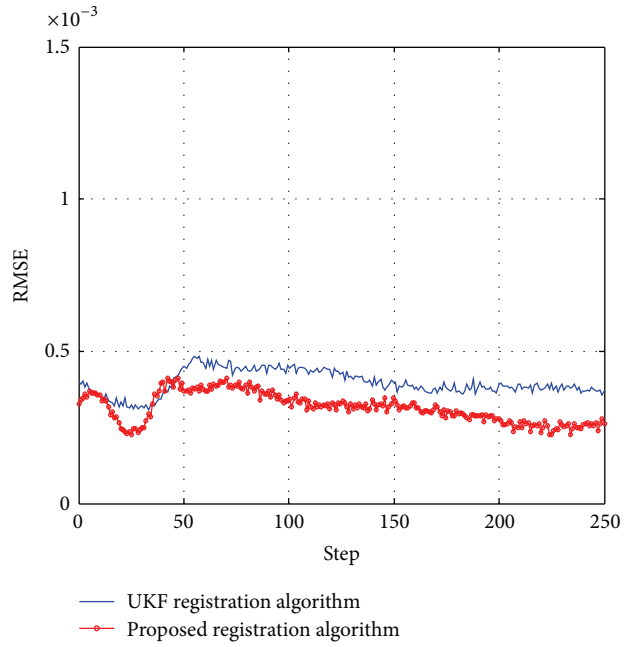

Figure 10: RMSE of the elevation bias estimation of IR.

7. Conclusions

This paper presents an improved deviation registration method based on federated filtering of unscented Kalman filter and standard Kalman filter. It takes the system deviation of sensors, position, and azimuth deviations relative to the common reference coordinate into consideration, modifies the covariance self-adaptively based on the real-time discrete situation, and performs precise deviation registering as per the data at different dimensions of 3D radar and IF sensors. At the same time it features a desirable computation speed. Therefore it has a promising future in heterogeneous sensor space registering field.

Conflict of Interests

The authors declare that there is no conflict of interests regarding the publication of this paper.

Acknowledgments

This work is partially supported by the Scientific Research Common Program of Beijing Municipal Commission of Education #KM200811417011, Funding Project for Academic Human Resources Development in Institutions of Higher Learning under the Jurisdiction of Beijing Municipality, PHR (IHLB) 200906126, PHR (IHLB) 200907120, and the Young Key Teacher Program of Beijing Municipal Commission of Education. Thanks are for the help.

References

[1] C. Yang, L. Kaplan, E. Blasch, and M. Bakich, "Optimal placement of heterogeneous sensors for targets with gaussian priors," *IEEE Transactions on Aerospace and Electronic Systems*, vol. 49, no. 3, pp. 1637–1653, 2013.

[2] M. Tummala and I. Glem, "Multisensor data fusion for the vessel traffic system," NPS EC-96-055, 1996.

[3] M. Tummala and S. A. Midwood, "A fuzzy associative data fusion algorithm for vessel traffic system," NPS EC-98-004, USA, 1998.

[4] S. Le Hegarat-Mascle, I. Bloch, and D. Vidal-Madjar, "Application of dempster-shafer evidence theory to unsupervised classification in multisource remote sensing," *IEEE Transactions on Geoscience and Remote Sensing*, vol. 35, no. 4, pp. 1018–1031, 1997.

[5] M. Datcu, F. Melgani, A. Piardi, and S. B. Serpico, "Multisource data classification with dependence trees," *IEEE Transactions on Geoscience and Remote Sensing*, vol. 40, no. 3, pp. 609–617, 2002.

[6] A. Mazeika, L. Jaulin, and C. Osswald, "A new approach for computing with fuzzy sets using interval analysis," in *Proceedings of the 9th International Conference on Information Fusion*, Florence, Italy, July 2006.

[7] H. Karniely and H. T. Siegelmann, "Sensor registration using neural networks," *IEEE Transactions on Aerospace and Electronic Systems*, vol. 36, no. 1, pp. 85–101, 2000.

[8] X. Lin, Y. Bar-Shalom, and T. Kirubarajan, "Multisensor-multitarget bias estimation for general asynchronous sensors," *IEEE Transactions on Aerospace and Electronic Systems*, vol. 41, no. 3, pp. 899–921, 2005.

[9] H. Leung and M. Blanchene, "A least squares fusion of multiple radar data," in *Proceedings of the RADAR*, pp. 364–369, Paris, France, 1994.

[10] N. Nabaa and R. H. Bishop, "Solution to a multisensor tracking problem with sensor registration errors," *IEEE Transactions on Aerospace and Electronic Systems*, vol. 35, no. 1, pp. 354–363, 1999.

[11] S. Dhar, "Application of a recursive method for registration error correction in tracking with multiple sensors," in *Proceedings of the American Control Conference*, pp. 869–874, San Francisco, Calif, USA, June 1993.

[12] H. E. Soken and C. Hajiyev, "Adaptive fading UKF with Q-adaptation: application to picosatellite attitude estimation," *Journal of Aerospace Engineering*, vol. 26, no. 3, pp. 628–636, 2013.

[13] W. Li, J. Wang, L. Lu, and W. Wu, "A novel scheme for DVL-aided SINS in-motion alignment using UKF techniques," *Sensors*, vol. 13, no. 1, pp. 1046–1063, 2013.

[14] H. Song, Y. Fu, and X. Liu, "An adaptive UKF algorithm for single observer passive location in Non-Gaussian environment," *Information Technology Journal*, vol. 11, no. 9, pp. 1251–1257, 2012.

[15] A. Vaccarella, E. De Momi, A. Enquobahrie, and G. Ferrigno, "Unscented Kalman filter based sensor fusion for robust optical and electromagnetic tracking in surgical navigation," *IEEE Transactions on Instrumentation and Measurement*, vol. 62, no. 7, pp. 2067–2081, 2013.

[16] L. Ye, J.-L. Wang, and Q. Zhang, "Genetic resampling particle filter," *Acta Automatica Sinica*, vol. 33, no. 8, pp. 885–887, 2007.

[17] X. Xu and B. Li, "Adaptive Rao-Blackwellized particle filter and its evaluation for tracking in surveillance," *IEEE Transactions on Image Processing*, vol. 16, no. 3, pp. 838–849, 2007.

[18] Y. Li, B. Bai, and Y. Zhang, "Improved particle swarm optimization algorithm for fuzzy multi-class SVM," *Journal of Systems Engineering and Electronics*, vol. 21, no. 3, pp. 509–513, 2010.

[19] W. Li, H. Leung, and Y. Zhou, "Space-time registration of radar and ESM using unscented Kalman filter," *IEEE Transactions on Aerospace and Electronic Systems*, vol. 40, no. 3, pp. 824–836, 2004.

Hindawi Publishing Corporation
Mathematical Problems in Engineering
Volume 2015, Article ID 457386, 9 pages
http://dx.doi.org/10.1155/2015/457386

Research Article

The Study on Detection Method of Water Vapor on Boundary Layer Based on Multiagent System

Xu Dongdong, Zhou Jie, Xia Jingming, Lu Zhenyu, and Huan Hai

Nanjing University of Information Science & Technology, Jiangsu 210044, China

Correspondence should be addressed to Zhou Jie; zhoujie45@hotmail.com

Received 12 July 2014; Revised 25 September 2014; Accepted 2 October 2014

Academic Editor: Wei Zhang

A method of detecting water vapor on boundary layer based on multiagent system is proposed in this paper. Multiagent system receives electromagnetic signals emitted by the telecommunication base station. Due to the analysis of the actual electromagnetic wave signal propagation path in the atmosphere, atmospheric refraction index and moisture inversion are discussed in this paper. And the feasibility of using electromagnetic detection method is also analyzed. A multiagent system is designed to receive the electromagnetic signals. The composition and function of the multiagent system are clearly described. The atmospheric refractivity is detected by the multiagent system in three weather conditions of sunny, foggy, and rainy days. The results demonstrate the feasibility of water vapor detection method of multiagent system boundary by comparing the result of experiment with traditional method.

1. Introduction

Water vapor is a kind of trace gas and mainly distributes in the bottom of the atmosphere. In particular when the height is less than 10–12 kilometers, water vapor accounts for 99% of all total. Even though the content is very small, it is the most active part in the atmosphere and is of great significance to life on Earth. Water vapor presents three states in the atmosphere varied from the temperature and is the material basis for the formation of clouds and rainfall. Water on Earth circulates between the atmosphere, land, and ocean and atmospheric water vapor plays an important role in the global water cycle. Most phenomena are the results of the changes of atmospheric water vapor while in the phase transition process water vapor absorbs and releases large amounts of latent heat which directly have impact on temperature of the ground and the air, hence affecting the stability of the atmosphere and the formation and evolution of atmospheric vertical stability and convective weather systems. Water vapor is a changeable parameter and plays a very important role in the atmospheric energy transfer and the evolution of weather systems. Atmospheric water vapor content is an essential parameter for forecasting rainfall of mesoscale or local scale [1]. Hence, obtaining atmospheric water vapor information in high precision and high space-time resolution is very important for accurately analyzing the formation and evolution of mesoscale severe weather system and medium-scale severe weather forecasting and disaster mitigation.

Factors in atmosphere which affect the distribution and water vapor content are very complex, and meanwhile the space-time change of water vapor is the most obvious factor in the atmosphere. Currently, the detection and requirement of water vapor data of high space-time resolution are still a difficult problem due to the limitation of detection funds, networking, and techniques. However, the water vapor data of high space-time resolution is the prerequisite for accurate numerical prediction. Hence, applying new technologies to improve the accuracy and resolution of water vapor observation is the most active research interest in the area of atmospheric sounding. Currently, the effective methods which have been used in sensing of atmospheric water vapor are the observation of hygrometers of ground weather station, solar spectrum water vapor analyzer, meteorological aircraft detection, laser detection, radar detection, satellite observation of water vapor, ground-based microwave radiometers detection, radio water vapor detection technology, and GPS measurements of water vapor. Among these methods, radio water vapor detection technology is the main mean which

is used in the high altitude meteorological data detection at present. The shortages of this method are that the cost of radiosondes is high and they have lower network distribution density. Meanwhile, the temporal resolution of observation data is very low which is not enough to distinguish the rapid space-time variation of water vapor. Furthermore, because of the restriction of sounding balloon tracking and locating technology as sounding balloon has low location resolution under high altitude complex turbulent condition and during the period of thunderstorms, we cannot detect the variation of water vapor during the process of convective weather effectively. The GPS used for measuring water vapor is a new method in atmospheric detection. The disadvantage of GPS measurement system is that the cost is high and it is hard to achieve high density distribution network. High resolution numerical weather prediction model of next generation needs meteorological date of 2–5 kilometers when forecasting mesoscale severe weather. However, GPS detection cannot satisfy this requirement [2, 3].

This paper provides a method which applies multiagent into the area of weather forecast and detection of water vapor content of atmospheric boundary layer. Multiagent receives electromagnetic signals from the communication base station. Then the atmospheric refractivity can be derived by using signal refraction phenomenon which resulted from the transmission of radio signals in the atmosphere. Since the atmospheric refractivity is a function of temperature, pressure, and water vapor pressure, the water vapor content can be derived from atmospheric refractivity under the assumption that the pressure and temperature are known [4]. Multiagent receiving signal from communication base station is a measurement method of a passive way. When the agent receives electromagnetic signal, multiple agents communicate with each other and sample the current location. Through the decision-making mechanism, the agent receives electromagnetic signal again after altering the location [5]. This method has its own superiorities compared with traditional detection methods.

(1) The method can be based on exiting communication network, such as mobile communication network and digital broadcasting network. Hence the observation network does not need to be reconfigured, and the cost of the observation could be decreased.

(2) Electromagnetic signal transmits linearly or quasi-linearly on the boundary layer without ionosphere reflection. Hence, there is no ionosphere delay interference phenomenon and the observation accuracy can be higher.

(3) Different transmission characteristics of electromagnetic signals of different wavelength can be used for enriching observation data.

(4) The time interval of multiagent receiving electromagnetic signals can be altered, which extends temporal resolution.

(5) Multiagent communication between the data generated according to the location information combined data.

Table 1: The level of sensitivity of electromagnetic waves of different wavelength to the water vapor.

Frequency (MHz)	Wavelength (m)	The level of sensitivity ($km^{-1}\,g^{-1}\,m^3$)
222	1.351	1.6
900	0.333	6.5
1800	0.166	13.01

(6) Data handling ability of multiagent individual can preprocess data, making it easy to post data processing.

2. Feasibility Analyses for Detection Method of Water Vapor of Boundary Layer Based on Multiagent

When propagating in the atmospheric environment, electromagnetic wave of different frequency has different level of sensitivity to water vapor which depends on the wavelength. Table 1 shows the level of sensitivity of electromagnetic waves of different wavelength to the water vapor [6].

From Table 1, it is obvious that the shorter the wavelength of electromagnetic wave, the higher the sensitivity of electromagnetic waves to the water vapor.

Electromagnetic wave is transported linearly in vacuum at a speed of 3×10^8 m/s. The electromagnetic wave will propagate in curve obviously which is called atmospheric refraction, when transmitted in the atmosphere, especially in remote transmission and atmospheric meteorological elements have abnormal vertical distribution. The index of atmospheric refraction has a very close relation to dielectric constant of atmosphere which depends on the material density, temperature, and the properties of molecules. The temperature, humidity, and atmospheric pressure vary along with molecules.

Electromagnetic wave has different velocity in inhomogeneous medium which is due to different physical properties of the propagation medium forming different levels. The essence of refraction is the deflection of electromagnetic wave in the propagation direction when the direction is not perpendicular to interface of medium. Investigating plane wave using Maxwell equation set can derive that

$$v = \frac{1}{\sqrt{\varepsilon\mu}}, \tag{1}$$

where v is the propagation velocity of electromagnetic wave in some homogeneous medium. ε and μ are absolute dielectric constant and absolute permeability, respectively. In a vacuum,

$$v = c = \frac{1}{\sqrt{\varepsilon_0\mu_0}} = 2.9979 \times 10^8 \text{ m/s}, \tag{2}$$

where $\varepsilon_0 = 8.85 \times 10^{-12}\,\text{C kg}^{-1}\,\text{m}^{-1}$ and $\mu_0 = 1.2566 \times 10^{-6}\,\text{C kg}^{-1}\,\text{m}^{-1}$.

The refractive index of medium n usually can be defined as

$$n = \frac{c}{v} = \sqrt{\frac{\varepsilon_0 \mu_0}{\varepsilon \mu}} = \sqrt{\varepsilon_r \mu_r}. \tag{3}$$

The magnetic permeability of most media satisfies $\mu_r \approx 1$; hence $n^2 = \varepsilon$.

It should be noted that the most common form of refractive index is a complex number as

$$m = n - ki, \tag{4}$$

where m is usually called complex refractive index. The real part n of m is ordinary refractive index and the imaginary part k of m is a coefficient which denotes the attenuation of electromagnetic wave signal. In this paper, we do not consider attenuation and use the refractive index n.

Considering the polarization of atmosphere in external electric field, when the medium consisting of nonpolar molecules is polarized, its molecules form an electric dipole of electric dipole moment $\vec{p}$. And $\vec{p}$ is proportional to the electric field which acts on molecules

$$\vec{p} = \beta \vec{E}' \approx \beta \vec{E}, \tag{5}$$

where β is the polarizability of molecules. $\vec{E}'$ denotes effective electric field acting on molecules. $\vec{E}$ is the average electric field. It can be approved that the relationship between β, $\vec{E}'$, and $\vec{E}$ can be written as

$$\begin{aligned} \vec{E}' &= \vec{E} + \frac{4}{3}\pi \vec{p} = \frac{1}{1 - (4/3)\,\pi\beta}, \\ \vec{p} &= \frac{\beta \vec{E}}{1 - (4/3)\,\pi\beta}. \end{aligned} \tag{6}$$

For polar molecules such as water vapor molecules, the electric dipole moment $\vec{p}$ can be derived into two parts as $\vec{p} = \overrightarrow{p_0} + \overrightarrow{p_1}$ where $\overrightarrow{p_0}$ is related to the orientation of polar molecules and has no relation to external field. Hence, $\overrightarrow{p_1}$ can be written as

$$\overrightarrow{p_1} = \frac{\beta \vec{E}}{1 - (4/3)\,\pi\beta}. \tag{7}$$

If the number of molecules per unit volume is N, then the total dipole moment $\vec{p}$ can be written as

$$\vec{p} = N\vec{p} = N\beta \vec{E}' = \frac{NP\vec{E}}{1 - (4/3)\,\pi N\beta}. \tag{8}$$

The intensity of electric induction in isotropic medium is

$$D = \varepsilon \vec{E} = \vec{E} + 4\pi \vec{p}. \tag{9}$$

Then we can derive the relationship between dielectric constant and molecular polarizability as

$$\frac{\varepsilon - 1}{\varepsilon + 2} = \frac{4}{3}\pi N\beta. \tag{10}$$

In the air comprising of multiple polar molecules, when external electric field $\vec{E} = 0$, the sum of inherent dipole moment equals 0 for random orientations. When external electric field $\vec{E} \neq 0$, natural pole moment of each molecules makes contribution to total dipole moment with certain probability. And the probability relates to absolute temperature T in the atmosphere. To quantify the relationship between the polarization of medium of polar molecules and the temperature, according to the statistical theory of Boltzmann, the number of polar molecules between U and $U + du$ in the energy per unit volume is as follows:

$$dN = Ce^{U/kT} dU, \tag{11}$$

where k is the Boltzmann constant, T is the absolute temperature of the atmosphere, and C is a proportional constant. It is known that the electrostatic energy of electric dipole with electric dipole moment $\vec{p}$ is

$$U = -pE\cos\theta, \tag{12}$$

where θ is the angle between electric axis and electric field $\vec{E}$. p and E are modulus of $\vec{p}$ and $\vec{E}$. Considering the polarization intensity of medium of polar molecules, we should take rotary and slight elastic deformation of each molecular dipole in external field into consideration. Hence, under the condition of weak electronic field and normal temperature, $\vec{p}$ can be expressed as

$$\frac{\varepsilon - 1}{\varepsilon + 2} = \frac{4\pi N}{3}\left(\beta + \frac{p^2}{3kT}\right). \tag{13}$$

The atmosphere consists of nonpolar molecules of dry air and polar molecules of water vapor. Hence, under the action of electric field, the electric polarization vector $\vec{p}$ of mixed gas can be expressed as

$$\vec{p} = \overrightarrow{p_n} + \overrightarrow{p_p} = K_n \vec{E} + K_p \vec{E}, \tag{14}$$

where $\overrightarrow{p_n}$, $\overrightarrow{p_p}$, K_n, and K_p denote polarization vectors and polarizabilities of nonpolar and polar molecules. Without regard to the difference between $\vec{E}$ and $\vec{E}'$, the polarizability K of mixed gas can be written as

$$K = N_n\beta_n + N_p\left(\beta + \frac{p^2}{3kT}\right). \tag{15}$$

It is known that the relationship between polarizability K and dielectric constant ε is

$$\varepsilon - 1 = 4\pi K. \tag{16}$$

While $\varepsilon^2 - 1 = n^2 - 1 \approx 2n - 1$, we can find that

$$n - 1 \approx 2\pi\left(N\beta_{np} + N_p\frac{p^2}{3kT}\right), \tag{17}$$

where $N = N_n + N_p$ denotes the number of molecules of mixed gas per unit volume and $\overrightarrow{\beta_{np}}((N_n\beta_n + N_p\beta_p)/(N_n + N_p))$

is the average number of polarizations of molecules of mixed gas.

The atmosphere is a mixture of gases and the atmospheric pressure is $P = P_d + e$. Assuming that the density is ρ, gram molecular weight is μ and ideal gas state equation per unit volume is $P = (\rho/\mu)\, RT$; according to the equation $\rho = N\mu$, it can be derived that

$$N = \frac{P}{RT}, \tag{18}$$

where P is the atmospheric pressure and its unit is hPa. R is universal gas constant with the value of $8.31\,\mathrm{J}\cdot\mathrm{mol}^{-1}\cdot\mathrm{k}^{-1}$.

Similarly, the number of molecules of water vapor per unit volume N_p can be derived as

$$N_p = \frac{e}{RT}, \tag{19}$$

where e is the water vapor pressure and its unit is hPa. Furthermore, it can be derived as

$$(n-1)\,10^6 = \frac{A}{T}\left(P + \frac{Be}{T}\right), \tag{20}$$

where A and B are coefficients which are determined by experiments, T is the absolute temperature, and the units of P and e are hPa.

While the value of n is small and bad for expression, the refraction unit N is always used actually which can be called refraction index N:

$$N = (n-1)\,10^6. \tag{21}$$

The refraction index N includes dry refractive components caused by atmospheric pressure P and temperature T and wet refractive components caused by water vapor pressure. The expression of atmospheric refractive index can be derived after decomposing dry and wet refractive components as

$$N = 77.6\frac{P}{T} + 3.75\times 10^5\frac{e}{T^2} = N_{\mathrm{dry}} + N_{\mathrm{wet}}, \tag{22}$$

where the first item N_{dry} is just connected with atmospheric pressure P and temperature T and the second item N_{wet} which is called wet refractive component is related to water vapor pressure. The variation range of N_{dry} is between 225 and 325 units and N_{wet} is between 0 and 150 units. And the change of humility has larger impact on refractive index than atmospheric pressure and temperature. The investigation in this paper is an inverse process actually which takes advantage of transmission feature of electromagnetic wave in the atmosphere to inverse refractive index. Then the value of water vapor pressure or the distribution of water vapor can be derived due to refractive index, temperature T, and atmospheric pressure P [7–9].

However the value of N during the actual inversion of water vapor cannot be obtained directly and it needs the comparison between the actual broadcasting distance and visual broadcasting distance (pseudorange) between electromagnetic transfer and receiver position. Lower atmosphere effects the transmission of electromagnetic wave in two ways, while the signal is transported near the ground and on the boundary layer. First, comparing to vacuum, the broadcasting velocity of electromagnetic wave becomes slower. The relationship between the velocities of electromagnetic wave in atmosphere and in vacuum is $n = c/v$, where n is the atmospheric refractive index. Second, the propagation path changes from linear to curved. These two influences are caused by the change of atmospheric refractive index N along with the propagation path. The delay of propagation of signal compared with vacuum equals the increase of propagation path length [10]. Therefore, the distance between agent and base station which is calculated according to the propagation delay and velocity is not the real distance actually but the visual broadcasting distance which is called pseudorange. Figure 1 shows the propagation path S of electromagnetic wave at the bottom of the atmosphere and distance G between agent and base station.

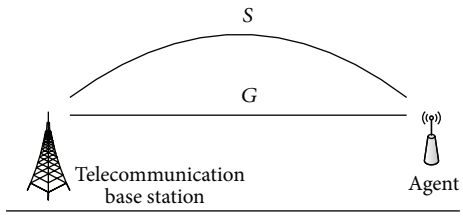

Figure 1: Propagation path S of electromagnetic wave at the bottom of the atmosphere and distance G between agent and base station.

The increased propagation path can be expressed as

$$\Delta L = c\Delta t - G = c\int_L \frac{ds}{v} - G = \int n(s)\,ds - G, \tag{23}$$

where c is the speed of light in vacuum, Δt is the actual propagation time of signal, v is the propagation velocity of signal in the atmosphere, and $n(s)$ is the average refractive index of the signal on the transmission path. The integral is performed along with the curved path of propagation of electromagnetic signals. G is the actual geometric distance between the transfer and the receiver stations. The formula can be rewritten in the following form:

$$\Delta L = \int_L [n(s) - 1 + 1]\,ds - G = \int_L [n(s) - 1]\,ds - (S - G), \tag{24}$$

where S is the length of propagation path. The first item is a slower one and is only related to atmospheric index n which is inversely proportional to the propagation velocity v. The second item is a signal bending one which is the difference between signal bending path S and linear propagation path G. The increasing of propagation path is mainly caused by signal slowing effect. Replacing atmospheric refractive index with refractivity, we can find that

$$\Delta L = 10^{-6}\times\int_L N(s)\,ds. \tag{25}$$

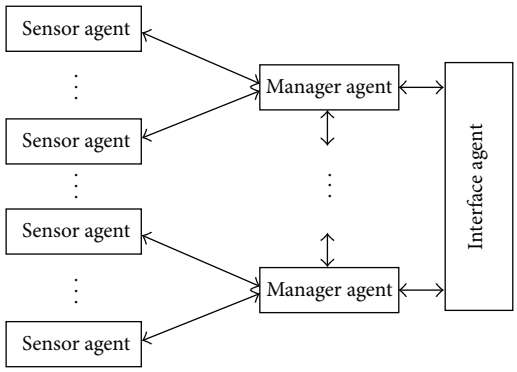

Figure 2: The architecture of multiagent system.

And ΔL can be decomposed as follows:

$$\Delta L = 10^{-6} \times \int_L \left(N_{\text{dry}} + N_{\text{wet}}\right) ds = \Delta L_d + \Delta L_w, \quad (26)$$

where ΔL_d and ΔL_w denote dry delay and wet delay, respectively. Compared with GPS system which is used in water vapor measurement, multiagent system could measure atmospheric refractive index of lower or boundary layer. Without ionospheric propagation of signal, it is not necessary to use the double-frequency method to correct the error caused by ionospheric delay which reduces the possibility of measurement error to some extent. In addition, multiagent detection system measures water vapor in low atmosphere and the water vapor content per volume is bigger than using GPS measurements which measure the whole atmospheric convection layer. Hence, it will cause larger delay under the same propagation distance. Besides, according to the measured refractive index N which is used to inverse water vapor pressure or intensity near the ground or boundary layer, we only need to combine it with observation data of atmospheric pressure and temperature near the ground and gradient distribution near the ground or boundary layer [11]. Hence, there is no need to consider the weighted average temperature of the whole atmosphere which makes a further error reduction of the source.

Therefore, the key of the inversion of atmospheric refraction index is to find the propagation path delay ΔL. The key issues of finding ΔL are to obtain signal propagation delay Δt in high accuracy and to eliminate error caused by noise and so forth [12].

3. The Architecture of Multiagent System

A multiagent system is designed to detect the vapor on boundary layer by calculating the refractive index of electromagnetic waves. The system has three components, such as sensor agent, manager agent, and interface agent. Figure 2 shows the architecture of multiagent system.

3.1. Sensor Agent. Sensor agent is the basic component of the multiagent system. The main task of sensor agent contains the following:

(1) receiving the electromagnetic waves of current position,

(2) acquiring the relevant information and data of current position,

(3) getting the information and data of current environment,

(4) calculating the corresponding water vapor content,

(5) uploading all data to manager agent.

There are some rules to help sensor agent work effectively:

(i) time resolution rules, which are used to control the time resolution of receiving the electromagnetic wave signal according to the preestablished time resolution or changed by instructions,

(ii) data acquiring rules, which are used to acquire the parameters of current position and environment such as GPS data, temperature, relative humidity, wind direction, wind speed, rainfall, air pressure, and solar radiation,

(iii) vapor calculating rules, which are used to set the different algorithms of calculating,

(iv) sensors connecting rules, which are used to connect with manager agent and other sensors agents nearby for data communication.

Sensor agent could only receive the very electromagnetic waves from telecommunication base station generally. But it also could receive several electromagnetic waves from different telecommunication base stations in other cases. When it happens, the sensor agent would provide several data. Each sensor agent associates with other sensor agents.

3.2. Manager Agent. All data collected from sensor agents upload to manager agent. The main task of manager agent contains the following:

(1) verifying the data of water vapor according to position information,

(2) sampling the verified data,

(3) merging the data based on position information,

(4) uploading all preprocessed data to interface agent,

(5) altering the frequency of sending data through the control instruction from the interface agent.

Some rules are used to make manager agents cooperate with each other:

(i) correlation rules, which are used to detect correspondences between data provided by several sensors to evaluate the quality of these data,

(ii) data sample rules, which are going to be used to set the different algorithms of data sampling,

(iii) data merge rules, which are used to merge the data from sensor agents with the data acquired in traditional method or historical data,

(iv) communication rules, which are used to define the communication protocol among sensor agents and interface agent.

The manager agent would standardize the data received from sensor agents and exclude the wrong data by comparing the data based on same position or nearby. Then the manager agent would get the valid data. Atmospheric water vapor content generally existed in the form of a continuous function, so the character of data acquired in same position or nearby should also show continuity [13]. This requires the use of the data associated with the agent.

The valid data acquired by sensor agents represent the character of selected area. But it is not necessary to analyse all valid data. So some data would be sampled from the valid data according to position information, which could also represent the character of selected area and distribute evenly. Here we use the method of stratified sampling. Firstly we stratify the sample space, then random sample at each layer [14]. Location-based sampling method is implemented as following.

(I) Stratification. The sample space is divided into nonoverlapping subspaces, called the layer of each subspace. In telecommunication base station as the center, the coverage is divided into several rings with the radius of r. Set distances $d_1, d_2, d_3, \ldots, d_k$ with the number of k to determine the space of each layer [15].

(II) Random Sampling. Randomly sample at each layer. Determine the number of each layer $n_1, n_2, n_3, \ldots, n_k$ and make sure the result of sample distributes evenly. Figure 3 shows the position of sensor agents and telecommunication base station and the sampling based on position.

The sample number in layer i is as follows:

$$n_i = n_e \times \frac{s(d_i)}{\sum_{j=1}^{k} s(d_j)}. \tag{27}$$

And n_e is the presetted sample number and $s(d_i)$ is the mumber of sample covered in layer i:

$$\begin{aligned} &S(d_1) = RQ(r_1), \\ &S(d_2) = RQ(r_2) - RQ(r_1), \ldots, \\ &S(d_i) = RQ(r_i) - RQ(r_{i-1}), \ldots, \\ &r_1 = d_1, \quad r_2 = r_1 + d_2, \ldots, \quad r_i = r_{i-1} + d_i, \ldots. \end{aligned} \tag{28}$$

The parameters $RQ(r_i)$ could be inquired by the range of sensor agents. Euclidean distance query and network distance query depend on the distribution of sensor agents. The range query refers to a query q where Q is the center point, a radius equal to the length of a subset of the query objects within a circle of radius r. In order to improve the efficiency of range query, algorithm of LUR-tree is used to build the index for the moving stored objects [16, 17].

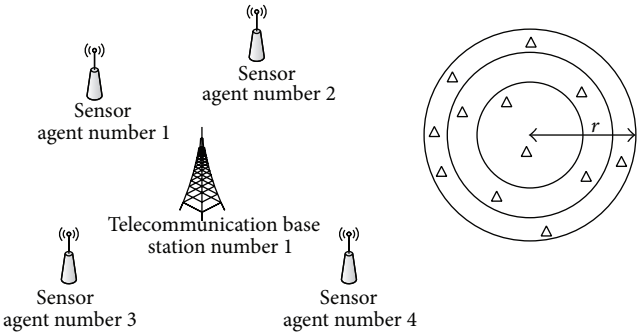

Figure 3: The position of sensor agents and telecommunication base station sampling based on position.

3.3. Interface Agent. The interface agent is the human-computer interface between human and multiagent. The main task of interface agent contains the following:

(1) showing the current position and status of all sensor agents on the map,

(2) setting the parameters of the system.

All valid data which are preprocessed by agents would upload to interface agent. The system's interface uses web application that displays all valid data and the status of all agents via Maps in Time [18]. The frequency of update valid date would be set by different time resolution.

4. Implementation

The system has been implemented using a JADE platform [19]. JADE is a software framework to develop agent applications in compliance with FIPA specifications for interoperable intelligent multiagent systems. The development of multi-agent system greatly simplifies by middleware. The inference engine for the rule-based system has been implemented using Drools [20].

In experiment, the sensor agents are settled on several vehicles, and the manager agents are placed in fixed position among the selected observation area. The vehicles select roads randomly during the processing of observation. The time resolution of uploading data is controlled by the instruction of interface agent.

Three different weather conditions are selected to verify the results of the measurement accuracy with the method of multiagents under sunny, foggy, and rainy weather. The atmospheric refraction index is calculated by the measured electromagnetic signals. The retrieval result with traditional measurement method and multiagent method is compared under the three weather conditions.

4.1. Retrieval and Analysis of Atmospheric Refractivity under Sunny Weather Condition. According to the result of retrieval atmospheric refractivity (Figure 4), the value of atmospheric refractivity acquired by multiagent method is entirely well fitted with the value of atmospheric refractivity acquired by observation. The average observation error of 96 samples which were observed in 24 hours is 42 percent of N. And the

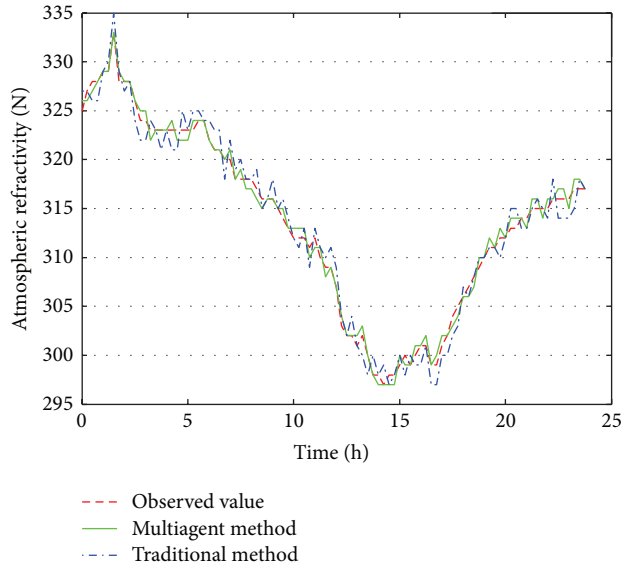

Figure 4: The comparison of the value of atmospheric refractivity N under sunny weather condition. Red line: the value of atmospheric refractivity acquired by observation. Green line: the value of atmospheric refractivity acquired by multiagent method. Blue line: the value of atmospheric refractivity acquired by traditional method.

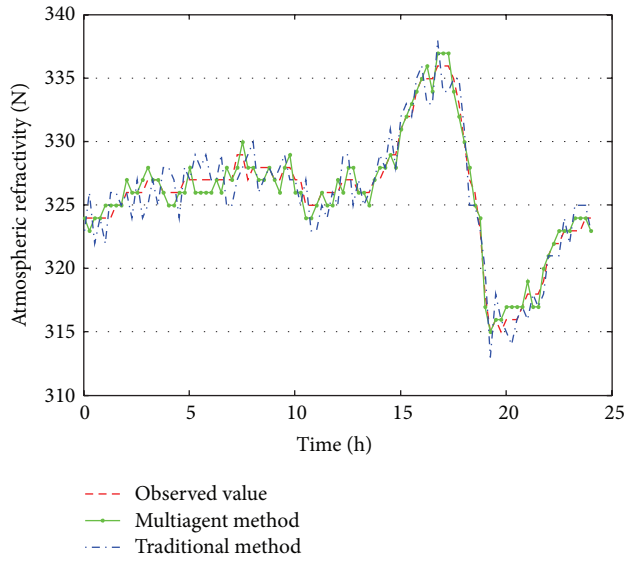

Figure 5: The comparison of the value of atmospheric refractivity N under foggy weather condition. Red line: the value of atmospheric refractivity acquired by observation. Green line: the value of atmospheric refractivity acquired by multiagent method. Blue line: the value of atmospheric refractivity acquired by traditional method.

average observation error of all samples is less than 100 percent of N. The correlation coefficient of the observed samples and calculated samples is 0.993, and the RMSE equals 1.072.

The difference between retrieval atmospheric refractivity by multiagent method and traditional method changes slightly. It reflects the high sensitivity of the electromagnetic signals. It is meaningful to analyse mesoscale convective weather or fog of boundary changes and transport of water vapor.

4.2. Retrieval and Analysis of Atmospheric Refractivity under Foggy Weather Condition. According to the result of retrieval atmospheric refractivity (Figure 5), the value of atmospheric refractivity acquired by multiagent method is entirely well fitted with the value of atmospheric refractivity acquired by observation. The average observation error of 96 samples which were observed in 24 hours is 49 percent of N. And the average observation error of all samples is less than 100 percent of N. The correlation coefficient of the observed samples and calculated samples is 0.993, and the RMSE equals 1.113.

The range of observation error under foggy weather condition is very close to observation error under sunny weather condition. It means that tiny liquid water droplets do not cause interference to retrieval results. And it is feasible to retrieve atmospheric refractivity by measuring the electromagnetic signals using multiagent system. Meanwhile according to retrieval, it can be found that the atmospheric refractivity would increase rapidly prior to significantly reducing visibility to develop into a very dense fog. Observation of this phenomenon can be used as early warning of approaching fog important reference index.

4.3. Retrieval and Analysis of Atmospheric Refractivity under Rainy Weather Condition. According to the result of retrieval atmospheric refractivity (Figure 6), the value of atmospheric refractivity acquired by multiagent method is entirely well fitted with the value of atmospheric refractivity acquired by observation. The average observation error of 96 samples which were observed in 24 hours is 57 percent of N. And the average observation error of all samples is less than 100 percent of N. The correlation coefficient of the observed samples and calculated samples is 0.991, and the RMSE equals 1.091.

Compared with the previous analysis, larger liquid water droplets do not interfere with the results of retrieval under rainy weather condition. Trends in rainfall and atmospheric vapor pressure of the index of refraction are consistent trends. Subtle changes in atmospheric refractivity of water vapor, temperature, and barometric pressure are very sensitive. The experimental validation of the method of the refractivity of atmospheric retrieval weather conditions in rainfall is possible and obtains higher retrieval accuracy.

5. Conclusions and Future Work

The refractivity of the low-altitude atmospheric inversion results fits well the results of the calculation of meteorological elements under sunny, foggy, and rainy weather condition according to the comparison. Tiny water droplets in the atmosphere almost have no impact on the results of the electromagnetic signal inversion of atmospheric refractive index. Therefore, electromagnetic measurement method based on multiagent is able to achieve real-time monitoring of water vapor near the ground changes under different weather

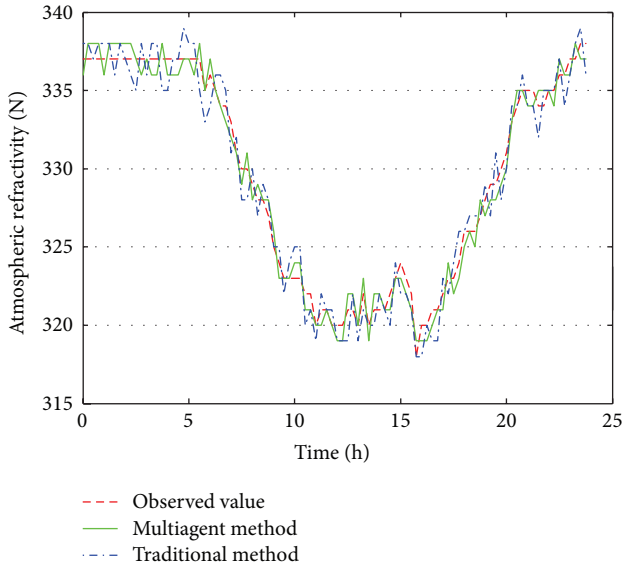

FIGURE 6: The comparison of the value of atmospheric refractivity N under rainy weather condition. Red line: the value of atmospheric refractivity acquired by observation. Green line: the value of atmospheric refractivity acquired by multiagent method. Blue line: the value of atmospheric refractivity acquired by traditional method.

conditions with a high time resolution. It exhibits a good electromagnetic wave signal variation of the moisture sensitivity of the results obtained in comparison with the conventional method results consistent.

A certain accuracy of moisture content of the boundary layer method by multiagent can be achieved according to the experiment. In future work, the following points could be improved.

(1) Sensor agents are mounted on the car body in the experiment, so the trajectory of the sensor agents is restricted in the trajectory of the car. The data only generated in the position where car can reach. Although the interpolation method can be used to fill with the position where the car cannot reach, this is not the actual measured data. Sensor agents will be settled to aerocraft in further work. And track of aerocraft would be controlled by manager agents. The more comprehensive data will be acquired.

(2) The only specific frequency which is electromagnetic is used in experiment. Previous studies showed that electromagnetic wave of different frequency has different level of sensitivity to water vapor which depends on the wavelength. Shorter wavelength electromagnetic would be selected to compare with result in further work.

(3) It would be worthy to research location sampling algorithm of sensor agents which are controlled by manager agents.

Conflict of Interests

The authors declare that there is no conflict of interests regarding the publication of this paper.

References

[1] F. Fabry, "The spatial variability of moisture in the boundary layer and its effect on convection initiation: project-long characterization," *Monthly Weather Review*, vol. 134, no. 1, pp. 79–91, 2006.

[2] B.-G. Jeon, Y. Moon, and T.-W. Ahn, "A study on 11 MHz ~ 1537 MHz DCO using tri-state inverter for DAB application," in *Proceedings of the IEEE Region 10 Conference (TENCON '09)*, pp. 1–5, Singapore, January 2009.

[3] J. Braun, C. Rocken, and R. Ware, "Validation of line-of-sight water vapor measurements with GPS," *Radio Science*, vol. 36, no. 3, pp. 459–472, 2001.

[4] B. L. Cheong, R. D. Palmer, T. Y. Yu, and C. Curtis, "Refractivity measurements from ground clutter using the National Weather Radar Testbed phased array radar," in *Proceedings of the 32nd Conference on Radar Meteorology*, Albuquerque, NM, USA, 2005.

[5] I. Martí, V. R. Tomás, L. A. García, and J. J. Martínez, "A multiagent system for managing adverse weather situations on the road network," *Integrated Computer-Aided Engineering*, vol. 17, no. 2, pp. 145–155, 2010.

[6] C. G. Someda, *Electromagnetic Waves*, CRC Press, New York, NY, USA, 2nd edition, 2006.

[7] J. Duan, M. Bevis, P. Fang et al., "GPS meteorology: direct estimation of the absolute value of precipitable water," *Journal of Applied Meteorology*, vol. 35, no. 6, pp. 830–838, 1996.

[8] A. E. Niell, A. J. Coster, F. S. Solheim et al., "Comparison of measurements of atmospheric wet delay by radiosonde, water vapor radiometer, GPS, and VLBI," *Journal of Atmospheric and Oceanic Technology*, vol. 18, no. 6, pp. 830–850, 2001.

[9] P. Miidla, K. Rannat, and P. Uba, "A mathematical model of troposphere water vapor tomography," in *Proceedings of the 2nd International Conference on Environmental and Computer Science (ICECS '09)*, pp. 183–187, Dubai, UAE, December 2009.

[10] S. Padmanabhan, S. C. Reising, J. Vivekanandan, and F. Iturbide-Sanchez, "Retrieval of atmospheric water vapor density with fine spatial resolution using three-dimensional tomographic inversion of microwave brightness temperatures measured by a network of scanning compact radiometers," *IEEE Transactions on Geoscience and Remote Sensing*, vol. 47, no. 11, pp. 3708–3721, 2009.

[11] R. J. Watson and C. J. Coleman, "The use of signals of opportunity for the measurement of atmospheric refractivity," in *Proceedings of the 4th European Conference on Antennas and Propagation (EuCAP '10)*, pp. 1–5, April 2010.

[12] W. Xu, R. Lv, X. Yu, Z. Yang, and L. Deng, "Synchronous orthogonal DAB spectrum layout scheme," in *Proceedings of the 2nd International Conference on Biomedical Engineering and Informatics (BMEI '09)*, October 2009.

[13] V. R. Tom and L. A. Garc, "A cooperative multiagent system for traffic management and control," in *Proceedings of the 4th International Joint Conference on Autonomous Agents and Multi-Agent Systems (AAMAS '05)*, pp. 52–59, Utrecht, The Netherlands, 2005.

[14] Z. Yan, D. Chakraborty, A. Misra, H. Jeung, and K. Aberer, "Sammple: detecting semantic indoor activities in practical

settings using locomotive signatures," in *Proceedings of the International Symposium on Wearable Computers*, pp. 37–40, Newcastle, UK, 2012.

[15] J. Zhu, P. Wu, X. Wang, and J. Zhang, "SenSec: mobile security through passive sensing," in *Proceedings of the International Conference on Computing, Networking and Communications (ICNC '13)*, pp. 1128–1133, IEEE, San Diego, Calif, USA, January 2013.

[16] D. Hasenfratz, O. Saukh, S. Sturzenegger, and L. Thiele, "Participatory air pollution monitoring using smartphones," in *Proceedings of the 1st International Workshop on Mobile Sensing: From Smartphones and Wearables to Big Data*, 2012.

[17] M. Faulkner, M. Olson, R. Chandy, J. Krause, K. M. Chandy, and A. Krause, "The next big one: detecting earthquakes and other rare events from community-based sensors," in *Proceedings of the 10th International Conference on Information Processing in Sensor Networks (IPSN '11)*, pp. 13–24, Chicago, Ill, USA, April 2011.

[18] P. Wu, H.-K. Peng, J. Zhu, and Y. Zhang, "Senscare: semi-automatic activity summarization system for elderly care," in *International Conference on Mobile Computing, Applications, and Services (MobiCASE '11)*, 2011.

[19] M. Rinard and M. Lam, "The design, implementation, and evaluation of Jade," *ACM Transactions on Programming Languages and Systems*, vol. 20, no. 3, pp. 483–545, 1998.

[20] M. Proctor, "Relational declarative programming with JBoss Drools," in *Proceedings of the 9th International Symposium on Symbolic and Numeric lgorithms for Scientific Computing (SYNASC '07)*, Timisoara, Romania, September 2007.

Hindawi Publishing Corporation
Mathematical Problems in Engineering
Volume 2014, Article ID 314920, 8 pages
http://dx.doi.org/10.1155/2014/314920

Research Article

Data Fusion Based Thermal Sensors for Mass Flow Measurement in Pneumatic Conveying

Hong Zhang, Wenqian Zhang, and Dan Ling

School of Automation, Huazhong University of Science and Technology, Wuhan 430074, China

Correspondence should be addressed to Hong Zhang; sunracer@mail.hust.edu.cn

Received 24 July 2014; Accepted 1 September 2014; Published 29 September 2014

Academic Editor: Wei Zhang

This paper mainly investigates the mass flow measurement of the gas-solid two-phase flow in pneumatic conveyor. A new data fusion method based on the thermal sensors is proposed, which can improve the overall accuracy of the flow rate of the gas-solid two-phase flow and the time resolution, that is, the overall response rate of the system. Based on this method, a model fusion used in time domain is obtained. Several examples are given to illustrate the advantages of the proposed method.

1. Introduction

The measurement of the gas-solid two-phase flow in pneumatic conveyor is of great significance, especially in the coil-fired station and steel production industry. The solid phase concentration measurement of gas-solid two-phase flow is one of the most difficult parameters to be measured, which has always been the research focus and difficulty in industrial detection over the last decade [1]. Recently, many sensors, such as capacitance sensor used in process tomography [2, 3], electrostatic sensor [4, 5], optical sensor [6, 7], microwave sensor [8, 9], and thermal sensor [10, 11], have been adopted in the research on gas-solid two-phase flow. A variety of data processing methods have been used in the measurement system to improve the accuracy, including neural network technique [12, 13], soft-sensing technique [14], and data fusion method [15].

The methods in thermology fell into two categories: heat balance method and heat transfer method. At present, the heat balance method, which has been employed for many years, is known as a comparatively mature measurement method. A lot of work has been done on the establishment of measurement models [16, 17], analysis of affecting error, and system implementation. Besides, several field devices with good practicality have been established. Despite its late start on the measurement of gas-solid two-phase flow, the heat transfer method is becoming popular gradually. Based on the heat transfer method, a noninvasive prototype system measuring the mass flow rate of two-phase flow can be first found in Moriyama [11]. The system can measure the mass flow rate of gas-solid from dilute phase to dense phase. Another noninvasive method measuring the mass of gas-solid, which measures the solid phase mass flow by heating the solid particles in the tube wall and measuring the temperature distribution of gas-solid two-phase flow, is well discussed in [18]. This method is similar to the principle for measurement of thermal distribution. A heat transfer probe method which is employed to measure pulverized coal concentration of the power feeding system in a power station is proposed in [19]. This method adopts elliptic probes with different placement to measure the concentration of pulverized coal and air volume. Yuan et al. [20] place a probe with electric heating in the flow to measure the solid flow rate. There are different heat transfer effects when the probe contacts the flow media with different flow velocities, concentrations, and particle diameters. In this case, the solid phase flow in the two-phase flow, given air volume, can be measured by the electrical heating power and the measured temperature of the probe. The heat transfer method has also been applied in [21]. They adopt the principle of heat dissipation type mass flowmeter in the plug-in probe consisting of platinum thermal resistance. The control circuit works in an environment of constant difference in temperature where it has a better response characteristic. Meanwhile, the thermal

sensor and temperature sensor in the same base can be formed into a compound transducer, which can not only acquire the flow signal but also decouple the temperature signal.

In terms of data processing technique, several key issues in indirect measurement method have been studied and discussed deeply, including spatial filtering effect, average effect, and the resolution and sensitivity of the tomographic imaging sensor array [22]. The BP artificial neural network has been used to predict the measurement of the solid flow rate of two-phase flow with heat transfer method and the prediction process is examined in [13]. Based on a lot of experimental data, it has been shown that the complicated nonlinear problem between the solid flow rate and the factors can be solved by the artificial neural network. The data fusion is attempted to deal with the measurement of heat balance method and heat transfer method via mathematical analysis, which has made some achievements [21]. Based on the result, this paper conducts further research.

The two different methods which measure gas-solid two-phase flow discussed in this paper are necessary to achieve data fusion and have something in common. First of all, not only are the two methods based on the principle of heat transfer, but also they have a direct relationship with the flow rate of air. Secondly, although each method has its own advantages and disadvantages, both of the measurement data are processed by reasonable data fusion method, which can improve the measurement accuracy, response speed, and robustness of the system.

The rest of the paper is organized as follows. Section 2 gives some problems in data fusion method and real-time measurement. Section 3 introduces the general model fusion method. Section 4 provides some main results. And Section 5 discusses the window size and the distribution of weights. The final section gives the conclusion of this paper.

2. Date Fusion Based Real-Time Measurement

For high performance, the measurement system has to provide not only high accuracy measured output information, but also a sufficiently high response speed in industrial process control, such as the boiler combustion control. This paper mainly investigates the real-time measurement via data fusion method, which can improve the overall accuracy of the flow rate of the gas-solid two-phase flow and the time resolution, that is, the overall response rate of the system. Date fusion based real-time measurement can be described as shown in Figure 1.

In Figure 1, when the sample data of system B with higher time resolution is measured in real-time, the corresponding sample data of system A could not be generated to fuse the data and modify the data of system B in time. If the window size is N, there will be a sample data $\widetilde{X}_1$ in $[N/2]$. In general, the data will be delayed in half of the window size and when the processing window is moving forward, $\widetilde{X}_1$ cannot stay in the correct place. The sample interval of $\widetilde{X}_1$ is too long to ensure that the sample value of $\widetilde{X}_1$ is proper in the processing window.

The sample time of heat balance method is about two minutes while the sample time of heat transfer method is five seconds because the probe of heat transfer method is placed in the fluid directly and the sensor has a speedy response. If the window size is set to be 16, the sampling point will not be inside some windows when the window is moving. If the window size is very large, the correlation among the measurements from the two measured methods will be reduced very much. If the sampling point is not in the middle of the window, it is difficult to satisfy the assumption of weighted average.

It is suggested that the measurements are processed by data fusion method after the sample value $\widetilde{X}$ with high accuracy is predicted by the preliminary data if the measurements are processed in real-time. For one sample value, we conclude

$$\widetilde{X}_1 \approx \sum_{i=1}^{n} w_{1,i} \cdot x_i, \tag{1}$$

where $\widetilde{X}$ expresses the weighted average of $\widetilde{x}$. $\widetilde{X}$ can be predicted by the modified sample value of system B.

After the sample value of system B is corrected, a new sample value X_{n+1} will be put into the processing window and the old sample value X_1 will be removed from the window. X_1 is the corrected sample value while X_{n+1} has not been corrected. In this paper, the estimate of $\widetilde{X}$ can be obtained by predicting the corrected measurement of X_{n+1} as follows:

$$\widetilde{X}_1' = \widetilde{X}_1 - w_{1,1}x_1 + w_{1,n}\widehat{x}_{n+1}, \tag{2}$$

where $\widehat{x}_{n+1}$ is the $(n+1)$th estimate which is predicted by the corrected measurement of system B.

3. Data Fusion

In the data fusion method [23], there are several methods to get the measured value of the same measurement x. Denote the ith measurement value of x as $\widetilde{x}^{(i)}$, $i = 1, \ldots, n$. Then, the corresponding measured error can be written as

$$\Delta x^{(i)} \overset{\text{def}}{=} \widetilde{x}^{(i)} - x, \tag{3}$$

where x represents the actual value of the measurement and $\Delta x^{(i)}$ is the measured error of the ith measured method.

If each measured error obeys normal distribution with zero mean and standard deviation $\sigma^{(i)}$, the probability density function of $\Delta x^{(i)}$ can be described as

$$f(x) = \frac{1}{\sqrt{2\cdot\pi}\cdot\sigma^{(i)}} \cdot \exp\left(-\frac{\left(\Delta x^{(i)}\right)^2}{2\cdot\left(\sigma^{(i)}\right)^2}\right) = \frac{1}{\sqrt{2\cdot\pi}\cdot\sigma^{(i)}} \cdot \exp\left(-\frac{\left(\widetilde{x}^{(i)} - x\right)^2}{2\cdot\left(\sigma^{(i)}\right)^2}\right). \tag{4}$$

If the measured error $\Delta x^{(i)}$ is independent, $\rho(x)$ expresses the joint probability destiny of x and it can be written as

$$\begin{aligned}\rho(x) &= \prod_{i=1}^{n} \frac{1}{\sqrt{2\cdot\pi}\cdot\sigma^{(i)}} \cdot \exp\left(-\frac{\left(\widetilde{x}^{(i)}-x\right)^2}{2\cdot\left(\sigma^{(i)}\right)^2}\right) \\ &= \left(\prod_{i=1}^{n} \frac{1}{\sqrt{2\cdot\pi}\cdot\sigma^{(i)}}\right) \cdot \exp\left(-\sum_{i=1}^{n} \frac{\left(\widetilde{x}^{(i)}-x\right)^2}{2\cdot\left(\sigma^{(i)}\right)^2}\right).\end{aligned} \tag{5}$$

It is reasonable to select the maximum likelihood estimate as the estimate of x when the probability $\rho(x)$ is the largest. Since $\exp(z)$ is an increasing function, maximizing $\rho(x) = A\cdot\exp(-B(x))$ is equivalent to minimizing $B(x)$, and then we can derive that

$$\min\left(\sum_{i=1}^{n} \frac{\left(\widetilde{x}^{(i)}-x\right)^2}{2\cdot\left(\sigma^{(i)}\right)^2}\right). \tag{6}$$

Differentiating (6) with respect to x and equating the derivative to zero, we can conclude the maximum value:

$$x = \frac{\sum_{i=1}^{n} \widetilde{x}^{(i)}\cdot\left(\sigma^{(i)}\right)^{-2}}{\sum_{i=1}^{n}\left(\sigma^{(i)}\right)^{-2}}. \tag{7}$$

The accuracy of this fused estimator can be described by the synthetic standard deviation σ as follows:

$$\sigma^{-2} = \sum_{i=1}^{n}\left(\sigma^{(i)}\right)^2. \tag{8}$$

It is assumed that there are two measurement systems, that is, the heat balance method and the heat transfer method, of which the accuracy and time (spatial) resolution are different. The accuracy of system with higher time resolution is higher, while the accuracy of system with lower time resolution is lower. Considering the individual and the mutual probability distribution, the data fusion method will use least squares (LS) algorithm to minimizing the deviation of the fused data.

In convenience, $\widetilde{X}_j$ is defined as the sample value (or estimated value) of system with low time resolution and high accuracy and the corresponding system is called system A. $\widetilde{x}_i$ expresses the sample value (or estimated value) of system with high time resolution and high accuracy and the corresponding system is system B. In this paper, system A uses the heat balance method and system B adopts the heat transfer method.

The following problems will be considered in this algorithm.

(A) Each sampling value $\widetilde{x}_i$ from system B is approximately equal to the actual value x_i at a certain probability in the corresponding time, with the standard deviation $\sigma_{h,i}$:

$$\widetilde{x}_i \approx x_i i. \tag{9}$$

(B) Each sampling value $\widetilde{X}_j$ from system A with a high time resolution is approximately equal to the weighted average of the actual values, with the standard deviation $\sigma_{l,i}$:

$$\widetilde{X}_j \approx \sum_i w_{j,i}\cdot x_i, \tag{10}$$

where $w_{j,i} \geq 0$ and $\sum_{i=1}^{n} w_{j,i} = 1$. In general, the weights are known. For example, these weights are equal in a joint inversion system and we get

$$\widetilde{X}_j \approx \frac{x_i(1,j) + \cdots + x_i\left(k_j, j\right)}{k_j}. \tag{11}$$

In this application, the influences on weights are different because the sampling intervals are different. So the weights will be different and the problem about the selection of weight will be discussed in the following sections.

(C) A prior estimate: if the system B has a prior estimate with higher time resolution, we get

$$x_i \approx x_{\mathrm{pr},i}, \tag{12}$$

where the standard deviation of $x_{\mathrm{pr},i}$ is $\sigma_{\mathrm{pr},i}$. In application, if there is no prior estimate, we can set $\sigma_{\mathrm{pr},i} = \infty$ and its influence can be eliminated.

(D) The sampling value $\widetilde{X}_j$ from system A is approximately equal to the actual value at the sampling time point with a high resolution at a certain probability, with the accuracy corresponding to the standard deviation $\sigma_{e,j}$:

$$\widetilde{X}_j \approx x_i(l,j). \tag{13}$$

The expectation can be estimated by the sampling value of system B:

$$E_j = \frac{1}{k_j}\cdot\sum_{l=1}^{k_j}\widetilde{x}_i(l,j). \tag{14}$$

The corresponding standard deviation is defined as $\sigma_{e,j}$ and it can be expressed as

$$\sigma_{e,j}^2 = \frac{1}{k_j}\cdot\sum_{l=1}^{k_j}\left(\widetilde{x}_i(l,j) - E_j\right)^2. \tag{15}$$

Next, the least squares (LS) technique will be applied to combine these approximate equalities and find the desirable estimate of the measurements by minimizing the resulting sum of weighted squared differences.

According to the LS approach, the sum of the different deviation in the above expression is minimized. In general case, we minimize the following expression:

$$\begin{aligned}&\sum_{i=1}^{n}\frac{\left(x_i-\widetilde{x}_i\right)^2}{\sigma_{h,i}^2} + \sum_{j=1}^{m}\frac{1}{\sigma_{l,j}^2}\left(\widetilde{X}_j - \sum_{i=1}^{n} w_{j,i}\cdot x_i\right)^2 \\ &\quad + \sum_{i=1}^{n}\frac{\left(x_i - x_{\mathrm{pr},i}\right)^2}{\sigma_{\mathrm{pr},i}^2} + \sum_{j=1}^{m}\sum_{l=1}^{k_j}\frac{\left(\widetilde{X}_j - x_i(l,j)\right)^2}{\sigma_{e,j}^2}.\end{aligned} \tag{16}$$

The solution of the LS approach includes the deviation of the measurements with high resolution (the first expression), the deviation of the prior estimate with high resolution (the third expression), the deviation of the weighted estimates of which low resolution are weighted by the sampling value of the high resolution (the fourth expression), and the deviation between the sampling value of high resolution and the corresponding area with the high resolution (the second expression). The synthesis results minimize the overall deviation in the above and the solution of the estimated x_i is equal to the value of data fusion.

Differentiation with respect to x_i leads to the following system of linear equations:

$$\begin{aligned}&\frac{1}{\sigma_{h,i}^2}\cdot\left(x_i-\widetilde{x}_i\right)+\sum_{j:j\ni i}\frac{1}{\sigma_{l,j}^2}\cdot w_{j,i}\cdot\left(\sum_{i'=1}^{n}w_{j,i'}\cdot x_{i'}-\widetilde{X}_j\right)\\&\quad+\frac{1}{\sigma_{\mathrm{pr},i}^2}\cdot\left(x_i-x_{\mathrm{pr},i}\right)+\sum_{j:j\ni i}\frac{1}{\sigma_{e,j}^2}\cdot\left(x_i-\widetilde{X}_j\right)=0,\end{aligned}\tag{17}$$

where $j \ni i$ means that the jth sampling value corresponding to a model with a low spatial resolution covers the ith sampling value.

In the above solution of LS approach, the prior estimate $x_{\mathrm{pr},i}$ and the estimate $\widetilde{x}_i$ from system A with a higher resolution have the general form. Then, they can be expressed into a unified form:

$$\frac{1}{\sigma_{h,i}^2}\cdot\left(x_i-\widetilde{x}_i\right)+\frac{1}{\sigma_{\mathrm{pr},i}^2}\cdot\left(x_i-x_{\mathrm{pr},i}\right)\tag{18}$$

Equation (18) can be expressed as follows:

$$\sigma_{f,i}^{-2}\cdot\left(x_i-x_{f,i}\right),\tag{19}$$

where

$$\begin{aligned}x_{f,i}&\stackrel{\mathrm{def}}{=}\frac{\widetilde{x}_i\cdot\sigma_{h,i}^{-2}+x_{\mathrm{pr},i}\cdot\sigma_{\mathrm{pr},i}^{-2}}{\sigma_{h,i}^{-2}+\sigma_{\mathrm{pr},i}^{-2}}\\\sigma_{f,i}^{-2}&\stackrel{\mathrm{def}}{=}\sigma_{h,i}^{-2}+\sigma_{\mathrm{pr},i}^{-2}.\end{aligned}\tag{20}$$

Similarly, if the standard deviation is set to infinity, the influence of the corresponding term will be eliminated. For example, we can set $\sigma_{h,i} = 0$ if only the prior estimates of the system are known.

After simplification, the LS expression is

$$\begin{aligned}&\sigma_{f,i}^{-2}\cdot\left(x_i-x_{f,i}\right)+\sum_{j:j\ni i}\frac{1}{\sigma_{l,j}^2}\cdot w_{j,i}\cdot\left(\sum_{i'=1}^{n}w_{j,i'}\cdot x_{i'}-\widetilde{X}_j\right)\\&\quad+\sum_{j:j\ni i}\frac{1}{\sigma_{e,j}^2}\cdot\left(x_i-\widetilde{X}_j\right)=0.\end{aligned}\tag{21}$$

Now, we consider the case of a single estimate with low resolution.

Let us consider the simplest case, when we have exactly one estimate from system A with a low resolution. In this case, (21) takes the following form:

$$\begin{aligned}&\sigma_{f,i}^{-2}\cdot\left(x_i-x_{f,i}\right)+\frac{1}{\sigma_{l,1}^2}\cdot w_{1,i}\cdot\left(\sum_{i'}w_{1,i'}\cdot x_{i'}-\widetilde{X}_1\right)\\&\quad+\frac{1}{\sigma_{e,1}^2}\left(x_i-\widetilde{X}_1\right)=0.\end{aligned}\tag{22}$$

If multiplying both sides of (22) by $\sigma_{f,i}^2$, we conclude that

$$\begin{aligned}&x_i-x_{f,i}+\frac{\sigma_{f,i}^2}{\sigma_{l,1}^2}\cdot w_{1,i}\cdot\left(\sum_{i'}w_{1,i'}\cdot x_{i'}-\widetilde{X}_1\right)\\&\quad+\frac{\sigma_{f,i}^2}{\sigma_{e,1}^2}\cdot\left(x_i-\widetilde{X}_1\right)=0.\end{aligned}\tag{23}$$

If we introduce an auxiliary variable μ as

$$\mu\stackrel{\mathrm{def}}{=}\frac{1}{\sigma_{l,1}^2}\cdot\left(\sum_{i'}w_{1,i'}\cdot x_{i'}-\widetilde{X}_1\right),\tag{24}$$

we get the equation

$$x_i-x_{f,i}+w_{1,i}\cdot\sigma_{f,i}^2\cdot\mu+\frac{\sigma_{f,i}^2}{\sigma_{e,1}^2}\cdot\left(x_i-\widetilde{X}_1\right)=0.\tag{25}$$

By keeping terms proportional to x_i in the left-hand side and by moving all the other terms to the right-hand side, we get

$$\left(1+\frac{\sigma_{f,i}^2}{\sigma_{e,1}^2}\right)\cdot x_i=x_{f,i}-w_{1,i}\cdot\sigma_{f,i}^2\cdot\mu+\frac{\sigma_{f,i}^2}{\sigma_{e,1}^2}\cdot\widetilde{X}_1.\tag{26}$$

Hence

$$\begin{aligned}x_i=&\frac{x_{f,i}}{1+\sigma_{f,i}^2/\sigma_{e,1}^2}-\frac{w_{1,i}\cdot\sigma_{f,i}^2}{1+\sigma_{f,i}^2/\sigma_{e,1}^2}\cdot\mu+\widetilde{X}_1\\&\cdot\frac{\sigma_{f,i}^2/\sigma_{e,1}^2}{1+\sigma_{f,i}^2/\sigma_{e,1}^2}.\end{aligned}\tag{27}$$

According to the definition of μ, it includes the actual value of random variable x_i. To make this expression practical, we must describe μ in terms of the given $\widetilde{x}_i$ and $\widetilde{X}_1$.

From (27), we get

$$\begin{aligned}\sum_{i=1}^{n}w_{1,i}\cdot x_i=&\sum_{i=1}^{n}\frac{w_{1,i}\cdot x_{f,i}}{1+\sigma_{f,i}^2/\sigma_{e,1}^2}-\mu\\&\cdot\sum_{i=1}^{n}\frac{w_{1,i}^2\cdot\sigma_{f,i}^2}{1+\sigma_{f,i}^2/\sigma_{e,1}^2}+\widetilde{X}_1\cdot\sum_{i=1}^{n}\frac{w_{1,i}\cdot\left(\sigma_{f,i}^2/\sigma_{e,1}^2\right)}{1+\sigma_{f,i}^2/\sigma_{e,1}^2}.\end{aligned}\tag{28}$$

According to definition of μ, we conclude that

$$\begin{aligned}\sigma_{l,1}^2 \cdot \mu &= \sum_{i=1}^{n} w_{1,i} \cdot x_i - \widetilde{X}_1 \\ &= \sum_{i=1}^{n} \frac{w_{1,i} \cdot x_{f,i}}{1 + \sigma_{f,i}^2/\sigma_{e,1}^2} - \mu \cdot \sum_{i=1}^{n} \frac{w_{1,i}^2 \cdot \sigma_{f,i}^2}{1 + \sigma_{f,i}^2/\sigma_{e,1}^2} + \widetilde{X}_1 \\ &\quad \cdot \sum_{i=1}^{n} \frac{w_{1,i} \cdot \left(\sigma_{f,i}^2/\sigma_{e,1}^2\right)}{1 + \sigma_{f,i}^2/\sigma_{e,1}^2} - \widetilde{X}_1.\end{aligned} \tag{29}$$

According the definition of weighted average, the sum of the weights is equal to one:

$$\sum_{i=1}^{n} w_{1,i} = 1. \tag{30}$$

Then the final two terms in the left-hand side of (29) can be merged into

$$\begin{aligned}&\widetilde{X} \cdot \sum_{i=1}^{n} \frac{w_{1,i} \cdot \left(\sigma_{f,i}^2/\sigma_{e,1}^2\right)}{1 + \sigma_{f,i}^2/\sigma_{e,1}^2} - \widetilde{X}_1 \\ &= \widetilde{X}_1 \cdot \left(\sum_{i=1}^{n} w_{1,i} \frac{\sigma_{f,i}^2/\sigma_{e,1}^2}{1 + \sigma_{f,i}^2/\sigma_{e,1}^2} - \sum_{i=1}^{n} w_{1,i} \right) \\ &= -\widetilde{X}_1 \cdot \sum_{i=1}^{n} \frac{w_{1,i}}{1 + \sigma_{f,i}^2/\sigma_{e,1}^2}.\end{aligned} \tag{31}$$

By taking (31) into (24) and moving all terms containing μ to the left-hand side, we get

$$\begin{aligned}&\mu \cdot \left(\sigma_{l,1}^2 + \sum_{i=1}^{n} \frac{w_{1,i}^2 \cdot \sigma_{f,i}^2}{1 + \sigma_{f,i}^2/\sigma_{e,1}^2} \right) \\ &= \sum_{i=1}^{n} \frac{w_{1,i} \cdot x_{f,i}}{1 + \sigma_{f,i}^2/\sigma_{e,1}^2} - \widetilde{X}_1 \cdot \sum_{i=1}^{n} \frac{w_{1,i}}{1 + \sigma_{f,i}^2/\sigma_{e,1}^2} \\ &= \sum_{i=1}^{n} \frac{w_{1,i} \left(x_{f,i} - \widetilde{X}_1\right)}{1 + \sigma_{f,i}^2/\sigma_{e,1}^2}.\end{aligned} \tag{32}$$

If we introduce two auxiliary variables N and D, the auxiliary variable μ can be computed as follows:

$$\mu = \frac{N}{D}, \tag{33}$$

where

$$\begin{aligned}D &= \left(\sigma_{l,1}^2 + \sum_{i=1}^{n} \frac{w_{1,i}^2 \cdot \sigma_{f,i}^2}{1 + \sigma_{f,i}^2/\sigma_{e,1}^2} \right) \\ N &= \sum_{i=1}^{n} \frac{w_{1,i} \left(x_{f,i} - \widetilde{X}_1\right)}{1 + \sigma_{f,i}^2/\sigma_{e,1}^2}.\end{aligned} \tag{34}$$

Then, under higher time resolution, we compute the more accurate estimate for x_i, $i = 1, \ldots, h$, as

$$\begin{aligned}\widehat{x}_i &= \frac{x_{f,i}}{1 + \sigma_{f,i}^2/\sigma_{e,1}^2} - \frac{w_{1,i} \cdot \sigma_{f,i}^2}{1 + \sigma_{f,i}^2/\sigma_{e,1}^2} \cdot \mu + \widetilde{X}_1 \\ &\quad \cdot \frac{\sigma_{f,i}^2/\sigma_{e,1}^2}{1 + \sigma_{f,i}^2/\sigma_{e,1}^2}.\end{aligned} \tag{35}$$

Equation (35) indicates that the sampling accuracy of the low accuracy system B will be improved by modifying the sampling value with the sampling value of higher accuracy system A if the noises of system A and B obey a Gaussian distribution and the standard deviation of system A is known.

The above method, using LS algorithm, shows the basic results by modifying the sampling value from a measurement system with a low accuracy when we have one estimate from system A with a higher accuracy. If all of the standard deviations in the resulting expression can be computed online or known in advance, they can be used to improve the accuracy of the system with a low accuracy.

We then solve the problem which is how to obtain the standard deviation of the above model in real-time. If this problem can be solved, the whole system will satisfy the need of the real-time measurement and this method will be applied into the polynomial prediction filter approach in the next section.

4. Main Results

4.1. Polynomial Prediction Filtering Method Based on FIR Scheme. In theory, the signal can be described by a M-order polynomial. Consider

$$x(n) = a_0 + a_1 n + \cdots + a_M n^M = \sum_{l=0}^{M} a_l n^l. \tag{36}$$

The polynomial filter method is that the measured signals are predicted and filtered by polynomial. A polynomial prediction filter method based on the finite impulse response (FIR) scheme has been proposed in Henry and Clarke [24]. And it is called H-N FIP predictor. This method can predict the signals with smoothness.

It is assumed that the first n measurements are known and the $(n + p)$th measurement can be predicted as follows:

$$\widehat{x}(n + p) = \sum_{k=0}^{N-1} h(k)\, x(n - k), \tag{37}$$

where p is the prediction horizon, which can be an integer or a decimal. $h(k)$ is a coefficient of the FIR scheme.

By taking (36) into (37), we can get

$$\hat{x}(n+p) = \sum_{l=0}^{M} a_l [n+p]^l, \tag{38}$$

$$\sum_{k=0}^{N-1} h(k)\, x(n-k) = \sum_{k=0}^{N-1} h(k) \sum_{l=0}^{M} a_l [n-k]^l, \tag{39}$$

$$\sum_{l=0}^{M} a_l [n+p]^l = \sum_{k=0}^{N-1} h(k) \sum_{l=0}^{M} a_l [n-k]^l. \tag{40}$$

Both sides of (40) are expended by the lth power subentry, respectively. The polynomial which includes a_l is that

$$a_l [n+p]^l = \sum_{k=0}^{N-1} h(k)\, a_l [n-k]^l = a_l \sum_{k=0}^{N-1} h(k)\, [n-k]^l. \tag{41}$$

If a_l is removed from (41), we can get

$$[n+p]^l = \sum_{k=0}^{N-1} h(k)\, [n-k]^l \tag{42}$$

or it can expressed as

$$[-p]^l = \sum_{k=0}^{N-1} h(k)\, [k]^l. \tag{43}$$

Equation (43) is one of the restrictions of $h(k)$.

The noise of signals can be sufficiently suppressed by minimizing the gain of the filter noise. If the noise is a white noise, the gain of signals for the digital filter based on FIR scheme can be expressed as

$$G_{\text{noise}} = \sum_{k=0}^{N-1} |h(k)|^2. \tag{44}$$

If the restriction is satisfied, we can minimize G_{noise} and the optimal solution of $h(k)$ can be obtained.

When $p = 1$ and $M = 1$, we can get

$$h(k) = \frac{4N - 6k - 4}{N(N-1)}. \tag{45}$$

When $p = 1$ and $M = 2$, we can get

$$h(k) = \frac{9N^2 + (9 - 36k)N + 30k^2 - 18k + 6}{N^3 - 3N^2 + 2N}. \tag{46}$$

According to (45) and (46), the coefficient of polynomial prediction filter is independent of $x(k)$. But it is simply a matter of the window size N, the order M of polynomial, and the prediction horizon p. All of the parameters are determined before computation. Therefore, this method is called one-step-prediction algorithm and it is applicable under the real-time condition.

4.2. Model Parameters Modification under the Prediction Model. In this paper, the measurements of heat balance method in data fusion are estimated. Therefore, there is a necessity of modifying the estimated signal parameter in order to adapt to the model fusion method. Once the prediction method is applied, we should consider whether all of the standard deviations defined in model fusion method need to be reestimated.

It is assumed that the corresponding standard deviations are known in a "real" fusion which is based on the actual measurements from heat balance method. The standard deviations include the standard deviation of the measurements with heat balance method and standard deviation of single measurement with heat transfer method. Both of them can be measured and calculated by experiments.

According to the principle of combination of error, assuming each measurement is independent,

$$\sigma_y^2 = \left(\frac{\partial f}{\partial x_1}\right)^2 \cdot \sigma_{x_1}^2 + \left(\frac{\partial f}{\partial x_2}\right)^2 \cdot \sigma_{x_2}^2 + \cdots + \left(\frac{\partial f}{\partial x_n}\right)^2 \cdot \sigma_{x_n}^2. \tag{47}$$

For one estimate of system A, we have

$$\widetilde{X}_1' = \widetilde{X}_1 - w_{1,1} x_1 + w_{1,n} \hat{x}_{n+1}. \tag{48}$$

The standard deviation can be computed as follows:

$$\sigma_{\widetilde{X}'}^2 = \sigma_{\widetilde{X}_1}^2 + \sigma_{x_1}^2 + \sigma_{x_{n+1}}^2, \tag{49}$$

where $\sigma_{\widetilde{X}_1}$ is the sampling standard deviation of one estimate for system A; σ_{x_1} is the standard deviation of modified measurement for system B in the fusing window; and $\sigma_{x_{n+1}}$ is the standard deviation of the $(n+1)$th modified measurement for system B. σ_{x_1} can be obtained from (15).

In the polynomial prediction algorithm, the standard deviation of $\hat{x}_{n+1}$ can be expressed as

$$\sigma_{n+1}^2 = \sigma_i^2 \sum_{i=1}^{k} h_0(i)^2, \tag{50}$$

where σ_i is the sample deviation.

By taking (49) into (50), the standard deviation of measurements from heat balance method can be estimated before model fusion.

5. Discussion

5.1. Window of the Data Fusion. The measurements of heat transfer method are estimated by polynomial prediction method; then the estimated value of heat balance method can be obtained. The estimated value will be used in the data fusion method.

Considering the polynomial prediction filtering method and the characteristic of signal, M is 2 and N is 16, and $\widetilde{X}$ can be estimated from (36) in most of the windows. The measured value of heat transfer method will be modified after the actual measurement enters into the window.

Table 1: The distribution of weights.

m	i															
	1	2	3	4	5	6	7	8	9	10	11	12	13	14	15	16
16	0.5	0.8	1.1	1.5	2	2.5	3	4	4	3	2.5	2	1.5	1.1	0.8	0.5
15	0.8	1.1	1.5	2	2.5	3	4	4	3	2.5	2	1.5	1.1	0.8	0.5	0.5
14	1.1	1.5	2	2.5	3	4	4	3	2.5	2	1.5	1.1	0.8	0.8	0.5	0.5
13	1.5	2	2.5	3	4	4	3	2.5	2	1.5	1.1	1.1	0.8	0.8	0.5	0.5

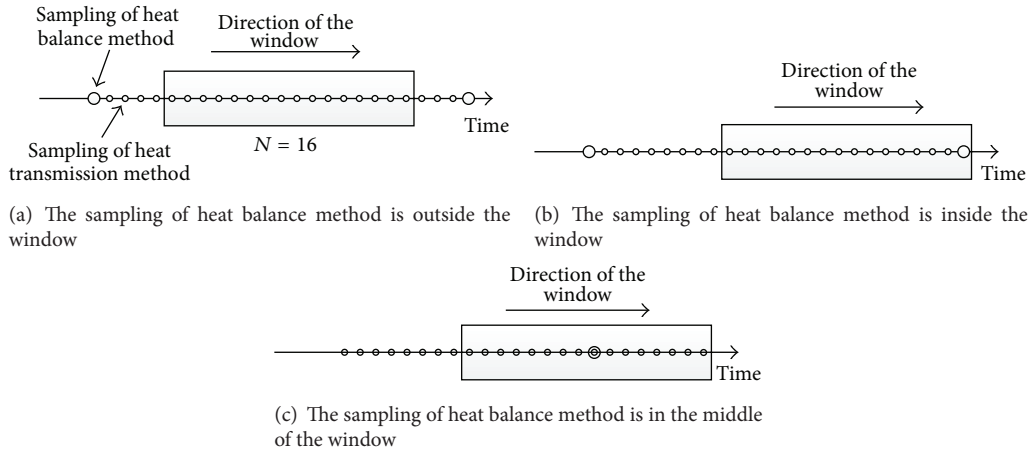

(a) The sampling of heat balance method is outside the window

(b) The sampling of heat balance method is inside the window

(c) The sampling of heat balance method is in the middle of the window

Figure 1: Window of data fusion.

The window adopted in this data fusion method is shown in Figure 1. Here, the sample time of the heat balance method is 2 minutes while the sample time of the heat transfer method can be 5 seconds which is much shorter than heat balance method. Therefore, there is no actual high accuracy sample value of heat balance method in the fusing window when the window is 16. As described in the previous section, the data used in the fusing window will be estimated by the polynomial prediction filtering method.

5.2. Distribution of Weight. In Figure 1, the actual sample value rather than the estimated value will be used to process by the data fusion method once a new sample value of heat balance method enters into the window. The new sample value of heat balance method stays in the window for a while and the position of the sampling point will change.

If the sampling point of heat balance method is in middle of the fusing window, the result is the average of the sampling value of heat balance in the window which can be seen in (11). In fact, the sampling point is often not in the middle of the fusing window where the weights should be assigned reasonably.

If the window size is 16, the weight $w_{1,i}$ of data fusion method can be expressed as follows:

$$w_{1,i} = \frac{w_{m,i}}{16}, \tag{51}$$

where i is the position of the sample value of system B in the fusing window. The position of the sample value of system A in the window is used here and it satisfies the following equation:

$$\sum_{m=1}^{16} w_{m,i} = 16. \tag{52}$$

When a new sample value of system A enters into the window, it is reasonable that the new sample value contains sixteen sample values of system B. In other words, it is a sample value which delays half of the window. When the position of the sampling value of system A is less than 13 in the window, its effect becomes weaker and the sampling value of system A will be decided by the prediction method which is used in the data fusion. The distribution of weights is shown in Table 1.

6. Conclusion

This paper investigates the measurement of the gas-solid two-phase flow in pneumatic conveyor. A new approach called data fusion based real-time measurement is proposed, which can improve the overall accuracy of the flow rate of the gas-solid two-phase flow and the time resolution. The proposed method also can be applied into the polynomial prediction filter for modifying the model parameters.

Conflict of Interests

The authors declare that there is no conflict of interests regarding the publication of this paper.

References

[1] Y. Yan, "Mass flow measurement of bulk solids in pneumatic pipelines," *Measurement Science & Technology*, vol. 7, no. 12, pp. 1687–1706, 1996.

[2] R. Deloughry and E. Pickup, "Investigation of the closed loop control of a pneumatic conveying system using tomographic imaging," in *Process Imaging for Automatic Control*, vol. 4188 of *Proceedings of SPIE*, pp. 103–113, November 2000.

[3] F. Q. Shao, Z. X. Lu, E. G. Wu, and S. Wang, "Study and industrial evaluation of mass flow measurement of pulverized coal for iron-making production," *Flow Measurement and Instrumentation*, vol. 11, no. 3, pp. 159–163, 2000.

[4] J. Ma and Y. Yan, "Design and evaluation of electrostatic sensors for the measurement of velocity of pneumatically conveyed solids," *Flow Measurement and Instrumentation*, vol. 11, no. 3, pp. 195–204, 2000.

[5] J. B. Gajewski, "Non-contact electrostatic flow probes for measuring the flow rate and charge in the two-phase gas-solids flows," *Chemical Engineering Science*, vol. 61, no. 7, pp. 2262–2270, 2006.

[6] E. Chenglin, C. Lu, C. Xu, J. Gao, and M. Shi, "A new method for measurement of local solid flux in gas-solid two-phase flow," *Chinese Journal of Chemical Engineering*, vol. 11, no. 6, pp. 617–621, 2003.

[7] L. Aísa, J. A. Garcia, L. M. Cerecedo, I. García Palacín, and E. Calvo, "Particle concentration and local mass flux measurements in two-phase flows with PDA. Applications to a study on the dispersion of spherical particles in a turbulent air jet," *International Journal of Multiphase Flow*, vol. 28, no. 2, pp. 301–324, 2002.

[8] T. G. Evans, N. G. Cutmore, E. Zoud, and F. J. Paolani, "Microwave techniques for on-line determination of pulverised coal mass flow," in *Proceedings of the AMPC Asia-Pacific Microwave Conference*, vol. 1, pp. 559–562, 1992.

[9] S. Bhusarapu, M. Al-Dahhan, and M. P. Dudukovic, "Quantification of solids flow in a gas-solid riser: single radioactive particle tracking," *Chemical Engineering Science*, vol. 59, no. 22-23, pp. 5381–5386, 2004.

[10] T. Moriyama, S. Fujii, K. Abe, and M. Kobayashi, "Mass flowmeter using heat transfer for dense phase solid gas two-phase flow," in *Proceedings of the International Conference on Fluid Control and Measurement*, vol. 33, pp. 1063–1066, 1985.

[11] T. Moriyama, "Mass flow measurement using heat transfer method for stand pipe," in *Proceedings of the SICE*, vol. 25, pp. 1063–1066, 1992.

[12] X. Wu and Z.-L. Yun, "Neural networks for on-line prediction of the solid flowrate in gas-solid two phase flow based on heat transfer," *Boiler Technology*, vol. 32, no. 12, pp. 8–11, 2001.

[13] S.-Z. Wu, Y.-J. Han, W.-X. Pu et al., "Investigation on prediction of solid flow-rate in gas-solid two phase by BP neural networks," *Power System Engineering*, vol. 19, no. 5, pp. 56–58, 2003.

[14] C. Xu, Y. Zhao, J. Huang et al., "The soft sensor model for mass flow rate measurement of pneumatically conveyed solids based on the artificial neural network," *Acta Metrologica Sinica*, vol. 27, no. 3, pp. 246–249, 2006.

[15] B. Menz, "Vortex flowmeter with enhanced accuracy and reliability by means of sensor fusion and self-validation," *Measurement*, vol. 22, no. 3-4, pp. 123–128, 1997.

[16] W. G. Pan and J. M. Cao, "Study on techniques for online measurement to air and pulverized coal mixture flow parameters of coal-fired boiler in power plant," *Proceedings of the CSEE*, vol. 24, no. 10, pp. 193–195, 2004.

[17] N. J. Zhou, Y. Q. Xue, and F. Q. Wang, "Improved energy balance method for monitoring the pulverized coal and air flow," *Thermal Power Generation*, vol. 34, no. 12, pp. 59–62, 2005.

[18] Y. Zheng, J. R. Pugh, D. McGlinchey, and R. O. Ansell, "Simulation and experimental study of gas-to-particle heat transfer for non-invasive mass flow measurement," *Measurement*, vol. 41, no. 4, pp. 446–454, 2008.

[19] L. Liu, Y. Wang, F. D. Zhou, and H. Qian, "Measurement of air flow and concentration of pulverized coal with two ellipse-shaped thermal probes," *Journal of Xi'an Jiaotong University*, vol. 42, no. 1, pp. 23–26, 2008.

[20] Z. L. Yuan and Z. J. Lu, "Heat transfer method for solid flow rate measurement in gas-solid two phase flow," *Journal of Southeast University*, vol. 13, no. 2, pp. 73–77, 1997.

[21] C. X. Li, Y. Shao, and W. Li, "Measuring gas-solid two-phase mass flow based on thermal sensors fusion," *Journal Huazhong University of Science and Technology*, vol. 29, no. 8, pp. 50–52, 2001.

[22] Y. N. Zheng and Q. Liu, "Review of techniques for the mass flow rate measurement of pneumatically conveyed solids," *Measurement*, vol. 44, no. 4, pp. 589–604, 2011.

[23] O. Ochoa, A. A. Velasco, and C. Servin, "Towards a fast, practical alternative to joint inversion of multiple datasets: model fusion," *Journal of Uncertain Systems*, vol. 5, no. 2, pp. 119–136, 2011.

[24] M. P. Henry and D. W. Clarke, "The self-validating sensor: rationale, definitions and examples," *Control Engineering Practice*, vol. 1, no. 4, pp. 585–610, 1993.

Hindawi Publishing Corporation
Mathematical Problems in Engineering
Volume 2014, Article ID 276373, 6 pages
http://dx.doi.org/10.1155/2014/276373

Research Article

Distributed Event-Triggered Control of Multiagent Systems with Time-Varying Topology

Jingwei Ma,[1,2] Jie Zhou,[1] and Yanping Gao[3]

[1] *Department of Automation, Tsinghua University, Beijing 100084, China*
[2] *NO. 7 Department, NAAU, Yantai 264001, China*
[3] *College of Computer and Information Engineering, Beijing Technology and Business University, Beijing 100048, China*

Correspondence should be addressed to Jingwei Ma; mjw08@mails.tsinghua.edu.cn

Received 9 July 2014; Accepted 31 August 2014; Published 28 September 2014

Academic Editor: Housheng Su

This paper studies the consensus of first-order discrete-time multiagent systems, where the interaction topology is time-varying. The event-triggered control is used to update the control input of each agent, and the event-triggering condition is designed based on the combination of the relative states of each agent to its neighbors. By applying the common Lyapunov function method, a sufficient condition for consensus, which is expressed as a group of linear matrix inequalities, is obtained and the feasibility of these linear matrix inequalities is further analyzed. Simulation examples are provided to explain the effectiveness of the theoretical results.

1. Introduction

The distributed control of multiagent systems has received much attention because of its wide applications in scheduling of automated highway systems, cooperation control of multiple vehicles/robots, design of sensor networks, and so forth, and consensus is one of the hot topics in distributed control of multiagent systems [1–3].

Consensus of multiagent systems has been studied by researchers from different viewpoints, such as the dynamics of agents [4–7], the interaction topology [8–10], the convergence rate [11], and the information transmission [12–15]. In [12], consensus of first-order multiagent systems is considered in the cases with sampling delay and without sampling delay, respectively, and some sufficient and necessary conditions are provided in the case of fixed topology. In [13], consensus is analyzed for second-order multiagent systems with time-varying sampling intervals by applying matrix theory and Lyapunov stability theory, respectively. In [14], consensus of second-order multiagent systems is also discussed, where the sampling periods of agents are different and the topology at each time may not have spanning tree. In [15], consensus of second-order multiagent systems with uniform and nonuniform sampling periods is considered, where only position information is transmitted among agents. It is noted that the work in [12–15] all assumes that the information received by agents at each time will be transmitted to controllers and thus consensus in these cases can be viewed as time-based consensus.

Compared with the time-based consensus, event-based consensus is more realistic, where the information received by agents is transmitted to controllers only when some events occur. Event-triggered control has some advantages such as reducing the number of transmissions and thus it is more suitable for cooperative control over networks with limited bandwidth [16]. There has been some work on event-based consensus of first-order continuous-time multiagent systems [17–22] and second-order continuous-time multiagent systems [20, 23–25]. In [17], a centralized event-triggering condition is provided and a sufficient condition of consensus is established in the cases of fixed topology and switching topology, where the topology at each time is strongly connected and balanced. In [18–20], a distributed event-triggering condition is given and some sufficient conditions for consensus are obtained in the case of fixed topology. Moreover, to avoid continuously monitoring whether the event-triggering

condition is satisfied, the self-trigged control, where the next update time of controller is predetermined, is also discussed. In [21, 22], each agent can only obtain information at some discrete times, and if the information at these discrete times satisfies the distributed event-triggering condition, then they will be used to update control input. Furthermore, sufficient conditions for consensus in the cases of fixed and switching topology, where the topology at each time is connected, are provided. In [20, 23, 24], some centralized or distributed event-triggering conditions are designed for second-order multiagent systems with fixed topology, where the position and velocity information of each agent share a common event-triggering condition. In addition, the leader-follower consensus based on event-triggered control is considered for the case of fixed topology in [25].

However, there is little work [26–28] on the event-based consensus of discrete-time multiagent systems. In [26], a centralized event-triggering condition is provided for first-order multiagent systems and some sufficient conditions are obtained. In [27, 28], the event-based consensus of heterogeneous discrete-time multiagent systems is discussed. Moreover, the above three papers all consider the fixed topology case. Based on the above observation, we study the event-based consensus of first-order discrete-time multiagent systems in the case of time-varying topology. The main contribution of our work is to design a distributed event-triggering condition and obtain a sufficient condition of consensus in the case of time-varying topology.

This paper is organized as follows. In Section 2, we present some concepts in graph theory and formulate the model to be studied. In Section 3, main results are stated. In Section 4, simulations are provided to illustrate the effectiveness of the theoretical results. Conclusion remarks are made in Section 5.

2. Preliminaries

2.1. Graph Theory. Graph plays a key role in modeling the interaction topology among agents. We first introduce some basic definitions in graph theory [29].

A directed graph $\mathcal{G}$ consists of a vertex set $\mathcal{V}(\mathcal{G})$ and an edge set $\mathcal{E}(\mathcal{G})$, where $\mathcal{V}(\mathcal{G}) = \{v_1, \ldots, v_n\}$ and $\mathcal{E}(\mathcal{G}) \subset \{(v_j, v_i) : v_j, v_i \in \mathcal{V}(\mathcal{G})\}$. For edge (v_j, v_i), v_j is called the parent vertex of v_i and v_i is called the child vertex of v_j. If two ends of an edge are the same vertex, then such an edge is called a self-loop. The set of neighbors of vertex v_i is defined by $N(\mathcal{G}, v_i) = \{v_j : (v_j, v_i) \in \mathcal{E}(\mathcal{G}) \text{ and } j \neq i\}$, and the associated index set is denoted by $N(\mathcal{G}, i) = \{j : v_j \in N(\mathcal{G}, v_i)\}$. A (directed) path from v_{i_1} to v_{i_k} is a sequence, $v_{i_1}, \ldots, v_{i_k}$, of distinct vertices such that $(v_{i_j}, v_{i_{j+1}}) \in \mathcal{E}(\mathcal{G})$, $j = 1, \ldots, k-1$. A directed graph $\mathcal{G}$ is strongly connected if there is a path from every vertex to every other vertex. A directed tree is a directed graph, where every vertex except one special vertex has exactly one parent vertex, and the special vertex, called root vertex, has no parent vertices and can be connected to any other vertices via paths. A subgraph $\mathcal{G}_s$ of $\mathcal{G}$ is a graph such that $\mathcal{V}(\mathcal{G}_s) \subset \mathcal{V}(\mathcal{G})$ and $\mathcal{E}(\mathcal{G}_s) \subset \mathcal{E}(\mathcal{G})$. $\mathcal{G}_s$ is said to be a spanning subgraph if $\mathcal{V}(\mathcal{G}_s) = \mathcal{V}(\mathcal{G})$. For any $v_i, v_j \in \mathcal{V}(\mathcal{G}_s)$, if $(v_i, v_j) \in \mathcal{E}(\mathcal{G}_s) \Leftrightarrow (v_i, v_j) \in \mathcal{E}(\mathcal{G})$, then $\mathcal{G}_s$ is said to be an induced subgraph of $\mathcal{G}$ and $\mathcal{G}_s$ is also said to be induced by $\mathcal{V}(\mathcal{G}_s)$. A spanning tree of $\mathcal{G}$ is a directed tree which is a spanning subgraph of $\mathcal{G}$. $\mathcal{G}$ is said to have a spanning tree if some edges form a spanning tree of $\mathcal{G}$.

A matrix is called nonnegative if each of its elements is nonnegative. A weighted directed graph $\mathcal{G}(A)$ is a directed graph $\mathcal{G}$ plus a nonnegative matrix $A = [a_{ij}] \in \mathbb{R}^{n\times n}$, where $a_{ij} > 0 \Leftrightarrow (v_j, v_i) \in \mathcal{E}(\mathcal{G})$, and a_{ij} is called the weight of edge (v_j, v_i). If $\sum_{j=1}^{n} a_{ij} = \sum_{j=1}^{n} a_{ji}$, $i = 1, \ldots, n$, then $\mathcal{G}(A)$ is called balanced. If $A = A^T$, then $\mathcal{G}(A)$ is also called undirected, and $\mathcal{G}(A)$ is said to be connected if it, as a directed graph, is strongly connected. The Laplacian matrix $L = [l_{ij}] \in \mathbb{R}^{n\times n}$ of $\mathcal{G}(A)$ is defined as

$$l_{ij} = \begin{cases} -a_{ij}, & i \neq j \\ \sum_{s=1, s\neq i}^{n} a_{is}, & i = j. \end{cases} \tag{1}$$

The Laplacian matrix of $\mathcal{G}(A)$ has the following properties.

Lemma 1 (see [9]). *Consider the following:*

(i) *zero is an eigenvalue of L and $\mathbf{1}_n$ is the associated right eigenvector;*

(ii) *zero is an algebraically simple eigenvalue of L and all the other eigenvalues are with positive real parts if and only if $\mathcal{G}(A)$ has a spanning tree.*

Remark 2. In the time-varying topology case, we use $\mathcal{G}(t)$ to denote the topology graph at time t.

2.2. Model. Consider a group of agents with first-order discrete-time dynamics:

$$x_i(k+1) = x_i(k) + u_i(k), \quad i = 1, \ldots, n, \ k = 0, 1, 2, \ldots, \tag{2}$$

where $x_i(k)$ is the state of agent i at time k and $u_i(k)$ is the control input, called the protocol, to be designed based on the information obtained by agent i. Without loss of generality, we assume $x_i \in \mathbb{R}$, $i = 1, \ldots, n$.

Given u_i, $i = 1, \ldots, n$, u_i or multiagent system (2) solves a consensus problem asymptotically if, for any initial states and any $i, j = 1, \ldots, n$, $\lim_{k\to\infty}(x_i(k) - x_j(k)) = 0$.

Different from the previous work on consensus, not all the information obtained by agent i is used by controller u_i in our work. For agent i, when it receives new information, it will validate whether some condition, which is called event-triggering condition, is satisfied. If the event-triggering condition is satisfied, then the received information will not be used by its controller, or else the received information will be transmitted to its controller. The following event-triggering condition is considered:

$$\left|e_i(k)\right| \leq \sigma_i \left| \sum_{j\in N_i(k)} a_{ij}(k)\left(x_j(k) - x_i(k)\right)\right|, \quad i = 1, 2, \ldots, n, \tag{3}$$

where $e_i(k) = \sum_{j\in N_i(t_l^i)} a_{ij}(t_l^i)(x_j(t_l^i) - x_i(t_l^i)) - \sum_{j\in N_i(k)} a_{ij}(k)(x_j(k) - x_i(k))$ and $t_0^i, t_1^i, \ldots$ are event times of agent i; namely, at these times, (3) is not satisfied and the controller of agent i will be updated. Hence, the controller has the following form:

$$u_i(k) = u_i\left(t_l^i\right), k \in \left\{t_l^i, t_l^i + 1, \ldots, t_{l+1}^i - 1\right\},\ i = 1, 2, \ldots, n, \tag{4}$$

where $u_i(t_l^i)$ is dependent on the information received at time t_l^i; namely,

$$u_i\left(t_l^i\right) = \varepsilon \sum_{j\in N_i(t_l^i)} a_{ij}\left(t_l^i\right)\left(x_j\left(t_l^i\right) - x_i\left(t_l^i\right)\right), \tag{5}$$

where $\varepsilon > 0$.

Remark 3. If (3) is satisfied at all times, then the consensus under consideration becomes the usual consensus of discrete time multiagent systems.

Remark 4. In the following analysis, we use another topology graph $\widehat{\mathcal{G}}(k)$, which is different from the actual topology graph $\mathcal{G}(k)$. $\widehat{\mathcal{G}}(k)$ is defined as follows: $\widehat{\mathcal{G}}(k)$ has the same vertex set as $\mathcal{G}(k)$; if $(v_j, v_i) \in \mathcal{E}(\mathcal{G}(t_l^i))$, then, for any $k \in \{t_l^i, t_l^i + 1, \ldots, t_{l+1}^i - 1\}$, $(v_j, v_i) \in \mathcal{E}(\widehat{\mathcal{G}}(k))$, or else, for any $k \in \{t_l^i, t_l^i + 1, \ldots, t_{l+1}^i - 1\}$, $(v_j, v_i) \notin \mathcal{E}(\widehat{\mathcal{G}}(k))$. For facilitating the following analysis, we assume that $\{\widehat{\mathcal{G}}(0), \widehat{\mathcal{G}}(1), \ldots\}$ is a finite set.

3. Main Results

Obviously, $\sum_{j\in N_i(t_l^i)} a_{ij}(t_l^i)(x_j(t_l^i) - x_i(t_l^i)) = e_i(k) + \sum_{j\in N_i(k)} a_{ij}(k)(x_j(k) - x_i(k))$; then the multiagent system (2) under event-triggering condition (3) and controller (4) can be written as

$$X(k+1) = \left(I - \varepsilon\widehat{L}_k\right)X(k) + \varepsilon e(k), \tag{6}$$

where $X(k) = (x_1(k), x_2(k), \ldots, x_n(k))^T$, $e(k) = (e_1(k), e_2(k), \ldots, e_n(k))^T$ and $\widehat{L}_k$ denotes the Laplacian matrix of $\widehat{\mathcal{G}}(k)$.

Assume $\widehat{\mathcal{G}}(k)$ has a spanning tree for any $k = 0, 1, \ldots$; then there exists an orthogonal matrix $U = [(1/\sqrt{n})\mathbf{1}_n, U_1] \in \mathcal{R}^{n\times n}$ such that

$$U^T\widehat{L}_k U = \begin{bmatrix} 0 & \widehat{h}_k \\ 0 & \widehat{H}_k \end{bmatrix}. \tag{7}$$

Let $\theta(k) = U^T X(k)$, where $\theta(k) = [\delta_1(k), \delta(k)^T]^T, \delta(k) \in \mathcal{R}^{n-1}$; then

$$\delta_1(k+1) = \delta_1(k) + \widehat{h}_k\delta(k) + \varepsilon\frac{1}{\sqrt{n}}\mathbf{1}_n^T e(k), \tag{8}$$

$$\delta(k+1) = \left(I_{n-1} - \varepsilon\widehat{H}_k\right)\delta(k) + \varepsilon U_1^T e(k). \tag{9}$$

By Remark 4, both $\{\widehat{H}_0, \widehat{H}_1, \ldots\}$ and $\{\widehat{L}_0, \widehat{L}_1, \ldots\}$ are finite sets; let

$$\begin{aligned} \left\{\widehat{L}_0, \widehat{L}_1, \ldots\right\} &= \left\{\overline{L}_1, \overline{L}_2, \ldots, \overline{L}_N\right\}, \\ \left\{\widehat{H}_0, \widehat{H}_1, \ldots\right\} &= \left\{\overline{H}_1, \overline{H}_2, \ldots, \overline{H}_N\right\}. \end{aligned} \tag{10}$$

By the result in [30], we obtain the following lemma.

Lemma 5. *Multiagent system* (2) *under event-triggering condition* (3) *and controller* (4) *solves a consensus problem asymptotically if system* (9) *is asymptotically stable.*

Hence, we can obtain the following main result by analyzing the stability of system (9). Because the topology graph is time-varying, we apply the common Lyapunov function to analyze the stability of system (9).

Theorem 6. *Assume $\widehat{\mathcal{G}}(k)$ has a spanning tree at all times. Multiagent system* (2) *under event-triggering condition* (3) *and controller* (4) *solves a consensus problem asymptotically if there exists $P > 0$ such that the following linear matrix inequalities are satisfied:*

$$\begin{pmatrix} \left(I_{n-1} - \varepsilon\overline{H}_i\right)^T P\left(I_{n-1} - \varepsilon\overline{H}_i\right) - P + \sigma^2 U_1^T\overline{L}_i^T\overline{L}_i U_1 & \varepsilon\left(I_{n-1} - \varepsilon\overline{H}_i\right)^T P U_1^T \\ * & \varepsilon^2 U_1 P U_1^T - I_{n-1} \end{pmatrix} < 0, \quad i = 1, 2, \ldots, N, \tag{11}$$

where $\sigma = \max\{\sigma_1, \ldots, \sigma_n\}$.

Proof. Let $V(k) = \delta(k)^T P\delta(k)$, where $P > 0$; then, by (9), we obtain

$$\begin{aligned} \Delta V(k) &= V(k+1) - V(k) \\ &= \delta(k)^T\left[\left(I_{n-1} - \varepsilon\widehat{H}_k\right)^T P\left(I_{n-1} - \varepsilon\widehat{H}_k\right) - P\right]\delta(k) \\ &\quad + \varepsilon^2 e(k)^T U_1 P U_1^T e(k) \\ &\quad + 2\varepsilon e(k)^T U_1 P\left(I_{n-1} - \varepsilon\widehat{H}_k\right)\delta(k). \end{aligned} \tag{12}$$

By event-triggering condition (3),

$$\begin{aligned} e(k)^T e(k) &\le X(k)^T\widehat{L}_k^T \operatorname{diag}\left\{\sigma_1^2, \ldots, \sigma_n^2\right\}\widehat{L}_k X(k) \\ &\le \sigma^2 X(k)^T\widehat{L}_k^T\widehat{L}_k X(k) \\ &= \sigma^2 X(k)^T U\left(U^T\widehat{L}_k^T\widehat{L}_k U\right)U^T X(k) \\ &= \sigma^2\delta(k)^T U_1^T\widehat{L}_k^T\widehat{L}_k U_1\delta(k). \end{aligned} \tag{13}$$

Thus,

$$\begin{aligned}\Delta V(k) \le{}& \delta(k)^T\left[\left(I_{n-1}-\varepsilon\widehat{H}_k\right)^T P\left(I_{n-1}-\varepsilon\widehat{H}_k\right)-P\right]\delta(k)\\&+\varepsilon^2 e(k)^T U_1 P U_1^T e(k)\\&+2\varepsilon e(k)^T U_1 P\left(I_{n-1}-\varepsilon\widehat{H}_k\right)\delta(k)\\&+\sigma^2\delta(k)^T U_1^T\widehat{L}_k^T\widehat{L}_k U_1\delta(k)-e(k)^T e(k)\\={}&\left(\delta(k)^T, e(k)^T\right)\Phi_k\left(\delta(k)^T, e(k)^T\right)^T,\end{aligned}\tag{14}$$

where

$$\Phi_k=\begin{pmatrix}\left(I_{n-1}-\varepsilon\widehat{H}_k\right)^T P\left(I_{n-1}-\varepsilon\widehat{H}_k\right)-P+\sigma^2U_1^T\widehat{L}_k^T\widehat{L}_k U_1 & \varepsilon\left(I_{n-1}-\varepsilon\widehat{H}_k\right)^T PU_1^T\\ * & \varepsilon^2U_1PU_1^T-I_{n-1}\end{pmatrix}.\tag{15}$$

By (11), $\Phi_k < 0, k = 0,1,2,\ldots$; that is, system (9) is asymptotically stable. Hence, multiagent system (2) under event-triggering condition (3) and controller (4) solves a consensus problem asymptotically. □

Remark 7. The feasibility of LMI (11) is explained as follows:

$$\begin{aligned}\begin{pmatrix}\left(I_{n-1}-\varepsilon H_i\right)^T P\left(I_{n-1}-\varepsilon H_i\right)-P+\sigma^2U_1^TL_i^TL_iU_1 & \varepsilon\left(I_{n-1}-\varepsilon H_i\right)^T PU_1^T\\ * & \varepsilon^2U_1PU_1^T-I_{n-1}\end{pmatrix}&=\begin{pmatrix}-\varepsilon\left(H_i^TP+PH_i\right)+\sigma^2U_1^TL_i^TL_iU_1 & \varepsilon PU_1^T\\ * & -I_{n-1}\end{pmatrix}\\&\quad+O\left(\varepsilon^2\right),\end{aligned}\tag{16}$$

where $O(\varepsilon^2)$ denotes a matrix, each element of which is the same order infinitesimal of ε^2. By Schur complement,

$$\begin{pmatrix}-\varepsilon\left(H_i^TP+PH_i\right)+\sigma^2U_1^TL_i^TL_iU_1 & \varepsilon PU_1^T\\ * & -I_{n-1}\end{pmatrix}<0\tag{17}$$

if and only if

$$\begin{aligned}-\varepsilon\left(H_i^TP+PH_i\right)+\sigma^2U_1^TL_i^TL_iU_1<0,\\-\varepsilon\left(H_i^TP+PH_i\right)+\sigma^2U_1^TL_i^TL_iU_1+\varepsilon^2PU_1^TU_1P<0.\end{aligned}\tag{18}$$

Hence, if there exists $P > 0$ such that $H_i^TP + PH_i > 0$, $i = 1,2,\ldots,N$, then (11) must be feasible in the case that ε and σ are small.

4. Simulations

Consider four agents and their interaction topology is time-varying. For convenience, assume that the topology is $\mathcal{G}_1$ and $\mathcal{G}_2$ at odd and even times, respectively. The Laplacian matrices of L_1 and L_2 are

$$\begin{aligned}L_1&=\begin{pmatrix}1&0&0&-1\\-1&1&0&0\\-1&-1&2&0\\0&0&-1&1\end{pmatrix},\\L_2&=\begin{pmatrix}1&0&0&-1\\-1&1&0&0\\0&0&0&0\\0&0&-1&1\end{pmatrix}.\end{aligned}\tag{19}$$

By the LMI Toolbox in Matlab, (11) is feasible for $\varepsilon = 0.1$ and $\sigma = 0.1$. Hence, by Theorem 6, consensus can be reached asymptotically for controller (4) with $\varepsilon = 0.1$ and event-triggering condition (3) with $\max\{\sigma_i\} < 0.1$. The state trajectories of four agents in the case of $\varepsilon = 0.1, \sigma_1 = 0.01, \sigma_2 = 0.02, \sigma_3 = 0.03$, and $\sigma_4 = 0.05$ are shown in Figure 1, which validate the result of Theorem 6.

5. Conclusion

This paper has studied the consensus problem of first-order discrete-time multiagent systems with time-varying topology. Based on the designed event-triggering condition, each agent updates its control input only at event times. By

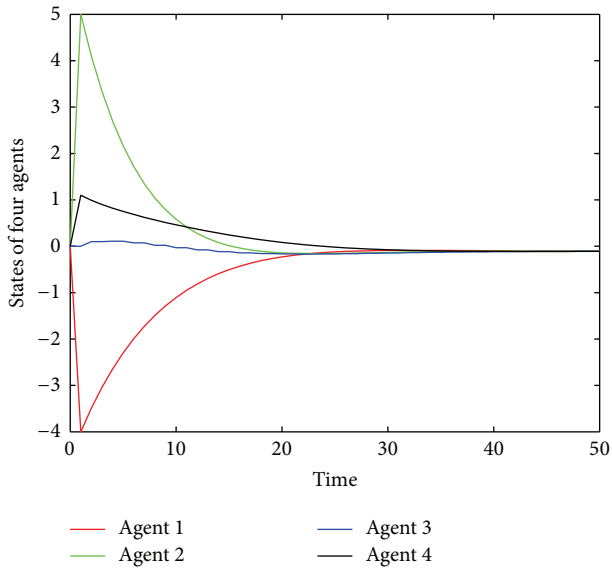

Figure 1: State trajectories of four agents.

applying a state transformation, consensus is transformed into the asymptotical stability of a time-varying system. In virtue of the common Lyapunov function method, we obtain that if the event-triggering conditions and controllers satisfy some linear matrix inequalities, then consensus can be reached asymptotically, and we further analyze the feasibility of these linear matrix inequalities. Our future work will focus on time delays and another time-varying tropology, namely, the jointly connected case.

Conflict of Interests

The authors declare that there is no conflict of interests regarding the publication of this paper.

Acknowledgments

This work was supported by National Natural Science Foundation (61203150, 61170113, and 61104141) and Beijing Natural Science Foundation (4122019).

References

[1] W. Ren, R. W. Beard, and E. M. Atkins, "Information consensus in multivehicle cooperative control," *IEEE Control Systems Magazine*, vol. 27, no. 2, pp. 71–82, 2007.

[2] H. Su, X. Wang, and Z. Lin, "Flocking of multi-agents with a virtual leader," *IEEE Transactions on Automatic Control*, vol. 54, no. 2, pp. 293–307, 2009.

[3] H. Su, N. Zhang, M. Z. Q. Chen, and X. Wang, "Adaptive flocking with a virtual leader of multiple agents governed by locally Lipschitz nonlinearity," *Nonlinear Analysis: Real World Applications*, vol. 14, no. 1, pp. 798–806, 2013.

[4] Y. Zheng and L. Wang, "Consensus of heterogeneous multi-agent systems without velocity measurements," *International Journal of Control*, vol. 85, no. 7, pp. 906–914, 2012.

[5] J. H. Seo, J. Back, H. Kim, and H. Shim, "Output feedback consensus for high-order linear systems having uniform ranks under switching topology," *IET Control Theory & Applications*, vol. 6, no. 8, pp. 1118–1124, 2012.

[6] H. Su, M. Z. Q. Chen, X. Wang, and J. Lam, "Semiglobal observer-based leader-following consensus with input saturation," *IEEE Transactions on Industrial Electronics*, vol. 61, no. 6, pp. 2842–2850, 2014.

[7] H. Su, M. Z. Q. Chen, J. Lam, and Z. Lin, "Semi-global leader-following consensus of linear multi-agent systems with input saturation via low gain feedback," *IEEE Transactions on Circuits and Systems I: Regular Papers*, vol. 60, no. 7, pp. 1881–1889, 2013.

[8] P. Lin, K. Qin, H. Zhao, and M. Sun, "A new approach to average consensus problems with multiple time-delays and jointly-connected topologies," *Journal of the Franklin Institute*, vol. 349, no. 1, pp. 293–304, 2012.

[9] W. Ren and R. W. Beard, "Consensus seeking in multiagent systems under dynamically changing interaction topologies," *IEEE Transactions on Automatic Control*, vol. 50, no. 5, pp. 655–661, 2005.

[10] N. Abaid and M. Porfiri, "Leader—follower consensus over numerosity-constrained random networks," *Automatica*, vol. 48, no. 8, pp. 1845–1851, 2012.

[11] Y. Zheng and L. Wang, "Finite-time consensus of heterogeneous multi-agent systems with and without velocity measurements," *Systems and Control Letters*, vol. 61, no. 8, pp. 871–878, 2012.

[12] G. Xie, H. Liu, L. Wang, and Y. Jia, "Consensus in networked multi-agent systems via sampled control: fixed topology case," in *Proceedings of the American Control Conference (ACC '09)*, pp. 3902–3907, St. Louis, Mo, USA, June 2009.

[13] S. Wang and D. Xie, "Consensus of second-order multi-agent systems via sampled control: undirected fixed topology case," *IET Control Theory & Applications*, vol. 6, no. 7, pp. 893–899, 2012.

[14] Y. Gao and L. Wang, "Sampled-data based consensus of continuous-time multi-agent systems with time-varying topology," *IEEE Transactions on Automatic Control*, vol. 56, no. 5, pp. 1226–1231, 2011.

[15] F. Xiao and T. Chen, "Sampled-data consensus for multiple double integrators with arbitrary sampling," *IEEE Transactions on Automatic Control*, vol. 57, no. 12, pp. 3230–3235, 2012.

[16] Q. Liu, Z. Wang, X. He, and D. Zhou, "A survey of event-based strategies on control and estimation," *Systems Science & Control Engineering*, vol. 2, pp. 90–97, 2014.

[17] Z. Liu and Z. Chen, "Reaching consensus in networks of agents via event-triggered control," *Journal of Information and Computational Science*, vol. 8, no. 3, pp. 393–402, 2011.

[18] D. V. Dimarogonas, E. Frazzoli, and K. H. Johansson, "Distributed event-triggered control for multi-agent systems," *IEEE Transactions on Automatic Control*, vol. 57, no. 5, pp. 1291–1297, 2012.

[19] Y. Fan, G. Feng, Y. Wang, and C. Song, "Distributed event-triggered control of multi-agent systems with combinational measurements," *Automatica*, vol. 49, no. 2, pp. 671–675, 2013.

[20] G. S. Seyboth, D. V. Dimarogonas, and K. H. Johansson, "Event-based broadcasting for multi-agent average consensus," *Automatica*, vol. 49, no. 1, pp. 245–252, 2013.

[21] X. Meng and T. Chen, "Event based agreement protocols for multi-agent networks," *Automatica*, vol. 49, no. 7, pp. 2125–2132, 2013.

[22] C. Ji, W. Zhou, and H. Liu, "Event-based control for average consensus of wireless sensor networks with stochastic communication noises," *Discrete Dynamics in Nature and Society*, vol. 2013, Article ID 610169, 8 pages, 2013.

[23] D. Xue and S. Hirche, "Event-triggered consensus of heterogeneous multi-agent systems with double-integrator dynamics," in *Proceedings of the 12th European Control Conference (ECC '13)*, pp. 1162–1167, July 2013.

[24] H. Yan, Y. Shen, H. Zhang, and H. Shi, "Decentralized event-triggered consensus control for second-order multi-agent systems," *Neurocomputing*, vol. 133, pp. 18–24, 2014.

[25] J. Hu, G. Chen, and H. Li, "Distributed event-triggered tracking control of leader-follower multi-agent systems with communication delays," *Kybernetika*, vol. 47, no. 4, pp. 630–643, 2011.

[26] X. Chen and F. Hao, "Event-triggered average consensus control for discrete-time multi-agent systems," *IET Control Theory and Applications*, vol. 6, no. 16, pp. 2493–2498, 2012.

[27] X. Yin and D. Yue, "Event-triggered tracking control for heterogeneous multi-agent systems with Markov communication delays," *Journal of the Franklin Institute. Engineering and Applied Mathematics*, vol. 350, no. 5, pp. 1312–1334, 2013.

[28] X. Yin, D. Yue, and S. Hu, "Distributed event-triggered control of discrete-time heterogeneous multi-agent systems," *Journal of the Franklin Institute*, vol. 350, no. 3, pp. 651–669, 2013.

[29] C. Godsil and G. Royle, *Algebraic Graph Theory*, Springer, New York, NY, USA, 2001.

[30] Y. Gao, B. Liu, J. Yu, J. Ma, and T. Jiang, "Consensus of first-order multi-agent systems with intermittent interaction," *Neurocomputing*, vol. 129, pp. 273–278, 2014.

Hindawi Publishing Corporation
Mathematical Problems in Engineering
Volume 2014, Article ID 248684, 7 pages
http://dx.doi.org/10.1155/2014/248684

Research Article

Consensus Analysis for a Class of Heterogeneous Multiagent Systems with Time Delay Based on Frequency Domain Method

Yi-Jie Sun, Guo-liang Zhang, and Jing Zeng

High-Tech Institute of Xi'an, Xi'an, Shanxi 710025, China

Correspondence should be addressed to Yi-Jie Sun; syjlxh@126.com

Received 4 May 2014; Accepted 17 August 2014; Published 28 September 2014

Academic Editor: Housheng Su

The consensus problem of heterogeneous multiagent systems composed of first-order and second-order agent is investigated. A linear consensus protocol is proposed. Based on frequency domain method, the sufficient conditions of achieving consensus are obtained. If communication topology contains spanning tree and some conditions can be satisfied on control gains, consensus can be achieved. Then, a linear consensus protocol with time delay is proposed. In this case, consensus is dependent only on system coupling strength, each agent input time delay, but independent of communication delay. Finally, numerical simulations are provided to illustrate the effectiveness of the theoretical result.

1. Introduction

Recently, multiagent systems have received significant attention due to their potential impact on numerous civilians, homeland securities, and military applications. Consensus plays an important role in achieving distributed coordination. The basic idea of consensus is that a team of agents reach an agreement on a common value by negotiating with their neighbors. Many literatures have investigated consensus problem on many cases, such as time variant topology, time delay, and nonlinearity [1–10].

Unfortunately, all the aforementioned multiagent systems are homogeneous; that is, all the agents share the same dynamics behavior. However, the dynamics of the agents are quite different because of various restrictions in the practical systems. Zheng et al. [11] studied the consensus problem of heterogeneous multiagent systems composed of first-order and second-order integrator agents. Zhu et al. [12] studied consensus problem of multiagent systems with two types of agents, namely, active agents and passive agents. Yin et al. [13] investigated the consensus problem for a set of discrete-time heterogeneous multiagent systems composed of two kinds of agents differed by their dynamics. Zhu et al. [14] investigated the finite-time consensus problem for heterogeneous multiagent systems composed of first-order and second-order agents. Zheng and Wang [15] studied finite-time consensus of heterogeneous multiagent systems with and without velocity measurements. C. Liu and F. Liu [16] considered stationary consensus of heterogeneous multiagent systems with bounded communication delays. Yan et al. [17] are concerned with the cooperative target pursuit problem by multiple agents based on directed acyclic graph. Kim et al. [18] studied the output consensus problem for a class of heterogeneous uncertain linear multiagent systems. Yin et al. [19] studied the consensus protocols design for a set of fractional-order heterogeneous agents, which is composed of two kinds of agents. Kim et al. [20] investigated the heterogeneous consensus problem for multiagent systems with random link failures between agents.

Consensus of heterogeneous multiagent systems is investigated in undirected graph generally. An important challenge is to study this problem in directed graph. However, this seems to be less studied in the literature. Meanwhile, frequency domain approach is an important method for analyzing stability of control system. In the existing literatures, there are so few literatures that use frequency domain method. Time delay appears in almost all practical systems, and times delay can degrade the systems performance or even destroy the system stability.

In this paper, we study consensus problem of heterogeneous multiagent systems with and without time delay. The model and algorithms in this paper are similar to [11], but in [11] they only consider the case in undirected graph mainly based on Lyapunov theory. Unlike [11], in this paper consider the cases with and without time delay in directed graph. Based on the frequency domain method, the sufficient conditions are given for the existence of consensus solution to heterogeneous multiagent systems. By these conditions, it is shown that consensus can be achieved when control gains satisfy some conditions in the case without time delay. In the case with time delay, the results show that the consensus is dependent only on system coupling strength, each agent input time delay, but independent of communication delay.

The rest of the paper is organized as follows. In Section 2, some preliminaries are introduced for the graph theory, and heterogeneous multiagent systems are formulated. Two consensus protocols are proposed in Section 3, and consensus analysis is shown for without delay time and with delay time, respectively. In Section 4, two numerical examples are studied. Finally, concluding remarks are given in Section 5.

2. Preliminaries

2.1. Graph Theory. Let $\mathcal{G}(\mathcal{V}, \mathcal{E}, \mathcal{A})$ be a weighted directed graph composed of a set of nodes $\mathcal{V} = \{v_1, v_2, \ldots, v_n\}$, set of edges $\mathcal{E} \subset \mathcal{V} \times \mathcal{V}$, and a weighted adjacency matrix $A = [a_{ij}]_{n\times n}$, with nonnegative adjacency elements a_{ij}. An edge of $\mathcal{G}$ is denoted by $e_{ij} = (v_i, v_j) \in \mathcal{E}$, which means that node v_i receives information from node v_j and v_j is called the parent of v_i. The adjacency elements associated with the edges of the graph are positive; that is, $e_{ij} \in \mathcal{E} \Leftrightarrow a_{ij} > 0$. Moreover, we assume $a_{ii} = 0$ for all $i \in 1, \ldots, n$. The set of neighbors of node v_i is denoted by $N_i = \{v_j \in \mathcal{V} : (v_i, v_j) \in \mathcal{E}\}$. The corresponding graph Laplacian $L = [l_{ij}]_{n\times n}$ can be defined as

$$l_{ij} = \begin{cases} -a_{ij}, & j \neq i, \\ \sum_{j\in N_i} a_{ij}, & j = i. \end{cases} \tag{1}$$

If $a_{ij} = a_{ji}$, then $\mathcal{G}$ becomes the undirected graph. If there is not isolated node in an undirected graph, the graph is said to be connected.

Graph with a Spanning Tree. For a directed graph, if every node, except a node called root, has exactly one parent, then it is called a directed tree. A spanning tree of a directed graph is a directed tree formed by graph edges that connect all the nodes of the graph.

In heterogeneous multiagent system, the neighbors of each second-order agent i include first-order and second-order agents, denoted by $N_i = N_i^s \cup N_i^f$, and the neighbors of each first-order agent are denoted by $N_l = N_l^s \cup N_l^f$. The Laplacian matrix can be denoted as follows:

$$L = \begin{bmatrix} \overline{L}_s & -A_{sf} \\ -A_{fs} & \overline{L}_f \end{bmatrix}, \tag{2}$$

where $\overline{L}_s = D_{sf} + L_s$, L_s is the Laplacian matrix of second-order agents, $D_{sf} = \mathrm{diag}(\sum_{j\in N_i^f} a_{ij}, i = 1, \ldots, m)$, and A_{sf} denotes the adjacency relations of second-order agent to first-order agent. Meanwhile, L_f is the Laplacian matrix of first-order agent, $D_{fs} = \mathrm{diag}(\sum_{j\in N_l^s} a_{lj}, l = m+1, \ldots, n)$, and A_{fs} denotes the adjacency relations of first-order agents to second-order agents.

2.2. The Heterogeneous Multiagent System. Suppose that the heterogeneous multiagent system consists of first-order and second-order integrator agents. The number of agents is n, labeled from 1 through n. Firstly, the heterogeneous multiagent system and concept of consensus are established. Suppose that the number of second-order integrator agents is m ($m < n$). The remainder is the first-order integrator agents; the number is $n - m$. Then, the system is given as follows:

$$\begin{aligned} \dot{x}_i &= v_i, \\ \dot{v}_i &= u_i, \quad i = 1, \ldots, m, \\ \dot{x}_l &= u_l, \quad l = m+1, \ldots, n, \end{aligned} \tag{3}$$

where x_i, v_i, u_i are the position, velocity, and control input, of second-order agent i, respectively. x_l, u_l are the position and control input of first-order agent l, respectively. The initial conditions are $\mathbf{x}(0) = [x_1(0), x_2(0), \ldots, x_n(0)]^T$ and $\mathbf{v}(0) = [v_1(0), v_2(0), \ldots, v_m(0)]^T$.

Definition 1. The heterogeneous multiagent system (3) is said to reach consensus asymptotically if, for any initial conditions $\mathbf{x}(0)$ and $\mathbf{v}(0)$, one has $\lim_{t\to\infty}\|x_j(t) - x_i(t)\| = 0$, $i, j = 1, \ldots, n$, $\lim_{t\to\infty}\|v_j(t) - v_i(t)\| = 0$, $i, j = 1, \ldots, m$.

Lemma 2 (see [5]). *Suppose that $\mathbf{z} = [z_1, z_2, \ldots, z_p]^T$ with $z_i \in R$ and $L \in R^{p\times p}$ is the Laplacian matrix. Then, the following four conditions are equivalent: (i) L has a simple zero eigenvalue with an associated eigenvector $\mathbf{1}_p$ and all of the other eigenvalues have positive real parts; (ii) $Lz = 0$ implies that $z_1 = z_2 \cdots = z_p$; (iii) consensus is reached asymptotically for a system $z = -Lz$; (iv) the directed graph of L has a directed spanning tree.*

Remark 3. Throughout the paper, we just take the positions and velocities of agents as scalars. However, all the following developments can be directly extended to the case of vectors by introducing the Kronecker product.

3. Main Results

3.1. Consensus Protocol without Time Delay. In this section, the protocol without time delay is proposed for system (3), as follows:

$$\begin{aligned} u_i &= \sum_{j\in N_i} a_{ij}\left(x_j - x_i\right) - k_1 v_i, \quad i = 1, \ldots, m, \\ u_l &= k_2 \sum_{j\in N_l} a_{ij}\left(x_j - x_l\right), \quad l = m+1, \ldots, n, \end{aligned} \tag{4}$$

where $k_1, k_2 > 0$ are control gains.

Theorem 4. *If the following conditions can hold, then consensus of system* (3) *with protocol* (4) *can be achieved.*

(i) The fixed topology contains spanning tree. (ii) The control gains satisfy conditions

$$k_1 \geq \sqrt{2\max\{d_i, i = 1, \ldots, m\}}, \qquad k_2 > 0. \tag{5}$$

Proof. The system (3) under protocol (4) can be written in a vector form as

$$\dot{z}(t) = \Lambda z(t), \tag{6}$$

where

$$\Lambda = \begin{bmatrix} 0 & I_m & 0 \\ -\left(L_s + D_{sf}\right) & -k_1 I_m & A_{sf} \\ k_2 A_{fs} & 0 & -k_2\left(L_f + D_{fs}\right) \end{bmatrix}, \tag{7}$$

where $\mathbf{z}(t) = [x_1(t), \ldots, x_m(t), v_1(t), \ldots, v_m(t), x_{m+1}(t), \ldots, x_n(t)]^{\mathrm{T}}$.

The Laplace transformation is imposed on system (6) and we have

$$\begin{aligned} s^2 x_s(s) &= -\left(L_s + D_{sf}\right) x_s(s) - k_1 s x_s(s) + A_{sf} x_f(s), \\ s x_f(s) &= -k_2\left(L_f + D_{fs}\right) x_f(s) + k_2 A_{fs} x_s(s). \end{aligned} \tag{8}$$

From (8), the following form is obtained:

$$\begin{aligned} s x_s(s) &= \frac{-\left(L_s + D_{sf}\right) x_s(s) - s^2 x_s(s) + A_{sf} x_f(s)}{k_1}, \\ s x_f(s) &= -\left(L_f + D_{fs}\right) x_f(s) + A_{fs} x_s(s). \end{aligned} \tag{9}$$

Let $x_s = [x_1, \ldots, x_m]^{\mathrm{T}}$, $x_f = [x_{m+1}, \ldots, x_n]^{\mathrm{T}}$, and $y = [x_s^{\mathrm{T}}, x_f^{\mathrm{T}}]^{\mathrm{T}}$; we have

$$\begin{aligned} s y(s) &= \Gamma(s)\, y(s), \\ \Gamma(s) &= \begin{bmatrix} \dfrac{-\left(L_s + D_{sf}\right) - s^2 I}{k_1} & \dfrac{A_{sf}}{k_1} \\ k_2 A_{fs} & -k_2\left(L_f + D_{fs}\right) \end{bmatrix}. \end{aligned} \tag{10}$$

Let $F(s) = \det(sI - \Gamma(s))$. It is the fact that the zero point of $F(s)$ is the eigenvalue of Λ. Consider the following.

(1) When $s = 0$, $F(0) = \det(\Gamma(0)) = (1/k_1)^m (k_2)^{n-m} \det(L)$. Zero is a simple eigenvalue of L owing to the topology that contains spanning tree based on Lemma 2. Then, $F(0) = 0$ and the zero point is $s = 0$.

(2) When $s \neq 0$, let $P(s) = \det(I + G(s))$, $G(s) = -\Gamma(s)/s$. Based on the generalized Nyquist criterion, if the point $(-1, 0j)$ is not encircled by Nyquist curve of $G(s)$, then zero points of $P(s)$ are all with negative real part.

Let $s = j\omega$, according to Gershgorin disk theorem, the eigenvalues $\lambda(G(j\omega))$ of matrix $G(j\omega)$ are all in below circles. One can see that

$$\begin{aligned} &\lambda\left(G\left(j\omega\right)\right) \in \{G_i, i = 1, \ldots, m\} \bigcup \{G_l, l = m+1, \ldots, n\}, \\ &G_i = \left\{\xi : \xi \in C \mid \left|\xi - \frac{\sum_{j\in N_i} a_{ij}}{j\omega k_1} - \frac{j\omega}{k_1}\right| \leq \sum_{j\in N_i}\left|\frac{a_{ij}}{j\omega k_1}\right|\right\}, \\ &\qquad i = 1, \ldots, m, \\ &G_l = \left\{\xi : \xi \in C \mid \left|\xi - \frac{k_2 \sum_{j\in N_i} a_{ij}}{j\omega}\right| \leq \sum_{j\in N_i}\left|\frac{k_2 a_{ij}}{j\omega}\right|\right\}, \\ &\qquad l = m+1, \ldots, n, \end{aligned} \tag{11}$$

where G_i, $i = 1, \ldots, m$, are considered firstly. Let $d_i = \sum_{j\in N_i} a_{ij}$,and the center of circle G_i is $G_{i0}(j\omega) = ((\omega/k_1) - (d_i/\omega k_1))j$.

If the point $(-a, 0j)$, $a \geq 1$, is not in G_i, then

$$\left|-a - \frac{d_i}{j\omega k_1} - \frac{j\omega}{k_1}\right| \geq \sum_{j\in N_i}\left|\frac{a_{ij}}{j\omega k_1}\right|. \tag{12}$$

Then, we have

$$2d_i - \omega^2 \leq k_1^2. \tag{13}$$

It is easy to see that if $k_1 \geq \sqrt{2\max\{d_i, i = 1, \ldots, m\}}$, then (20) can be established.

Therefore, $k_1 \geq \sqrt{2\max\{d_i, i = 1, \ldots, m\}}$, and the point $(-1, 0j)$ is not encircled by G_i, $i = 1, \ldots, m$.

Next, G_l, $l = m+1, \ldots, n$, will be considered. If the point $(-a, 0j)$, $a \geq 1$, is not in G_l, then

$$\left|-a - \frac{k_2 d_l}{j\omega}\right| \geq \sum_{j\in N_l}\left|\frac{k_2 a_{ij}}{j\omega}\right|. \tag{14}$$

It is easy to verify that if $k_2 > 0$, (14) can be established.

From the above analysis, we can get that matrix Λ only has a simple eigenvalue and all nonzero eigenvalues with negative real part. Then, system (6) can converge a stable state, $\lim_{t\to\infty} \mathbf{z}(t) = \mathbf{z}^*(t)$, and $\Lambda \mathbf{z}^*(t) = 0$, where $\mathbf{z}^*(t) = [x_1^*(t), \ldots, x_m^*(t), v_1^*(t), \ldots, v_m^*(t), x_{m+1}^*(t), \ldots, x_n^*(t)]^{\mathrm{T}}$. It is easy to verify that the vector $c[\mathbf{1}_m^{\mathrm{T}}, \mathbf{0}_m^{\mathrm{T}}, \mathbf{1}_{n-m}^{\mathrm{T}}]^{\mathrm{T}}$ is eigenvector of matrix Λ associated with eigenvalue 0. So, the solution of $\Lambda \mathbf{y}^*(t) = 0$ is $c[\mathbf{1}_m^{\mathrm{T}}, \mathbf{0}_m^{\mathrm{T}}, \mathbf{1}_{n-m}^{\mathrm{T}}]^{\mathrm{T}}$, where c is a constant. We can get that $\lim_{t\to\infty} x_i(t) = c$, $i = 1, \ldots, n$, $\lim_{t\to\infty} v_i(t) = 0$, $i = 1, \ldots, m$. Based on Definition 1, the system achieves the consensus. It can be observed from Theorem 4 that the control gains k_1, k_2 play important roles in achieving consensus. □

3.2. Consensus Protocol with Time Delay. In this section, the case with time delay is considered. A consensus protocol with time delay is proposed for system (3). The different

communication time delay and identical input time delay among agents are considered in following protocol:

$$u_i = \sum_{j\in N_i} a_{ij}\left(x_j\left(t-\tau_{ij}\right)-x_i\left(t-\tau\right)\right)-k_1 v_i\left(t-\tau\right), \quad i=1,\ldots,m,$$
$$u_l = k_2\sum_{j\in N_l} a_{ij}\left(x_j\left(t-\tau_{ij}\right)-x_l\left(t-\tau\right)\right), \quad l=m+1,\ldots,n, \tag{15}$$

where $k_1, k_2 > 0$ are control gains, τ_{ij} is communication time delay, and τ is input time delay.

Theorem 5. *If the following conditions can be hold, then consensus of system* (3) *with protocol* (15) *can be achieved.*

(i) The fixed topology contains spanning tree. (ii) The following conditions can be established: $k_1 \geq \sqrt{2\max\{d_i, i=1,\ldots,m\}}$, $k_2 > 0$, *and* $\tau \leq \min\{1/2k_1, 1/2k_2\max\{d_l, l=m+1,\ldots,n\}\}$.

Proof. The Laplace transformation is imposed on system (3) with protocol (15), and we have

$$sx_i(s) = v_i(s),$$
$$sv_i(s) = \sum_{j\in N_i} a_{ij}\left(e^{-\tau_{ij}s}x_j(s)-e^{-\tau s}x_i(s)\right)-k_1 e^{-\tau s}v_i(s), \quad i=1,\ldots,m,$$
$$sx_l(s) = \sum_{j\in N_l} a_{ij}\left(e^{-\tau_{ij}s}x_j(s)-e^{-\tau s}x_l(s)\right), \quad l=m+1,\ldots,n. \tag{16}$$

Let $\widetilde{L} = [\widetilde{l}_{ij}]_{n\times n}$

$$\widetilde{l}_{ij} = \begin{cases} e^{-\tau_{ijs}}a_{ij}, & i\neq j, \\ \sum_{j\in N_i} a_{ij}e^{-\tau s}, & i=j. \end{cases} \tag{17}$$

We have

$$s^2 x_s(s) = -\left(\widetilde{L}_s+\widetilde{D}_{sf}\right)x_s(s)-k_1 e^{-\tau s}sx_s(s)+\widetilde{A}_{sf}x_f(s),$$
$$sx_f(s) = -k_2\left(\widetilde{L}_f+\widetilde{D}_{fs}\right)x_f(s)+k_2\widetilde{A}_{fs}x_s(s). \tag{18}$$

Let $x_s = [x_1,\ldots,x_m]^{\mathrm{T}}$, $x_f = [x_{m+1},\ldots,x_n]^{\mathrm{T}}$, and $y = [x_s^{\mathrm{T}}, x_f^{\mathrm{T}}]^{\mathrm{T}}$; we have

$$sy(s) = \widetilde{\Gamma}y(s),$$
$$\widetilde{\Gamma}(s) = \begin{bmatrix} \dfrac{-\left(\widetilde{L}_s+\widetilde{D}_{sf}\right)-s^2 I}{k_1 e^{-\tau s}} & \dfrac{\widetilde{A}_{sf}}{k_1 e^{-\tau s}} \\ k_2\widetilde{A}_{fs} & -k_2\left(\widetilde{L}_f+\widetilde{D}_{fs}\right) \end{bmatrix}. \tag{19}$$

Let $\widetilde{F}(s) = \det(sI-\widetilde{\Gamma}(s))$. Next, the zero point of $F(s)$ will be analyzed. Consider the following.

(1) When $s=0$, $\widetilde{F}(0) = \det(\widetilde{\Gamma}(0)) = (1/k_1)^m(k_2)^{n-m}\det(L)$. Zero is a simple eigenvalue of L owing to the topology that contains spanning tree based on Lemma 2. Then, $F(0)=0$ and the zero point is $s=0$.

(2) When $s\neq 0$, let $\widetilde{P}(s) = \det(I+\widetilde{G}(s))$, $\widetilde{G}(s) = -\widetilde{\Gamma}(s)/s$. Based on the generalized Nyquist criterion, if the point $(-1, 0j)$ is not encircled by Nyquist curve of $\widetilde{G}(s)$, then zero points of $\widetilde{P}(s)$ are all with negative real part.

Let $s = j\omega$; according to Gershgorin disk theorem, the eigenvalues $\lambda(\widetilde{G}(j\omega))$ of matrix $\widetilde{G}(j\omega)$ are all in below circles. Consider

$$\lambda\left(\widetilde{G}\left(j\omega\right)\right)\in\left\{\widetilde{G}_i, i=1,\ldots,m\right\}\bigcup\left\{\widetilde{G}_l, l=m+1,\ldots,n\right\},$$
$$\widetilde{G}_i = \left\{\xi:\xi\in C \mid \left|\xi-\frac{\sum_{j\in N_i}a_{ij}}{j\omega k_1}-\frac{j\omega e^{\tau\omega j}}{k_1}\right| \leq \sum_{j\in N_i}\left|\frac{a_{ij}e^{-(\tau_{ij}-\tau)\omega j}}{j\omega k_1}\right|\right\}, \quad i=1,\ldots,m,$$
$$\widetilde{G}_l = \left\{\xi:\xi\in C \mid \left|\xi-\frac{\sum_{j\in N_l}a_{lj}e^{-\tau\omega j}}{j\omega}\right| \leq \sum_{j\in N_l}\left|\frac{a_{lj}e^{-\tau_{lj\omega j}}}{j\omega}\right|\right\}, \quad l=m+1,\ldots,n. \tag{20}$$

Firstly, $\widetilde{G}_i$, $i=1,\ldots,m$, are considered. Let $d_i = \sum_{j\in N_i}a_{ij}$, and the center of circle is $\widetilde{G}_{i0} = -((\omega\sin\omega\tau)/k_1) + (((\omega\cos\omega\tau)/k_1)-(d_i/k_1\omega))j$.

If the point $(-a, 0j)$, $a\geq 1$, is not in $\widetilde{G}_i$, then

$$\left|-a-\frac{\sum_{j\in N_i}a_{ij}}{j\omega k_1}-\frac{j\omega e^{\tau\omega j}}{k_1}\right| \geq \sum_{j\in N_i}\left|\frac{a_{ij}e^{-(\tau_{ij}-\tau)\omega j}}{j\omega k_1}\right|. \tag{21}$$

We have

$$1-2\frac{\omega\sin\omega\tau}{k_1}+\frac{\omega^2}{k_1^2}-2\frac{\cos\omega\tau d_i}{k_1^2}\geq 0, \tag{22}$$
$$\omega^2\left(1-2k_1\tau\frac{\sin\omega\tau}{\omega\tau}\right)+k_1^2-2\cos\omega\tau d_i\geq 0. \tag{23}$$

If the following inequalities can hold, then (22) will be established:

$$\left(1-2k_1\tau\frac{\sin\omega\tau}{\omega\tau}\right)\geq 0, \quad k_1^2-2\cos\omega\tau d_i\geq 0. \tag{24}$$

Note that $\sin x/x \leq 1$ can be established for all $x \in R$ and $-1 \leq \cos x \leq 1$. Therefore, if the following conditions are satisfied, then the point $(-1, 0j)$ is not encircled by Nyquist curve of $\widetilde{G}_i(j\omega)$, $i = 1, \ldots, m$:

$$\tau \leq \frac{1}{2k_1}, \qquad k_1 \geq \sqrt{2 \max\{d_i, i = 1, \ldots, m\}}. \tag{25}$$

Next, $\widetilde{G}_l$, $l = m+1, \ldots, n$, are considered. If the point $(-a, 0j)$, $a \geq 1$, is not in $\widetilde{G}_l$, $l = m+1, \ldots, n$, then

$$\left| -a - \frac{k_2 \sum_{j \in N_l} a_{lj} e^{-\tau \omega j}}{j\omega} \right| \geq \sum_{j \in N_l} \left| \frac{k_2 a_{lj} e^{-\tau_{lj\omega} j}}{j\omega} \right|. \tag{26}$$

We have

$$a^2 - 2ak_2 \frac{\sin \omega \tau d_l}{\omega} \geq 0, \tag{27}$$

$$2k_2 \frac{\tau \sin \omega \tau d_l}{\omega \tau} \leq 1. \tag{28}$$

It is obvious that $\sin x/x \leq 1$ can be established for all $x \in R$. So, (29) can be satisfied, and (28) will hold:

$$\tau \leq \frac{1}{2k_2 \max\{d_l, l = m+1, \ldots, n\}}. \tag{29}$$

Combining the above analysis, Theorem 5 is demonstrated. □

Remark 6. From Theorem 5, it can be seen that consensus condition of system (3) with time delay only is dependent on input time delay of each agent, but is independent of communication time delay.

In Theorem 5, each agent with identical input time delay is assumed. From the above analysis, the conclusion with different input time delay among agents can also be deduced from the conclusion of Theorem 5. Consider

$$u_i = \sum_{j \in N_i} a_{ij} \left(x_j \left(t - \tau_{ij} \right) - x_i \left(t - \tau_i \right) \right) - k_1 v_i \left(t - \tau_i \right), \quad i = 1, \ldots, m,$$
$$u_l = k_2 \sum_{j \in N_l} a_{ij} \left(x_j \left(t - \tau_{ij} \right) - x_l \left(t - \tau_i \right) \right), \quad l = m+1, \ldots, n. \tag{30}$$

Corollary 7. *If the following conditions can hold, then consensus of system* (3) *with protocol* (30) *can be achieved.*

(i) The fixed topology contains spanning tree. (ii) The following conditions can be established: $k_1 \geq \sqrt{2 \max\{d_i, i = 1, \ldots, m\}}$, $k_2 > 0$, *and* $\tau_i \leq 1/2k_1$, $i = 1, \ldots, m$, $\tau_l \leq 1/2k_2 d_l$, *and* $l = m+1, \ldots, n$.

From Corollary 7, the upper bound of each τ_i, $i = 1, \ldots, n$, can be established.

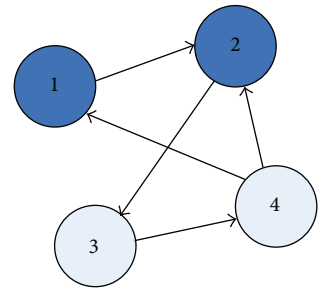

Figure 1: Interconnection graph.

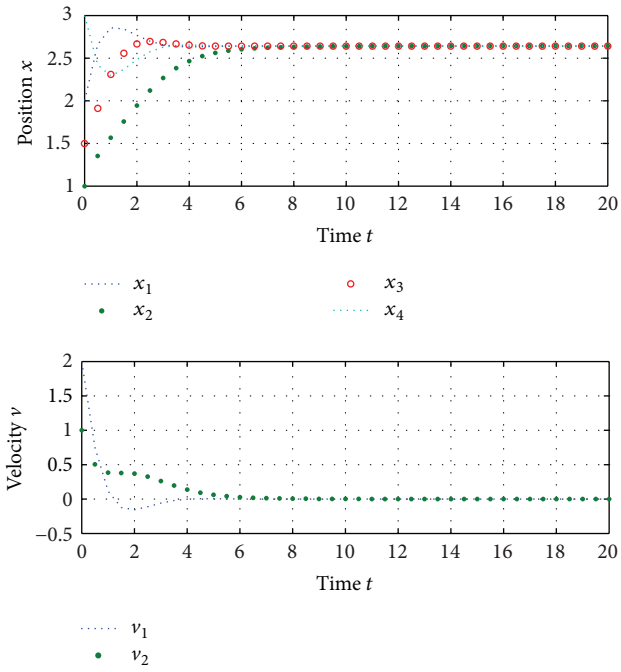

Figure 2: The state information of agents.

4. Simulation

In this section, several simulation results are presented to illustrate the proposed consensus algorithm introduced in Section 3.

Example 8. Consider a heterogeneous multiagent system with 4 agents, shown in Figure 1, where nodes 1, 2 are second-order agents and nodes 3, 4 are first-order agents. The graph has a directed spanning tree apparently. If $e_{ji} \in \mathcal{E}$, then $a_{ij} = 1$; else $a_{ij} = 0$. The Laplacian matrix is given as follows:

$$L = \begin{bmatrix} 1 & 0 & 0 & -1 \\ -1 & 2 & 0 & -1 \\ 0 & -1 & 1 & 0 \\ 0 & 0 & -1 & 1 \end{bmatrix}. \tag{31}$$

According to the conditions in Theorem 4, we select $k_1 = 2.1$, $k_2 = 1.2$. The initial conditions are $\mathbf{x}(0) = [2, 1, 1.5, 3]^{\mathrm{T}}$, $\mathbf{v}(0) = [2, 1]^{\mathrm{T}}$. The simulation results (Figure 2) show that

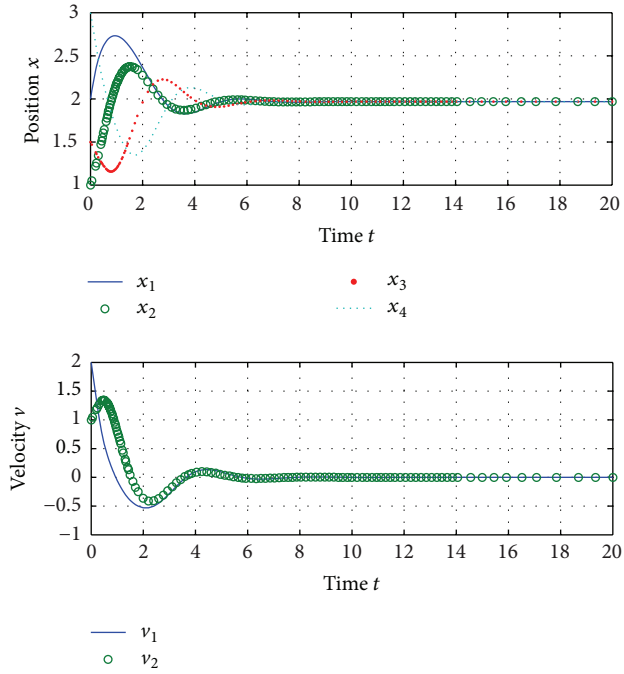

FIGURE 3: The state information of agents.

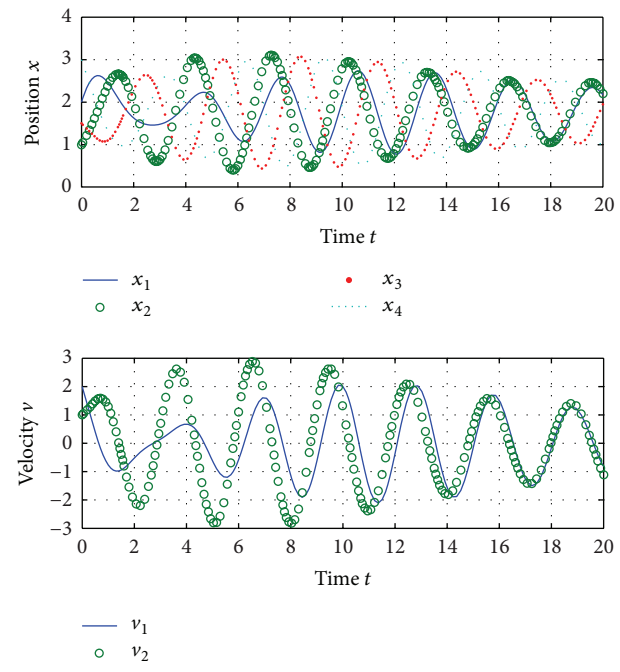

FIGURE 4: The state information of agents.

the positions of all agents and the velocities of second-order agents reach consensus asymptotically.

Example 9. These are the same communication topology and initial conditions as Example 8. The consensus protocol with time delay is considered. Firstly, control gains are selected as $k_1 = 2.1$, $k_2 = 1.2$. Based on the conditions in Theorem 5,

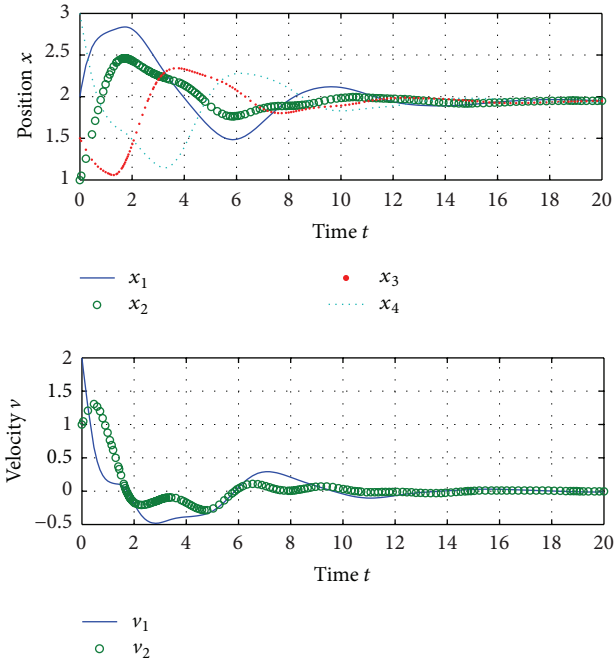

FIGURE 5: The state information of agents.

the upper bound of input time delay can be obtained and $\tau < 0.2381$ can be derived. We selected $\tau = 0.23$. The communication time delay among agents is set as $\tau_{12} = 0.2$, $\tau_{23} = 0.6$, $\tau_{34} = 0.4$, $\tau_{41} = 0.5$, and $\tau_{42} = 0.3$. The simulation results (Figure 3) show that the positions of all agents and the velocities of second-order agents reach consensus asymptotically. It can be seen that the speed of convergence of system with time delay is slower than the system without time delay.

Based on Example 9, input time delay is set as $\tau = 0.5$, and the simulation result (Figure 4) shows that the system is divergent. So, consensus condition is dependent on input time delay.

Meanwhile, we selected $\tau = 0.23$, and the communication time delays are enlarged as $\tau_{12} = 1.5$, $\tau_{23} = 1.2$, $\tau_{34} = 1.6$, $\tau_{41} = 1.4$, and $\tau_{42} = 1.2$. The simulation result (Figure 5) shows that the system is convergent. Consensus condition is dependent on input time delay. But, communication time delays can affect the speed of convergence of system obviously.

5. Conclusion

This paper focuses on the consensus problem of heterogeneous multiagent composed of first-order agent and second-order agent. The protocols with time delay and without time delay are investigated, respectively. The sufficient conditions of consensus are obtained in two cases. Consensus of the protocol without time delay is dependent on control gains and communication topology. If the control gains satisfy some conditions and communication topology contains spanning tree, then the consensus can be achieved. Consensus of the protocol with time delay is dependent only

on system coupling strength, each agent input time delay, but independent of communication delay. Finally, numerical simulations are provided to illustrate the effectiveness of the theoretical result. From simulation, it can be seen that all communication time delays and input time delay can affect the speed of convergence of system obviously. In the future work, discrete-time heterogeneous with time delay will be considered.

Conflict of Interests

The authors declare that there is no conflict of interests regarding the publication of this paper.

Acknowledgments

The authors would like to thank the associate editor and the anonymous reviewers for their valuable comments and suggestions that have improved the presentation of this paper.

References

[1] T. Vicsek, A. Czirok, E. B. Jacob, I. Cohen, and O. Schochet, "Novel type of phase transition in a system of self-driven particles," *Physical Review Letters*, vol. 75, no. 6, pp. 1226–1229, 1995.

[2] A. Jadbabaie, J. Lin, and A. S. Morse, "Coordination of groups of mobile autonomous agents using nearest neighbor rules," *IEEE Transactions on Automatic Control*, vol. 48, no. 6, pp. 988–1001, 2003.

[3] R. Olfati-Saber and R. M. Murray, "Consensus problems in networks of agents with switching topology and time-delays," *IEEE Transactions on Automatic Control*, vol. 49, no. 9, pp. 1520–1533, 2004.

[4] W. Ren and R. W. Beard, "Consensus seeking in multi-agent systems under dynamically changing interaction topologies," *IEEE Transactions on Automatic Control*, vol. 50, no. 5, pp. 655–661, 2005.

[5] L. Wang and F. Xiao, "A new approach to consensus problems in discrete-time multiagent systems with time-delays," *Science in China F: Information Sciences*, vol. 50, no. 4, pp. 625–635, 2007.

[6] F. Xiao and L. Wang, "State consensus for multi-agent systems with switching topologies and time-varying delays," *International Journal of Control*, vol. 79, no. 10, pp. 1277–1284, 2006.

[7] F. Xiao and L. Wang, "Asynchronous consensus in continuous-time multi-agent systems with switching topology and time-varying delays," *IEEE Transactions on Automatic Control*, vol. 53, no. 8, pp. 1804–1816, 2008.

[8] H. Su, X. Wang, and Z. Lin, "Flocking of multi-agents with a virtual leader," *IEEE Transactions on Automatic Control*, vol. 54, no. 2, pp. 293–307, 2009.

[9] H. Su, M. Z. Q. Chen, J. Lam, and Z. Lin, "Semi-global leader-following consensus of linear multi-agent systems with input saturation via low gain feedback," *IEEE Transactions on Circuits and Systems. I: Regular Papers*, vol. 60, no. 7, pp. 1881–1889, 2013.

[10] H. Su, M. Z. Chen, X. Wang, and J. Lam, "Semiglobal observer-based leader-following consensus with input saturation," *IEEE Transactions on Industrial Electronics*, vol. 61, no. 6, pp. 2842–2850, 2014.

[11] Y. Zheng, Y. Zhu, and L. Wang, "Consensus of heterogeneous multi-agent systems," *IET Control Theory & Applications*, vol. 5, no. 16, pp. 1881–1888, 2011.

[12] S. Zhu, C. Chen, and X. Guan, "Consensus protocol for heterogeneous multi-agent systems: a Markov chain approach," *Chinese Physics B*, vol. 22, no. 1, Article ID 018901, 2013.

[13] X. Yin, D. Yue, and S. Hu, "Distributed event-triggered control of discrete-time heterogeneous multi-agent systems," *Journal of the Franklin Institute*, vol. 350, no. 3, pp. 651–669, 2013.

[14] Y. Zhu, X. Guan, and X. Luo, "Finite-time consensus of heterogeneous multi-agent systems," *Chinese Physics B*, vol. 22, no. 3, Article ID 038901, 2013.

[15] Y. Zheng and L. Wang, "Finite-time consensus of heterogeneous multi-agent systems with and without velocity measurements," *Systems & Control Letters*, vol. 61, no. 8, pp. 871–878, 2012.

[16] C. Liu and F. Liu, "Stationary consensus of heterogeneous multi-agent systems with bounded communication delays," *Automatica*, vol. 47, no. 9, pp. 2130–2133, 2011.

[17] J. Yan, X. Guan, and X. Luo, "Consensus pursuit of heterogeneous multi-agent systems under a directed acyclic graph," *Chinese Physics B*, vol. 20, no. 4, Article ID 048901, 2011.

[18] H. Kim, H. Shim, and J. H. Seo, "Output consensus of heterogeneous uncertain linear multi-agent systems," *IEEE Transactions on Automatic Control*, vol. 56, no. 1, pp. 200–206, 2011.

[19] X. Yin, D. Yue, and S. Hu, "Consensus of fractional-order heterogeneous multi-agent systems," *IET Control Theory & Applications*, vol. 7, no. 2, pp. 314–322, 2013.

[20] J. M. Kim, J. B. Park, and Y. H. Choi, "Leaderless and leader-following consensus for heterogeneous multi-agent systems with random link failures," *IET Control Theory & Applications*, vol. 8, no. 1, pp. 51–60, 2014.

Hindawi Publishing Corporation
Mathematical Problems in Engineering
Volume 2014, Article ID 498630, 8 pages
http://dx.doi.org/10.1155/2014/498630

Research Article

Distributed Fault Detection for a Class of Nonlinear Stochastic Systems

Bingyong Yan, Huazhong Wang, and Huifeng Wang

Department of Automation, East China University of Science and Technology(ECUST), 130 Meilong Road, Shanghai 200237, China

Correspondence should be addressed to Huifeng Wang; nsisyy@163.com

Received 6 July 2014; Accepted 5 August 2014; Published 25 September 2014

Academic Editor: Fanglai Zhu

A novel distributed fault detection strategy for a class of nonlinear stochastic systems is presented. Different from the existing design procedures for fault detection, a novel fault detection observer, which consists of a nonlinear fault detection filter and a consensus filter, is proposed to detect the nonlinear stochastic systems faults. Firstly, the outputs of the nonlinear stochastic systems act as inputs of a consensus filter. Secondly, a nonlinear fault detection filter is constructed to provide estimation of unmeasurable system states and residual signals using outputs of the consensus filter. Stability analysis of the consensus filter is rigorously investigated. Meanwhile, the design procedures of the nonlinear fault detection filter are given in terms of linear matrix inequalities (LMIs). Taking the influence of the system stochastic noises into consideration, an outstanding feature of the proposed scheme is that false alarms can be reduced dramatically. Finally, simulation results are provided to show the feasibility and effectiveness of the proposed fault detection approach.

1. Introduction

In recent years, with the increasing complexity of modern dynamic systems, more and more researchers are now investigating new fault detection and identification (FDI) schemes to ensure safety and reliability of these modern complex dynamic systems. Effective FDI schemes can help find the early indication of system faults and avoid breakdowns of these complicated plants. The model-based analytical redundancy approaches have been proved to be an effective way to detect and diagnose faults for linear systems in the last two decades [1, 2].

However, in many practical applications, a large number of dynamic systems are inherently nonlinear systems with some uncertainty, which include the transformer, some chemical processes, and robotic manipulators with homonymic constraints. There are fruitful research results on fault diagnosis schemes for nonlinear systems in recent years. In [3], Donghua and Yinzhong proposed a novel FDI scheme for a class of nonlinear systems. Strong tracking filter was employed for parameter estimation to achieve fault detection. Fault estimation and accommodation scheme for nonlinear time-delay systems was developed using adaptive fault diagnosis observer in literature [4]. A novel fast adaptive fault estimation algorithm was proposed to improve the accuracy of fault estimation. The existence of the proposed adaptive fault diagnosis observer was given in terms of matrix inequality. More recently, by combining adaptive learning control theory with neural network, Polycarpou et al. in [5–8] proposed an online learning approximator to detect and isolate system faults. These approaches were based on generic function approximator with adjustable parameters. In [7], Zhang et al. developed a sensor fault isolation scheme for a class of nonlinear systems using online learning approximator. In the presence of modeling uncertainties, Vemuri used adaptive techniques to estimate an unknown sensor bias for a class of nonlinear discrete-time systems. The robustness, sensitivity, and stability properties were rigorously investigated [8]. Chen and Saif in [9] proposed an iterative learning observer (ILO) based fault diagnosis approach for fault detection, identification, and accommodation. The states of the ILO were updated using the previous output errors and the control input vectors.

Due to the existence of some Gaussian or non-Gaussian noises, fault detection and identification for nonlinear stochastic systems are always challenging tasks [10–12]. There are fewer research results on FDI for nonlinear stochastic systems compared with fruitful research results for linear systems. An effective FDI method for linear stochastic systems is to apply Kalman filters or extended Kalman filters. For nonlinear stochastic systems, this situation turns to be much more complicated. Zhang et al. investigated a fault detection and isolation scheme for a class of Lipschitz nonlinear systems with nonlinear and unstructured modeling uncertainty using adaptive estimation techniques [10]. The fault detection and isolation scheme was composed of a fault detection estimator and a bank of fault isolation estimators. The fault detectability and isolability were also rigorously investigated. For fault isolation problems, Guo and Wang proposed a novel fault isolation scheme for nonlinear non-Gaussian stochastic systems with multiple faults [11]. In this work, the fault isolation problem was converted into an entropy optimization problem using a state estimator. By building output probability density functions (PDFs) of the stochastic error, a novel data-driven fault isolation algorithm was derived. For those unmeasurable system outputs, square root B-spline expansion approach was applied to find the relationship of entropy of the system outputs with system faults and noises [12].

The main difficulty of designing an effective fault detection observer is the influence of stochastic noises on residual signals, which can give rise to false alarm and reduce the accuracy of fault detection. In this paper, we present a novel distributed fault detection scheme for a class of nonlinear stochastic systems. The objective of the fault detection scheme is to minimize the influence of system stochastic noises on residual signals using parameter optimization techniques. Firstly, by constructing a consensus filter to filter system outputs, a novel fault detection filter is proposed to estimate system states and generate residual signals. Secondly, the properties of the consensus filter are analyzed in detail, and the existence of the proposed fault detection filter is rigorously investigated in terms of linear matrix inequalities. An outstanding feature of the proposed scheme is that the influence of system stochastic noises on residual signals is reduced greatly, and, as a result, fault detection accuracy can be improved dramatically.

An outline of this paper is as follows. In Section 2, we define a class of nonlinear stochastic systems and give some preliminaries. In Section 3, a fault detection observer is proposed to detect system faults. The stability analysis of the consensus filter and the existence of the proposed fault detection filter are rigorously investigated. Finally, in Section 4, some simulation results are reported to illustrate the effectiveness of the proposed fault detection scheme. Some conclusion remarks are provided in Section 5.

2. Problem Statement and Preliminaries

Consider a class of nonlinear stochastic systems described by

$$\dot{x}(t) = Ax(t) + \Phi(x,u) + B_d d(t) + B_f f(t), \quad (1)$$

$$y(t) = Cx(t), \quad (2)$$

where $x(t) \in R^n$ is the system state vector, $u(t) \in R^m$ is the control input vector, $y(t) \in R^q$ is the measurement output vector, $d(t)$ is a zero-mean Gaussian white-noise process, $f(t) \in R^m$ is the system fault to be detected, and $\Phi(x,u)$ is a known nonlinear function. A, B_f, B_d, and C are known parameter matrices with appropriate dimensions. Throughout this paper, we take the following assumptions.

Assumption 1. System faults $f(t)$ and stochastic noises $d(t)$ are bounded, that is, $\|f(t)\| \le N_1$, and $\|d(t)\| \le N_2$.

Assumption 2. The nonlinear function $\Phi(\cdot)$ satisfies Lipschitz condition: that is,

$$\left\|\Phi(x(t),t) - \Phi(y(t),t)\right\| \le a\left\|(x(t) - y(t))\right\|, \quad \forall x(t), y(t) \in D, \quad (3)$$

where a is a known real constant.

In order to estimate system states, one gives the following full order Luenberger-like observer [13–16]:

$$\dot{\hat{x}}(t) = A\hat{x}(t) + \Phi(\hat{x},u) + H\left(y - C\hat{x}\right), \quad (4)$$

where H is a gain matrix to be determined. In order to detect system faults, one constructs the nonlinear fault detection filter as follows:

$$\dot{\hat{x}}(t) = A\hat{x}(t) + \Phi(\hat{x},u) + H\left(y - C\hat{x}\right), \quad (5)$$

$$\hat{y}(t) = C\hat{x}(t), \quad (6)$$

$$r(t) = y(t) - \hat{y}(t), \quad (7)$$

where $\hat{x}(t) \in R^n$ and $\hat{y}(t) \in R^q$ represent the estimated states and outputs vectors, respectively. H is a $n \times q$ design gain matrix. $r(t)$ is the so-called generated residual signal. Define states estimation error $e(t) = x(t) - \hat{x}(t)$, and it follows from (1) to (7) that

$$\dot{e}(t) = (A - HC)e(t) + B_f f(t) + B_d d(t) + \Phi - \widehat{\Phi}, \quad (8)$$

$$r(t) = Ce(t), \quad (9)$$

where $\Phi \triangleq \Phi(x,u)$ and $\widehat{\Phi} \triangleq \Phi(\hat{x},u)$. The gain matrix H is to be designed such that systems (5)–(7) are asymptotically stable.

We can clearly see from (5) to (7) that estimation errors of system states and system outputs are all corrupted by stochastic noises, which will lead to false alarms. In order to improve fault detection accuracy, a nonlinear fault detection observer is needed to minimize the influence of the system stochastic noise on residual signals. Therefore, we convert this problem to the following optimization problem: finding a gain matrix H, such that system (8) and (9) remains asymptotically stable, and the performance index $J = \|T_{rd}\|_\infty$ is minimized. Here, T_{rd} denotes the transfer function from system stochastic noises to residual signals. From (8) and (9), we can see that dynamics of the residual signals depend not only on $f(t)$ and $d(t)$ but also on nonlinear part: $\Phi - \widehat{\Phi}$. So the existing design techniques for fault detection observer cannot

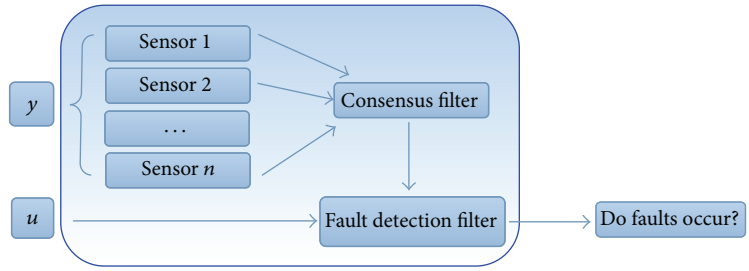

Figure 1: Architecture of fault detection observer.

be used here. In this paper, we propose a novel distributed fault detection approach by combining a consensus filter with a nonlinear fault detection filter. The selection of matrix H will be given in terms of LMIs in Section 3.

3. Main Results

In this section, we will give detailed design procedures for fault detection observer. The stability analysis of consensus filter and the existence of the fault detection filter are rigorously investigated.

3.1. Fault Detection Observer Design. Generally speaking, it is often difficult to get an exact description of a real plant system. Some unavoidable stochastic noises will have an influence on the practical engineering systems. As a result, some false alarms will be generated using the existing fault detection techniques. Also, with the increasing complexity of a real plant system, it is inevitable to use distributed sensors to measure system outputs at the same time. Take the high voltage direct current transmission system, for instance, we have to use distributed sensors to measure voltages, currents, and resistors along the transmission lines. Therefore, distributed fault diagnosis schemes are now attracting a lot of attentions from researchers.

In this work, we propose a novel distributed fault detection observer for a class of nonlinear stochastic systems. From (5) to (7), we can clearly see that the estimation errors of system states and outputs are affected by stochastic noises. It is difficult to detect the nonlinear stochastic systems faults using residual signals generated by a fault detection filter. To improve the fault detection accuracy, we develop a novel fault detection observer to detect system faults, which consists of a consensus filter and a fault detection filter. Firstly, a bank of distributed sensors is used to measure the system outputs. Secondly, each sensor sends its data to the consensus filter. The consensus filter acts as a data fusion center to reduce the influence of stochastic noises on residual signals. Then, a novel fault detection filter is developed by combining system control inputs with outputs of the consensus filter. Due to the existence of stochastic noises, one thing we have to consider is that to what extent the stochastic noises will have an influence on the residual signals. The whole architecture of the proposed fault detection scheme is shown in Figure 1.

For the convenience of designing the fault detection observer, we rewrite (5)–(7) as follows:

$$\dot{\hat{x}}(t) = A\hat{x}(t) + \Phi(\hat{x}, u) + L(\overline{y} - C\hat{x}), \tag{10}$$

$$\hat{y}(t) = C\hat{x}(t), \tag{11}$$

$$z_i(t) = \widetilde{y}_i(t) - y(t), \quad (i = 0, 1, \ldots, n), \tag{12}$$

$$r(t) = \overline{y}(t) - \hat{y}(t), \tag{13}$$

where $\overline{y}(t)$ is outputs of the consensus filter. $\widetilde{y}(t)$ is the state of each node in consensus filter. To minimize the influence of nonlinear system stochastic noises on residual signals, it leads to the following optimization problem: finding gain matrix L, such that system (10)–(13) remains asymptotically stable, and the performance index $J = \|T_{rd}\|_{\infty}$ is minimized.

3.2. Stability Analysis of Consensus Filter. In recent years, the study of information flow and coordination among different dynamic agents had aroused a larger amount of interests for researchers from all over the world. Among them, how to control each agent in a group to reach consensus is the key point in the condition that information exchange is limited and unreliable. The conceptions and ideas of consensus filter can be found in [17–29] and references therein.

Theorem 3. *Suppose that system* (1) *and* (2) *satisfies the Assumptions 1 and 2, and the fault diagnosis observer holds the form of* (10)–(13). *Then the consensus filter is asymptotically* ε *stable with each node state* $\eta^* = z(t)P$, *where*

$$\begin{aligned}\varepsilon = &\left(\|C\|\left[(\|A - LC\| + \alpha)\sigma + N_1\left\|B_f\right\| + N_2\left\|B_d\right\|\right]\right.\\ &\left.\times\sqrt{n}\left(1 + d_{\max}\right)\lambda_{\min}^{1/2}(M)\right)\\ &\times\left(\lambda_{\min}^{5/2}(M)\right)^{-1},\end{aligned} \tag{14}$$

η denotes the node of a small world networks G, $M = \{m_{ij}\}$ is the relation topology matrix of G, $Z(t)$ is the expected output of the consensus filter, and $P = \underbrace{[1, 1, \ldots, 1]}_{n}^{T}$.

Proof. From (10)–(12) and the definition of state estimation errors $e(t) = x(t) - \hat{x}(t)$, the maximum estimation errors of system states can be expressed as follows: $\sigma = \mathrm{MAX}(e(t))$.

We choose small world networks G as the weighed graph of the consensus filter. Let η denote a set of nodes in graph G with size n. $z(t)$ is the input of the consensus filter, that is, the state of each node is $z(t)P$.

Let $\delta = \eta - z(t)P$, then we have

$$\dot{\delta} = -M\delta + \dot{z}(t)P, \tag{15}$$

where M is a positive definite matrix with property

$$\left(1 + d_{\min}\right) \le \lambda_{\min}(M) \le \lambda_{\max}(M) \le \left(1 + 3d_{\max}\right). \tag{16}$$

For system (12), we select the Lyapunov function as follows:

$$V = \frac{1}{2}\delta^T M\delta. \tag{17}$$

Then we have

$$\begin{aligned}
\dot{V} &= -\|M\delta\|^2 + \dot{z}(t)\left(P^T M\delta\right) \\
&= -\|M\delta\|^2 \\
&\quad + C\left[(A - LC)e(t) + \Phi - \widehat{\Phi} + B_f f(t) + B_d d(t)\right] \\
&\quad \times \left[\left(1 + d_1, 1 + d_2, \ldots, 1 + d_n\right)\delta\right] \\
&\le -\lambda_{\min}^2(M)\|\delta\|^2 \\
&\quad + \|C\|\left(\|A - LC\|\sigma + \alpha\sigma + N_1\left\|B_f\right\| + N_2\left\|B_d\right\|\right) \\
&\quad \times \left[\sum_i \left(1 + d_i\right)^2\right]^{1/2}\|\delta\| \\
&\le -\lambda_{\min}^2(M)\|\delta\|^2 \\
&\quad + \|C\|\left[\left(\|A - LC\| + \alpha\right)\sigma + N_1\left\|B_f\right\| + N_2\left\|B_d\right\|\right] \\
&\quad \times \sqrt{n}\left(1 + d_{\max}\right)\|\delta\| \\
&= -\left\{\lambda_{\min}(M)\|\delta\|\right. \\
&\qquad - \left(\|C\|\left[\left(\|A - LC\| + \alpha\right)\sigma + N_1\left\|B_f\right\| + N_2\left\|B_d\right\|\right]\right. \\
&\qquad\quad \left.\left. \times \sqrt{n}\left(1 + d_{\max}\right)\right)\left(2\lambda_{\min}(M)\right)^{-1}\right\}^2 \\
&\quad + \left(\left(\|C\|\left[\left(\|A - LC\| + \alpha\right)\sigma + N_1\left\|B_f\right\| + N_2\left\|B_d\right\|\right]\right.\right. \\
&\qquad \left.\left. \times\sqrt{n}\left(1 + d_{\max}\right)\right)\left(2\lambda_{\min}(M)\right)^{-1}\right)^2.
\end{aligned} \tag{18}$$

Define a closed ball X which is centered at zero point, and the radius of the closed ball is

$$\begin{aligned}
r = \Big(&\|C\|\left[\left(\|A - LC\| + \alpha\right)\sigma + N_1\left\|B_f\right\| + N_2\left\|B_d\right\|\right] \\
&\times\sqrt{n}\left(1 + d_{\max}\right)\Big)\left(2\lambda_{\min}(M)\right)^{-1}.
\end{aligned} \tag{19}$$

Define a set of Lyapunov functions:

$$\Delta = \left\{\delta : V(\delta) \le \frac{1}{2}\lambda_{\max}(M)r^2\right\}. \tag{20}$$

Then we have $X \subset \Delta$,

$$\|\delta\| \le r \Longrightarrow V(\delta) = \frac{1}{2}\delta^T M\delta \le \frac{1}{2}\lambda_{\max}(M)\delta^2. \tag{21}$$

Thus we have $\delta \in \Delta$. Therefore, the solution of $\dot{\delta} = -M\delta + \dot{z}(t)P$ satisfies $\dot{V}(\rho) < 0$.

This completes the proof. □

According to Theorem 3, we can draw the conclusion that the consensus filter for the nonlinear stochastic systems is asymptotically convergent.

3.3. Design of Fault Detection Filter. In this section, design procedures of fault detection filter are given in details. The matrix parameters are designed in terms of linear matrix inequality using robust control theory and nonlinear matrix inequality methods.

Lemma 4 (see [1]). *Let A and B be real matrices with appropriate dimensions. For any scalar $\varepsilon > 0$ and vectors x, $y \in R^n$, one has $2x^T ABy \le \varepsilon^{-1}x^T AA^T x + \varepsilon y^T B^T By$.*

Theorem 5. *Suppose that the systems* (1) *and* (2) *satisfy Assumptions 1 and 2, and the fault detection observer holds the form of* (10)–(13). *Given a constant $\gamma > 0$, the system* (10)–(13) *satisfies $\|r(t)\|_\infty \le \gamma\|d(t)\|_\infty$, if there exist a positive symmetrical matrix P and a scalar $\varepsilon_1 > 0$, satisfying the following LMI:*

$$\begin{bmatrix}
P(A - LC) + (A - LC)^T P + C^T C + \varepsilon_1\alpha^2 I & 0 & P \\
0 & -\gamma^2 I & \\
P^T & & -\varepsilon_1 I
\end{bmatrix} < 0. \tag{22}$$

Proof. Considering the system (10)–(13), we choose a Lyapunov function of the following form: $V(t) = e^T(t)Pe(t)$, where P is a positive symmetrical matrix. In fault-free case, when system uncertainty $d(t) = 0$, we have

$$\begin{aligned}
\dot{V}(t) &= e^T(t)P\dot{e}(t) + \dot{e}^T(t)Pe(t) \\
&= e^T(t)P\left[(A - LC)e(t) + \Phi - \widehat{\Phi}\right] + \dot{e}^T(t)Pe(t) \\
&= e^T(t)P\left[(A - LC)e(t) + \Phi - \widehat{\Phi}\right] \\
&\quad + \left[(A - LC)e(t) + \Phi - \widehat{\Phi}\right]^T Pe \\
&= e^T(t)\left[P(A - LC) + (A - LC)^T P\right]e(t) \\
&\quad + e^T(t)P\left[\Phi - \widehat{\Phi}\right] + \left[\Phi - \widehat{\Phi}\right]^T Pe.
\end{aligned} \tag{23}$$

According to Lemma 4 and Assumption 2, we have

$$\begin{aligned}
&2e^T(t)P\left[\Phi - \widehat{\Phi}\right] \\
&\le \varepsilon_1^{-1}e^T(t)PP^T e(t) + \varepsilon_1\left(\Phi - \widehat{\Phi}\right)^T\left(\Phi - \widehat{\Phi}\right) \\
&\le \varepsilon_1^{-1}e^T(t)PP^T e(t) + \varepsilon_1\alpha^2 e^T(t)e(t).
\end{aligned} \tag{24}$$

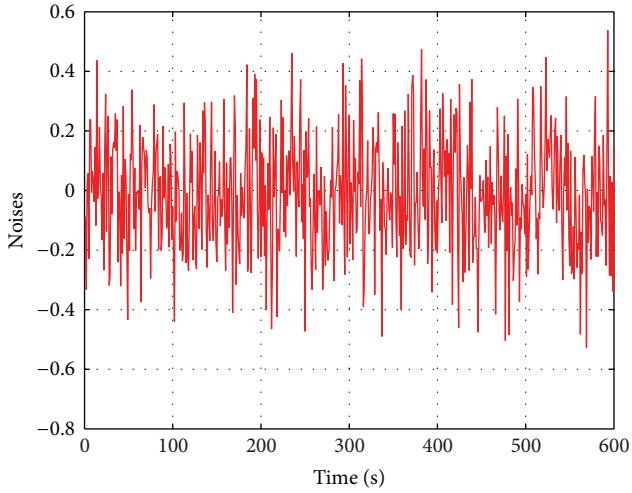

Figure 2: Stochastic noises.

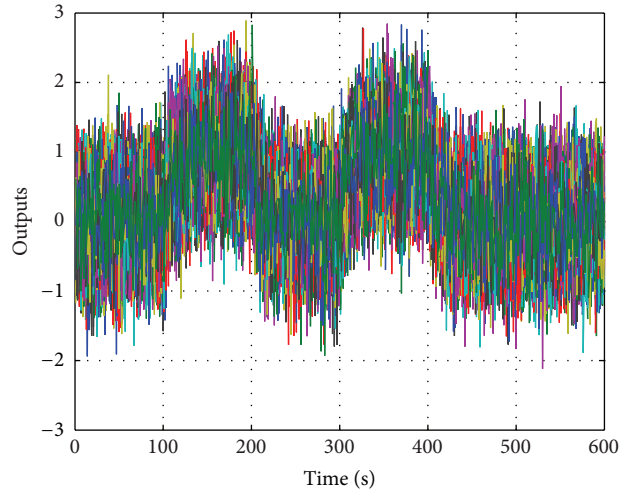

Figure 3: System outputs.

Thus,

$$\dot{V}(t) \le e^T(t)\left[P(A-LC)+(A-LC)^TP+\varepsilon_1^{-1}PP^T + \varepsilon_1\alpha^2 I\right]e(t). \tag{25}$$

From (22), we can obtain that $\dot{V}(t) \le 0$.

So the system described by (10)–(13) is asymptotically stable in the condition of no fault.

When the system uncertainty $d(t) \neq 0$, by defining

$$H(e,d) = \dot{V}(t) + \|r(t)\|_\infty - \gamma^2\|d(t)\|_\infty \tag{26}$$

we have

$$\begin{aligned} H(e,d) &= e^T(t)P\dot{e}(t) + \dot{e}^T(t)Pe(t) + e^T(t)C^TCe(t) \\ &\quad - \gamma^2 d^T(t)d(t) \\ &= e^T(t)P\left[(A-LC)e(t) + B_d d(t) + \Phi - \widehat{\Phi}\right] \\ &\quad + \left[(A-LC)e(t) + \Phi - \widehat{\Phi} + B_d d(t)\right]^T Pe(t) \\ &\quad + e^T(t)C^TCe(t) - \gamma^2 d^T(t)d(t) \\ &\le e^T(t)\left[P(A-LC) + (A-LC)^TP + \varepsilon_1^{-1}PP^T + C^TC \right. \\ &\quad \left. + \varepsilon_1\alpha^2 I\right]e(t) - \gamma^2 d^T(t)d(t) \\ &= \begin{bmatrix} e(t) \\ d(t) \end{bmatrix}^T \begin{bmatrix} \Lambda & 0 \\ 0 & -\gamma^2 I \end{bmatrix} \begin{bmatrix} e(t) \\ d(t) \end{bmatrix}, \end{aligned} \tag{27}$$

where

$$\Lambda = P(A-LC) + (A-LC)^TP + C^TC + \varepsilon_1^{-1}PP^T + \varepsilon_1\alpha^2 I. \tag{28}$$

From the known condition (22), by using Schur theory we have

$$H(e,d) = \dot{V}(t) + r^T(t)r(t) - \gamma^2 d^T(t)d(t) < 0. \tag{29}$$

For any given time $t > 0$, integration of (29) from 0 to t yields

$$\int_0^{+\infty} r^T(t)r(t) < \gamma^2 \int_0^{+\infty} d^T(t)d(t). \tag{30}$$

Thus, the inequality $\|r(t)\|_\infty \le \gamma\|d(t)\|_\infty$ holds.

This completes the proof. □

Remark 6. Theorem 5 gives the existence of the fault detection filter. This optimization problem (22) can be solved by using Matlab software toolboxes. In the presence of system stochastic noises, the effects of faults on residual signals are hidden in the stochastic noises. It is difficult to distinguish a real one from the residual signals. Theorem 5 gives us a method to select an approximate gain matrix to design the fault detection filter. One can use residual evaluation function $\|r(t)\|_2$ to detect system faults. As a result, the fault detection accuracy can be improved dramatically.

4. Simulation Results

We consider a class of nonlinear stochastic systems:

$$\begin{aligned} \dot{x}(t) &= \begin{bmatrix} -0.46 & 0 \\ 0 & -0.53 \end{bmatrix} x(t) + \begin{bmatrix} 1 \\ 1 \end{bmatrix} u \\ &\quad + \begin{bmatrix} 0.3\sin(x(t)) & \\ & 0.2\sin(x(t)) \end{bmatrix} \\ &\quad + \begin{bmatrix} 0.3 \\ 0.2 \end{bmatrix} d(t) + \begin{bmatrix} 1 \\ 0 \end{bmatrix} f(t), \\ y(t) &= \begin{bmatrix} 1 & 1 \end{bmatrix} x(t), \end{aligned} \tag{31}$$

where $d(t)$ is a zero-mean Gaussian white noise. Let $\gamma = 0.3$, $\varepsilon_1 = 0.7$. According to Theorem 5, we determine the gain matrix L with Matlab toolbox: $L = [0.2511, 0.1279]$.

In the simulation study, we take the step-function fault into consideration. Figure 2 shows the zero-mean Gaussian white noises generated by Matlab software. Figure 3 shows

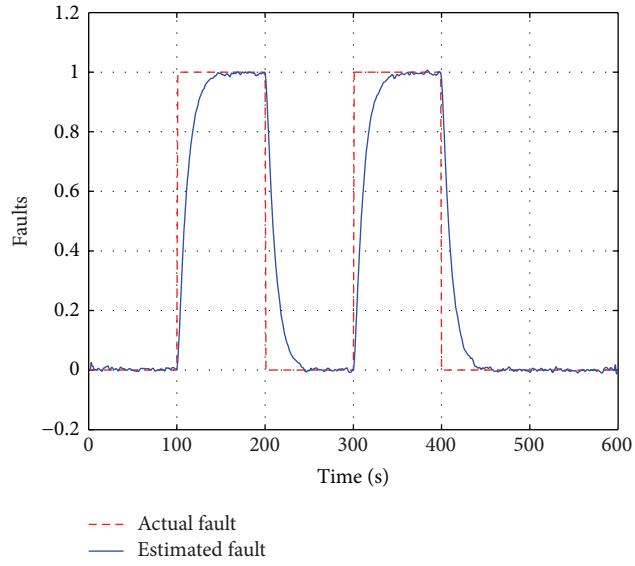

Figure 4: Outputs of fault detection filter.

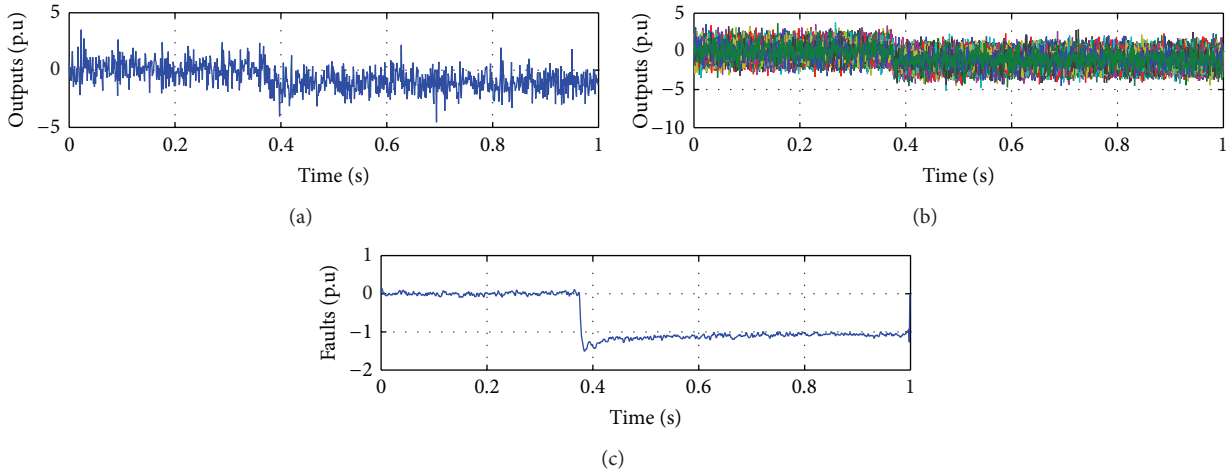

Figure 5: (a) System outputs, (b) measurements by distributed sensors, and (c) outputs of fault detection filter.

the system outputs measured by 100 distributed sensors. Figure 4 shows the outputs of the fault detection filter using the outputs of the consensus filter. From Figure 3, we can see that system outputs are corrupted by stochastic noises, and it is difficult to detect system faults using these system outputs. From Figure 4 we can clearly see that system faults occur at time $t = 100$ s and $t = 300$ s, respectively. As a result, we can detect system faults at time $t = 100$ s and $t = 300$ s, respectively. Figure 5 shows another simulation study by using 100 distributed sensors. In this simulation study, we investigate a step-function fault which occurs at $t = 0.38$ s. From Figure 5(a), we can see that the system faults seem to be hidden by system stochastic noises. Some false alarms may be generated using existing fault detection approaches. We use 100 distributed sensors to measure the system outputs at the same time and then send the measured system outputs to the consensus filter, as is shown in Figure 5(b). A fault detection filter is constructed using outputs of the consensus filter and the system control inputs. Comparing Figure 5(a) with Figure 5(c), we can see that the residual signals generated by fault detection filter can reflect real system faults. Therefore, fault detection accuracy can be improved dramatically.

5. Conclusions

This paper has proposed a novel distributed fault detection scheme for a class of nonlinear stochastic systems. A novel fault detection observer is developed using a consensus filter and a nonlinear fault detection filter. By combining these two kinds of filters, a distributed fault detection observer is designed to minimize the influence of stochastic noises on residual signals. The stability of consensus filter is rigorously analyzed in detail. Meanwhile, the parameter optimization of the fault detection filter is given in terms of LMIs.

In the simulation study, numerical examples are given to demonstrate the validity and applicability of the proposed approach.

Conflict of Interests

The authors declare that there is no conflict of interests regarding the publication of this paper.

Acknowledgments

This work was supported by the Special Fund of East China University of Science and Technology for Basic Scientific Research (WH14027 and WJ1313004-1) and National Natural Science Foundation of China (nos. 21327807, H200-4-13192, and 51207007). The authors would like to thank the reviewers for the detailed comments that have helped us significantly improve the quality of our presentation.

References

[1] P. M. Frank, "Fault diagnosis in dynamic systems using analytical and knowledge-based redundancy: a survey and some new results," *Automatica*, vol. 26, no. 3, pp. 459–474, 1990.

[2] R. Isermann, "Process fault detection based on modeling and estimation methods: a survey," *Automatica*, vol. 20, no. 4, pp. 387–404, 1984.

[3] Z. Donghua and Y. Yinzhong, *Modern Fault Diagnosis and Fault Tolerant Control*, Publishing Company of Tsinghua University, Beijing, China, 2000.

[4] K. Zhang, B. Jiang, and V. Cocquempot, "Fast adaptive fault estimation and accommodation for nonlinear time-varying delay systems," *Asian Journal of Control*, vol. 11, no. 6, pp. 643–652, 2009.

[5] M. M. Polycarpou and A. B. Trunov, "Learning approach to nonlinear fault diagnosis: detectability analysis," *IEEE Transactions on Automatic Control*, vol. 45, no. 4, pp. 806–812, 2000.

[6] X. D. Zhang, M. M. Polycarpou, and T. Parisini, "A robust detection and isolation scheme for abrupt and incipient faults in nonlinear systems," *IEEE Transactions on Automatic Control*, vol. 47, no. 4, pp. 576–593, 2002.

[7] X. D. Zhang, T. Parisini, and M. M. Polycarpou, "Sensor bias fault isolation in a class of nonlinear systems," *IEEE Transactions on Automatic Control*, vol. 50, no. 3, pp. 370–376, 2005.

[8] A. T. Vemuri, "Sensor bias fault diagnosis in a class of nonlinear systems," *IEEE Transactions on Automatic Control*, vol. 46, no. 6, pp. 949–954, 2001.

[9] W. Chen and M. Saif, "An iterative learning observer for fault detection and accommodation in nonlinear time-delay systems," *International Journal of Robust and Nonlinear Control*, vol. 16, no. 1, pp. 1–19, 2006.

[10] X. Zhang, M. M. Polycarpou, and T. Parisini, "Fault diagnosis of a class of nonlinear uncertain systems with Lipschitz nonlinearities using adaptive estimation," *Automatica*, vol. 46, no. 2, pp. 290–299, 2010.

[11] L. Guo and H. Wang, "Fault detection and diagnosis for general stochastic systems using B-spline expansions and nonlinear filters," *IEEE Transactions on Automatic Control*, vol. 52, no. 8, pp. 1644–1652, 2005.

[12] Y. Bingyong, T. Zuohua, and L. Dongmei, "Fault diagnosis for a class of nonlinear stochastic time-delay systems," *Control and Instruments in Chemical Industry*, vol. 34, no. 1, pp. 12–15, 2007.

[13] W. Zhang, H. Su, H. Wang, and Z. Han, "Full-order and reduced-order observers for one-sided lipschitz nonlinear systems using Riccati equations," *Communications in Nonlinear Science and Numerical Simulation*, vol. 17, no. 12, pp. 4968–4977, 2012.

[14] W. Zhang, H.-S. Su, Y. Liang, and Z.-Z. Han, "Non-linear observer design for one-sided Lipschitz systems: an linear matrix inequality approach," *IET Control Theory and Applications*, vol. 6, no. 9, pp. 1297–1303, 2012.

[15] W. Zhang, H. Su, and J. Wang, "Computation of upper bounds for the solution of continuous algebraic Riccati equations," *Circuits, Systems, and Signal Processing*, vol. 32, no. 3, pp. 1477–1488, 2013.

[16] W. Zhang, X.-S. Cai, and Z.-Z. Han, "Robust stability criteria for systems with interval time-varying delay and nonlinear perturbations," *Journal of Computational and Applied Mathematics*, vol. 234, no. 1, pp. 174–180, 2010.

[17] H. Su, X. Wang, and Z. Lin, "Flocking of multi-agents with a virtual leader," *IEEE Transactions on Automatic Control*, vol. 54, no. 2, pp. 293–307, 2009.

[18] H. Su, X. Wang, G. Chen, and Z. Lin, "Adaptive second-order consensus of networked mobile agents with nonlinear dynamics," *Automatica*, vol. 47, no. 2, pp. 368–375, 2011.

[19] H. Su, Z. Rong, M. Z. Q. Chen, X. Wang, G. Chen, and H. Wang, "Decentralized adaptive pinning control for cluster synchronization of complex dynamical networks," *IEEE Transactions on Cybernetics*, vol. 43, no. 1, pp. 394–399, 2013.

[20] H. Su, M. Z. Q. Chen, J. Lam, and Z. Lin, "Semi-global leader-following consensus of linear multi-agent systems with input saturation via low gain feedback," *IEEE Transactions on Circuits and Systems I: Regular Papers*, vol. 60, no. 7, pp. 1881–1889, 2013.

[21] H. Su, M. Z. Q. Chen, X. Wang, and J. Lam, "Semiglobal observer-based leader-following consensus with input saturation," *IEEE Transactions on Industrial Electronics*, vol. 61, no. 6, pp. 2842–2850, 2014.

[22] J. A. Fax and R. M. Murray, "Information flow and cooperative control of vehicle formations," *IEEE Transactions on Automatic Control*, vol. 49, no. 9, pp. 1465–1476, 2004.

[23] A. Jadbabaie, J. Lin, and A. S. Morse, "Coordination of groups of mobile autonomous agents using nearest neighbor rules," *IEEE Transactions on Automatic Control*, vol. 48, no. 6, pp. 988–1001, 2003.

[24] R. Olfati-Saber and R. M. Murray, "Consensus problems in networks of agents with switching topology and time-delays," *IEEE Transactions on Automatic Control*, vol. 49, no. 9, pp. 1520–1533, 2004.

[25] W. Ren, R. W. Beard, and D. B. Kingston, "Multi-agent kalman consensus with relative uncertainty," in *Proceedings of the American Control Conference (ACC '05)*, pp. 1865–1870, Portland, Ore, USA, June 2005.

[26] R. Olfati-Saber and J. S. Shamma, "Consensus filters for sensor networks and distributed sensor fusion," in *Proceeding of the 44th IEEE Conference on Decision and Control, and the European Control Conference (CDC-ECC '05)*, pp. 6698–6703, December 2005.

[27] D. Bauso, L. Giarré, and R. Pesenti, "Distributed consensus protocols for coordinating buyers," in *Proceedings of the IEEE Conference on Decision and Control*, pp. 588–592, December 2003.

[28] R. Olfati-Saber, "Distributed Kalman filter with embedded consensus filters," in *Proceedings of the 44th IEEE Conference on Decision and Control, and the European Control Conference (CDC-ECC '05)*, pp. 8179–8184, December 2005.

[29] R. Olfati-Saber, "Distributed Kalman filtering and sensor fusion in sensor networks," in *Proceedings of the Workshop on Network Embedded Sensing and Control*, Notre Dame University, South Bend, Ind, USA, October 2005.

Hindawi Publishing Corporation
Mathematical Problems in Engineering
Volume 2014, Article ID 269031, 9 pages
http://dx.doi.org/10.1155/2014/269031

Research Article

Pinning-Like Adaptive Consensus for Networked Mobile Agents with Heterogeneous Nonlinear Dynamics

Chengjie Xu,[1,2] Yanwei Wang,[3] Hong Zhang,[2] and Xiaoqi Zhou[1]

[1] *School of Science, Hunan University of Technology, Zhuzhou 412007, China*
[2] *School of Automation, Huazhong University of Science and Technology, Wuhan 430074, China*
[3] *School of Mechanical and Electrical Engineering, Wuhan Institute of Technology, Wuhan 430073, China*

Correspondence should be addressed to Yanwei Wang; ywwang.cad@gmail.com

Received 26 June 2014; Accepted 15 August 2014; Published 25 September 2014

Academic Editor: Michael Chen

This paper investigates the adaptive consensus for networked mobile agents with heterogeneous nonlinear dynamics. Using tools from matrix, graph, and Lyapunov stability theories, sufficient consensus conditions are obtained under adaptive control protocols for both first-order and second-order cases. We design an adaptive strategy on the coupling strengths, which can guarantee that the consensus conditions do not require any global information except a connection assumption. The obtained results are also extended to networked mobile agents with identical nonlinear dynamics via adaptive pinning control. Finally, numerical simulations are presented to illustrate the theoretical findings.

1. Introduction

In recent years, distributed cooperative control for multiagent systems has been intensively investigated by researchers from various disciplines. This is due to its broad potential applications in sensor networks, combat intelligence, surveillance, and so forth [1, 2]. Various scenarios about distributed cooperative control are studied, such as leaderless consensus [3–5], leader-following consensus [6–8], containment [9–13], and flocking [14, 15].

Consensus is one of the most fundamental problems in distributed cooperative control, which means that the states of the agents reach an agreement on a common physical quantity of interest by implementing an appropriate consensus protocol based on the information from local neighbors. Numerous interesting results about consensus algorithm were presented in the past decade. The earlier studies on consensus problem are mainly about multiagent systems with first-order dynamics [16–18]. And consensus for multiagent systems with second-order dynamics has been investigated recently [19–21], which is more challenging than the first-order case. Meanwhile, consensus for linear multiagent systems is discussed in [22, 23], which is considered more general than first-order and second-order multiagent systems.

However, in reality, mobile agents may be governed by more complicated intrinsic dynamics, so second-order consensus problems for multiagent with nonlinear dynamics have been investigated [24–33], in which the authors assume that all the agents have identical nonlinear dynamics. Recently, second-order consensus of multiagent systems with heterogeneous nonlinear dynamics and time-varying delay was investigated by introducing novel decentralized adaptive control in [28]. In [29], a distributed cooperative tracking problem was studied for a group of second-order multiagents networked system with nonidentical nonlinear dynamics and bounded external disturbances. Impulsive consensus for first-order multiagent with heterogeneous nonlinear dynamics was discussed [30], in which the information of the leader is known by every following agent. This assumption is also adopted in [31]. Motivated by [28–33], we investigate the second-order consensus for networked mobile agents with heterogeneous nonlinear dynamics without assuming that all the nonlinear functions have a common equilibrium solution. A distributed adaptive strategy and a pinning-like control is introduced in the consensus protocol. The protocol is composed of two parts. One is designed to compensate the errors of the nonlinear dynamics and the other one is designed like a pinning controller.

The rest of the paper is organized as follows. In Section 2, we state the model considered in the paper and give some basic definitions, lemmas, and assumptions. In Section 3, new results on the second-order consensus problem are addressed. And numerical example is given in Section 4. Finally, we conclude the paper in Section 5.

2. Preliminaries and Model Description

In this section, some notations and preliminaries are introduced. The following notations are used throughout this paper. I_n denotes the $n \times n$ identity matrix. For a matrix A (or a vector x), A^T (or x^T) represents the transpose of A (or x).

Let $\mathcal{G} = (\mathcal{V}, \mathcal{E}, \mathcal{A})$ be a directed graph with a nonempty set of nodes $\mathcal{V} = (v_1, v_2, \ldots, v_{N+M})$, a set of edges $\mathcal{E} \subseteq \mathcal{V} \times \mathcal{V}$, and a weighted adjacent matrix $\mathcal{A} = [a_{ij}]$. An edge is denoted by (v_i, v_j) in a directed graph which means that vertex j can obtain information from vertex i but not necessarily vice versa. a_{ij} represents the weight of the edge (v_j, v_i) and $a_{ij} > 0 \Leftrightarrow (v_j, v_i) \in \mathcal{E}$. Node v_j is called the parent node, node v_i is the child node, and v_j is a neighbor of v_i. The neighbor set $\mathcal{N}_i = \{v_j \mid (v_j, v_i) \in \mathcal{E}\}$. A graph is undirected if $(v_j, v_i) \in \mathcal{E}$ implies $(v_i, v_j) \in \mathcal{E}$. The elements l_{ij} of Laplace matrix L is defined as $l_{ij} = -a_{ij}$, $i \neq j$, and $l_{ii} = \sum_{j \neq i, j=1}^{N} a_{ij}$.

Before moving on, some assumptions and Lemmas are introduced.

Assumption 1. Suppose that the undirected graph G is connected.

Lemma 2 (see [33]). *If $L = (l_{ij}) \in R^{N \times N}$ is a symmetric irreducible matrix with $l_{ii} = -\sum_{j=1, j \neq i}^{N} l_{ij}$, $l_{ij} = l_{ji} \leq 0$ $(i \neq j)$, then L is semipositive definite and then for any matrix $E = \mathrm{diag}(e, 0, \ldots, 0)$ with $e > 0$, all eigenvalues of the matrix $(L+E)$ are positive.*

Lemma 3 (see [34]). *The matrix A of an undirected graph G is irreducible if and only if the undirected graph is connected.*

Lemma 4 (see [35]). *If a scalar function $V(x,t)$ satisfies the following conditions, then $\dot{V}(x,t) \to 0$, as $t \to \infty$. (a) $V(x,t)$ is lower bounded; (b) $\dot{V}(x,t)$ is negative semidefinite; (c) $\dot{V}(x,t)$ is uniformly continuous in t.*

3. Main Results

In this section, consensus conditions for both first-order and second-order multiagent systems with heterogeneous nonlinear dynamics are obtained by designing pinning-like adaptive control protocols. Pinning-like adaptive consensus for first-order multiagent systems with heterogeneous nonlinear dynamics is investigated in the first subsection and the second-order case is investigated in the second subsection. For the first-order case, the ith node can be described as

$$\dot{x}_i = f_i\left(t, x_i\left(t\right)\right) + u_i, \tag{1}$$

where $i = 1, 2, \ldots, N$, $t \in R^+$, $x_i = (x_{i1}, x_{i2}, \ldots, x_{in})^T \in R^n$ is the state vector of the ith node. $f_i : R \times R^n \to R^n$ is a continuous vector-value function, which describes the local dynamics of the nodes in the ith node.

For the second-order case, the ith node can be described as

$$\begin{aligned} \dot{x}_i\left(t\right) &= v_i\left(t\right), \\ \dot{v}_i\left(t\right) &= f_i\left(t, x_i\left(t\right), v_i\left(t\right)\right) + u_i\left(t\right), \\ & \qquad i = 1, \ldots, N, \end{aligned} \tag{2}$$

where $t \in R^+$, $x_i, v_i, u_i \in R^n$ are the position, velocity, and input vector of the ith follower, respectively. $f_i : R \times R^n \times R^n \to R^n$ is a continuous vector-value function, which describes the local dynamics of the nodes in the ith node.

3.1. Pinning-Like Adaptive Consensus for First-Order Multiagent Systems with Heterogeneous Nonlinear Dynamics. In this subsection, we investigate consensus criteria for first-order multiagent systems with heterogeneous nonlinear dynamics via distributed adaptive pinning control.

As mentioned in many literatures, consensus or synchronization for networked systems with nonidentical nodes cannot be realized without control if the nonidentical dynamic functions do not have a common solution. Thereby, a distributed adaptive pinning-like control protocol is proposed, under which leader-following consensus for networked system (1) can be achieved; that is, there exists a desired state s, such that

$$\lim_{t \to \infty} \left\| x_i\left(t\right) - s\left(t\right) \right\| = 0, \quad i = 1, 2, \ldots, N, \tag{3}$$

where s satisfies $\dot{s} = f(t, s(t))$, and s can be an equilibrium, a limit cycle, or even a chaotic attractor.

The following assumption is necessary for our main results.

Assumption 5. For arbitrary $x, y \in R^n$ and every $i \in \{1, 2, \ldots, N\}$, there exists a constant $\omega > 0$ such that

$$\left(x - y\right)^T \left(f_i\left(t, x\right) - f_i\left(t, y\right)\right) \leq \omega \left(x - y\right)^T \left(x - y\right). \tag{4}$$

We choose the control protocol as

$$\begin{aligned} u_i\left(t\right) = \dot{s}\left(t\right) - f_i\left(t, s\left(t\right)\right) &+ \sum_{j \in \mathcal{N}_i} c_{ij} a_{ij} \left(x_j\left(t\right) - x_i\left(t\right)\right) \\ &+ h_i c_i\left(t\right) \left(s\left(t\right) - x_i\left(t\right)\right). \end{aligned} \tag{5}$$

In the controller (4), $h_i = 1$ for some i, then the ith node is named as pinning-like node and $h_i = 0$ for others. $c_i > 0$ and $c_{ij} > 0$ are determined by the following equations:

$$\begin{aligned} \dot{c}_i\left(t\right) &= h_i k_i \left(s\left(t\right) - x_i\left(t\right)\right)^T \left(s\left(t\right) - x_i\left(t\right)\right), \\ \dot{c}_{ij}\left(t\right) &= a_{ij} k_{ij} \left(x_j\left(t\right) - x_i\left(t\right)\right)^T \left(x_j\left(t\right) - x_i\left(t\right)\right), \\ & \qquad i \neq j, \quad i, j = 1, 2, \ldots, N, \end{aligned} \tag{6}$$

where $k_{ij} = k_{ji} > 0$, $k_i > 0$ are the weights of adaptive laws for parameters $c_{ij}(t)$ and $c_i(t)$. $c_{ij} > 0$ denotes the coupling strength between node i and node $j, i, j = 1, \ldots, N$. We define a new matrix, named adaptive weighted Laplace matrix of the network topology, as the following:

$$\widetilde{L} = \begin{bmatrix} \widetilde{l}_{11} & \widetilde{l}_{12} & \cdots & \widetilde{l}_{1N} \\ \widetilde{l}_{21} & \widetilde{l}_{22} & \cdots & \widetilde{l}_{2N} \\ \vdots & \vdots & \vdots & \vdots \\ \widetilde{l}_{N1} & \widetilde{l}_{N2} & \cdots & \widetilde{l}_{NN} \end{bmatrix}. \tag{7}$$

The elements $\widetilde{l}_{ij}$ is defined as $\widetilde{l}_{ij} = c_{ij} l_{ij}$, $i \neq j$, $i, j = 1, 2, \ldots, N$, and c_{ii} is defined as $\widetilde{l}_{ii} = c_{ii} l_{ii} = \sum_{j \neq i, j=1}^{N} c_{ij} a_{ij}$, so $\widetilde{L}$ is zero-row-sum. The initial values of the elements of $\widetilde{L}$ should be chosen symmetrically for the symmetry of $\widetilde{L}$.

Remark 6. From Lemmas 2 and 3, if the undirected topology graph G is connected, the adaptive weighted Laplace matrix is semipositive definite.

The controlled network for system (1) under protocol (5) with adaptive strategy (6) can be rewritten as

$$\begin{aligned} \dot{x}_i = {} & f_i\left(t, x_i(t)\right) + \sum_{j \in \mathcal{N}_i} c_{ij} a_{ij} \left(x_j(t) - x_i(t)\right) \\ & + \dot{s}(t) - f_i(t, s(t)) + h_i c_i(t) \left(s(t) - x_i(t)\right). \end{aligned} \tag{8}$$

Let error state e_i be defined as

$$e_i = x_i - s, \quad i = 1, 2, \ldots, N. \tag{9}$$

From (1) and ((8)-(9)), the error systems can be described as

$$\begin{aligned} \dot{e}_i = {} & f_i\left(t, x_i(t)\right) - f_i(t, s(t)) \\ & + \sum_{j \in \mathcal{N}_i} c_{ij} a_{ij} \left(x_j(t) - x_i(t)\right) - h_i c_i(t) e_i(t). \end{aligned} \tag{10}$$

Noting that $\widetilde{L}$ is zero-row-sum, (10) can be rewritten as

$$\dot{e}_i = f_i\left(t, x_i(t)\right) - f_i(t, s(t)) - \sum_{j=1}^{N} \widetilde{l}_{ij} x_j - h_i c_i(t) e_i. \tag{11}$$

Theorem 7. *Suppose that Assumptions 1 and 5 hold. Then consensus for multiagent system* (1) *can be achieved under the control protocol* (5) *with adaptive strategy* (6) *if there exists at least one pinned-like node in the network.*

Proof. Let $H = \operatorname{diag}(h_1, h_2, \ldots, h_N)$, according to Lemma 2, $L + H$ is positive definite. Consider the following Lyapunov function candidate:

$$\begin{aligned} V\left(e_i, c_{ij}, c_i\right) = {} & \frac{1}{2} \sum_{i=1}^{N} e_i^T e_i \\ & + \frac{1}{2} \sum_{i=1}^{N} \left[\sum_{j=1, j \neq i}^{N} \frac{\left(c_{ij} - m\right)^2}{2k_{ij}} + \frac{\left(c_i - m\right)^2}{k_i} \right], \end{aligned} \tag{12}$$

where $m > \omega / \lambda_1(L+H)$, and $\lambda_1(L+H)$ denotes the minimum eigenvalue of $L + H$.

Differentiating $V(t)$ with respect to t along (11), we have

$$\begin{aligned} \dot{V}(t) = {} & \sum_{i=1}^{N} e_i^T \left(f_i\left(t, x_i(t)\right) - f_i(t, s(t))\right) \\ & - \sum_{i=1}^{N} e_i^T \left[\sum_{j=1}^{N} \widetilde{l}_{ij} x_j(t) + h_i c_i(t) e_i(t) \right] \\ & + \frac{1}{2} \sum_{i=1}^{N} \sum_{j=1, j \neq i}^{N} \left(c_{ij} - m\right) a_{ij} \left(x_j - x_i\right)^T \left(x_j - x_i\right) \\ & + \sum_{i=1}^{N} \left(c_i - m\right) h_i e_i^T e_i \\ \leq {} & \sum_{i=1}^{N} \left[\omega e_i^T e_i - m h_i e_i^T e_i - \sum_{j=1}^{N} \widetilde{l}_{ij} e_i^T x_j(t) \right. \\ & \left. + \frac{1}{2} \sum_{j=1, j \neq i}^{N} \left(c_{ij} - m\right) a_{ij} \left(x_j - x_i\right)^T \left(x_j - x_i\right) \right]. \end{aligned} \tag{13}$$

Noting that $\widetilde{L}$ is symmetric and zero-row-sum, we have

$$\begin{aligned} \sum_{i=1}^{N} \sum_{j \neq i}^{N} \left(c_{ij} - m\right) a_{ij} e_j^T e_j &= \sum_{i=1}^{N} \sum_{j \neq i}^{N} \left(c_{ij} - m\right) a_{ij} e_i^T e_i \\ &= \sum_{i=1}^{N} \left(c_{ii} - m\right) l_{ii} e_i^T e_i. \end{aligned} \tag{14}$$

According to (14), we have

$$\begin{aligned} & \sum_{i=1}^{N} \sum_{j=1, j \neq i}^{N} \left(c_{ij} - m\right) a_{ij} \left(x_j - x_i\right)^T \left(x_j - x_i\right) \\ & = \sum_{i=1}^{N} \sum_{j \neq i}^{N} \left(c_{ij} - m\right) a_{ij} \left(e_j - e_i\right)^T \left(e_j - e_i\right) \\ & = \sum_{i=1}^{N} \sum_{j \neq i}^{N} \left(c_{ij} - m\right) a_{ij} \left(e_j^T e_j + e_i^T e_i - 2 e_i^T e_j\right) \\ & = 2 \sum_{i=1}^{N} \left(c_{ii} - m\right) l_{ii} e_i^T e_i + 2 \sum_{i=1}^{N} \sum_{j \neq i}^{N} \left(c_{ij} - m\right) l_{ij} e_i^T e_j \\ & = 2 \sum_{i=1}^{N} \sum_{j=1}^{N} \left(c_{ij} - m\right) l_{ij} e_i^T e_j. \end{aligned} \tag{15}$$

So we have

$$\sum_{i=1}^{N}\sum_{j=1}^{N}\left(c_{ij}-m\right)l_{ij}e_i^Te_j = \frac{1}{2}\sum_{i=1}^{N}\sum_{j\neq i}^{N}\left(c_{ij}-m\right)a_{ij}\left(e_j-e_i\right)^T\left(e_j-e_i\right). \tag{16}$$

From ((14)–(16)), one can easily conclude the following:

$$\sum_{i=1}^{N}\sum_{j=1}^{N}\widetilde{l}_{ij}e_i^Te_j = \frac{1}{2}\sum_{i=1}^{N}\sum_{j\neq i}^{N}c_{ij}a_{ij}\left(e_j-e_i\right)^T\left(e_j-e_i\right). \tag{17}$$

From (13), (16), and (17), we have

$$\begin{aligned}\dot{V}(t) &\le \sum_{i=1}^{N}\omega e_i^Te_i - \sum_{i=1}^{N}\sum_{j=1}^{N}\widetilde{l}_{ij}e_i^Te_j \\ &\quad + \frac{1}{2}\sum_{i=1}^{N}\sum_{j=1,j\neq i}^{N}\left(c_{ij}-m\right)a_{ij}\left(e_j-e_i\right)^T\left(e_j-e_i\right) \\ &\quad - m\sum_{i=1}^{N}h_ie_i^Te_i \\ &= \sum_{i=1}^{N}\omega e_i^Te_i - \sum_{i=1}^{N}\sum_{j=1}^{N}ml_{ij}e_i^Te_j - m\sum_{i=1}^{N}h_ie_i^Te_i \\ &= e^T\left[\omega I - m\left(L+H\right)\right]e.\end{aligned} \tag{18}$$

Since $m > \omega/\lambda_1(L+H)$, $\omega I - m(L+H)$ is negative definite, which means $\dot{V}(t) \le 0$. This implies that $V(e(t), c_ij(t), c_i(t)) \le V(e(0), c_ij(0), c_i(0))$, for all $t > 0$. Therefore, e, c_ij, and c_i are bounded. Noting that c_ij and c_i are dependent on e and e is bounded, then, from Assumption 1, (13), and (18), one can know that $\ddot{V}$ is bounded. This means that $\dot{V}$ is uniformly continuous in t. Hence, according to Lemma 4, $\dot{V}(e(t), c_ij(t), c_i(t)) \to 0$ as $t \to \infty$. Again noting that $\omega I - m(L+H)$ is negative definite, one can conclude that $e(t) \to 0$, as $t \to \infty$, which means that the consensus of networked system (1) is achieved. □

Remark 8. From Theorem 7, we can know all the nodes in network (1) will asymptotically converge to the desired node s. When all the nonlinear dynamic f_i have a common solution, that is, there exists a vector $y \in R^n$, satisfied $\dot{y} = f_i(t, y)$, we can choose y as the desired node. And if all the nonlinear dynamic f_i do not have a common solution, we can choose $\overline{x} = \sum_{i=1}^{N} x_i/N$ as the desired node. And we also can obtain the distributed consensus protocol for nonlinear multiagent systems with identical nodes. Considering the network with identical nodes, the ith node of which is described as

$$\dot{x}_i = f\left(t, x_i(t)\right). \tag{19}$$

We choose the control protocol as

$$u_i(t) = \sum_{j\in N_i}c_{ij}a_{ij}\left(x_j-x_i\right) + h_ic_i\left(s-x_i\right), \tag{20}$$

where the desired state s satisfies $\dot{s} = f(t, s)$ and the adaptive strategy is designed as (6).

According to Theorem 7, we have the following corollary.

Corollary 9. *Suppose that the topology is undirected and connected and f satisfies Lipschitz condition with a Lipschitz constant $\gamma > 0$. Then, under the control protocol* (20) *with adaptive strategy* (6)*, consensus for multiagent system* (19) *can be achieved if there exists at least one pinned node in the network.*

3.2. Pinning-Like Adaptive Consensus for Second-Order Multiagent Systems with Heterogeneous Nonlinear Dynamics. In this subsection, we investigate second-order consensus of networked nonlinear multiagent system (2) via pinning-like adaptive control.

Assumption 10. For every f_i in (2) and arbitrary $u, v, x, y \in R^n$, there exist corresponding constants $\theta > 0$ such that

$$\left\|f_i(t,u,v) - f_i(t,x,y)\right\| \le \theta\left(\|u-x\| + \|v-y\|\right). \tag{21}$$

Remark 11. Choosing $\theta = \max\{\rho_1, \rho_2\}$ in [24], we can get the well-definition of Assumption 10. In fact, this condition can be satisfied by many systems. Examples include the pendulum system with a control torque, car-like robots, the Chuas circuit, the Lorenz system, and the Chen system and so forth [27].

Let

$$\widetilde{x}_i = x_i - x_0, \quad \widetilde{v}_i = v_i - v_0, \quad i = 1, 2, \ldots, N. \tag{22}$$

Synchronization or consensus for network with nonidentical nodes cannot be realized without control if the nonidentical dynamic functions do not have a common equilibrium. The purpose of this paper is to design distributed tracking consensus algorithm for networked system (1). Therefore, a distributed adaptive control protocol is proposed, under which leader-following second-order consensus for network (1) can be achieved; that is, there exists a desired state $s = (x_0^T, v_0^T)^T$, satisfying $\dot{x}_i(t) = v_0(t), \dot{v}_0(t) = f_0(t, x_0(t), v_0(t))$, such that

$$\begin{aligned}\lim_{t\to\infty}\left\|x_i(t) - x_0(t)\right\| &= 0, \\ \lim_{t\to\infty}\left\|v_i(t) - v_0(t)\right\| &= 0, \\ i &= 1, 2, \ldots, N.\end{aligned} \tag{23}$$

The following consensus protocol is designed for networked system (2):

$$\begin{aligned}u_i(t) &= \dot{v}_0(t) - f_i\left(t, x_0(t), v_0(t)\right) \\ &\quad + \sum_{j=1,j\neq i}^{N}c_{ij}a_{ij}\left(x_j-x_i\right) + h_ic_i(t)\left(x_0(t)-x_i(t)\right) \\ &\quad + \sum_{j=1,j\neq i}^{N}c_{ij}a_{ij}\left(v_j-v_i\right) + h_ic_i(t)\left(v_0(t)-v_i(t)\right), \\ &\quad i = 1, 2, \ldots, N.\end{aligned} \tag{24}$$

In the controller (3), $h_i = 1$ for some i, then the ith node is named as pinning-like node and $h_i = 0$ for others. The adaptive weights $c_{ij} > 0$, $c_i > 0$, $i, j = 1, 2, \ldots, N$ are determined by the following equations:

$$\begin{aligned}\dot{c}_{ij}(t) &= h_{ij}a_{ij}\left[\left(x_j(t) - x_i(t)\right)^T\left(x_j(t) - x_i(t)\right)\right.\\ &\quad\left. + \left(v_j(t) - v_i(t)\right)^T\left(v_j(t) - v_i(t)\right)\right],\\ &\quad i \neq j, \quad i, j = 1, 2, \ldots, N,\\ \dot{c}_i(t) &= h_i d_i\left[\left(x_0(t) - x_i(t)\right)^T\left(x_0(t) - x_i(t)\right)\right.\\ &\quad\left. + \left(v_0(t) - v_i(t)\right)^T\left(v_0(t) - v_i(t)\right)\right],\\ &\quad i = 1, 2, \ldots, N,\end{aligned} \tag{25}$$

where $h_{ij} = h_{ji} > 0$, $d_i > 0$ are the weights of adaptive laws for parameters $c_{ij}(t)$ and $c_i(t)$.

Under consensus protocol (24), the error systems can be rewritten as

$$\begin{aligned}\dot{\widetilde{x}}_i(t) &= \widetilde{v}_i(t),\\ \dot{\widetilde{v}}_i(t) &= f_i\left(t, x_i(t), v_i(t)\right) - f_i\left(t, x_0(t), v_0(t)\right)\\ &\quad + \sum_{j=1, j\neq i}^{N} c_{ij}(t)\, a_{ij}\left(\widetilde{x}_j(t) - \widetilde{x}_i(t)\right) - h_i c_i(t)\,\widetilde{x}_i(t)\\ &\quad + \sum_{j=1, j\neq i}^{N} c_{ij}(t)\, a_{ij}\left(\widetilde{v}_j(t) - \widetilde{v}_i(t)\right) - h_i c_i(t)\,\widetilde{v}_i(t),\\ &\quad i = 1, \ldots, N.\end{aligned} \tag{26}$$

The following theorem addresses a sufficient condition for the consensus of networked system (2).

Theorem 12. *Suppose that Assumptions 1 and 5 hold. Then consensus of heterogeneous nonlinear networked system* (2) *can be achieved under the control protocol* (24) *with adaptive strategy* (25) *if there exists at least one pinned-like node in the network.*

Proof. Let $Q = \begin{bmatrix} 2\widetilde{L} + 2\Delta + I_N & I_N \\ I_N & I_N \end{bmatrix}$, $\Delta = \operatorname{diag}(c_1 h_1, \ldots, c_N h_N)$. According to [19, Theorem 6.2.24], for an undirected graph G, the Laplace matrix L is irreducible if and only if G is connected. Noting that the corresponding graph of $\widetilde{L}$ has the same connectivity with L, $\widetilde{L}$ is irreducible under Assumption 5. Then one can conclude that $\widetilde{L}$ is semipositive definite according to Lemma 2. And then by virtue of *Schur* Complement Lemma, we can know that Q is positive definite.

Consider the following Lyapunov function candidate:

$$\begin{aligned}V\left(e_i, c_{ij}, c_i\right) &= \frac{1}{2}\begin{pmatrix}\widetilde{x}^T & \widetilde{v}^T\end{pmatrix} Q \begin{pmatrix}\widetilde{x} \\ \widetilde{v}\end{pmatrix}\\ &\quad + \frac{1}{2}\sum_{i=1}^{N}\left[\sum_{j=1, j\neq i}^{N}\frac{\left(c_{ij} - \alpha\right)^2}{2h_{ij}} + \frac{\left(c_i - \alpha\right)^2}{d_i}\right],\end{aligned} \tag{27}$$

where $\alpha > (2\theta + 1)/\lambda_1(L + H)$, $H = \operatorname{diag}(h_1, \ldots, h_N)$, and $\lambda_1(L + H)$ denotes the minimum eigenvalue of $(L + H)$.

Differentiating $V(t)$ with respect to t along (28), we have

$$\begin{aligned}\dot{V}(t) &= \widetilde{x}^T\left(2\widetilde{L} + 2\Delta + I_N\right)\widetilde{v} + \widetilde{x}^T\dot{\widetilde{v}} + \widetilde{v}^T\widetilde{v} + \widetilde{v}^T\dot{\widetilde{v}}\\ &\quad + \sum_{i=1}^{N}\left[\sum_{j=1, j\neq i}^{N}\frac{\left(c_{ij} - \alpha\right)\dot{c}_{ij}}{2h_{ij}} + \frac{\left(c_i - \alpha\right)\dot{c}_i}{d_i}\right]\\ &= \widetilde{x}^T\left(2\widetilde{L} + 2\Delta + I_N\right)\widetilde{v} + \widetilde{v}^T\widetilde{v}\\ &\quad + \sum_{i=1}^{N}\left(\widetilde{x}_i + \widetilde{v}_i\right)^T\left(f_i\left(t, x_i, v_i\right) - f_i\left(t, x_0, v_0\right)\right)\\ &\quad + \sum_{i=1}^{N}\left(\widetilde{x}_i + \widetilde{v}_i\right)^T\left(\sum_{j=1, j\neq i}^{N} c_{ij}a_{ij}\left(x_j - x_i\right)\right.\\ &\qquad + \sum_{j=1, j\neq i}^{N} c_{ij}a_{ij}\left(v_j - v_i\right)\\ &\qquad \left. - c_i h_i\widetilde{x}_i - c_i h_i\widetilde{v}_i\right)\\ &\quad + \frac{1}{2}\sum_{i=1}^{N}\sum_{j=1, j\neq i}^{N}\left[\left(c_{ij} - \alpha\right)a_{ij}\left(x_j - x_i\right)^T\left(x_j - x_i\right)\right.\\ &\qquad + \left(c_{ij} - \alpha\right)a_{ij}\left(v_j - v_i\right)^T\\ &\qquad \left.\times\left(v_j - v_i\right)\right]\\ &\quad + \sum_{i=1}^{N}\left(c_i - \alpha\right)h_i\widetilde{x}_i^T\widetilde{x}_i + \sum_{i=1}^{N}\left(c_i - \alpha\right)h_i\widetilde{v}_i^T\widetilde{v}_i.\end{aligned} \tag{28}$$

Noting that $\widetilde{L}$ is symmetric and zero-row-sum, similarly as (16), we have

$$\begin{aligned}&\sum_{i=1}^{N}\sum_{j=1, j\neq i}^{N}\left(c_{ij} - \alpha\right)a_{ij}\left(\widetilde{x}_j - \widetilde{x}_i\right)^T\left(\widetilde{x}_j - \widetilde{x}_i\right)\\ &\quad = 2\sum_{i=1}^{N}\sum_{j=1}^{N}\left(\widetilde{l}_{ij} - \alpha l_{ij}\right)\widetilde{x}_i^T\widetilde{x}_j,\\ &\sum_{i=1}^{N}\sum_{j=1, j\neq i}^{N}\left(c_{ij} - \alpha\right)a_{ij}\left(\widetilde{v}_j - \widetilde{v}_i\right)^T\left(\widetilde{v}_j - \widetilde{v}_i\right)\\ &\quad = 2\sum_{i=1}^{N}\sum_{j=1}^{N}\left(\widetilde{l}_{ij} - \alpha l_{ij}\right)\widetilde{v}_i^T\widetilde{v}_j.\end{aligned} \tag{29}$$

From ((11)–(13)), we have

$$\begin{aligned}\dot{V}(t) &= \tilde{x}^T\left(2\tilde{L}+2\Delta+I_N\right)\tilde{v}+\tilde{v}^T\tilde{v}\\ &\quad+\sum_{i=1}^{N}\left(\tilde{x}_i+\tilde{v}_i\right)^T\left(f_i(t,x_i,v_i)-f_i(t,x_0,v_0)\right)\\ &\quad+\sum_{i=1}^{N}\left(\tilde{x}_i+\tilde{v}_i\right)^T\left[\sum_{j=1}^{N}\left(-\tilde{l}_{ij}\left(\tilde{x}_j+\tilde{v}_j\right)\right)-c_ih_i\left(\tilde{x}_i+\tilde{v}_i\right)\right]\\ &\quad+\sum_{i=1}^{N}\sum_{j=1,j\neq i}^{N}\left[\left(\tilde{l}_{ij}-\alpha l_{ij}\right)\tilde{x}_i^Tx_j+\left(\tilde{l}_{ij}-\alpha l_{ij}\right)\tilde{v}_i^T\tilde{v}_i\right]\\ &\quad+\sum_{i=1}^{N}\left(c_i-\alpha\right)h_i\tilde{x}_i^T\tilde{x}_i+\sum_{i=1}^{N}\left(c_i-\alpha\right)h_i\tilde{v}_i^T\tilde{v}_i\\ &\le(2\theta+1)\left(\tilde{x}^T\tilde{x}+\tilde{v}^T\tilde{v}\right)\\ &\quad-\alpha\tilde{x}^T(L+H)\tilde{x}-\alpha\tilde{v}^T(L+H)\tilde{v}\\ &=\tilde{x}^T\left[(2\theta+1)I-\alpha(L+H)\right]\tilde{x}\\ &\quad+\tilde{v}^T\left[(2\theta+1)I-\alpha(L+H)\right]\tilde{v}.\end{aligned}\tag{30}$$

According to Lemma 2, $(L+H)$ is positive definite. Since $\alpha>(2\theta+1)/\lambda_1(L+H)$, $(2\theta+1)I-\alpha(L+H)$ is negative definite, which means $\dot{V}(t)\le 0$. The same to Theorem 7, by in virtue of Lemma 4, one can conclude that $\tilde{x}_i\to 0$ and $\tilde{v}_i\to 0$, as $t\to\infty$, which means that the consensus of networked system (2) is achieved. □

Remark 13. From Theorem 12, we can know that all the nodes in network (2) will asymptotically converge to the desired node s. When all the nonlinear dynamic f_i have a common solution, we can choose it as the desired node. And if all the nonlinear dynamics f_i do not have a common solution, we can choose average state as the desired node. And we also can obtain the pinning adaptive consensus control protocol for nonlinear mobile agents networked system with identical nonlinear dynamics.

When all the nonlinear function f_i, $i=1,\ldots,N$ are identical, that is, the ith node in system (1) can be described as

$$\begin{aligned}\dot{x}_i(t)&=v_i(t),\\ \dot{v}_i(t)&=f\left(t,x_i(t),v_i(t)\right)+u_i(t),\\ &\qquad i=1,\ldots,N.\end{aligned}\tag{31}$$

We choose the control protocol as

$$\begin{aligned}u_i(t)&=\sum_{j=1,j\neq i}^{N}c_{ij}a_{ij}\left(x_j-x_i\right)+h_ic_i(t)\left(x_0-x_i\right)\\ &\quad+\sum_{j=1,j\neq i}^{N}c_{ij}a_{ij}\left(v_j-v_i\right)+h_ic_i(t)\left(v_0-v_i\right),\\ &\qquad i=1,2,\ldots,N.\end{aligned}\tag{32}$$

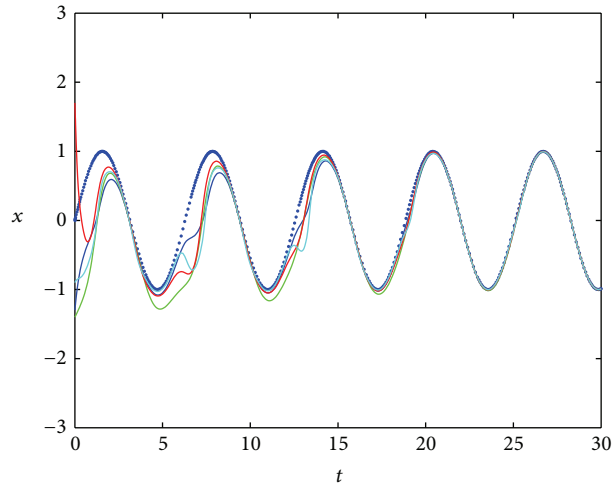

Figure 1: State trajectories of the four nodes with the reference state.

In the protocol, the adaptive weights $c_{ij}>0$, $c_i>0$, $i,j=1,2,\ldots,N$, are determined by (25). Then, from Theorem 12, one can easily obtain the following corollary.

Corollary 14. *Suppose that Assumptions 1 and 5 hold. Then consensus for nonlinear mobile multiagent networked system* (31) *can be achieved under the control protocol* (32) *with adaptive strategy* (25) *if there exists at least one pinned node in the network.*

4. Simulations

In this section, several simulation results are presented to illustrate the previous theoretical results.

Example 1. We choose a network with 4 nodes and the reference node is chosen as $\dot{v}_0(t)=\sin t$. The nonlinear dynamic functions are chosen as $f_i=\sin(ix_i+\pi/i)$, $i=1,2,3,4$, and nonlinear coupled function $g(x)=x+\tanh x$. The topology is described by the following adjacent matrix:

$$A=\begin{pmatrix}0&1&0&1\\1&0&1&0\\0&1&0&1\\1&0&1&0\end{pmatrix}.\tag{33}$$

In Figure 1, the dash dotted line denotes the state of the reference node. And other lines represent the trajectories of the nodes in the network. The trajectories of the adaptive gains are drawn in Figure 2. According to the simulation, we can know that the consensus for the proposed network can be achieved rapidly, which results in that the adaptive gains are stabilized rapidly.

Example 2. The topology is chosen the same as Example 1 and the reference node is chosen as

$$\begin{aligned}\dot{x}_0(t)&=\sin t,\\ \dot{v}_0(t)&=\cos t.\end{aligned}\tag{34}$$

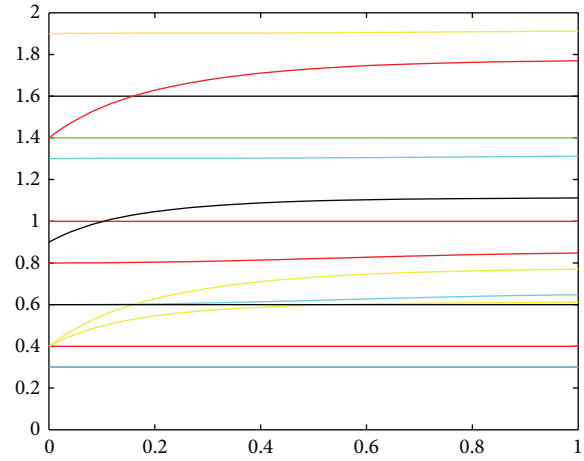

Figure 2: Trajectories of the adaptive gains.

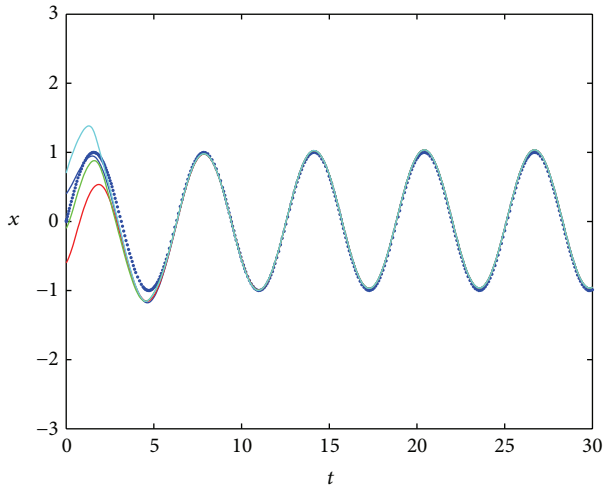

Figure 3: Trajectories for position.

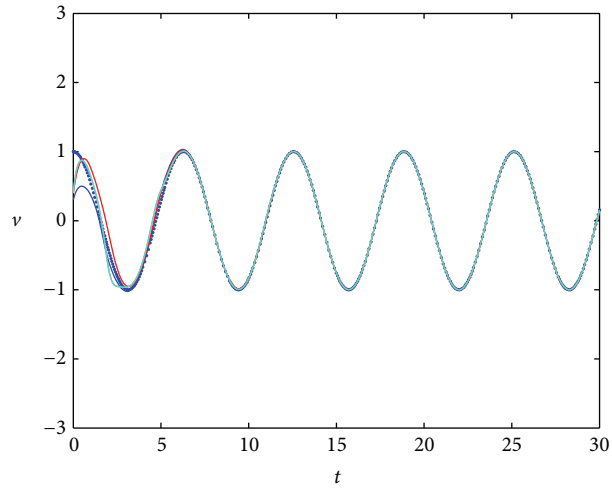

Figure 4: Trajectories for velocity.

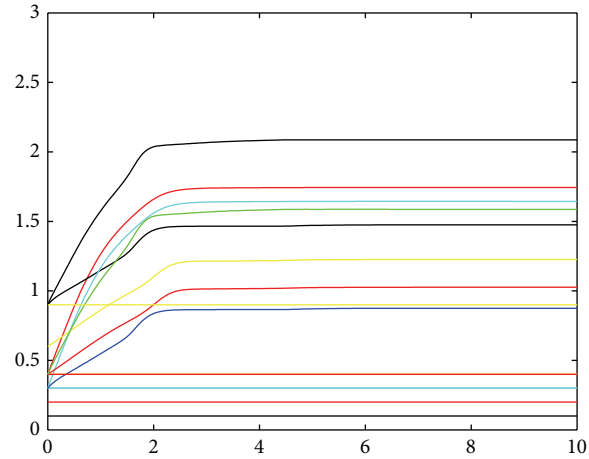

Figure 5: Trajectories of the adaptive gains.

The nonlinear dynamic functions are chosen as $f_i = \sin(ix_i + \pi/i)$, $i = 1, 2, 3, 4$. We choose the first node as the pinning-like node. In Figures 3 and 4, the dash dotted line denotes the position trajectory and the velocity trajectory of the reference node. And other lines represent the trajectories of the nodes in the network. The trajectories of the adaptive gains are drawn in Figure 5. According to Figures 3 and 4, the consensus can be achieved.

5. Conclusions

Adaptive consensus for networked mobile agents with heterogeneous nonlinear dynamics was investigated in this paper. Sufficient consensus conditions for both first-order and second-order networked mobile agents with heterogeneous nonlinear dynamics were obtained. By designing an adaptive strategy on the coupling strengths, the consensus can be achieved without requiring any global information except a connection assumption. We also extended the results to the consensus for nonlinear mobile agents with identical nonlinear dynamics. Simulation examples were given to demonstrate the feasibility and effectiveness of the proposed consensus scheme.

Conflict of Interests

The authors declare that there is no conflict of interests regarding the publication of this paper.

Acknowledgments

This work is supported by National Natural Science Foundation (NNSF) of China under Grant no. 61174075, 51375186, Natural Science Foundation of Ministry of Education in Hunan Province (12C0077), and NSF of Hunan University of Technology (2012HZX18).

References

[1] R. Olfati-Saber, J. A. Fax, and R. Murray, "Consensus and cooperation in networked multi-agent systems," *Proceedings of the IEEE*, vol. 95, no. 1, pp. 215–233, 2007.

[2] D. V. Dimarogonas and K. J. Kyriakopoulos, "On the rendezvous problem for multiple nonholonomic agents," *IEEE Transactions on Automatic Control*, vol. 52, no. 5, pp. 916–922, 2007.

[3] W. Ren and R. W. Beard, "Consensus seeking in multiagent systems under dynamically changing interaction topologies," *IEEE Transactions on Automatic Control*, vol. 50, no. 5, pp. 655–661, 2005.

[4] Y. Chen, J. Lü, and Z. Lin, "Consensus of discrete-time multi-agent systems with transmission nonlinearity," *Automatica*, vol. 49, no. 6, pp. 1768–1775, 2013.

[5] P. Lin and Y. M. Jia, "Multi-agent consensus with diverse time-delays and jointly-connected topologies," *Automatica*, vol. 47, no. 4, pp. 848–856, 2011.

[6] Z. J. Tang, T. Z. Huang, J. L. Shao, and J. P. Hu, "Leader-following consensus for multi-agent systems via sampled-data control," *IET Control Theory & Applications*, vol. 5, no. 14, pp. 1658–1665, 2011.

[7] Y. G. Hong, J. P. Hu, and L. Gao, "Tracking control for multi-agent consensus with an active leader and variable topology," *Automatica*, vol. 42, no. 7, pp. 1177–1182, 2006.

[8] H. S. Su, G. Chen, X. F. Wang, and Z. L. Lin, "Adaptive second-order consensus of networked mobile agents with nonlinear dynamics," *Automatica*, vol. 47, no. 2, pp. 368–375, 2011.

[9] M. Ji, G. Ferrari-Trecate, M. Egerstedt, and A. Buffa, "Containment control in mobile networks," *IEEE Transactions on Automatic Control*, vol. 53, no. 8, pp. 1972–1975, 2008.

[10] Y. Cao, W. Ren, and M. Egerstedt, "Distributed containment control with multiple stationary or dynamic leaders in fixed and switching directed networks," *Automatica*, vol. 48, no. 8, pp. 1586–1597, 2012.

[11] J. Li, W. Ren, and S. Xu, "Distributed containment control with multiple dynamic leaders for double-integrator dynamics using only position measurements," *IEEE Transactions on Automatic Control*, vol. 57, no. 6, pp. 1553–1559, 2012.

[12] K. Hengster-Movric and F. Lewis, "Cooperative observers and regulators for discrete-time multiagent systems," *International Journal of Robust and Nonlinear Control*, vol. 23, no. 14, pp. 1545–1562, 2013.

[13] C. Xu, Y. Zheng, H. Su, C. Zhang, and M. Chen, "Necessary and sufficient conditions for dis tributed containment control of multi-agent systems without velocity measurement," *IET Control Theory & Applications*, 2014.

[14] R. Olfati-Saber, "Flocking for multi-agent dynamic systems: algorithms and theory," *IEEE Transactions on Automatic Control*, vol. 51, no. 3, pp. 401–420, 2006.

[15] H. S. Su, X. F. Wang, and Z. L. Lin, "Flocking of multi-agents with a virtual leader," *IEEE Transactions on Automatic Control*, vol. 54, no. 2, pp. 293–307, 2009.

[16] R. Olfati-Saber and R. M. Murray, "Consensus problems in networks of agents with switching topology and time-delays," *IEEE Transactions on Automatic Control*, vol. 49, no. 9, pp. 1520–1533, 2004.

[17] G. Xie and L. Wang, "Consensus control for a class of networks of dynamic agents," *International Journal of Robust and Nonlinear Control*, vol. 17, no. 10-11, pp. 941–959, 2007.

[18] Y. Tian and C. Liu, "Consensus of multi-agent systems with diverse input and communication delays," *IEEE Transactions on Automatic Control*, vol. 53, no. 9, pp. 2122–2128, 2008.

[19] A. Abdessameud and A. Tayebi, "On consensus algorithms for double-integrator dynamics without velocity measurements and with input constraints," *Systems & Control Letters*, vol. 59, no. 12, pp. 812–821, 2010.

[20] W. Ren, "On consensus algorithms for double-integrator dynamics," *IEEE Transactions on Automatic Control*, vol. 53, no. 6, pp. 1503–1509, 2008.

[21] Q. Ma, S. Xu, and F. L. Lewis, "Second-order consensus for directed multi-agent systems with sampled data," *International Journal of Robust and Nonlinear Control*, 2013.

[22] H. S. Su, M. Z. Q. Chen, J. Lam, and Z. Lin, "Semi-global leader-following consensus of linear multi-agent systems with input saturation via low gain feedback," *IEEE Transactions on Circuits and Systems I: Regular Papers*, vol. 60, no. 7, pp. 1881–1889, 2013.

[23] H. S. Su, M. Z. Q. Chen, X. F. Wang, and J. Lam, "Semiglobal observer-based leader-following consensus with input saturation," *IEEE Transactions on Industrial Electronics*, vol. 61, no. 6, pp. 2842–2850, 2013.

[24] W. W. Yu, G. R. Chen, M. Cao, and J. Kurths, "Second-Order consensus for multiagent systems with directed topologies and nonlinear dynamics," *IEEE Transactions on Systems, Man, and Cybernetics B: Cybernetics*, vol. 40, no. 3, pp. 881–891, 2010.

[25] Q. Jia and W. K. S. Tang, "Consensus of nonlinear agents in directed network with switching topology and communication delay," *IEEE Transactions on Circuits and Systems I: Regular Papers*, vol. 59, no. 12, pp. 3015–3023, 2012.

[26] Q. Song, J. Cao, and W. Yu, "Second-order leader-following consensus of nonlinear multi-agent systems via pinning control," *Systems and Control Letters*, vol. 59, no. 9, pp. 553–562, 2010.

[27] J. Mei, W. Ren, and G. Ma, "Distributed coordination for second-order multi-agent systems with nonlinear dynamics using only relative position measurements," *Automatica*, vol. 49, no. 5, pp. 1419–1427, 2013.

[28] B. Liu, X. L. Wang, H. S. Su, Y. P. Gao, and L. Wang, "Adaptive second-order consensus of multi-agent systems with heterogeneous nonlinear dynamics and time-varying delays," *Neurocomputing*, vol. 118, pp. 289–300, 2013.

[29] Z. Y. Meng, Z. L. Lin, and W. Ren, "Robust cooperative tracking for multiple non-identical second-order nonlinear systems," *Automatica*, vol. 49, no. 8, pp. 2363–2372, 2013.

[30] B. Liu and D. J. Hill, "Impulsive consensus for complex dynamical networks with nonidentical nodes and coupling time-delays," *SIAM Journal on Control and Optimization*, vol. 49, no. 2, pp. 315–338, 2011.

[31] J. H. Qin, W. X. Zheng, and H. J. Gao, "Consensus of multiple second-order vehicles with a time-varying reference signal under directed topology," *Automatica*, vol. 47, no. 9, pp. 1983–1991, 2011.

[32] H. S. Su, Z. H. Rong, M. Z. Q. Chen, X. F. Wang, G. R. Chen, and H. W. Wang, "Decentralized adaptive pinning control for cluster synchronization of complex dynamical networks," *IEEE Transactions on Cybernetics*, vol. 43, no. 1, pp. 394–399, 2013.

[33] M. Wang, H. Su, M. Zhao, M. Z. Q. Chen, and H. Wang, "Flocking of multiple autonomous agents with preserved network connectivity and heterogeneous nonlinear dynamics," *Neurocomputing*, vol. 115, pp. 169–177, 2013.

[34] R. A. Horn and C. R. Johnson, *Matrix analysis*, Cambridge University Press, Cambridge, UK, 1985.

[35] J. J. E. Slotine and W. Li, *Applied Nonlinear Control*, Prentice-Hall, Englewood Cliffs, NJ, USA, 1991.

Hindawi Publishing Corporation
Mathematical Problems in Engineering
Volume 2014, Article ID 834698, 7 pages
http://dx.doi.org/10.1155/2014/834698

Research Article

Design of the Congestion Control for TCP/AQM Network with Time-Delay

Dazhong Wang and Shujing Wu

Shanghai University of Engineering Science, Shanghai 201620, China

Correspondence should be addressed to Dazhong Wang; wdzh168@hotmail.com

Received 8 July 2014; Accepted 20 August 2014; Published 25 September 2014

Academic Editor: Housheng Su

The purpose of this paper is to design congestion controller for TCP/AQM (transmission control protocol/active queue management) networks using model following control; the equilibrium of a class of TCP/AQM networks with time-delay is investigated, and the effect of communication time-delay on the stability is addressed. The features of this design method are bounded property of the internal states of the control system being given and the utility of this control. Such design exhibits important attributes including fast convergence with high accuracy to a desired queue length. Simulation results show that the time-delay nonlinear behavior of the system can be controlled by this method.

1. Introduction

In recent years, with the rapid growth of throughput-demanding applications, congestion control has emerged as a major issue in computer and communication network design [1]. So many researchers are seeking some methods to effectively control congestion. TCP congestion control mechanism is used to prevent congestion collapse.

AQM schemes have been proposed to complement the TCP network congestion control [2]. Several mathematical models are developed by some researchers [3–5] and a variety of control theory-based AQM schemes are proposed based on these models. The simulated approaches contain a wide range of variations in network topologies, topological parameters, load and capacity, and traffic mixtures. The outperformance of the PFC-AQM in comparison with the commonest AQM methods such as the RED (random early detection), PI, and REM (random early marking) emphasizes the proper applicability of PFC as an AQM method [6–9]. Based on the system model for congestion control in transmission control protocol TCP/AQM networks, control theory-based approaches are utilized either to analyze or to design the AQM schemes. Based on the system model, several conventional controllers [10–15] are designed as AQM methods in TCP networks.

The design of some communication systems requires the implementation of time-delays within the system. These time-delays can be accomplished with a variety of optics technologies, which could be readily fabricated and integrated into the communication system without significant impacts on the system design [16–19]. Time-delay is very important for the modeling of networks, occurring both in the control of networks and in the control over networks [20]. In the context of communication networks, the term "congestion control" is generally used to refer to the action of regulating various flows within a network. In recent years, intense research efforts are devoted to the application of the Smith predictor for queue length control of ATM (asynchronous transfer mode) networks [21]. The TCP was designed in the late 1983s by Jacobson, which is a critical part of the internet machinery.

The purpose of this paper is to design a congestion controller based on the model following control system (MFCS) [22, 23] control theory. The features of this design method are that bounded property of the internal state of the system, which is given and confirmed on basis of a numerical example of the network congestion system in which the output signal of the control system asymptotically follows the reference model signal in the case of the existence of disturbances.

The paper is organized as follows. In Section 2, the TCP/AQM network in congestion control model is described. In Section 3, controller design of the network congestion system with time-delay is proposed. In Section 4, bounded analysis of control system internal state is shown. Section 5 is the simulation results. The paper is concluded in Section 6.

2. The TCP/AQM Networks in Congestion Control Model

In this paper, the network in Figure 1 is considered. The network consists of n nodes (sender), 1 node (receiver), and 1 bottleneck router. The bottleneck router sends packets from these senders to the receiver. This network topology denotes 1 server machine to multiple client machines in a computer network. TCP is only the communication protocol in Figure 1. Large-scale networks can be simplified as in Figure 1 in case of designing congestion controllers if only one router is bottleneck in the large-scale computer network.

In this approach, we overview the dynamical fluid-flow model developed by [24–29] to describe the behavior of TCP/AQM networks. A simplified version of that system model is considered, which ignores the timeout and slow start mechanism of TCP. The model involves the average value of key network variables and is described by the following coupled nonlinear differential equations with time-delay [25]:

$$\dot{W}(t) = \frac{1}{R(t)} - \frac{W(t)}{2}\frac{W(t-R(t))}{R(t-R(t))}p(t-R(t)), \quad (1)$$

$$\dot{q}(t) = \frac{W(t)}{R(t)}N(t) - D(t), \quad (2)$$

$$R(t) = \frac{q(t)}{D(t)} + T_p, \quad (3)$$

where $W(t)$ is the congestion window size in packets at time t, $q(t)$ is the queue length at the congested router in packets, $R(t)$ is the RTT (round trip time) which represents the time-delay in TCP dynamics in seconds, $D(t)$ is the link capacity in packets per second, T_p is the propagation time-delay in seconds, $N(t)$ is the number of active TCP connections, and $p(t)$ is the packet mark/drop probability.

These differential equations in the block diagram of Figure 2 are taken from [24] highlighting TCP window-control and queue dynamics.

Set up a model for nonlinear TCP networks dynamic model. Let $x_1(t) = q(t) - q_0$, $x_2(t) = \dot{x}_1(t)$, and $u(t) = p(t)$, where q_0 is a desired queue length in the router. Assume that the rate of the change for $x_1(t)$, $N(t)$, $C(t)$, and $R(t)$ is slower than $W(t)$, $q(t)$; (1) can be expressed in the following form [30]:

$$\dot{x}(t) = f(x(t)) + g(x(t))\,u(t-R(t)), \quad (4)$$

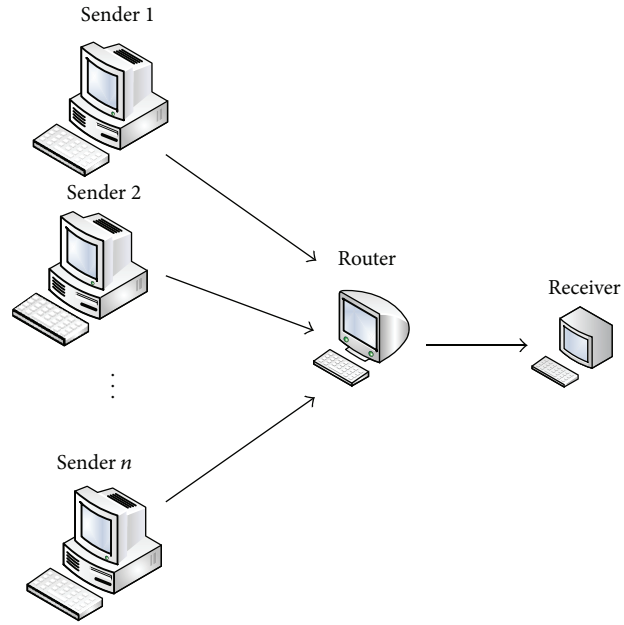

Figure 1: The network of the congestion control.

where

$$\begin{aligned} x(t) &= [x_1(t) \;\; x_2(t)]^T, \\ f(x(t)) &= [f_1(x(t)) \;\; f_2(x(t))]^T, \\ g(x(t)) &= [g_1(x(t)) \;\; g_2(x(t))]^T, \\ f_1(x(t)) &= x_2(t), \\ f_2(x(t)) &= \frac{N(t)}{R^2(t)}, \\ g_1(x(t)) &= -\frac{[(x_2(t) + C(t)] + [x_2(t-R(t)) + C(t)]}{2N(t)}. \end{aligned} \quad (5)$$

Therefore, the system is defined by

$$\dot{x}(t) = f(x(t), u(t-R(t))), \quad (6)$$

$$y(t) = [0 \;\; 1]\,x(t). \quad (7)$$

3. Controller Design of the Network Congestion System with Time-Delay

Based on (6), the system in (4) can be rewritten in equivalent form as follows:

$$\begin{aligned} \dot{x}(t) &= A_{11}x(t) + A_{12}u(t) + f_1(x(t), u(t-R(t))), \\ \dot{u}(t) &= A_{21}x(t) + A_{22}u(t) + g_1(x(t), u(t)) + Bu_1(t), \end{aligned} \quad (8)$$

where $A_{11} \in R^{n\times n}$, $A_{12} \in R^{n\times l}$, $A_{21} \in R^{l\times n}$, and $A_{22} \in R^{l\times l}$.

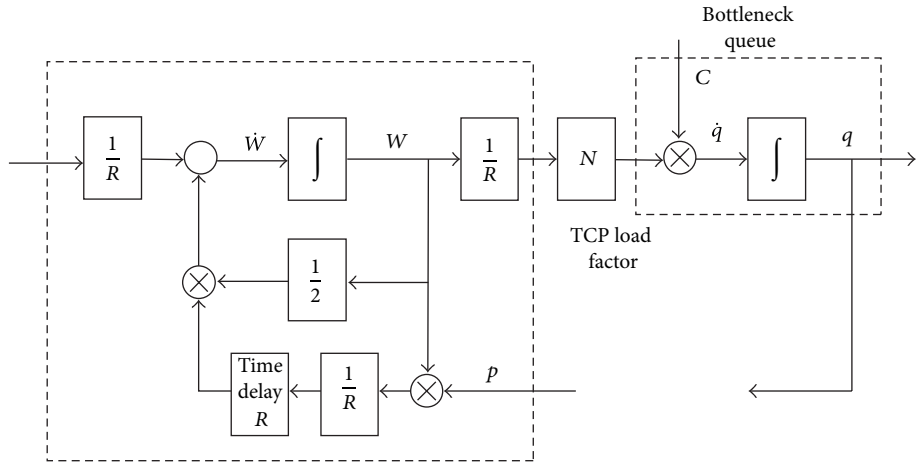

Figure 2: Block diagram of TCP congestion avoidance mode.

Then, from (8), we can obtain the following system:

$$\dot{x}_1(t) = A_1 x_1(t) + B_1 u_1(t) + f_2(x_1(t)), \quad y(t) = C_1 x_1(t), \tag{9}$$

where

$$\begin{aligned} x_1(t) &= [x(t) \;\; u(t)]^T, \\ f_2(x_1(t)) &= [f_1(x_1(t)) \;\; g_1(x_1(t))]^T, \\ f_1(x_1(t)) &= f(x_1(t)) - A_{11}x(t) - A_{12}u(t), \\ A_1 &= \begin{bmatrix} A_{11} & A_{12} \\ A_{21} & A_{22} \end{bmatrix}, \\ B_1 &= [0 \;\; B]^T, \\ C_1 &= [C \;\; 0]. \end{aligned} \tag{10}$$

Let $p = d/dt$; we have

$$y(t) = C_1[pI - A_1]^{-1}B_1 u_1(t) + C_1[pI - A_1]^{-1} f_2(x_1(t)). \tag{11}$$

Then the representations of input-output are given as

$$\begin{aligned} D(p)\,y(t) &= N(p)\,u_1(t) + N_f(p)\,f_2(x_1(t)) \\ &= N_r p^{n+l-2} u_1(t) + N_1(p)\,u_1(t) \\ &\quad + C_1 p^{n+l-2} \frac{d}{dt} f_2(x_1(t)) + N_{f_1}(p)\,f_2(x_1(t)), \end{aligned} \tag{12}$$

where $N(p)/D(p) = C_1[pI - A_1]^{-1}B_1$,

$$\begin{aligned} N_f(p) &= C_1 \mathrm{adj}(pI - A_1), \\ N(p) &= N_r p^{n+l-2} + N_1(p), \\ N_f(p) &= C_1 p^{n+l-1} + N_{f_1}(p). \end{aligned} \tag{13}$$

Now we have

$$\begin{aligned} D(p)\,y(t) &= p^{n+l-2}\left(C\frac{\partial f(x_1(t))}{\partial u^T(t)}B\right)u_1(t) \\ &\quad + N_1(p)\,u_1(t) + p^{n+l-2} \\ &\quad \times \left\{C\left(\frac{\partial f(x_1(t))}{\partial u^T(t)} - A_{12}\right)\right. \\ &\qquad \times (A_{21}x(t) + A_{22}u(t) + g_1(x_1(t))) \\ &\qquad \left. + C\left(\frac{\partial f(x_1(t))}{\partial x^T(t)} - A_{11}\right) f(x_1(t))\right\} \\ &\quad + N_{f_1}(p)\,f_2(x_1(t)) \\ &= p^{n+l-2}\left(C\frac{\partial f(x_1(t))}{\partial u^T(t)}B\right)u_1(t) + N_1(p)\,u_1(t) \\ &\quad + p^{n+l-2}\left\{C\left(\frac{\partial f(x_1(t))}{\partial u^T(t)} - A_{12}\right)\right. \\ &\qquad \times (A_{21}x(t) + A_{22}u(t) + g_1(x_1(t))) \\ &\qquad \left. + C\left(\frac{\partial f(x_1(t))}{\partial x^T(t)} - A_{11}\right) f(x_1(t))\right\} \\ &\quad + C_1\Gamma_{n+l-2}p^{n+l-2} f_2(x_1(t)) \\ &\quad + N_{f_2}(p)\,f_2(x_1(t)), \end{aligned} \tag{14}$$

where $N_{f_1}(p) = C_1\Gamma_{n+l-2}p^{n+l-2} + N_{f_2}(p)$.

Let

$$\begin{aligned}\Gamma_{n+l-1} &= I,\\ \Gamma_{n+l-2} &= A_1\Gamma_{n+l-1} + \alpha_{n+l-1}I\\ &= A_1 + \alpha_{n+l-1}I\\ &= A_1 - T_r(A_1)I,\end{aligned} \tag{15}$$

where $\alpha_{n+l-1} = -T_r(A_1)$.

Now the representations of input-output (12) are given as follows:

$$\begin{aligned}D(p)y(t) &= p^{n+l-2}\left(C\frac{\partial f(x_1(t))}{\partial u^T(t)}B\right)u_1(t)\\ &\quad + N_1(p)u_1(t) + p^{n+l-2}f_4(x_1(t))\\ &\quad + N_{f_2}(p)f_2(x_1(t)),\end{aligned} \tag{16}$$

where

$$\begin{aligned}f_4(x_1(t)) &= C\left\{\left(\frac{\partial f(x_1(t))}{\partial x^T(t)} - T_r(A_1)I\right)f(x_1(t))\right.\\ &\quad + \left(\frac{\partial f(x_1(t))}{\partial u^T(t)}\right)g_1(x_1(t))\\ &\quad + \left(\frac{\partial f(x_1(t))}{\partial u^T(t)} - A_{12}\right)\\ &\quad \cdot (A_{21}x(t) + A_{22}u(t)) + (T_r(A_1)I - A_{11})\\ &\quad \left.\cdot (A_{11}x(t) + A_{12}u(t))\right\}.\end{aligned} \tag{17}$$

Let $N_r v_z(t) = (C(\partial f(x_1(t))/\partial u^T(t))B)u_1(t) + f_4(x_1(t))$.

We have

$$\begin{aligned}D(p)y(t) &= p^{n+l-2}N_r v_z(t) + N_1(p)u_1(t)\\ &\quad + N_{f_2}(p)f_2(x_1(t)).\end{aligned} \tag{18}$$

The reference model is given as

$$\begin{aligned}\dot{x}_m(t) &= A_m x_m(t) + B_m r_m(t)\\ y_m(t) &= C_m x_m(t).\end{aligned} \tag{19}$$

Choose a stable polynomial $T(p)$ which satisfies the following conditions. (1) The degree of $T(p)$ is $\rho \geq n_d + 2n - n_m - 2 - \eta_i$. (2) The coefficient of the maximum degree term of $T(p)$ is the same as $D(p)$.

Consider the following equation:

$$T(p)D_m(p) = D_d(p)D(p)R(p) + S(p), \tag{20}$$

where the degree of each polynomial is $\partial T(p) = \rho$, $\partial D_m(p) = n_m$, $\partial D_d(p) = n_d$, $\partial D(p) = n$, $\partial R(p) = \rho + n_m - n_d - n$, and $\partial S(p) \leq n_d + n - 1$. $T(p)$, $D_m(p)$, $D_d(p)$, $D(p)$, and $R(p)$ are monic polynomials.

In this paper, we propose a design of model following control system with disturbances. We can prove that all the internal states are bounded and output error

$$e(t) = y(t) - y_m(t) \tag{21}$$

converges to zero asymptotically. Then the following form is obtained:

$$\begin{aligned}&T(p)D_m(p)e(t)\\ &\quad = D_d(p)R(p)\left\{p^{n+l-2}N_r v_z(t)\right.\\ &\qquad \left. + N_1(p)u_1(t) + N_{f_2}(p)f_2(x_1(t))\right\}\\ &\qquad + S(p)y(t) - T(p)D_m(p)y_m(t),\end{aligned} \tag{22}$$

where $N_1(p) = \sum_{k=0}^{n+l-3} C_1\Gamma_k p^k B_1 = N_{f_2}(p)B_1$.

The control law (controller) $v_z(t)$ can be obtained by making the right-hand side of (22) equal to zero.

Thus,

$$\begin{aligned}v_z(t) &= -N_r^{-1}Q(p)^{-1}\left\{D_d(p)R(p)p^{n+l-2} - Q(p)\right\}N_r v_z(t)\\ &\quad - N_r^{-1}Q(p)^{-1}D_d(p)R(p)N_{f_2}(p)\\ &\quad \cdot \{B_1u_1 + f_2(x_1(t))\}\\ &\quad - N_r^{-1}Q(p)^{-1}S(p)y(t) + r_m(t),\\ v_m(t) &= N_r^{-1}Q(p)^{-1}T(p)N_m(p)r_m(t).\end{aligned} \tag{23}$$

Therefore, $v_z(t)$ of (22) is obtained from $e(t) = 0$. The model following control system can be realized if the system internal states are bounded.

4. Bounded Analysis of Control System Internal State

Let $z_1(t) = \left[x_1^T(t)\ \ \xi_1^T(t)\ \ \xi_2^T(t)\ \ \xi_3^T(t)\right]^T$; then the system is defined by

$$\begin{aligned}\dot{z}_1(t) &= A_s + \psi(z_1(t)),\\ x_1(t) &= C_s z_1(t),\end{aligned} \tag{24}$$

where

$$A_s = \begin{bmatrix} A_1 - B_1E_2C_1 & -B_1H_1 & -B_1H_2 & -B_1H_3 \\ -G_1E_2C_1 & F_1 - G_1H_1 & -G_1H_2 & -G_1H_3 \\ G_2C_1 & 0 & F_2 & 0 \\ -G_3B_1E_2C_1 & -G_3B_1H_1 & -G_3B_1H_2 & F_3 - G_3B_1H_3 \end{bmatrix},$$

$$C_s = \begin{bmatrix} I & 0 & 0 & 0 \end{bmatrix},$$

$$\psi(z_1(t)) = f_2(x_1(t)) - B_1\left(C\frac{\partial f(x_1(t))}{\partial u^T(t)}B\right)^{-1} \cdot \left(W(x_1(t))\, v_z(t) + f_4(x_1(t))\right),$$

$$\psi(z_2(t)) = G_3\left(f_2(x_1(t)) - B_1\left(C\frac{\partial f(x_1(t))}{\partial u^T(t)}B\right)^{-1} f_4(x_1(t))\right) = G_3B_1\left(C\frac{\partial f(x_1(t))}{\partial u^T(t)}B\right)^{-1} W(x_1(t))\, v_z,$$

$$C\frac{\partial f(x_1(t))}{\partial u^T(t)}B = N_r + W(x_1(t)). \tag{25}$$

The characteristic polynomial $|pI - A_s|$ can be calculated as follows:

$$|pI - A_s| = |Q(p)|^2 V_s(p)\, T(p)^l D_m(p)^l \tag{26}$$

with stable polynomials of $T(p)$, $D_m(p)$, $|Q(p)|$, and $V_s(p)$. Therefore, A_s is also a stable system matrix.

Now, the system can be rewritten as

$$\dot{z}_2(t) = A_s z_2(t) + \psi(z_1(t)), \tag{27}$$

$$x_1(t) = C_s z_2(t). \tag{28}$$

Consider a quadratic Lyapunov function candidate:

$$V(t) = \frac{1}{2} z_2^T(t)\, P_s z_2(t), \tag{29}$$

$$\dot{V}(t) = z_2^T(t)\, P_s\left(A_s z_2(t) + \psi(z_1(t))\right) = -\frac{1}{2} z_2^T(t)\, Q_s z_2(t) + z_2^T(t)\, P_s \psi(z_1(t)) \le z_2^T(t)\, P_s \psi(z_1(t)) < 0, \tag{30}$$

$$P_s A_s + A_s^T P_s = -Q_s, \tag{31}$$

where Q_s and P_s are symmetric positive definite matrices defined by (27). If A_s is a stable matrix, we can get a unique P_s from (31) when Q_s is given. Therefore, $z_2(t)$ is bounded.

5. Simulation Results

This simulation, which proposes static state feedback AQM controller for the time-delay system, verifies the performance.

Table 1: Sender 1-2 node and receiver node parameters.

Parameter	Value
Application	ftp
Transport layer protocol	TCP
TCP agent SACK bit	False
Packet size	1448 (byte)
Acknowledgment size	40 (byte)
Flow number (TCP session number) (disturbance)	8 (+1) (flow)

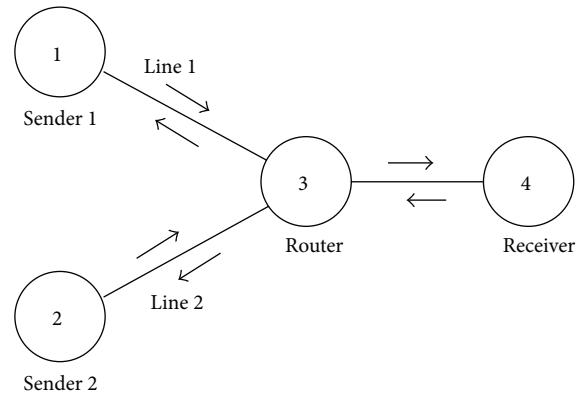

Figure 3: The network topology.

The network topology is simple and it is shown in Figure 3. But this small-scale network is developed by using four computers, and some experiments are carried out.

This network consists of two senders with four data flows (this means four sessions and $N = 8$), one bottleneck router, and one receiver, which receives data from senders through the bottleneck router (see Table 1).

In the responses (Figures 4, 5, and 6) of the congestion system with time-delay, the output errors converge to zero. So the effectiveness of this method is verified.

6. Conclusions

In this paper, a new design method for the congestion controller of the TCP/AQM networks is introduced. The developed approach can theoretically guarantee the system performances, including the disturbance rejection and the implied stability of the closed-loop system. This property is useful for congestion controller design. This paper studies a control system with time-delay using a model following method which is one of the effective means of solving time-delay problems in a control system. The method can efficaciously control time-delay under disturbances and has excellent practicability.

By using this model, the nonlinear input time-delay system, which describes a TCP/AQM network, is transformed into an equivalent nonlinear system, and it is possible to design controllers based on nonlinear control theories. For a congestion control problem, a round packet trip time is

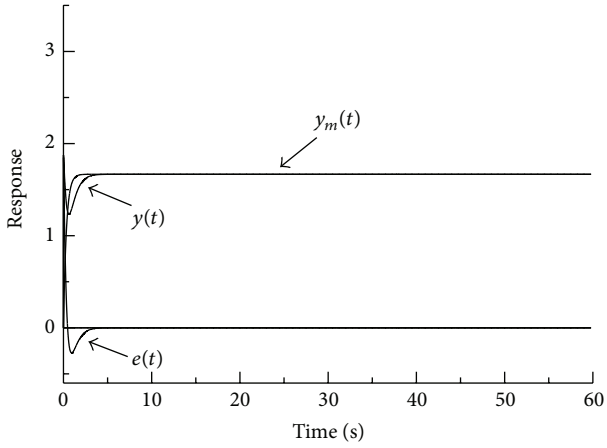

Figure 4: Responses of the congestion system with time-delay (the reference queue size is $\overline{q}_0 = 1.7$ (packets); time-delay is 0.12 (ms)).

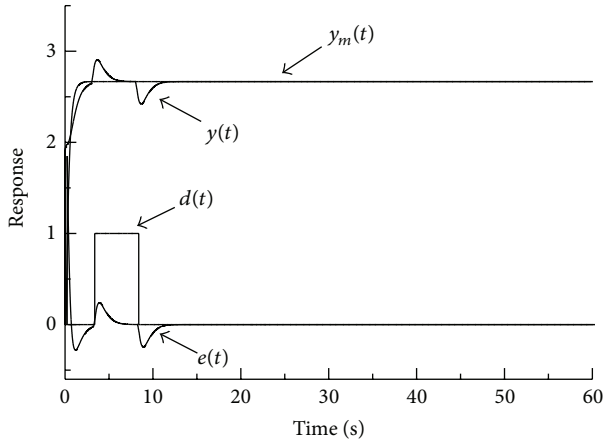

Figure 5: Responses of the congestion system with time-delay (the reference queue size is $\overline{q}_0 = 2.7$ (packets), time-delay is 12 (ms), and $d(t)$ is white noises).

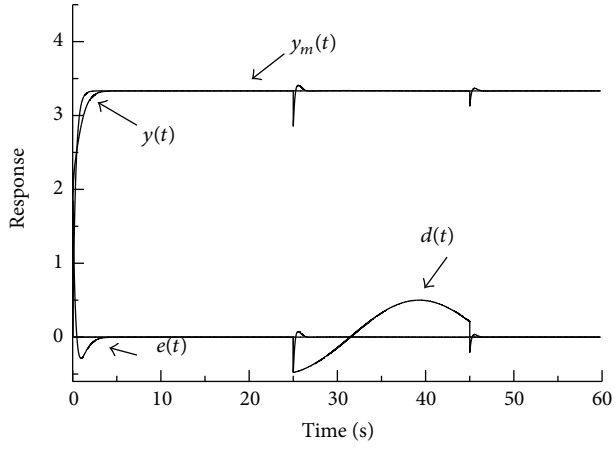

Figure 6: Responses of the congestion system with time-delay (the reference queue size is $\overline{q}_0 = 3.3$ (packets), time-delay is 0.1 (ms), and $d(t)$ is white noises).

not stationary and depends on the actual traffic. Finally, it is pointed out that the effectiveness of the proposed approach is only verified via simulations.

Conflict of Interests

The authors declare that there is no conflict of interests regarding the publication of this paper.

Acknowledgments

This work was financially supported by the Shanghai University of Engineering Science Development Fund to cultivate high-level special project (2012gp02). The authors would like to thank the editor and the reviewers for their constructive comments and suggestions which improved the quality of the paper.

References

[1] R. Barzamini, M. Shafiee, and A. Dadlani, "Adaptive generalized minimum variance congestion controller for dynamic TCP/AQM networks," *Computer Communications*, vol. 35, no. 2, pp. 170–178, 2012.

[2] Y. Jing, H. Wang, W. Pan, and X. Liu, "Robust stability analysis for uncertain state and input delay TCP/AQM network systems," in *Proceedings of the American Control Conference (ACC '08)*, pp. 2643–2647, Seattle, Wash, USA, June 2008.

[3] F. P. Kelly, A. K. Maulloo, and D. Tan, "Rate control for communication networks: shadow prices, proportional fairness and stability," *Journal of the Operational Research Society*, vol. 49, no. 3, pp. 237–252, 1998.

[4] S. H. Low, "A duality model of TCP and queue management algorithms," *IEEE/ACM Transactions on Networking*, vol. 11, no. 4, pp. 525–536, 2003.

[5] C. V. Hollot, Y. Liu, V. Misra, and D. Towsly, "Unresponsive flows and AQM performance," in *Proceedings of the 22nd Annual Joint Conference of the IEEE Computer and Communications (INFOCOM '03)*, vol. 1, pp. 85–95, March-April 2003.

[6] N. Bigdeli and M. Haeri, "Predictive functional control for active queue management in congested TCP/IP networks," *ISA Transactions*, vol. 48, no. 1, pp. 107–121, 2009.

[7] S. Manfredi, M. di Bernardo, and F. Garofalo, "Design, validation and experimental testing of a robust AQM control," *Control Engineering Practice*, vol. 17, no. 3, pp. 394–407, 2009.

[8] F. Zheng and J. Nelson, "An H_∞ approach to the controller design of AQM routers supporting TCP flows," *Automatica*, vol. 45, no. 3, pp. 757–763, 2009.

[9] K. Tsumura, S. Hara, and A. Nakajima, "H_2 performance limitation of congestion controller for TCP/AQM network systems," in *Proceedings of the 44th IEEE Conference on Decision and Control, and the European Control Conference (CDC-ECC '05)*, pp. 6768–6773, Seville, Spain, December 2005.

[10] J. Sun, K.-T. Ko, G. Chen, S. Chan, and M. Zukerman, "PD-RED: to improve the performance of RED," *IEEE Communications Letters*, vol. 7, no. 8, pp. 406–408, 2003.

[11] M. F. Firuzi and M. Haeri, "Adaptive generalized predictive control of active queue management in TCP networks," in *Proceedings of the The International Conference on Computer as a Tool (EUROCON 2005)*, pp. 676–679, Belgrade, Serbia, November 2005.

[12] L. Tan, W. Zhang, G. Peng, and G. Chen, "Stability of TCP/RED systems in AQM routers," *IEEE Transactions on Automatic Control*, vol. 51, no. 8, pp. 1393–1398, 2006.

[13] N. Bigdeli and M. Haeri, "CDM-based design and performance evaluation of a robust AQM method for dynamic TCP/AQM networks," *Computer Communications*, vol. 32, no. 1, pp. 213–229, 2009.

[14] V. Misra, W. B. Gong, and D. Towsley, "Fluid-based analysis of a network of AQM routers supporting TCP flows with an application to RED," in *Proceedings of the ACM SIGCOMMConference*, pp. 151–160, September 2000.

[15] C. Hollot, V. Misra, D. Towsley, and W. Gong, "On designing improved controllers for AQM routers supporting TCP flows," in *Proceedings of 20th Annual Joint Conference of the IEEE Computer and Communications Societies (INFOCOM '01)*, vol. 3, pp. 1726–1734, IEEE, Anchorage, Alaska, USA, 2001.

[16] S. Floyd and V. Jacobson, "Random early detection gateways for congestion avoidance," *IEEE/ACM Transactions on Networking*, vol. 1, no. 4, pp. 397–413, 1993.

[17] D. Anick, D. Mitra, and M. M. Sondhi, "Stochastic theory of a data-handling system with multiple sources," *The Bell System Technical Journal*, vol. 61, no. 8, pp. 1871–1894, 1982.

[18] S. Mascolo, "Congestion control in high-speed communication networks using the Smith principle," *Automatica*, vol. 35, no. 12, pp. 1921–1935, 1999.

[19] Y. G. Zheng and Z. H. Wang, "Stability and Hopf bifurcation of a class of TCP/AQM networks," *Nonlinear Analysis: Real World Applications*, vol. 11, no. 3, pp. 1552–1559, 2010.

[20] J. Chiasson and J. Loiseau, *Applications of Time Delay Systems*, Springer, Berlin, Germany, 2007.

[21] S. Mascolo, "Smith's principle for congestion control in high-speed data networks," *IEEE Transactions on Automatic Control*, vol. 45, no. 2, pp. 358–364, 2000.

[22] S. Wu, S. Okubo, and D. Wang, "Design of a model following control system for nonlinear descriptor system in discrete time," *Kybernetika*, vol. 44, no. 4, pp. 546–556, 2008.

[23] D. Wang, S. Wu, and S. Okubo, "The state predictive model following control system for linear time delays," *International Journal of Automation and Computing*, vol. 6, no. 2, pp. 186–191, 2009.

[24] C. V. Hollot, V. Misra, D. Towsley, and W. Gong, "Analysis and design of controllers for AQM routers supporting TCP flows," *IEEE Transactions on Automatic Control*, vol. 47, no. 6, pp. 945–959, 2002.

[25] C. V. Hollot, V. Misra, D. Towsely, and W. B. Gong, "A control theoretic analysis of RED," in *Proceedings of the INFOCOM 12th Annual Joint Conference of the IEEE Computer and Communications Societies*, pp. 1510–1519, Anchorage, Alaska, USA, 2001.

[26] B. Marami and M. Haeri, "Implementation of MPC as an AQM controller," *Computer Communications*, vol. 33, no. 2, pp. 227–239, 2010.

[27] T. Azuma, T. Fujita, and M. Fujita, "Congestion control for TCP/AQM networks using state predictive control," *EEE Transactions on Electronics, Information and Systems*, vol. 125, no. 9, pp. 1491–1496, 2005.

[28] T. Azuma, T. Fujita, and M. Fujita, "A design of state predictive H_∞ congestion controllers for TCP/AQM networks," *Transactions of the Institute of Systems, Control and Information Engineers*, vol. 18, no. 10, pp. 373–375, 2005.

[29] T. Azuma, H. Naito, and M. Fujita, "Experimental verification of stabilizing congestion controllers using the network testbed," in *Proceedings of the American Control Conference*, pp. 1841–1846, Portland, Ore, USA, 2005.

[30] Y. Jing, Z. Chen, and G. M. Dimirovski, "Robust fuzzy observer-based control for TCP/AQM network systems with state delay," in *Proceedings of the American Control Conference (ACC '10)*, pp. 1350–1355, Marriott Waterfront, Baltimore, Md, USA, July 2010.

Hindawi Publishing Corporation
Mathematical Problems in Engineering
Volume 2014, Article ID 967578, 9 pages
http://dx.doi.org/10.1155/2014/967578

Research Article

Hybrid Structure Based Tracking and Consensus for Multiple Motors

Changfan Zhang,[1] Han Wu,[1] Bin Liu,[2] Jing He,[1,3] and Baiyan Li[4]

[1] *College of Electrical and Information Engineering, Hunan University of Technology, Zhuzhou, Hunan 412007, China*
[2] *College of Sciences, Hunan University of Technology, Zhuzhou, Hunan 412007, China*
[3] *College of Mechatronic Engineering and Automation, National University of Defense Technology, Changsha, Hunan 410073, China*
[4] *Department of Information Engineering, Huanghuai University, Zhumadian, Henan 463000, China*

Correspondence should be addressed to Jing He; hejing@263.net

Received 2 July 2014; Accepted 3 August 2014; Published 1 September 2014

Academic Editor: Housheng Su

This paper investigates a hybrid structure based synchronous control strategy for multimotor system of shaftless-driven printing press. Many existing algorithms can obtain a stable synchronous system; however, the obtained stable system may encounter a large enough disturbance that can destroy the synchronization. Focusing on this challenging technological problem about how to receive more robust synchronization during steady-state process, this paper first proposes a state-dependent-switching based leader-following control approach, in which synchronization includes two parts, one associated with tracking control for all members, and the other one associated with consensus maintained among followers in the case that one follower loses synchronization with the leader during steady-state motion. By employing the algebra graph theory, matrix theory, and Lyapunov analysis, the convergence and stability of the given multimotor system are proved. Finally, simulation examples are presented to demonstrate the effectiveness and robustness of the theoretical results.

1. Introduction

Recent years have witnessed increasing interests in the study of shaftless-driven systems. Owing to excellent synchronous performance, shaftless-driven printing presses play a central role in printing industry [1, 2]. However, the accuracy of multiaxis synchronization has a direct effect on production quality and efficiency [3]. Accordingly, finding more advanced multiaxis synchronous control technology remains a challenge.

Existing synchronization related literatures for multiaxis printing presses are mostly directed toward coupling control [4, 5] and virtual line shaft control [6, 7]. In the past years, considerable algorithms on synchronization for multiple motors pose advantages as well as limitations. References [4, 5] achieved synchronization by introducing parameter coupling into control strategies. However, the increasing coordinated axes induce intensive online computational work. References [6, 7] presented novel synchronous control laws with a virtual line shaft. However, there is no information exchange among followers, and it is difficult to find a satisfactory solution for the measurement of acceleration.

Meanwhile, we notice that consensus of multiagent system is arousing extensive attention in various disciplines, including biology, computer science, and control engineering [8–10]. Many existing papers have made great contributions in distributed coordinated control. Vicsek et al. first proposed the emergence of self-ordered motion in systems of particles with biologically motivated interaction and received interesting results [11]. Jadbabaie et al. provided a theoretical explanation for this convergence behavior and derived several other similar models [12]. Cortes extended the application of consensus algorithms to general continuous functions [13]. Thereafter, various consensus algorithms were investigated, ranging from single-integrator dynamics to double-integrator and high-order-integrator dynamics [14–16], from continuous time to discrete time [17, 18], from fixed topologies to switching topologies [19], from average consensus to

consensus tracking [20–22], and so forth. Extension consensus algorithms that considered many other extra conditions were studied afterwards, and an adaptive synchronization algorithm of coupled oscillators was proposed [23]. In [24], an adaptive algorithm of coupled oscillators with multiple leaders was investigated. In [25], a superior decentralized adaptive cluster synchronization was introduced to investigate the pinning-control problem of complex dynamical networks. In [26, 27], input saturation was taken into account in the leader-following consensus of agents described by general linear systems. Due to different versions of consensus algorithms, various cooperation control capabilities were developed; examples include flocking [28, 29], task assignment [30, 31], containment control [32, 33], formation control [34–36], and rendezvous [37].

To our knowledge, many existing algorithms can obtain a stable synchronous system; however, when the obtained stable system encounters these unanticipated situations, such as parameter perturbations, external load disturbances, and model nonlinearities, the created consistent system may be inconsistent. Moreover, amounts of wastes would be produced in the high speed printing process. Therefore, in industrial manufacturing areas, one of the main challenges is how to find a control strategy that keeps all motors maintaining consensus all the time, especially in the case that one follower loses synchronization with reference signal. If the other followers turn to track the faulty one rather than the given reference in this circumstance, the problem would be solved. Inspired by the aforementioned researches and industrial requirement, based on a state-dependent-switching law, this paper proposes a virtual-leader-based consensus tracking control with hybrid structure for multimotor system.

The remainder of this paper is organized as follows. Section 2 states the problems to be solved according to a multimotor system. Section 3 establishes the control strategy and presents theoretical analysis. Simulation results are given in Section 4. Finally, Section 5 draws a conclusion.

2. Preliminaries and Problem Statement

Consider a shaftless-driven printing press (SDPP), which can be regarded as a multimotor system (MMS). Let each printing roller be driven by a servomotor, and each servomotor system stands for an agent with actual motion ability; multiple servo systems compose a multiagent system.

Let R denote the set of real number. The SDPP consists of n different motors, together with an additional motor labeled $0(L)$, which acts as the unique virtual leader of the group, and motors $1, 2, \ldots, n$ are followers.

The motion of each DC motor is described by [38]

$$\begin{aligned} \dot{\theta}_i &= \omega_i \\ \dot{\omega}_i &= -\frac{K_{ti}K_{ei}}{J_iR_i}\omega_i + \frac{K_{ti}}{J_iR_i}u_i - \frac{1}{J_i}T_{Li} \quad (i = 0, 1, \ldots, n), \end{aligned} \tag{1}$$

where θ_i is the position of motor i, ω_i is the speed of motor i, u_i is the control input of motor i, R_i is total armature resistance of motor i, K_{ei} is the voltage feedback coefficient of motor i, J_i is inertia of motor i, K_{ti} is the electromagnetic torque coefficient of motor i, and T_{Li} is the load torque of motor i.

Let $a_i = -K_{ti}K_{ei}/J_iR_i$, $b_i = K_{ti}/J_iR_i$, and $c_i = -1/J_i$; here, $a_i = \overline{a}_i + \Delta a_i$, $b_i = \overline{b}_i + \Delta b_i$, and $c_i = \overline{c}_i + \Delta c_i$. $\overline{a}_i$, $\overline{b}_i$, and $\overline{c}_i$ denote the nominal value of a_i, b_i, and c_i, respectively. Δa_i, Δb_i, and Δc_i denote the uncertain value.

Equation (1) can be rewritten as

$$\begin{aligned} \dot{\theta}_i &= \omega_i \\ \dot{\omega}_i &= \overline{a}_i\omega_i + \overline{b}_iu_i + F_i. \end{aligned} \tag{2}$$

Here, $i = 0, 1, \ldots, n$, $F_i = \Delta a_i\omega_i + \Delta b_iu_i + c_iT_{Li}$ is a time-varying uncertainty.

Define

$$S = \begin{bmatrix} \theta_0 & \theta_1 & \cdots & \theta_n \end{bmatrix}^T \tag{3}$$

to be the actual output position of each motor in MMS (2). Let θ^d be the given reference, which is only transmitted to virtual leader. The output of leader $\theta_0(\theta_L)$ acts as the reference of followers. Since the power of inverter is limited, the driven control system provides a limited torque; that is, θ_i $(i = 0, 1, \ldots, n)$ is bounded. Our results will rely on the following assumption.

Assumption 1. The uncertainty F_i $(i = 0, 1, \ldots, n)$, θ_i, $\dot{\theta}_i$, and $\ddot{\theta}_i$ $(i = 1, \ldots, n)$ are bounded in an actual SDPP.

The interaction topology of MMS (2) is represented by graph $G_{n+1} = (v_{n+1}, \varepsilon_{n+1})$, where $v_{n+1} = \{0, 1, \ldots, n\}$ is the set of nodes and $\varepsilon_{n+1} \subseteq v_{n+1} \times v_{n+1}$ is the set of edges. Let $A_{n+1} = [a_{ij}] \in R^{(n+1)\times(n+1)}$ be the adjacency matrix related to G_{n+1}; $a_{ij} > 0$ implies that information flows from node j to i; otherwise, $a_{ij} = 0$. Here we assume $a_{ii} = 0, \forall i = 0, 1, \ldots, n$. a_{i0} is positive if $(0, i) \in \varepsilon_{n+1}$; otherwise, $a_{i0} = 0, \forall i = 1, 2, \ldots, n$. Consider $a_{0j} = 0, \forall j = 0, 1, \ldots, n$. When we need to focus only on followers 1 to n, we use a follower graph $G_n = (v_n, \varepsilon_n)$, letting $\overline{A}_n = [a_{ij}] \in R^{n\times n}$ be the adjacency matrix associated with G_n. The Laplacian matrix $\overline{L}_n = [l_{ij}] \in R^{n\times n}$ associated with $\overline{A}_n$ is defined as $l_{ii} = \sum_{j=1, j\neq i}^{n} a_{ij}$ and $l_{ij} = -a_{ij}$, where $i \neq j$. In this paper, we suppose $\theta_0(\theta_L)$ is available to all the followers, and the followers have only local interactions with their neighbors and graphs G_{n+1} and G_n are fixed and have a spanning tree.

Problems to be addressed in this paper can be divided into two parts. One is the tracking control of all group members, under normal circumstances (i.e., the followers can track the motion trajectory of virtual leader with the given tracking control law), designing a tracking control algorithm to achieve $\|\theta_i - \theta_L\| \to 0$ $(i = 1, 2, \ldots, n)$, such that all followers will track the trajectory of virtual leader. The other one is consensus control among followers, under abnormal circumstance (i.e., at least one follower cannot follow the virtual leader during large enough disturbances), designing a consensus algorithm to guarantee that the other followers can track the faulty one; if it satisfies $\|\theta_i - \theta_j\| \to 0$ $(i, j = 1, 2, \ldots, n)$, then followers would maintain consensus. It

contributes to solving the technological problem about how to reduce the production of vast amounts of wastes due to the existent printing-registration deviation when a high speed SDPP is in response to local environment disturbances.

3. Main Results

In this section, we design control algorithms to satisfy the conditions proposed in Section 2 and give the theoretical analysis.

Lemma 2 (see [39]). *Given a matrix $L_n = [l_{ij}] \in R^{n\times n}$, where $l_{ii} \le 0$, $l_{ij} \ge 0$, $\forall i \ne j$, and $\sum_{j=1}^{n} l_{ij} = 0$ for each i, then L_n has at least one zero eigenvalue with an associated eigenvector 1_n, and all nonzero eigenvalues are in the open left half plane. Furthermore, L_n has exactly one zero eigenvalue if and only if the directed graph of L_n has a directed spanning tree.*

Corollary 3 (see [39]). *The nonsymmetrical Laplacian matrix L_n of a directed graph has a simple zero eigenvalue with an associated eigenvector 1_n and all of the other eigenvalues are in the open right half plane if and only if the directed graph has a directed spanning tree.*

Define synchronous coordinated matrix $\overline{D} = [\overline{D}_{ij}] \in R^{n\times n}$ $(i, j = 1, 2, \ldots, n)$, where

$$\overline{D}_{ij} = \theta_i - \theta_j. \tag{4}$$

Let $\overline{e} = [e_1 \ e_2 \ \cdots \ e_n]^T$ represent the tracking error of each member, where

$$e_i = \theta_i - \theta_L \quad (i = 1, 2, \ldots, n). \tag{5}$$

Let $E_i = \sum_{j=1, j\ne i}^{n} a_{ij}(\theta_i - \theta_j)$ be the element of $E^{n\times 1}$, which represents the synchronous coordinated error of each follower, and $E^{n\times 1}$ can be expressed in a vector form

$$E = \left(\overline{A} \circ \overline{D}\right) 1_{n\times 1}. \tag{6}$$

Here, operator $\circ$ expresses the Hadamard product of matrix.

Theorem 4. *Consider the MMS* (2) *and suppose graphs G_{n+1} and G_n are connected and both have a spanning tree, under normal circumstance; n followers track the virtual leader if and only if $\overline{e} = 0$; under abnormal circumstance, the followers maintain consensus if and only if $E = 0$.*

Proof. From (5), $\overline{e} = [e_i]_{n\times 1} = [\theta_i - \theta_L]_{n\times 1}$, and we have $\overline{e} = 0 \Leftrightarrow \theta_i = \theta_L$ $(i = 1, 2, \ldots, n)$. Thus, each follower can follow the motion state of virtual leader if and only if $\overline{e} = 0$.

Consider the related properties of adjacency matrix and (5); (6) is equivalent to

$$E = \left(\overline{A} \circ \overline{D}\right) 1_{n\times 1} = \overline{L}\overline{e}. \tag{7}$$

If we have $E = 0$, according to Lemma 2 and Corollary 3, we can also have $\overline{e} \in \text{span}\{1\}$, it means that each element of $\overline{e}$ is nonzero and the same as the others; that is, $\theta_1 = \cdots = \theta_i = \cdots = \theta_n \ne \theta_L$. It follows that $E = 0$ infers $\theta_1 = \cdots = \theta_i = \cdots = \theta_n$ and vice versa. Therefore, we can conclude that followers maintain consensus under abnormal circumstance if and only if synchronous coordination error E asymptotically converges to zero.

This completes the proof. □

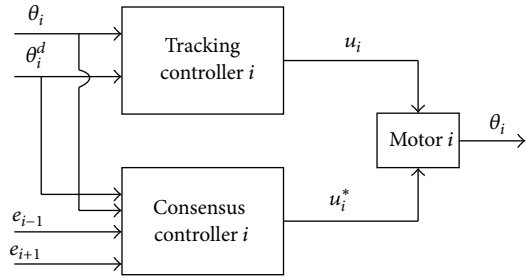

Figure 1: Structure diagram of the position controller.

Our control scheme is composed by tracking control under normal circumstance and coordinated consensus control under abnormal circumstance. The position controller structure of the follower servomotor i $(i = 1, 2, \ldots, n)$ is shown in Figure 1. Define a state-dependent-switching law

$$U_i = \begin{cases} u_i & \dfrac{1}{2}\displaystyle\sum_{i,j=1}^{n} \left|e_i - e_j\right| < \delta \\ u_i^* & \dfrac{1}{2}\displaystyle\sum_{i,j=1}^{n} \left|e_i - e_j\right| \ge \delta, \end{cases} \tag{8}$$

where δ is a positive constant, and u_i and u_i^* are designed as equations (9) and (10).

The tracking control law of each motor is given by

$$u_i = \frac{1}{\overline{b}_i}\left(-\lambda_i \dot{e}_i - \overline{a}_i \dot{\theta}_i + \ddot{\theta}_L - \overline{F}_i \operatorname{sgn}(\sigma_i) - h_i(\sigma_i + \beta_i \operatorname{sgn}(\sigma_i))\right) \quad (i = 0, 1, \ldots, n), \tag{9}$$

where the gains λ_i, h_i, and β_i are to be designed, $\overline{F}_i$ is the upper bound of F_i, and $\operatorname{sgn}(\sigma_i)$ denotes a signum function, where $\sigma_i = \lambda_i e_i + \dot{e}_i$.

The consensus control law is given by

$$u_i^* = k_p E_i + k_i \int E_i dt + k_d \frac{dE_i}{dt} \quad (i = 1, 2, \ldots, n), \tag{10}$$

where the gains k_p, k_i, and k_d are to be designed.

Theorem 5. *Consider the MMS* (2). *Let each motor be steered by the control input* (8). *Then choose arbitrary proper gains k_p, k_i, k_d, and δ and positive gains λ_i, h_i, and β_i satisfying $\lambda_i h_i > 1/4$; the multimotor system asymptotically synchronizes with a common evolution with the following:*

(i) *under normal circumstances, $\|\theta_i - \theta_L\| \to 0$ $(i = 1, 2, \ldots, n)$, as $t \to \infty$;*

(ii) *under abnormal circumstances, $\|\theta_i - \theta_j\| \to 0$ $(i = 1, 2, \ldots, n)$, as $t \to \infty$.*

Proof. Case (i). Under the normal circumstances (i.e., when unanticipated environmental disturbances can be tolerated by followers, that is, $(1/2)\sum_{i,j=1}^{n}|e_i - e_j| < \delta$), define vector

$$\alpha_i^T = \begin{bmatrix} e_i & \sigma_i \end{bmatrix}. \tag{11}$$

Consider a Lyapunov function candidate

$$V(t) = \sum_{i=1}^{n} V_i(t), \tag{12}$$

where

$$V_i(t) = \frac{1}{2}\alpha_i^T \alpha_i \tag{13}$$

which is a positive definite function and radially unbounded with respect to α_i^T.

Differentiating $V(t)$ with respect to time gives

$$\begin{aligned} \dot{V}(t) &= \sum_{i=1}^{n} \alpha_i^T \dot{\alpha}_i \\ &= \sum_{i=1}^{n} \left(e_i \dot{e}_i + \sigma_i \dot{\sigma}_i\right) \\ &= \sum_{i=1}^{n} \left(e_i \dot{e}_i + \sigma_i \left(\lambda_i \dot{e}_i + \ddot{e}_i\right)\right). \end{aligned} \tag{14}$$

From (2) and (5), we obtain

$$\ddot{e}_i = \ddot{\theta}_i - \ddot{\theta}_L = \overline{a}_i \dot{\theta}_i + \overline{b}_i u_i + F_i - \ddot{\theta}_L. \tag{15}$$

Substituting (15) and (9) into (14) yields

$$\begin{aligned} \dot{V}(t) &= \sum_{i=1}^{n} \left(e_i \dot{e}_i + \sigma_i \left(\lambda_i \dot{e}_i + \overline{a}_i \dot{\theta}_i + \overline{b}_i u_i + F_i - \ddot{\theta}_L\right)\right) \\ &= \sum_{i=1}^{n} \Big[e_i \dot{e}_i + \sigma_i \Big(\lambda_i \dot{e}_i + \overline{a}_i \dot{\theta}_i + F_i - \ddot{\theta}_L \\ &\qquad + \left(-\lambda_i \dot{e}_i - \overline{a}_i \dot{\theta}_i + \ddot{\theta}_L\right) \\ &\qquad -\overline{F}_i \operatorname{sgn}(\sigma_i) - h_i \left(\sigma_i + \beta_i \operatorname{sgn}(\sigma_i)\right)\Big)\Big] \\ &= \sum_{i=1}^{n} \left(e_i \dot{e}_i + F_i \sigma_i - \overline{F}_i |\sigma_i| - h_i \sigma_i^2 - h_i \beta_i |\sigma_i|\right) \\ &\le \sum_{i=1}^{n} \left(e_i \left(\sigma_i - \lambda_i e_i\right) + \left(|F_i| - \overline{F}_i\right)|\sigma_i| - h_i \sigma_i^2 - h_i \beta_i |\sigma_i|\right) \\ &\le \sum_{i=1}^{n} \left(-\lambda_i e_i^2 + e_i \sigma_i - h_i \sigma_i^2 - h_i \beta_i |\sigma_i|\right). \end{aligned} \tag{16}$$

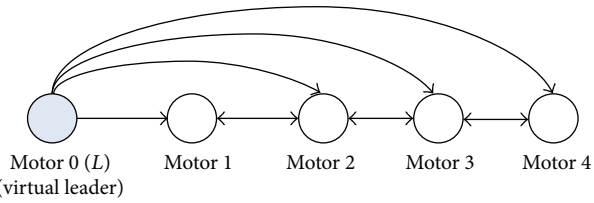

Figure 2: Interaction topology among five motors where θ_L is available to all the followers.

Letting $Q_i = \begin{bmatrix} \lambda_i & -1/2 \\ -1/2 & h_i \end{bmatrix}$, we have $|Q_i| = \lambda_i h_i - 1/4$ and supposing $\lambda_i h_i > 1/4$, then, $|Q_i| > 0$, Q_i is a positive definite matrix

$$\begin{aligned} \alpha_i^T Q_i \alpha_i &= \begin{bmatrix} e_i & \sigma_i \end{bmatrix} \begin{bmatrix} \lambda_i & -\frac{1}{2} \\ -\frac{1}{2} & h_i \end{bmatrix} \begin{bmatrix} e_i \\ \sigma_i \end{bmatrix} \\ &= \lambda_i e_i^2 - e_i \sigma_i + h_i \sigma_i^2. \end{aligned} \tag{17}$$

Substituting (17) into (16) yields

$$\begin{aligned} \dot{V}(t) &\le \sum_{i=1}^{n} \left(-\alpha_i^T Q_i \alpha_i - h_i \beta_i |\sigma_i|\right) \\ &\le \sum_{i=1}^{n} -\alpha_i^T Q_i \alpha_i \\ &\le \sum_{i=1}^{n} -\lambda_{\min}(Q_i) \left\|\alpha_i^T\right\|^2 \le 0, \end{aligned} \tag{18}$$

where $\lambda_{\min}(Q_i)$ is the minimum eigenvalue of Q_i.

It implies that $V(t) \le V(0)$; that is, e_i, δ_i are bounded; $\dot{e}_i$ is bounded since δ_i is bounded. $\ddot{e}_i$ is bounded from (15) and Assumption 1, and thus $\dot{e}_i$, $\dot{\sigma}_i$ are bounded, and then e_i, σ_i are uniformly continuous; from Barbalat lemma, $\alpha_i^T = \begin{bmatrix} e_i & \sigma_i \end{bmatrix} \to 0$ as $t \to \infty$; that is, $\theta_i \to \theta_L$, which is equivalent to $\|\theta_i - \theta_L\| \to 0$.

Case (ii). Under the abnormal circumstances (i.e., when unanticipated environmental disturbances cannot be tolerated by followers, at least one member fails to follow the reference motion state; that is, it satisfies $(1/2)\sum_{i,j=1}^{n}|e_i - e_j| \ge \delta$), when $(1/2)\sum_{i,j=1}^{n}|e_i - e_j|$ is above a specified threshold δ, the system will switch to consensus control law u_i^* which is shown in (10), controller u_i^* provides $E \to 0$, as the proof of Theorem 4, and $E \to 0$ is equivalent to $e_1 = \cdots = e_i = \cdots = e_n \ne 0$ (i.e., $\theta_1 = \cdots = \theta_i = \cdots = \theta_n$). Thus $\|\theta_i - \theta_j\| \to 0$, and all the followers maintain consensus. In the regulation of switching law and consensus control law, the system ultimately switches to tracking control and converges to the leader again.

This completes the proof. □

4. Simulations

In this section, three different cases are considered to validate the theoretical results. The network topology of MMS (2)

Table 1: Parameters of five driven motors.

Motor	0 (L)	1	2	3	4
R (Ω)	0.2	0.5	0.4	0.6	0.7
K_t	0.005	0.01	0.008	0.015	0.02
J (Kg·m^2)	0.02	0.03	0.025	0.05	0.04
K_e	0.1	0.2	0.2	0.18	0.25
Initial position (rad)	0.5	−0.8	1.3	−2.0	−2.4

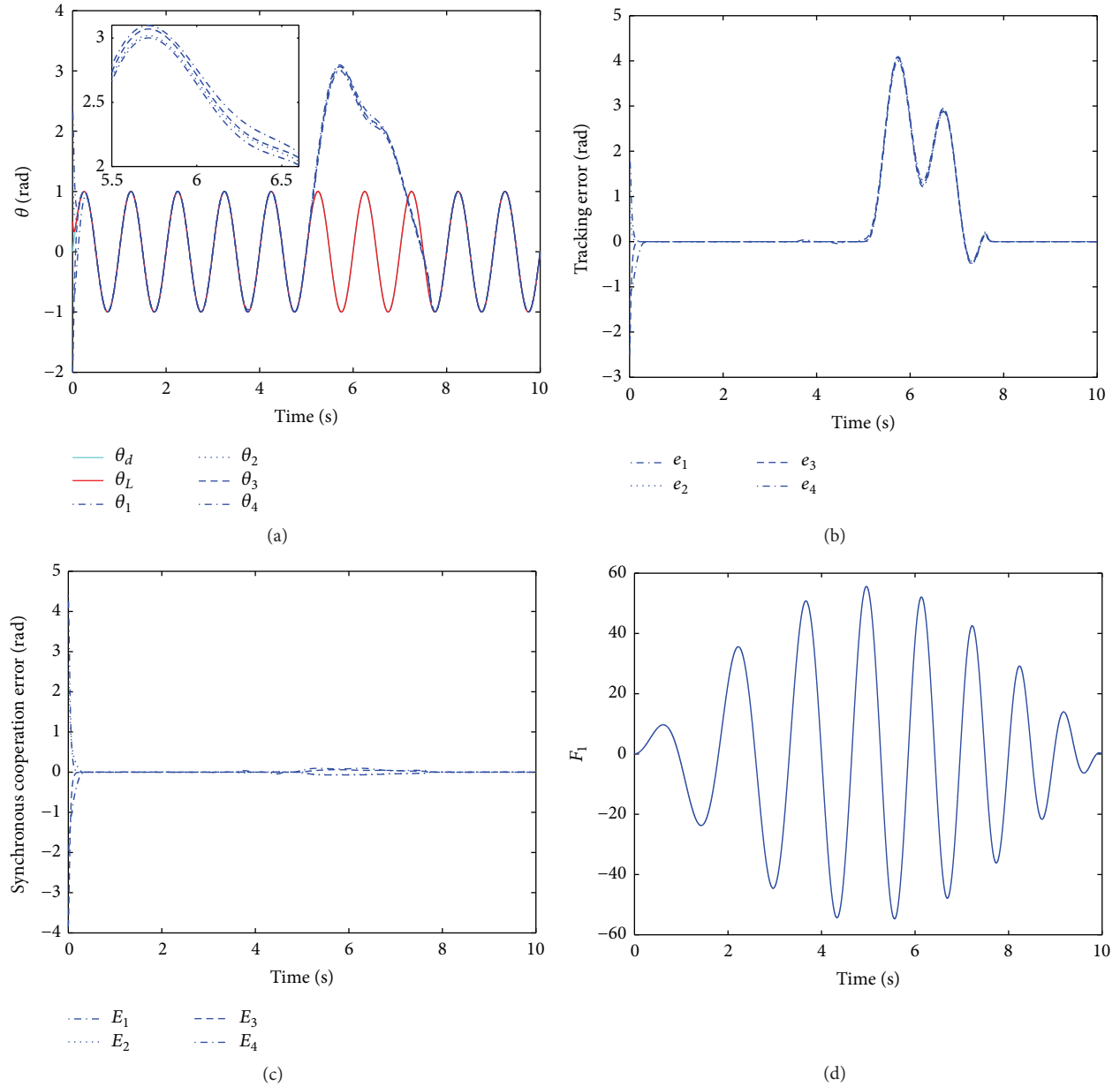

Figure 3: Simulation results for motor 1 with a slowly varying disturbance under protocol (8) corresponding to topology in Figure 2.

is shown in Figure 2. Apparently, it has a spanning tree in this graph, for which the virtual leader $0(L)$ acts as the root node, and the reference state θ_L is available to all the followers. Follower motor 1 is selected to be added to various disturbances. The parameters of the five driven motors are given in Table 1. Let each motor be steered by the control input (8), set $\delta = 0.075$, and let the consensus reference state of virtual leader be $\theta^d = \sin(2\pi t)$rad.

From Figure 2, let

$$A = \begin{bmatrix} 0 & B \\ C & \overline{A} \end{bmatrix}, \tag{19}$$

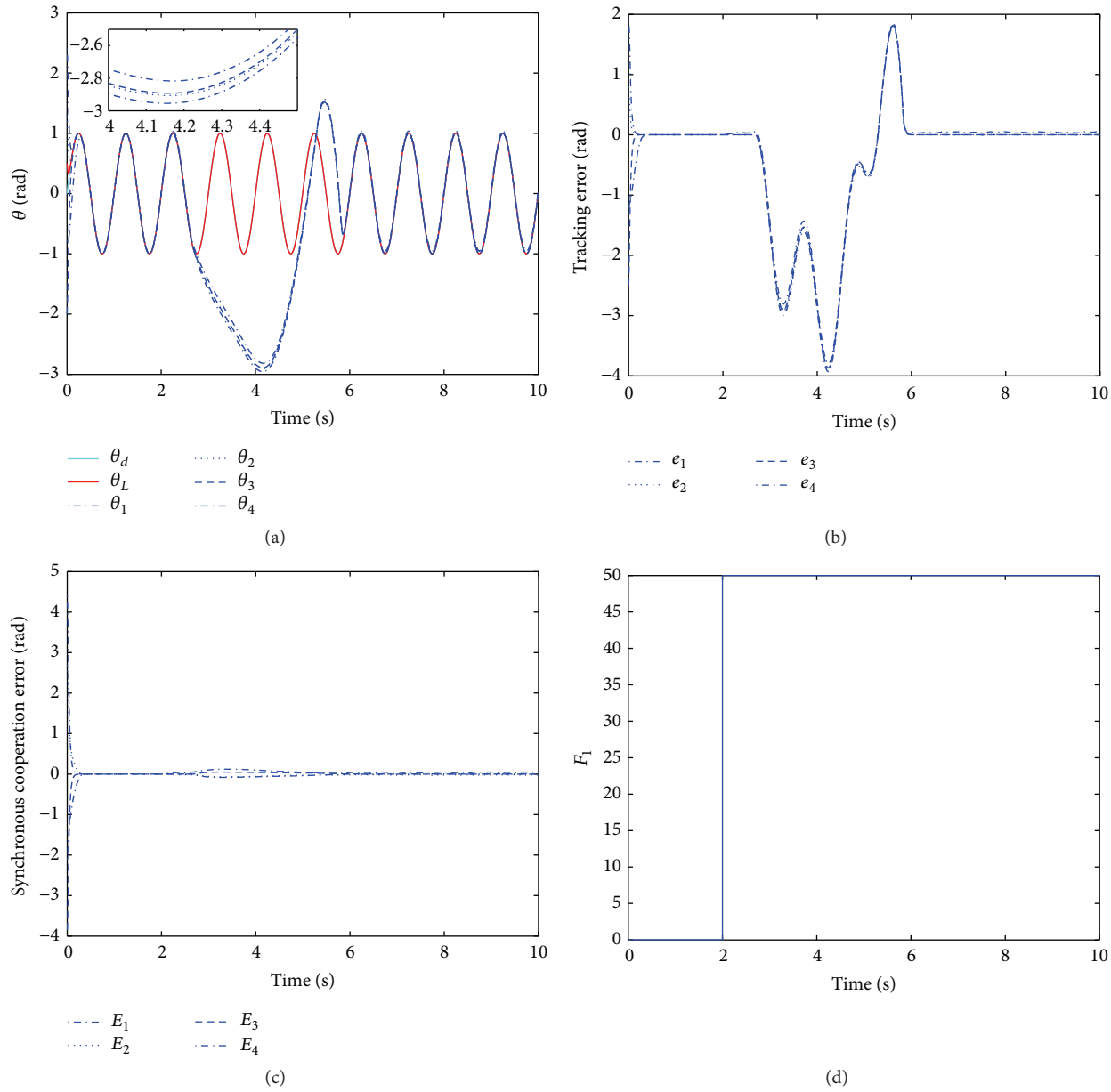

FIGURE 4: Simulation results for motor 1 with a step disturbance under protocol (8) corresponding to topology in Figure 2.

and supposing all the neighbors have the same effect on each motor, we have

$$B = \begin{bmatrix} 0 & 0 & 0 & 0 \end{bmatrix}, \qquad C = \begin{bmatrix} 1 & 1 & 1 & 1 \end{bmatrix}^T,$$
$$\overline{A} = \begin{bmatrix} 0 & 1 & 0 & 0 \\ 0.5 & 0 & 0.5 & 0 \\ 0 & 0.5 & 0 & 0.5 \\ 0 & 0 & 1 & 0 \end{bmatrix}. \tag{20}$$

Case (1). In the first case, we choose a slowly varying disturbance that is shown in subplot 3(d). Subplot 3(a) shows the position tracking of each motor, subplot 3(b) is the tracking error of each team member, and subplot (c) in Figure 3 shows the synchronous cooperation error of each follower. From subplot 3(a), each follower can follow the reference state at first. As the disturbance F_1 increases gradually, motor 1 will lose tracking. Simultaneously, from subplots 3(a) and 3(b), we can see that other followers maintain consensus with motor 1 in this situation.

Case (2). In the second case, we consider a step disturbance

$$F_1 = \begin{cases} 0N \cdot m & t < 2s \\ 50N \cdot m & t \geq 2s, \end{cases} \tag{21}$$

which is shown in subplot 4(d). It is obvious from subplot 4(a) that the control protocol (8) is capable of tracking the virtual leader and that the followers maintain a consensus state even

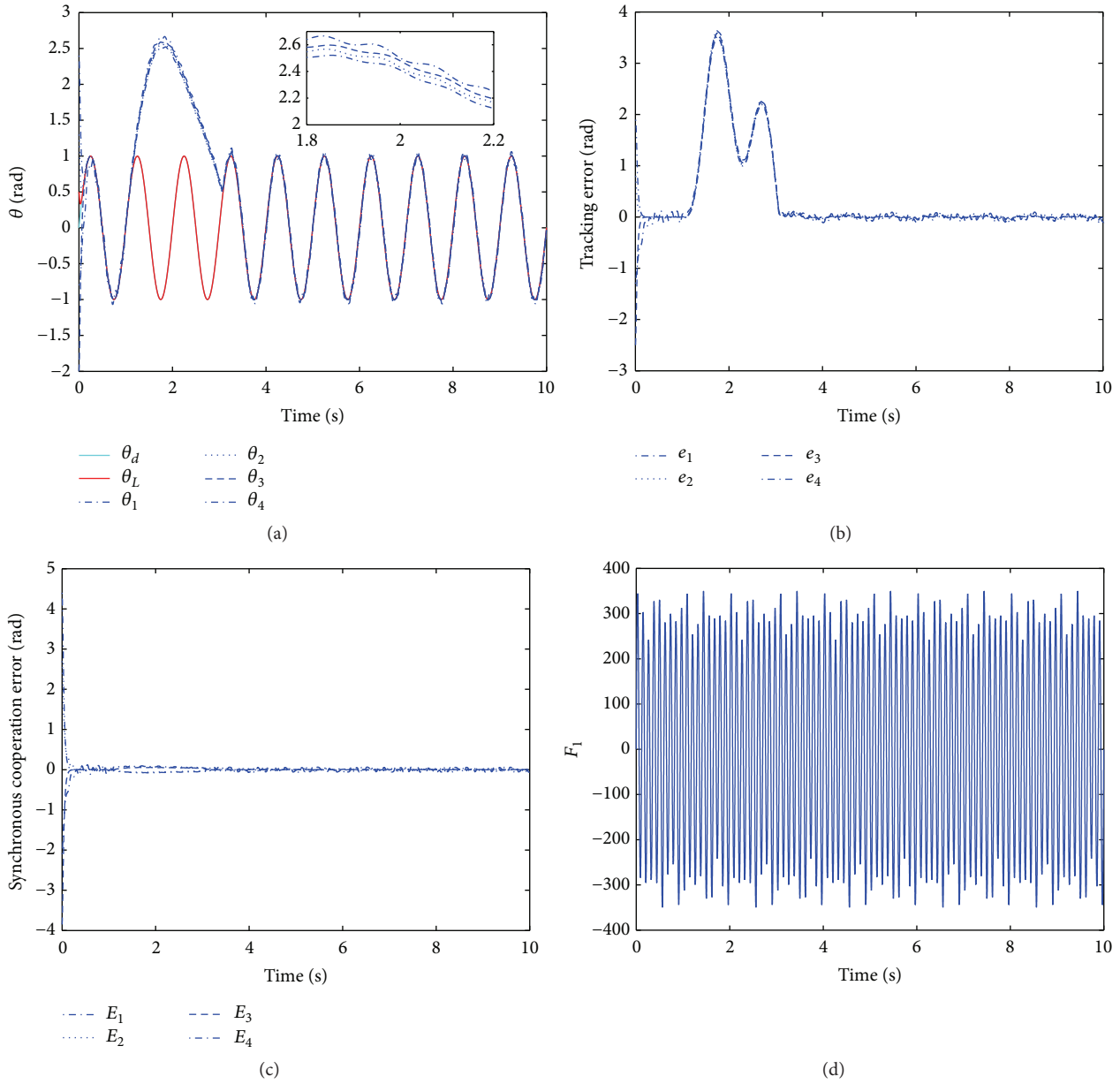

FIGURE 5: Simulation results for motor 1 with a high-frequency disturbance under protocol (8) corresponding to topology in Figure 2.

during a step disturbance. Subplot 4(b) corresponds to the tracking error of each motor and subplot 4(c) corresponds to the synchronous cooperation error of each follower.

Case (3). The third case considers a high-frequency disturbance shown in subplot 5(d). It is clear from subplot (a) in Figure 5 that the control protocol (8) is capable of tracking the virtual leader at first and followers maintain consensus even during high-frequency disturbance F_1 in 5(d). Subplot 5(b) presents the tracking error of each motor, and subplot 5(c) shows the synchronous cooperation error of each follower.

5. Conclusion

In this paper, we have studied approaches of improving synchronous accuracy for multiple motors. Compared with other relevant results which refer only to a final synchronization, our novel control strategy in this paper additionally considers the synchronous process by integrating tracking with consensus control based on hybrid structure. Theoretical analysis has shown that all followers asymptotically converge to a consistent state even when one follower fails to follow the virtual leader during a large enough disturbance. Simulation results show good performance of synchronization control accuracy, interference immunity, and convergence for the suggested algorithms.

Conflict of Interests

The authors declare that there is no conflict of interests regarding the publication of this paper.

Acknowledgments

This work was supported by the Natural Science Foundation of China (nos. 61273157, 61104024, and 61473117), Hunan Provincial Natural Science Foundation of China (nos. 13JJ8020 and 14JJ5024), and Hunan Province Education Department (nos. 12A040 and 13CY018).

References

[1] S. Tang, "Application of shaftless drive in gravure," *Micromotors Servo Technique*, vol. 39, no. 5, pp. 69–74, 2006.

[2] M. Yang, "Analysis and simulation of winding tension control system in shaftless web press," in *Proceeding of the 31st Chinese Control Conference (CCC '12)*, pp. 1826–1830, Hefei, China, July 2012.

[3] Y. Xiao, Y. Pang, X. Ge, and J. Sun, "Synchronous control for high-accuracy biaxial motion systems," *Journal of Control Theory and Applications*, vol. 11, no. 2, pp. 294–298, 2013.

[4] C. Chen and L. Chen, "Robust cross-coupling synchronous control by shaping position commands in multiaxes system," *IEEE Transactions on Industrial Electronics*, vol. 59, no. 12, pp. 4761–4773, 2012.

[5] L. Zeng and Z. Li, "Double-motor synchronous control system based on deviation coupling strategy," in *Unifying Electrical Engineering and Electronics Engineering*, pp. 849–855, Springer, 2014.

[6] G. Liu, S. Li, and L. Zhang, "The synchronization control of the hydraulic press brake based on the virtual shaft control algorithm," *Advanced Materials Research*, vol. 383-390, pp. 574–579, 2012.

[7] R. G. Anderson, A. J. Meyer, M. A. Valenzuela, and R. D. Lorenz, "Web machine coordinated motion control via electronic lineshafting," *IEEE Transactions on Industry Applications*, vol. 37, no. 1, pp. 247–254, 2001.

[8] J. Toner and Y. Tu, "Flocks, herds, and schools: a quantitative theory of flocking," *Physical Review E*, vol. 58, no. 4, pp. 4828–4858, 1998.

[9] W. Ren and R. W. Beard, "Consensus seeking in multiagent systems under dynamically changing interaction topologies," *IEEE Transactions on Automatic Control*, vol. 50, no. 5, pp. 655–661, 2005.

[10] H. Su, X. Wang, and Z. Lin, "Flocking of multi-agents with a virtual leader," *IEEE Transactions on Automatic Control*, vol. 54, no. 2, pp. 293–307, 2009.

[11] T. Vicsek, A. Czirk, E. Ben-Jacob, I. Cohen, and O. Shochet, "Novel type of phase transition in a system of self-driven particles," *Physical Review Letters*, vol. 75, no. 6, pp. 1226–1229, 1995.

[12] A. Jadbabaie, J. Lin, and A. S. Morse, "Coordination of groups of mobile autonomous agents using nearest neighbor rules," *IEEE Transactions on Automatic Control*, vol. 48, no. 6, pp. 988–1001, 2003.

[13] J. Cortés, "Distributed algorithms for reaching consensus on general functions," *Automatica*, vol. 44, no. 3, pp. 726–737, 2008.

[14] G. Xie and L. Wang, "Consensus control for a class of networks of dynamic agents," *International Journal of Robust and Nonlinear Control*, vol. 17, no. 10-11, pp. 941–959, 2007.

[15] H. Su, X. Wang, G. Chen, and Z. Lin, "Adaptive second-order consensus of networked mobile agents with nonlinear dynamics," *Automatica*, vol. 47, no. 2, pp. 368–375, 2011.

[16] W. He and J. Cao, "Consensus control for high-order multi-agent systems," *IET Control Theory & Applications*, vol. 5, no. 1, pp. 231–238, 2011.

[17] L. Wang and F. Xiao, "Finite-time consensus problems for networks of dynamic agents," *IEEE Transactions on Automatic Control*, vol. 55, no. 4, pp. 950–955, 2010.

[18] M. Zhu and S. Martnez, "Discrete-time dynamic average consensus," *Automatica*, vol. 46, no. 2, pp. 322–329, 2010.

[19] W. Ni and D. Cheng, "Leader-following consensus of multi-agent systems under fixed and switching topologies," *Systems & Control Letters*, vol. 59, no. 3-4, pp. 209–217, 2010.

[20] J. Qin, H. Gao, and W. X. Zheng, "On average consensus in directed networks of agents with switching topology and time delay," *International Journal of Systems Science*, vol. 42, no. 12, pp. 1947–1956, 2011.

[21] F. Zhang and G. Duan, "Integrated relative position and attitude control of spacecraft in proximity operation missions," *International Journal of Automation and Computing*, vol. 9, no. 4, pp. 342–351, 2012.

[22] Y. Xia, Z. Zhu, M. Fu, and S. Wang, "Attitude tracking of rigid spacecraft with bounded disturbances," *IEEE Transactions on Industrial Electronics*, vol. 58, no. 2, pp. 647–659, 2011.

[23] H. Su, X. Wang, and Z. Lin, "Synchronization of coupled harmonic oscillators in a dynamic proximity network," *Automatica*, vol. 45, no. 10, pp. 2286–2291, 2009.

[24] H. Su, M. Z. Q. Chen, X. Wang, H. Wang, and N. V. Valeyev, "Adaptive cluster synchronisation of coupled harmonic oscillators with multiple leaders," *IET Control Theory & Applications*, vol. 7, no. 5, pp. 765–772, 2013.

[25] H. Su, Z. Rong, M. Z. Q. Chen, X. Wang, G. Chen, and H. Wang, "Decentralized adaptive pinning control for cluster synchronization of complex dynamical networks," *IEEE Transactions on Systems, Man, and Cybernetics B: Cybernetics*, vol. 43, no. 1, pp. 394–399, 2013.

[26] H. Su, M. Z. Q. Chen, J. Lam, and Z. Lin, "Semi-global leader-following consensus of linear multi-agent systems with input saturation via low gain feedback," *IEEE Transactions on Circuits and Systems I: Regular Papers*, vol. 60, no. 7, pp. 1881–1889, 2013.

[27] H. Su, M. Z. Q. Chen, X. Wang, and J. Lam, "Semi-global observer-based leader-following consensus with input saturation," *IEEE Transactions on Industrial Electronics*, vol. 61, no. 6, pp. 2842–2850, 2014.

[28] H. G. Tanner, A. Jadbabaie, and G. J. Pappas, "Flocking in fixed and switching networks," *IEEE Transactions on Automatic Control*, vol. 52, no. 5, pp. 863–868, 2007.

[29] W. Yu, G. Chen, and M. Cao, "Distributed leader-follower flocking control for multi-agent dynamical systems with time-varying velocities," *Systems & Control Letters*, vol. 59, no. 9, pp. 543–552, 2010.

[30] K. L. Moore and D. Lucarelli, "Decentralized adaptive scheduling using consensus variables," *International Journal of Robust and Nonlinear Control*, vol. 17, no. 10-11, pp. 921–940, 2007.

[31] D. Zou, L. Gao, S. Li, J. Wu, and X. Wang, "A novel global harmony search algorithm for task assignment problem," *Journal of Systems and Software*, vol. 83, no. 10, pp. 1678–1688, 2010.

[32] Z. Meng, W. Ren, and Z. You, "Distributed finite-time attitude containment control for multiple rigid bodies," *Automatica*, vol. 46, no. 12, pp. 2092–2099, 2010.

[33] C. Xu, Y. Zheng, H. Su, C. Zhang, and M. Chen, "Necessary and sufficient conditions for distributed containment control of multi-agent systems without velocity measurement," *IET Control Theory & Applications*, 2014.

[34] W. Ren, "Consensus strategies for cooperative control of vehicle formations," *IET Control Theory and Applications*, vol. 1, no. 2, pp. 505–512, 2007.

[35] A. Karimoddini, H. Lin, B. M. Chen, and T. H. Lee, "Hybrid formation control of the unmanned aerial vehicles," *Mechatronics*, vol. 21, no. 5, pp. 886–898, 2011.

[36] C. S. Ho, Q. H. Nguyen, Y. Ong, and X. Chen, "Autonomous multi-agents in flexible flock formation," *Lecture Notes in Computer Science*, vol. 6459, pp. 375–385, 2010.

[37] H. Su, X. Wang, and G. Chen, "Rendezvous of multiple mobile agents with preserved network connectivity," *Systems & Control Letters*, vol. 59, no. 5, pp. 313–322, 2010.

[38] W. P. Aung, "Analysis on modeling and Simulink of DC motor and its driving system used for wheeled mobile robot," *World Academy of Science, Engineering and Technology*, vol. 32, pp. 299–306, 2007.

[39] W. Ren and R. W. Beard, *Distributed Consensus in Multi-vehicle Cooperative Control: Theory and Applications*, Springer, New York, NY, USA, 2007.

Hindawi Publishing Corporation
Mathematical Problems in Engineering
Volume 2014, Article ID 616024, 7 pages
http://dx.doi.org/10.1155/2014/616024

Research Article

Consensus of the Multiagent System with a Dynamic Leader Based on Directed Topology Using Laplace Transform

Bo Liu,[1] Fei Han,[2] Yang Mei,[3] and Xinmao Zhu[1]

[1] *College of Science, North China University of Technology, Beijing 100144, China*
[2] *College of Mechanical and Electrical Engineering, North China University of Technology, Beijing 100144, China*
[3] *Power Electronics and Motor Driving Engineering Center, North China University of Technology, Beijing 100144, China*

Correspondence should be addressed to Bo Liu; liubo2014@yeah.net

Received 26 June 2014; Accepted 19 July 2014; Published 5 August 2014

Academic Editor: Wei Zhang

The consensus of the multiagent system with directed topology and a leader is investigated, in which the leader is dynamic. Based on Laplace transform method, the accurate upper error bound between the leader and the followers can be obtained. It is also proved that all agents of the system will aggregate and eventually form a cohesive cluster following the leader if the leader is globally reachable. Finally, some simulation examples are given to illustrate the theoretical results.

1. Introduction

In recent years, the consensus problem of multiagent systems has become a hot topic due to their broad applications, such as cooperative unmanned air vehicles, automated highway systems, air traffic control, and autonomous underwater vehicles [1–22].

Various algorithms and models about multiagent systems have been discussed based on different tasks or interests. The leader-following system is one of the most interesting topics in the motion control of the multiagent systems. Vicsek et al. [1] proposed a simple model about autonomous agents moving with a constant identical speed and tending to the average direction of its neighbors. It is demonstrated numerically that all the agents will move in the same direction at the same speed eventually. Jadbabaie et al. [2] gave the theoretical explanation for the numerical results of the Vicsek model by algebraic graph theory. Based on the Vicsek model, some researchers designed the leader-following model, where the leader agent can be regarded as the control input used to control the other agents in such system. Shi et al. [5] regarded the reference signal as a virtual leader for guiding the agent group to move at the desired constant velocity. Hong et al. [7] discussed the leader-following system with variable coupling topology. Olfati-Saber [3] used virtual leaders to accomplish obstacle avoidance.

The coupling topology plays an important role in the studies of multiagent systems. Because of the complexity in the consensus analysis with directed topology, most researchers focus on the undirected topology or balance topology to simplify the problem [7–22]. In this paper, we will discuss the consensus problem with directed topology and give a weak condition for reaching network consensus. According to Laplace transform, the accurate upper error bound between the leader and followers can be calculated and some assumptions needed in Lyapunov approach can be simplified. Finally, some simulation examples are provided to illustrate the theoretical results.

This paper is organized as follows. Section 2 proposes the model formulation and some preliminaries of graph theory. Section 3 gives the analysis of the convergence of the model. Section 4 gives simulations of the theoretical results. Finally, the main contribution of this paper is summarized in Section 5.

2. Model and Preliminaries

2.1. Model. Consider a multiagent system of $n+1$ agents, where the leader is labeled with 0 and the followers are labeled with $1, 2, \ldots, n$. The motion of the system is described by

$$\dot{x}_i = -\sum_{j\in\mathcal{N}_i} a_{ij}\left(x_i - x_j\right) + b_i\left(x_0 - x_i\right), \quad i = 1, 2, \ldots, n,$$
$$\dot{x}_0 = v(t), \tag{1}$$

where $x_i \in \mathbb{R}^m$ represents the state of agent i; $\mathcal{N}_i$ is the neighbor set of agent i. $A = [a_{ij}] \in \mathbb{R}^{n\times n}$ is the coupling matrix, where a_{ij} is the weight parameter with $a_{ij} \geq 0$ and $a_{ii} = 0$. $b_i(x_0 - x_i)$ is the term performing attractive effect from leader agent 0 to agent i. Define $B = \mathrm{diag}\{b_1, b_2, \ldots, b_n\} \in \mathbb{R}^{n\times n}$. $b_i > 0$ means agent i can measure the information of the leader with strength b_i, while $b_i = 0$ means there is no information from the leader to agent i. $v(t)$ is the velocity of the leader, which is a bounded function.

2.2. Preliminaries. To discuss the coordinated control among the agents, graph theory is a very effective tool. Regard the agent as a node and the connection link between any two agents as an edge; the coupling topology is conveniently described by a directed graph. Let $\mathcal{G} = (\mathcal{V}, \mathcal{E}, A)$ be a weighted digraph of order n with the set of nodes $\mathcal{V} = \{1, 2, 3, \ldots, n\}$ and set of arcs $\mathcal{E} \subseteq \mathcal{V}\times\mathcal{V}$. $A = [a_{ij}]$ is adjacency matrix of graph $\mathcal{G}$. An arc of $\mathcal{G}$ is denoted by (i, j), which starts from i and ends at j. The set of neighbors of node i is denoted by $\mathcal{N}_i = \{j \in \mathcal{V} : (i, j) \in \mathcal{E}\}$. A digraph $\mathcal{G}$ is strongly connected if there exists a path between any two distinct nodes. For a node j, if there exists at least a path from every other node i in $\mathcal{G}$ to node j, we say that node j is globally reachable.

A diagonal matrix $D = \mathrm{diag}\{d_1, d_2, \ldots, d_n\} \in \mathbb{R}^{n\times n}$ is a degree matrix of $\mathcal{G}$ with its diagonal elements $d_i = \sum_{j\in\mathcal{N}_i} a_{ij}$, $i = 1, 2, \ldots, n$. Then the Laplacian of the weighted digraph $\mathcal{G}$(or matrix A) is defined as

$$L = D - A \in \mathbb{R}^{n\times n}. \tag{2}$$

In order to study the leader-following problem, a multiagent system with directed topology is considered, which is consisting of n agents and one leader. In $\overline{\mathcal{G}}$, if there exists at least one path from every node in $\mathcal{G}$ to the leader, we say that the leader is globally reachable in $\overline{\mathcal{G}}$.

It is easy to see that L has a zero eigenvalue corresponding to the right eigenvector $\mathbf{1} = (1, 1, \ldots, 1)^T$.

Lemma 1 (see [9]). *A digraph $\mathcal{G}$ has a globally reachable node if and only if 0 is a simple eigenvalue of L (i.e.,* $\mathrm{rank}(L) = n-1$*).*

Lemma 2. *The nonzero eigenvalues of L have positive real parts.*

Proof. The proof is similar to that of [3]; it is omitted here. □

Lemma 3. *The eigenvalues of $L + B$ have positive real parts if and only if the leader is a globally reachable node in digraph $\overline{\mathcal{G}}$.*

Proof. If node 0 is globally reachable, the Laplacian matrix of $\overline{\mathcal{G}}$ can be written as

$$\overline{L} = \begin{pmatrix} 0 & 0 & 0 & \cdots & 0 \\ l_{10} & l_{11} & l_{12} & \cdots & l_{1n} \\ l_{20} & l_{21} & l_{22} & \cdots & l_{2n} \\ \vdots & \vdots & \vdots & \ddots & \vdots \\ l_{n0} & l_{n1} & l_{n2} & \cdots & l_{nn} \end{pmatrix} \in \mathbb{R}^{(n+1)\times(n+1)}. \tag{3}$$

According to Lemma 1, then $\mathrm{rank}(\overline{L}) = n$.

Notice that the block matrix of $\overline{L}$ is

$$\begin{pmatrix} l_{11} & l_{12} & \cdots & l_{1n} \\ l_{21} & l_{22} & \cdots & l_{2n} \\ \vdots & \vdots & \ddots & \vdots \\ l_{n1} & l_{n2} & \cdots & l_{nn} \end{pmatrix} = L + B \in \mathbb{R}^{n\times n}. \tag{4}$$

Then, we can have $\mathrm{rank}(L + B) = n$, where L is the Laplacian matrix of $\mathcal{G}$. □

3. Coordinated Control Analysis

In this section, we focus on the coordinated control problem of model (1). Denote $X = (x_1, x_2, \ldots, x_n)^T$, $X_0 = (x_0, x_0, \ldots, x_0)^T$, and $V = (v, v, \ldots, v)^T = \mathbf{1}v$; then the model can be rewritten into matrix form

$$\dot{X} = -LX - B\left(X - X_0\right). \tag{5}$$

Based on system (5), we can derive the following theorem.

Theorem 4. *If leader 0 is globally reachable in digraph $\overline{\mathcal{G}}$, all the agents described by* (1) *will converge and form a cohesive cluster following the leader asymptotically. Moreover, the errors between the leader and followers will be included in a fixed bound.*

Proof. To solve this problem, we introduce the Laplace transform, succinctly denoted by $\mathcal{L}(\cdot)$ in this paper. System (5) can be transformed as

$$\dot{X} - \dot{X}_0 = -(L + B)\left(X - X_0\right) - V. \tag{6}$$

Define $X - X_0 = Y$ as the error vector; then (6) can be written as

$$\dot{Y} = -(L + B)Y - V. \tag{7}$$

Applying $\mathcal{L}$ to (7), then we have

$$\mathcal{L}\left(\dot{Y}\right) = \mathcal{L}\left(-(L + B)Y - V\right). \tag{8}$$

That is,

$$\left[sI_n + (L + B)\right]\mathcal{L}(Y) = Y(0) - \mathcal{L}(V). \tag{9}$$

For simplicity, denote $\mathcal{L}(Y) = \mathcal{Y}(s)$ and $\mathcal{L}(V) = \mathcal{V}(s)$, where s is the Laplace variable; then

$$\left[sI_n + (L + B)\right]\mathcal{Y}(s) = Y(0) - \mathcal{V}(s). \tag{10}$$

According to *Cramer rule*, we can get solutions of (10):

$$\mathscr{Y}_i(s) = \frac{\Delta[sI_n + (L+B)]^i}{\Delta[sI_n + (L+B)]}, \quad i = 1, 2, \ldots, n, \tag{11}$$

where I_n is the identity matrix of order n; $\Delta[sI_n + (L+B)]^i$ is the determinant of matrix $sI_n + (L+B)$ in which the ith column has been replaced by $Y(0) - \mathscr{V}(s)$; and $\Delta[sI_n + (L+B)]$ is the determinant of matrix $sI_n + (L+B)$. We can separate (11) into two parts as follows:

$$\mathscr{Y}_i(s) = \frac{\Delta[sI_n + (L+B)]_1^i}{\Delta[sI_n + (L+B)]} - \frac{\Delta[sI_n + (L+B)]_2^i}{\Delta[sI_n + (L+B)]}, \tag{12}$$

where $\Delta[sI_n + (L+B)]_1^i$ is the determinant of matrix $sI_n + (L+B)$ in which the ith column has been replaced by $Y(0)$; $\Delta[sI_n + (L+B)]_2^i$ is the determinant of matrix $sI_n + (L+B)$ in which the ith column has been replaced by $\mathscr{V}(s)$. Because $\mathscr{V}(s) = \mathscr{L}[v(t)]\mathbf{1}$, determinant $\Delta[sI_n + (L+B)]_2^i$ can be transformed as

$$\Delta[sI_n + (L+B)]_2^i = \mathscr{L}[v(t)] \cdot \Delta[sI_n + (L+B)]_3^i, \tag{13}$$

where $\Delta[sI_n + (L+B)]_3^i$ is the determinant of matrix $sI_n + (L+B)$ in which the ith column has been replaced by $\mathbf{1}$. Since $\Delta[sI_n + (L+B)]_1^i$, $\Delta[sI_n + (L+B)]_3^i$, and $\Delta[sI_n + (L+B)]$ are polynomials about s, for simplicity, we denote $P_{i1}(s) = \Delta(sI + L)^{i1}$, $P_{i3}(s) = \Delta[sI_n + (L+B)]_3^i$, and $Q(s) = \Delta(sI + L)$, respectively. Then (12) can be rewritten as

$$\begin{aligned}\mathscr{Y}_i(s) &= \frac{\Delta[sI_n + (L+B)]_1^i}{\Delta[sI_n + (L+B)]} - \frac{\mathscr{L}[v(t)]\,\Delta[sI_n + (L+B)]_3^i}{\Delta[sI_n + (L+B)]} \\ &= \frac{P_{i1}(s)}{Q(s)} - \frac{\mathscr{L}[v(t)]\,P_{i3}(s)}{Q(s)}.\end{aligned} \tag{14}$$

According to Lemma 3, the eigenvalues of $L + B$ have positive real parts, denoted as

$$\lambda_1, \lambda_2, \ldots, \lambda_j, \tag{15}$$

with multiplicity as $p, q, \ldots, r$. So we have

$$\Delta(sI + L + B) = (s+\lambda_1)^p (s+\lambda_2)^q \cdots (s+\lambda_j)^r. \tag{16}$$

If the fractional expressions in (14) are reducible, we should make reduction of the fraction expressions. In the following discussion, we assume that the fractional expressions in (14) are irreducible. Applying *Heaviside's Method*, (14) can be expanded into

$$\begin{aligned}\mathscr{Y}_i(s) = {} & \frac{c_{1p}^i}{(s+\lambda_1)^p} + \frac{c_{1(p-1)}^i}{(s+\lambda_1)^{(p-1)}} + \cdots + \frac{c_{11}^i}{(s+\lambda_1)} \\ & + \frac{c_{2q}^i}{(s+\lambda_2)^q} + \frac{c_{2(q-1)}^i}{(s+\lambda_2)^{(q-1)}} + \cdots + \frac{c_{21}^i}{(s+\lambda_2)} \\ & + \cdots + \frac{c_{jr}^i}{(s+\lambda_j)^r} + \frac{c_{j(r-1)}^i}{(s+\lambda_j)^{(r-1)}} \\ & + \cdots + \frac{c_{j1}^i}{(s+\lambda_j)} - \mathscr{L}[v(t)] \\ & \times \left(\frac{d_{1p}^i}{(s+\lambda_1)^p} + \frac{d_{1(p-1)}^i}{(s+\lambda_1)^{(p-1)}} + \cdots + \frac{d_{11}^i}{(s+\lambda_1)} \right. \\ & \quad + \frac{d_{2q}^i}{(s+\lambda_2)^q} + \frac{d_{2(q-1)}^i}{(s+\lambda_2)^{(q-1)}} + \cdots \\ & \quad + \frac{d_{21}^i}{(s+\lambda_2)} + \cdots + \frac{d_{jr}^i}{(s+\lambda_j)^r} \\ & \quad \left. + \frac{d_{j(r-1)}^i}{(s+\lambda_j)^{(r-1)}} + \cdots + \frac{d_{j1}^i}{(s+\lambda_j)} \right),\end{aligned} \tag{17}$$

where

$$\begin{aligned}c_{1k}^i &= \frac{d^{p-k}}{ds^{p-k}} \left[(s+\lambda_1)^{(p-k)} \frac{P_{i1}(s)}{Q(s)} \right]\Bigg|_{s=\lambda_1}, \quad k = 1, 2, \ldots, p, \\ c_{2k}^i &= \frac{d^{q-k}}{ds^{q-k}} \left[(s+\lambda_2)^{(q-k)} \frac{P_{i1}(s)}{Q(s)} \right]\Bigg|_{s=\lambda_2}, \quad k = 1, 2, \ldots, q, \\ &\vdots \\ c_{jk}^i &= \frac{d^{r-k}}{ds^{r-k}} \left[(s+\lambda_j)^{(r-k)} \frac{P_{i1}(s)}{Q(s)} \right]\Bigg|_{s=\lambda_j}, \quad k = 1, 2, \ldots, r, \\ d_{1k}^i &= \frac{d^{p-k}}{ds^{p-k}} \left[(s+\lambda_1)^{(p-k)} \frac{P_{i3}(s)}{Q(s)} \right]\Bigg|_{s=\lambda_1}, \quad k = 1, 2, \ldots, p, \\ d_{2k}^i &= \frac{d^{q-k}}{ds^{q-k}} \left[(s+\lambda_2)^{(q-k)} \frac{P_{i3}(s)}{Q(s)} \right]\Bigg|_{s=\lambda_2}, \quad k = 1, 2, \ldots, q, \\ &\vdots \\ d_{jk}^i &= \frac{d^{r-k}}{ds^{r-k}} \left[(s+\lambda_j)^{(r-k)} \frac{P_{i3}(s)}{Q(s)} \right]\Bigg|_{s=\lambda_j}, \quad k = 1, 2, \ldots, r.\end{aligned} \tag{18}$$

Applying *Inverse Laplace transform* to (17), we obtain

$$\begin{aligned} y_i(t) = & \left(c_{11}^i + \frac{c_{12}^i}{1!}t + \cdots + \frac{c_{1p}^i}{(p-1)!}t^{(p-1)}\right)e^{(-\lambda_1 t)} \\ & + \left(c_{21}^i + \frac{c_{22}^i}{1!}t + \cdots + \frac{c_{2q}^i}{(q-1)!}t^{(q-1)}\right)e^{(-\lambda_2 t)} + \cdots \\ & + \left(c_{j1}^i + \frac{c_{j2}^i}{1!}t + \cdots + \frac{c_{jr}^i}{(r-1)!}t^{(r-1)}\right)e^{(-\lambda_j t)} \\ & + \int_0^t \left[\left(d_{11}^i + \frac{d_{12}^i}{1!}\xi + \cdots + \frac{d_{1p}^i}{(p-1)!}\xi^{(p-1)}\right)e^{(-\lambda_1 \xi)}\right. \\ & \quad + \left(d_{21}^i + \frac{d_{22}^i}{1!}\xi + \cdots + \frac{d_{2q}^i}{(q-1)!}\xi^{(q-1)}\right) \\ & \quad \times e^{(-\lambda_2 \xi)} + \cdots \\ & \quad + \left(d_{j1}^i + \frac{d_{j2}^i}{1!}\xi + \cdots + \frac{d_{jr}^i}{(r-1)!}\xi^{(r-1)}\right) \\ & \quad \left.\times e^{(-\lambda_j \xi)}\right] \nu(t-\xi)\, d\xi. \end{aligned} \tag{19}$$

According to integral property, it is easy to have

$$\begin{aligned} y_i(t) \le & \left(c_{11}^i + \frac{c_{12}^i}{1!}t + \cdots + \frac{c_{1p}^i}{(p-1)!}t^{(p-1)}\right)e^{(-\lambda_1 t)} \\ & + \left(c_{21}^i + \frac{c_{22}^i}{1!}t + \cdots + \frac{c_{2q}^i}{(q-1)!}t^{(q-1)}\right)e^{(-\lambda_2 t)} + \cdots \\ & + \left(c_{j1}^i + \frac{c_{j2}^i}{1!}t + \cdots + \frac{c_{jr}^i}{(r-1)!}t^{(r-1)}\right)e^{(-\lambda_j t)} + |\nu(t)| \\ & \times \left|\int_0^t \left[\left(d_{11}^i + \frac{d_{12}^i}{1!}\xi + \cdots + \frac{d_{1p}^i}{(p-1)!}\xi^{(p-1)}\right)e^{(-\lambda_1 \xi)}\right.\right. \\ & \quad + \left(d_{21}^i + \frac{d_{22}^i}{1!}\xi + \cdots + \frac{d_{2q}^i}{(q-1)!}\xi^{(q-1)}\right) \\ & \quad \times e^{(-\lambda_2 \xi)} + \cdots \\ & \quad + \left(d_{j1}^i + \frac{d_{j2}^i}{1!}\xi + \cdots + \frac{d_{jr}^i}{(r-1)!}\xi^{(r-1)}\right) \\ & \quad \left.\left.\times e^{(-\lambda_j \xi)}\right] d\xi\right|. \end{aligned} \tag{20}$$

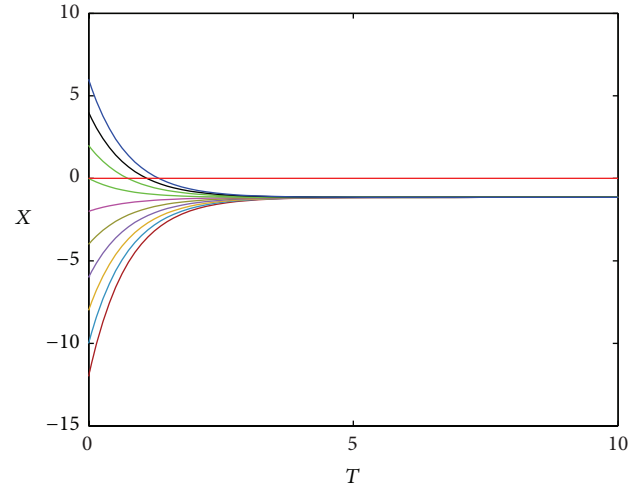

Figure 1: Errors between leader and followers about system (1), in which 0 is globally reachable in $\overline{\mathcal{G}}$ and $\nu(t) = 1.3$.

Since as $t \to +\infty$, we have $e^{(-\lambda t)} \to 0$, then we can get the following inequality:

$$\begin{aligned} & |y_i(t)| \\ & \le \varepsilon + H\left|\frac{d_{11}^i}{\lambda_1} + \frac{d_{12}^i}{\lambda_1^2} + \cdots + \frac{d_{1p}^i}{\lambda_1^p} + \frac{d_{21}^i}{\lambda_2} + \frac{d_{22}^i}{\lambda_2^2}\right. \\ & \qquad \left. + \cdots + \frac{d_{2q}^i}{\lambda_2^q} + \cdots + \frac{d_{j1}^i}{\lambda_j} + \frac{d_{j2}^i}{\lambda_j^2} + \cdots + \frac{d_{jr}^i}{\lambda_j^r}\right| \\ & = \varepsilon + HM_i, \end{aligned} \tag{21}$$

as $t \to +\infty$ where ε is a function close to 0, H is the upper bound of $\nu(t)$, and $M_i = |(d_{11}^i/\lambda_1) + (d_{12}^i/\lambda_1^2) + \cdots + (d_{1p}^i/\lambda_1^p) + (d_{21}^i/\lambda_2) + (d_{22}^i/\lambda_2^2) + \cdots + (d_{2q}^i/\lambda_2^q) + \cdots + (d_{j1}^i/\lambda_j) + (d_{j2}^i/\lambda_j^2) + \cdots + (d_{jr}^i/\lambda_j^r)|$. It shows that the upper bound of $y_i(t)$ is influenced by $\nu(t)$ and the coupling matrix A. Define $M = \max_{i=1,2,\ldots,n}\{M_i\}$ and choose $\varepsilon = 0$; we have

$$|x_i(t) - x_0(t)| = |y_i(t)| \le HM, \tag{22}$$

as $t \to +\infty$. Then, any agent of the system will enter into a region with the leader as the center bounded by HM within sufficient time.

This completes the proof. □

Remark 1. In Theorem 4, the error between the leader 0 and any agent is bounded. If the velocity of leader is zero, we can get that the error will tend to zero, which implies that all the agents will asymptotically approach the same states of the leader. If the velocity of the leader is nonzero and bounded, it is easy to see that the states and velocities of all the followers will keep in a bounded region following the leader.

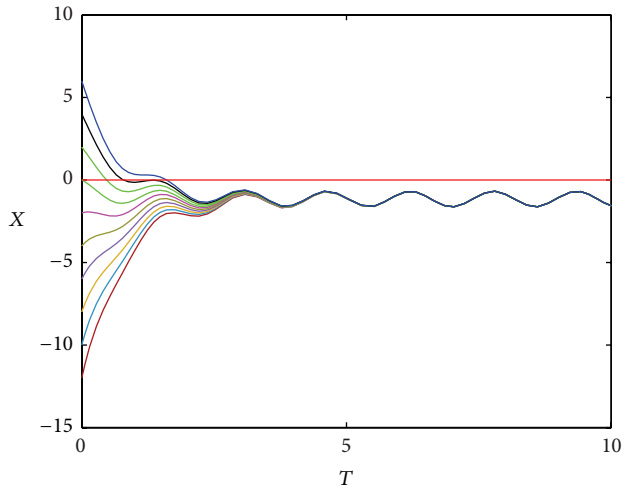

Figure 2: Errors between leader and followers about system (1), in which 0 is globally reachable in $\overline{\mathcal{G}}$ and $v(t) = 1.5 + 2\sin(4t)$.

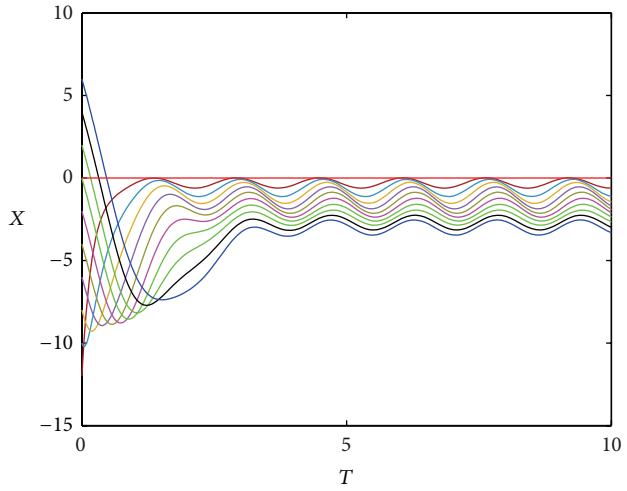

Figure 3: Errors between leader and followers about system (1), in which 0 is globally reachable in $\overline{\mathcal{G}}$ and $v(t) = 0.7$.

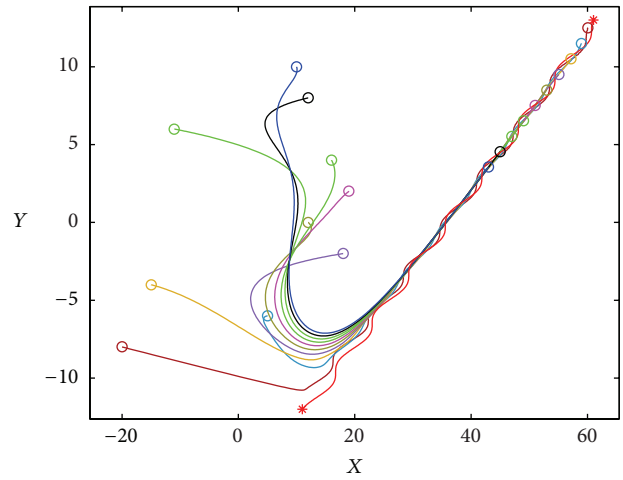

Figure 4: Trajectories of the agents about system (1), in which 0 is globally reachable in $\overline{\mathcal{G}}$ and $v(t) = 0.7 + \sin(t)$.

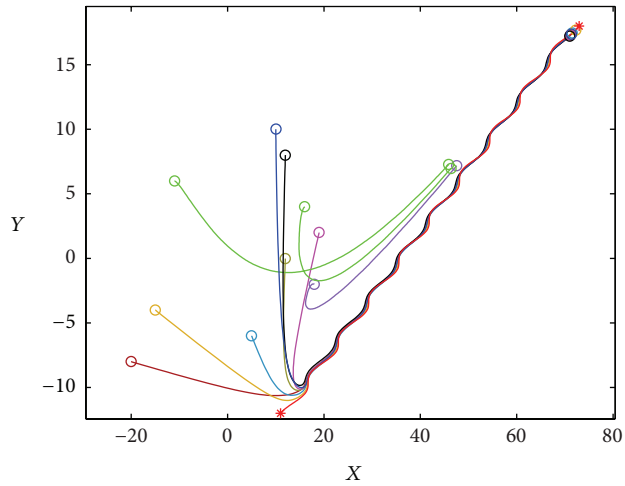

Figure 5: Trajectories of the agents about system (1), in which 0 is globally reachable in $\overline{\mathcal{G}}$ and $v(t) = 0.7$.

4. Numerical Simulations

In order to verify the above theoretical analysis, we present some numerical simulations to illustrate the systems. These simulations are performed with ten followers and one leader, and the initial positions of the agents are chosen randomly. The coupling matrix A is given based on certain conditions.

Figures 1, 2, and 3 show the errors between leader and followers about system (1), under different coupling topology and control. It is easy to see that the states of the error are contained in a bounded region. Figures 4 and 5 depict the trajectories of the agents in 2-dimensional Euclidian space. If leader agent in the coupling topology is globally reachable, then the followers in the system will reach synchronization with the leader within sufficient time. Figures 6 and 7 show the trajectories of the agents in 3-dimensional Euclidian space, in which the states of the followers are influenced by the state of leader, and all agents in the system can achieve consensus eventually.

5. Conclusion

In this paper, we have investigated the coordinated control of leader-following multiagent systems. It is proved that the agents of the systems will aggregate and form a cluster following the leader asymptotically. Meanwhile, we have studied the coupling topology among the agents in the general case. The systems considered in this paper can better reflect the collective behavior in practice. It is clear that the ideas and approaches about graph theory and linear dynamical system theory will play an important role in the analysis of the multiagent system. Finally, simulations give an effective demonstration of the leader-following systems.

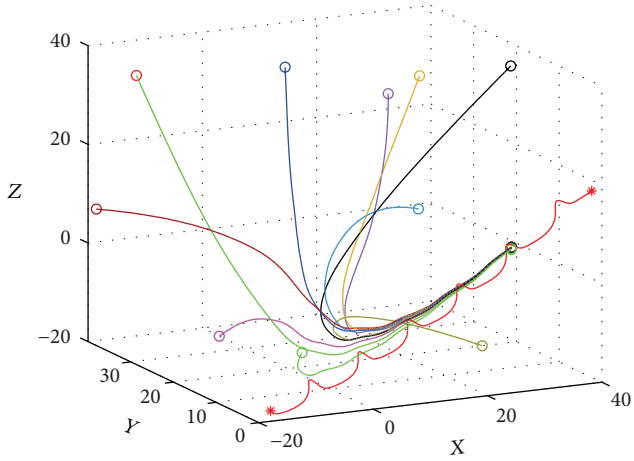

Figure 6: Trajectories of the agents about system (1), in which 0 is globally reachable in $\overline{\mathcal{G}}$.

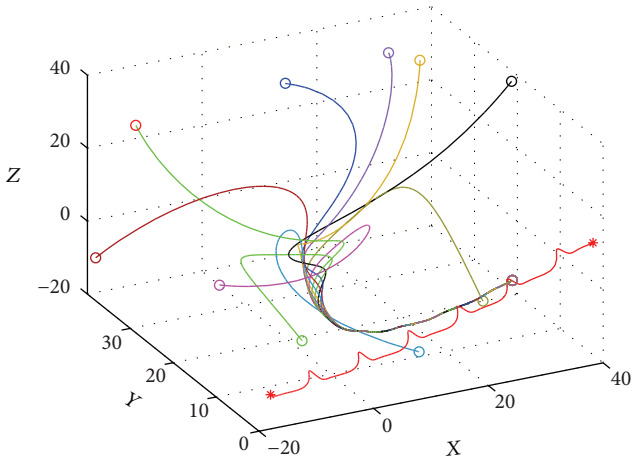

Figure 7: Trajectories of the agents about system (1), in which 0 is globally reachable in $\overline{\mathcal{G}}$.

Conflict of Interests

The authors declare that there is no conflict of interests regarding the publication of this paper.

Acknowledgments

This work was supported by the National Natural Science Foundation of China under Grant no. 61304049, the Science and Technology Development Plan Project of Beijing Education Commission (no. KM201310009011), and the Plan training project of excellent young teacher of North China University of Technology.

References

[1] T. Vicsek, A. Czirk, E. Ben-Jacob, I. Cohen, and O. Shochet, "Novel type of phase transition in a system of self-driven particles," *Physical Review Letters*, vol. 75, no. 6, pp. 1226–1229, 1995.

[2] A. Jadbabaie, J. Lin, and A. S. Morse, "Coordination of groups of mobile autonomous agents using nearest neighbor rules," *IEEE Transactions on Automatic Control*, vol. 48, no. 6, pp. 988–1001, 2003.

[3] R. Olfati-Saber, "Flocking for multi-agent dynamic systems: algorithms and theory," *IEEE Transactions on Automatic Control*, vol. 51, no. 3, pp. 401–420, 2006.

[4] H. Su, X. Wang, and Z. Lin, "Flocking of multi-agents with a virtual leader," *IEEE Transactions on Automatic Control*, vol. 54, no. 2, pp. 293–307, 2009.

[5] H. Shi, L. Wang, and T. Chu, "Virtual leader approach to coordinated control of multiple mobile agents with asymmetric interactions," *Physica D: Nonlinear Phenomena*, vol. 213, no. 1, pp. 51–65, 2006.

[6] H. Su, X. Wang, and G. Chen, "A connectivity-preserving flocking algorithm for multi-agent systems based only on position measurements," *International Journal of Control*, vol. 82, no. 7, pp. 1334–1343, 2009.

[7] Y. Hong, J. Hu, and L. Gao, "Tracking control for multi-agent consensus with an active leader and variable topology," *Automatica*, vol. 42, no. 7, pp. 1177–1182, 2006.

[8] H. Su, X. Wang, and W. Yang, "Flocking in multi-agent systems with multiple virtual leaders," *Asian Journal of Control*, vol. 10, no. 2, pp. 238–245, 2008.

[9] V. Gazi and K. M. Passino, "Stability analysis of swarms," *Institute of Electrical and Electronics Engineers. Transactions on Automatic Control*, vol. 48, no. 4, pp. 692–697, 2003.

[10] W. Ren, "Collective motion from consensus with Cartesian coordinate coupling," *IEEE Transactions on Automatic Control*, vol. 54, no. 6, pp. 1330–1335, 2009.

[11] H. Su, X. Wang, and G. Chen, "Rendezvous of multiple mobile agents with preserved network connectivity," *Systems and Control Letters*, vol. 59, no. 5, pp. 313–322, 2010.

[12] V. Gazi and K. M. Passino, "Stability analysis of social foraging swarms," *IEEE Transactions on Systems, Man, and Cybernetics B: Cybernetics*, vol. 34, no. 1, pp. 539–557, 2004.

[13] H. Su, G. Chen, X. Wang, and Z. Lin, "Adaptive second-order consensus of networked mobile agents with nonlinear dynamics," *Automatica*, vol. 47, no. 2, pp. 368–375, 2011.

[14] B. Liu, T. Chu, and L. Wang, "Stability and oscillation of swarm with interaction time delays," in *Proceedings of the American Control Conference (ACC '07)*, pp. 4600–4605, July 2007.

[15] J. Y. Yu and L. Wang, "Group consensus of multi-agent systems with undirected communication graphs," in *Proceedings of the 7th Asian Control Conference*, pp. 105–110, 2009.

[16] H. Su, M. Chen, J. Lam, and Z. Lin, "Semi-global leader-following consensus of linear multi-agent systems with input saturation via low gain feedback," *IEEE Transactions on Circuits and Systems. I: Regular Papers*, vol. 60, no. 7, pp. 1881–1889, 2013.

[17] B. Liu, T. G. Chu, L. Wang, and Z. Wang, "Collective motion of a class of social foraging swarms," *Chaos, Solitons and Fractals*, vol. 38, no. 1, pp. 277–292, 2008.

[18] B. Liu, X. M. Zhu, and J. Zhang, "Consensus analyss of the multi-agent sysem," in *Proceedings of the 3rd International Workshop on Chaos-Fractals Theories and Applications, (IWCFTA '10)*, pp. 383–387, October 2010.

[19] H. Shi, L. Wang, and T. G. Chu, "Stability behavior of multi-agent system," *Journal of Control Theory and Applications*, vol. 4, pp. 313–318, 2004.

[20] H. Su, Z. Rong, M. Z. Q. Chen, X. Wang, G. Chen, and H. Wang, "Decentralized adaptive pinning control for cluster synchronization of complex dynamical networks," *IEEE Transactions on Cybernetics*, vol. 43, pp. 394–399, 2013.

[21] Z. Yang, Z. Liu, Z. Chen, and Z. Yuan, "Tracking control for multi-agent consensus with an active leader and directed topology," in *Proceeding of the 7th World Congress on Intelligent Control and Automation (WCICA '08)*, pp. 1037–1041, Chongqing, China, June 2008.

[22] V. Gazi and K. M. Passino, "Stability analysis of swarms in an environment with an attractant/repellent Profile," in *Proceedings of the American Control Conference*, pp. 1819–1824, 2002.

Hindawi Publishing Corporation
Mathematical Problems in Engineering
Volume 2014, Article ID 697895, 11 pages
http://dx.doi.org/10.1155/2014/697895

Research Article

Risk-Sensitive Multiagent Decision-Theoretic Planning Based on MDP and One-Switch Utility Functions

Wei Zeng, Hongtao Zhou, and Mingshan You

School of Automation, Huazhong University of Science and Technology, Wuhan 430074, China

Correspondence should be addressed to Wei Zeng; zengwei@mail.hust.edu.cn

Received 28 April 2014; Accepted 16 June 2014; Published 7 July 2014

Academic Editor: Wei Zhang

In high stakes situations decision-makers are often risk-averse and decision-making processes often take place in group settings. This paper studies multiagent decision-theoretic planning under Markov decision processes (MDPs) framework with considering the change of agent's risk attitude as his wealth level varies. Based on one-switch utility function that describes agent's risk attitude change with his wealth level, we give the additive and multiplicative aggregation models of group utility and adopt maximizing expected group utility as planning objective. When the wealth level approaches infinity, the characteristics of optimal policy are analyzed for the additive and multiplicative aggregation model, respectively. Then a backward-induction method is proposed to divide the wealth level interval from negative infinity to initial wealth level into subintervals and determine the optimal policy in states and subintervals. The proposed method is illustrated by numerical examples and the influences of agent's risk aversion parameters and weights on group decision-making are also analyzed.

1. Introduction

Decision-theoretic planning is to compute optimal policy that is formed by courses of action to maximize expected reward with considering actions that have uncertain outcomes [1]. In high stakes situations with the possibility of high wins and losses, such as emergency and crisis response, business and investment decision, military battle, and lottery, decision-makers are often risk-averse. In the risk-sensitive decisions, exponential utility function is one of the typical utility functions to model decision-maker's risk aversion and maximizing expected utility is the most commonly used rule instead of maximizing expected reward. However, the risk attitude of a decision-maker modeled by exponential utility function is independent of his wealth level and does not change as his wealth level varies, while in reality personal risk attitude often changes with his wealth level [2–4]. Bell proposes a kind of utility function, named one-switch utility function, to model an agent who is always risk-averse but becomes risk neutral as his wealth increases [2]. Bell and Fishburn take further studies on the characteristics of a form of one-switch utility function that is a combination of linear utility function and exponential utility function [5]. Liu and Koenig give a form of one-switch utility function with considering agent's risk aversion parameter γ ($0 < \gamma < 1$); that is, $u(w) = w - D\gamma^w$, where w denotes the wealth level and D is a parameter to adjust tradeoff between risk neutrality and risk aversion. This form of one-switch utility function not only describes the change of agent's risk attitude, but also presents the degree of agent's risk aversion by the quantitative risk aversion parameter γ [6–8].

For decision-theoretic planning problems, Markov decision processes (MDPs) framework is adopted broadly as an underlying model. Howard and Matheson in their seminal paper introduce risk-sensitive MDPs based on maximizing the expected exponential utility [9]. In the follow-up related studies structural properties of optimal solution and algorithms to compute optimal policy are investigated based on exponential utility function [10–12]. If an agent is risk-sensitive, it is necessary to consider the possible change of agent's risk attitude when his wealth level varies and further influence on the decisions in the next stage. Liu and Koenig

study Markov decision processes with considering agent's risk-sensitive attitude modeled by one-switch utility function and propose an exact backward-induction algorithm to compute optimal policy [8].

In reality decision-making processes often take place in group settings due to a single decision-maker's limited decision-making ability. For the group decision-making problem, group utility is usually got by aggregating personal utilities and then group decisions are made based on the group utility. The aggregation methods include additive value model and multiplicative value rule. Other methods such as multiobjective linear programming [13], fuzzy sets method [14, 15], and interactive approach [16, 17] are used to aggregate individual decision information including attribute weights and attribute values into group decisions. Besides, some researches on group decision-making problem take time into consideration. Xu investigates multistage multiattribute group decision-making problems in which the weight information on a collection of attributes and the decision information on a finite set of alternatives with respect to the attributes are collected at different stages [18].

This paper focuses on decision-theoretic planning problem in which sequential decisions are made by a group of risk-sensitive members. Considering agent's risk-sensitive attitude and wealth level, this paper studies the risk-sensitive multiagent decision-theoretic planning problem based on one-switch utility function and MDP framework. Two group utility functions based, respectively, on additive value model and multiplicative value model of one-switch utility functions are given. Backward-induction algorithms for these two kinds of group utility functions to compute optimal policy of risk-sensitive group decision-making under MDP framework are proposed.

The rest of this paper is organized as follows. One-switch utility function and risk-sensitive MDP model augmented with wealth level are introduced in Section 2. In Section 3, additive and multiplicative aggregation model of one-switch utility functions are given. We analyze the characteristics of optimal policy when the wealth level approaches negative infinity for additive and multiplicative aggregation model, respectively, in Section 3. In Section 4, detailed backward-induction algorithms are proposed to solve the multiagent decision-theoretic planning problem based, respectively, on additive and multiplicative aggregation model. Numerical examples are used to illustrate the proposed method and analyze the influences of agent's risk aversion parameters and weights on group decision-making in Section 5. Finally, a conclusion of this paper and suggested topics for future research are presented in Section 6.

2. Risk-Sensitive MDP Model Augmented with Wealth Level

2.1. One-Switch Utility Function. One-switch utility function is a kind of utility function to describe the change of agent's risk attitude as his wealth level varies. In detail, there exists a wealth level w; when the agent's wealth level is below w, the agent is risk-averse, but when his wealth level increases and becomes higher than w, the agent becomes risk neutral. For agent i, one-switch utility function given by Liu and Koenig is shown as follows [6–8]:

$$u_i(w) = w - D_i {\gamma_i}^w = u_l + D \cdot u_{i,e}(w), \quad (1)$$

where w is wealth level, γ_i is agent i's risk aversion parameter, and $0 < \gamma_i < 1$. D_i is a constant that provides an adjustable tradeoff between risk neutrality (linear term) and risk aversion (exponential term). $u_l = w$ is a linear utility function. $u_{i,e}(w) = -{\gamma_i}^w$ is agent i's exponential utility function.

2.2. Risk-Sensitive MDP Model Augmented with Wealth Level. In the paper goal directed Markov decision problem (GDMDP) is adopted as underlying model of decision-theoretic planning problem [8]. GDMDP is a kind of MDP with a finite set of goal states. When an agent reaches a goal state, he stops acting and receives no more rewards thereafter. One-switch utility function is used to describe the agent's risk-sensitive attitude and maximizing expected utility is adopted as planning objective instead of maximizing expected reward. As wealth level is included in the one-switch utility function, it is necessary to consider the wealth level as a component of the system state of GDMDP.

Formally, a GDMDP consists of a finite set of states S with wealth levels W, so the augmented state set of GDMDP is denoted by (S, W). Goal state set is (G, W), where $G \subseteq W$. Nongoal state set is (S', W), where $S' = S \setminus G$.

The agent's action set is A_s. The agent chooses an action $a \in A_s$ to execute in its current state $s \in S$.

The agent's execution of action a in state s results in a finite reward $r(s, a, s')$ and a transition to successor state $s' \in S$ with probability $P(s' \mid s, a)$. In the paper only cost is considered and assumed reward is strictly negative, $r(s, a, s') < 0$.

We also use s_t and a_t to denote the state and action at time step t $(t = 0, 1, 2, \ldots)$. $r_t = r(s_t, a_t, s_{t+1})$ is used to denote the reward for executing action a_t. After the agent reaches a goal state, $r_t = 0$.

$w_t = w_0 + \sum_{i=0}^{i=t-1} r_i$ is the agent's wealth level at time step t, where the initial wealth level is denoted by w_0.

For the MDP model augmented with wealth level, the optimal policy maps every combination of a state $s \in S'$ and wealth level w to an action $a \in A_s$ that an agent in state s with wealth level w should execute to maximize expected utility.

For agent i's exponential utility function $u_{i,e}(w)$ and all policies π, we define the value $v_{i,e}^{\pi}(s, w) = \lim_{t \to \infty} E_{s,w}^{\pi}[u_{i,e}(w_t)]$ as the expected exponential utility of agent i with initial state s and initial wealth level w that follows policy π.

The optimal value $v_{i,e}^{*}(s, w) = \max_{\pi} v_{i,e}^{\pi}(s, w)$ is defined as the highest possible expected exponential utility of agent i with initial state s and initial wealth level w. Assume $v_{i,e}^{*}(s, w)$ is finite for all state $s \in S$ and wealth levels w.

An optimal policy $\pi_{i,e}^{*}(s, w)$ is defined as a policy with $v_{i,e}^{\pi_{i,e}^{*}}(s, w) = v_{i,e}^{*}(s, w)$ for all state $s \in S$ and wealth levels w.

Similarly, for linear utility function $u_l(w)$, we use $v_l^{\pi}(s, w)$, $v_l^{*}(s, w)$, and $\pi_l^{*}(s, w)$ to denote expected utility, optimal value, and optimal policy, respectively.

It is worth noting that differently from Liu and Koenig [8], the paper focuses on the decision-making in group setting. So the value function in MDP will be replaced by group utility function which is the aggregation of personal one-switch utilities and the planning objective is to maximize the expected group utility.

3. Utility Aggregation Model of One-Switch Utility Functions

Group utility is the aggregation of personal utilities. The common methods include additive value model and multiplicative value model. In the following sections we will discuss additive and multiplicative value model for the aggregation of personal one-switch utility functions, respectively.

3.1. Additive Aggregation Model of One-Switch Utility Functions. In general, additive aggregation model of group utility is defined as follows:

$$u(w) = \sum_{i=1}^{n} k_i u_i(w), \tag{2}$$

where k_i is the weight of agent i's utility, $0 < k_i < 1$, and $\sum_{i=1}^{n} k_i = 1$.

Thus the additive aggregation model of one-switch utility functions is defined as follows:

$$\begin{aligned} u(w) &= \sum_{i=1}^{n} k_i u_i(w) \\ &= w - k_1 D_1 {\gamma_1}^w - k_2 D_2 {\gamma_2}^w - \cdots - k_n D_n {\gamma_n}^w. \end{aligned} \tag{3}$$

According to MDP, the expected group utility for all policies π and state (s, w) is presented as follows:

$$\begin{aligned} v^\pi(s,w) &= u(w) \\ &= w - k_1 D_1 {\gamma_1}^w \\ &\quad - k_2 D_2 {\gamma_2}^w - \cdots - k_n D_n {\gamma_n}^w \quad \forall s \in G,\ \forall w \\ v^\pi(s,w) &= \sum_{s' \in S} P\left(s' \mid s, \pi(s,w)\right) \\ &\quad \cdot v^\pi\left(s', w + r\left(s, \pi(s,w), s'\right)\right) \quad \forall s \in S',\ \forall w. \end{aligned} \tag{4}$$

Then, the optimal value $v^*(s, w)$ is presented as follows:

$$\begin{aligned} v^*(s,w) &= u(w) \\ &= w - k_1 D_1 {\gamma_1}^w \\ &\quad - k_2 D_2 {\gamma_2}^w - \cdots - k_n D_n {\gamma_n}^w \quad \forall s \in G,\ \forall w \\ v^*(s,w) &= \max_{a \in A_s} \sum_{s' \in S} P\left(s' \mid s, a\right) \\ &\quad \cdot v^*\left(s', w + r\left(s, a, s'\right)\right) \quad \forall s \in S',\ \forall w. \end{aligned} \tag{5}$$

Next, we will derive the relationship between the expected group utility and the expected personal linear and exponential utility for the additive aggregation model.

For all policies π, the expected group utility of the additive aggregation model of one-switch utility functions is presented as follows:

$$\begin{aligned} v^\pi(s,w) &= \lim_{t\to\infty} E^\pi_{s,w}\left[u(w_t)\right] \\ &= \lim_{t\to\infty} E^\pi_{s,w}\left[u_l(w_t) + k_1 D_1 u_{1,e}(w_t) \right. \\ &\qquad + k_2 D_2 u_{2,e}(w_t) \\ &\qquad \left. + \cdots + k_n D_n u_{n,e}(w_t)\right] \\ &= \lim_{t\to\infty} E^\pi_{s,w}\left[u_l(w_t)\right] \\ &\quad + \lim_{t\to\infty} E^\pi_{s,w}\left[k_1 D_1 u_{1,e}(w_t)\right] \\ &\quad + \cdots + \lim_{t\to\infty} E^\pi_{s,w}\left[k_n D_n u_{n,e}(w_t)\right] \\ &= \lim_{t\to\infty} E^\pi_{s,w}\left[w + \sum_{i=0}^{t-1} r_i\right] \\ &\quad + \lim_{t\to\infty} E^\pi_{s,w}\left[k_1 D_1 {\gamma_1}^{w+\sum_{i=0}^{t-1} r_i}\right] \\ &\quad + \cdots + \lim_{t\to\infty} E^\pi_{s,w}\left[k_n D_n {\gamma_n}^{w+\sum_{i=0}^{t-1} r_i}\right] \\ &= w + \lim_{t\to\infty} E^\pi_{s,w}\left[\sum_{i=0}^{t-1} r_i\right] \\ &\quad + k_1 D_1 {\gamma_1}^w \lim_{t\to\infty} E^\pi_{s,w}\left[{\gamma_1}^{\sum_{i=0}^{t-1} r_i}\right] \\ &\quad + \cdots + k_n D_n {\gamma_n}^w \lim_{t\to\infty} E^\pi_{s,w}\left[{\gamma_n}^{\sum_{i=0}^{t-1} r_i}\right] \\ &= w + v^\pi_l(s) + k_1 D_1 {\gamma_1}^w v^\pi_{1,e}(s) \\ &\quad + \cdots + k_n D_n {\gamma_n}^w v^\pi_{n,e}(s), \end{aligned} \tag{6}$$

where $v^\pi_l(s)$ and $v^\pi_{i,e}(s)$ satisfy the following policy-evaluation equations, respectively, [8, 19, 20]:

$$\begin{aligned} v^\pi_l(s) &= 0 \quad s \in G \\ v^\pi_l(s) &= \sum_{s' \in S} P\left(s' \mid s, \pi(s)\right)\left[r\left(s, \pi(s), s'\right) + v^\pi_l\left(s'\right)\right] \quad s \in S' \\ v^\pi_{i,e}(s) &= -1 \quad s \in G \\ v^\pi_{i,e}(s) &= \sum_{s' \in S} P\left(s' \mid s, \pi(s)\right)\left[{\gamma_i}^{r(s,\pi(s),s')} \cdot v^\pi_{i,e}\left(s'\right)\right] \quad s \in S'. \end{aligned} \tag{7}$$

From the above policy-evaluation equation (6), we obtain the relationship between $v^\pi(s, w)$ and expected linear utility $v^\pi_l(s)$ and expected personal exponential utility $v^\pi_{i,e}(s)$ for the additive aggregation model, where $v^\pi_l(s)$ and $v^\pi_{i,e}(s)$ are independent of the wealth level w.

3.2. Multiplicative Aggregation Model of One-Switch Utility Functions. In the paper we adopt the following multiplicative aggregation model of group utility:

$$u(w) = \sum_{i=1}^{n} k_i u_i(w) + \sum_{i=1, j>i}^{n} k_{ij} u_i(w) u_j(w) + \cdots + k_{123\cdots n} u_1(w) u_2(w) \cdots u_n(w), \tag{8}$$

where $k_1, k_2, \ldots, k_n, k_{12}, k_{23}, \ldots, k_{123\cdots n}$ are constants and $0 < k_i < 1$.

For simplicity, in the paper we only consider the case $n = 2$. For $n > 2$, the derivation of multiplicative aggregation model is similar.

For $n = 2$, multiplicative aggregation model of one-switch utility functions is simplified as follows:

$$\begin{aligned} u(w) &= k_1 u_1(w) + k_2 u_2(w) + k_{12} u_1(w) u_2(w) \\ &= k_{12} w^2 - k_{12} D_1 w \gamma_1{}^w - k_{12} D_2 w \gamma_2{}^w \\ &\quad + k_{12} D_1 D_2 (\gamma_1 \gamma_2)^w + k_1 w + k_2 w \\ &\quad - k_1 D_1 \gamma_1{}^w - k_2 D_2 \gamma_2{}^w. \end{aligned} \tag{9}$$

According to MDP, the optimal value $v^*(s, w)$ is presented as follows:

$$\begin{aligned} v^*(s, w) &= u(w) \quad \forall s \in G, \ \forall w \\ v^*(s, w) &= \max_{a \in A_s} \sum_{s' \in S} P(s' \mid s, a) \\ &\quad \cdot v^*(s', w + r(s, a, s')) \quad \forall s \in S', \ \forall w. \end{aligned} \tag{10}$$

For the multiplicative aggregation model of one-switch utility functions and all policies π, the expected group utility is

$$\begin{aligned} v^\pi(s, w) &= \lim_{t \to \infty} E^\pi_{s,w}[u(w_t)] \\ &= \lim_{t \to \infty} E^\pi_{s,w}[k_1 u_1(w) + k_2 u_2(w) + k_{12} u_1(w) u_2(w)] \\ &= k_1 \lim_{t \to \infty} E^\pi_{s,w}[u_1(w)] + k_2 \lim_{t \to \infty} E^\pi_{s,w}[u_2(w)] \\ &\quad + k_{12} \lim_{t \to \infty} E^\pi_{s,w}[u_1(w)] \cdot \lim_{t \to \infty} E^\pi_{s,w}[u_2(w)]. \end{aligned} \tag{11}$$

According to the fact that $\lim_{t \to \infty} E^\pi_{s,w}[u_i(w)] = w + v^\pi_l(s) + D_1 \gamma_1{}^w v^\pi_{i,e}(s)$ [8], we have

$$\begin{aligned} v^\pi(s, w) &= k_1 (w + v^\pi_l(s) + D_1 \gamma_1{}^w v^\pi_{1,e}(s)) \\ &\quad + k_2 (w + v^\pi_l(s) + D_2 \gamma_2{}^w v^\pi_{2,e}(s)) \\ &\quad + k_{12} (w + v^\pi_l(s) + D_1 \gamma_1{}^w v^\pi_{1,e}(s)) \\ &\quad \times (w + v^\pi_l(s) + D_2 \gamma_2{}^w v^\pi_{2,e}(s)). \end{aligned} \tag{12}$$

From the above policy-evaluation equation (12), we obtain the relationship between expected group utility $v^\pi(s, w)$ and expected linear utility $v^\pi_l(s)$ and expected personal exponential utility $v^\pi_{i,e}(s)$ for the multiplicative aggregation model.

4. Preparation for Backward-Induction Method

To solve the optimal policy of the additive and multiplicative aggregation model of one-switch utility functions, backward-induction method is adopted. In the paper the value range of wealth level is a continuous interval $(-\infty, w_0]$; we first compute the optimal policy when wealth level $w \to -\infty$ that is represented by $\pi^*_{-\infty}$. Then increase the wealth level until $\pi^*_{-\infty}$ is no longer an optimal policy and get a wealth level threshold. Increase further the wealth level and get the next wealth level threshold similarly. The backward-induction method ends when the wealth level is larger than initial wealth level w_0. Thus the continuous wealth level interval is divided into subintervals by the thresholds. We use $((s, (w^i, w^{i+1}]), a)$ to denote action a executed in state s and wealth level interval $(w^i, w^{i+1}]$ (w^i denotes a wealth level threshold and $i = 0, 1, 2, \ldots$). In this section we will analyze the characteristics of optimal policy when the wealth level w approaches negative infinity for additive and multiplicative aggregation model, respectively.

Lemma 1. *For additive aggregation model of one-switch utility functions, if agent i is the most risk-averse one, that is, $\gamma_i < \gamma_j$, for any $j \neq i$, $i, j = 1, 2, \ldots, n$, then*

$$\lim_{w \to -\infty} v^*(s, w) \gamma_i{}^{-w} = k_i D_i v^*_{i,e}(s) \quad \text{for all states } s \in S. \tag{13}$$

Proof. For all optimal policies π^*, we have

$$\begin{aligned} \lim_{w \to -\infty} v^*(s, w) \gamma_i{}^{-w} &= \lim_{w \to -\infty} v^{\pi^*}(s, w) \gamma_i{}^{-w} \\ &= \lim_{w \to -\infty} \left[w \gamma_i{}^{-w} + v^{\pi^*}_l(s) \gamma_i{}^{-w} + k_1 D_1 \left(\frac{\gamma_1}{\gamma_i} \right)^w v^{\pi^*}_{1,e}(s) \right. \\ &\quad \left. + \cdots + k_i D_i v^{\pi^*}_{i,e}(s) + \cdots + k_n D_n \left(\frac{\gamma_n}{\gamma_i} \right)^w v^{\pi^*}_{n,e}(s) \right]. \end{aligned} \tag{14}$$

As $\gamma_j / \gamma_i > 1$, $j \neq i$, we can derive $\lim_{w \to -\infty} k_j D_j (\gamma_j / \gamma_i)^w v^{\pi^*}_{j,e}(s) = 0$.

Thus $\lim_{w \to -\infty} v^*(s, w) \gamma_i{}^{-w} = k_i D_i v^{\pi^*}_{i,e}(s) \leq k_i D_i v^*_{i,e}(s)$.

On the other hand, for all optimal policies $\pi^*_{i,e}$, according to the fact that $v^*(s, w) \geq v^\pi(s, w)$ for all policies π, we have

$$\begin{aligned} \lim_{w \to -\infty} v^*(s, w) \gamma_i{}^{-w} &\geq \lim_{w \to -\infty} v^{\pi^*_{i,e}}(s, w) \gamma_i{}^{-w} \\ &= \lim_{w \to -\infty} \left[w \gamma_i{}^{-w} + v^{\pi^*_{i,e}}_l(s) \gamma_i{}^{-w} \right. \\ &\quad \left. + k_1 D_1 \left(\frac{\gamma_1}{\gamma_i} \right)^w v^{\pi^*_{i,e}}_{1,e}(s) \right. \end{aligned}$$

$$+\cdots+k_iD_iv_{i,e}^{*\pi_{i,e}^*}(s)+\cdots+k_nD_n\left(\frac{\gamma_n}{\gamma_i}\right)^w v_{n,e}^{*\pi_{i,e}^*}(s)\Big]=k_iD_iv_{i,e}^{*}(s). \tag{15}$$

Therefore, the lemma holds. □

Lemma 1 implies that the optimal policy for the additive aggregation model of one-switch utility functions is the same as the most risk-averse agent's optimal policy for the exponential utility function as the wealth level $w \to -\infty$.

Lemma 2. *For multiplicative aggregation model of one-switch utility functions,* $\lim_{w\to-\infty}v^*(s,w)\gamma_3^{-w}=k_{12}D_1D_2v_{3,e}^*(s)$ *for all states* $s\in S$ *and* $\gamma_3=\gamma_1\gamma_2$, *where* $v_{3,e}^*(s,w)$ *is the highest expected exponential utility with risk aversion parameter* γ_3.

Proof. For all optimal policies π^*, we have

$$\begin{aligned}\lim_{w\to-\infty}v^*(s,w)\gamma_3^{-w}&=\lim_{w\to-\infty}v^{\pi^*}(s,w)\gamma_3^{-w}\\&=\lim_{w\to-\infty}\gamma_3^{-w}\Big[k_1\left(w+v_l^{\pi^*}(s)+D_1{\gamma_1}^w v_{1,e}^{\pi^*}(s)\right)\\&\quad+k_2\left(w+v_l^{\pi^*}(s)+D_2{\gamma_2}^w v_{2,e}^{\pi^*}(s)\right)\\&\quad+k_{12}\left(w+v_l^{\pi^*}(s)+D_1{\gamma_1}^w v_{1,e}^{\pi^*}(s)\right)\\&\quad\times\left(w+v_l^{\pi^*}(s)+D_2{\gamma_2}^w v_{2,e}^{\pi^*}(s)\right)\Big].\end{aligned} \tag{16}$$

As $\gamma_i/\gamma_3>1, i=1,2,$

Then $\lim_{w\to-\infty}k_iD_i(\gamma_i/\gamma_3)^w v_{i,e}^{\pi^*}(s)=0, \lim_{w\to-\infty}k_iD_iw(\gamma_i/\gamma_3)^w v_{i,e}^{\pi^*}(s)=0.$

Therefore,

$$\begin{aligned}&\lim_{w\to-\infty}v^*(s,w)\gamma_3^{-w}\\&=k_{12}D_1D_2v_{1,e}^{\pi^*}(s)\,v_{2,e}^{\pi^*}(s)\\&=k_{12}D_1D_2\lim_{w\to-\infty}E_{s,w}^{\pi^*}\left[\gamma_1^{\sum_{i=0}^{t-1}r_i}\right]\cdot\lim_{w\to-\infty}E_{s,w}^{\pi}\left[\gamma_2^{\sum_{i=0}^{t-1}r_i}\right]\\&=k_{12}D_1D_2\lim_{w\to-\infty}E_{s,w}^{\pi^*}\left[(\gamma_1\gamma_2)^{\sum_{i=0}^{t-1}r_i}\right]\\&\le k_{12}D_1D_2v_{3,e}^*(s).\end{aligned} \tag{17}$$

On the other hand, for all optimal policies $\pi_{3,e}^*$, according to the fact that $v^*(s,w)\ge v^{\pi}(s,w)$ for all policies π, we have

$$\begin{aligned}&\lim_{w\to-\infty}v^*(s,w)\gamma_3^{-w}\\&\ge\lim_{w\to-\infty}v^{\pi_{3,e}^*}(s,w)\gamma_3^{-w}\\&=\lim_{w\to-\infty}\gamma_3^{-w}\Big[k_1\left(w+v_l^{\pi_{3,e}^*}(s)+D_1{\gamma_1}^w v_{1,e}^{\pi_{3,e}^*}(s)\right)\\&\quad+k_2\left(w+v_l^{\pi_{3,e}^*}(s)+D_2{\gamma_2}^w v_{2,e}^{\pi_{3,e}^*}(s)\right)\\&\quad+k_{12}\left(w+v_l^{\pi_{3,e}^*}(s)+D_1{\gamma_1}^w v_{1,e}^{\pi_{3,e}^*}(s)\right)\\&\quad\times\left(w+v_l^{\pi_{3,e}^*}(s)+D_2{\gamma_2}^w v_{2,e}^{\pi_{3,e}^*}(s)\right)\Big]\\&=k_{12}D_1D_2v_{1,e}^{\pi_{3,e}^*}(s)\,v_{2,e}^{\pi_{3,e}^*}(s)=k_{12}D_1D_2v_{3,e}^*(s).\end{aligned} \tag{18}$$

Therefore, the lemma holds. □

Lemma 2 implies that the optimal policy for the multiplicative aggregation of one-switch utility functions is the same as the optimal policy for a virtual agent's exponential utility function as the wealth level $w \to -\infty$. The virtual agent's risk aversion parameter is the product of every agent's risk aversion parameter in the group.

5. Division of Wealth Level Interval and Backward-Induction Method

The above section gives the optimal policy as the wealth level approaches negative infinity for additive and multiplicative aggregation model of one-switch utility functions, respectively. The next step is to divide the wealth level interval and determine the wealth level thresholds and optimal policies in the intervals by using backward-induction method. In this section we will discuss the backward-induction method in the cases of additive and multiplicative aggregation model.

5.1. The Case of Additive Aggregation Model. For the additive aggregation model of one-switch utility functions, we first give the following theorem to prove the existence of a wealth level threshold $\underline{w}$ and then give the backward-induction algorithm.

Theorem 3. *For all optimal policies* π^*, *there exists a wealth level threshold* $\underline{w}$ *such that it holds for all states* $s\in S'$ *and all wealth levels* $w\le\underline{w}$ *that*

$$\begin{aligned}v_l^*(s,w)=v_l^{\pi^*}(s),\quad v_{i,e}^*(s,w)=v_{i,e}^{\pi^*}(s),\\v^*(s,w)=v^{\pi^*}(s,w),\quad i=1,2,\ldots n.\end{aligned} \tag{19}$$

Please see Appendix A for the proof of Theorem 3.

Theorem 3 shows the existence of the wealth level threshold $\underline{w}$. Next we will show how to determine the wealth level threshold $\underline{w}$.

After getting $\pi_{-\infty}^*$ when wealth level $w \to -\infty$, assume $\pi_{-\infty}^*$ is the optimal policy for the wealth level interval $(-\infty,\underline{w}]$; then for wealth level w in the interval $(\underline{w}, \min_{a\in A_s}(\underline{w}-r(s,a,s')))$, where $r(s,a,s')$ is the reward got by executing one step action, $\pi_{-\infty}^*$ is no longer the optimal

policy, and assume π' is the optimal policy; according to (5); for all nongoal states, we have

$$v^*(s,w) = \max_{a\in A_s} \sum_{s'\in S} P\left(s' \mid s,a\right) \cdot v^{\pi^*_{-\infty}}\left(s', w + r\left(s,a,s'\right)\right). \tag{20}$$

As $w + r(s,a,s') < \underline{w}$,

$$\begin{aligned} v^*(s,w) &= \max_{a\in A_s} \sum_{s'\in S} P\left(s' \mid s,a\right) \cdot v^{\pi^*_{-\infty}}\left(s', w + r\left(s,a,s'\right)\right) \\ &= \max_{a\in A_s} \sum_{s'\in S} P\left(s' \mid s,a\right) \cdot \left(w + r\left(s,a,s'\right) + v_l^{\pi^*_{-\infty}}(s) \right. \\ &\qquad + k_1 D_1 {\gamma_1}^{w+r(s,a,s')} v_{1,e}^{\pi^*_{-\infty}}(s) \\ &\qquad \left. + \cdots + k_n D_n {\gamma_n}^{w+r(s,a,s')} v_{n,e}^{\pi^*_{-\infty}}(s)\right) \\ &= \max_{a\in A_s} \left[w + v_l^{\pi^*_{-\infty}}(s,a) + k_1 D_1 {\gamma_1}^{w} v_{1,e}^{\pi^*_{-\infty}}(s,a) \right. \\ &\qquad \left. + \cdots + k_n D_n {\gamma_n}^{w} v_{n,e}^{\pi^*_{-\infty}}(s,a)\right], \end{aligned} \tag{21}$$

where

$$\begin{aligned} v_l^*(s,a) &= \sum_{s'\in S} P\left(s' \mid s,a\right)\left[r\left(s,a,s'\right) + v_l^*\left(s'\right)\right], \\ v_{i,e}^*(s,a) &= \sum_{s'\in S} P\left(s' \mid s,a\right)\left[{\gamma_i}^{r(s,a,s')} v_{i,e}^*\left(s'\right)\right]. \end{aligned} \tag{22}$$

For $s \in S' \setminus G$, $a_j \in A_s \setminus \pi^*_{-\infty}(s)$, because the optimal policy is π', not $\pi^*_{-\infty}$ now under assumption, we have

$$\begin{aligned} &\sum_{s'\in S} P\left(s' \mid s, \pi^*_{-\infty}(s)\right) \cdot v^{\pi^*_{-\infty}}\left(s', w + r\left(s, \pi^*_{-\infty}(s), s'\right)\right) \\ &\quad \geq \sum_{s'\in S} P\left(s' \mid s, a_j\right) \cdot v^{\pi^*_{-\infty}}\left(s', w + r\left(s, a_j, s'\right)\right) \end{aligned} \tag{23}$$

or, equivalently,

$$\begin{aligned} &w + v_l^{\pi^*_{-\infty}}\left(s, \pi^*_{-\infty}(s)\right) + k_1 D_1 {\gamma_1}^{w} v_{1,e}^{\pi^*_{-\infty}}\left(s, \pi^*_{-\infty}(s)\right) \\ &\qquad + \cdots + k_n D_n {\gamma_n}^{w} v_{n,e}^{\pi^*_{-\infty}}\left(s, \pi^*_{-\infty}(s)\right) \\ &\geq w + v_l^{\pi^*_{-\infty}}\left(s, a_j\right) + k_1 D_1 {\gamma_1}^{w} v_{1,e}^{\pi^*_{-\infty}}\left(s, a_j\right) \\ &\qquad + \cdots + k_n D_n {\gamma_n}^{w} v_{n,e}^{\pi^*_{-\infty}}\left(s, a_j\right). \end{aligned} \tag{24}$$

We can get a wealth level threshold $\underline{w}_{\pi^*_{-\infty},s,a_j}$ in equality case of the above weak inequality.

From the algorithm above, we can get the wealth level threshold $\underline{w}$:

$$\underline{w} = \min_{s\in s'} \min_{a_j\in A_s\setminus\pi^*_{-\infty}(s)} \min\left(w_0, \underline{w}_{\pi^*_{-\infty},s,a_j}\right). \tag{25}$$

After getting $\underline{w}$, the next step is to divide further the wealth level interval $(\underline{w}, w_0]$ into subintervals and solve the optimal policy for each subinterval similarly to the above algorithm. The main procedure of the backward-induction algorithm for group decision-making in the case of additive aggregation model is listed as follows.

Step 1. By maximizing the expected exponential utility, get the optimal policy $\pi^*_{i,e}$ of the most risk-averse agent when $w \to -\infty$.

Step 2. According to (6), we have

$$\begin{aligned} v^*(s,w) = \max_{a\in A^*_{i,e}(s)} &\left\{w + v_l^{\pi^*_{i,e}}(s,a) + k_1 D_1 {\gamma_1}^{w} v_{1,e}^{\pi^*_{i,e}}(s,a) \right. \\ &\left. + \cdots + k_n D_n {\gamma_n}^{w} v_{n,e}^{\pi^*_{i,e}}(s,a)\right\}, \end{aligned} \tag{26}$$

where $A^*_{i,e}(s) = \arg\max_{a\in A_s} \sum_{s\in S} P(s' \mid s,a)[{\gamma_i}^{r(s,a,s')} \cdot v^*_{i,e}(s')]$; get the optimal value $v^*(s,w)$ and the values of $v^*_{1,e}(s), v^*_{2,e}(s), \ldots, v^*_{n,e}(s), v^*_l(s)$ for all states $s \in s'$ when $w \to -\infty$.

Step 3. For all states $s \in s'$, $a \in A_s \setminus \pi^*_{-\infty}(s)$, get the values of $v_l^{\pi^*_{-\infty}}(s,a), v_{1,e}^{\pi^*_{-\infty}}(s,a), \ldots, v_{n,e}^{\pi^*_{-\infty}}(s,a)$ by (7); then get $\underline{w}_{\pi^*_{-\infty},s,a_j}$ by Expression (24).

Step 4. Calculate the wealth level threshold $\underline{w}$ according to (25).

Step 5. For the wealth level interval $(\underline{w}, w_0]$, increase further the wealth level according to the reward got by executing one step action, and determine the wealth level threshold and optimal policy similarly to the above steps.

Step 6. If, for all $s \in s'$, the wealth level w is larger than w_0, then end the algorithm.

5.2. The Case of Multiplicative Aggregation Model. For the multiplicative aggregation model of one-switch utility functions, we also have the following theorem that shows the existence of a wealth level threshold $\underline{w}$.

Theorem 4. *For all optimal policies π^*, there exists a wealth threshold $\underline{w}$. For any state $s \in S'$, wealth level $w \leq \underline{w}$,*

$$\begin{aligned} v_l^*(s,w) = v_l^{\pi^*}(s), \quad v_{i,e}^*(s,w) = v_{i,e}^{\pi^*}(s), \\ v^*(s,w) = v^{\pi^*}(s,w), \quad i = 1,2. \end{aligned} \tag{27}$$

Please see Appendix B for the proof of Theorem 4.

Similarly to additive aggregation model, we determine the wealth level threshold $\underline{w}$ for the multiplicative aggregation model. Assume that $\pi^*_{-\infty}$ is the optimal policy for the wealth level interval $(-\infty, \underline{w}]$; then for the wealth level w in the interval $(\underline{w}, \min_{a\in A_s}(\underline{w} - r(s,a,s')))]$, $\pi^*_{-\infty}$ is no longer

the optimal policy, and assuming π' is the optimal policy, according to (10), for all nongoal states, we have

$$v^*(s,w) = \max_{a\in A_s} \sum_{s'\in S} P\left(s' \mid s,a\right) \cdot v^{\pi^*_{-\infty}}\left(s', w + r\left(s,a,s'\right)\right). \tag{28}$$

As $w + r(s,a,s') < \underline{w}$,

$$\begin{aligned} v^*(s,w) &= \max_{a\in A_s} \sum_{s'\in S} P\left(s' \mid s,a\right) \\ &\quad \cdot \Big[k_1\Big(w + r\left(s,a,s'\right) + v_l^{\pi^*_{-\infty}}(s) + D_1{\gamma_1}^{w+r(s,a,s')} v_{1,e}^{\pi^*_{-\infty}}(s)\Big) \\ &\quad + k_2\Big(w + r\left(s,a,s'\right) + v_l^{\pi^*_{-\infty}}(s) + D_2{\gamma_2}^{w+r(s,a,s')} v_{2,e}^{\pi^*_{-\infty}}(s)\Big) \\ &\quad + k_{12}\Big(w + r\left(s,a,s'\right) + v_l^{\pi^*_{-\infty}}(s) + D_1{\gamma_1}^{w+r(s,a,s')} v_{1,e}^{\pi^*_{-\infty}}(s)\Big) \\ &\quad \times \Big(w + r\left(s,a,s'\right) + v_l^{\pi^*_{-\infty}}(s) + D_2{\gamma_2}^{w+r(s,a,s')} v_{2,e}^{\pi^*_{-\infty}}(s)\Big)\Big] \\ &= \max_{a\in A_s} \Big[k_1\Big(w + v_l^{\pi^*_{-\infty}}(s) + D_1{\gamma_1}^{w} v_{1,e}^{\pi^*_{-\infty}}(s)\Big) \\ &\quad + k_2\Big(w + v_l^{\pi^*_{-\infty}}(s) + D_2{\gamma_2}^{w} v_{2,e}^{\pi^*_{-\infty}}(s)\Big) \\ &\quad + k_{12}\Big(w + v_l^{\pi^*_{-\infty}}(s) + D_1{\gamma_1}^{w} v_{1,e}^{\pi^*_{-\infty}}(s)\Big) \\ &\quad \times \Big(w + v_l^{\pi^*_{-\infty}}(s) + D_2{\gamma_2}^{w} v_{2,e}^{\pi^*_{-\infty}}(s)\Big)\Big]. \end{aligned} \tag{29}$$

For w, because the optimal policy is π', not $\pi^*_{-\infty}$ now under assumption, we have

$$\begin{aligned} &\sum_{s'\in S'} P\left(s' \mid s, \pi^*_{-\infty}(s)\right) \cdot v^{\pi^*_{-\infty}}\left(s', w + r\left(s, \pi^*_{-\infty}(s), s'\right)\right) \\ &\quad \le \sum_{s'\in S'} P\left(s' \mid s, a_j\right) \cdot v^{\pi^*_{-\infty}}\left(s', w + r\left(s, a_j, s'\right)\right) \end{aligned} \tag{30}$$

or, equivalently,

$$\begin{aligned} &k_1\Big(w + v_l^{\pi^*_{-\infty}}\left(s, \pi^*_{-\infty}(s)\right) + D_1{\gamma_1}^{w} v_{1,e}^{\pi^*_{-\infty}}\left(s, \pi^*_{-\infty}(s)\right)\Big) \\ &\quad + k_2\Big(w + v_l^{\pi^*_{-\infty}}\left(s, \pi^*_{-\infty}(s)\right) + D_2{\gamma_2}^{w} v_{2,e}^{\pi^*_{-\infty}}\left(s, \pi^*_{-\infty}(s)\right)\Big) \\ &\quad + k_{12}\Big(w + v_l^{\pi^*_{-\infty}}\left(s, \pi^*_{-\infty}(s)\right) + D_1{\gamma_1}^{w} v_{1,e}^{\pi^*_{-\infty}}\left(s, \pi^*_{-\infty}(s)\right)\Big) \\ &\quad \times \Big(w + v_l^{\pi^*_{-\infty}}\left(s, \pi^*_{-\infty}(s)\right) + D_2{\gamma_2}^{w} v_{2,e}^{\pi^*_{-\infty}}\left(s, \pi^*_{-\infty}(s)\right)\Big) \\ &\le k_1\Big(w + v_l^{\pi^*_{-\infty}}\left(s,a_j\right) + D_1{\gamma_1}^{w} v_{1,e}^{\pi^*_{-\infty}}\left(s,a_j\right)\Big) \\ &\quad + k_2\Big(w + v_l^{\pi^*_{-\infty}}\left(s,a_j\right) + D_2{\gamma_2}^{w} v_{2,e}^{\pi^*_{-\infty}}\left(s,a_j\right)\Big) \\ &\quad + k_{12}\Big(w + v_l^{\pi^*_{-\infty}}\left(s,a_j\right) + D_1{\gamma_1}^{w} v_{1,e}^{\pi^*_{-\infty}}\left(s,a_j\right)\Big) \\ &\quad \times \Big(w + v_l^{\pi^*_{-\infty}}\left(s,a_j\right) + D_2{\gamma_2}^{w} v_{2,e}^{\pi^*_{-\infty}}\left(s,a_j\right)\Big). \end{aligned} \tag{31}$$

We can get a wealth level point $\underline{w}_{\pi^*_{-\infty},s,a_j}$ in equality case of the above weak inequality.

Then, we can get the wealth level threshold $\underline{w}$ according to (25).

After getting $\underline{w}$, the next step is to divide further the interval $(\underline{w}, w_0]$ into subintervals and compute the optimal policy for each subinterval. The main procedure of the backward-induction algorithm for group decision-making in the case of multiplicative aggregation model is listed as follows.

Step 1. By maximizing the expected exponential utility, get the optimal policy $\pi^*_{3,e}$ of the visual agent when $w \to -\infty$.

Step 2. According to (12), we have

$$\begin{aligned} v^*(s,w) = \max_{a\in A^*_{3,e}(s)} \Big\{&k_1\Big(w + v_l^{\pi^*_{3,e}}(s) + D_1{\gamma_1}^{w} v_{1,e}^{\pi^*_{3,e}}(s)\Big) \\ &+ k_2\Big(w + v_l^{\pi^*_{3,e}}(s) + D_2{\gamma_2}^{w} v_{2,e}^{\pi^*_{3,e}}(s)\Big) \\ &+ k_{12}\Big(w + v_l^{\pi^*_{3,e}}(s) + D_1{\gamma_1}^{w} v_{1,e}^{\pi^*_{3,e}}(s)\Big) \\ &\times \Big(w + v_l^{\pi^*_{3,e}}(s) + D_2{\gamma_2}^{w} v_{2,e}^{\pi^*_{3,e}}(s)\Big)\Big\}, \end{aligned} \tag{32}$$

where $A^*_{3,e}(s) = \arg\max_{a\in A_s} \sum_{s\in S} P(s' \mid s,a)[{\gamma_3}^{r(s,a,s')} \cdot v^*_{3,e}(s')]$; get the optimal value $v^*(s,w)$ and the values of $v^*_{1,e}(s)$, $v^*_{2,e}(s)$, $v^*_l(s)$ for all states $s \in s'$ when $w \to -\infty$.

Step 3. For all states $s \in s'$, $a \in A_s \setminus \pi^*_{-\infty}(s)$, get the values of $v_l^{\pi^*_{-\infty}}(s,a)$, $v_{1,e}^{\pi^*_{-\infty}}(s,a)$, $v_{2,e}^{\pi^*_{-\infty}}(s,a)$ by (7); then get $\underline{w}_{\pi^*_{-\infty},s,a_j}$ by Expression (31).

Step 4. Calculate the wealth level threshold $\underline{w}$ according to (25).

Step 5. For the wealth level interval $(\underline{w}, w_0]$, increase further the wealth level according to the reward got by executing one step action and determine the wealth level threshold and optimal policy similarly to the above steps.

Step 6. If, for all $s \in s'$, the wealth level w is larger than w_0, then end the algorithm.

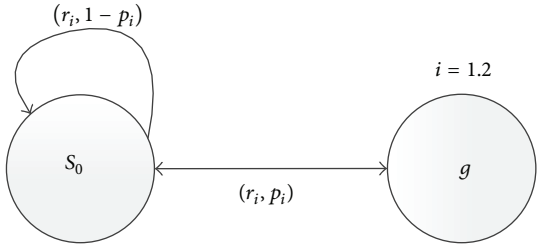

Figure 1: System state transitions.

6. Numerical Examples

Consider a simple GDMDP model. There are two agents named Agent_1 and Agent_2 with risk aversion parameters γ_1 and γ_2, respectively. The state set of the GDMDP model includes initial state s_0 and goal state g. Agent's action set is $\{a_1, a_2\}$. In state s_0 executing action a_i $(i = 1, 2)$ results in a finite reward r_i and a transition to goal state g with possibility p_i. When agent reaches the goal state g it stops acting and receives no more rewards thereafter. Figure 1 shows the transitions of system states. Agents need to make an optimal policy together to reach the goal state.

Without loss of generality, the GDMDP model's parameters are assumed as follows: $p_1 = 0.4$, $p_2 = 0.005$, $r_1 = -15$, and $r_2 = -40$; the one-switch utility functions of two agents are defined as $u_1(w) = w - 0.952^w$ and $u_2(w) = w - 0.93^w$ with $\gamma_1 = 0.952$ and $\gamma_2 = 0.93$, respectively. Initial wealth level of each agent is set 0.

First, consider the situation that each agent makes decisions alone. The agent's optimal policy and the wealth level threshold are solved by utilizing the method proposed by Liu and Koenig [8]. The results are shown as follows:

$$\begin{aligned} \text{Agent}_1\text{: } \pi^*(s_0, w) &= \begin{cases} a_1 & w \in (-106.5, 0] \\ a_2 & w \in (-\infty, -106.5] \end{cases} \\ \text{Agent}_2\text{: } \pi^*(s_0, w) &= \begin{cases} a_1 & w \in (-6.9, 0] \\ a_2 & w \in (-\infty, -6.9] \end{cases}. \end{aligned} \tag{33}$$

Next, we consider the group decision-making based on additive and multiplicative aggregation model of one-switch utility functions. In the case of additive aggregation model, assume each agent has equal weight; that is, $k_1 = k_2 = 0.5$; then the optimal policy and the wealth level threshold based on the proposed method in the paper are solved as follows:

$$\pi^*(s_0, w) = \begin{cases} a_1 & w \in (-16.4, 0] \\ a_2 & w \in (-\infty, -16.4] \end{cases}. \tag{34}$$

The above result shows that, in the wealth level interval $(-106.5, -16.4)$, if Agent_1 makes decisions alone, the optimal policy is taking action a_1 in state s_0 but a_2 if Agent_2 makes decisions alone. If they make decisions together, then action a_2 is taken.

Now we consider how the wealth level threshold $\underline{w}$ of group decision-making changes as the weights of agents vary. In detail, k_1 changes from 0.05 to 0.95; meanwhile $k_2 = 1 - k_1$ changes from 0.95 to 0.05. The change of the wealth level threshold of group decision-making is shown in Figure 2.

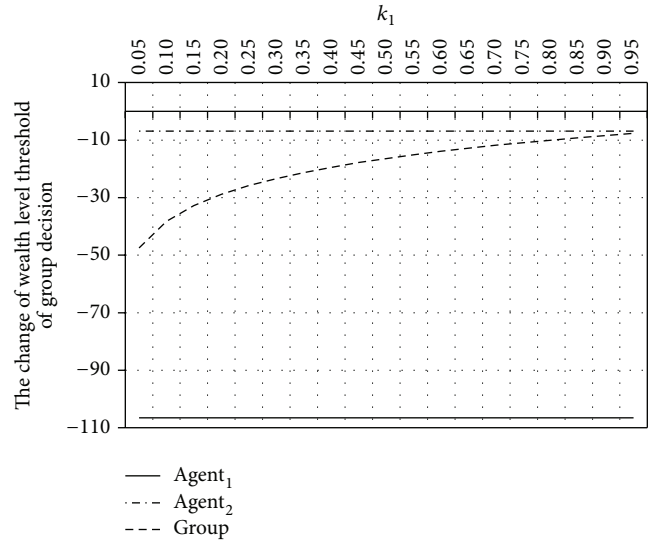

Figure 2: The change of the wealth level threshold of group decision-making with different risk aversion parameters of agents.

Figure 2 shows that the values of the wealth level threshold $\underline{w}$ of group decision-making are near to the wealth level threshold of Agent_2 who is more risk-averse even if k_2 is small and $k_1 = k_2 - 1$ is large. This means that the influence of weights on group decision-making is not obvious if the risk aversion parameters of agents are different, while the risk aversion parameters play an important role in this situation.

Consider the situation that two agents have similar risk attitude; that is, their risk aversion parameters are similar; for example, their one-switch utility functions are $u_1(w) = w - 0.952^w$ and $u_2(w) = w - 0.95^w$, respectively. When each agent makes decisions alone their optimal policies and the wealth level thresholds are solved as follows:

$$\begin{aligned} \text{Agent}_1\text{: } \pi^*(s_0, w) &= \begin{cases} a_1 & w \in (-106.5, 0] \\ a_2 & w \in (-\infty, -106.5] \end{cases} \\ \text{Agent}_2\text{: } \pi^*(s_0, w) &= \begin{cases} a_1 & w \in (-71.5, 0] \\ a_2 & w \in (-\infty, -71.5] \end{cases}. \end{aligned} \tag{35}$$

Change the values of weights in the same way as Figure 2; the result is shown in Figure 3. Difference from Figures 2 and 3 shows that the values of the wealth level threshold $\underline{w}$ of group decision-making are near to the wealth level threshold of Agent_1 when k_2 is small and $k_1 = k_2 - 1$ is large. So if the difference between the risk aversion parameters of agents is not obvious, the weights of agents will play a critical role.

Finally, we consider group decision-making based on the multiplicative aggregation model and especially focus on the influence of product term of group utility, that is, $k_{12}u_1(w)u_2(w)$, on the group decision-making. Given the same one-switch utility functions of agents in Figure 3 and assuming two sets of k_1 and k_2 value, in detail, $k_1 = 0.85$, $k_2 = 0.1$ and $k_1 = 0.1$, $k_2 = 0.85$. If the value of k_{12} is changed

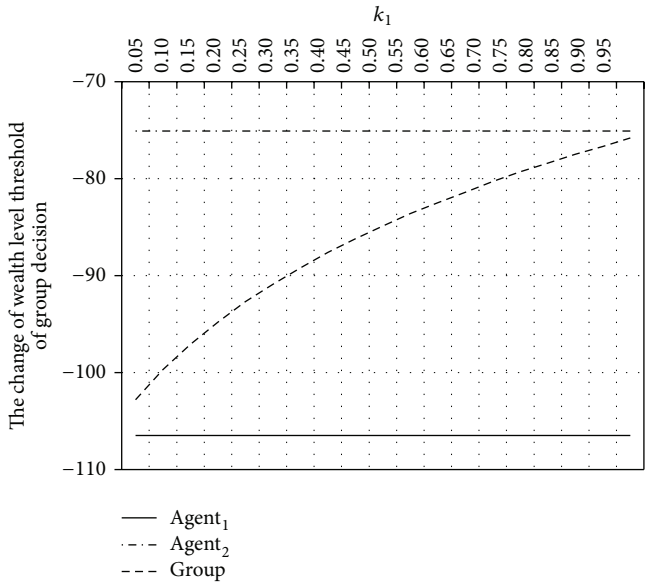

Figure 3: The change of the wealth level threshold of group decision-making with similar risk aversion parameters of agents.

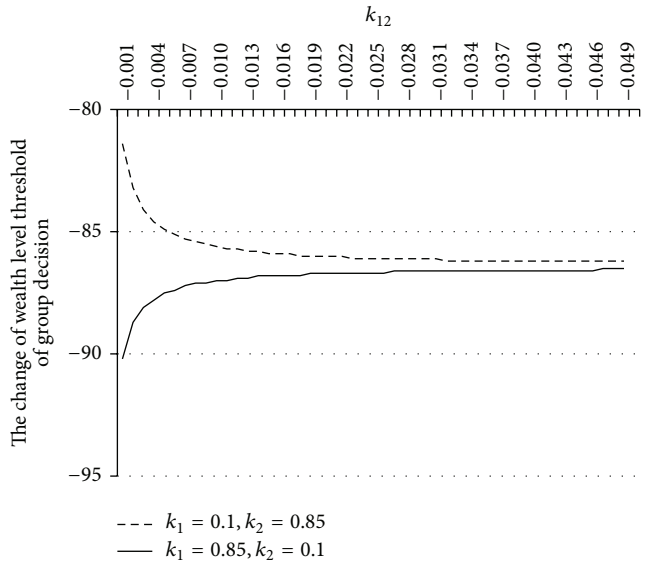

Figure 4: The change of the wealth level threshold of group decision-making based on the multiplicative aggregation model.

from −0.001 to −0.05, we get two curved lines of wealth level threshold of group decision-making in Figure 4.

The two curved lines gradually approach each other to a point when the absolute value of k_{12} increases from 0.001 to 0.05. If compared with the result of additive aggregation model, we can find that the point is very close to the wealth level threshold of additive aggregation model with $k_1 = k_2 = 0.5$. This is because when the absolute value of k_{12} is small the absolute values of $k_1u_1(w)$ and $k_2u_2(w)$ in group utility are larger than the absolute value of $k_{12}u_1(w)u_2(w)$, so $k_{12}u_1(w)u_2(w)$ has little influence on group decision-making. When the absolute value of k_{12} increases enough $k_{12}u_1(w)u_2(w)$ will mainly influence the group decision-making; furthermore, $k_{12}u_1(w)u_2(w)$ has same influence on Agent$_1$ and Agent$_2$; therefore the wealth level threshold of multiplicative aggregation model will approach the threshold of additive aggregation model with $k_1 = k_2 = 0.5$. This implies that the multiplicative aggregation model avoids group decision-making being dominated by the weights of individuals completely.

7. Conclusion and Future Works

This paper has put an effort on how to extend a single agent's risk-sensitive decision-theoretic planning under the MDP framework to the multiagent problem. Based on one-switch utility function that is used to describe agent's risk-sensitive attitude, the additive and multiplicative aggregation models of group utility have been proposed in this paper. According to the characteristics of group utility, a backward-induction method has been presented to divide the wealth level interval and compute the optimal policy. The paper has also offered numerical examples and discussed how the weights and risk aversion parameters influence the group decision-making. From numerical examples we can observe that, for the additive aggregation model, if the risk aversion parameters of agents are different, the risk aversion parameters will have an obvious influence on the group decision-making, while the weights of agents will play a critical role if the risk aversion parameters are similar. For the multiplicative aggregation model, group decision-making will not be dominated by the weights of individuals completely. The product term of group utility will also influence the group decision-making.

In the future we intend to further study multiattribute group decision-making under the MDP framework with one-switch utility function. Based on the work of Tsetlin and Winkler [21], we will further study how to extend our method to the group decision-making problem.

Appendices

A. Proof of Theorem 3

Proof. Let $A^*_{i,e}(s) = \arg\max_{a\in A_s} \sum_{s\in S} P(s' \mid s,a)[\gamma_i^{r(s,a,s')} \cdot v^*_{i,e}(s')]$,

$$\varepsilon = \min_{s\in S}\left(v^*_{i,e}(s) - \max_{a\in A_s\setminus A^*_{i,e}(s)} \sum_{s\in S} P\left(s' \mid s,a\right) \times \left[\gamma_i^{r(s,a,s')} \cdot v^*_{i,e}\left(s'\right)\right]\right). \tag{A.1}$$

As $v^*_{i,e}(s) = \max_{a\in A_s} \sum_{s\in S} P(s' \mid s,a)[\gamma_i^{r(s,a,s')} \cdot v^*_{i,e}(s')]$, and

$$\lim_{w\to-\infty} v^*(s,w)\,\gamma_i^{-w} = k_i D_i v^*_{i,e}(s), \tag{A.2}$$

thus there exists a wealth level w_0, for wealth level $w \le w_0$, $s \in S$,

$$k_i D_i v_{i,e}^*(s) - v^*(s,w)\,\gamma_i^{-w} \le \frac{k_i D_i}{2}\varepsilon. \tag{A.3}$$

On the other hand, for all wealth levels $w \le w_0$, $s \in S$, let $f^{\pi}(s,w) = w + v_l^{\pi}(s) + k_1 D_1 {\gamma_1}^w v_{1,e}^{\pi}(s) + \cdots + k_{i-1} D_{i-1} {\gamma_{i-1}}^w v_{i-1,e}^{\pi}(s) + k_{i+1} D_{i+1} {\gamma_{i+1}}^w v_{i+1,e}^{\pi}(s) + \cdots + k_n D_n {\gamma_n}^w v_{n,e}^{\pi}(s)$; then $v^{\pi_{i,e}^*}(s,w) = f^{\pi_{i,e}^*}(s,w) + k_i D_i v_{i,e}^*(s)$.

Assume that there exists a state $s' \in S'$; $\pi'(s)$ does not belong to $A_{i,e}^*(s)$; then

$$\begin{aligned} v_{i,e}^{\pi'}(s') &= \sum_{s'' \in S} P\left(s'' \mid s', \pi'(s')\right) \\ &\quad \times \left[{\gamma_i}^{r(s',\pi'(s'),s'')} \cdot v_{i,e}^{\pi'}(s'')\right] \\ &\le \sum_{s'' \in S} P\left(s'' \mid s', \pi_{i,e}^*(s')\right) \\ &\quad \times \left[{\gamma_i}^{r(s',\pi_{i,e}^*(s'),s'')} \cdot v_{i,e}^*(s'')\right]. \end{aligned} \tag{A.4}$$

According to the fact that w, $v_l^{\pi'}(s')$, and $v_{j,e}^{\pi'}(s')$ ($j = 1, 2, \ldots, n$) are all less than 0, we have

$$\begin{aligned} v^{\pi'}(s', w) &= f^{\pi'}(s,w) + k_i D_i v_{i,e}^{\pi'}(s) \le k_i D_i v_{i,e}^{\pi'}(s) \\ &\le \sum_{s'' \in S} P\left(s'' \mid s', \pi_{i,e}^*(s')\right) \\ &\quad \times \left[{\gamma_i}^{r(s',\pi_{i,e}^*(s'),s'')} \cdot v_{i,e}^*(s'')\right]. \end{aligned} \tag{A.5}$$

Therefore,

$$\begin{aligned} k_i D_i v_{i,e}^{\pi'}(s') - v^*(s', w)\,\gamma_i^{-w} &\ge k_i D_i \\ &\times \left(v_{i,e}^{\pi'}(s') - \sum_{s'' \in S} P\left(s'' \mid s', \pi_{i,e}^*(s')\right) \right. \\ &\quad \left. \times \left[{\gamma_3}^{r(s',\pi_{i,e}^*(s'),s'')} \cdot v_{i,e}^*(s'')\right] \right) \ge k_i D_i \varepsilon. \end{aligned} \tag{A.6}$$

This is contradictory to (A.3). Thus for $w \le w_0$, $s \in S$, optimal action $\pi^*(s,w) \in A_{i.e}^*(s)$.

Additionally, as $v_{i,e}^{\pi_{i,e}^*}(s) = v_{i,e}^*(s)$, and $f^{\pi_{i,e}^*}(s,w) \le f^{\pi^*}(s,w)$, then

$$\begin{aligned} v^{\pi_{i,e}^*}(s,w) &= f^{\pi_{i,e}^*}(s,w) + k_i D_i v_{i,e}^{\pi_{i,e}^*}(s) \\ &\le f^{\pi^*}(s,w) + k_i D_i v_{i,e}^*(s) = v^{\pi^*}(s,w). \end{aligned} \tag{A.7}$$

Therefore, for $w \le w_0$, $s \in S$, $v^*(s,w) = v^{\pi^*}(s,w)$. □

B. Proof of Theorem 4

Proof. Let $A_{3,e}^*(s) = \arg\max_{a \in A_s} \sum_{s \in S} P(s' \mid s, a)[{\gamma_3}^{r(s,a,s')} \cdot v_{3,e}^*(s')]$,

$$\begin{aligned} \varepsilon = \min_{s \in S} \left(v_{3,e}^*(s) - \max_{a \in A_s \setminus A_{3,e}^*(s)} \sum_{s \in S} P\left(s' \mid s, a\right) \right. \\ \left. \times \left[{\gamma_3}^{r(s,a,s')} \cdot v_{3,e}^*\left(s'\right)\right] \right). \end{aligned} \tag{B.1}$$

As $v_{3,e}^*(s) = \max_{a \in A_s} \sum_{s \in S} P(s' \mid s, a)[{\gamma_3}^{r(s,a,s')} \cdot v_{3,e}^*(s')]$, and

$$\lim_{w \to -\infty} v^*(s,w)\,{\gamma_3}^{-w} = k_{12} D_1 D_2 v_{3,e}^*(s), \tag{B.2}$$

there exists a wealth level w_0, for all $w \le w_0$, $s \in S$,

$$k_{12} D_1 D_2 v_{3,e}^*(s) - v^*(s,w)\,{\gamma_3}^{-w} \le \frac{k_{12} D_1 D_2}{2}\varepsilon. \tag{B.3}$$

On the other hand, for all $w \le w_0$, $s \in S$, let

$$\begin{aligned} f^{\pi}(s,w) &= \left(w + v_l^{\pi}(s)\right) + k_1 D_1 {\gamma_1}^w v_{1,e}^{\pi}(s) \\ &\quad + k_2 D_2 {\gamma_2}^w v_{2,e}^{\pi}(s) \\ &\quad + k_{12}\left(w + v_l^{\pi}(s)\right)^2 + k_{12}\left(w + v_l^{\pi}(s)\right) \\ &\quad \times \left(D_1 {\gamma_1}^w v_{1,e}^{\pi}(s) + D_2 {\gamma_2}^w v_{2,e}^{\pi}(s)\right); \end{aligned} \tag{B.4}$$

then $v^{\pi_{3,e}^*}(s,w) = f^{\pi_{3,e}^*}(s,w) + k_{12} D_1 D_2 v_{3,e}^*(s)$.

Assume that there exists some state $s' \in S'$; $\pi'(s)$ does not belong to $A_{3,e}^*(s)$; then

$$\begin{aligned} v_{3,e}^{\pi'}(s') &= \sum_{s'' \in S} P\left(s'' \mid s', \pi'(s')\right)\left[{\gamma_3}^{r(s',\pi'(s'),s'')} \cdot v_{3,e}^{\pi'}(s'')\right] \\ &\le \sum_{s'' \in S} P\left(s'' \mid s', \pi_{3,e}^*(s')\right) \\ &\quad \times \left[{\gamma_3}^{r(s',\pi_{3,e}^*(s'),s'')} \cdot v_{3,e}^*(s'')\right]. \end{aligned} \tag{B.5}$$

According to the fact that w, $v_l^{\pi'}(s')$, and $v_{i,e}^{\pi'}(s')$ are all less than 0, we have

$$\begin{aligned} v^{\pi'}(s', w) &= f^{\pi'}(s,w) + k_{12} D_1 D_2 v_{3,e}^{\pi'}(s) \\ &\le k_{12} D_1 D_2 v_{3,e}^{\pi'}(s) \\ &\le \sum_{s'' \in S} P\left(s'' \mid s', \pi_{3,e}^*(s')\right) \\ &\quad \times \left[{\gamma_3}^{r(s',\pi_{3,e}^*(s'),s'')} \cdot v_{3,e}^*(s'')\right]. \end{aligned} \tag{B.6}$$

Therefore,

$$\begin{aligned} & k_{12}D_1D_2v^*_{3,e}\left(s'\right) - v^*\left(s',w\right)\gamma_3{}^{-w} \\ & \geq k_{12}D_1D_2\left(v^*_{3,e}\left(s'\right) - \sum_{s''\in S} P\left(s'' \mid s', \pi^*_{3,e}\left(s'\right)\right) \right. \\ & \qquad \left. \times \left[\gamma_3{}^{r(s',\pi^*_{3,e}(s'),s'')} \cdot v^*_{3,e}\left(s''\right)\right]\right) \\ & \geq k_{12}D_1D_2\varepsilon. \end{aligned} \tag{B.7}$$

This is contradictory to (B.3). So for all $w \leq w_0$, $s \in S$, optimal policy $\pi^*(s,w) \in A^*_{3,e}(s)$.

Additionally, as $v^{\pi^*_{3,e}}_{3,e}(s) = v^*_{3,e}(s)$, and $f^{\pi^*_{3,e}}(s,w) \leq f^{\pi^*}(s,w)$, so

$$\begin{aligned} v^{\pi^*_{3,e}}(s,w) &= f^{\pi^*_{3,e}}(s,w) + k_{12}D_1D_2v^{\pi^*_{3,e}}_{3,e}(s) \\ &\leq f^{\pi^*}(s,w) + k_{12}D_1D_2v^*_{3,e}(s) = v^{\pi^*}(s,w). \end{aligned} \tag{B.8}$$

Therefore, for all $w \leq w_0$, $s \in S$, $v^*(s,w) = v^{\pi^*}(s,w)$. □

Conflict of Interests

The authors declare that there is no conflict of interests regarding the publication of this paper.

Acknowledgment

This work was supported by the National Natural Science Foundation of China under Grant 70971048.

References

[1] C. Boutilier, T. Dean, and S. Hanks, "Decision-theoretic planning: structural assumptions and computational leverage," *Journal of Artificial Intelligence Research*, vol. 11, pp. 1–94, 1999.

[2] D. E. Bell, "One-switch utility functions and a measure of risk," *Management Science*, vol. 34, no. 12, pp. 1416–1424, 1988.

[3] G. M. Gelles and D. W. Mitchell, "Broadly decreasing risk aversion," *Management Science*, vol. 45, no. 10, pp. 1432–1439, 1999.

[4] Y. Nakamura, "Sumex utility functions," *Mathematical Social Sciences*, vol. 31, no. 1, pp. 39–47, 1996.

[5] D. E. Bell and P. C. Fishburn, "Strong one-switch utility," *Management Science*, vol. 47, no. 4, pp. 601–604, 2001.

[6] Y. Liu, *Decision-theoretic planning under risk-sensitive planning objectives [Ph.D. thesis]*, College of Computing, Georgia Institute of Technology, 2005.

[7] Y. Liu and S. Koenig, "Risk-sensitive planning with one-switch utility functions: value iteration," in *Proceedings of the 20th National Conference on Artificial Intelligence*, pp. 993–999, 2005.

[8] Y. Liu and S. Koenig, "An exact algorithm for solving MDPs under risk-sensitive planning objectives with one-switch utility functions," in *Proceedings of the 7th International Conference on Autonomous Agents and Multi-Agent Systems*, 2008.

[9] R. A. Howard and J. E. Matheson, "Risk-sensitive Markov decision processes," *Management Science*, vol. 18, no. 7, pp. 356–369, 1972.

[10] S. D. Patek, "On terminating Markov decision processes with a risk-averse objective function," *Automatica*, vol. 37, no. 9, pp. 1379–1386, 2001.

[11] D. Hernandez-Hernández and S. I. Marcus, "Risk sensitive control of Markov processes in countable state space," *Systems and Control Letters*, vol. 29, no. 3, pp. 147–155, 1996.

[12] Y. Le and L. Tallec, *Robust, risk-sensitive, and data-driven control of Markov decision processes [Ph.D dissertation]*, Sloan School of Management , Massachusetts Institute of Technology, 2007.

[13] P. H. Iz, "Two multiple criteria group decision support systems based on mathematical programming and ranking methods," *European Journal of Operational Research*, vol. 61, no. 1-2, pp. 245–253, 1992.

[14] S. J. Chen and C. L. Hwang, *Fuzzy Multiple Attribute Decision Making: Methods and Applications*, vol. 375 of *Lecture Notes in Economics and Mathematical Systems*, Springer, New York, NY, USA, 1992.

[15] R. J. Li, "Fuzzy method in group decision making," *Computers & Mathematics with Applications*, vol. 38, no. 1, pp. 91–101, 1999.

[16] R. Benayoun, J. de Montgolfier, and J. Tergny, "Linear programming with multiple objective functions: step method (stem)," *Mathematical Programming*, vol. 1, no. 1, pp. 366–375, 1971.

[17] A. M. Geoffrion, J. S. Dyer, and A. Feinberg, "An interactive approach for multi-criterion optimization, with an application to the operation of academic department," *Management Science*, vol. 19, no. 4, pp. 357–368, 1972.

[18] Z. Xu, "Approaches to multi-stage multi-attribute group decision making," *International Journal of Information Technology and Decision Making*, vol. 10, no. 1, pp. 121–146, 2011.

[19] D. P. Bertsekas and J. N. Tsitsiklis, "An analysis of stochastic shortest path problems," *Mathematics of Operations Research*, vol. 16, no. 3, pp. 580–595, 1991.

[20] S. D. Patek, "On terminating Markov decision processes with a risk-averse objective function," *Automatica*, vol. 37, no. 9, pp. 1379–1386, 2001.

[21] I. Tsetlin and R. L. Winkler, "Multiattribute one-switch utility," *Management Science*, vol. 58, no. 3, pp. 602–605, 2012.

Hindawi Publishing Corporation
Mathematical Problems in Engineering
Volume 2014, Article ID 917903, 10 pages
http://dx.doi.org/10.1155/2014/917903

Research Article

A Dynamical Reliability Prediction Algorithm for Composite Service

Chunli Xie and Jianguo Ren

Department of Computer Science and Technology, Jiangsu Normal University, Xuzhou 221116, China

Correspondence should be addressed to Chunli Xie; xcl_bhb@163.com

Received 31 March 2014; Accepted 4 June 2014; Published 6 July 2014

Academic Editor: Housheng Su

Dynamic selection and dynamic binding and rebinding at runtime are new characters of composite services. The traditional static reliability prediction models are unsuitable to dynamic composite services. A new reliability predicting algorithm for composite services is proposed in this paper. Firstly, a composite service is decomposed into composition unites (executing path, composite module and atomic service) according to their constituents. Consequently, a hierarchical graph of all composite units is constructed. Lastly, a new dynamic reliability prediction algorithm is presented. Comparing with the traditional reliability model, the new dynamic reliability approach is more flexible, which does not recompute reliability for all composite units and only computes the reliability of the effected composite units. In addition, an example to show how to measure the reliability based on our algorithm is designed. The experimental results show our proposed methods can give an accurate estimation of reliability. Furthermore, a more flexible sensitivity analysis is performed to determine which service component has the most significant impact on the improvement of composite service reliability.

1. Introduction

With the rapid development and widespread use of web services, more and more businesses are achieved by composite services which can be created by aggregating a number of atomic or composite services (called service components) by following certain composition pattern and rules. Thus, how to ensure the reliability of composite services has become an important problem. In addition, a large amount of function-equivalent services has been in the Internet, which make more services be selected. Users can translate their requirements for services to the constraints of some QoS properties [1]. Then, different users may select different service to realize the same function based on different QoS constraints. There are two methods for web service composition: static composition and dynamic composition. In static web service composition, composition is performed manually; that is, each web service is selected and bound before execution. Static composition is sufficient for constructing applications with well-defined specific requirements that are not likely to change frequently. But, it is not flexible and agile enough when the requirements are changed frequently. Dynamic web service composition can achieve this goal as, in dynamic composition, services components are selected at runtime from a set of service components and when the selected service components failed, the new selected service components will replace them while keeping the running services constantly available to users [2]. Dynamic service composition provides an ability to rapidly adapt to changes that were not envisioned during design time.

Dynamic binding and rebinding are the basis for the dynamic composition. There are three kinds of binding: early binding, local binding at runtime, and rebinding at runtime [3–6]. In early binding, the service is selected and bound before execution, which is also called static binding. In local binding, when a composite service is running, one of its service components is bound to a selected service according to some QoS properties before it is invoked. Local binding can help service components to avoid binding to failed services and reduce the failure probability of composite services. During the execution of a composite service, when the QoS

of some service components do not satisfy the requirements of the user or the bound services fail, the composite service will pause, and after new services are bound to the service components, the composite service continues to run; the binding in this process is called rebinding at runtime.

To address the above problems of dynamic composition, traditional static reliability model to predict the reliability is not applicable to services with dynamic composition. A new dynamic reliability model is presented for the dynamic service composition in this paper. The new model makes the computation simple when the reliability of some service components is changed frequently.

The remaining sections of the paper are organized as follows. Section 2 describes the related works. Section 3 discusses some concepts about composite units. Section 4 describes the reliability of the composite units. Section 5 presents the dynamic reliability prediction approaches based on the hierarchical graph. Section 6 conducts some experiments to verify our reliability algorithm. Section 7 presents the conclusion and our future works.

2. Related Works

The existing reliability predicting models can be divided into two categories: black-box and white-box [7, 8]. The black-box models, such as the Bayesian models, the SRGM (software reliability growth models), and the statistical models, only consider the functionality of software while ignoring its internal structure. The white-box models estimate the reliability of a software system based on its internal structure. The structures are often described by Markov chain [9–19] or Petri net [20, 21]. These white-box models can be further divided into three categories: state-based models, path-based models, and additive models. As these models are often developed for component-based software systems, they are also called component-based reliability models (CBRM). The state-based models which are the common models usually model the system as a discrete-time Markov chain (DTMC), a continuous-time Markov chain (CTMC), or a semi-Markov process Markov chain (SMP). Wang et al. presented a typical state-based model which described four common architecture styles, including batch-sequential, parallel/pipe-filter, call-and-return, and fault-tolerance styles, and proposed a transformation from architecture view to state view to perform reliability analysis [10]. S. Gokhale et al. classified the state-based models from three aspects: the architecture of the application, the failure behavior of components, and the analysis methods. The architectures were CTMC or DTMC and the Markov chain was irreducible or absorbing. The failure behavior was represented by reliability, constant failure rate, or time-dependent failure intensity. The analysis method was composite or hierarchical. In sum, they gave seven kinds of DTMC-based models and CTMC-based models.

The emergency of web services makes the software system be dynamic discovery and binding, which make the development and the execution be more complex. Then, web services are more prone to failure than traditional distributed software. It is necessary to develop new methods to predict the reliability of services [17–19]. Tsai et al. extended the components based reliability models to services reliability analysis [20, 21]. The structure of services is also described as Markov chain. Wang et al. proposed a hierarchical reliability model which divided the reliability of services into data reliability, service components reliability, service pool reliability and composite services reliability [22, 23]. Zheng and Lyu proposed a collaborative reliability prediction approach, which employs the past failure data of other similar users to predict the web service reliability for the current user [24, 25]. This method needs large amount of user data; when the number of user is small, it is difficult to classify a user to its similar group. The composition process of web services is actually a workflow process; then a workflow-based model is also a usual method to predict the reliability [26]. Moreover, there are also other approaches to estimate the reliability of composite services from the ports, message delivery, or network transition [27–31]. Web services are different from general software system, as they are dynamic composition. Most of the existing reliability models are based on the service components in the design phase, without considering the dynamic selection and binding. In this paper, we would propose a new dynamic approach to predict the reliability of services.

3. Composite Units

Composite services are divided into *atomic service, composite unit, execution path,* and composite *service* according to their different constituents. We will discuss the four composite units in detail.

3.1. Atomic Service (AS). An atomic service is the smallest organization unit of web service. In other words, it would be impractical to decompose an atomic service. An atomic service has a fine-grained structure which can be designed, implemented, and tested independently. A composite service is a composite process; in dynamical composition, the service component in composite process is called abstract service. When the service is invoked, the abstract service is bound to the concrete service. There are several concrete services offering the same piece of functionality, which means that several concrete services may match an abstract service in service specification. So, the reliability of atomic service is changed in the execution process.

3.2. Basic Composite Module (BCM). Service composite module is composed of a set of services according to some operations. The constituted services may be atomic services, composite modules, or composite services. The operations are *sequence, choice, loop,* and *concurrent*. According to the operations, the service composite modules can be divided into four categories, that is, *sequence module (SM)*, *choice module (CM)*, *loop module (LP),* and *concurrent module (CoM)*. If all services in a composite module are atomic services, the composite module is called a basic composite module (BCM). Let $BCM = \{Ass, OP\}$, Ass is the set of

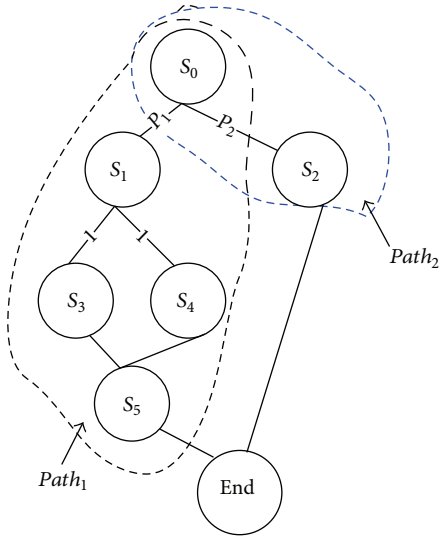

Figure 1: Execution path graph.

atomic services, and OP is the operator of atomic services, $OP \in \{sequence, choice, loop, concurrent\}$.

3.3. Execution Path (Path). All services invoked sequentially are defined as an execution path when completing a task. Let $Path = \{S_1, S_2, \ldots, S_n\}$, $S_i \in BCM$, $i = 1, 2, \ldots, n$, and the S_i in $Path$ is sequential.

3.4. Composite Service (CS). The execution of a composite service is combined by several paths. Let $CS = \{\langle Path_1, P_1\rangle, \langle Path_2, P_2\rangle, \ldots, \langle Path_n, P_n\rangle\}$, where $Path_i$ is the ith execution path, $i = 1, 2, 3, \ldots, n$, and P_i is the execution probability of $Path_i$. An example of a composite service is shown in Figure 1; the composite service has two execution paths, $Path_1, Path_2$, $CS = \{\langle Path_1, P_1\rangle, \langle Path_2, P_2\rangle\}$. Services in an execution path of composite services may be atomic services, service module, or composite services; then they have $AS \in BCM \in Path \in CS$. A composite service includes several paths and the composite modules in a path may be BCM or other composite modules which have some $BCMs$. Any composite service can be finally divided into several execution paths consisting of several $BCMs$. We will prove the theorem.

Proposition 1. *Any composite service can be finally divided into some execution paths which consist of several BCMs.*

Proof. As a composite service constitutes several execution paths by the probability, suppose that a $Path_i$ includes another composite module A which consists of several atomic services and a BCM, $A = \{As_{a1}, As_{a2}, \ldots, As_{an}, B, OP_A\}$ and $B = \{As_{b1}, As_{b2}, \ldots, As_{bn}, OP_B\}$, where $OP_A \in \{sequence, loop, choice, concurrent\}$ and $OP_B \in \{sequence, loop, choice, concurrent\}$. We use $OP_A = sequence$ and $OP_B = sequence$ as an example to illustrate the problem. If we introduce composite module B into A, we will get $A = \{As_{a1}, As_{a2}, \ldots, As_{an}, As_{b1}, As_{b2}, \ldots, As_{bn}, sequence\}$. Then, a composite module A can be deeply divided into $an + bn$ atomic services and the decomposition does not affect its execution path. If one of the operations is *choice*, the execution path $Path_i$ can be replaced by more execution paths. As OP_A, OP_B are one of the four operations, the execution path is not affected except when one of the operations is *choice*. One composite module can be decomposed into one or more $BCMs$, and the corresponding execution path can be extended into more execution paths. So, a composite service can be finally divided into some execution paths which consist of several $BCMs$. □

3.5. Hierarchical Graph of Composite Units. In this section, we will describe a hierarchical graph to represent the composite unit: *composite service, path, basic composite module,* and *atomic service*, while the following section describes how to calculate the graph attributes.

Definition 2 (hierarchical graph). A hierarchical graph is defined by a 2-tuple $\langle V, E\rangle$, where $\langle V, E\rangle$ is a DAG (directed acyclic graph). V is a set of nodes in the graph, $V = \{v_i\}, i = 1 \cdots |V|$, and E is a set of directed edges in the graph, $E = \{e_i\}$, $i = 1 \cdots |E|$.

Definition 3 (node). A node $v \in V$ models a composite unit i and is defined by a 2-tuple $\langle N_i, R_i\rangle$, where N_i is the name of composite unit i and R_i is the reliability of composite unit i.

Definition 4 (edge). A directed edge $e \in E$ models the constitution of composite units v_i and is defined by the tuple $\langle v_i, v_j, w_{i,j}\rangle$, where v_i, v_j are nodes, the node v_j is one of the components of node v_i, and $w_{i,j}$ is the weight of edge from node v_i to v_j which describes the constitution of v_i and v_j. If $w_{i,j} < 1$, the edge represents the node v_i consisting of v_j according to *choice* structure, if $w_{i,j} = 1$, the edge represents the node v_i consisting of v_j according to *sequence* or *concurrent* structure, and if $w_{i,j} > 1$, the edge represents the node v_i consisting of v_j according to *loop* structure.

As shown in Figure 2, the node $\langle CS, R_1\rangle$ is the composite service, the nodes $\langle Path_1, R_{path1}\rangle$ and $\langle Path_2, R_{path2}\rangle$ in level 2 are the execution paths of composite service CS, the nodes $\langle BCM_1, R_{BCM1}\rangle$, $\langle BCM_2, R_{BCM2}\rangle$, and $\langle BCM_3, R_{BCM3}\rangle$ in level 3 are the $BCMs$ of CS, the nodes $\langle AS_1, R_{AS1}\rangle$, $\langle AS_2, R_{AS2}\rangle$, $\langle AS_3, R_{AS3}\rangle$, $\langle AS_4, R_{AS4}\rangle$, and $\langle AS_5, R_{AS5}\rangle$ in level 4 are atomic services, and the nodes in the last level are the matched concrete services of atomic service AS_1.

4. Reliability of Composite Units

4.1. Reliability of Atomic Services. An abstract service may have several concrete services to be matched; then, different user may select different concrete service to be bound for the same abstract service as they have different QoS requirement [24]. For example, there are an abstract service AS and three matched concrete services AS_1, AS_2, and AS_3. The reliability of the three concrete services is $\{0.98, 0.9, 0.75\}$, and one of the QoS $\{high, general, low\}$. The reliability and price of AS_1 are the highest, and AS_3 is the lowest. If a user only

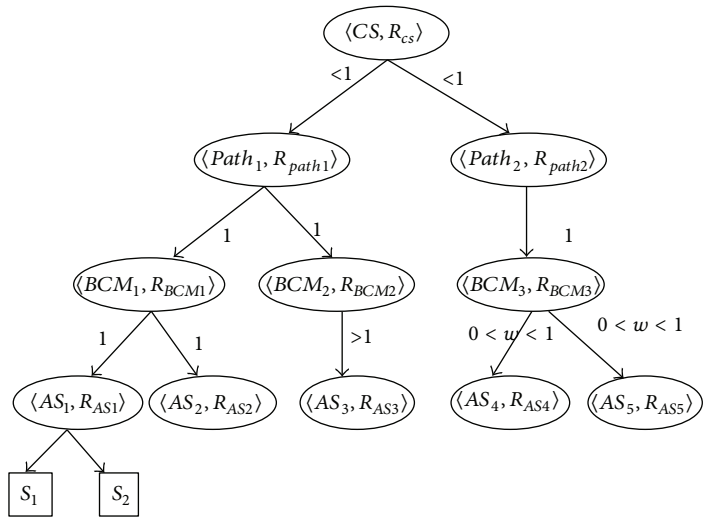

Figure 2: Hierarchical graph of composite service.

cares about the reliability and has no claim for price, he may select AS_1 to be invoked. Other users may have different choice considering the price. The binding information can be recorded by monitor mechanism, and the binding probability can be computed from this information [27]. Here, we assume that the binding probability is known. As shown in Figure 3, the reliability of atomic service v_i can be computed by the following:

$$R_{AS} = R_i = \sum_{j=1}^{n} R_j * w_{i,j}, \tag{1}$$

where R_i is the reliability of an abstract atomic service node V_i, R_j is the reliability of v_j, $j = 1, \ldots, n$, which is a concrete atomic service to be bound to v_i, and $w_{i,j}$ is the binding probability of node v_i to node v_j. After the binding changed, the reliability of atomic service AS must be recomputed according to the above formula.

4.2. Reliability of Basic Composite Module. Sequence module (SM), choice module (CoM), loop module (LM), and concurrent module (CoM) are four kinds of composite modules. Next, we will discuss their reliability in a dynamic environment.

4.2.1. Sequence Module/Concurrent Module. As shown in Figure 3(a), node v_i is SM or CM, nodes $v_1, \ldots, v_n$ are the atomic services which compose the SM or CoM, and the weight of edge from node v_i to v_j, $j = 1, \ldots, n$, is 1. The reliability of SM or CoM is

$$R_{SM} = R_{CoM} = R_i = \prod_{j=1}^{n} R_j. \tag{2}$$

In the equation, if the binding probability of an atomic service v_k is changed, then the reliability of v_i will be changed, and the reliability of SM will be changed. Let ΔR_k be the changed value of v_k; then the new value of node v_i can be represented by

$$\begin{aligned} R_i' &= \prod_{j=1, j\neq k}^{n} R_j \left(R_k + \Delta R_k\right) \\ &= R_i + \Delta R_k \prod_{j=1, j\neq k}^{n} R_j \\ &= \left(1 + \frac{\Delta R_k}{R_k}\right) R_i. \end{aligned} \tag{3}$$

From the equation, we can see that when the binding of a service has been changed, it does not need to recalculate the reliability of the entire services. As long as the changed value is calculated, the whole reliability can be known.

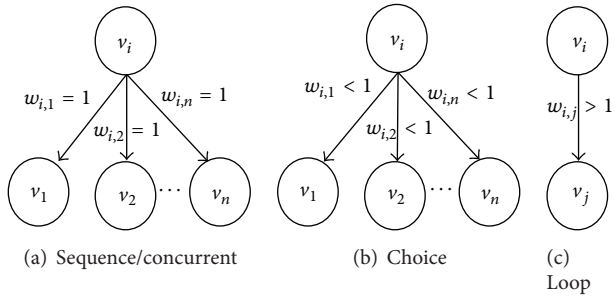

(a) Sequence/concurrent (b) Choice (c) Loop

Figure 3: Hierarchical graph of composite module.

4.2.2. Choice Module. As shown in Figure 3(b), the weight of edge from node v_i to node v_j is less than 1; the composite module is CM. The reliability of CM can be computed by the following expression:

$$R_{CM} = R_i = \sum_{j=1}^{n} R_j w_{i,j}. \tag{4}$$

If a binding probability of an atomic service (e.g., v_k) is changed, the reliability of the atomic service must be recomputed, $R'_k = R_k + \Delta R_k$, where ΔR_k is the changed value of node v_k. Thus, the new reliability of CM can be expressed by the following:

$$\begin{aligned} R'_{CM} = R'_i &= \sum_{j=1, j\neq k}^{n} \left(R_j w_{i,j}\right) + \Delta R_k w_{i,k} \\ &= R_i + \Delta R_k w_{i,k} \end{aligned} \tag{5}$$

and $\Delta R_k = \Delta R_k w_{i,k}$.

4.2.3. Loop Module. As shown in Figure 3(c), the weight of edge from node v_i to node v_j is larger than 1, the composite module is LM, and the weight of edge is the number of times. The reliability of LM can be computed by the following expression:

$$R_{LM} = R_i = R_j^{w_{i,j}}. \tag{6}$$

If the binding probability of v_j is changed, ΔR_j is the changed value of node v_j. The new reliability of LM can be expressed by the following:

$$\begin{aligned} R'_i &= \left(R_i + \Delta R_j\right)^{w_{i,j}} \\ &= R_i\left(1 + \frac{\Delta R_j}{R_i}\right)^{w_{i,j}}. \end{aligned} \tag{7}$$

From (7), we also can see that when the reliability of an abstract service in LM is changed there is no need to recalculate all reliabilities of services in LM to get the reliability of the entire service. It is easy to get the reliability of the entire service as long as the changed value has been got. In a word, the incremental reliability of BCM is

$$\Delta R_i = \begin{cases} \dfrac{\Delta R_k}{R_k} R_i & sequence/concurrent \\ \Delta R_k w_{i,k} & choice \\ \left[\left(1 + \dfrac{\Delta R_k}{R_k}\right)^{w_{i,k}} - 1\right] R_i & loop. \end{cases} \tag{8}$$

4.3. Reliability of Path. As shown in Figure 2, an execution path is a sequence structure of all its $BCMs$ in the path. The weight of edge from execution paths to its $BCMs$ is 1. So, the reliability of execution path is the same as SM:

$$\begin{aligned} R_{Path} = R_i &= \prod_{j=1}^{n} R_j, \\ R'_{Path} &= R_i + \Delta R_i, \end{aligned} \tag{9}$$

where $\Delta R_{Path} = \Delta R_i = (\Delta R_k / R_k) R_i$.

4.4. Reliability of Composite Service. The execution of a composite service can be divided into several paths, and each path is executed according to a probability. Assume that node v_0 is a composite service CoS in Figure 2 that has several execution paths, $Path_1, \ldots, Path_n$; their execution probabilities are $P_1, \ldots, P_n$ and their nodes are $v_1, v_2, \ldots, v_n$. Then, the reliability of composite service CS can be calculated by

$$R_{CS} = R_0 = \sum_{i=1}^{n} R_i w_{0,i}. \tag{10}$$

If the reliability of $Path_k$ has been changed, and ΔR_k is the changed value of $Path_k$, the new reliability of composite service can be recalculated similar to the CM:

$$R'_{CS} = R'_0 = R_0 + \Delta R_0, \tag{11}$$

where $\Delta R_{CS} = \Delta R_0 = \Delta R_k w_{0,k}$ and $Delta\ R_0$ is the changed value of composite service.

```
(1) {
(2) double R = R_i;
(3) for (v_j = v_i.firstneighbor();
(4) v_j != NULL; v_j = v_i.nextneighbor())
(5) if (visited[v_j] == false);
(6) {
(7) if (w_{i,j} < 1)
(8) R = R + CalRel(G, v_j) * w_{i,j};
(9) else if (w_{i,j} = 1)
(10) R = R * CalRel(G, v_j) * w_{i,j};
(11) else R = R * (CalRel(G, v_j))^{w_{i,j}};;
(12) }
(13) return R;
(14) }
```

Algorithm 1: Double *CalRel* (graph G, vertex v_i).

5. Reliability Prediction of Composite Service

Composite services can be decomposed into three layers, that is, *path* layer, *BCM* layer, and *atomic service* layer. Thus, the reliability of composite services can be calculated by the reliability of *path, BCM,* and *atomic service*. In this section, we will discuss how to compute the reliability of composite services.

5.1. Reliability Algorithm for Composite Service. The nodes in different layer in Figure 2 represent different composite units. We assume that the reliability of atomic services is known, and the reliability of other nodes can be derived from the reliability of their next layer nodes. We can get all the reliabilities of nodes from bottom to up. The algorithm $CalRel(G, v)$ calculates the reliability of all nodes in the hierarchical graph of the composite service CS (Algorithm 1). The parameter G is the hierarchical graph and v_i is a node, $\langle v_i, v_j \rangle \in E$, whose initial value is

$$R_i = \begin{cases} 0 & w_{i,j} < 1 \\ 1 & w_{i,j} \geq 1. \end{cases} \tag{12}$$

```
(1) {
(2) double ΔR = 0;
(3) for (v_j = v_i.firstneighbor();
(4) v_j != NULL; v_j = v_i.nextneighbor())
(5) if (!visited[v_j]);
(6) {ΔR_j = CalDeltaRel(G', v_j)
(7) if (w_{i,j} < 1)
(8) ΔR = Δv_j w_{i,j};
(9) else if (w_{i,j} = 1)
(10) ΔR = Δv_j / R_j R_i;
(11) else
(12) ΔR = [(1 + Δv_j / R_j)^{w_{i,j}} − 1]R_i;
(13) }
(14) return ΔR;
(15) }
```

Algorithm 2: Double *CalDeltaRel* (graph G', vertex v_i).

When the algorithm is invoked, parameter v_i is the composite service node v_0. The calculation process is the traverse process and all reliabilities of nodes are calculated in traverse of graph. Then the time complexity is the same as the traverse process, which is $O(n + e)$, n is the number of nodes, and e is the number of edges.

5.2. Dynamic Reliability Algorithm for Composite Services. If the reliability of an atomic service is changed, the composite service will be affected. In this section, we will discuss how to perform our dynamic reliability model to evaluate the reliability of composite services. Not all composite units are affected by the atomic service; we only recalculate the reliability of the influenced nodes. For example, in Figure 4, the nodes with bold line are the affected nodes. The first step is to find all affected nodes, for example, *CS*, $Path_1$, $Path_2$, $Path_3$, $Path_4$, BCM_1, and AS_1 in Figure 4. Then, all the affected nodes are extracted to a subgraph G' in Figure 5. We present an algorithm *CalDeltaRel* to calculate the reliability of the affected nodes (Algorithm 2). The parameter G' is the subgraph and v_i is a node in subgraph G'. Variable R_i is the reliability of node v_i. The returned result (ΔR_{CS}) is the incremental reliability of a composite service and $R'_{CS} = \Delta R_{CS} + R_{CS}$.

6. Case Study

6.1. Experimental Setup. We demonstrate the reliability prediction model with a typical example of a service for travel. In this example, the composite consists of 11 atomic services, and we assume that their reliability is known. As shown in Figure 6 the composite service can be divided into 4 execution paths and 7 basic composite modules. Its hierarchical graph is Figure 7.

6.2. Comparison of Prediction Accuracy. The prediction reliability of the composite units in travel service according to formula (2) to (10) is shown in Table 1.

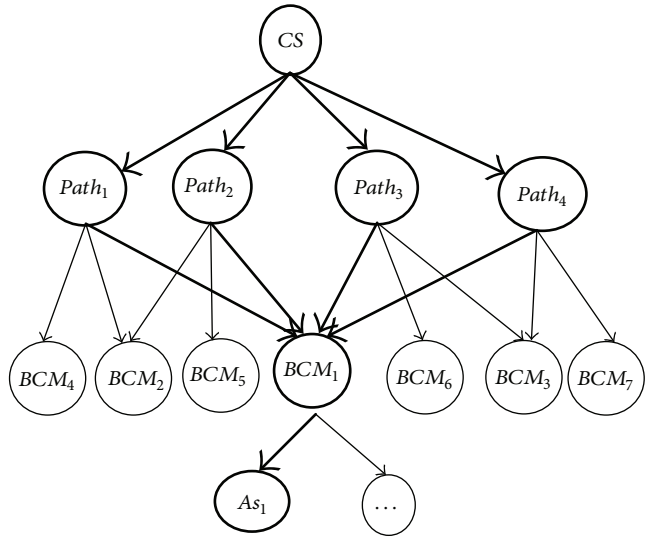

Figure 4: Hierarchical graph of composite service.

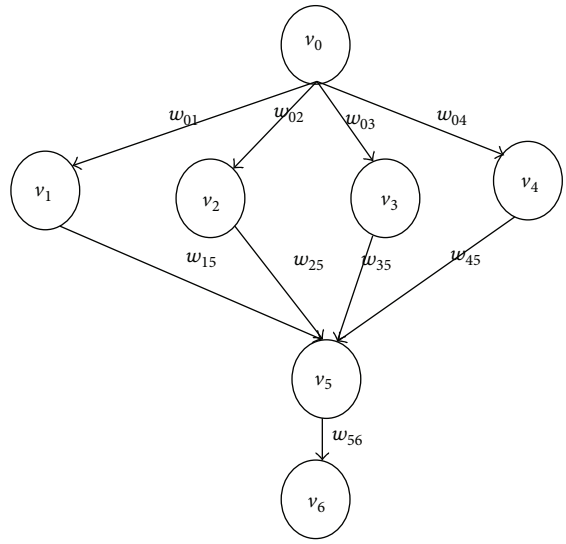

Figure 5: Subgraph of composite service.

To study our method performance, we compare our prediction approach with the user-object reliability model (UORM). As shown in Figure 8, success and failure states are added to the state diagram of UORM, the transition matrix is P, and the reliability is

$$R_{\text{UORM}} = R_{\text{END}}(I - Q)^{-1}_{1,n} = 0.422. \tag{13}$$

From Table 1, we can see that the result of our approach is the same as that of UORM.

6.3. Dynamic Reliability Prediction. If the reliability of atomic service AS_3 is changed, the affected composite units are

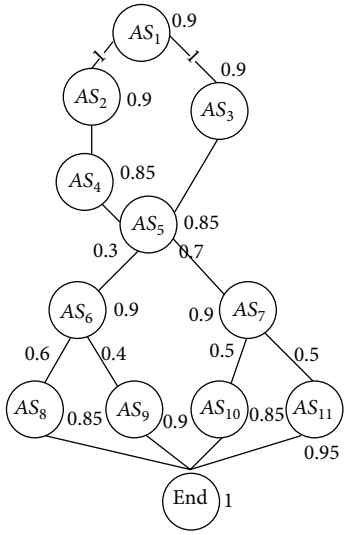

Figure 6: Travel service.

Table 1: Reliability of composite units.

Composite unit	R
AS_1	0.9
AS_2	0.9
AS_3	0.9
AS_4	0.85
AS_5	0.85
AS_6	0.9
AS_7	0.9
AS_8	0.85
AS_9	0.9
AS_{10}	0.85
AS_{11}	0.95
BCM_1	0.5267
BCM_2	0.9
BCM_3	0.9
BCM_4	0.85
BCM_5	0.9
BCM_6	0.85
BCM_7	0.95
$path_1$	0.4029
$path_2$	0.4266
$path_3$	0.4029
$path_4$	0.4503
CS	0.422

BCM_1, $Path_1$, $Path_2$, $Path_3$, and $Path_4$. According to (11), we have

$$\Delta R_{CS} = \sum_{i=1}^{4} \left(\Delta R_{Path_i} w_{0,i}\right),$$

$$\Delta R_{Path_i} = \frac{\Delta R_{BCM1}}{R_{BCM1}} R_{Path_i},$$

$$\Delta R_{BCM1} = \frac{\Delta R_{AS3}}{R_{AS3}} R_{BCM1}. \tag{14}$$

If $\Delta R_{AS3} = 0.02$, the new reliability of composite service v_0 is $R'_{CS} = R_{CS} + \Delta R_{CS} = 0.41298$. The computing process is very simple, but, according to UORM, the transition matrix P' must be rebuilt. The new reliability $R'_{\text{UORM}} = R_{\text{END}}(I - Q)'^{-1}_{1,n} = 0.41298$. From the results of two methods, we can see that our dynamic approach is simpler than UORM, especially when the atomic services are not fixed; then our approach is more applicable to dynamic web services.

6.4. Sensitivity Analysis. Sensitivity analysis helps to understand the impact of the reliability of service components with respect to the system or composite service reliability [28]. The sensitivity of composite service reliability based on our approach with respect to a given atomic service AS_i can be defined as

$$C_i = \frac{\Delta R_{CS}}{\Delta R_{ASi}},$$

$$P = \begin{bmatrix} Q & D \\ 0 & I \end{bmatrix}$$

$$= \begin{bmatrix} 0 & 0.158 & 0.369 & 0 & 0 & 0 & 0 & 0 & 0 & 0.474 \\ 0 & 0 & 0 & 0.54 & 0.36 & 0 & 0 & 0 & 0 & 0.1 \\ 0 & 0 & 0 & 0 & 0 & 0.45 & 0.45 & 0 & 0 & 0.1 \\ 0 & 0 & 0 & 0 & 0 & 0 & 0 & 0.85 & 0 & 0.15 \\ 0 & 0 & 0 & 0 & 0 & 0 & 0 & 0.9 & 0 & 0.1 \\ 0 & 0 & 0 & 0 & 0 & 0 & 0 & 0.85 & 0 & 0.15 \\ 0 & 0 & 0 & 0 & 0 & 0 & 0 & 0.95 & 0 & 0.05 \\ 0 & 0 & 0 & 0 & 0 & 0 & 0 & 0 & 1 & 0 \\ 0 & 0 & 0 & 0 & 0 & 0 & 0 & 0 & 1 & 0 \\ 0 & 0 & 0 & 0 & 0 & 0 & 0 & 0 & 0 & 1 \end{bmatrix},$$

$$P' = \begin{bmatrix} Q' & D' \\ 0 & I \end{bmatrix}$$

$$= \begin{bmatrix} 0 & 0.154 & 0.360 & 0 & 0 & 0 & 0 & 0 & 0 & 0.474 \\ 0 & 0 & 0 & 0.54 & 0.36 & 0 & 0 & 0 & 0 & 0.1 \\ 0 & 0 & 0 & 0 & 0 & 0.45 & 0.45 & 0 & 0 & 0.1 \\ 0 & 0 & 0 & 0 & 0 & 0 & 0 & 0.85 & 0 & 0.15 \\ 0 & 0 & 0 & 0 & 0 & 0 & 0 & 0.9 & 0 & 0.1 \\ 0 & 0 & 0 & 0 & 0 & 0 & 0 & 0.85 & 0 & 0.15 \\ 0 & 0 & 0 & 0 & 0 & 0 & 0 & 0.95 & 0 & 0.05 \\ 0 & 0 & 0 & 0 & 0 & 0 & 0 & 0 & 1 & 0 \\ 0 & 0 & 0 & 0 & 0 & 0 & 0 & 0 & 1 & 0 \\ 0 & 0 & 0 & 0 & 0 & 0 & 0 & 0 & 0 & 1 \end{bmatrix}. \tag{15}$$

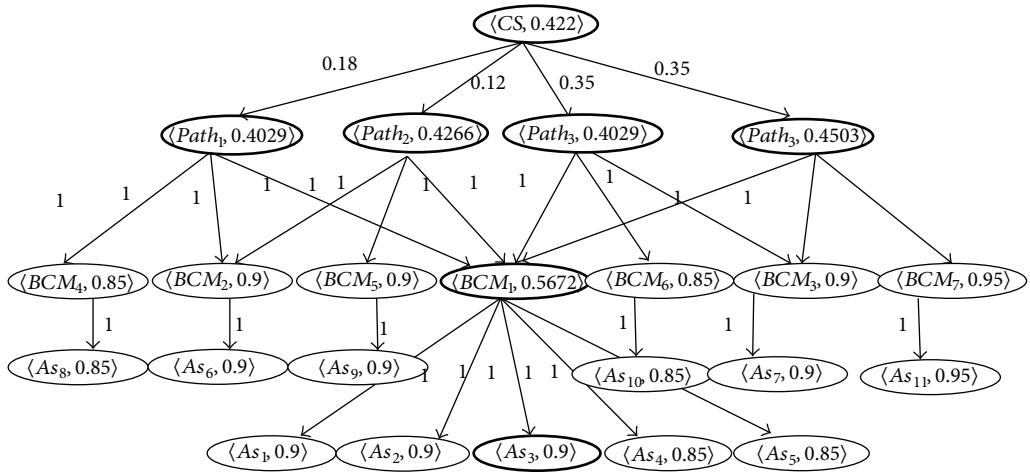

Figure 7: Hierarchical graph of travel service.

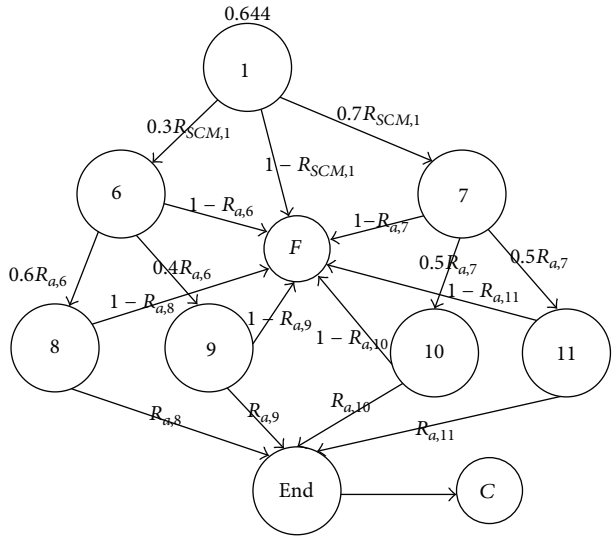

Figure 8: State diagram of composite service.

Table 2: Sensitivity results.

AS	C_i
AS_1	0.7351
AS_2	0.7351
AS_3	0.7351
AS_4	0.7351
AS_5	0.7351
AS_6	0.2205
AS_7	0.5146
AS_8	0.1323
AS_9	0.0882
AS_{10}	0.2537
AS_{11}	0.2537

The higher sensitivity indicates the greater impact on the reliability of composite service. The results of sensitivity analysis are shown in Table 2. From Table 2, we can see that sensitivity of atomic services AS_1, AS_2, AS_3, AS_4, and AS_5 is the same. The atomic service AS_9 has the lowest sensitivity among all abstract services, because the atomic service AS_9 in the execution path $Path_2$ and the execution probability of $Path_2$ is the smallest. We will try to improve the reliability of some critical atomic services to improve the reliability of the composite service.

7. Conclusion and Future Works

In this paper, a new approach has been proposed to evaluate the reliability of composite services based on the hierarchical graph of composite units. The composite services can be decomposed into four different kinds of composite units, and they are *AS*, *BCM*, *Path*, and *CS* nodes in the hierarchical graph from bottom to top layer. We proposed a recursive algorithm to compute the reliability for the four kinds of nodes from down to up, which simplifies the whole computational process. We also proposed an algorithm to compute the reliability of some affected nodes when some atomic service nodes are changed. The approach firstly searches the affected path in the hierarchical graph from the changed atomic service node to the root node and all nodes in the path are affected by the atomic service. The reliability of nodes in the affected path is recalculated, and the reliability of composite service is recalculated based on the reliability of paths, instead of recalculating the reliability of all nodes. A case study illustrates how to apply the proposed methods to estimate the composite service reliability. The results of case study show the effectiveness and usefulness of our approach. The proposed approach has some limitations. Currently, a composite service may have more than one decomposition. Which decomposition is the best way and how to select the best decomposition are our new future works.

Conflict of Interests

The authors declare that there is no conflict of interests regarding the publication of this paper.

Acknowledgment

This work is supported partially by the National Natural Science Foundation of China under Grant nos. 61304174 and 61304117.

References

[1] V. Agarwal and P. Jalote, "From specification to adaptation: an integrated QoS-driven approach for dynamic adaptation of web service compositions," in *Proceedings of the IEEE 8th International Conference on Web Services (ICWS '10)*, pp. 275–282, Miami, Fla, USA, July 2010.

[2] I. Satoh, "Spatial connector: loosely bind ing contextual changes and non-context-aware services," in *Proceedings of the 8th International Joint Conference on Software Technologies*, pp. 50–57, Reykjavłk, Iceland, 2013.

[3] G. Canfora, M. Di Penta, R. Esposito, and M. L. Villani, "A framework for QoS-aware binding and re-binding of composite web services," *Journal of Systems and Software*, vol. 81, no. 10, pp. 1754–1769, 2008.

[4] G. Canfora, M. D. Penta, R. Esposito et al., "Service composition (re)binding driven by application-specific QoS. Service-oriented computing," in *Proceedings of the 4th In ternational Conference Service-Oriented Computing*, pp. 141–152, Chicago, Ill, USA, December 2006.

[5] G. Canfora, M. di Penta, R. Esposito, and M. L. Villani, "QoS-aware replanning of composite web services," in *Proceedings of the IEEE International Conference on Web Services (ICWS '05)*, pp. 121–129, Orlando, Fla, USA, July 2005.

[6] M. D. Penta, R. Esposito, M. L. Villani, R. Codato, M. Colombo, and E. Di Nitto, "WS-Binder: a framework to enable dynamic binding of composite web services," in *Proceedings of the International Workshop on Service-Oriented Software Engineering*, pp. 74–80, Jhongli, Taiwan, December 2008.

[7] K. Goševa-Popstojanova and K. S. Trivedi, "Architecture-based approach to reliability assessment of software systems," *Performance Evaluation*, vol. 45, no. 2-3, pp. 179–204, 2001.

[8] S. S. Gokhale, "Architecture-based software reliability analysis: overview and limitations," *IEEE Transactions on Dependable and Secure Computing*, vol. 4, no. 1, pp. 32–40, 2007.

[9] R. C. Cheung, "A user-oriented software reliability model," *IEEE Transaction on Software Engineering*, vol. 6, no. 2, pp. 118–125, 1980.

[10] W.-L. Wang, D. Pan, and M.-H. Chen, "Architecture-based software reliability modeling," *Journal of Systems and Software*, vol. 79, no. 1, pp. 132–146, 2006.

[11] S. S. Gokhale and K. S. Trivedi, "Analytical models for architecture-based software reliability prediction: a unification framework," *IEEE Transactions on Reliability*, vol. 55, no. 4, pp. 578–590, 2006.

[12] Q. Yu, X. Liu, A. Bouguettaya, and B. Medjahed, "Deploying and managing Web services: issues, solutions, and directions," *Very Large Data Bases Journal*, vol. 17, no. 3, pp. 537–572, 2008.

[13] C. Li, X. Fu, Q. Tian, W. Wang, and Y. Xia, "Optimal reliability allocation with minimum cost for Web service composition," in *Proceedings of the 25th Chinese Control and Decision Conference (CCDC '13)*, pp. 58–63, Guiyang, China, May 2013.

[14] R. Albu and F. Popentiu-Vladicescu, "A prototype for web services reliability prediction," *International Journal of Information and Communication Technology*, vol. 5, no. 1, pp. 64–74, 2013.

[15] X. Liu and J. Cao, "Robust state estimation for neural networks with discontinuous activations," *IEEE Transactions on Systems, Man, and Cybernetics B: Cybernetics*, vol. 40, no. 6, pp. 1425–1437, 2010.

[16] X. Liu and J. Cao, "On periodic solutions of neural networks via differential inclusions," *Neural Networks*, vol. 22, no. 4, pp. 329–334, 2009.

[17] R. Yingxin, Q. Gu, Q. Jingxian, and D. Chen, "Reliability prediction of web service composition based on DTMC," in *Proceedings of the 3rd IEEE International Conference on Secure Software Integration Reliability Improvement (SSIRI '09)*, pp. 369–375, Shanghai, China, July 2009.

[18] G. Fan, H. Yu, L. Chen, and D. Liu, "Petri net based techniques for constructing reliable service composition," *Journal of Systems and Software*, vol. 86, no. 4, pp. 1089–1106, 2013.

[19] Y. N. Xia, X. Luo, J. Li, and Q. S. Zhu, "A petri-net-based approach to reliability determination of ontology-based service compositions," *IEEE Transactions on Systems, Man, and Cybernetics: Systems*, vol. 43, no. 5, pp. 1240–1247, 2013.

[20] W. T. Tsai, D. Zhang, Y. Chen, H. Huang, R. Paul, and N. Liao, "A software reliability model for web services," in *Proceedings of the 8th IASTED International Conference on Software Engineering and Applications*, pp. 144–149, MIT Cambridge, November 2004.

[21] V. Grassi and S. Patella, "Reliability prediction for service-oriented computing environments," *IEEE Internet Computing*, vol. 10, no. 3, pp. 43–49, 2006.

[22] L. Wang, X. Bai, L. Zhou, and Y. Chen, "A hierarchical reliability model of service-based software system," in *Proceedings of the 33rd Annual IEEE International Computer Software and Applications Conference (COMPSAC '09)*, pp. 199–208, Seattle, Wash, USA, July 2009.

[23] Y.-S. Dai, Y. Pan, and X. Zou, "A hierarchical modeling and analysis for grid service reliability," *IEEE Transactions on Computers*, vol. 56, no. 5, pp. 681–691, 2007.

[24] Z. B. Zheng and M. R. Lyu, "Collaborative reliability prediction for service-oriented systems," in *Proceedings of the 32nd ACM/IEEE International Conference on Software Engineering*, pp. 35–44, Cape Town, South Africa, May 2010.

[25] Z. B. Zheng and M. R. Lyu, "Personalized reliability prediction of web services," *ACM Transactions on Software Engineering and Methodology*, vol. 22, no. 2, article 12, 2013.

[26] L. Coppolino, L. Romano, N. Mazzocca, and S. Salvi, "Web services workflow reliability estimation through reliability patterns," in *Proceedings of the 3rd International Conference on Security and Privacy in Communication Networks (SecureComm '07)*, pp. 107–115, Nice, France, September 2007.

[27] H. Zo, D. L. Nazareth, and H. K. Jain, "End-to-end reliability of service oriented applications," *Information Systems Frontiers*, vol. 14, no. 5, pp. 971–986, 2012.

[28] Z. H. Ding, M. Y. Jiang, and A. Kandel, "Port-based reliability computing for service composition," *IEEE Transactions on Services Computing*, vol. 5, no. 3, pp. 422–436, 2012.

[29] C. J. Prakash, P. M. Rohini, R. B. Ganesh, and V. Maheswari, "Hybrid reliability model to enhance the efficiency of composite web services," in *Proceedings of the IEEE International*

Conference on Emerging Trends in Computing, Communication and Nanotechnology (ICE-CCN '13), pp. 79–83, Tuticorin, India, March 2013.

[30] S. Hwang and C. Lee, "Reliable Web service selection in choreographed environments," *Decision Support Systems*, vol. 54, no. 3, pp. 1463–1476, 2013.

[31] M. Silic, G. Delac, and S. Srbljic, "Prediction of atomic web services reliability based on K-means clustering," in *Proceedings of the 9th Joint Meeting of the European Software Engineering Conference and the ACM SIGSOFT Symposium on the Foundations of Software Engineering*, pp. 70–80, Saint Petersburg, Russia, August 2013.

Hindawi Publishing Corporation
Mathematical Problems in Engineering
Volume 2014, Article ID 437819, 7 pages
http://dx.doi.org/10.1155/2014/437819

Research Article

Consensus of Multiagent Systems with Directed Topology and Communication Time Delay Bases on the Laplace Transform

Bo Liu,[1] Li Wang,[2] Dehui Sun,[2] and Xinmao Zhu[1]

[1] *College of Science, North China University of Technology, Beijing 100144, China*
[2] *Key Laboratory of Beijing for Field-Bus Technology & Automation, North China University of Technology, Beijing 100144, China*

Correspondence should be addressed to Bo Liu; liuboangle@163.com

Received 6 May 2014; Accepted 18 June 2014; Published 1 July 2014

Academic Editor: Wei Zhang

This paper investigates the consensus problem of multiagent systems with directed topologies. Different from the literatures, a new method, the Laplace transform, to study the consensus of multiagent systems with directed topology and communication time delay is proposed. The accurate state of the consensus center and the upper bound of the communication delay to make the agents reach consensus are given. It is proved that all the agents could aggregate and eventually form a cohesive cluster in finite time under certain conditions, and the consensus center is only determined by the initial states and the communication configuration among the agents. Finally, simulations are given to illustrate the theoretical results.

1. Introduction

In recent years, there has been an increasing interest in the study of consensus and rendezvous problems in the multiagent systems [1–16]. This is partly due to the wide applications in cooperative control of unmanned air vehicles, formation control of mobile robots, design of sensor networks, flocking of ants and birds, distributed decision making, and so on [5–10]. Vicsek et al. [1] proposed a discrete model of autonomous agents. Each agent of such model was moving at a constant identical velocity, and the direction was updated via a local rule based on the average of the directions of its neighbors. At the same time, they gave some numerical simulations to describe the dynamic behavior of the model. Jadbabaie et al. [3] gave a theoretical explanation for the numerical results of Vicsek's model. In [5], Olfati-Saber and Murray analyzed the consensus problem of multiagent systems with time delay and obtained the accurate bound of the time delay with undirected topology. In [7, 9], the authors discussed the consensus of second-order multiagent systems with time delay by Lyapunov approach. However, due to certain limitations, the bound of delay in those papers is not specific.

The analysis of the coupling topology plays an important part in discussing the consensus problems. Jadbabaie et al. [3] discussed the communication information by applying an undirected graph to model the coupling topology among the agents. Olfati-Saber and Murray [5] investigated the average consensus problem with directed topology, where the coupling topology is undirected and needs to satisfy the balance condition, which is a strong condition for the consensus. Ren and Beard [11] introduced the definition of spanning tree to depict the coupling topology. It was shown that consensus can be achieved asymptotically if the directed interaction graph contains a spanning tree as the system evolves. A useful Lemma about the Laplacian matrix was given in [11], and Laplacian matrix has a simple zero eigenvalue if and only if the directed graph has a spanning tree. Lin et al. [12] introduced the definition of globally reachable node to describe the coupling topology and gave a similar lemma about the Laplacian matrix; that is, the digraph has a globally reachable node if and only if 0 is a simple eigenvalue of Laplacian matrix.

In this paper, we discuss the consensus problem of the multiagent system mentioned in [5] with directed topology and time delay. Compared with the previous references, the main contribution of this paper is to study the coupling topology in a more general case. According to the Laplace transform, we can not only have the specific consensus center of the model but also obtain the accurate upper bound of

the communication delay value to achieve consensus. By the Laplace transform, we can eliminate some assumptions used in the Lyapunov approach and give further simplification of the assumptions.

This paper is organized as follows. Section 2 presents some preliminaries of graph theory. Section 3 proposes the model and gives the analysis for the consensus of the model. In Section 3, some extensions of the studies are discussed. Section 4 gives simulations to verify the theoretical results. Finally, we summarize our main contribution in Section 5.

2. Some Preliminaries

To discuss the coupling topology of the communication configuration of the agents, graph theory is a very effective tool. If each agent is regarded as a node, then the coupling topology is conveniently described by a directed graph. In particular, in the definition of the directed graph, self-loops are excluded. Let $\mathcal{G} = (\mathcal{V}, \mathcal{E}, A)$ be a weighted digraph of order n with the set of nodes $\mathcal{V} = \{1, 2, 3, \ldots, n\}$ and set of arcs $\mathcal{E} \subseteq \mathcal{V} \times \mathcal{V}$, and $A = [a_{ij}]$ is the adjacency matrix of graph $\mathcal{G}$. An arc of $\mathcal{G}$ is denoted by (i, j), which is from i to j. The set of neighbors of node i is denoted by $\mathcal{N}_i = \{j \in \mathcal{V} : (i, j) \in \mathcal{E}\}$. A digraph $\mathcal{G}$ is strongly connected if there exists a path between any two distinct nodes. For a node j, if there exists at least a path from every other node i in $\mathcal{G}$ to node j, we say that node j is globally reachable.

A diagonal matrix $D = \mathrm{diag}\{d_1, d_2, \ldots, d_n\} \in R^{n\times n}$ is a degree matrix of $\mathcal{G}$, and its diagonal elements $d_i = \sum_{j\in\mathcal{N}_i} a_{ij}$ for $i = 1, 2, \ldots, n$. The Laplacian of the weighted digraph $\mathcal{G}$ (or matrix A) is denoted as

$$L = D - A \in R^{n\times n}. \tag{1}$$

It is obvious that the digraph $\mathcal{G}$, the adjacency matrix A, and the Laplacian matrix L are peer-to-peer. Some basic properties of the Laplacian matrix need to be introduced in the following.

Lemma 1 (see [12]). *The digraph $\mathcal{G}$ has a globally reachable node if and only if the Laplacian matrix L has a simple zero eigenvalue (with eigenvector $\mathbf{1} = (1, 1, \ldots, 1)^T \in \mathbb{R}^n$).*

Lemma 2 (see [5]). *The nonzero eigenvalues of L are of positive real part.*

Lemma 3. *For arbitrary row of the Laplacian matrix L, the cofactor of any elements is equal.*

Proof. For Laplacian L

$$\begin{pmatrix} l_{11} & l_{12} & \cdots & l_{1n} \\ l_{21} & l_{22} & \cdots & l_{2n} \\ \vdots & \vdots & \ddots & \vdots \\ l_{n1} & l_{n2} & \cdots & l_{nn} \end{pmatrix}, \tag{2}$$

without loss of generality, the first row of L is chosen to discuss. The cofactors of element l_{1j} and $l_{1(j+1)}$, $j \in \{1, 2, \ldots, n-1\}$, are, respectively, denoted by

$$\begin{aligned} M_{1j} &= (-1)^{1+j} \begin{vmatrix} l_{21} & l_{22} & \cdots & l_{2(j-1)} & l_{2(j+1)} & \cdots & l_{2n} \\ l_{31} & l_{32} & \cdots & l_{3(j-1)} & l_{3(j+1)} & \cdots & l_{3n} \\ \vdots & \vdots & \cdots & \vdots & \vdots & \ddots & \vdots \\ l_{n1} & l_{n2} & \cdots & l_{n(j-1)} & l_{n(j+1)} & \cdots & l_{nn} \end{vmatrix}, \\ M_{1(j+1)} &= (-1)^{1+j+1} \begin{vmatrix} l_{21} & l_{22} & \cdots & l_{2j} & l_{2(j+2)} & \cdots & l_{2n} \\ l_{31} & l_{32} & \cdots & l_{3j} & l_{3(j+2)} & \cdots & l_{3n} \\ \vdots & \vdots & \cdots & \vdots & \vdots & \ddots & \vdots \\ l_{n1} & l_{n2} & \cdots & l_{nj} & l_{n(j+2)} & \cdots & l_{nn} \end{vmatrix}. \end{aligned} \tag{3}$$

For $M_{1(j+1)}$, adding all the other columns to the jth column, we can have

$$\begin{aligned} & M_{1(j+1)} \\ &= (-1)^{1+j+1} \begin{vmatrix} l_{21} & l_{22} & \cdots & -l_{2(j+1)} & l_{2(j+2)} & \cdots & l_{2n} \\ l_{31} & l_{32} & \cdots & -l_{3(j+1)} & l_{3(j+2)} & \cdots & l_{3n} \\ \vdots & \vdots & \cdots & \vdots & \vdots & \ddots & \vdots \\ l_{n1} & l_{n2} & \cdots & -l_{n(j+1)} & l_{n(j+2)} & \cdots & l_{nn} \end{vmatrix} \\ &= (-1)^{1+j+1+1} \begin{vmatrix} l_{21} & l_{22} & \cdots & l_{2(j+1)} & l_{2(j+2)} & \cdots & l_{2n} \\ l_{31} & l_{32} & \cdots & l_{3(j+1)} & l_{3(j+2)} & \cdots & l_{3n} \\ \vdots & \vdots & \cdots & \vdots & \vdots & \ddots & \vdots \\ l_{n1} & l_{n2} & \cdots & l_{n(j+1)} & l_{n(j+2)} & \cdots & l_{nn} \end{vmatrix} \\ &= M_{1j}. \end{aligned} \tag{4}$$

Since j is arbitrary, we can obtain $M_{11} = M_{12} = \cdots = M_{1n}$. Similarly, we can have $M_{21} = M_{22} = \cdots = M_{2n}, \cdots, M_{n1} = M_{n2} = \cdots = M_{nn}$.

This completes the proof. □

3. Model Formulation and Analysis

Consider a multiagent system consisting of n agents in m-dimensional Euclidian space whose motion is governed by the following delay differential equations:

$$\dot{x}_i(t) = -\sum_{j\in\mathcal{N}_i} a_{ij}\left(x_i(t-\tau) - x_j(t-\tau)\right), \quad i = 1, 2, \ldots, n, \tag{5}$$

where $x_i \in \mathbb{R}^m$ represents the state of agent i, $\mathcal{N}_i$ is the neighbor set of agent i, $A = (a_{ij})$ is the coupling weight matrix, and a_{ij} is weight parameter with $a_{ij} > 0$, if agent i has information with agent j; otherwise, $a_{ii} = 0$; the time delay $\tau > 0$ is a constant.

For simplicity of discussion, we take $m = 1$ in model (5). Then, model (5) can be rewritten into a matrix form:

$$\dot{X}(t) = -LX(t-\tau), \tag{6}$$

where $X(t) = (x_1(t), x_2(t), \ldots, x_n(t))^T \in R^n$ and L is the Laplacian matrix.

For system (6), we can have the following main results by Laplace transform.

Theorem 4. *For system* (6)*, if there exists at least one globally reachable node in* $\mathcal{G}$ *and the time delay parameter* τ *satisfies*

$$\tau < \min_{i=2,3,\ldots,n} \frac{\pi/2 - \left|\arg\left(\lambda_i\right)\right|}{\left\|\lambda_i\right\|}, \tag{7}$$

then the states of all agents of the system will asymptotically converge to a constant value; that is,

$$c = \frac{\begin{vmatrix} x_1(0) & l_{12} & \cdots & l_{1n} \\ x_2(0) & l_{22} & \cdots & l_{2n} \\ \vdots & \vdots & \ddots & \vdots \\ x_n(0) & l_{n2} & \cdots & l_{nn} \end{vmatrix}}{\lambda_1\lambda_2\ldots\lambda_n}, \tag{8}$$

where $\lambda_1\lambda_2\ldots\lambda_n$ *are the nonzero eigenvalues of* L *and* $\arg(\lambda_i)$ *and* $\|\lambda_i\|$ *are the argument and modulus of* λ_i*, respectively.*

Proof. Applying Laplace transform on (6), succinctly denoted as $\mathcal{L}(\cdot)$, we can obtain

$$\begin{aligned} s\mathcal{L}\left(X\left(t\right)\right) - X\left(0\right) &= -L\int_0^\infty e^{-st}X\left(t-\tau\right)dt \\ &= -L\int_\tau^\infty e^{-st}X\left(t-\tau\right)dt \\ &= -L\int_0^\infty e^{-s(\xi+\tau)}X\left(t\right)d\xi \\ &= -e^{-s\tau}L\mathcal{L}\left(X\left(t\right)\right); \end{aligned} \tag{9}$$

that is,

$$\left(sI + e^{-s\tau}L\right)\mathcal{L}\left(X\left(t\right)\right) = X\left(0\right), \tag{10}$$

where s is the Laplace variable. For simplicity, $\mathcal{L}X(t)$ is denoted as $\mathcal{X}(s)$.

According to *Cramer rule*, we can get the solutions of (10):

$$\mathcal{X}_i\left(s\right) = \frac{\Delta\left(sI + e^{-s\tau}L\right)^i}{\Delta\left(sI + e^{-s\tau}L\right)}, \quad i = 1, 2, \ldots, n, \tag{11}$$

where $\Delta(sI + e^{-s\tau}L)^i$ is the determinant of $sI + e^{-s\tau}L$ in which the ith column has been replaced by $X(0)$; $\Delta(sI + e^{-s\tau}L)$ is the determinant of matrix $(sI + e^{-s\tau}L)$.

By calculating, we can obtain

$$\mathcal{X}_i\left(s\right) = \frac{e^{-(n-1)s\tau}\Delta\left(se^{s\tau}I + L\right)^i}{e^{-ns\tau}\Delta\left(se^{s\tau}I + L\right)} = \frac{e^{s\tau}\Delta\left(se^{s\tau}I + L\right)^i}{\Delta\left(se^{s\tau}I + L\right)}. \tag{12}$$

That is fractional expression about variable $se^{s\tau}$. If there are common factors between $\Delta(se^{s\tau}I + L)^i$ and $\Delta(se^{s\tau}I + L)$, we can reduce them and make them irreducible. In the following, assume that $\Delta(se^{s\tau}I + L)^i$ and $\Delta(se^{s\tau}I + L)$ are irreducible. For simplicity, we denote $P_i(s) = \Delta(se^{s\tau}I + L)^i$ and $Q(s) = \Delta(se^{s\tau}I + L)$.

According to Lemma 1, the zero eigenvalue of L is simple and the eigenvalues of L are denoted as

$$0, \lambda_2, \lambda_3, \ldots, \lambda_h, \lambda_j, \ldots, \lambda_l, \tag{13}$$

where $\lambda_j, \ldots, \lambda_l$ are the multiple eigenvalues corresponding with the multiplicity as $q, \ldots, p$, respectively. Then, it follows that

$$\begin{aligned} &\Delta\left(se^{s\tau}I + L\right) \\ &\quad = se^{s\tau}\left(se^{s\tau} + \lambda_2\right)\cdots\left(se^{s\tau} + \lambda_h\right)\left(se^{s\tau} + \lambda_j\right)^p\cdots\left(s + \lambda_l\right)^q. \end{aligned} \tag{14}$$

By *Heaviside's method*, (12) can be expanded into

$$\begin{aligned} \mathcal{X}_i\left(s\right) &= e^{s\tau}\left(\frac{c_1^i}{se^{s\tau}} + \frac{c_2^i}{se^{s\tau} + \lambda_2} + \cdots + \frac{c_h^i}{se^{s\tau} + \lambda_h}\right. \\ &\qquad + \frac{c_{jp}^i}{\left(se^{s\tau} + \lambda_j\right)^p} + \frac{c_{j(p-1)}^i}{\left(se^{s\tau} + \lambda_j\right)^{(p-1)}} \\ &\qquad + \cdots + \frac{c_{j1}^i}{\left(se^{s\tau} + \lambda_j\right)} + \cdots \\ &\qquad + \frac{c_{lq}^i}{\left(se^{s\tau} + \lambda_l\right)^q} + \frac{c_{l(q-1)}^i}{\left(se^{s\tau} + \lambda_l\right)^{(q-1)}} \\ &\qquad \left. + \cdots + \frac{c_{l1}^i}{\left(se^{s\tau} + \lambda_l\right)}\right) \\ &\triangleq \frac{c_1^i}{s} + \frac{c_2^i}{s + \lambda_2 e^{-s\tau}} + \cdots + \frac{c_h^i}{s + \lambda_h e^{-s\tau}} \\ &\qquad + \frac{c_{jp}^i}{\left(s + \lambda_j e^{-s\tau}\right)^p} + \frac{c_{j(p-1)}^i}{\left(s + \lambda_j e^{-s\tau}\right)^{(p-1)}} \\ &\qquad + \cdots + \frac{c_{j1}^i}{\left(s + \lambda_j e^{-s\tau}\right)} + \cdots \\ &\qquad + \frac{c_{lq}^i}{\left(s + \lambda_l e^{-s\tau}\right)^q} + \frac{c_{l(q-1)}^i}{\left(s + \lambda_l e^{-s\tau}\right)^{(q-1)}} \\ &\qquad + \cdots + \frac{c_{l1}^i}{\left(s + \lambda_l e^{-s\tau}\right)}, \end{aligned} \tag{15}$$

where

$$c_1^i = s\frac{P_i(s)}{Q(s)}\bigg|_{s=0}, \quad c_e^i = (s+\lambda_e)\frac{P_i(s)}{Q(s)}\bigg|_{s=\lambda_e}, \quad e = 2,\ldots,h,$$

$$c_{jf}^i = \frac{d^{p-f}}{ds^{p-f}}\left[\left(s+\lambda_j\right)^{(p-f)}\frac{P_i(s)}{Q(s)}\right]\bigg|_{s=\lambda_j}, \quad f = 1,2,\ldots,p,$$

$$\vdots$$

$$c_{lg}^i = \frac{d^{q-g}}{ds^{q-g}}\left[\left(s+\lambda_l\right)^{(q-g)}\frac{P_i(s)}{Q(s)}\right]\bigg|_{s=\lambda_l}, \quad g = 1,2,\ldots,q. \tag{16}$$

Equation (15) is the transfer function of $x_i(t)$; the Laplace reverse transform of the first term is a constant value c_1^i. In order to make $x_i(t)$ asymptotically stable, the real part of the denominators' roots must be negative, which implies that the roots of transcendental equation $s + \lambda_k e^{-s\tau} = 0$ must have negative real part. Then, the roots of

$$s + \lambda_k e^{-s\tau} = 0 \tag{17}$$

will be analyzed in the following. To solve (17), we let $s = x + iy$, and $\lambda_k = u + iv$, where $u > 0$, and $i = \sqrt{-1}$ is the plural unit. Then,

$$x + iy + ue^{-(x+iy)\tau} + ive^{-(x+iy)\tau} = 0, \tag{18}$$

which can be expanded as

$$\begin{aligned} &x + iy + ue^{-x\tau}\left(\cos\left(-y\tau\right) + i\sin\left(-y\tau\right)\right) \\ &\quad + ive^{-x\tau}\left(\cos\left(-y\tau\right) + i\sin\left(-y\tau\right)\right) = 0; \end{aligned} \tag{19}$$

that is,

$$\begin{aligned} &x + ue^{-x\tau}\cos\left(-y\tau\right) - ve^{-x\tau}\sin\left(-y\tau\right) \\ &\quad + i\left(y + ue^{-x\tau}\sin\left(-y\tau\right) + ve^{-x\tau}\cos\left(-y\tau\right)\right) = 0. \end{aligned} \tag{20}$$

Separating the real and imaginary parts, then we can have

$$\begin{aligned} x + ue^{-x\tau}\cos\left(-y\tau\right) - ve^{-x\tau}\sin\left(-y\tau\right) = 0, \\ y + ue^{-x\tau}\sin\left(-y\tau\right) + ve^{-x\tau}\cos\left(-y\tau\right) = 0. \end{aligned} \tag{21}$$

Solving the above equations, we can get

$$\begin{aligned} x + \sqrt{u^2+v^2}e^{-x\tau}\cos\left(-y\tau+\varphi\right) = 0, \\ y + \sqrt{u^2+v^2}e^{-x\tau}\sin\left(-y\tau+\varphi\right) = 0, \end{aligned} \tag{22}$$

where $\varphi = \arg(\lambda_k) = \arctan(v/u)$ is the argument of λ and $\varphi \in (-\pi/2, \pi/2)$.

According to (22), we can know that

$$\begin{aligned} x^2 + y^2 &= \left(u^2+v^2\right)e^{-2x\tau}, \\ y\tau &= \pm\tau\sqrt{\left(u^2+v^2\right)e^{-2x\tau} - x^2}. \end{aligned} \tag{23}$$

Substituting those into the first equation of (22), we have

$$x + \sqrt{u^2+v^2}e^{-x\tau}\cos\left(\mp\tau\sqrt{\left(u^2+v^2\right)e^{-2x\tau} - x^2} + \varphi\right) = 0; \tag{24}$$

that is,

$$x + \sqrt{u^2+v^2}e^{-x\tau}\cos\left(\tau\sqrt{\left(u^2+v^2\right)e^{-2x\tau} - x^2} \pm \varphi\right) = 0. \tag{25}$$

Let x be equal to the critical value; that is, $x = 0$; then

$$\tau\sqrt{\left(u^2+v^2\right)} \pm \varphi = \frac{\pi}{2} + m\pi, \quad m = 0, \pm1, \pm2, \ldots. \tag{26}$$

In order to get the smallest positive value of τ, we have $m = 0$, and $\tau\sqrt{(u^2+v^2)} + |\varphi| = \pi/2$, since $\tau\sqrt{(u^2+v^2)} \geq 0$ and the sign of φ is decided by u and v. So, we can get the critical value of the time delay, denoted as τ_0, and

$$\tau_0 = \frac{\pi/2 - |\varphi|}{\sqrt{u^2+v^2}}. \tag{27}$$

In the following, we will show that the roots of (17) have negative real part when $\tau < \tau_0$.

Since the complex eigenvalues of L are conjugated, their imaginary signs arguments are opposite. According to (25), we define the function as

$$\begin{aligned} &f(x) \\ &= x + \sqrt{u^2+v^2}e^{-x\tau}\cos\left(\tau\sqrt{\left(u^2+v^2\right)e^{-2x\tau} - x^2} + |\varphi|\right). \end{aligned} \tag{28}$$

For arbitrary $\tau_1 > (\pi/2 - |\varphi|)/(\sqrt{u^2+v^2})$, let $x = 0$, and if $\tau = \tau_1$, then

$$f(0) = \sqrt{u^2+v^2}\cos\left(\tau_1\sqrt{u^2+v^2} + |\varphi|\right) < 0. \tag{29}$$

For function $\sqrt{(u^2+v^2)e^{-2x\tau_1} - x^2}$, there exists a positive root $b > 0$, and it decreases monotonically in the interval $[0, b]$.

Taking

$$\tau_1\sqrt{\left(u^2+v^2\right)e^{-2x\tau_1} - x^2} + |\varphi| = \frac{\pi}{2}, \tag{30}$$

there exists only one solution in the interval $(0, b)$, denoted as x_1.

Then

$$f\left(x_1\right) = x_1 > 0. \tag{31}$$

From (29) and (31), there exists a root of $f(x)$ between 0 and x_1. Moreover, if $\tau = \tau_1$, the same result holds.

For arbitrary $\tau_2 < \tau_0$, then

$$f(0) = \sqrt{u^2+v^2}\cos\left(\tau_2\sqrt{u^2+v^2} + |\varphi|\right) > 0. \tag{32}$$

Because $\sqrt{(u^2+v^2)e^{-2x\tau_2}-x^2}$ is a monotonically decreasing function in the interval $(0,b)$, $0<\tau_2\sqrt{(u^2+v^2)e^{-2x\tau_2}-x^2}+|\varphi|<\pi/2$ and $f(x)>0,(x\in(0,b))$, which implies that they have no positive roots of (28) but have infinite negative roots of (28).

Define

$$h=\min_{k=\{2,3,\ldots,n\}}\frac{\pi/2-\left|\arg\left(\lambda_k\right)\right|}{\left\|\lambda_k\right\|}, \tag{33}$$

for arbitrary $\tau<h$; the roots of the denominator of each term of (15) must have negative real part.

Take arbitrary term of (15), simply denoted as

$$G(s)=\frac{c}{(s+\lambda e^{-s\tau})^r}, \tag{34}$$

where c is the coefficient, r is the degree, and $\tau<h$. It has infinite singular points which have negative real part. The Laplace inverse transform of the function asymptotically tends to 0; that is, for the function,

$$g(t)=\mathscr{L}^{-1}\left(G(s)\right), \tag{35}$$

when $t\to+\infty$ and $g(t)\to 0$. So, we can obtain

$$x_i(t)=\mathscr{L}^{-1}\left(\mathscr{X}_i(s)\right)\longrightarrow c_1^i, \tag{36}$$

when $t\to+\infty$; that is, $X(t)\to(c_1^1,c_2^1,\ldots,c_n^1)^T$ as $t\to+\infty$.

According to Lemma 1, we can get

$$\begin{aligned} c&=c_1^1=c_1^2=\cdots=c_1^n\\ &=s\frac{P_1(s)}{Q(s)}\bigg|_{s=0}=\frac{\begin{vmatrix} x_1(0) & l_{12} & \cdots & l_{1n}\\ x_2(0) & l_{22} & \cdots & l_{2n}\\ \vdots & \vdots & \ddots & \vdots\\ x_n(0) & l_{n2} & \cdots & l_{nn}\end{vmatrix}}{\lambda_1\lambda_2\ldots\lambda_n}. \end{aligned} \tag{37}$$

This completes the proof. □

Remark 5. If matrix A is symmetrical, then the imaginary parts of the eigenvalues are equal to zero; that is, $\varphi_k=0$. The critical value of the time delay is $h=\pi/2\lambda_{\max}$.

Furthermore, the multiagent system is described by

$$\dot{x}_i(t)=-\sum_{j\in\mathscr{N}_i}a_{ij}\left(x_i\left(t-\tau_{ji}(t)\right)-x_j\left(t-\tau_{ij}(t)\right)\right),\quad i=1,2,\ldots,n. \tag{38}$$

We can also have the same result as follows.

Theorem 6. *For model* (38)*, if there exists at least one globally reachable node in digraph $\mathcal{G}$ and the time delay parameter τ satisfies*

$$\tau(t)<\min_{i=2,3,\ldots,n}\frac{\pi/2-\left|\arg\left(\lambda_i\right)\right|}{\left\|\lambda_i\right\|}, \tag{39}$$

then all the agents of the system can achieve asymptotically consensus.

In model (5), we regarded the feedback gain value as 1. If the feedback gain value is a, then the model can be described as

$$\dot{x}_i(t)=-a\sum_{j\in\mathscr{N}_i}a_{ij}\left(x_i(t-\tau)-x_j(t-\tau)\right),\quad i=1,2,\ldots,n, \tag{40}$$

which can be rewritten as the matrix form

$$\dot{X}(t)=-aLX(t-\tau). \tag{41}$$

It can be easy to get that the consensus center is not changed; then, we have the following theorem.

Theorem 7. *For model* (40)*, if there exists at least one reserve tree in the digraph $\mathcal{G}$ associated with matrix A and the time delay parameter τ satisfies*

$$\tau<\min_{i=2,3,\ldots,n}\frac{\pi/2-\left|\arg\left(\lambda_i\right)\right|}{a\left\|\lambda_i\right\|}, \tag{42}$$

then all the agents of the system will asymptotically converge upon a fixed point c, where

$$c=\frac{\begin{vmatrix} x_1(0) & l_{12} & \cdots & l_{1n}\\ x_2(0) & l_{22} & \cdots & l_{2n}\\ \vdots & \vdots & \ddots & \vdots\\ x_n(0) & l_{n2} & \cdots & l_{nn}\end{vmatrix}}{\lambda_1\lambda_2\ldots\lambda_n}. \tag{43}$$

Remark 8. The feedback gain a can be used to adjust the consensus velocity of the agents and the critical value of delay.

4. Numerical Simulations

In this section, we will give some numerical simulations to illustrate the theoretical results.

Consider a multiagent system with ten agents, where the initial states of agents are chosen randomly. The coupling matrices are given as follows, respectively:

$$A_1=\begin{pmatrix} 0&0&0&0&0&0&0&0&0&0\\ 1&0&0&0&0&0&0&0&0&0\\ 1&0&0&0&0&0&0&0&0&0\\ 1&0&0&0&0&0&0&0&0&0\\ 1&0&0&0&0&0&0&0&0&0\\ 1&0&0&0&0&0&0&0&0&0\\ 1&0&0&0&0&0&0&0&0&0\\ 1&0&0&0&0&0&0&0&0&0\\ 1&0&0&0&0&0&0&0&0&0\\ 1&0&0&0&0&0&0&0&0&0 \end{pmatrix},$$

$$A_2=\begin{pmatrix} 0&0&0&0&0&0&0&0&0&1\\ 1&0&0&0&0&0&0&0&0&0\\ 0&1&0&0&0&0&0&0&0&0\\ 0&0&1&0&0&0&0&0&0&0\\ 0&0&0&1&0&0&0&0&0&0\\ 0&0&0&0&1&0&0&0&0&0\\ 0&0&0&0&0&1&0&0&0&0\\ 0&0&0&0&0&0&1&0&0&0\\ 0&0&0&0&0&0&0&1&0&0\\ 0&0&0&0&0&0&0&0&1&0 \end{pmatrix}. \tag{44}$$

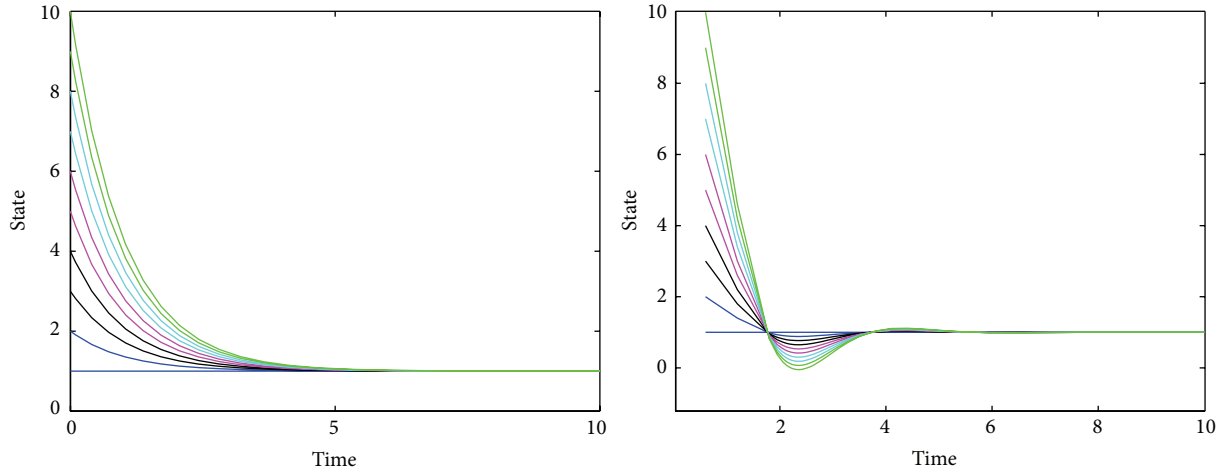

Figure 1: States of the agents about model (5) with the coupling matrix A_1, when $\tau = 0$ and 0.6, respectively.

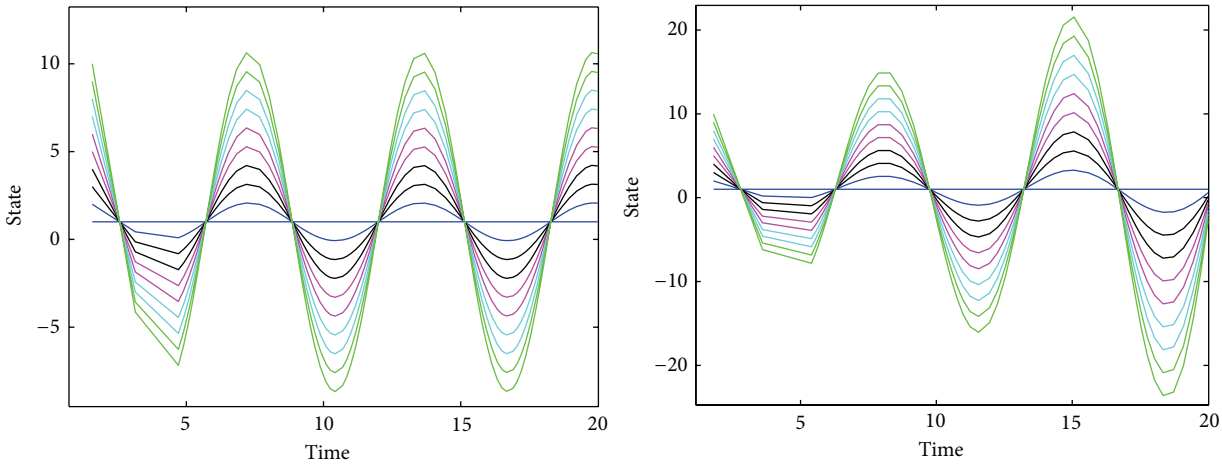

Figure 2: States of the agents about model (5) with the coupling matrix A_1, when $\tau = \pi/2$ and 1.8, respectively.

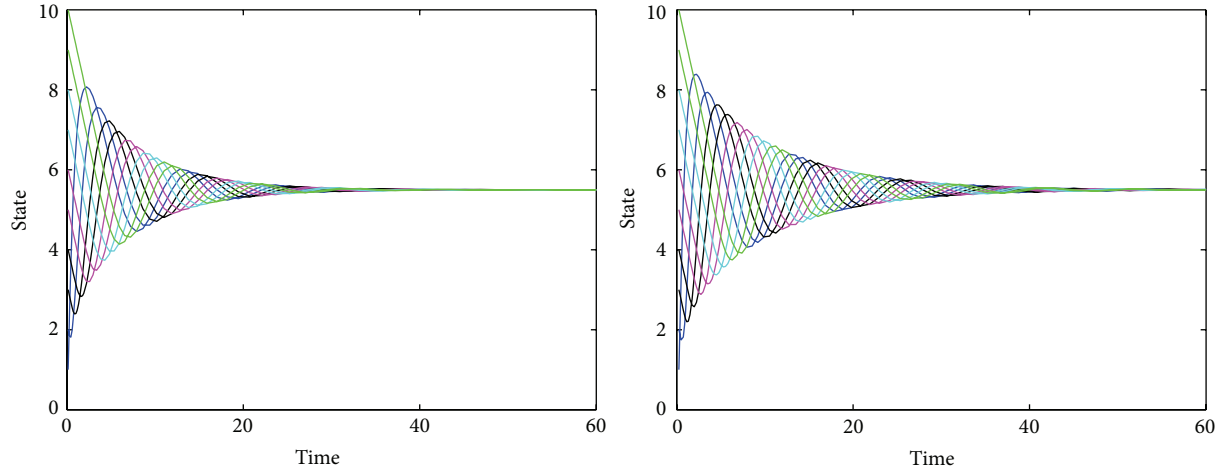

Figure 3: States of the agents about model (38) with the coupling matrix A_2 and the feedback gain $a = 0.5$, when $\tau = 0.3$ and 0.5089, respectively.

Matrix A_1 is the associated Laplacian matrix with only one zero eigenvalue, and the other eigenvalues are all equal to 1. And the critical value of delay is $h_1 = \pi/2$.

For matrix A_2, the associated digraph $\mathcal{G}$ is strongly connected, and the eigenvalues of L are

$$0.0000, 2.0000, 1.8090 + 0.5878i, 1.8090 - 0.5878i;$$
$$1.3090 + 0.9511i, 1.3090 - 0.9511i, 0.6910 + 0.9511i;$$
$$0.6910 - 0.9511i, 0.1910 + 0.5878i, 0.1910 - 0.5878i.$$

The critical value of delay $h_3 = \min_{i=2,3,\ldots,n}((\pi/2 - |\arg(\lambda_i)|)/a\|\lambda_i\|) = 0.5089$.

Figures 1 and 2 show the simulation results, where the coupling matrix is A_1. We can find that, from Figure 1, the states of all agents of model (5) will asymptotically converge to a constant value when $\tau = 0, 0.6$ ($\tau < \pi/2$), respectively; however, from Figure 2, the states of all agents of the system will diverge when $\tau = \pi/2, 1.8$ ($\tau \geq \pi/2$), respectively. Figure 3 shows, for model (38), the states of all agents of the system with the coupling matrix A_2, and the feedback gain will asymptotically converge to a constant value when $\tau = 0.3, 0.5089$ ($\tau < \pi/2$), respectively.

5. Conclusion

In this paper, we have considered the consensus of multiagent systems with directed topology and communication time delay. We have proved that the system aggregates and forms a cluster in finite time if the time delays are smaller than the critical value. The methods and results of this paper can be extended to discuss the leader-follower second-order multiagent system with time delay.

Conflict of Interests

The authors declare that there is no conflict of interests regarding the publication of this paper.

Acknowledgments

This work was supported by the National Natural Science Foundation of China under Grant (nos. 61304049, 61174116, and 51308005) and Science and Technology Development Plan Project of Beijing Education Commission (no. KM201310009011).

References

[1] T. Vicsek, A. Czirk, E. Ben-Jacob, I. Cohen, and O. Shochet, "Novel type of phase transition in a system of self-driven particles," *Physical Review Letters*, vol. 75, no. 6, pp. 1226–1229, 1995.

[2] H. Su, X. Wang, and G. Chen, "Rendezvous of multiple mobile agents with preserved network connectivity," *Systems & Control Letters*, vol. 59, no. 5, pp. 313–322, 2010.

[3] A. Jadbabaie, J. Lin, and A. S. Morse, "Coordination of groups of mobile autonomous agents using nearest neighbor rules," *IEEE Transactions on Automatic Control*, vol. 48, no. 6, pp. 988–1001, 2003.

[4] H. Su, G. Chen, X. Wang, and Z. Lin, "Adaptive second-order consensus of networked mobile agents with nonlinear dynamics," *Automatica*, vol. 47, no. 2, pp. 368–375, 2011.

[5] R. Olfati-Saber and R. M. Murray, "Consensus problems in networks of agents with switching topology and time-delays," *IEEE Transactions on Automatic Control*, vol. 49, no. 9, pp. 1520–1533, 2004.

[6] H. Su, X. Wang, and G. Chen, "A connectivity-preserving flocking algorithm for multi-agent systems based only on position measurements," *International Journal of Control*, vol. 82, no. 7, pp. 1334–1343, 2009.

[7] J. Hu and Y. Hong, "Leader-following coordination of multi-agent systems with coupling time delays," *Physica A: Statistical Mechanics and its Applications*, vol. 374, no. 2, pp. 853–863, 2007.

[8] H. Su, X. Wang, and Z. Lin, "Flocking of multi-agents with a virtual leader," *IEEE Transactions on Automatic Control*, vol. 54, no. 2, pp. 293–307, 2009.

[9] J. Wang, J. Hu, Y. Hong, and D. Cheng, "Consensus of a class of multi-agent systems with active leader and time delay," *Graduate School of Chinese Academy of Sciences*, vol. 25, no. 3, pp. 320–328, 2008.

[10] H. Su, N. Zhang, M. Z. Q. Chen, and X. Wang, "Adaptive flocking with a virtual leader of multiple agents governed by locally Lipschitz nonlinearity," *Nonlinear Analysis: Real World Applications*, vol. 14, no. 1, pp. 798–806, 2013.

[11] W. Ren and R. W. Beard, "Consensus seeking in multiagent systems under dynamically changing interaction topologies," *IEEE Transactions on Automatic Control*, vol. 50, no. 5, pp. 655–661, 2005.

[12] Z. Lin, B. Francis, and M. Maggiore, "Necessary and sufficient graphical conditions for formation control of unicycles," *IEEE Transactions on Automatic Control*, vol. 50, no. 1, pp. 121–127, 2005.

[13] H. Su, M. Chen, X. Wang, and J. Lam, "Semiglobal observer-based leader-following consensus with input saturation," *IEEE Transactions on Industrial Electronics*, vol. 61, no. 6, pp. 2842–2850, 2014.

[14] H. Su, Z. Rong, M. Z. Q. Chen, X. Wang, G. Chen, and H. Wang, "Decentralized adaptive pinning control for cluster synchronization of complex dynamical networks," *IEEE Transactions on Systems, Man, and Cybernetics B: Cybernetics*, vol. 43, no. 1, pp. 394–399, 2013.

[15] H. Su, M. Z. Q. Chen, J. Lam, and Z. Lin, "Semi-global leader-following consensus of linear multi-agent systems with input saturation via low gain feedback," *IEEE Transactions on Circuits and Systems I*, vol. 60, no. 7, pp. 1881–1889, 2013.

[16] L. Ji and X. Liao, "Consensus problems of first-order dynamic multi-agent systems with multiple time delays," *Chinese Physics B*, vol. 22, no. 4, Article ID 040203, 2013.

Hindawi Publishing Corporation
Mathematical Problems in Engineering
Volume 2014, Article ID 418594, 6 pages
http://dx.doi.org/10.1155/2014/418594

Research Article

Solving the Fuzzy BiLevel Linear Programming with Multiple Followers through Structured Element Method

Shengyue Deng,[1] Liqian Zhou,[2] and Xinfan Wang[1]

[1] *School of Science, Hunan University of Technology, Zhuzhou, Hunan 412007, China*
[2] *School of Computer and Communication, Hunan University of Technology, Zhuzhou, Hunan 412007, China*

Correspondence should be addressed to Liqian Zhou; zhoulq11@163.com

Received 10 May 2014; Accepted 11 June 2014; Published 29 June 2014

Academic Editor: Housheng Su

The optimal solution of fuzzy bilevel linear programming with multiple followers (MFFBLP) model is shown to be equivalent to the optimal solution of the bilevel linear programming with multiple followers by using fuzzy structured element theory. The optimal solution to this model is found out by adopting the Kuhn-Tucker approach. Finally, an illustrative numerical example for this model is also provided to demonstrate the feasibility and efficiency of the proposed method.

1. Introduction

Bilevel programming introduced by Stackelberg in 1952 [1] has been developed to solve the decentralized planning problem in which decision makers are often arranged within a hierarchical administrative structure. A bilevel programming problem occurs when two decision makers are located at different hierarchical levels. In general, a decision maker at the upper level is termed as the leader and the lower level is termed as the follower [2, 3]. In the context of bilevel programming, the leader first specifies a strategy; the follower then specifies a strategy so as to optimize the objective with full knowledge of the action of the leader.

Many researches on bilevel programming so far have centered on the linear version of the problem [2–7]. Also two fundamental issues in theory and practice of both bilevel programming problems are mostly concerned: one is how to model a real world bilevel programming and the other is how to find properties and an optimal solution to the bilevel programming problem. There are many such hierarchical optimization problems in the fields of industry, agriculture, finance transportation, and so on [8–11]. But in many practical hierarchical decision making systems, the coefficients of objective functions and constraints sometimes cannot be described by precise values. Hence, it is necessary for us to formulate the decentralized decision making problem with uncertainty as fuzzy models.

At present, the linear bilevel programming in which the coefficients are characterized by fuzzy numbers is called fuzzy linear bilevel programming [12, 13]. Sakawa et al. [4, 5, 14–17] formulated cooperative fuzzy bilevel programming problems and proposed an interactive fuzzy programming approach to solve the problems. From this approach, the concept of a bilevel programming was introduced based on fuzzy number λ-level sets. At the same time, some researches applied fuzzy set technique to deal with bilevel programming problems. Shih and Stanely Lee [18] applied fuzzy set theory to overcome the computational difficulties in solving bilevel problems. Sinha [19] started from the fuzzy mathematical programming approach to obtain the solution of multilevel linear programming problems. Recently, Zhang et al. [13, 20–22] studied fuzzy bilevel programming problem, which focuses on the situation where the leader or the follower has multiple objectives with fuzzy parameters and all followers share their decision variables, and provided related algorithms based on the y function in fuzzy set theory. Moreover, they have first solved the fuzzy linear bilevel programming problems with a specialized form of membership functions, triangular form, in the fuzzy parameters [6, 12]. Nevertheless so far the fuzzy linear bilevel programming problem remains the focus of fuzzy multilevel programming problem.

This paper discusses the fuzzy bilevel linear programming with multiple followers (MFFBLP) model. Based on the homeomorphism properties between the bounded real fuzzy

number and the monotone functions on $[-1, 1]$, the comparison of a fuzzy number is changed into a new comparison of monotone function by the definition of fuzzy numbers structured element weighted order. Then the optimal solutions of new derived model is proved equivalent to the optimal solution of the MFFBLP model. The feasibility of the proposed approach is proved by giving a numerical example.

The following of this paper is arranged as follows. In Section 2, some concepts and properties of the fuzzy numbers structured element weighted order are introduced. In Section 3, we study the optimal solution of the MFFBLP model. In Section 4, one numerical example is shown for illustrating the proposed models and approach. Finally, we give some conclusions in Section 5.

2. Preliminaries

In this section, some necessary backgrounds and notions of fuzzy structured element theory are presented.

Definition 1 (see [23]). Let E be a fuzzy set on R and $E(x)$ the membership function of E. Then, E is called a fuzzy structured element, if (i) $E(0) = 1$; (ii) $E(x)$ is a function of monotonous increasing and right continuous on $[-1, 0]$ and monotone decreasing and left continuous on (0,1]; (iii) $E(x) = 0$ $(-\infty < x < -1$ or $1 < x < +\infty)$.

Definition 2 (see [23]). E is called a canonical fuzzy structured element, if (i) $\forall x \in (-1, 1), E(x) > 0$; (ii) $E(x)$ is continuous and strictly monotone increasing on $[-1, 0]$ and strictly monotone decreasing and continuous on $(0, 1]$.

Definition 3 (see [23]). E is called a symmetrical fuzzy structured element, if $E(-x) = E(x)$.

Lemma 4 (see [23]). *Let E be a fuzzy structured element and $E(x)$ is its membership function; the function $f(x)$ is continuous and monotone on $[-1, 1]$; then $f(E)$ is a fuzzy number, and the membership function of $f(E)$ is $E(f^{-1}(x))$, where $f^{-1}(x)$ is rotational symmetry function for variables x and y, if f is a strictly monotone function, then $f^{-1}(x)$ is the inverse function of $f(x)$.*

Lemma 5 (see [24]). *For a given canonical fuzzy structured element E and any finite fuzzy number $\widetilde{A}$, there always exists a monotone bounded function f on $[-1, 1]$, having the form $\widetilde{A} = f(E)$.*

Lemma 6 (see [25]). *Let the triangular fuzzy number $\widetilde{A} = (a, b, c)$, E is a fuzzy structured element, and its membership function is*

$$E(x) = \begin{cases} 1 + x, & -1 \le x \le 0, \\ 1 - x, & 0 \le x \le 1, \\ 0, & others. \end{cases} \tag{1}$$

Then arbitrary bounded triangular fuzzy number can be generated by E and the monotone bounded function is

$$f(x) = \begin{cases} (b - a)\, x + b, & -1 \le x \le 0, \\ (c - b)\, x + b, & 0 \le x \le 1, \\ 0, & others. \end{cases} \tag{2}$$

Therefore, we easily get the conclusion $\widetilde{A} = f(E)$.

Remark 7. The class of all bounded fuzzy numbers is denoted by $\widetilde{N}_C(R)$, and let E be a canonical fuzzy structured element.

Definition 8 (see [23]). Suppose $\widetilde{A}_1, \widetilde{A}_2 \in \widetilde{N}_C(R)$. Its structured element representation is $\widetilde{A}_i = f_i(E)$, $i = 1, 2$, respectively, where E is given a canonical fuzzy structured element and its membership function is $E(x)$, $f_1(x)$ and $f_2(x)$ are the same sequence monotonic functions on $[-1, 1]$, respectively. By the following formula

$$\begin{aligned} \widetilde{A}_1 \le \widetilde{A}_2 &\Longleftrightarrow F\left(\widetilde{A}_1, \widetilde{A}_2\right) \\ &= \int_{-1}^{1} E(x) \left(f_1(x) - f_2(x)\right) dx \\ &= \int_{-1}^{1} E(x)\, f_1(x)\, dx - \int_{-1}^{1} E(x)\, f_2(x)\, dx \le 0 \end{aligned} \tag{3}$$

to determine the binary relation "$\le$" is a total order on $\widetilde{N}_C(R)$ and then called fuzzy numbers structured element weighted order.

Lemma 9 (see [23]). *Let E be a symmetrical fuzzy structured element, $f_1(x)$ and $f_2(x)$ are the same sequence monotonic functions on $[-1, 1]$, the fuzzy number $\widetilde{A}_1 = f_1(E)$, and $\widetilde{A}_2 = f_2(E)$, then*

$$\begin{aligned} \widetilde{A}_1 + \widetilde{A}_2 &= f_1(E) + f_2(E), \\ \widetilde{A}_1 - \widetilde{A}_2 &= f_1(E) + f_2^{\tau}(E), \\ k\widetilde{A}_1 &= |k|\, f_1^{\tau}(E), \\ k\widetilde{A}_2 &= |k|\, f_2^{\tau}(E), \end{aligned} \tag{4}$$

when $k \ge 0$, $f_1^{\tau}(E) = f_1(E)$, and $f_2^{\tau}(E) = f_2(E)$; when $k < 0$, $f_1^{\tau}(E) = -f_1(-E)$, and $f_2^{\tau}(E) = -f_2(-E)$.

The proof of above Lemmas can be found in reference [23–25].

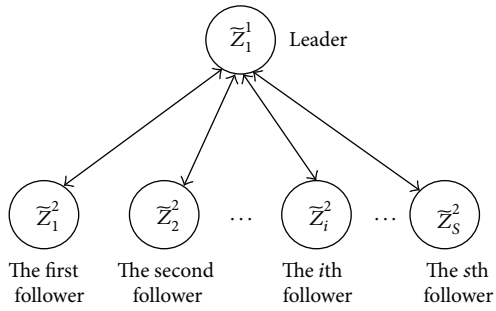

Figure 1: Fuzzy bilevel linear programming with multiple followers.

3. Fuzzy Bilevel Linear Programming with Multiple Followers

Figure 1 shows the fuzzy bilevel linear programming with multiple followers model (MFFBLP), and this mathematical model is defined as follows:

$$\begin{aligned}
&\min_{x_i} \quad \widetilde{Z}_1^1 = \sum_{i=1}^{N} \widetilde{c}_i^1 x_i + \sum_{s=1}^{S}\sum_{j=1}^{M} \widetilde{d}_{sj}^1 y_{sj};\\
&\text{s.t.} \quad \text{where } y_{sj}\,(s = 1, 2, \ldots, S;\ j = 1, 2, \ldots, M)\\
&\qquad \text{is the solution of the lower level problem:}\\
&\min_{y_{sj}} \quad \widetilde{Z}_s^2 = \sum_{i=1}^{N} \widetilde{c}_{si}^2 x_i + \sum_{j=1}^{M} \widetilde{d}_{sj}^2 y_{sj}\\
&\text{s.t} \quad \sum_{i=1}^{N} \widetilde{a}_{ti}^s x_i + \sum_{j=1}^{M} \widetilde{b}_{tj}^s y_{sj} \le \widetilde{e}_t^s;\\
&\qquad\qquad x_i \ge 0;\ \ y_{sj} \ge 0;\\
&i = 1, 2, \ldots, N; \quad j = 1, 2, \ldots, M; \quad s = 1, 2, \ldots, S;\\
&\qquad\qquad\qquad\qquad t = 1, 2, \ldots, T,
\end{aligned} \tag{5}$$

where $\widetilde{Z}_1^1$ is the leader's objective function and $\widetilde{Z}_s^2$ is the sth follower's objective function; x_i, $y_{sj} \in R$; $\widetilde{c}_i^1, \widetilde{c}_{si}^2, \widetilde{d}_{sj}^1, \widetilde{d}_{sj}^2, \widetilde{a}_{ti}^s, \widetilde{b}_{tj}^s, \widetilde{e}_t^s \in \widetilde{N}_C(R)$.

Theorem 10. *Suppose that* $\widetilde{Z}_1^1 = G_1^1(E)$, $\widetilde{Z}_s^2 = G_s^2(E)$, $\widetilde{c}_i^1 = f_i^1(E)$, $\widetilde{c}_{si}^2 = f_{si}^2(E)$, $\widetilde{d}_{sj}^1 = F_{sj}^1(E)$, $\widetilde{d}_{sj}^2 = F_{sj}^2(E)$, $\widetilde{a}_{ti}^s = \varphi_{ti}^s(E)$, $\widetilde{b}_{tj}^s = g_{tj}^s(E)$, $\widetilde{e}_t^s = \psi_t^s(E)$, *and* $M_1^1 = \int_{-1}^{1} E(t) G_1^1(t)dt$, *if* E *is a canonical fuzzy structured element,* $G_1^1(t)$, $G_s^2(t)$, $f_i^1(t)$, $f_{si}^2(t)$, $F_{sj}^1(t)$, $F_{sj}^2(t)$, $\varphi_{ti}^s(t)$, $g_{tj}^s(t)$, *and* $\psi_t^s(t)$ *are monotonous increasing functions, then the model* (5) *is equivalent to the following model:*

$$\begin{aligned}
&\min_{x_i} M_1 = \sum_{i=1}^{N} x_i \int_{-1}^{1} E(t)\, f_i^1(t)\, dt + \sum_{s=1}^{S}\sum_{j=1}^{M} y_{sj} \int_{-1}^{1} E(t)\, F_{sj}^1(t)\, dt;\\
&s.t. \quad \text{where } y_{sj}\,(s = 1, 2, \ldots, S;\ j = 1, 2, \ldots, M) \text{ is the}\\
&\qquad \text{solution of the lower level problem:}\\
&\min_{y_{sj}} M_s^2 = \sum_{i=1}^{N} x_i \int_{-1}^{1} E(t)\, f_{si}^2(t)\, dt + \sum_{j=1}^{M} y_{sj} \int_{-1}^{1} E(t)\, F_{sj}^2(t)\, dt\\
&s.t \quad \sum_{i=1}^{N} x_i \int_{-1}^{1} E(t)\, \varphi_{ti}^s(t)\, dt + \sum_{j=1}^{M} y_{sj} \int_{-1}^{1} E(t)\, g_{tj}^s(t)\, dt\\
&\qquad \le \int_{-1}^{1} E(t)\, \psi_t^s(t)\, dt;\\
&\qquad x_i \ge 0;\ \ y_{sj} \ge 0;\\
&\qquad i = 1, 2, \ldots, N; \quad j = 1, 2, \ldots, M; \quad s = 1, 2, \ldots, S;\\
&\qquad\qquad\qquad\qquad t = 1, 2, \ldots, T.
\end{aligned} \tag{6}$$

Proof. By Definition 8, we know that comparing the size of fuzzy number $\widetilde{Z}_1^1$ by $M_1^1 = \int_{-1}^{-1} E(t) G_1^1(t)\, dt$ in model (5), then

$$\begin{aligned}
\widetilde{Z}_1^1 = G_1^1(E) &= \sum_{i=1}^{N} \widetilde{c}_i^1 x_i + \sum_{s=1}^{S}\sum_{j=1}^{M} \widetilde{d}_{sj}^1 y_{sj}\\
&= \sum_{i=1}^{N} f_i^1(E)\, x_i + \sum_{s=1}^{S}\sum_{j=1}^{M} F_{sj}^1(E)\, y_{sj};
\end{aligned} \tag{7}$$

because $f_i^1(t)$ and $F_{sj}^1(t)$ are monotonous increasing functions; then

$$\begin{aligned}
M_1^1 &= \int_{-1}^{1} E(t)\, G_1^1(t)\, dt\\
&= \int_{-1}^{1} E(t) \left[\sum_{i=1}^{N} f_i^1(t)\, x_i + \sum_{s=1}^{S}\sum_{j=1}^{M} F_{sj}^1(t)\, y_{sj} \right] dt\\
&= \int_{-1}^{1} E(t) \sum_{i=1}^{N} f_i^1(t)\, x_i\, dt + \int_{-1}^{1} E(t) \sum_{s=1}^{S}\sum_{j=1}^{M} F_{sj}^1(t)\, y_{sj}\, dt\\
&= \sum_{i=1}^{N} x_i \int_{-1}^{1} E(t)\, f_i^1(t)\, dt + \sum_{s=1}^{S}\sum_{j=1}^{M} y_{sj} \int_{-1}^{1} E(t)\, F_{sj}^1(t)\, dt.
\end{aligned} \tag{8}$$

In the same way, we get

$$\begin{aligned}
M_s^2 &= \int_{-1}^{1} E(t)\, G_s^2(t)\, dt\\
&= \sum_{i=1}^{N} x_i \int_{-1}^{1} E(t)\, f_{si}^2(t)\, dt + \sum_{j=1}^{M} y_{sj} \int_{-1}^{1} E(t)\, F_{sj}^2(t)\, dt.
\end{aligned} \tag{9}$$

By Lemmas 6 and 9, we obtain that

$$\sum_{i=1}^{N} x_i \int_{-1}^{1} E(t)\,\varphi_{ti}^{s}(t)\,dt + \sum_{j=1}^{M} y_{sj} \int_{-1}^{1} E(t)\,g_{tj}^{s}(t)\,dt \le \int_{-1}^{1} E(t)\,\psi_{t}^{s}(t)\,dt. \tag{10}$$

The proof is completed. □

4. Algorithm and Numerical Example

4.1. Algorithm. By using Theorem 10, we give all steps of the approach for the proposed MFFBLP model.

Step 1. If the fuzzy number is triangular fuzzy number, according to Lemma 6 and E expression, we have $\mu_{\widetilde{A}}(t) = E(f^{-1}(t))$ and then get $f_i^1(t)$, $f_{si}^2(t)$, $F_{sj}^1(t)$, $F_{sj}^2(t)$, $\varphi_{ti}^s(t)$, $g_{tj}^s(t)$, and $\psi_t^s(t)$.

Step 2. Computation formula is as follows: $\int_{-1}^{1} E(t) f_i^1(t)dt$, $\int_{-1}^{1} E(t) f_{si}^2(t)dt$, $\int_{-1}^{1} E(t) F_{sj}^1(t)dt$, $\int_{-1}^{1} E(t) F_{sj}^2(t)dt$, $\int_{-1}^{1} E(t)\varphi_{ti}^s(t)dt$, $\int_{-1}^{1} E(t) g_{tj}^s(t)dt$, and $\int_{-1}^{1} E(t)\psi_t^s(t)dt$, and plug in model (5).

Step 3. According to Theorem 10, the MFFBLP model is transformed into the classical bilevel linear programming with multiple followers model whose optimal solution of model (6) can be derived from Kuhn-Tucker's approach [7].

Step 4. After the optimal solution of model (6) is plugged into model (5), we get the optimal solution of the MFFBLP model.

4.2. Numerical Example. Consider the following MFFBLP problem with $x_1 \in R^1$, $x_2 \in R^1$, $y_{11} \in R^1$, and $y_{21} \in R^1$. Consider

$$\begin{aligned}
&\min_{x_1,x_2} \quad \widetilde{Z}_1^1(x_1, x_2, y_{11}, y_{21}) = \widetilde{3.1}x_1 + \widetilde{8}x_2 + \widetilde{6.9}y_{11} + \widetilde{11}y_{21};\\
&\text{s.t.} \quad \text{where given } x_1,\ x_2, \text{and } y_{11}, y_{21} \text{ solve}\\
&\qquad \text{the following problem.}\\
&\min_{y_{11}} \quad \widetilde{Z}_1^2(x_1, x_2, y_{11}) = \widetilde{2}x_1 + \widetilde{1}x_2 - \widetilde{1}y_{11};\\
&\text{s.t.} \quad \widetilde{6}x_1 - \widetilde{1}x_2 + \widetilde{13}y_{11} \le \widetilde{15},\\
&\qquad \widetilde{5}x_1 + \widetilde{6.9}y_{11} \le \widetilde{15},\\
&\qquad -\widetilde{4}x_2 + \widetilde{25}y_{11} \le \widetilde{3.1};
\end{aligned}$$

$$\begin{aligned}
&\min_{y_{21}} \quad \widetilde{Z}_2^2(x_1, x_2, y_{21}) = \widetilde{15}x_1 - \widetilde{1}x_2 + \widetilde{80}y_{21};\\
&\text{s.t.} \quad \widetilde{1}x_1 + \widetilde{1}x_2 - \widetilde{6.9}y_{21} \le \widetilde{10},\\
&\qquad \widetilde{40}x_1 + \widetilde{1}y_{21} \le \widetilde{5};\\
&\qquad x_1 \ge 0,\ x_2 \ge 0,\ y_{11} \ge 0,\ y_{21} \ge 0,
\end{aligned} \tag{11}$$

where the triangular fuzzy numbers $\widetilde{1} = (0, 1, 2)$, $\widetilde{2} = (1.5, 2, 2.5)$, $\widetilde{3.1} = (2, 3.1, 3.6)$, $\widetilde{4} = (2, 4, 6)$, $\widetilde{5} = (4.7, 5, 5.3)$, $\widetilde{6} = (5, 6, 7)$, $\widetilde{6.9} = (6.5, 6.9, 7.9)$, $\widetilde{8} = (7.5, 8, 8.5)$, $\widetilde{10} = (8, 10, 12)$, $\widetilde{11} = (10.7, 11, 11.3)$, $\widetilde{13} = (12, 13, 14)$, $\widetilde{15} = (14.5, 15, 15.5)$, $\widetilde{25} = (23, 25, 27)$, $\widetilde{40} = (39, 40, 41)$, and $\widetilde{80} = (77, 80, 83)$.

Step 1. By Lemma 6, we have

$$f_1^1(t) = \psi_3^1(t) = \begin{cases} 1.1t + 3.1, & -1 \le t \le 0\\ 0.5t + 3.1, & 0 \le t \le 1\\ 0, & \text{others,} \end{cases}$$

$$f_2^1(t) = \begin{cases} 0.5t + 8, & -1 \le t \le 0\\ 0.5t + 8, & 0 \le t \le 1\\ 0, & \text{others,} \end{cases}$$

$$F_{11}^1(t) = g_{21}^1(t) = \begin{cases} 0.4t + 6.9, & -1 \le t \le 0\\ t + 6.9, & 0 \le t \le 1\\ 0, & \text{others,} \end{cases}$$

$$F_{21}^1(t) = \begin{cases} 0.3t + 11, & -1 \le t \le 0\\ 0.3t + 11, & 0 \le t \le 1\\ 0, & \text{others,} \end{cases}$$

$$f_{11}^2(t) = \begin{cases} 0.5t + 2, & -1 \le t \le 0\\ 0.5t + 2, & 0 \le t \le 1\\ 0, & \text{others,} \end{cases}$$

$$f_{12}^2(t) = \varphi_{11}^2(t) = \varphi_{12}^2(t) = g_{21}^2(t) = \begin{cases} t + 1, & -1 \le t \le 0\\ t + 1, & 0 \le t \le 1\\ 0, & \text{others,} \end{cases}$$

$$F_{11}^2(t) = \varphi_{12}^1(t) = f_{22}^2(t) = \begin{cases} t - 1, & -1 \le t \le 0\\ t - 1, & 0 \le t \le 1\\ 0, & \text{others,} \end{cases}$$

$$\varphi_{11}^1(t) = \begin{cases} t + 6, & -1 \le t \le 0\\ t + 6, & 0 \le t \le 1\\ 0, & \text{others,} \end{cases}$$

$$g_{11}^1(t) = \begin{cases} t + 13, & -1 \le t \le 0\\ t + 13, & 0 \le t \le 1\\ 0, & \text{others,} \end{cases}$$

$$\psi_1^1(t) = \psi_2^1(t) = f_{21}^2(t) = \begin{cases} 0.5t + 15, & -1 \le t \le 0 \\ 0.5t + 15, & 0 \le t \le 1 \\ 0, & \text{others,} \end{cases}$$

$$\varphi_{21}^1(t) = \psi_1^2(t) = \begin{cases} 0.3t + 5, & -1 \le t \le 0 \\ 0.3t + 5, & 0 \le t \le 1 \\ 0, & \text{others,} \end{cases}$$

$$\varphi_{32}^1(t) = \begin{cases} 2t - 4, & -1 \le t \le 0 \\ 2t - 4, & 0 \le t \le 1 \\ 0, & \text{others,} \end{cases}$$

$$g_{31}^1(t) = \begin{cases} 2t + 25, & -1 \le t \le 0 \\ 2t + 25, & 0 \le t \le 1 \\ 0, & \text{others,} \end{cases}$$

$$F_{21}^2(t) = \begin{cases} 3t + 80, & -1 \le t \le 0 \\ 3t + 80, & 0 \le t \le 1 \\ 0, & \text{others,} \end{cases}$$

$$g_{11}^2(t) = \begin{cases} t - 6.9, & -1 \le t \le 0 \\ 0.4t - 6.9, & 0 \le t \le 1 \\ 0, & \text{others,} \end{cases}$$

$$\psi_1^2(t) = \begin{cases} 2t + 10, & -1 \le t \le 0 \\ 2t + 10, & 0 \le t \le 1 \\ 0, & \text{others,} \end{cases}$$

$$\varphi_{11}^2(t) = \begin{cases} t + 40, & -1 \le t \le 0 \\ t + 40, & 0 \le t \le 1 \\ 0, & \text{others.} \end{cases} \tag{12}$$

Step 2. Compute $\int_{-1}^{1} f_1^1(t)E(t)dt = 3$, $\int_{-1}^{1} f_2^1(t)E(t)dt = 8$, $\int_{-1}^{1} F_{11}^1(t)E(t)dt = 7$, $\int_{-1}^{1} F_{21}^1(t)E(t)dt = 11$, $\int_{-1}^{1} f_{11}^2(t)E(t)dt = 2$, $\int_{-1}^{1} f_{12}^1(t)E(t)dt = 1$, $\int_{-1}^{1} F_{11}^2(t)E(t)dt = -1$, $\int_{-1}^{1} \varphi_{11}^1(t)E(t)dt = 6$, $\int_{-1}^{1} g_{11}^1(t)E(t)dt = 13$, $\int_{-1}^{1} \psi_1^1(t)E(t)dt = 15$, $\int_{-1}^{1} \varphi_{21}^1(t)E(t)dt = 5$, $\int_{-1}^{1} \varphi_{32}^1(t)E(t)dt = -4$, $\int_{-1}^{1} g_{31}^1(t)E(t)dt = 25$, $\int_{-1}^{1} F_{21}^2(t)E(t)dt = 80$, $\int_{-1}^{1} g_{11}^2(t)E(t)dt = -7$, $\int_{-1}^{1} \psi_1^2(t)E(t)dt = 10$, and $\int_{-1}^{1} \varphi_{11}^2(t)E(t)dt = 40$.

Step 3. By Theorem 10, the original problem is equivalent to the following bilevel linear programming with multiple followers' problem:

$$\begin{aligned} \min_{x_1,x_2} \quad & M_1^1(x_1, x_2, y_{11}, y_{21}) = 3x_1 + 8x_2 + 7y_{11} + 11y_{21}; \\ \text{s.t.} \quad & \text{where given } x_1, x_2, \text{ and } y_{11}, y_{21} \text{ solve} \\ & \text{the following problem.} \end{aligned}$$

$$\begin{aligned} \min_{y_{11}} \quad & M_1^2(x_1, x_2, y_{11}) = 2x_1 + x_2 - y_{11}; \\ \text{s.t.} \quad & 6x_1 - x_2 + 13y_{11} \le 15, \\ & 5x_1 + 7y_{11} \le 15, \\ & -4x_2 + 25y_{11} \le 3; \\ \min_{y_{21}} \quad & M_2^2(x_1, x_2, y_{21}) = 15x_1 - x_2 + 80y_{21}; \\ \text{s.t.} \quad & x_1 + x_2 - 7y_{21} \le 10, \\ & 40x_1 + y_{21} \le 5; \\ & x_1 \ge 0, \quad x_2 \ge 0, \quad y_{11} \ge 0, \quad y_{21} \ge 0. \end{aligned} \tag{13}$$

Step 4. We use the Kuhn-Tucker approach to get an optimal solution; the solution of the problem is as follows:

$$\begin{aligned} & (x_1, x_2, y_{11}, y_{21}) = (0.1182, 11.7878, 2.0061, 0.2723), \\ & M_1^1 = 111.6946, \qquad M_1^2 = 10.0181, \qquad M_2^2 = 11.7692 \\ & \overline{Z}_1^1 = \left(\underline{Z}_1^1, Z_1^1, \overline{Z}_1^1\right) = (104.5982, 111.5062, 119.5470), \\ & \overline{Z}_1^2 = \left(\underline{Z}_1^2, Z_1^2, \overline{Z}_1^2\right) = (-3.8349, 10.0181, 23.8711), \\ & \overline{Z}_2^2 = \left(\underline{Z}_2^2, Z_2^2, \overline{Z}_2^2\right) = (-0.8946, 11.7692, 24.4330). \end{aligned} \tag{14}$$

The example illustrates how to solve a MFFBLP problem and obtains an optimal solution by using the proposed approach.

5. Conclusions

A real world bilevel decision problem may be modeled to have fuzzy coefficients. In this paper, we investigated the MFFBLP model and solved this complex problem by using the fuzzy structured element method. Further study includes the development of models and methods for fuzzy multilevel programming. We will also explore effective applications of the proposed techniques.

Conflict of Interests

The authors declare that there is no conflict of interests regarding the publication of this paper.

Acknowledgments

The work was supported by the Scientific Research Fund of Hunan Provincial Education Department of China (Grant nos. 14C0350 and 13A004), the NSF of Hunan Province of China (Grant nos. 13JJ3109 and 14JJ3127), and the Humanities and Social Science Foundation of the Ministry of Education of China (Grant no. 12YJA630114).

References

[1] H. V. Stackelberg, *The Theory of the Market Economy*, Oxford University Press, Oxford, UK, 1952.

[2] W. F. Bialas and M. H. Karwan, "Two-level linear programming," *Management Science*, vol. 30, no. 8, pp. 1004–1020, 1984.

[3] S. Dempe, *Foundations of Bilevel Programming*, vol. 61 of *Nonconvex Optimization and its Applications*, Kluwer Academic, Dordrecht, The Netherlands, 2002.

[4] M. Sakawa and I. Nishizaki, "Interactive fuzzy programming for decentralized two-level linear programming problems," *Fuzzy Sets and Systems*, vol. 125, no. 3, pp. 301–315, 2002.

[5] M. Sakawa, H. Katagiri, and T. Matsui, "Stackelberg solutions for fuzzy random two-level linear programming through probability maximization with possibility," *Fuzzy Sets and Systems*, vol. 188, pp. 45–57, 2012.

[6] G. Zhang and J. Lu, "The definition of optimal solution and an extended Kuhn-Tucker approach for fuzzy linear bilevel programming," *The IEEE Computational Intelligence Bulletin*, vol. 5, pp. 1–7, 2005.

[7] J. Lu, C. Shi, and G. Zhang, "On bilevel multi-follower decision making: general framework and solutions," *Information Sciences: An International Journal*, vol. 176, no. 11, pp. 1607–1627, 2006.

[8] H. A. Gil, F. D. Galiana, and E. L. da Silva, "Nodal price control: a mechanism for transmission network cost allocation," *IEEE Transactions on Power Systems*, vol. 21, no. 1, pp. 3–10, 2006.

[9] H. Yang, X. Zhang, and Q. Meng, "Stackelberg games and multiple equilibrium behaviors on networks," *Transportation Research Part B: Methodological*, vol. 41, no. 8, pp. 841–861, 2007.

[10] K. Kogan and C. S. Tapiero, "Optimal co-investment in supply chain infrastructure," *European Journal of Operational Research*, vol. 192, no. 1, pp. 265–276, 2009.

[11] Z. Yao, S. C. H. Leung, and K. K. Lai, "Manufacturer's revenue-sharing contract and retail competition," *European Journal of Operational Research*, vol. 186, no. 2, pp. 637–651, 2008.

[12] G. Zhang and J. Lu, "Model and approach of fuzzy bilevel decision making for logistics planning problem," *Journal of Enterprise Information Management*, vol. 20, no. 2, pp. 178–197, 2007.

[13] Y. Gao, G. Zhang, J. Ma, and J. Lu, "A λ-cut and goal-programming-based algorithm for fuzzy-linear multiple-objective bilevel optimization," *IEEE Transactions on Fuzzy Systems*, vol. 18, no. 1, pp. 1–13, 2010.

[14] M. Sakawa, I. Nishizaki, and Y. Uemura, "Interactive fuzzy programming for multi-level linear programming problems with fuzzy parameters," *Fuzzy Sets and Systems*, vol. 109, no. 1, pp. 3–19, 2000.

[15] M. Sakawa and K. Yauchi, "Interactive decision making for multiobjective nonconvex programming problems with fuzzy numbers through coevolutionary genetic algorithms," *Fuzzy Sets and Systems*, vol. 114, no. 1, pp. 151–165, 2000.

[16] M. Sakawa and I. Nishizaki, "Interactive fuzzy programming for two-level linear fractional programming problems," *Fuzzy Sets and Systems*, vol. 119, no. 1, pp. 31–40, 2001.

[17] M. Sakawa and I. Nishizaki, "Interactive fuzzy programming for two-level nonconvex programming problems with fuzzy parameters through genetic algorithms," *Fuzzy Sets and Systems*, vol. 127, no. 2, pp. 185–197, 2002.

[18] H. Shih and E. Stanley Lee, "Compensatory fuzzy multiple level decision making," *Fuzzy Sets and Systems*, vol. 114, no. 1, pp. 71–87, 2000.

[19] S. Sinha, "Fuzzy programming approach to multi-level programming problems," *Fuzzy Sets and Systems*, vol. 136, no. 2, pp. 189–202, 2003.

[20] G. Zhang, J. Lu, and T. Dillon, "Decentralized multi-objective bilevel decision making with fuzzy demands," *Knowledge-Based Systems*, vol. 20, no. 5, pp. 495–507, 2007.

[21] G. Zhang, J. Lu, and Y. Gao, "Fuzzy bilevel programming: multi-objective and multi-follower with shared variables," *International Journal of Uncertainty, Fuzziness and Knowledge-Based Systems*, vol. 16, pp. 105–133, 2008.

[22] G. Zhang, J. Lu, and Y. Gao, "An algorithm for fuzzy multi-objective multi-follower partial cooperative bilevel programming," *Journal of Intelligent and Fuzzy Systems*, vol. 19, no. 4-5, pp. 303–319, 2008.

[23] S. Guo, *Principle of Mathematical Analysis Based on Structured Element*, Northeast University Press, Shenyang, China, 2004.

[24] S. Z. Guo, "Common representation method for fuzzy-valued functions based on structured elements," *Fuzzy Systems and Mathematics*, vol. 19, no. 1, pp. 82–86, 2005.

[25] S. Guo, "Comparison and sequencing of fuzzy numbers based on the method of structured element," *System Engineering Theory and Practice*, vol. 29, no. 3, pp. 106–111, 2009.

Hindawi Publishing Corporation
Mathematical Problems in Engineering
Volume 2014, Article ID 108024, 6 pages
http://dx.doi.org/10.1155/2014/108024

Research Article

Punishment Effect of Prisoner Dilemma Game Based on a New Evolution Strategy Rule

Dehui Sun and Xiaoliang Kou

Key Laboratory of Beijing for Field-Bus Technology & Automation, North China University of Technology, Beijing 100144, China

Correspondence should be addressed to Dehui Sun; sundehui7@126.com

Received 11 March 2014; Accepted 6 April 2014; Published 27 April 2014

Academic Editor: Wei Zhang

We discuss the effect of the punishment in the prisoner's dilemma game. We propose a new evolution strategy rule which can reflect the external factor for both players in the evolution game. In general, if the punishment exists, the D (defection-defection) structure (i.e., both of the two players choose D-D strategy) which is the Nash equilibrium for the game can keep stable and never let the cooperation emerge. However, if a new evolution strategy rule is adopted, we can find that the D-D structure can not keep stable and it will decrease during the game from the simulations. In fact, the punishment mainly affects the C-D (cooperation-defection) structure in the network. After the fraction of the C-D structure achieved some levels, the punishment can keep the C-D structure stable and prevent it from transforming into C-C (cooperation-cooperation) structure. Moreover, in light of the stability of structure and the payoff of the individual gains, it can be found that the probability which is related to the payoff can affect the result of the evolution game.

1. Introduction

Game theory is ubiquitous in the real world [1–23] in nature and society, such as the invasion of alien species and the conflict of trade between two countries. However, how to settle up with the contradiction between the selfish individual and the social wellbeing and make maximum benefit for the whole society have confused scientists for some decades. There are two classic models in game theory: the public goods game (PGG) and the prisoner's dilemma game (PDG). PGG can be used to study the problem about the cooperation in game [3]. Wang et al. [5] studied the evolutionary dynamics of PGG in finite populations. Under the evolutionary dynamics, players who contributed more could successfully defend the invasion and invade others. It could help us understand cooperative behaviors about the contributions in the real world. Furthermore, Wang et al. [6] considered the effect of wealth distribution about PGG under collective risk to analyze the cooperation among rich and poor individuals. On the other hand, PDG has been used to study how to eliminate the dilemma between the person and the society [8]. Nowak and May [9] found that the spatial structure could benefit the cooperators against defectors' invasion, which inaugurated a new field-complex network, to study the game theory. The vertex nodes represent the individuals and the edges represent the interactions among the players. Tomassini et al. [11] used two kinds of models of complex network-regular lattices and random graphs to research the Hawk-Dove game and found that the fraction of cooperators in the network was related to the gain-to-cost ratio. Heterogeneity, one of the most important properties in complex network, plays a very important role in the evolution game. Fu et al. [12] found that in small world network the underlying network topological organization could help in enhancing and sustaining the cooperative behaviors. Furthermore, Fu et al. [13] presented a punished strategy having the high heterogeneity property which could make the cooperators survive and wipe out the defectors. Perc and Szolnoki [15] found that the distribution of the wealth and social status could promote the cooperation in the evolution game. Ishibuchi and Namikawa [16] researched the evolution strategies about iterated PDG. The players in the game were located in a cell of grid world. They found that the structure could benefit from promoting the cooperation with random pairing. Roca et al. [18] discussed

the effect of spatial structure about the evolution cooperation. Despite the results, they offered some new insights like the relation between the intensities of selection.

In this paper, we pay our attention to the effect of the defection's payoff for the evolution game. In order to simplify the process of the game of PDG, most of the literature usually adopts the limit PDG model, in which the punishment is zero. Here, we consider the factor about the punishment for the evolution game. The reminder of this paper is organized as follows. Section 2 gives the model and the strategy rule. Section 3 presents the simulation results and the explanations. And the conclusion is made in Section 4.

2. The Model and the Strategy Rule of the Evolution Game

There are only two strategies, C (cooperation) and D (defection), in the PDG. According to the strategy selected, the two players will get the benefits, respectively. If one player chooses the C and the other chooses the D, the individual choosing the strategy C will get the lowest payoff S. Meanwhile, the individual choosing the strategy D will gain the highest payoff T. If both of the two players choose the strategy C or strategy D, they will gain the payoff R or P, with $T > R > P > S$ and $2R > T + S$. We use a 2×2 matrix denoting the possible strategies and payoff as follows:

$$\begin{pmatrix} R & S \\ T & P \end{pmatrix}. \tag{1}$$

In order to study the processing of the game theory concisely, researches usually take the limited payoff matrix; that is, let element P be zero, which is introduced by Nowak and May [19]. Here, we use the normal payoff matrix as follows:

$$A = \begin{pmatrix} 1 & 0 \\ b & p \end{pmatrix}, \quad 1 < b < 2,\ 0 < p < 1. \tag{2}$$

Now, we give the strategy rule on lattice network for the evolution game; that is, if one individual's payoff is larger than its neighbor's, it will keep its strategy; otherwise, it will randomly imitate the other individuals' strategy in which one of its neighbors interacts with itself. Note that this evolution rule can reflect the external effect for the individuals in the game as in Figure 1. If the individual E's payoff is larger than F's, E will keep its strategy unchanged. Otherwise, E will imitate H's, I's, or G's strategy randomly. At the same time, we can regard H, I, or G as the environment for E who does not interact with them. In the evolution game, the probability of the strategy changed between individuals x and y depended on the payoff difference [13]:

$$W\left[s_x \longleftarrow s_y\right] = \frac{1}{1 + \exp\left(U_x - U_y\right)/\beta}, \tag{3}$$

where β characterizes the noise for permitting irrational choices. In iterated PDG, both of the two players will choose the strategy D gradually, so the strategy (D, D) is the only Nash equilibrium for the PGD. Usually, the researches

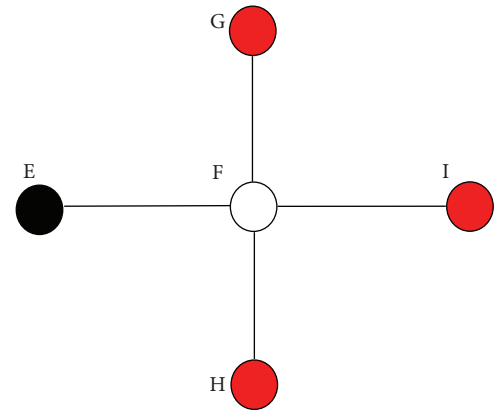

Figure 1: The imitating strategy rule.

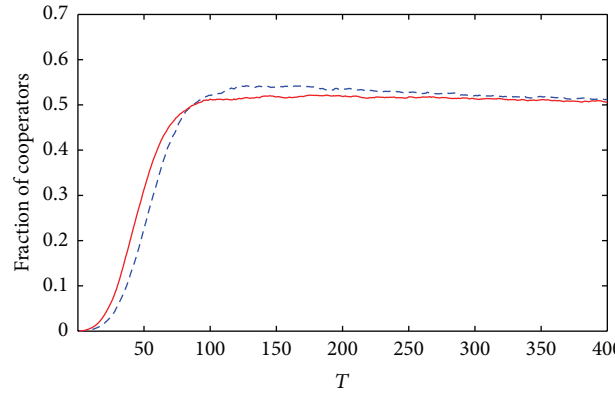

Figure 2: The solid line represents the fraction of cooperators in the network with $b = 1.35$ for $p = 0$ and the dashed line represents that for $p = 0.3$.

can let the punishment benefit be zero for simplifying the processing of the evolution game. However, in real world, the punishment benefit is not always zero. When the external effect becomes a very important factor in the evolution game, the effect of punishment can never be ignored. Moreover, sometimes the effect of punishment may not affect the evolution game in negative degree.

3. Main Result and Simulations

In this section, we will illustrate some simulations on the lattice network with the size $N = 50 \times 50$; let the final time step $T = 400$; and all individuals' strategies selected are D in the initial network. We run 100 simulations independently and take the average data of the 100 simulations for Figures 2–12. It is easy to see that b in the payoff matrix can affect the result of the evolution game from the model. Therefore, we will discuss the two different cases for $1 < b < 1.5$ and $1.5 < b < 2$, respectively. First, we take $b = 1.35$, $p = 0.3$, and $\beta = 0.1$. For $b = 1.35$, the result of the game will evolute to the equilibrium state which is the cooperators and defectors located on the lattice alternatively for the evolution strategy rule. With the punishment element p existing, one individual

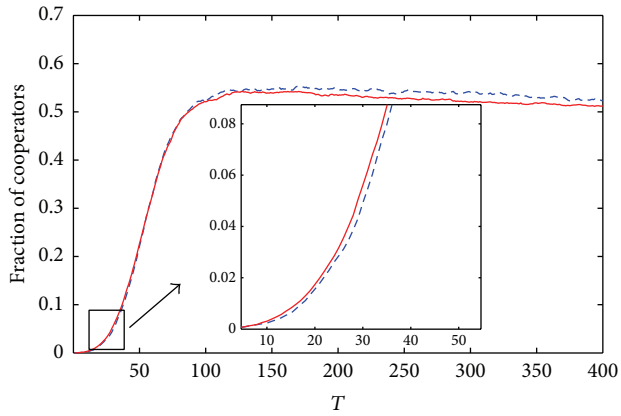

Figure 3: The solid line represents the fraction of cooperators in the network with $b = 1.35$ and $\beta = 0.1$ for $p_1 = 0.3$ and the dashed line represents that for $p_2 = 0.5$.

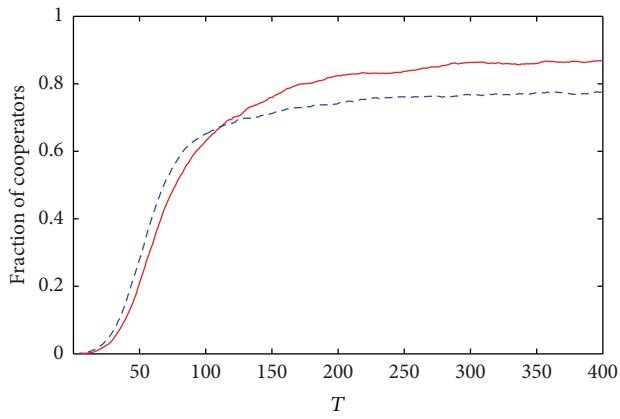

Figure 4: The solid line represents the fraction of cooperators in the network with $b = 1.55$ and $\beta = 0.1$ for $p_1 = 0.3$ and the dashed line represents that for $p_2 = 0.5$.

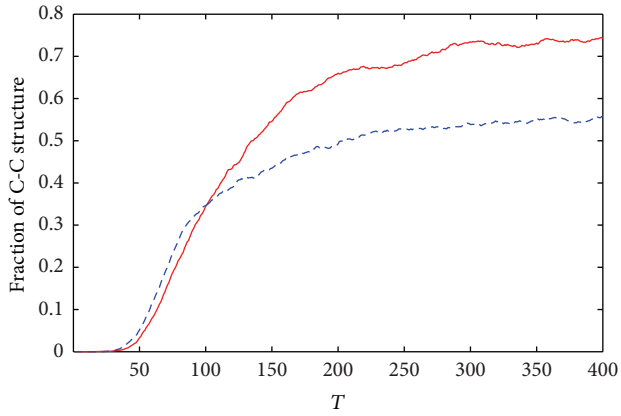

Figure 5: The solid line represents the fraction of C-C structure in the network with $b = 1.55$ and $\beta = 0.1$ for $p_1 = 0.3$ and the dashed line represents that for $p_2 = 0.5$.

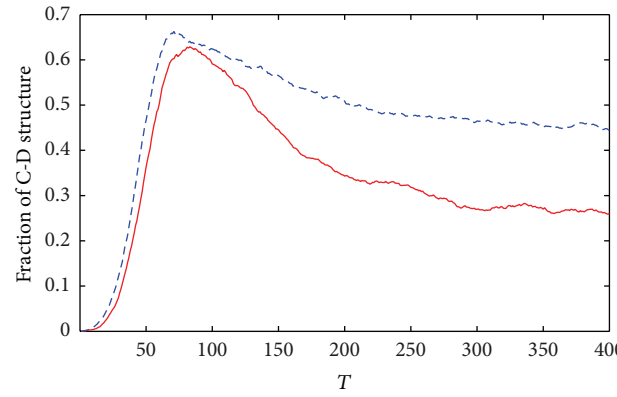

Figure 6: The solid line represents the fraction of C-D structure in the network with $b = 1.55$ and $\beta = 0.1$ for $p_1 = 0.3$ and the dashed line represents that for $p_2 = 0.5$.

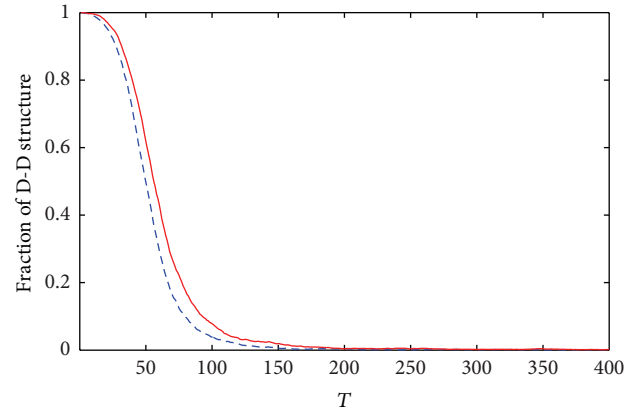

Figure 7: The solid line represents the fraction of D-D structure in the network with $b = 1.55$ and $\beta = 0.1$ for $p_1 = 0.3$ and the dashed line represents that for $p_2 = 0.5$.

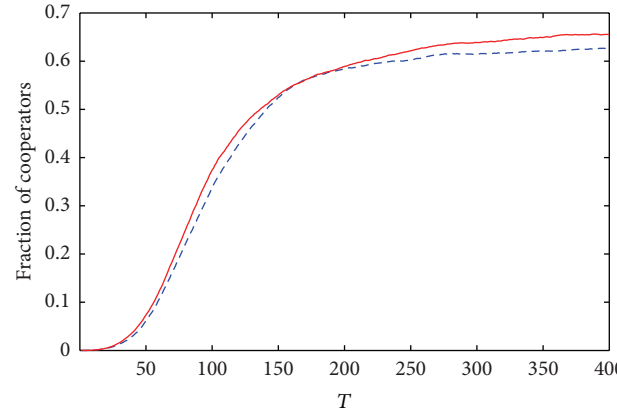

Figure 8: The solid line represents the fraction of cooperators in the network with $b = 1.55$ and $\beta = 0.0015$ for $p_1 = 0.3$ and the dashed line represents that for $p_2 = 0.5$.

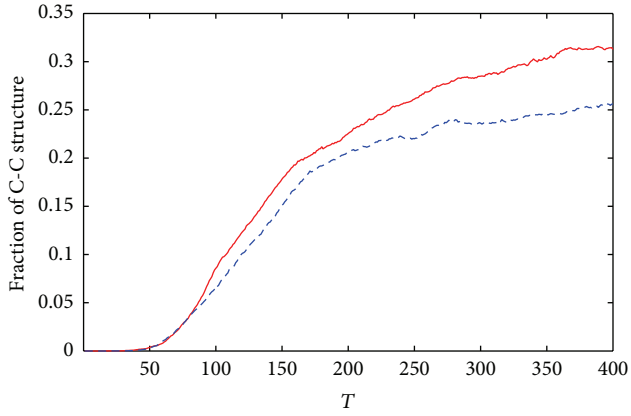

Figure 9: The solid line represents the fraction of C-C structure in the network with $b = 1.55$ and $\beta = 0.0015$ for $p_1 = 0.3$ and the dashed line represents that for $p_2 = 0.5$.

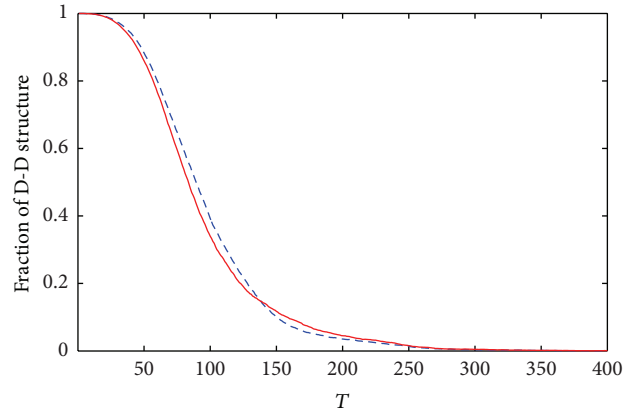

Figure 11: The solid line represents the fraction of D-D structure in the network with $b = 1.55$ and $\beta = 0.0015$ for $p_1 = 0.3$ and the dashed line represents that for $p_2 = 0.5$.

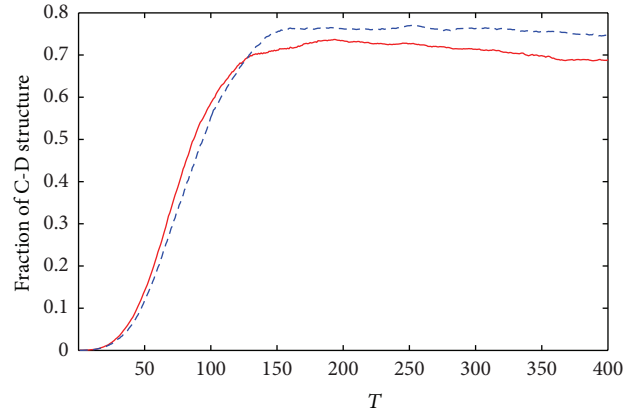

Figure 10: The solid line represents the fraction of C-D structure in the network with $b = 1.55$ and $\beta = 0.0015$ for $p_1 = 0.3$ and the dashed line represents that for $p_2 = 0.5$.

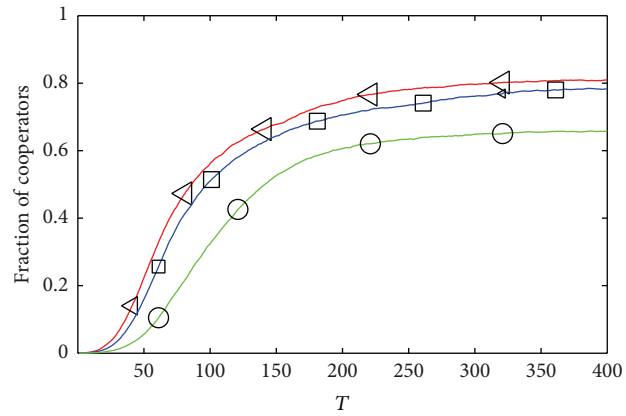

Figure 12: The triangle line represents the fraction of cooperators in the network with $b = 1.55$ for $\beta = 0.1$, the square line represents the fraction of cooperators in the network for $\beta = 0.03$, and the circle line represents the fraction of cooperators in the network for $\beta = 0.0015$.

will not choose the strategy C. Because others choose the strategy D, it means that the one selecting strategy C will gain no payoff; moreover, both of the two players selecting strategy D will also get payoffs. And, in PDG, both of the two players choose the strategy D which is the dilemma of the game. Generally, the punishment can help the D-D structure keep stability. From Figure 3, comparing to $p = 0$, the appearance of cooperators in the network will increase slowly in the initial network. As the game goes, we can see that the faction of the cooperators for $p = 0.3$ will be larger than that of $p = 0$. But, from the common sense, the result of the game for $p = 0$ should be better than $p = 0.3$. Why can this unusual situation happen? If one individual on lattice selects strategy C, its neighbors can get the maximum payoff. However, the ones connected with the neighbors whose payoffs are less than the neighbors', according to the evolution rule, may select the strategy C. In addition, the strategy of changing probability depends on the individual's payoff. For the effect of the punishment element p, the probability of the strategy D transforming to strategy C will be large for formula (3). At the same time, the probability of the strategy C changing to strategy D will be less contrarily. So, the C-D structure formed for $p = 0.3$ is more stable than for $p = 0$, which is the reason why the percentage of the cooperators for $p = 0.3$ is more than that for $p = 0$ at the end of the game. And then we find that the strategy D-D structure cannot stop the cooperation in the network for the evolution strategy rule. For a fixed b, we will see that the different p can affect the evolution game. Here, let $b = 1.35$, $\beta = 0.1$, $p_1 = 0.3$, and $p_2 = 0.5$. From Figure 3, being similar to the above analysis, for $p_2 = 0.5$, we can see that the fraction of cooperators will increase more slowly and achieve more profit than $p_1 = 0.3$. Therefore, the punishment does not always take negative effect. In some particular evolution rules, the punishment can help in promoting the cooperation.

Next, for $1.5 < b < 2$, the result of the evolution game is different from the situation for $1 < b < 1.5$. The cooperators can form triangle clusters to fight against

the defectors' invasion efficiently and can expand more in the network [21, 22]. So, the cooperators can break up the equilibrium state who can take advantage obviously at the end of the game. Let $b = 1.55$, $\beta = 0.1$, $p_1 = 0.3$, and $p_2 = 0.5$. From Figure 4, for $p_2 = 0.5$, the fraction of the cooperators will increase firstly and then when the percentage of the cooperators achieves some levels, the growth of the cooperators will slow down. Furthermore, at the end of the evolution game, the percentage of the cooperators will be less than $p_1 = 0.3$.

We will illustrate it together in Figures 5–7. Because of the evolution rule, if someone chooses the strategy C, others who are the neighbors of the C individual's neighbors may select the strategy C. Therefore, the D-D structure cannot keep stable and then the D-D structure will transform to the C-D structure and drop obviously as the game goes. We can also see that, for higher p, the fraction of D-D structure decreases faster and more in Figure 8. With the cooperators increased in the network, the C-D structure will increase and, accordingly, the C-C structure will also increase. Because the cooperators can form the triangle structure to defend the defectors' invasion and the cluster of the cooperators can be larger, so the fraction of the C-C structure can increase. From velocity of increasing for cooperators in Figures 6 and 7, the C-D structure will increase fast. After achieving the summit, the C-D structure will transform to C-C structure fast and then decrease as the evolution game goes. The effect of the C-C cluster will enhance. That is the reason why the fraction of C-C structure will increase as the game goes. With the effect of the punishment, the C-D structure will decrease more slowly for $p_2 = 0.5$ than for $p_1 = 0.3$. For higher p, the C-D structure can better keep stable. This situation means that the punishment p can defend the cluster of the cooperators and keep the C-D structure stable. Therefore, the fraction of the cooperators for $p_1 = 0.3$ will be larger than $p_2 = 0.5$'s at the end of the evolution game. In conclusion, for the particular evolution rule, the effect of the punishment can affect certain strategy structure. Here, we give the data about the the changing of the fraction of C-D structure on lattice network as in Table 1.

From the above analysis, we can find that the changing of the payoff which the individual gains can affect the probability. And then we will focus on the effect of the probability. So, we can use the parameter β in formula (3). Here, for $b = 1.55$ and $\beta = 0.0015$, let $p_1 = 0.3$ and $p_2 = 0.5$. When the parameter β turns to be small, the probability of the strategy changing will also be small. In Figure 8, for $p_1 = 0.3$, the fraction of the cooperators will increase firstly and will be larger than $p_2 = 0.5$ at the end of the game. From Figures 9–11, we can see that the C-D and C-C structure for $p_1 = 0.3$ will increase firstly and the D-D structure will decrease firstly. And, then, the C-D structure for $p_2 = 0.5$ achieves the summit more; after that, the fraction of the C-D structure decreases less than $p_1 = 0.3$ and the fraction of C-C structure for $p = 0.3$ in the network will almost be more than $p_2 = 0.5$. Comparing with Figures 4–7, we can see the difference. In Figure 8, the faction of cooperators will increase slowly for higher p, but the situation is in contrast to that in Figure 4. Why can this difference happen? For the smaller probability, the changing of strategy is not often. It will help the strategy D-D structure in keeping stable. However, for the evolution strategy rule, the D-D structure cannot keep stable and it will transform to C-D structure. In another way, the smaller probability can reduce the effect of evolution rule in some degree. From Figures 9–11, we also can see that the effect of the punishment mainly affects the fraction of the C-D structure. For higher p, the C-D strategy can gain more and keep more stable. In Figure 12, we can find that the more the β is, the more the fraction of the cooperators is. Moreover, with the β increased, the fraction of the cooperators in the network will increase fast, which implies that the probability can affect the result of the evolution game.

Table 1: The data about changing of the fraction of C-D structure in network.

C-D	$T = 20$	$T = 40$	$T = 60$	$T = 80$
$p = 0.3$	0.035862	0.246115	0.554025	0.643101
$p = 0.5$	0.035819	0.245783	0.557239	0.636969
C-D	$T = 100$	$T = 120$	$T = 140$	$T = 160$
$p = 0.3$	0.611341	0.567636	0.515405	0.470873
$p = 0.5$	0.602177	0.557766	0.519670	0.485273
C-D	$T = 180$	$T = 200$	$T = 220$	$T = 240$
$p = 0.3$	0.443957	0.418154	0.400718	0.394343
$p = 0.5$	0.473424	0.446014	0.423388	0.420653
C-D	$T = 260$	$T = 280$	$T = 300$	$T = 320$
$p = 0.3$	0.381033	0.368123	0.353101	0.351371
$p = 0.5$	0.415273	0.406363	0.400152	0.390591
C-D	$T = 340$	$T = 360$	$T = 380$	$T = 400$
$p = 0.3$	0.348811	0.336239	0.334177	0.33415
$p = 0.5$	0.397233	0.393287	0.389619	0.37703

4. Conclusion

In this paper, we have discussed the problem of the effect of the punishment for the evolution game on lattice. We proposed an evolution strategy rule which can reflect the external factors. Under the evolution rule, we can find that the punishment can affect the evolution game. The punishment can help the cooperators to increase firstly which is contrary to the common sense that the D-D structure will keep stable. Actually, the D-D structure cannot be stable for the evolution rule. Moreover, the punishment through the C-D structure affects the result of the evolution game. For higher p, when the C-D structure achieves the summit, it will keep more stable and decrease less. Despite the payoff the players gain, we also find that the probability is related to the evolution game. The more the probability is, the more and faster the fraction of cooperators increases.

Conflict of Interests

The authors declare that there is no conflict of interests regarding the publication of this paper.

Acknowledgment

This work was supported by the National Natural Science Foundation of China under Grant no. 61174116.

References

[1] A. M. Colman, *Game Theory and Its Applications in the Social and Biological Sciences*, Butterworth-Heinemann, Oxford, UK, 1995.

[2] E. Pennisi, "How did cooperative behavior evolve," *Science*, vol. 309, no. 5731, p. 93, 2005.

[3] M. Olson, *The Logic of Collective Action: Public Goods and the Theory of Groups*, Harvard University Press, Cambrigdge, Mass, USA, 1965.

[4] H. Su, X. Wang, and Z. Lin, "Flocking of multi-agents with a virtual leader," *IEEE Transactions on Automatic Control*, vol. 54, no. 2, pp. 293–307, 2009.

[5] J. Wang, B. Wu, X. Chen, and L. Wang, "Evolutionary dynamics of public goods games with diverse contributions in finite populations," *Physical Review E*, vol. 81, no. 5, Article ID 056103, 8 pages, 2010.

[6] J. Wang, F. Fu, and L. Wang, "Effects of heterogeneous wealth distribution on public cooperation with collective risk," *Physical Review E*, vol. 82, no. 1, Article ID 016102, 13 pages, 2010.

[7] H. Su, N. Zhang, M. Z. Q. Chen, H. Wang, and X. Wang, "Adaptive flocking with a virtual leader of multiple agents governed by locally Lipschitz nonlinearity," *Nonlinear Analysis: Real World Applications*, vol. 14, no. 1, pp. 798–806, 2013.

[8] W. Poundstone, *The Prisoner's Dliemma*, Doubleday, New York, NY, USA, 1992.

[9] M. A. Nowak and R. M. May, "Evolutionary games and spatial chaos," *Nature*, vol. 359, no. 6398, pp. 826–829, 1992.

[10] H. Su, M. Chen, X. Wang, and J. Lam, "Semiglobal observer-based leaderfollowing consensus with input saturation," *IEEE Transactions on Industrial Electronics*, vol. 61, no. 6, pp. 2842–2850, 2014.

[11] M. Tomassini, L. Luthi, and M. Giacobini, "Hawks and Doves on small-world networks," *Physical Review E*, vol. 73, no. 1, Article ID 016132, 10 pages, 2006.

[12] F. Fu, X. Chen, L. Liu, and L. Wang, "Social dilemmas in an online social network: the structure and evolution of cooperation," *Physics Letters A*, vol. 371, no. 1-2, pp. 58–64, 2007.

[13] F. Fu, X. Chen, L. Liu, and L. Wang, "Promotion of cooperation induced by the interplay between structure and game dynamics," *Physica A*, vol. 383, no. 2, pp. 651–659, 2007.

[14] H. Su, Z. Rong, M. Chen, X. Wang, G. Chen, and H. Wang, "Decentralized adaptive pinning control for cluster synchronization of complex dynamical networks," *IEEE Transactions on Cybernetics*, vol. 43, no. 1, pp. 394–399, 2013.

[15] M. Perc and A. Szolnoki, "Social diversity and promotion of cooperation in the spatial prisoner's dilemma game," *Physical Review E*, vol. 77, no. 1, Article ID 011904, 5 pages, 2008.

[16] H. Ishibuchi and N. Namikawa, "Evolution of iterated prisoner's dilemma game strategies in structured demes under random pairing in game playing," *IEEE Transactions on Evolutionary Computation*, vol. 9, no. 6, pp. 552–561, 2005.

[17] H. Su, M. Z. Q. Chen, J. Lam, and Z. Lin, "Semi-global leader-following consensus of linear multi-agent systems with input saturation via low gain feedback," *IEEE Transactions on Circuits and Systems. I. Regular Papers*, vol. 60, no. 7, pp. 1881–1889, 2013.

[18] C. P. Roca, J. A. Cuesta, and A. Sanchez, "Effect of spatial structure on the evolution of cooperation," *Physical Review E*, vol. 80, no. 4, Article ID 046106, 16 pages, 2009.

[19] M. A. Nowak and R. M. May, "The spatial dilemmas of evolution," *International Journal of Bifurcation and Chaos in Applied Sciences and Engineering*, vol. 3, no. 1, pp. 35–78, 1993.

[20] B. Liu, X. L. Kou, and J. Zhang, "The imitating strategy rule about prisoner's dillema game on lattice," in *Proceedings of the 5th International Conference on Intelligent Computation Technology and Automation (ICICTA '12)*, pp. 719–722, Hunan, China, January 2012.

[21] J. Vukov, G. Szabó, and A. Szolonoki, "Cooperation in the noisy case: Prisoner's dilemma game on two types of regular random graphs," *Physical Review E*, vol. 73, no. 6, Article ID 067103, 4 pages, 2006.

[22] C. K. Chan and K. Y. Szeto, "Decay of invincible clusters of cooperators in the evolutionary prisoner's dilemma game," in *Applications of Evolutionary Computing*, vol. 5484 of *Lecture Notes in Computer Science*, pp. 243–252, Springer, 2009.

[23] J. Du, B. Wu, P. M. Altrock, and L. Wang, "Aspiration dynamics of multiplayer games in finite populations," *Journal of the Royal Society Interface*, vol. 11, no. 94, Article ID 20140077, 2014.

Hindawi Publishing Corporation
Mathematical Problems in Engineering
Volume 2014, Article ID 304126, 6 pages
http://dx.doi.org/10.1155/2014/304126

Research Article

Average Consensus in Multiagent Systems with the Problem of Packet Losses When Using the Second-Order Neighbors' Information

Mei Yu,[1] Lijuan Li,[2] Guangming Xie,[3] and Hong Shi[4]

[1] *School of Control and Computer Engineering, North China Electric Power University, Beijing 102206, China*
[2] *Tianjin Electric Power Design Institute, Tianjin 300400, China*
[3] *State Key Laboratory for Turbulence and Complex Systems and College of Engineering, Peking University, Beijing 100871, China*
[4] *Department of Mathematics and Physics, Beijing Institute of Petrochemical Technology, Beijing 102617, China*

Correspondence should be addressed to Guangming Xie; xiegming@pku.edu.cn

Received 17 February 2014; Accepted 18 March 2014; Published 10 April 2014

Academic Editor: Housheng Su

This paper mainly investigates the average consensus of multiagent systems with the problem of packet losses when both the first-order neighbors' information and the second-order neighbors' information are used. The problem is formulated under the sampled-data framework by discretizing the first-order agent dynamics with a zero-order hold. The communication graph is undirected and the loss of data across each communication link occurs at certain probability, which is governed by a Bernoulli process. It is found that the distributed average consensus speeds up by using the second-order neighbors' information when packets are lost. Numerical examples are given to demonstrate the effectiveness of the proposed methods.

1. Introduction

In recent years, there has been an increasing research in coordination control of multiagent systems. Information consensus has attracted more and more attentions from many engineering application fields, such as formation control, flocking, artificial intelligence, and automatic control [1–4]. A critical problem in distributed control is to develop distributed protocols under which agents can reach an agreement on a common decision.

An excellent protocol can reduce cost, increase efficiency, and can optimize performance. Convergence rate is an important index to evaluate the performance of consensus. There has been much research interest in dealing with this issue. In [5], the authors pointed out that the second smallest eigenvalue of its Laplacian matrix was a measure of speed of solving consensus problems. From [6], we know that the convergence speeds up by finding the optimal weight associated with each communication link, where the global structure of the network must be known beforehand. Reference [7] accelerated the convergence rate by using the polynomial filtering algorithms. In [8], the authors presented randomized gossip algorithm on an arbitrary connected network and showed its performance precisely in the terms of the second largest eigenvalue of an appropriate stochastic matrix. The above literatures all tried to seek a suitable topology communication to achieve a fast convergence. However, in practice, it is more useful to design a protocol to obtain a better convergence performance under a given topology. In order to get a better convergence speed without changing the topology and edge weights, the authors in [9] proposed a protocol in an unchanged topology network that each node got its state value updated by using the information of multihop communication and showed that the protocol increased the convergence speed effectively for the first time. Then, in [10], the authors discussed that the node in the network topology updated its current state value not only from its immediate neighbors but also from its second-order neighbors for both the discrete-time case and the continuous-time case. Further, the authors in [11] extended the systems to second-order

case and made comparisons between the convergence rate of second-order neighbor protocol and the general protocol. What is more, the delay margins of general protocol and second-order neighbor protocol were derived.

It is noted that the literatures mentioned above mainly focus on consensus problem for agents under first-order dynamics with time delay. In reality, the agents exchange data over fading communication channels instead of ideal ones. In fact, in many practical applications, this data exchange between sensors is done by wireless communication, which has a possibility of packets lost. Thereby, the packet losses should be taken into consideration. Many related works have been reported. Reference [12] dealt with consensus with random delay and data losses. Reference [13] compared the memory and memoryless consensus protocols in the presence of uniform packet losses. In [14, 15], the authors discussed the average consensus in first-order agents and analyzed the convergence speed under data losses. Furthermore, [16] showed that packet dropouts can be treated as an absence of a communication link over time. In addition, [17–19] studied stochastic consensus subject to a random process.

Inspired by the above references, we consider multiagent systems with the problem of packet losses based on the second-order neighbors' information. We construct a group of agents, which can communicate with their second-order neighbors and each communication link has a probability of failure. We assume that all channels are independent and subject to a distributed random process. Thereby, they have the same probability of data loss. Each agent is equipped with a sampler and a zero-order hold, which are synchronized in time. Then, by converting the system to the equivalent error dynamics, stochastic stability of the error dynamic system is studied. Here, a Lyapunov function is constructed and a sufficient condition is established to guarantee the average consensus in the form of linear matrix inequality (LMI). We are curious about whether the protocol based on the second-order neighbors' information can accelerate the convergence speed with the problem of packet losses. Then, a simulation comparison of the convergence rate between the protocol based on the second-order neighbors and the one in general linear is shown. Comparison of the convergence speed between different probabilities of packet losses is also simulated.

The rest of this paper is organized as follows. Section 2 provides some preliminaries on graph theory and gives the designed protocol. Section 3 analyses the average consensus and gives a sufficient condition. Section 4 includes some numerical examples, which demonstrate the effectiveness of the proposed approach. Finally, Section 5 offers the concluding remarks.

Notations. The set of real numbers is denoted by $\mathbb{R}$. For any matrix $Q \in \mathbb{R}^{n\times n}$, $\mathrm{sym}(Q) = Q + Q^T$. The index set $\Lambda_n = \{1, 2, \ldots, n\}$ is a group of consecutive integers from 1 to n. The vector $1_n = [1, 1, \ldots, 1]^T \in \mathbb{R}^n$ has all of its elements equal to 1. The mathematical expectation is denoted by $E\{\cdot\}$ and $P\{\cdot\}$ is the probability operator.

2. Problem Formation

2.1. Preliminaries on Graph Theory. In this paper, the interaction among n agents is modeled by an undirected graph $G = \{\nu, \varepsilon, A\}$, where $\nu = \{\nu_1, \nu_2, \ldots, \nu_n\}$ is the node set. The edge set $\varepsilon \subseteq \nu \times \nu$ contains ordered pairs of nodes. The neighbor set of agent i is denoted by N_i, which includes agents from which agent i receives information. The adjacency matrix $A = [w_{ij}] \in \mathbb{R}^{n\times n}$ is a nonnegative matrix, where $w_{ij} > 0$ if and only if $(\nu_j, \nu_i) \in \varepsilon$; otherwise, $w_{ij} = 0$. We assume that there is no self-loop, so $w_{ii} = 0$. The Laplacian matrix $L = [l_{ij}] \in \mathbb{R}^{n\times n}$ is defined as

$$\begin{aligned} l_{ij} &= -w_{ij}, \quad \text{if } i \neq j; \\ l_{ij} &= \sum_{k\in N_i} w_{ik}. \end{aligned} \tag{1}$$

From the above definitions, we know some facts: A and L determine each other uniquely, and L has nonnegative eigenvalues. Moreover, L has at least one zero eigenvalue with the associated eigenvector 1_n^T ($L1_n^T = 0$); that is, $\mathrm{span}\{1_n^T\} \subseteq \mathrm{null}\{L\}$, where $\mathrm{null}\{L\}$ is the null space of L. For the undirected graph, we further have $L = L^T$, $1_n^T L = 0$. From [20], it is known that $\mathrm{span}\{1_n^T\} = \mathrm{null}\{L\}$ if and only if the undirected graph G is connected.

2.2. Protocols Based on Second-Order Neighbor with Packet Losses. Consider the following first-order dynamics:

$$\dot{x}_i = u_i, \quad i \in \Lambda_n, \tag{2}$$

where $x_i, u_i \in \mathbb{R}$ are the state and the input of agent i, respectively. With sampling period T and a zero-order hold, the agent dynamics is discretized as

$$x_i(k+1) = x_i(k) + Tu_i(k), \quad i \in \Lambda_n. \tag{3}$$

Considering the protocol based on second-order neighbors' information, if there is no communication constraint taken into account, the following control protocol can be used:

$$u_i(k) = -r_c \sum_{j\in N_i} w_{ij} \left[\left(x_i(k) - x_j(k)\right) + \sum_{h\in N_j} w_{jh} \left(x_i(k) - x_h(k)\right) \right], \tag{4}$$

where the control gain r_c is to be designed.

Next, we consider the packet losses among agents. The following control protocol is designed:

$$u_i(k) = -r_c \left\{ \sum_{j \in N_i} \gamma_{ij}(k) w_{ij} \left[\left(x_i(k) - x_j(k) \right) + \sum_{h \in N_j} \gamma_{jh}(k) w_{jh} \times \left(x_i(k) - x_h(k) \right) \right] \right\}, \tag{5}$$

where $\gamma_{ij}(k) = 1$, if there is no packet loss between agents i and j; $\gamma_{ij}(k) = 0$, otherwise.

Furthermore, we assume that the occurrence of packet loss is governed by a Bernoulli process with uniform probability p satisfying $0 < p < 1$; that is,

$$P\left\{\gamma_{ij}(k) = 1\right\} = p, \quad P\left\{\gamma_{ij}(k) = 0\right\} = 1 - p, \quad \forall i \neq j. \tag{6}$$

As a result, we have $E\{\gamma_{ij}(k)\} = p$.

Assumption 1. The undirected topology is coupled; that is, for any pair of agents i and j, the communication channels between them exist or vanish simultaneously.

Assumption 1 ensures that the communication topology is always symmetric, so the average of agents' states can be retained during dynamic evolution.

We define two sets of matrices $L_1(k) = [l_{1ij}(k)] \in \mathbb{R}^{n \times n}$ and $L_2(k) = [l_{2ij}(k)] \in \mathbb{R}^{n \times n}$ as follows:

$$\begin{aligned} l_{1ij}(k) &= -\gamma_{ij}(k) w_{ij}, \\ l_{2ij}(k) &= -\sum_{\substack{h \in N_i \\ j \in N_h}} \gamma_{ih}(k) w_{ih} \gamma_{hj}(k) w_{hj}, \quad i \neq j, \\ l_{1ii}(k) &= \sum_{j \in N_i} \gamma_{ij}(k) w_{ij}, \\ l_{2ii}(k) &= \sum_{h \in N_i} \gamma_{ih}(k) w_{ih} \sum_{l \in N_h} \gamma_{hl}(k) w_{hl}. \end{aligned} \tag{7}$$

Denote the vectors $x(k)$ and $u(k)$ by

$$\begin{aligned} x(k) &= \left[x_1(k), x_2(k), \ldots, x_n(k)\right]^T, \\ u(k) &= \left[u_1(k), u_2(k), \ldots, u_n(k)\right]^T. \end{aligned} \tag{8}$$

Then, the control protocol can be rewritten as

$$u(k) = -r_c L(k) x(k), \tag{9}$$

where $L(k) = L_1(k) + L_2(k)$.

So, the system dynamics can be written as

$$x(k+1) = x(k) - r_c TL(k) x(k) = \left[I - r_c TL(k)\right] x(k). \tag{10}$$

By taking the mathematical expectation of $L_1(k)$ and $L_2(k)$, we have $E\{L_1(k)\} = p \times L^{(1)}$, $E\{L_2(k)\} = p^2 \times L^{(2)}$, where $L^{(1)}$ is the nominal Laplacian matrix of full weights where there is no packet loss and $L^{(2)}$ is the nominal Laplacian matrix of the system which is only based on the second-order neighbors' information with full weights and without packet loss.

Assumption 2. The nominal communication topologies $G^{(1)}$ associated with $L^{(1)}$ and $G^{(2)}$ associated with $L^{(2)}$ are all connected.

The above assumption is necessary for consensus because if the undirected graph is not connected, then it does not have a spanning tree. From [21, Lemma 1] and [22, Theorem 5], we know that there exist two nonempty, disjoint groups of agents that have no communication with each other at any time. In this case, consensus cannot be reached.

3. Consensus Analysis

The average states of the agents

$$\alpha = \mathrm{Ave}(x(k)) = \frac{1}{n}\sum_{i=1}^{n} x_i(k) = \frac{1}{n} 1_n^T x(k) \tag{11}$$

are invariant. We say the *average consensus* problem is solved, if

$$\lim_{k \to +\infty} x_i(k) = \alpha, \quad i = 1, \ldots, n. \tag{12}$$

Each agent state can be presented by the form

$$x(k) = \alpha 1_n + \delta(k), \tag{13}$$

where the variable $\delta(k) = [\delta_1(k), \delta_2(k), \ldots, \delta_n(k)]^T$ satisfies

$$1_n^T \delta = 0. \tag{14}$$

The following error dynamics are obtained:

$$\delta(k+1) = \delta(k) - r_c TL(k) \delta(k) = \left[I - r_c TL(k)\right] \delta(k). \tag{15}$$

Obviously, the stability of (15) is equivalent to the consensus in (2). Then, we introduce the following lemma, which plays an important role in the stability analysis of (15).

Lemma 3 (see [16]). *For an undirected graph, given the Laplacian matrix $L_1(k)$, $L_2(k)$, and a symmetric matrix*

$Q = Q^T$, $E\{(L_1(k)+L_2(k))\ \ Q(L_1(k)+L_2(k))\}$ can be calculated as follows:

$$\begin{aligned}
&E\left\{\left(L_1(k)+L_2(k)\right)\ \ Q\left(L_1(k)+L_2(k)\right)\right\}\\
&\quad= E\left\{\mathrm{I}\begin{bmatrix}L_1(k) & 0\\ 0 & L_2(k)\end{bmatrix}\mathrm{I}^T Q \mathrm{I}\begin{bmatrix}L_1(k) & 0\\ 0 & L_2(k)\end{bmatrix}\mathrm{I}^T\right\}\\
&\quad= \mathrm{I}E\left\{\begin{bmatrix}L_1(k) & 0\\ 0 & L_2(k)\end{bmatrix}\Gamma\begin{bmatrix}L_1(k) & 0\\ 0 & L_2(k)\end{bmatrix}\right\}\mathrm{I}^T \qquad (16)\\
&\quad= \mathrm{I}\Big\{\hat{P}\left(L^{(0)}\right)\hat{P}\left(L^{(0)}\right)L^{(0)}\Gamma L^{(0)}\\
&\qquad+\hat{P}\left(L^{(0)}\right)\left(I-\hat{P}\left(L^{(0)}\right)\right)\Xi(\Gamma)\Big\}\mathrm{I}^T,
\end{aligned}$$

where $L^{(0)} = \begin{bmatrix}L^{(1)} & 0\\ 0 & L^{(2)}\end{bmatrix}$, $\mathrm{I}^T = \begin{bmatrix}I\\ I\end{bmatrix}_{2n*n}$, $\hat{P}\left(L^{(0)}\right) = \begin{bmatrix}p & 0\\ 0 & p^2\end{bmatrix}$, $\Gamma = \begin{bmatrix}Q & Q\\ Q & Q\end{bmatrix}$, and $\Xi(\Gamma)$ is a function of Q, defined as

$$\begin{aligned}
&\Xi(\Gamma)\\
&= \sum_{m=1}^{n}\sum_{q=1}^{n}\begin{bmatrix}E_{1(m,q)}^T & 0\\ 0 & E_{2(m,q)}^T\end{bmatrix}\Gamma\begin{bmatrix}E_{1(m,q)} & 0\\ 0 & E_{2(m,q)}\end{bmatrix}\\
&\qquad\times\begin{bmatrix}a_{1(m,q)}^2 & 0\\ 0 & a_{2(m,q)}^2\end{bmatrix}\\
&\quad+\sum_{m=1}^{n}\sum_{q=1}^{n}\begin{bmatrix}E_{1(m,m)}^T & 0\\ 0 & E_{2(m,m)}^T\end{bmatrix}\Gamma\begin{bmatrix}E_{1(m,m)} & 0\\ 0 & E_{2(m,m)}\end{bmatrix}\\
&\qquad\times\begin{bmatrix}a_{1(m,q)}^2 & 0\\ 0 & a_{2(m,q)}^2\end{bmatrix}\\
&\quad-\sum_{m=1}^{n}\sum_{q=1}^{n}\mathrm{sym}\left(\begin{bmatrix}E_{1(m,q)}^T & 0\\ 0 & E_{2(m,q)}^T\end{bmatrix}\Gamma\begin{bmatrix}E_{1(m,m)} & 0\\ 0 & E_{2(m,m)}\end{bmatrix}\right)\\
&\qquad\times\begin{bmatrix}a_{1(m,q)}^2 & 0\\ 0 & a_{2(m,q)}^2\end{bmatrix}\\
&\quad+\sum_{j=1}^{n}\sum_{m=j+1}^{n}\mathrm{sym}\left(2\begin{bmatrix}E_{1(j,j)}^T & 0\\ 0 & E_{2(j,j)}^T\end{bmatrix}\Gamma\begin{bmatrix}E_{1(m,m)} & 0\\ 0 & E_{2(m,m)}\end{bmatrix}\right.\\
&\qquad-\begin{bmatrix}E_{1(j,j)}^T & 0\\ 0 & E_{2(j,j)}^T\end{bmatrix}\Gamma\begin{bmatrix}E_{1(m,j)} & 0\\ 0 & E_{2(m,j)}\end{bmatrix}\\
&\qquad-\begin{bmatrix}E_{1(j,m)}^T & 0\\ 0 & E_{2(j,m)}^T\end{bmatrix}\\
&\qquad\times\Gamma\begin{bmatrix}E_{1(m,m)} & 0\\ 0 & E_{2(m,m)}\end{bmatrix}\Big)\\
&\qquad\times\begin{bmatrix}a_{1(m,q)}^2 & 0\\ 0 & a_{2(m,q)}^2\end{bmatrix}. \qquad (17)
\end{aligned}$$

The following theorem gives a sufficient condition on the average consensus of the system (2).

Theorem 4. *Given the scalar r_c, the average consensus of the system (2) is achieved if there exists a matrix $Q > 0$, such that the following LMI holds:*

$$\begin{aligned}
&-\left[L^{(1)}Q+QL^{(1)}+p\left(L^{(2)}Q+QL^{(2)}\right)\right]\\
&\quad+r_c T\mathrm{I}\Big\{\hat{P}\left(L^{(0)}\right)\hat{P}\left(L^{(0)}\right)L^{(0)}\Gamma L^{(0)}\\
&\qquad+\hat{P}\left(L^{(0)}\right)\left(I-\hat{P}\left(L^{(0)}\right)\right)\Xi(\Gamma)\Big\}\mathrm{I}^T<0. \qquad (18)
\end{aligned}$$

Proof. Construct the candidate Lyapunov function as $V(k) = \delta^T(k)Q\delta(k)$. We have

$$\begin{aligned}
&E\{\Delta V(k)\}\\
&\quad= E\{V(k+1)-V(k)\}\\
&\quad= E\left\{\delta^T(k+1)Q\delta(k+1)-\delta^T(k)Q\delta(k)\right\}\\
&\quad= E\left\{\delta^T(k)\left[I-r_cTL(k)\right]Q\left[I-r_cTL(k)\right]\delta(k)\right.\\
&\qquad\left.-\delta^T(k)Q\delta(k)\right\}\\
&\quad= E\left\{\delta^T(k)\left[-r_cTL(k)Q-r_cTQL(k)\right.\right.\\
&\qquad\left.\left.+r_c^2TL(k)QL(k)\right]\delta(k)\right\}\\
&\quad= -r_cT\delta^T(k)\left(pL^{(1)}+p^2L^{(2)}\right)Q\delta(k)\\
&\qquad-r_cT\delta^T(k)Q\left(pL^{(1)}+p^2L^{(2)}\right)\delta(k)\\
&\qquad+r_c^2T^2\delta^T(k)E\{L(k)QL(k)\}\delta(k)\\
&\quad= -r_cTp\delta^T(k)\left[L^{(1)}Q+QL^{(1)}\right.\\
&\qquad\left.+p\left(L^{(2)}Q+QL^{(2)}\right)\right]\delta(k)\\
&\qquad+r_c^2T^2\delta^T(k)\mathrm{I}\Big\{\hat{P}\left(L^{(0)}\right)\hat{P}\left(L^{(0)}\right)L^{(0)}\Gamma L^{(0)}\\
&\qquad+\hat{P}\left(L^{(0)}\right)\left(I-\hat{P}\left(L^{(0)}\right)\right)\Xi(\Gamma)\Big\}\\
&\qquad\times\mathrm{I}^T\delta(k). \qquad (19)
\end{aligned}$$

Thus, from the Lyapunov stability theory, we know that if $E\{\Delta V(k)\}$ is negative, then (15) is asymptotically stable. Thereby, the states of all agents will converge to their average state; that is, the average consensus of the system (2) is achieved. □

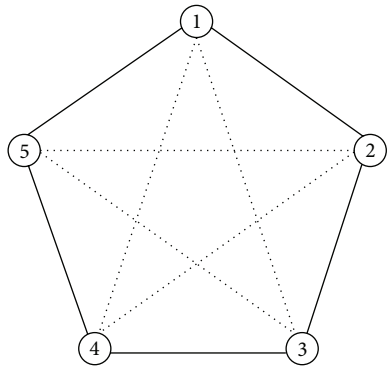

FIGURE 1: Nominal communication topology and topology based on the second-order neighbors' information.

4. Simulations and Analyses

To illustrate the average consensus of the system (2) under the condition of packet losses and fast convergence rate of the protocol based on second-order neighbors' information, a numerical example is provided. The nominal interaction topology $G^{(1)}$ and topology only based on second-order neighbors' information $G^{(2)}$ among five agents are shown in Figure 1.

The weights are set to unity for simplicity here. We set the corresponding Laplacian matrices $L^{(1)}$ and $L^{(2)}$ as follows:

$$L^{(1)} = \begin{bmatrix} 2 & -1 & 0 & 0 & -1 \\ -1 & 2 & -1 & 0 & 0 \\ 0 & -1 & 2 & -1 & 0 \\ 0 & 0 & -1 & 2 & -1 \\ -1 & 0 & 0 & -1 & 2 \end{bmatrix},$$
$$L^{(2)} = \begin{bmatrix} 2 & 0 & -1 & -1 & 0 \\ 0 & 2 & 0 & -1 & -1 \\ -1 & 0 & 2 & 0 & -1 \\ -1 & -1 & 0 & 2 & 0 \\ 0 & -1 & -1 & 0 & 2 \end{bmatrix}. \quad (20)$$

We choose the sampling period as $T = 0.05$ sec, control gain as $r_c = 0.5$, and the probability of successfully receiving information as $P = 0.9$. The initial condition is set to be $x(0) = [1, 2, 3, 4, 5]^T$, and it will be shown that the agents' states finally converge to the average value $\alpha = \text{Ave}(x(0)) = (1+2+3+4+5)/5 = 3$. Then, by solving the LMI in Theorem 4, the result shows that it is feasible. Thus, consensus will be achieved. The time history of the Bernoulli variable $\gamma_{ab}(k)$ is shown in Figure 2. Figure 3 compares the convergence speed of the nominal communication and the topology based on second-order neighbors' information with $P = 0.9$, from which we can see that the protocol we designed is more effective. Figure 4 compares the convergence speed based on second-order neighbors' information with $P = 0.9$ and $P = 0.5$, from which we can see the influence of packet losses.

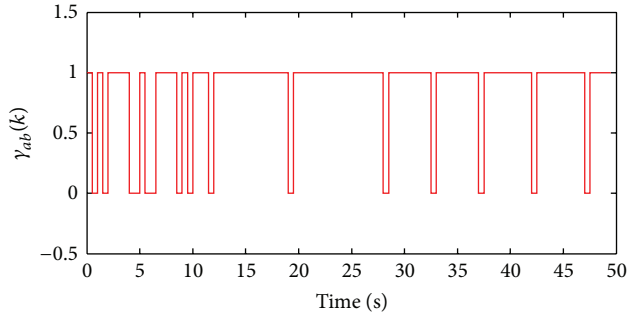

FIGURE 2: Time history of the Bernoulli variable $\gamma_{ab}(k)$.

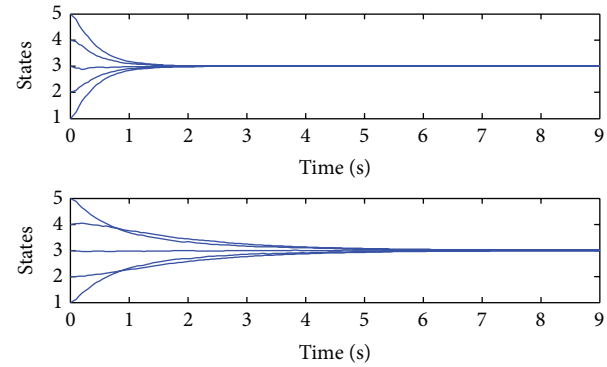

FIGURE 3: Nominal communication and the topology based on second-order neighbors' information with $P = 0.9$.

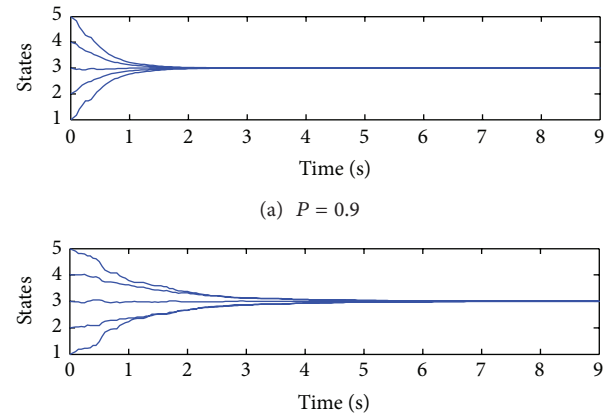

FIGURE 4: Comparison of the convergence speed based on second-order neighbors' information with different package loss probability.

5. Conclusions

In this paper, we have investigated the average consensus in multiagent systems with the problem of packet losses when second-order neighbors' information was used. The convergence rates of general protocol and second-order neighbor protocol with packet losses have been compared and it is concluded that second-order neighbor protocol speeds up the consensus rate. What is more, we can see

the influence of packet losses. Future work will extend the agent dynamics to second-order or higher-order dynamics with data loss and time-varying delay.

Conflict of Interests

The authors declare that there is no conflict of interests regarding the publication of this paper.

Acknowledgments

This work is supported by the National Natural Science Foundation (NNSF) of China under Grants no. 61004031, no. 61174096, and no. 61104141, Beijing Municipal Commission of Education Science and Technology Program (KM201310017006), and the Fundamental Research Funds for the Central Universities.

References

[1] H. Su, X. Wang, and Z. Lin, "Flocking of multi-agents with a virtual leader," *IEEE Transactions on Automatic Control*, vol. 54, no. 2, pp. 293–307, 2009.

[2] H. Su, N. Zhang, M. Z. Q. Chen, H. Wang, and X. Wang, "Adaptive flocking with a virtual leader of multiple agents governed by locally Lipschitz nonlinearity," *Nonlinear Analysis: Real World Applications*, vol. 14, no. 1, pp. 798–806, 2013.

[3] H. Michael, Z. Chen, X. Wang, and J. Lam, "Semi-global observer-based leader-following consensus with input saturation," *IEEE Transactions on Industrial Electronics*, vol. 61, no. 6, pp. 2842–2850, 2014.

[4] H. Su, M. Z. Q. Chen, J. Lam, and Z. Lin, "Semi-global leader-following consensus of linear multi-agent systems with input saturation via low gain feedback," *IEEE Transactions on Circuits and Systems I: Regular Papers*, vol. 60, no. 7, pp. 1881–1889, 2013.

[5] R. Olfati-Saber and R. M. Murray, "Consensus problems in networks of agents with switching topology and time-delays," *IEEE Transactions on Automatic Control*, vol. 49, no. 9, pp. 1520–1533, 2004.

[6] L. Xiao and S. Boyd, "Fast linear iterations for distributed averaging," *Systems & Control Letters*, vol. 53, no. 1, pp. 65–78, 2004.

[7] E. Kokiopoulou and P. Frossard, "Polynomial filtering for fast convergence in distributed consensus," *IEEE Transactions on Signal Processing*, vol. 57, no. 1, pp. 342–354, 2009.

[8] S. Boyd, A. Ghosh, B. Prabhakar, and D. Shah, "Randomized gossip algorithms," *IEEE Transactions on Information Theory*, vol. 52, no. 6, pp. 2508–2530, 2006.

[9] Z. Jin and R. M. Murray, "Multi-hop relay protocols for fast consensus seeking," in *Proceedings of the 45th IEEE Conference on Decision and Control 2006 (CDC '06)*, pp. 1001–1006, December 2006.

[10] D. Yuan, S. Xu, H. Zhao, and Y. Chu, "Accelerating distributed average consensus by exploring the information of second-order neighbors," *Physics Letters A*, vol. 374, no. 24, pp. 2438–2445, 2010.

[11] H. Pan and X. Nian, "Second-order consensus in multi-agent systems based on second-order neighbors' information," *International Journal of Systems Science*, pp. 1–22, 2012.

[12] Y. Zhang and Y.-P. Tian, "Consensus of data-sampled multi-agent systems with random communication delay and packet loss," *IEEE Transactions on Automatic Control*, vol. 55, no. 4, pp. 939–943, 2010.

[13] S. Wang, C. An, X.-X. Sun, and X. Du, "Average consensus over communication channels with uniform packet losses," in *Proceedings of the IEEE Control and Decision Conference (CCDC '10)*, pp. 114–119, May 2010.

[14] F. Fagnani and S. Zampieri, "Randomized consensus algorithms over large scale networks," *IEEE Journal on Selected Areas in Communications*, vol. 26, no. 4, pp. 634–649, 2008.

[15] F. Fagnani and S. Zampieri, "Average consensus with packet drop communication," *SIAM Journal on Control and Optimization*, vol. 48, no. 1, pp. 102–133, 2009.

[16] J. Wu and Y. Shi, "Average consensus in multi-agent systems with time-varying delays and packet losses," in *Proceedings of the American Control conference*, pp. 1579–1584, 2012.

[17] Y. Hatano and M. Mesbahi, "Agreement over random networks," *IEEE Transactions on Automatic Control*, vol. 50, no. 11, pp. 1867–1872, 2005.

[18] C. W. Wu, "Synchronization and convergence of linear dynamics in random directed networks," *IEEE Transactions on Automatic Control*, vol. 51, no. 7, pp. 1207–1210, 2006.

[19] M. Porfiri and D. L. Stilwell, "Consensus seeking over random weighted directed graphs," *IEEE Transactions on Automatic Control*, vol. 52, no. 9, pp. 1767–1773, 2007.

[20] W. Ren and R. W. Beard, "Consensus seeking in multiagent systems under dynamically changing interaction topologies," *IEEE Transactions on Automatic Control*, vol. 50, no. 5, pp. 655–661, 2005.

[21] Z. Lin, B. Francis, and M. Maggiore, "Necessary and sufficient graphical conditions for formation control of unicycles," *IEEE Transactions on Automatic Control*, vol. 50, no. 1, pp. 121–127, 2005.

[22] L. Moreau, "Stability of multiagent systems with time-dependent communication links," *IEEE Transactions on Automatic Control*, vol. 50, no. 2, pp. 169–182, 2005.